frontiers | Research Topics

Advances in estuarine and coastal nitrogen cycle

Edited by
Xianbiao Lin, Xiyang Dong, Shuting Liu and Jing Wei

Published in
Frontiers in Marine Science

ISSN 1664-8714
ISBN 978-2-83251-521-1
DOI 10.3389/978-2-83251-521-1

About Frontiers

Frontiers is more than just an open access publisher of scholarly articles: it is a pioneering approach to the world of academia, radically improving the way scholarly research is managed. The grand vision of Frontiers is a world where all people have an equal opportunity to seek, share and generate knowledge. Frontiers provides immediate and permanent online open access to all its publications, but this alone is not enough to realize our grand goals.

Frontiers journal series

The Frontiers journal series is a multi-tier and interdisciplinary set of open-access, online journals, promising a paradigm shift from the current review, selection and dissemination processes in academic publishing. All Frontiers journals are driven by researchers for researchers; therefore, they constitute a service to the scholarly community. At the same time, the *Frontiers journal series* operates on a revolutionary invention, the tiered publishing system, initially addressing specific communities of scholars, and gradually climbing up to broader public understanding, thus serving the interests of the lay society, too.

Dedication to quality

Each Frontiers article is a landmark of the highest quality, thanks to genuinely collaborative interactions between authors and review editors, who include some of the world's best academicians. Research must be certified by peers before entering a stream of knowledge that may eventually reach the public - and shape society; therefore, Frontiers only applies the most rigorous and unbiased reviews. Frontiers revolutionizes research publishing by freely delivering the most outstanding research, evaluated with no bias from both the academic and social point of view. By applying the most advanced information technologies, Frontiers is catapulting scholarly publishing into a new generation.

What are Frontiers Research Topics?

Frontiers Research Topics are very popular trademarks of the *Frontiers journals series*: they are collections of at least ten articles, all centered on a particular subject. With their unique mix of varied contributions from Original Research to Review Articles, Frontiers Research Topics unify the most influential researchers, the latest key findings and historical advances in a hot research area.

Find out more on how to host your own Frontiers Research Topic or contribute to one as an author by contacting the Frontiers editorial office: frontiersin.org/about/contact

Advances in estuarine and coastal nitrogen cycle

Topic editors

Xianbiao Lin — Ocean University of China, China

Xiyang Dong — Third Institute of Oceanography of the Ministry of Natural Resources, China

Shuting Liu — Kean University, United States

Jing Wei — Sun Yat-sen University, China

Citation

Lin, X., Dong, X., Liu, S., Wei, J., eds. (2023). *Advances in estuarine and coastal nitrogen cycle*. Lausanne: Frontiers Media SA. doi: 10.3389/978-2-83251-521-1

Table of contents

frontiers | Frontiers in Marine Science

TYPE Editorial
PUBLISHED 17 January 2023
DOI 10.3389/fmars.2023.1130839

OPEN ACCESS

EDITED AND REVIEWED BY
Eric 'Pieter Achterberg,
Helmholtz Association of German
Research Centres (HZ), Germany

*CORRESPONDENCE
Shuting Liu
liushut@kean.edu
Xianbiao Lin
linxianbiao@ouc.edu.cn

SPECIALTY SECTION
This article was submitted to
Marine Biogeochemistry,
a section of the journal
Frontiers in Marine Science

RECEIVED 23 December 2022
ACCEPTED 09 January 2023
PUBLISHED 17 January 2023

CITATION
Wei J, Dong X, Liu S and Lin X
(2023) Editorial: Advances in
estuarine and coastal nitrogen cycle.
Front. Mar. Sci. 10:1130839.
doi: 10.3389/fmars.2023.1130839

Editorial: Advances in estuarine and coastal nitrogen cycle

Jing Wei[1,2], Xiyang Dong[2,3], Shuting Liu[4]* and Xianbiao Lin[5]*

[1]School of Atmospheric Sciences, Sun Yat-sen University, Zhuhai, Guangdong, China, [2]Southern Marine Science and Engineering Guangdong Laboratory (Zhuhai), Zhuhai, Guangdong, China, [3]Key Laboratory of Marine Genetic Resources, Third Institute of Oceanography, Ministry of Natural Resources, Xiamen, China, [4]Department of Environmental & Sustainability Sciences, Kean University, Union, NJ, United States, [5]Frontiers Science Center for Deep Ocean Multispheres and Earth System, and Key Laboratory of Marine Chemistry Theory and Technology, Ministry of Education, Ocean University of China, Qingdao, China

KEYWORDS

organic nitrogen, inorganic nitrogen, N forms, N fluxes, nitrous oxide, microbial metabolisms, climate change, estuarine and coastal ecosystems

Editorial on the Research Topic
Advances in estuarine and coastal nitrogen cycle

Dramatically increased reactive nitrogen (N) inputs over the past decades caused numerous eco-environmental problems in coastal marine ecosystems (Wei et al., 2022; Wei et al., 2023). Estuarine and coastal ecosystems are not only critical zones connecting terrestrial and marine ecosystems, but also a hotpot for greenhouse gas nitrous oxide (N_2O) emissions and diverse N biogeochemical processes such as denitrification, anammox, and N burial in sediment (Figure 1). In estuarine and coastal ecosystems, N cycling is temporally and spatially complex and dynamically influenced by multiple interrelated ecosystem components (Liu et al., 2020; Murray et al., 2020). It is necessary to deepen our knowledge of N cycle in estuarine and coastal ecosystems (Tian et al., 2020; Harris et al., 2022). Within this aspect, this Research Topic focuses on spatiotemporal N variations, N fluxes, as well as their controlling factors and environmental implications. Sixteen articles were finally collected in this Research Topic as summarized below.

Variations in natural forcing and environmental conditions affect spatiotemporal patterns of nitrogen cycle processes. Zhang et al. investigated the influence of the tidal cycle on total nitrogen (TN) and N speciation in a coastal bay. They reported that while TN concentrations during the spring and neap tides did not differ, significant differences in particulate nitrogen (PN) and NO_2^- were observed between the spring and neap tides. Furthermore, the net exchange flux of TN during spring tide was 4.3 times higher than that of neap tide. They also reported an above 50% contribution of the total dissolved nitrogen (TDN) pool in TN. Among TDN, dissolved organic nitrogen (DON) accounted for higher proportion during the spring tides compared to neap tides. Xu et al. show that both local and remote forcing, such as winds, upwelling, and climate factors like El Niño-Southern Oscillation, Pacific Decadal Oscillation, and North Pacific Gyre Oscillation, affected the variations of sedimentary nitrogen isotope ($\delta^{15}N_{sed}$) in the Santa Barbara Basin (SBB). Sedimentary nitrogen isotopes has often been used as a proxy for the denitrification process to track temporal record. For instance, the long-term variations of the SBB $\delta^{15}N_{sed}$ signature with decreasing and increasing trend from 1940 to 2019 reflect changes in denitrification

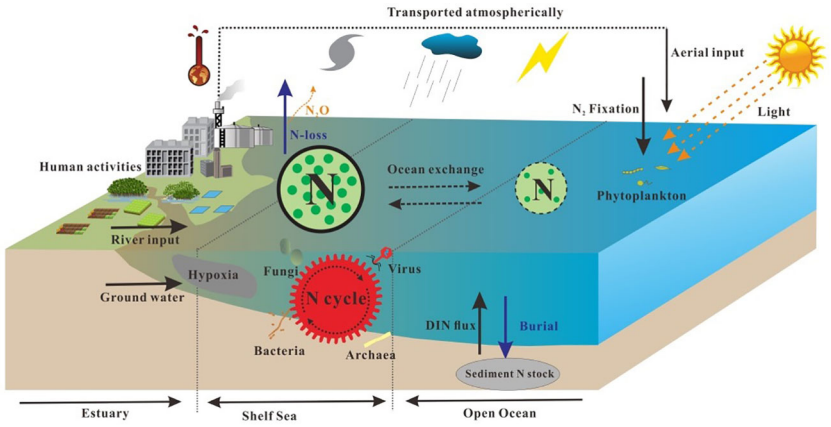

FIGURE 1
N cycle in estuarine and coastal ecosystem.

induced by the strength of tropical trade winds in the eastern tropical North Pacific. Yan et al. studied high-resolution N dynamics in the upper water column of the South China Sea to interpret mechanisms controlling N cycling in the water. They resolved the dominant N sources and processes, including atmospheric N deposition (AND)/N_2-fixation, assimilative fractionation, and nitrification, and quantitatively evaluated their contributions in the vertical distribution of NO_3^- in the water column. They showed variations in nitrification and AND/N_2 fixation sources of NO_3^- assimilated by phytoplankton between different water layers.

In addition to natural processes, human activities can affect nitrogen stocks and fluxes in estuarine and coastal ecosystems. Dun et al. found that seawater intrusion and human activities affect the hydrochemical characteristics of groundwater in the Pearl River Estuary, which resulted in elevated NO_3^- concentrations. They also revealed zonation of groundwater depending on distinct major controlling factors of groundwater characteristics. Li et al. found that long-term grazing prohibition significantly increased nitrification and denitrification rates in the salt marsh on Chongming Island, which indicated that the implementation of reasonable grazing prohibition policies in salt marshes has great potential to restore their ecosystem functions and achieve their goal of sustainable development. Qin et al. examined seasonal changes in various N subpools of plant-soil subsystems in embanked and adjacent S. alterniflora natural salt marshes on the coast of Eastern China. The embankment with purpose of holding seawater back from salt marshes significantly reduced both litter and root N storage by varying extent over either all or specific seasons. The different nitrogen pools such as soil organic nitrogen (SON), labile organic nitrogen (LON), recalcitrant organic nitrogen (RON), and ammonium concentrations also declined significantly by different levels, over the four seasons following the embankment construction. Liu et al. found that the conversion of natural marshland to shrimp aquaculture ponds significantly promoted sediment N fixation rates, which may be mainly attributed to the change of sediment electrical conductivity (EC), total organic carbon (TOC) and Fe^{2+}/Fe^{3+} rather than the change of N fixation gene abundance. In addition, increasing inhibiting effect of inorganic N concentration with reclamation time has been revealed from no obvious difference in sediment N fixation rates between 5-year-old shrimp ponds and 18-year-old shrimp ponds. In another shrimp aquaculture study, Sun et al. reported that denitrification was responsible for the majority of the total NO_3^- reduction, surpassing anammox in the sediment from eight studied shrimp ponds. Their results of high NO_3^- reduction rate and N loss indicate that coastal reclamation is a non-negligible way to remove nitrogen in the artificial aquatic environment of shrimp ponds. In three types of aquaculture ecosystems (seabass, white shrimp, and green crab ponds), Lin et al. showed higher fluxes of total mineralized N relative to immobilized N fluxes in aquaculture surface sediment from the Guangdong-Hong Kong-Macao Greater Bay Area, indicating that the sediment serves as an important source of eutrophication in reclaimed aquaculture system of coastal wetland.

Microbes such as bacteria, archaea, and fungi are key components responsible for many N transformation and consumption processes. The review by Wei et al. who conducted a scientometric analysis on a co-citation network consisting of 835 references derived from 354 citing articles and summarized the distribution of denitrifying anaerobic methane oxidation (DAMO) in both freshwater and coastal environments. DAMO involves two possible pathways mediated either by bacteria or archaea. They found archaea pathway is generally under-studied compared to bacteria pathway and coastal systems are generally under-studied in comparison to freshwater systems. The emerging research topics in this area include coupling of alternative electron acceptors with AMO processes and their role as CH_4 sinks. Several areas that require further research were identified from Wei et al. and future research including comparisons of DAMO with other N cycling pathways and environmental conditions in the context of the river-estuary sea continuum has been proposed. Tang et al. investigated microbial uptake and oxidation processes of two reduced N forms, ammonium and urea, in a eutrophic estuary. They showed that shallow light penetration depth leaves 76% of estuary water bodies to stay in dark throughout a day and thus ammonium oxidation, which favors dark conditions, dominates the estuarine regenerated-N cycle. Microorganisms' high preference for ammonium over urea showed the following rank: ammonia oxidation > ammonium uptake >> urea

uptake ≈ urea oxidation. Maxwell Lazo-Murphy et al. isolated four fungi strains (*Purpureocillium lilacinum, Trichoderma harzianum, Trichoderma virens*, and *Rhodotorula glutinis*) from salt marsh sediments in North Inlet, South Carolina, USA and discovered that up to 22.8% of nitrite provided in growth media was converted to N_2O by isolated fungal strains, implying of an additional significant source of N_2O emission from fungi. Using isotope mass balance approach, they showed that the site preference (SP) of N_2O produced by salt marsh sediment fungi, which changes in intramolecular distribution of ^{15}N and is used as a tracer to identify the source of N_2O among bacteria, archaea, and fungi, ranged from 7.5 ± 1.6‰ to 33.4 ± 1.2‰ in the four isolates and expanded our standing of relative contribution of fungi to N_2O production in salt marsh sediments.

Detection of microbial targeted genes can also indicate N-related dynamics. For examples, copper-containing nitrite reductase gene (*nirK*) and cytochrome cd1-containing nitrite reductase gene (*nirS*) are two gene markers that are widely used to study denitrifying microbes (Wolsing and Priemé, 2004; Santoro et al., 2006). Zhao et al. showed that the *nirK*-type denitrifying bacteria were more sensitive to a macroalgae green tide than the *nirS*-type denitrifying bacteria, as bacterial community structures differed depending on the algal bloom stages with the more stable and complex *nirK*-type denitrifying bacterial interactions during the bloom outbreak phase in contrast to the more stable and complex *nirS*-type denitrifying bacterial interactions during the bloom decline phase. Their results demonstrated that different type denitrifying bacteria may occupy different niches during the green tide in coastal Qingdao areas. Comparing gene markers between two nitrogen removal processes (denitrification and anammox) in the surface sediments from Yangtze Estuary and adjacent sea, results from Teng et al. suggested that the gene abundances of *nirS* and *nirK* for denitrifiers were higher than that of AMX 16S rRNA for anammox bacteria, indicating of denitrification as the dominant nitrogen removal pathway in the studied region. Teng et al. also found different spatial distribution patterns between the genera composition of *nirS*- and *nirK*-encoding denitrifiers communities. Furthermore, they discovered novel bacteria genera with anammox oxidation capacity in marine sediments. Besides nitrogen removal, nitrogen fixation process can also be studied through targeted genes such as *nifH* gene. Song et al. demonstrated the main soil physicochemical factors shaping diazotroph communities in coastal saline soils. For instance, they showed that the copy number of *nifH* gene, which encodes the Fe protein subunit of the nitrogenase in the nitrogen fixation process, was significantly affected by soil physiochemical factors, the abundance of diazotrophs in the rhizospheric soil samples was positively related with soil physicochemical properties, and diazotrophic community structure significantly varied with environmental parameters including soil salinity, moisture, pH and total nitrogen, carbon, sulphur and nitrite content.

N cycle is sometimes intertwined with other elemental cycles. Hu et al. demonstrated that the facilitation effect on litter accumulative CO_2 release by N amendments was more and more obvious over the litter decomposition time in the estuarine marsh. Increase of accumulative CO_2 release varied among N amendment treatments with different dose. These observations highlight that N deposition could cause high losses of litter C and emissions of greenhouse gas CO_2.

Overall, these articles presented in this research topic represent important progress, datasets, as well as novel methodologies in understanding of N cycle in estuarine and coastal ecosystem.

Author contributions

XL invited the other guest editors JW, SL, and XD to design this Research Topic. All guest editors have edited and reviewed the editorial article, and approved the submitted version.

Funding

This study was supported by Guangdong Major Project of Basic and Applied Basic Research (2020B0301030004), Fundamental Research Funds for the Central Universities (202262007), Guangdong Province Key Laboratory for Climate Change and Natural Disaster Studies (Grant 2020B1212060025), Innovation Group Project of Southern Marine Science and Engineering Guangdong Laboratory (Zhuhai) (No. 311021009), and the National Natural Science Foundation of China (U21A6001).

Conflict of interest

The authors declare that the research was conducted in the absence of any commercial or financial relationships that could be construed as a potential conflict of interest.

Publisher's note

References

Harris, E., Yu, L., Wang, Y. P., Mohn, J., Henne, S., Bai, E., et al. (2022). Warming and redistribution of nitrogen inputs drive an increase in terrestrial nitrous oxide emission factor. *Nat. Commun.* 13, 4310. doi: 10.1038/s41467-022-32001-z

Liu, Q., Liang, Y., Cai, W.-J., Wang, K., Wang, J., and Yin, K. (2020). Changing riverine organic C:N ratios along the pearl river: Implications for estuarine and coastal carbon cycles. *Sci. Total Environ.* 709, 136052. doi: 10.1016/j.scitotenv.2019.136052

Murray, R., Erler, D. V., Rosentreter, J., Wells, N. S., and Eyre, B. D. (2020). Seasonal and spatial controls on N_2O concentrations and emissions in low-nitrogen estuaries: Evidence from three tropical systems. *Mar. Chem.* 221, 103779. doi: 10.1016/j.marchem.2020.103779

Santoro, A. E., Boehm, A. B., and Francis, C. A. (2006). Denitrifier community composition along a nitrate and salinity gradient in a coastal aquifer. *Appl. Environ. Microbiol.* 72, 2102–2109. doi: 10.1128/AEM.72.3.2102-2109.2006

Tian, H., Xu, R., Canadell, J. G., Thompson, R. L., Winiwarter, W., Suntharalingam, P., et al. (2020). A comprehensive quantification of global nitrous oxide sources and sinks. *Nature* 586, 248–256. doi: 10.1038/s41586-020-2780-0

Wei, J., Knicker, H., Zhou, Z., Eckhardt, K.-U., Leinweber, P., Wissel, H., et al. (2023). Nitrogen immobilization caused by chemical formation of black- and amide-n in soil. *Geoderma* 429, 116274. doi: 10.1016/j.geoderma.2022.116274

Wei, J., Zhang, X., Xia, L., Yuan, W., Zhou, Z., and Brüggmann, N. (2022). Role of chemical reactions in the nitrogenous trace gas emissions and nitrogen retention: A meta-analysis. *Sci. Total Environ.* 808, 152141. doi: 10.1016/j.scitotenv.2021.152141

Wolsing, M., and Priemé, A. (2004). Observation of high seasonal variation in community structure of denitrifying bacteria in arable soil receiving artificial fertilizer and cattle manure by determining T-RFLP of nir gene fragments. *FEMS Microbiol. Ecol.* 48, 261–271. doi: 10.1016/j.femsec.2004.02.002

frontiers | Frontiers in Marine Science

ORIGINAL RESEARCH
published: 14 July 2022
doi: 10.3389/fmars.2022.945330

Hydrochemical Evolution and Nitrogen Behaviors in Coastal Groundwater Suffered From Seawater Intrusion and Anthropogenic Inputs

*Yu Dun[1], Junhong Ling[2], Rui Wang[3], Jun Wei[3], Qianyi Zhou[4], Yingjie Cao[4], Yizhang Zhang[2,5] and Yingxue Xuan[4]**

[1] Institute of Hydrogeology & Environmental Geology, Chinese Academy of Geological Sciences & Key Laboratory of Groundwater Remediation of Hebei Province and China Geological Survey, Shijiazhuang, China, [2] Research Institute for Environmental Innovation (Tianjin Binhai), Tianjin, China, [3] Shenzhen Branch of PowerChina HuaDong Engineering Corporation Limited, Hangzhou, China, [4] School of Environmental Science and Engineering, Sun Yat-Sen University & Southern Marine Science and Engineering Guangdong Laboratory (Zhuhai), Guangzhou, China, [5] State Key Laboratory of Environmental Criteria and Risk Assessment, Chinese Research Academy of Environmental Sciences, Beijing, China*

OPEN ACCESS

Edited by:
Xianbiao Lin,
Ocean University of China, China

Reviewed by:
Dengzhou Gao,
East China Normal University, China
Xiaoli Zhang,
Yantai Institute of Coastal Zone Research (CAS), China

***Correspondence:**
Yingxue Xuan
xuanyx3@mail.sysu.edu.cn

Specialty section:
This article was submitted to Marine Biogeochemistry, a section of the journal Frontiers in Marine Science

Received: *16 May 2022*
Accepted: *01 June 2022*
Published: *14 July 2022*

Citation:
Dun Y, Ling J, Wang R, Wei J, Zhou Q, Cao Y, Zhang Y and Xuan Y (2022) Hydrochemical Evolution and Nitrogen Behaviors in Coastal Groundwater Suffered From Seawater Intrusion and Anthropogenic Inputs. Front. Mar. Sci. 9:945330. doi: 10.3389/fmars.2022.945330

Coastal aquifers play key roles in providing freshwater resources to maintain the social and economic development in coastal areas. However, climate change and human activities have dramatically affected the quantities and qualities of groundwater in coastal aquifers. In this study, stoichiometric analysis of hydrogeochemistry, multivariate analysis, and isotopic trancing techniques were used to reveal the local hydrochemistry characteristics, the natural and anthropogenic origins, and the major hydrochemical evolution in a typical coastal aquifer located in the Pearl River estuary. According to hydrogeological conditions and groundwater burial conditions, the aquifer was divided into three zones, namely, semiconfined fissure groundwater (SFGW), recharged fissure groundwater (RFGW), and porous medium groundwater (PGW). Seawater intrusion, ion exchange, water–rock reaction, and human activities were the main controlling factors affecting the characteristics of groundwater, but there were significant differences in the main controlling effects of different zones. Among them, the samples from the SFGW was severely affected by seawater intrusion, and the contributions of seawater ranged from 6% to 97%. Obvious cation exchange process occurred during the seawater intrusion. The hydrochemical characteristics of the PGW and the RFGW were mainly controlled by water–rock interaction. In addition, human activities had further influence on the hydrochemical characteristics of groundwater, which resulted in elevated nitrate–nitrogen (NO_3^-–N). The mean NO_3–N concentrations in the PGW and the SFGW were 6.58 and 3.07 mg/L, respectively. Furthermore, the $\delta^{15}N$–NO_3^- and $\delta^{18}O$–NO_3^- values in these two regions ranged from +2.35‰ to +27.54‰ and from +0.39‰ to +18.95‰, respectively, indicating that the anthropogenic input contributed to the increased nitrate. Redox analysis and dual nitrogen isotopic evidence indicated that denitrification was the predominant biogeochemical process in the PGW and the RFGW. This study highlights the impacts of seawater intrusion and anthropogenic inputs on hydrochemical evolution

and nitrogen behaviors in coastal groundwater, which provides a scientific basis for the management of groundwater resources in coastal aquifers.

Keywords: coastal aquifers, nitrogen cycling, groundwater, seawater intrusion, anthropogenic inputs

1 INTRODUCTION

Globally, population concentrating in coastal areas has significantly increased due to the geographical advantages provided in these areas and the large development of industrial activities (Xiong et al., 2020). It is estimated that 50%–70% of the global population lives along coastal areas that only account for approximately 5% of world's surface area (Council, 2007; Steyl and Dennis, 2010). Water resources are key factors of sustainable development, and coastal aquifers provide freshwater to more than one billion people lived in these areas (Small and Nicholls, 2003; Ferguson and Gleeson, 2012). However, climate change and human activities have dramatically affected the quantities and qualities of groundwater in coastal aquifers. For example, saltwater intrusion exacerbated by groundwater extraction and rising sea levels would degrade the quality and the quantity of freshwater available in coastal aquifers (Argamasilla et al., 2017; Parizi et al., 2019; Abd-Elaty et al., 2020; Rakib et al., 2020). Human activities, such as industry, agriculture, and urbanization would also affect groundwater resources (Wakida and Lerner, 2005; Wei et al., 2020). Among these factors, the impact of human activities on water resources is anticipated to increase over the next few decades and to be more significant than that of climate change (Vörösmarty et al., 2000; Lin et al., 2016). Urbanized coastal aquifer acts as a reservoir for "pollution collection" and "pollution transport," which records changes in pollutants under anthropogenic impacts and has become pools of reactive major or trace elements and hotspots of regional pollution (Hale et al., 2014; Zhang et al., 2015; Lin et al., 2017; Huang et al., 2021). Therefore, it is essential to investigate the groundwater quality, distribution, and transformations of major pollutants in a highly urbanized coastal aquifer suffered from both the seawater intrusion and the anthropogenic pollutant inputs, which could be helpful to the groundwater resource management.

In general, the environmental fate of major pollutants such as nitrogen, organic matters, and trace metals depends on redox condition in aquifers (Appelo and Dimier, 2004; Wang et al., 2016). The redox processes in groundwater generally include the reduction of O_2, NO_3^-, Mn(IV), Fe(III), SO_4^{2-}, and CO_2 (Froelich et al., 1979; Schüring et al., 2000). Among these processes, denitrification (reduction of NO_3^- to N_2O/N_2), methanogenesis, and sulfate reduction are the major redox processes in the coastal aquifer due to the lack of O_2 (Huang et al., 2022b). However, the redox processes in the coastal aquifer have relatively spatial and temporal heterogeneity that are mainly influenced by terrestrial pollutants and saltwater intrusion (Wei and Lin, 2021). How to reveal the redox processes in groundwater and clarify the controlling factors are a huge challenge. Stable isotopic technology is recognized as a powerful tool for understanding the origins of water and dissolved constituents, and the biogeochemical processes in the groundwater (Kendall, 1998; Cook and Herczeg, 2000). For example, dual isotopes ($\delta^{15}N$ and $\delta^{18}O$) of nitrate have commonly been utilized to quantify the nitrate sources and to identify the occurrence of nitrogen transformations (Fukada et al., 2003; Choi et al., 2007; Hosono et al., 2013; Weng et al., 2017; Lin et al., 2021). The ratios of the $\delta^{15}N$ and $\delta^{18}O$ values in the remaining nitrate are assumed to be close to 1.5:1 or even 2:1 if denitrification occurred (Mengis et al., 1999; Kendall et al., 2007). Thus, in order to identify the redox processes and the environmental fate of major pollutants in the groundwater, coupled nitrogen and oxygen isotopes technique of nitrate was used in this study.

Shenzhen, located along the east bank of the Pearl River Estuary in China, is a typical city that has undergone rapid urbanization. Because of the special geographical conditions, there are no large rivers, large lakes, and large reservoirs in Shenzhen. The per capita water resources are<200 m^3, which is roughly 1/11 of the average level of China and lower than the world water crisis standard (Chen et al., 2020), showing a serious shortage of local water resources. The groundwater resources in the coastal aquifer of Shenzhen are underutilized, and the amount of groundwater supply was only 2.8×10^6 m^3/year (SMWB, 2019). Regional groundwater budget and numerical simulation showed that estimated average groundwater recharge was approximately 12% of annual precipitation (Lancia et al., 2019). As a strategic water resource and environmental asset, it is urgent to evaluate the water quality and major pollutants in the local aquifer. Although recent studies on the evolution of resources and chemistry in the groundwater have been conducted in Shenzhen city, including the effects of sewers on the amount of groundwater (Lancia et al., 2020), and the groundwater chemistry and its main geochemical factors (Shi et al., 2018), it is still unclear which major biogeochemical processes are likely to contribute to the environmental fate of major pollutants under the impacts of seawater intrusion and anthropogenic activities. Therefore, in this study, hydrogeochemical and isotope techniques were used in the coastal aquifer to (1) characterize the hydrogeochemistry, (2) identify the sources of major and trace elements, and (3) identify the major biogeochemical processes of the hydrochemical evolution suffered from seawater intrusion and anthropogenic disturbance.

2 STUDY SITE

The study area is located in the east coast of the Pearl River Estuary (**Figure 1**). The total area is 186.88 km^2 with a 29.9-km-long coastline. The topography of the study area is

generally steep, declining from the east hill zone (100–150 m) to the west coastline (5–25 m). The climate is a typical subtropical monsoon climate with annual average precipitation of 1,935.8 mm and annual average temperature of 23.0°C.

Triassic–Jurassic sedimentary formation contains interbedded sedimentary successions of glutenite, sandstones, and siltstones outcrops in the north and the east part of this study area (**Figure 1**). The west part is mainly overlaid by a thin clay layer (aquitard) and quaternary sediment with a thickness of 2–5 m in sequence (**Figure 1**). This fissure medium constitutes the major part of aquifer (FGW, fissure groundwater) in the study area (Han et al., 2009). The characteristics of the aquitard in this study indicated that the west region is the semiconfined fissure groundwater, and the north and east regions are the recharge zone of fissure groundwater. Therefore, the FGW could be further defined as two subzones, the FGW that could be recharged by precipitation (RFGW) and the semiconfined FGW (SFGW) (**Figure 1**). The overlaying quaternary sediment is recognized as the porous medium aquifer (PGW, porous groundwater, **Figure 1**). The PGW has relatively poor vertical hydraulic connection with the FGW but receives lateral recharge from the FGW. In addition, diffuse recharge by precipitation and river are also important recharge sources for the FGW.

As one of China's current national key economic development regions, Shenzhen city is a complex urbanized region with population dynamics, intense economic activities, and innovative clusters (Hui et al., 2018; Gao, 2019). In the study area, the gross domestic product (GDP) has increased from 182.95 billion in 2007 to 345.32 billion in 2017. The rapid economic and social development caused remarkable increased sewage inputs in the past decades, which resulted in the deterioration of local groundwater system.

3 MATERIALS AND METHODS

3.1 Field Procedures

The spatial distributions of major elements, trace metals, and pollutants in the study area were investigated based on 57 sampling sites those that were collected in June 2015 (**Figure 1**). Groundwater samples were mainly collected from domestic and industrial wells. The well information, such as well depth, location, and operating interval, was recorded by questionnaire surveys. Based on the geology conditions, groundwater samples were classified into two groups: groundwater from the north and east recharge zone of fissure aquifer (RFGW, 20 samples) and groundwater from the west porous aquifer (PGW, 37 samples). Hydrochemistry data of 12 samples from the semiconfined fissure aquifer (SFGW) were compiled and reported by Jiang et al. (2009).

Field parameters for groundwater samples, including temperature (T), pH, electric conductivity (EC), redox potential (Eh), oxidation reduction potential (ORP), and dissolved oxygen (DO), were measured *in situ* using portable equipment (YSI EXO2 Multiparameter Sondes). Alkalinity was also determined on-site using the Gran titration method. Before sampling, the groundwater was pumped from the well until the EC value remained constant. Samples used for testing NH_4^+ concentrations were filtered by a 0.45-μm syringe-tip filter and then were acidified with reagent-quality HCl to a pH of approximately 4.0 to

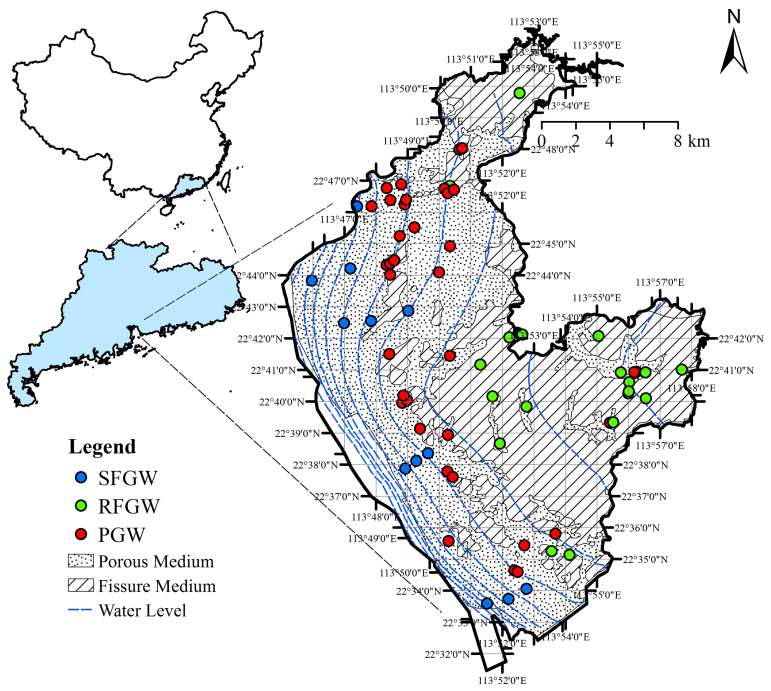

FIGURE 1 | Sampling and geology map and groundwater flow field.

avoid NH_4^+ volatilization. Samples for trace metal analysis were filtered through vacuum filtration with 0.45-μm membranes and acidified with reagent-quality HNO_3 to pH<2 on site. Samples for analyses of the major ion (Na^+, K^+, Mg^{2+}, Ca^{2+}, Cl^-, SO_4^{2-}, and NO_3^-) concentrations and the isotopes of nitrate ($\delta^{15}N–NO_3^-$ and $\delta^{18}O–NO_3^-$) were filtered by 0.45-μm membranes and collected in 100-ml polyethylene bottles. Once filtered and acidified, the samples were kept cold by an ice bag in the field. All samples were brought back to the laboratory and stored at 4°C before further analysis.

3.2 Laboratory and Statistical Analysis

Dissolved cations (Na^+, K^+, Mg^{2+}, and Ca^{2+}) and anions (Cl^-, SO_4^{2-}, and NO_3^-) concentrations were measured using ion chromatography (Thermo Fisher ICS-900) with limit of detection of 0.01 mg/L. Sample replicates were chosen at random, and all fell within 5% for major compositions. Trace metals including Fe and Mn were analyzed by inductively coupled plasma mass spectrometry (ICP-MS, NexION 350D, PerkinElmer, USA).

The $\delta^{15}N–NO_3^-$ and $\delta^{18}O–NO_3^-$ values were determined using the bacterial denitrifier method (Sigman et al., 2001; Casciotti et al., 2002). Briefly, the NO_3^- in the groundwater samples was converted to N_2O by denitrifying bacteria that lack N_2O-reductase activity. Then, the N_2O was extracted and purified through a precon system, and $\delta^{15}N–NO_3^-$ and $\delta^{18}O–NO_3^-$ were analyzed using an isotope ratio mass spectrometer (Thermo Fisher DELTA-V Advantage). Three international references (IAEA-N3, USGS34, and USG35) were used to correct the isotope values of samples. The analytical precisions for $\delta^{15}N–NO_3^-$ and $\delta^{18}O–NO_3^-$ were ±0.4‰ and ±0.5‰, respectively.

Descriptive statistics and factor analysis were conducted using SPSS version 22.0. One-way ANOVA was used to test the spatial differences in major ion concentrations, trace metal concentrations, pollutant concentrations, and nitrogen and oxygen isotopes in nitrate with significance at $p<0.05$. Factor analysis was employed to unravel the underlying data set through the reduced new variables, and the significant factors affecting the characteristics of water chemistry were analyzed. The map of sampling sites was generated using ArcGIS 10.2.

4 RESULTS

4.1 Field Parameter and Major Element

During the sampling period, for the samples from the FGW, the temperature ranged from 25.0. to 28.9°C. Wide ranges for EC, pH, and ORP were observed. EC ranged from 62 to 534 μs/cm, with an average of 197 μs/cm. Most samples were acidic with an averaged pH value of 5.45. ORP ranged from −116 to +311 mV, and its mean value was −53 mV. For the samples from the PGW, the temperature was relatively higher, with a range from 26.5°C to 31.5°C. Elevated EC has been observed and ranged from 283 to 2220 μs/cm, with an average of 793 μs/cm. The pH was also higher than that from the fissure groundwater, with an average of 6.44. The ORP had a wide range from −602 to +281 mV.

The Piper plot was employed here to identify groundwater hydrochemical patterns (**Figure 2**). For the samples from the PGW, the cation was dominated by Ca^{2+} (mean=1.68 mmol/L) and Na^+ (mean=2.10 mmol/L), and the anion was dominated by HCO_3^- (mean=0.79 mmol/L). The hydrochemical pattern was Ca–HCO_3. The order of abundance (expressed by meq/L) of the major cations was $Ca^{2+}>Na^+>Mg^{2+}>K^+$, and the order of abundance for the major anions was $HCO_3^->Cl^->SO_4^{2-}$. For the samples from the RFGW, the cation was also dominated by Ca^{2+} (mean=0.35 mmol/L) and Na^+ (mean=0.46 mmol/L), and the anion was dominated by HCO_3^- (mean=0.79 mmol/L). The hydrochemical pattern was Ca–HCO_3, which was similar to that in the PGW. The order of abundance of major cations was $Ca^{2+}>Na^+>Mg^{2+}>K^+$, and the order of abundance for the major anions was $HCO_3^->Cl^->SO_4^{2-}$. High salinization was identified in the SFGW samples, and the hydrochemical pattern was Na–Cl. Prevalent cations were Na^+ and K^+, and the most abundant anion was Cl^-.

4.2 Trace Metals Concentrations

Groundwater trace metal concentrations had a wide range within the aquifer (**Figure 3**), for instance, Fe (3.60–2,687.66 μg/L), Mn (0.65–569.86 μg/L), Ba (3.30–174.32 μg/L), Zn (0.23–99.28 μg/L), Al (0.11–80.91 μg/L), Cr (0.73–17.06 μg/L), As (0.25–38.04 μg/L), Ni (0.21–28.15 μg/L), Mo (0.02–14.21 μg/L), Se (0.00–6.99 μg/L), Cu (0.17–3.93 μg/L), Co (0.0.1–13.22 μg/L), Pb (0.00–7.86 μg/L), Cd (0.00–0.37 μg/L), and Be (0.00–1.00 μg/L). Among the 15 trace metals analyzed, Ni, Pb, and Cd are the most toxic. According to the WHO drinking water guidelines (WHO, 2011), the highest admissible concentrations of Ni, Pb, and Cd are 70, 10, and 3 μg/L, respectively. In our study area, concentrations of Ni and Pb in all the samples were below the guideline values of WHO; only one sample had Cd of 0.375 ug/L that was higher than the guideline value.

4.3 Pollutant Concentrations and Isotope Signatures

Nitrogen (NH_4–N, NO_2–N, NO_3–N, and TN) concentrations showed significant spatial distributions (**Figure 4**). The NO_3–N was detected in both the PGW and the SFGW with averaged concentrations of 6.58 and 3.07 mg/L, respectively. The NH_4–N was mainly detected in the PGW with an averaged concentration of 8.21 mg/L. The NO_2–N was also detected in PGW with an averaged concentration of 0.40 mg/L. As a whole, NO_3–N was the predominant species of dissolved inorganic nitrogen in the RFGW, and NH_4–N was the predominant species in the PGW, while the DFGW samples were free of nitrogen contamination. The COD concentrations of groundwater ranged from 0.1 to 75.0 mg/L, which showed spatial variations. The range of COD concentrations in the PGW was from 0.1 to 75.0 mg/L with an average of 21.9 mg/L, while the range of COD concentrations was from 0.1 to 57 mg/L with an average of 26.7 mg/L in the RFGW. The $\delta^{15}N–NO_3^-$ and $\delta^{18}O–NO_3^-$ values in the PGW ranged from +12.81‰ to +27.54‰ and from 7.54‰ to +18.95‰, respectively, while for the samples from the RFGW,

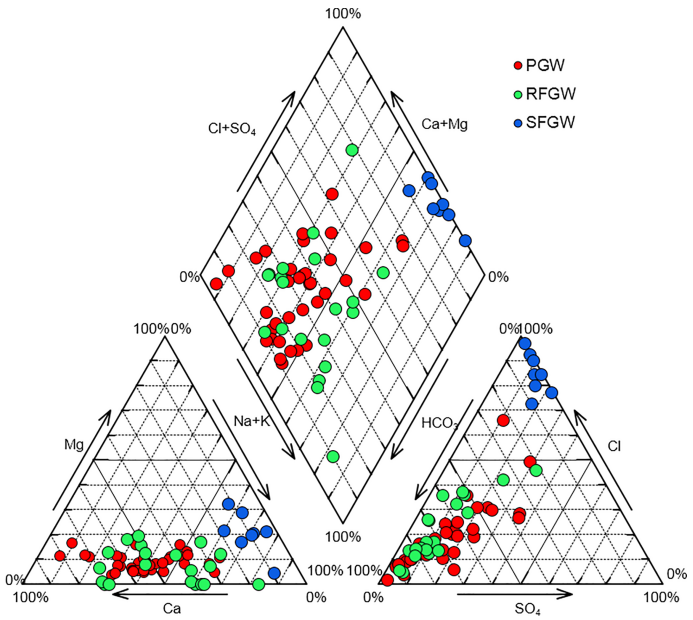

FIGURE 2 | Piper Plot of groundwater samples in the study area.

the $\delta^{15}N–NO_3^-$ and $\delta^{18}O–NO_3^-$ values ranged from +2.35‰ to +15.79‰ and from +0.39‰ to +9.96‰, respectively.

5 DISCUSSION

5.1 Characteristics of Dual Isotopes in Nitrate in Coastal Groundwater

As results showed, NO_3^-–N was the dominant N form and major pollutant in the coastal groundwater. The characteristics of dual isotopes of NO_3^- ($\delta^{15}N–NO_3^-$ and $\delta^{18}O–NO_3^-$) could provide evidence of origins and major transformation process of nitrate. In this study, the mean values of $\delta^{15}N–NO_3^-$ and $\delta^{18}O–NO_3^-$ in this study were 16.4 ± 5.7‰ and 10.0 ± 3.6‰, respectively. These values were comparable to those reported in previous studies on groundwater in the Pearl River Delta. For example, the $\delta^{15}N–NO_3^-$ and $\delta^{18}O–NO_3^-$ in coastal aquifer system of Guangzhou ranged from +9.25‰ to +31.99‰ and from −2.83‰ to +16.74‰, respectively (Li et al., 2019b); the $\delta^{15}N–NO_3^-$ and $\delta^{18}O–NO_3^-$ in shallow groundwater of Dongguan ranged from +6.68‰ to +26.23‰ and from −6.59‰ to +13.72‰, respectively (Li et al., 2020). In addition, the mean values of $\delta^{15}N–NO_3^-$ and $\delta^{18}O–NO_3^-$ in the coastal groundwater of this study was higher than those reported in the shallow groundwater (+12.4 ± 0.4‰ and +8.2 ± 0.1‰) and was lower than those reported in the deep groundwater of the southern ocean (+21 ±

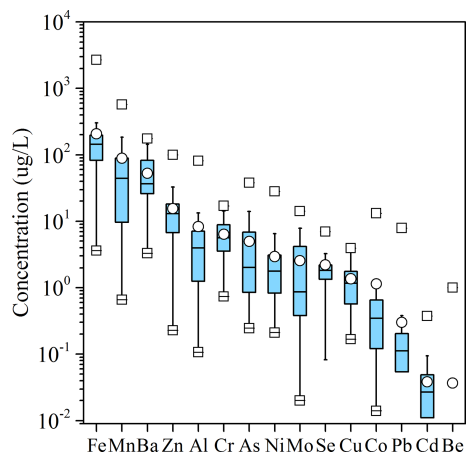

FIGURE 3 | Boxplots of trace metal concentrations (μg/L) in groundwater in the study area. Logarithmic coordinates are used for the y-axis due to the large variation in concentration ranges.

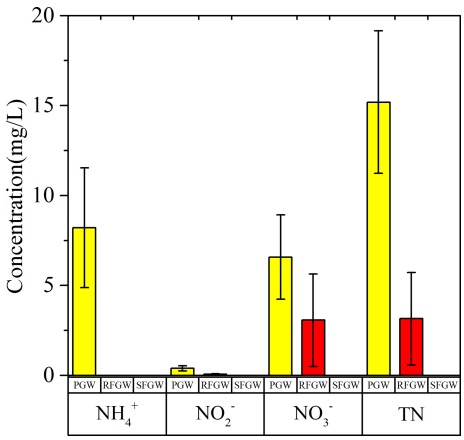

FIGURE 4 | Nitrogen variations in the groundwater of the study area.

0.7‰ and +11 ± 0.9‰) (Wong et al., 2014). However, compared to surface water in the estuarine and coastal ecosystems, the $\delta^{15}N–NO_3^-$ in groundwater showed higher values (Ye et al., 2016; Archana et al., 2018). This finding suggested that sewage effluents ($\delta^{15}N>+10‰$) or denitrification was likely to be responsible for the elevated $\delta^{15}N–NO_3^-$ values in the groundwater.

5.2 Origins of Major and Trace Elements

The data set for the three groups was analyzed separately by R-mode factor analysis, and different factors were identified for the RFGW, the PGW, and the SFGW. ORP is excluded from all the analysis because it is highly skewed and has no improvement by BOX-COX transformation. NH_4^+ is also excluded from the analysis for the RFGW and the SFGW because the samples in the RFGW and the SFGW were free of ammonium pollution. COD and NO_3^- data are missing for SFGW so that only major ions such as Na^+, K^+, Ca^{2+}, Mg^{2+}, HCO_3^-, Cl^-, and SO_4^{2-} are included for the SFGW factor analysis. Four factors are identified for the RFGW and the PGW, while only two factors were identified for the SFGW. The parameters with factor loadings >0.6 or<−0.6 and factor meanings are listed in **Table 1**. Based on the loadings, the first and second factors can be grouped as the groundwater salinization factors, and the third and fourth factors can be grouped as the pollution factors.

5.2.1 Natural Origin

(1) Natural origin of major elements

The first factor group (factor 1 and 2) identified was mainly related to the groundwater salinization processes, although each has some different meanings for the RFGW, the PGW and the SFGW (**Table 1**). In the recharge zone of fissure aquifer (RFGW), factor 1 had high positive loadings on TDS, Na^+, Ca^{2+}, Mg^{2+}, Cl^-, NO_2^- and NO_3^- and was recognized as "rock weathering" factor, which indicated that the water-rock reaction was the main factor contributing to TDS. The sea water indicator SO_4^{2-} showed a negative loading, which indicated that the increase of TDS had no relation with the sea water. In addition, NO_3^- showed a positive loading on factor 1, implying natural (non-anthropogenic) origin of NO_3^- such as precipitation deposition. Factor 2 with high positive loadings on HCO_3^- and negative loadings on DO represented the occurrence of DOM oxidation and DO consumption processes. The corrosive CO_2 released by oxidation of DOM could promote the dissolution of carbonate and silicate, which resulted in the increases of HCO_3^- and Ca^{2+}. The first factor identified for the PGW had positive loadings on TDS, Na^+, K^+, Ca^{2+}, Mg^{2+}, Cl^- and SO_4^{2-} (**Table 1**) and was recognized as "rock weathering and evaporation concentration" factor. Factor 2 for the PGW had high loadings on T, pH, Ca^{2+} and HCO_3^-. This factor was recognized as "carbonate dissolution factor". The factor analysis results indicated that carbonate dissolution, mixing with seawater and evaporation were major factors that resulted in the increase of TDS for the PGW. The first factor identified for the SFGW had positive loadings on TDS, Na^+, K^+, Ca^{2+}, Mg^{2+}, Cl^- and SO_4^{2-} (**Table 1**) and was recognized as "sea water intrusion" factor. In addition, the Gibbs plot showed that all the samples came from the SFGW were located in the sea water zone, which indicated that the major elements in the SFGW was affected by severe seawater intrusion (**Figure 5**).

(2) Natural origin of trace elements

Because the relative low concentrations and low mobility of trace metals, the origin of trace metals were expected to originating natural input rather than anthropogenic input in this study area. Previous studies have documented the contents of trace metal in the Quaternary sediments of the Pearl River Delta (PRD) (Wang et al., 2016), which found that Fe and Mn showed the largest abundance, followed by Ba, Cr, Zn, Ni, Cu, Pb, Co, Mo, Cd in the solid phase. Similar abundance of trace metals with Fe > Mn > Ba > Zn > Al > Cr >As > Ni > Mo > Se >Cu >Co >Pb >Cd > Be were observed in the dissolved phase in this study area (**Figure 3**), which indicated that the origin of trace elements in the groundwater was sedimentary deposits. In addition, previous studies suggested that the mobility of trace metals in the groundwater was limited by adsorption on various solid phases of sediments, including sedimentary organic matter, carbonate phases, Fe-Mn oxides, and other minerals, which was strongly depended on pH variability (Wang et al., 2016; Liénart et al., 2018). Trace metals would mobilize when pH values were low, and most of heavy metals would be entirely adsorbed when pH values were as high as 7 (Appelo and Postma, 2005b). Although significant amounts of heavy metals were found in the groundwater in this study, no significant correlation was identified between the concentrations of any heavy metal and the pH (**Figure 6**), which indicated that pH was not the major factor affecting the mobility of heavy metals in this groundwater system. This results was likely because pH values were circum-neutral or slightly alkaline caused by marine influences and the

TABLE 1 | Results of factors analysis in the different aquifers.

Item	Groundwater salinization group		Pollution group	
	Factor 1	**Factor 2**	**Factor 3**	**Factor 4**
RFGW	Rock weathering factor: TDS, Na^+, Mg^{2+}, Cl^-, NO_3^-, SO_4^{2-}*	DOM oxidation and DO consumption factor: HCO_3^-, Ca^{2+}, DO*	T, pH	COD pollution factor: COD
PGW	Evaporation concentration factor: TDS, Na+, K+, Mg2+, Cl–, SO_4^{2-}	Carbonate dissolution factor: T, pH, Ca^{2+}, HCO_3^-	Nitrogen pollution factor: DO, NO_3^-	COD pollution factor: COD
SFGW	Sea water intrusion factor: TDS, Na^+, K^+, Ca^{2+}, Mg^{2+}, Cl^-, SO_4^{2-}	HCO_3^-	–	–

**Implies the parameter with factor loading<−0.5.*

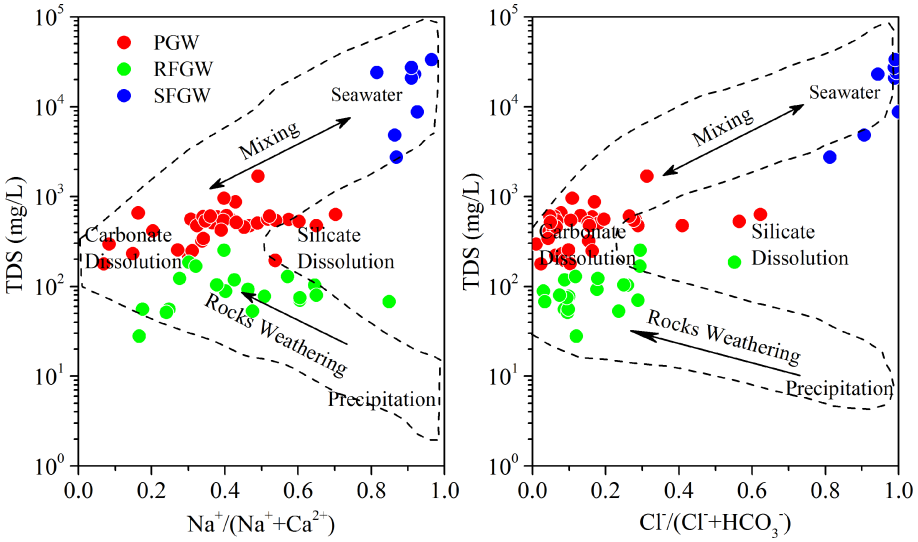

FIGURE 5 | Modified Gibbs plot. The $Na^+/(Na^+ + Ca^{2+})$, $Cl^-/(Cl^- + HCO_3^-)$ is calculated by weight concentrations in mg/L.

possible presence of dissolved ammonia in the groundwater (Wang et al., 2016; Huang et al., 2022a).

5.2.2 Anthropogenic Input

Deterioration of groundwater quality could be expressed by the pollution factor group (factors 3 and 4 in **Table 1**. Factor 4 with loading on COD was identified for both the RFGW and the PGW, indicating ubiquitous organic pollution in the local groundwater. Averaged COD concentrations of the RFGW and the PGW were 26.65 and 21.85 mg/L, respectively. In addition, factor 3 showed different meanings for the RFGW and the PGW. For the RFGW, only nitrate was detected, and the averaged concentration was approximately 0.22 mmol/L (3.08 mg N/L), which was lower than that of the WHO drinking water standard (10 mg N/L). As described by factor 1, the natural origin of nitrate came from precipitation deposition. Compared with the RFGW, elevated nitrate, nitrite, and ammonium were detected in the samples from the PGW. For the PGW, the averaged concentrations of nitrate, nitrite, and ammonium were 0.47, 0.03, and 0.59 mmol/L, respectively. From the N loading perspective, 20% of the PGW samples have exceeded the WHO drinking water standard. The isotope signals of $\delta^{15}N–NO_3^-$ and $\delta^{18}O–NO_3^-$ values in the PGW showed higher values and within the expected range of manure and sewage zones (**Figure 10A**), indicating that the infiltration

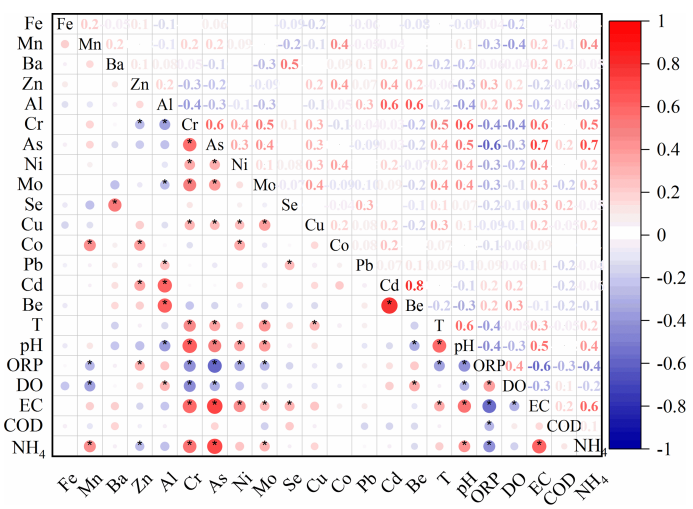

FIGURE 6 | Matrixes of Person correlations between trace metals and other field parameters in this study area. Red and blue dots inside the squares correspond to the negative and positive correlations with $p<0.05$, respectively. Light-colored small dots represent low correlations, while darker-colored large dots correspond to higher correlations. Missing dots inside the squares indicate an insignificant relationship between the pairwise variables.

of manure and sewage caused by human activities was mainly responsible for the increase in nitrate in the groundwater. In addition, the more severe environmental problem for the PGW samples was caused by high ammonium concentrations. Averaged NH_4^+ concentration of the PGW samples was 0.59 mmol/L (8.26 mg N/L), which was higher than the values that were defined by the standard for groundwater quality in China (type V: 1.5 mg N/L). Previous studies have showed that the extremely high ammonium concentration originated from N-bearing organic matter mineralization in the west bank of the Pearl River estuary (Jiao et al., 2010; Wang and Jiao, 2012; Wang et al., 2013; Li et al., 2019b). This study found that the high ammonium with natural origins also existed in the east bank of the Pearl River estuary. However, our previous study showed that mineral dissolution was mainly controlled by acid rain caused by human activities in the eastern Pearl River Delta (Li et al., 2020). Therefore, the indirect impact of anthropogenic activities (e.g., acid rain) on groundwater chemistry might be more responsible for the accumulation of nitrogen in the groundwater.

5.3 Hydrochemical Evolution and Nitrogen Behaviors

Gibbs plots displaying the weight ratios of $Na^+/(Na^+{+}Ca^{2+})$ and $Cl^-/(Cl^-{+}HCO_3^-)$ against the TDS values have been widely employed to assess the dominant factors of soluble ions in the surface waters, such as precipitation, river water, and bedrock mineralogy (Gibbs, 1970; Feth and Gibbs, 1971). However, total key factors that controlled hydrochemical evolution in the groundwater were unlikely to be identified from the original Gibbs diagram due to the complexity of groundwater environments. Therefore, the natural processes defining the hydrochemical evolution of groundwater have been reassessed by Marandi and Shand (2018), which are shown in a modified version (**Figure 5**). It was observed that all groundwater samples from the PGW and the RFGW fell into the rock weathering dominance zone. Among the rock weathering processes, carbonate dissolution was recognized as the dominant factor, while silicate dissolution by precipitation was responsible for some of the samples. The samples from the SFGW were located in the region of seawater, which evidenced seawater intrusion. In addition, the large variations of $Na^+/(Na^+{+}Ca^{2+})$ suggested that cation exchange might have an influence on the cation exchange of Na^+ and Ca^{2+} content in the groundwater (Liu et al., 2015). Therefore, the cation exchange during mixing, water–rock interaction, and redox processes could not be revealed by Gibbs plot but are important factors affecting the specification and behavior of redox couples.

5.3.1 Mixing Process and Ion Exchange

Generally, Cl^- can be used to estimate the contribution of seawater in the confined aquifers by the mixing equation shown below (Appelo and Postma, 2005a):

$$f_{sea} = (m_{Cl,sample} - m_{Cl,fresh}) / (m_{Cl,sea} - m_{Cl,fresh}) \quad (1)$$

where $m_{Cl,sample}$, $m_{Cl,fresh}$, and $m_{Cl,sea}$ are the Cl^- concentration in the sample, freshwater, and seawater, respectively. f_{sea} is the fraction of seawater in the aquifer. Based on mixing Equation 1, the fraction of seawater contributions in the groundwater ranged from<1% to 97%. Specifically, the semiconfined fissure aquifer (SFGW, 12 samples) suffered from severe seawater intrusion with seawater fraction from 6% to 97%. Samples from the PGW and the RFGW were almost free of seawater intrusion with seawater fraction smaller than 1.5%.

During the mixing of seawater and fresh groundwater, the cation-exchange process could significantly alter the major cation compositions according to the Equations 2 and 3:

$$Na^+ + \frac{1}{2}Ca{\bullet}X_2 \rightarrow Na{\bullet}X + \frac{1}{2}Ca^{2+} \quad (2)$$

$$Ca^{2+} + 2Na{\bullet}X \rightarrow Ca{\bullet}X_2 + 2Na^+ \quad (3)$$

The plot of $(Na^+{+}K^+{-}Cl^-)$ against $[Ca^{2+}{+}Mg^{2+}{-}(HCO_3^-{+}CO_3^{2-}{+}SO_4^{2-})]$ was usually used to explain the possibility of cation exchange in groundwater (Liu et al., 2015; Li et al., 2019c). However, carbonic, sulfuric, and nitric acid participated in carbonate mineral and silicate mineral weathering, which resulted in the enrichment of Ca^{2+} and Mg^{2+} contents in the groundwater in this study area. Thus, we regarded $[Ca^{2+}{+}Mg^{2+}{-}(HCO_3^-{+}CO_3^{2-}{+}NO_3^-{+}SO_4^{2-})]$ as one of the coordinate axes. The diagram of $(Na^+{+}K^+{-}Cl^-)$ versus $[Ca^{2+}{+}Mg^{2+}{-}(HCO_3^-{+}CO_3^{2-}{+}NO_3^-{+}SO_4^{2-})]$ depicted a negative linear correlation (**Figure 7A**), which demonstrated that the cation exchange between Na^+, K^+ and Ca^{2+}, Mg^{2+} occurred in the groundwater. However, in the SFGW, the excess Ca^{2+} came from cation exchange that precipitated with HCO_3^- into $CaCO_3$, leading to the SFGW samples deviating from the 1:1 line as shown in **Figure 7A**.

The chloro-alkaline indices CAI1 = $[Cl^-{-}(Na^+{+}K^+)]/Cl^-$ and CAI2 = $[Cl^-{-}(Na^+{+}K^+)]/(HCO_3^-{+}CO_3^{2-}{+}SO_4^{2-}{+}NO_3^-)$ (Schoeller, 1964; Schoeller, 1977) were also applied to analyze cation-exchange processes (**Figure 7B**). The positive values of the two indices suggested the occurrence of cation exchange expressed as Equation 2, while negative values of the two indices could be obtained when cation exchange expressed as Equation 3 occurred. The CAI1 and CAI2 for all samples from the SFGW showed positive values, which ranged from 0.21 to 0.40 and from 0.77 to 6.30, respectively. The exchange of Na^+ and K^+ from the water with Ca^{2+} and Mg^{2+} of the aquifer medium in the SFGW did occur during the seawater infiltration. However, the CAI1 and CAI2 for the RFGW and the PGW samples showed negative values, indicating that the process could be expressed by Equation 3.

5.3.2 Water–Rock Interaction

The stoichiometric relationships among major ions could give further explanation of the influence of water–rock interaction on hydrochemistry in groundwater. The ratios of Na^+ and Cl^- (in meq/L) in seawater was close to 0.86, while the congruent dissolution of halite or exogenous input of NaCl resulted in the ratios of Na^+ and Cl^- close to 1:1. In **Figure 8A**, the ratios of Na^+

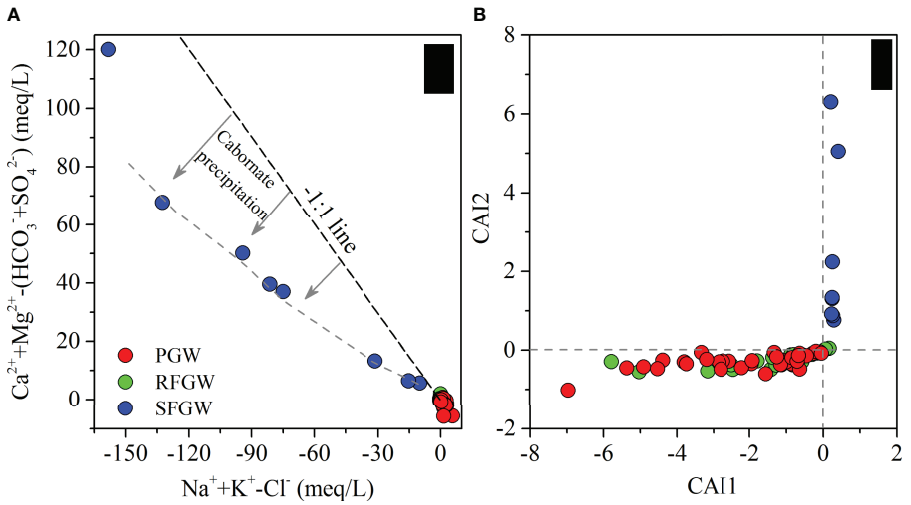

FIGURE 7 | Stoichiometric relation between major ions **(A)** and scatter plot of CAI1 and CAI2 for groundwater samples **(B)**.

and Cl^- of the SFGW samples were close to 0.86, which confirmed the occurrence of seawater intrusion. For the PGW and the RFGW, some samples located along the 1:1 line, indicating the existence of halite or exogenous input of NaCl. The excess of Na^+ implied the dissolution of albite ($NaAlSi_3O_8$) and Na-feldspar ($NaAlSi_3O_8$) caused by carbonic, sulfuric, and even nitric acid, which are the sources of (Na^++K^+) contents in groundwater. In **Figure 8B**, most of the samples deviated from the 1:1 line of Ca^{2+} and SO_4^{2-}, indicating the absence of gypsum in the aquifer. The excess of Ca^{2+} indicated that the carbonate dissolution was the dominant process that contributed most of Ca^{2+}. This result could be further proved by the stoichiometric analysis of (Ca^{2+}+Mg^{2+}) and HCO_3^-. In **Figure 8C**, most of the samples from the PGW and the RFGW were located along the 1:1 carbonate dissolution line, which demonstrated that the dissolution of calcite and dolomite dominated in this study area. However, acid rain emerged as an important environmental problem in Southern China since the 1980s, as previous studies documented (He et al., 2002; Larssen et al., 2006; Zhang et al., 2010). SO_2 and NO_x are the main components in acid rain, which participate in carbonate mineral and silicate mineral weathering (Cao et al., 2020). In this study, the stoichiometric relation between (Ca^{2+}+Mg^{2+}) and (HCO_3^-+SO_4^{2-}) showed that lots of samples were located above the 1:1 line (**Figure 8D**). The excess of (HCO_3^-+SO_4^{2-}) compared to (Ca^{2+}+Mg^{2+}) illustrated the occurrence of silicate weathering in the PGW and the RFGW.

5.3.3 Redox Process and Nitrogen Behaviors

(1) The Redox Conditions

The fates of nitrogen and trace metals in groundwater are determined by the redox conditions. Under the ample supply of organic matter, the sequence of redox reactions is arranged as the depletion of dissolved oxygen (DO), reduction of nitrate (NO_3^-), emergence of manganese (Mn) and iron (Fe) with lower valence (+2), reduction of sulfate (SO_4^{2-}), and finally the generation of methane (CH_4) (Appelo and Postma, 2005b; Rivett et al., 2008). In this study, redox diagrams (pH–pe diagrams) were employed to evaluate the groundwater redox conditions and dominant species of nitrogen and trace metals. The dominant species theoretically controlled by the pH and pe was N_2 for nitrogen (**Figure 9A**), Fe (+2) in the RFGW and Fe (+3) in the PGW for iron (**Figure 9B**), and SO_4^{2-} (+6) for sulfur (**Figure 9C**). Thus, it could be deduced that the redox condition was in the state of reduction in NO_3^- (denitrification) and even reduction in Fe and Mn in the RFGW. However, due to the complex interaction of the electron acceptor and donor and lack of equilibrium between different redox couples in the aquifer, NO_3^- was still represented as the electron acceptor in the groundwater. The following part is mainly focused on the fate of NO_3^-.

(2) NO_3^- Behavior Revealed by Stable Isotopes Technique

The stable isotopic signatures of NO_3^- ($\delta^{15}N$–NO_3^- and $\delta^{18}O$–NO_3^-) were widely used to identify the nitrate sources and the occurrence of denitrification (Xue et al., 2009; Lin and Lin, 2022). Source identification showed that the $\delta^{15}N$–NO_3^- and $\delta^{18}O$–NO_3^- values in the groundwater fell in the range of manure and sewage zone (**Figure 10A**), which suggested that anthropogenic origin such as manure and sewage dominated in both the RFGW and the PGW. This result indicated that the local groundwater quality has been deteriorated by human activities. The deviation of both $\delta^{15}N$–NO_3^- and $\delta^{18}O$–NO_3^- forms the characteristic values of a typical pollutant source, indicating that the nitrogen transformations, such as denitrification, have been altering the initial N and O isotopes values.

Denitrification generally resulted in the removal of NO_3^- in aquifer. Based on the Rayleigh fractionation principle, the heavy isotopes ^{18}O and ^{15}N is more enriched in the residual nitrate when the removal of NO_3^- occurred. Thus, during the denitrification, a negative linear relationship between $\delta^{15}N$–NO_3^- and Ln(NO_3^-) (Fenton et al., 2009; Otero et al., 2009; Li et al., 2019a), and the ratios of fractionation factors ($\Delta\delta^{15}N/\Delta\delta^{18}O$) varying from 1.3 to

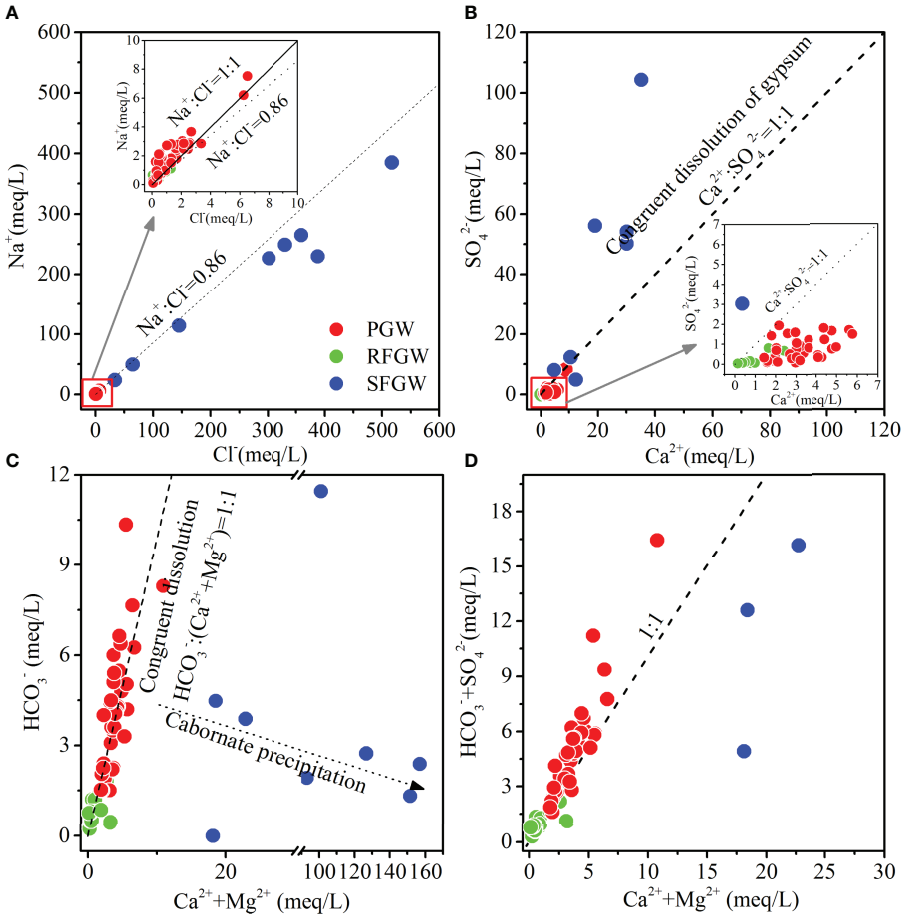

FIGURE 8 | Stoichiometric relation between Na^+ and Cl^- **(A)**, SO_4^{2-}, and Ca^{2+} **(B)**, Ca^{2+}+Mg^{2+} and HCO_3^- **(C)**, and Ca^{2+}+Mg^{2+} and HCO_3^-+SO_4^{2-} **(D)**.

2.1 (Fukada et al., 2003), could be detected. In our study area, for both the PGW and the RFGW, significant positive correlations between $\delta^{15}N$–NO_3^- and $\delta^{18}O$–NO_3^- (**Figure 10A**) combined with the negative correlations between $\delta^{15}N$–NO_3^- values and Ln(NO_3^-) (**Figure 10B**) were observed, which confirmed the existence of denitrification in these regions. In addition, the ratios between $\delta^{15}N$–NO_3^- and $\delta^{18}O$–NO_3^- were 1.85 for the PGW and 3.03 for the RFGW, respectively, which indicated that the

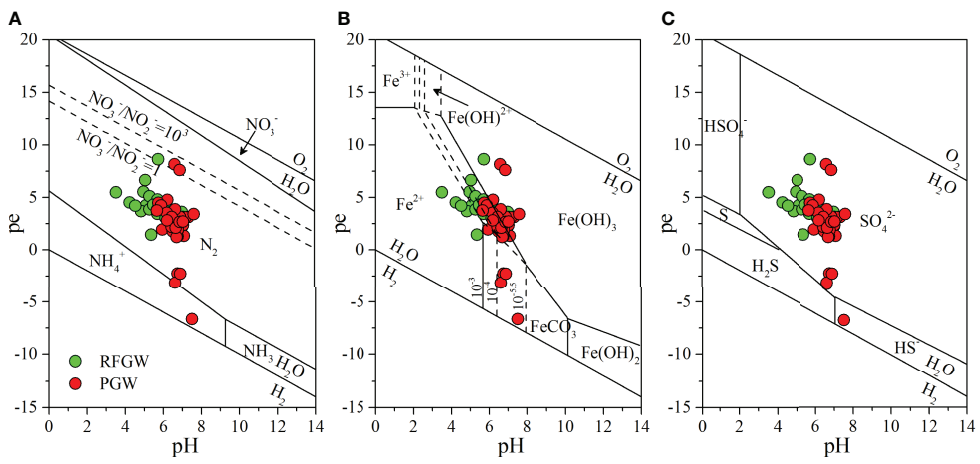

FIGURE 9 | Redox diagram of nitrogen **(A)**, iron **(B)**, and sulfur **(C)**.

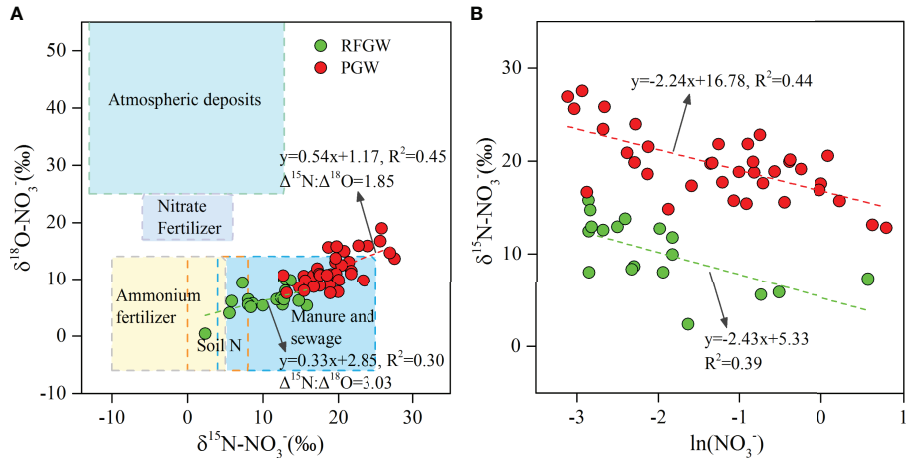

FIGURE 10 | Plot of $\delta^{15}N–NO_3^-$ versus $\delta^{18}O–NO_3^-$ **(A)** and $\delta^{15}N–NO_3^-$ versus $Ln(NO_3^-)$ **(B)**. The typical ranges of potential nitrate sources were taken from Xue et al. (2009).

denitrification signal was stronger for the PGW than that of the RFGW. This result acted in accordance with the redox condition analysis, which has found that the reduced environment was stronger for the PGW than that for the RFGW. Therefore, denitrification was a non-negligible biogeochemical process for the removal of NO_3^- in the aquifer, and our study highlights the elevated denitrification process in coastal groundwater that suffered from seawater intrusion and anthropogenic inputs.

6 CONCLUSION

Coastal aquifers play key roles in providing freshwater resources to maintain the social and economic development in coastal areas. As one of the current national key economic development regions in China, Shenzhen city is a complex urbanized region with population dynamics, intense economic activities, and innovative clusters. It is of great scientific and practical significance to evaluate the possibility of coastal groundwater resources as strategic reserve water resources. In this study, stoichiometric analysis of hydrogeochemistry, multivariate analysis, and isotopic trancing techniques were combined to reveal the local hydrochemistry characteristics, its natural and human-activity-induced controlling factors, and the major hydrochemical evolution in a typical coastal aquifer located in the Pearl River estuary.

Seawater intrusion, ion exchange, water–rock reaction, and human activities were the main controlling factors that affected the characteristics of groundwater in this study area, but there were significant differences in the predominant controlling effects of different zones. High salinization was identified in the SFGW samples, and the hydrochemical pattern was Na–Cl. Prevalent cations were Na^+ and K^+, and the most abundant anion was Cl^-. It revealed that SFGW was severely affected by seawater intrusion. Mass balance analysis based on Cl^- showed that the contribution of seawater was between 6% and 97%. Obvious cation exchange process occurred during the seawater intrusion. The hydrochemical characteristics of the PGW and the RFGW were mainly controlled by water–rock interaction. Human activities had further influences on the hydrochemical characteristics of groundwater, resulting in elevated nitrate. Redox analysis deduced that the redox condition was in the state of reduction in NO_3^- (denitrification) and even reduction in Fe and Mn in the RFGW. Furthermore, dual nitrogen isotope tracing techniques reveal that the denitrification did occur in the PGW and the RFGW. Denitrification was the major process that controlled the transformation of nitrogen. This research provides a scientific basis for the management of groundwater resources in coastal aquifers.

DATA AVAILABILITY STATEMENT

The raw data supporting the conclusions of this article will be made available by the authors, without undue reservation.

AUTHOR CONTRIBUTIONS

YD: formal analysis, investigation, writing—original draft, and writing—review and editing. JL: formal analysis, investigation, and writing—reviewing. RW: methodology investigation and writing—reviewing. JW: investigation and writing—editing; QZ: formal analysis and investigation. YC: funding acquisition, investigation, and writing—review and editing; YZ: methodology, writing—review and editing. YX: supervision, methodology, project administration, and writing—review and editing.

FUNDING

This study was supported by the National Natural Science Foundation of China (Grant No. 42077154), the GuangDong Basic and Applied Basic Research Foundation of China (Grant No. 2021A1515110372), the China Postdoctoral Science Foundation (2021M693588), and National Key Research and Development Program of China (2019YFC1805304).

REFERENCES

Abd-Elaty, I., Abd-Elhamid, H. F. and Qahman, K. (2020). Coastal Aquifer Protection From Saltwater Intrusion Using Abstraction of Brackish Water and Recharge of Treated Wastewater: Case Study of the Gaza Aquifer. *J. Hydrolog. Eng.* 25 (7). 05020012. doi:10.1061/(ASCE)HE.1943-5584.0001927

"Appelo and Dimier, 2004": Prepared for: Division of Systems Analysis and Regulatory Effectiveness Office of Nuclear Regulatory Research US Nuclear Regulatory Commission Washington, DC 20555-0001.

Appelo, C. A. J. and Postma, D. (2005). Geochemistry, Groundwater and Pollution. Sediment. *Geol.* 220 (3), 256–270. doi: 10.2136/vzj2005.1110br

Archana, A., Thibodeau, B., Geeraert, N., Xu, M. N., Kao, S. J., and Baker, D. M. (2018). Nitrogen Sources and Cycling Revealed by Dual Isotopes of Nitrate in a Complex Urbanized Environment. *Water Res.* 142, 459–470. doi: 10.1016/j.watres.2018.06.004

Argamasilla, M., Barberá, J. A. and Andreo, B. (2017). Factors Controlling Groundwater Salinization and Hydrogeochemical Processes in Coastal Aquifers From Southern Spain. *Sci. Total. Environ.* 580, 50–68. doi: 10.1016/j.scitotenv.2016.11.173

Cao, Y., Xuan, Y., Tang, C., Guan, S. and Peng, Y. (2020). Temporary and Net Sinks of Atmospheric CO_2 Due to Chemical Weathering in Subtropical Catchment With Mixing Carbonate and Silicate Lithology. *Biogeosciences* 17 (14), 3875–3890. doi:10.5194/bg-17-3875-2020

Casciotti, K. L., Sigman, D. M., Hastings, M. G., Böhlke, J. K. and Hilkert, A. (2002). Measurement of the Oxygen Isotopic Composition of Nitrate in Seawater and Freshwater Using the Denitrifier Method. *Analytical. Chem.* 74 (19), 4905–4912. doi: 10.1021/ac020113w

Chen, X. C., Li, F., Li, X. Q., Hu, Y. H. and Hu, P. P. (2020). Evaluating and Mapping Water Supply and Demand for Sustainable Urban Ecosystem Management in Shenzhen, China. *J. Clean. Product.* 251, 11. doi: 10.1016/j.jclepro.2019.119754

Choi, W-J., Han, G-H., Lee, S-M., Lee G-T., Yoon, K-S, Choi, S-M., et al. (2007). Impact of Land-Use Types on Nitrate Concentration and δ15n in Unconfined Groundwater in Rural Areas of Korea. *Agricult. Ecosyst. Environ.* 120 (2-4), 259–268. doi:10.1016/j.agee.2006.10.002

Cook, P. G. and Herczeg, A. L. (2000). *Environmental Tracers in Subsurface Hydrology* Kluwer, Dordrecht (Springer US), 397–424.

Council, N. R. (2007). *Mitigating Shore Erosion Along Sheltered Coasts* Vol. 188 (Washington, DC: The National Academies Press).

Fenton, O., Richards, K. G., Kirwan, L., Khalil, M. I. and Healy, M. G. (2009). Factors Affecting Nitrate Distribution in Shallow Groundwater Under a Beef Farm in South Eastern Ireland. *J. Environ. Manag.* 90 (10), 3135–3146. doi: 10.1016/j.jenvman.2009.05.024

Ferguson, G. and Gleeson, T. (2012). Vulnerability of Coastal Aquifers to Groundwater Use and Climate Change. *Nat. Climate Change* 2 (5), 342–345. doi:10.1038/nclimate1413

Feth, J. H. and Gibbs, R. J. (1971). Mechanisms Controlling World Water Chemistry: Evaporation-Crystallization Process. *Science* 172 (3985), 870–872. doi: 10.1126/science.172.3985.870

Froelich, P. N. , Klinkhammer, G. P. , Bender, M. L. , Luedtke, N. A. , Heath, G. R. , Cullen, D. , et al. (1979). Early Oxidation of Organic Matter in Pelagic Sediments of the Eastern Equatorial Atlantic: Suboxic Diagenesis. *Geochimica. Cosmochimica. Acta* 43 (7), 1075–1090. doi: 10.1016/0016-7037(79)90095-4

Fukada, T., Hiscock, K. M., Dennis, P. F. and Grischek, T. (2003). A Dual Isotope Approach to Identify Denitrification in Groundwater at a River-Bank Infiltration Site. *Water Res.* 37 (13), 3070–3078. doi: 10.1016/S0043-1354(03)00176-3

Gao, T., (2019). *A Review of Research on Tourism Integration in Guangdong-Hong Kong-Macao Greater Bay Area, Proceedings of the 2019 3rd International Conference on Education, Culture and Social Development (ICECSD 2019)*. Atlantis Press, 253-262.

Gibbs, R. J. (1970). Mechanisms Controlling World Water Chemistry. *Science* 17, 1088–1090. doi:10.1126/science.170.3962.1088

Hale, R. L., Turnbull, L., Earl, S., Grimm, N., Riha, K., Michalski. G., et al. (2014). Sources and Transport of Nitrogen in Arid Urban Watersheds. *Environ. Sci. Technol.* 48 (11), 6211–6219. doi: 10.1021/es501039t

Han, H. F., Jiang, F. Y. and Wang, Y. (2009). Groundwater Chemistry Evolution and Its Indication Under the Effect of Seawater Intrusion:A Case Study at Bao'an District of Shenzhen City. *Saf. Environ. Eng.* 16(04). 1-5. doi: 1671-1556(2009)04-0001-05

He, K., Huo, H. and Zhang, Q. (2002). Urban Air Pollution in China: Current Status, Characteristics, and Progress. *Annu. Rev. Energy Environ.* 27 (1), 397–431. doi:10.1146/annurev.energy.27.122001.083421

Hosono, T., Tokunaga, T., Kagabu, M., Nakata, H., Orishikida, T., Lin, I. T., et al. (2013). The Use of Delta15n and Delta18o Tracers With an Understanding of Groundwater Flow Dynamics for Evaluating the Origins and Attenuation Mechanisms of Nitrate Pollution. *Water Res.* 47 (8), 2661–2675. doi: 10.1016/j.watres.2013.02.020

Huang, F., Lin, X., Hu, W., Zeng, F., and Yin, K. (2021). Nitrogen cycling processes in sediments of the pearl river estuary: spatial variations, controlling factors, and environmental implications. *Catena*, 206, 105545. doi:10.1016/j.catena.2021.105545

Huang, F., Lin, X. and Yin, K. (2022a). Effects of Algal-Derived Organic Matter on Sediment Nitrogen Mineralization and Immobilization in a Eutrophic Estuary. *Ecol. Indic.* 138, 108813. doi:10.1016/j.ecolind.2022.1088131

Huang, F., Lin, X. and Yin, K. (2022b). Effects of Marine Produced Organic Matter on the Potential Estuarine Capacity of NO_x^- Removal. *Sci. Total. Environ.* 812, 151471. doi: 10.1016/j.scitotenv.2021.151471

Hui, E. C. M., Li, X., Chen, T. and Lang, W. (2018). Deciphering the Spatial Structure of China's Megacity Region: A New Bay Area-The Guangdong-Hong Kong-Macao Greater Bay Area in the Making. *Cities.* 105: 102168. doi:10.1016/j.cities.2018.10.011

Jiang, F., Han, H., Chen, J. and Wang, Y. (2009). Indication of Trace Elements and Isotopes in Groundwater to Seawater Intrusion and Groundwater Origin: A Case Study at Bao'an District of Shenzhen City, Guangdong Province. *J. East. China Univ. Technol. (Natural. Science).* 32 (3), 253–260. doi:1674-3504(2009)03-253-08

Jiao, J., Wang, Y., Cherry, J., Wang, X., Zhi, B., Du, H., et al. (2010). Abnormally High Ammonium of Natural Origin in a Coastal Aquifer-Aquitard System in the Pearl River Delta, China. *Environ. Sci. Technol.* 44 (19), 7470–7475. doi: 10.1021/es1021697

Kendall, C. (1998). *Tracing Nitrogen Sources and Cycling in Catchments*.

Kendall, C., Elliott, E. M. and Wankel, S. D. (2007). *Tracing Anthropogenic Inputs of Nitrogen to Ecosystems, Stable Isotopes in Ecology and Environmental Science*, 2nd Edn. Blackwell Publishing, London 375–449.

Lancia, M., Zheng, C., He, X., Lerner, D. N. and Andrews, C. (2020). Groundwater Complexity in Urban Catchments: Shenzhen, Southern China. *Groundwater* 58 (3), 470–481. doi: 10.1111/gwat.12935

Lancia, M., Zheng, C., Yi, S., Lerner, D. N. and Andrews, C. (2019). Analysis of Groundwater Resources in Densely Populated Urban Watersheds With a Complex Tectonic Setting: Shenzhen, Southern China. *Hydrogeol. J.* 27 (1), 183–194. 10.1007/S10040-018-1867-2

Larssen, T. , Lydersen, E. , Tang, D. , He, Y. , Gao, J. , Liu, H. , et al. (2006). Acid Rain in China. *Environ. Sci. Technol.* 40 (2), 418–425. doi:10.1021/es0626133

Liénart, Savoye, N. , Bozec, Y. , Breton, E. , Conan, P. , David, V. , et al. (2018). Dynamics of Particulate Organic Matter Composition in Coastal Systems: Forcing of Spatio-Temporal Variability at Multi-Systems Scale. *Prog. Oceanogr.* 162, 271–289. doi:10.13140/RG.2.2.35042.94405

Li, C., Li, S. L., Yue, F. J., Liu, J., Zhong, J., Yan, Z. F., et. al. (2019a). Identification of Sources and Transformations of Nitrate in the Xijiang River Using Nitrate Isotopes and Bayesian Model. *Sci. Total. Environ.* 646, 801–810. doi: 10.1016/j.scitotenv.2018.07.345

Li, X.,Tang, C., Cao, Y. and Li, X. (2019b).Carbon, Nitrogen and Sulfur Isotopic Features and the Associated Geochemical Processes in a Coastal Aquifer System of the Pearl River Delta,China. *J. Hydrol.* 575, 986-998. doi:10.1016/j.jhydrol.2019.05.092

Li, Z., Yang, Q., Ma, H., Li, S., and Martin, J. D. (2019c). Isotopic and Geochemical Interpretation of Groundwater Under the Influences of Anthropogenic Activities. *J. Hydrol.* 576, 685–697. doi:10.1016/j.jhydrol.2019.06.037

Lin, X., Jiang, X., Li, X., Gao, J., Liu, M., Hou, L., et al. (2016). Nitrogen Mineralization and Immobilization in Sediments of the East China Sea: Spatiotemporal Variations and Environmental Implications. *J. Geophys. Res.: Biogeosci.* 121 (11), 2842–2855. doi:10.1002/2016JG003499

Lin, X., Lu, K., Hardison, A. K., Liu, Z., and Gardner, W. S. (2021). Membrane Inlet Mass Spectrometry Method (REOX/MIMS) to Measure 15N-Nitrate in Isotope-Enrichment Experiments. *Ecol. Indic.* 126, 107639. doi:10.1016/j.ecolind.2021.107639

Lin, X., Li, X., Gao, D., Liu, M. and Cheng, L. (2017). Ammonium Production and Removal in the Sediments of Shanghai River Networks: Spatiotemporal Variations, Controlling Factors, and Environmental Implications. *J. Geophys. Res.: Biogeosci.* 122 (10), 2461–2478. doi:10.1002/2017JG003769

Lin, G. and Lin, X. (2022). Bait Input Altered Microbial Community Structure and Increased Greenhouse Gases Production in Coastal Wetland Sediment. *Water Res.*, 118520 218. doi:10.1016/j.watres.2022.118520.

Li, X., Tang, C., Cao, Y. and Li, D. (2020). A Multiple Isotope (H, O, N, C and S) Approach to Elucidate the Hydrochemical Evolution of Shallow Groundwater in a Rapidly Urbanized Area of the Pearl River Delta, China. *Sci. Total. Environ.* 724, 137930. doi: 10.1016/j.scitotenv.2020.137930

Liu, F., Song, X., Yang, L., Han, D., Zhang, Y., Ma, Y., et. al (2015). The Role of Anthropogenic and Natural Factors in Shaping the Geochemical Evolution of Groundwater in the Subei Lake Basin, Ordos Energy Base, Northwestern China. *Sci. Total. Environ.* 538, 327–340. doi: 10.1016/j.scitotenv.2015.08.057

Marandi, A. and Shand, P. (2018). Groundwater Chemistry and the Gibbs Diagram. *Appl. Geochem.* 97, 209–212. doi: 10.1016/j.apgeochem.2018.07.009

Mengis, M. , Schif, S. L. , Harris, M. , English, M. C. , and Maclean, A. (1999). Multiple Geochemical and Isotopic Approaches for Assessing Ground Water NO_3- Elimination in a Riparian Zone. *Groundwater* 37 (3), 448–457. doi:10.1111/j.1745-6584.1999.tb01124.x

Otero, N., Torrentó, C., Soler, A., Menció, A. and Mas-Pla, J. (2009). Monitoring Groundwater Nitrate Attenuation in a Regional System Coupling Hydrogeology With Multi-Isotopic Methods: The Case of Plana De Vic (Osona, Spain). *Agricult. Ecosyst. Environ.* 133 (1-2), 103–113. doi: 10.1016/j.agee.2009.05.007

Parizi, E., Hosseini, S. M., Ataie-Ashtiani, B. and Simmons, C. T. (2019). Vulnerability Mapping of Coastal Aquifers to Seawater Intrusion: Review, Development and Application. *J. Hydrol.* 570, 555–573. doi:10.1016/j.jhydrol.2018.12.021

Rakib, M. A., Sasaki, J., Matsuda, H., Quraishi, S. B., Mahmud, M. J., Bodrud-Doza, M., et. al. (2020). Groundwater Salinization and Associated Co-Contamination Risk Increase Severe Drinking Water Vulnerabilities in the Southwestern Coast of Bangladesh. *Chemosphere* 246, 125646. doi:10.1016/j.chemosphere.2019.125646

Rivett, M. O., Buss, S. R., Morgan, P., Smith, J. W. N. and Bemment, C. D. (2008). Nitrate Attenuation in Groundwater: A Review of Biogeochemical Controlling Processes. *Water Res.* 42 (16), 4215–4232. doi: 10.1016/j.watres.2008.07.020

Schoeller, H. (1964). *La classification géochimique des eaux*. IASH publication, Iahs.Info 64, 16-24.

Schoeller, H. J. (1977). "Charpter 15-Geochemistry of Ground Water," in *Ground-Water Studies - An International Guide for Research and Practice*. Eds. Brown, R. H., Konoplyantsev, A. A., Ineson, J. and Kovalevsky, V. S. (Paris: The UNESCO Press).

Schüring, J., Schlieker, M. and Hencke, J. (2000). *Redox Fronts in Aquifer Systems and Parameters Controlling Their Dimensions* (Berlin Heidelberg: Springer), 135–151.

Shi, X., Wang, Y., Jiao, J. J., Zhong, J., Wen, H., and Dong, R. (2018). Assessing Major Factors Affecting Shallow Groundwater Geochemical Evolution in a Highly Urbanized Coastal Area of Shenzhen City, China. *J. Geochem. Explor.* 184, 17–27. doi:10.1016/j.gexplo.2017.10.003

Sigman, D. M., Casciotti, K. L., Andreani, M., Barford, C., Galanter, M. B. J. K., and Böhlke, J. K. (2001). A Bacterial Method for the Nitrogen Isotopic Analysis of Nitrate in Seawater and Freshwater. *Analytical. Chem.* 73 (17), 4145–4153. doi: 10.1021/ac010088e

Small, C. and Nicholls, R. J. (2003). A Global Analysis of Human Settlement in Coastal Zones. *J. Coast. Res.* 19 (3), 584–599. doi:10.2307/4299200

SMWB (2019). *Shenzhen Water Resources Bulletin* (Bureau, S.M.W) Shenzhen, China.

Steyl, G. and Dennis, I. (2010). Review of Coastal-Area Aquifers in Africa. *Hydrogeol. J.* 18 (1), 217–225. doi:10.1007/s10040-009-0545-9

Vörösmarty, C. J., Green, P., Salisbury, J. and Lammers, R. B. (2000). Global Water Resources: Vulnerability From Climate Change and Population Growth. *Science* 289 (5477), 284. doi: 10.1126/science.289.5477.284

Wakida, F. T. and Lerner, D. N. (2005). Non-Agricultural Sources of Groundwater Nitrate: A Review and Case Study. *Water Res.* 39 (1), 3–16. doi: 10.1016/j.watres.2004.07.026

Wang, Y. and Jiao, J. J. (2012). Origin of Groundwater Salinity and Hydrogeochemical Processes in the Confined Quaternary Aquifer of the Pearl River Delta, China. *J. Hydrol.* 438-439, 112–124. doi:10.1016/j.jhydrol.2012.03.008

Wang, Y., Jiao, J. J., Cherry, J. A. and Lee, C. M. (2013). Contribution of the Aquitard to the Regional Groundwater Hydrochemistry of the Underlying Confined Aquifer in the Pearl River Delta, China. *Sci. total. Environ.* 461-462, 663–671. doi: 10.1016/j.scitotenv.2013.05.046

Wang, Y., Jiao, J. J., Zhang, K. and Zhou, Y. (2016). Enrichment and Mechanisms of Heavy Metal Mobility in a Coastal Quaternary Groundwater System of the Pearl River Delta, China. *Sci. Total. Environ.* 545–546, 493–502. doi: 10.1016/j.scitotenv.2015.12.019

Wei, H., Gao, D., Liu, Y. and Lin, X. (2020). Sediment Nitrate Reduction Processes in Response to Environmental Gradients Along an Urban River-Estuary-Sea Continuum. *Sci. Total. Environ.* 718, 137185. doi: 10.1016/j.scitotenv.2020.137185

Wei, H. and Lin, X. (2021). Shifts in the Relative Abundance and Potential Rates of Sediment Ammonia-Oxidizing Archaea and Bacteria Along Environmental Gradients of an Urban River–Estuary–Adjacent Sea Continuum. *Sci. Total. Environ.* 771, 144824. doi: 10.1016/j.scitotenv.2020.144824

Weng, T. N., Liu, C. W., Kao, Y. H. and Hsiao, S. S. (2017). Isotopic Evidence of Nitrogen Sources and Nitrogen Transformation in Arsenic-Contaminated Groundwater. *Sci. Total. Environ.* 578, 167–185. doi: 10.1016/j.scitotenv.2016.11.013

World Health Organization, Geneva (2011). *Guidelines for Drinking-Water Quality*, 4th ed.

Wong, W. W., Grace, M. R., Cartwright, I. and Cook, P. L. M. (2014). Sources and Fate of Nitrate in a Groundwater-Fed Estuary Elucidated Using Stable Isotope Ratios of Nitrogen and Oxygen. *Limnol. Oceanogr.* 59 (5), 1493–1509. doi:10.4319/lo.2014.59.5.1493

Xiong, G. Y., Chen, G. Q., Xu, X. Y., Liu, W. Q., Fu, T. F., Khokiattiwong, S., et. al. (2020). A Comparative Study on Hydrochemical Evolution and Quality of Groundwater in Coastal Areas of Thailand and Bangladesh. *J. Asian Earth Sci.* 195, 104336. doi:10.1021/ac010088e

Xue, D., Botte, J., Baets, B. D., Accoe, F., and Boeckx, P. (2009). Present Limitations and Future Prospects of Stable Isotope Methods for Nitrate Source Identification in Surface- and Groundwater. *Water Res.* 43 (5), 1159–1170. doi:10.1016/j.watres.2008.12.048

Ye, F., Jia, G., Xie, L., Wei, G. and Xu, J. (2016). Isotope Constraints on Seasonal Dynamics of Dissolved and Particulate N in the Pearl River Estuary, South China. *J. Geophys. Res.* 121 (12) 8689-8705. doi:10.1002/2016JC012066

Zhang, X. M., Chai, F. H., Wang, S. L. and Sun, X. Z. (2010). Research Progress of Acid Precipitation in China. *Res. Environ. Sci* 23(5): 527-532. doi: 1001-6929 (2010) 05-0527-06

Zhang, X., Wu, Y. and Gu, B. (2015). Urban Rivers as Hotspots of Regional Nitrogen Pollution. *Environ. pollut.* 205, 139–144. doi: 10.1016/j.envpol.2015.05.031

Conflict of Interest: Authors RW and JW are/were employed by PowerChina Huadong Engineering Corporation Limited.

The remaining authors declare that the research was conducted in the absence of any commercial or financial relationships that could be construed as a potential conflict of interest.

Publisher's Note: All claims expressed in this article are solely those of the authors and do not necessarily represent those of their affiliated organizations, or those of the publisher, the editors and the reviewers. Any product that may be evaluated in this article, or claim that may be made by its manufacturer, is not guaranteed or endorsed by the publisher.

frontiers | Frontiers in Marine Science

ORIGINAL RESEARCH
published: 18 July 2022
doi: 10.3389/fmars.2022.958803

The Nitrogen Removal Ability of Salt Marsh Improved After Grazing Prohibition

Niu Li[1,2], *Ming Nie*[2], *Ming Wu*[1] *and Jihua Wu*[2]*

[1]Wetland Ecosystem Research Station of Hangzhou Bay, Research Institute of Subtropical Forestry, Chinese Academy of Forestry, Hangzhou, China, [2]Ministry of Education Key Laboratory for Biodiversity Science and Ecological Engineering, Coastal Ecosystems Research Station of Yangtze River Estuary, Institute of Biodiversity Science and Institute of Eco-Chongming, School of Life Sciences, Fudan University, Shanghai, China

Grazing prohibition has been used for some conservation purposes in salt marshes. However, the impact of this measure on microbe-mediated key nitrogen removal processes remains poorly understood. Therefore, this study assessed the impact of grazing prohibition on potential rates of nitrification and denitrification under short- and long-term grazing prohibition in high and middle elevation of the Dongtan salt marsh on Chongming Island, China. Compared with short-term grazing prohibition, we found that long-term grazing prohibition significantly increased nitrification and denitrification (except for nitrification in the high marsh), which indicates that the nitrogen removal ability of the salt marsh was improved along with the grazing prohibition time. Furthermore, we found that nitrification and denitrification in the high marsh were largely affected by NH4+ and soil moisture, respectively. Nitrification and denitrification in the middle marsh were mainly controlled by soil organic carbon (SOC) and nirS gene abundances, respectively. Our results indicate that the implementation of scientific and reasonable grazing prohibition policies in salt marshes has great potential to restore their ecosystem functions, maintain their ecosystem balance and realize their sustainable development.

Keywords: grazing prohibition, nitrification, denitrification, salt marshes, Chongming Island

OPEN ACCESS

Edited by:
Xianbiao Lin, Ocean University of China, China

Reviewed by:
Hengchen Wei, Nanjing Tech University, China
Jiapeng Wu, Guangzhou University, China

***Correspondence:**
Jihua Wu
jihuawu@fudan.edu.cn

Specialty section:
This article was submitted to Marine Biogeochemistry, a section of the journal Frontiers in Marine Science

Received: *01 June 2022*
Accepted: *20 June 2022*
Published: *18 July 2022*

Citation:
Li N, Nie M, Wu M and Wu J (2022) The Nitrogen Removal Ability of Salt Marsh Improved After Grazing Prohibition. Front. Mar. Sci. 9:958803. doi: 10.3389/fmars.2022.958803

INTRODUCTION

Salt marshes are located at the transition zone between terrestrial and marine ecosystems, providing various ecosystem services (Costanza et al., 1997; Valiela and Cole, 2002). Salt marshes, acting as filters, are of interest because they can remove large amounts of terrestrial N inputs from marine ecosystems, as such inputs adversely affect human and ecosystem health (Mitsch et al., 2001; Yang et al., 2015). However, these environments are under increasing anthropogenic pressure; for example, livestock grazing decreases aboveground plant material, potentially impairs coastal protection, and reduces invertebrate richness (Eldridge and Delgado-Baquerizo, 2017; Huang et al., 2021). Many regions of the world where livestock grazing is permitted have experienced great salt marsh erosion (Pagès et al., 2019). Thus, to eliminate the negative effects of continuous grazing, grazing prohibition has been extensively employed around the world and has been used as a management tool for protecting and restoring degraded salt marshes (Law et al., 2014).

Most of the world's research on grazing prohibition has focused on grassland and forest ecosystems and has concentrated on studies related to plant community composition, primary production,

soil properties and carbon cycling (Chen et al., 2012; Chen et al., 2016; Hu et al., 2016; Väisänen et al., 2021). For example, Hu et al. (2016) found that grazing prohibition increased vegetation biomass and soil carbon content by synthesizing the results of 51 sites in grasslands in China; Olofsson et al. (2006) revealed that herbivore exclusion increased primary production in the long term; Moradi et al. (2021) showed that soil physicochemical properties had a significant improvement after livestock exclusion. However, in contrast to the above research, there are fewer studies on the effects of grazing exclusion on nitrogen cycling processes, especially in salt marsh ecosystem. Although studies in grassland ecosystems had demonstrated that grazing prohibition could have a significant effect on the nitrogen cycle through changes in soil physicochemical properties (Li et al., 2021a), microbial community composition (Song et al., 2019) and soil nutrient content (Walker et al., 2009 ; Li et al., 2017), and some of these effects are positive and some are negative. However, salt marshes have distinct environmental characteristics that vary from those of terrestrial grasslands, such as high salinity, low redox potential, and the occurrence of periodic tidal inundation (Zhang et al., 2021 ; Martin and Reddy, 1997). These discrepancies may result in different responses of salt marshes to grazing prohibition, and the regulator of grazing prohibition impacts may differ between these ecosystems.

Nitrification and denitrification are two key nitrogen removal processes occurring in salt marshes (Valiela and Teal, 1979; Eriksson et al., 2003). Nitrification can affect the internal circulation of nitrogen, while denitrification combined with tidal water exchange results in nitrogen removal from salt marshes. Several studies have demonstrated the effects of grazing prohibition practices on nitrogen cycling processes (Walker et al., 2009; Wang et al., 2010; Liao et al., 2019). However, these studies have tended to focus on grasslands (Cheng et al., 2016; Che et al., 2018; Pan et al., 2016), alpine meadows (Yin et al., 2019), and riparian zones (Walker et al., 2009) and have ignored this issue in salt marshes. Given the essential roles of nitrification and denitrification in nitrogen cycling, discerning their responses to grazing prohibition, especially in salt marshes, is important for improving our understanding of the mechanisms of salt marsh restoration. Such knowledge can also enhance our capacity to forecast the responses of salt marsh ecosystems to anthropogenic effects.

In this study, we selected the Dongtan salt marsh on Chongming Island, China, as the study area. This region has long suffered from high nitrogen loading (Huang et al., 2006). This area has also been experiencing intensive human activities, including livestock grazing, which has reduced plant biomass, negatively affected soil decomposers, altered carbon resources, and disturbed the habitats of birds (Yang et al., 2017). The Chinese government imposed a policy of grazing prohibition, but it is largely unknown how grazing affects key nitrogen removal processes. To address these knowledge gaps, we conducted a field experiment in the Dongtan salt marsh on Chongming Island to investigate the effects of grazing prohibition on nitrogen removal processes. Our specific objectives were to (i) analyze how nitrification and denitrification respond to grazing prohibition in the high and middle marsh after short- and long-term grazing prohibition and (ii) identify the major drivers of nitrification and denitrification.

MATERIALS AND METHODS

Study Site and Soil Sampling

This study was conducted in the Dongtan salt marsh on Chongming Island, China (31°69′N, 121°65′E) (**Figure 1**). The Dongtan salt marsh covers an area of approximately 4000 km^2, is located at the mouth of the Yangtze Estuary in eastern China, and is an important stopover and wintering site for migratory birds. It is representative of salt marsh landscapes in China with high sediment deposition rates (Tang et al., 2020). This region has a subtropical monsoon climate, and the annual precipitation and temperature are 1145 mm and 15.3°C, respectively (Yang et al., 2017). Tidal fluctuations in the vicinity of Dongtan salt marsh are regular and semidiurnal. Ebb and flood tides are the two obvious diurnal

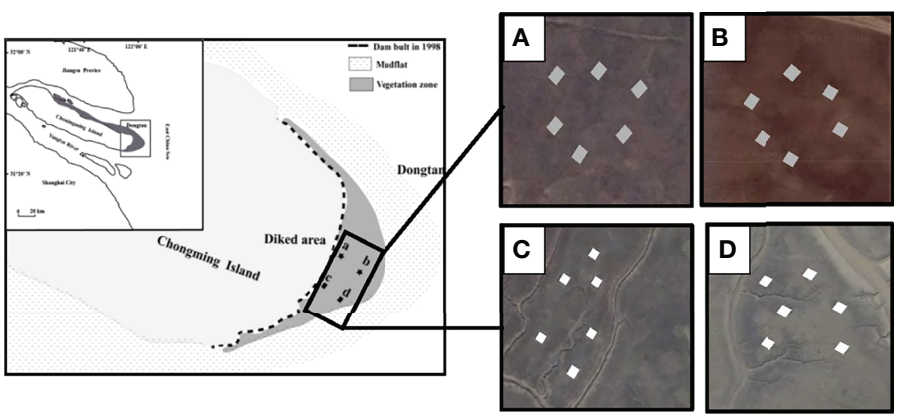

FIGURE 1 | Locations of experimental site. **(A)** LGA (long-term grazing prohibition) in the high marsh; **(B)** LGA (long-term grazing prohibition) in the middle marsh; **(C)** SGA (short-term grazing prohibition) in the high marsh; **(D)** SGA (short-term grazing prohibition) in the middle marsh.

tidal periods. The average elevations of the high and middle marsh are 380 cm and 330 cm above sea level, respectively, resulting in average monthly inundation frequencies of 17 and 39, respectively. The grazing history of Dongtan can be traced back to 1949 before the founding of the People's Republic of China. From the beginning of April to the end of October, cattle were grazed in this region with a stocking density of one head of cattle per ha (Yang et al., 2017). Grazing by cattle disturbs the habitats of birds, changes the plant community composition and structure, and damages the environment in this area (Yang et al., 2017). To relieve these problems, the local government implemented a policy of grazing prohibition in 2011. Given the interests and acceptance of herders, grazing activities were not completely banned and were restricted to the southern portion of the Dongtan salt marsh (**Figures 1C, D**). In 2017, total comprehensive grazing prohibition was achieved. Salt marshes undergoing different durations of grazing prohibition time were selected in August 2018. Grazing has been prohibited at these sites since 2011 (**Figures 1A, B**) or 2017 (**Figures 1C, D**), corresponding to grazing prohibition for 7 years (long-term grazing prohibition, LGA) and 1 year (short-term grazing prohibition, SGA), respectively (**Figure 1**). Four soil cores (3.8 cm diameter, 15 cm depth) were randomly taken from each plot (15 m × 15 m) in August 2018 and mixed to obtain one composite sample. A total of 24 composite soil samples (6 replicates × 2 marsh zones × 2 grazing prohibition treatments) were collected and transported to the laboratory in an ice box.

Soil Characteristics and Biomass Measurements

Soil temperature and redox potential (Eh) were measured *in situ* with a multiple digital meter (IQ Scientific Instruments, CA, USA) (Li et al, 2020). The pH and salinity of the samples were determined from soil suspensions at the soil water ratio was 1:5 (w/w) by using a conductivity meter (SevenExcellence S479-uMix, Mettler-Toledo, Switzerland) (Li et al., 2009). Soil moisture was determined by oven drying 50 g of fresh soil to a constant weight at 105°C (Cui et al., 2017). The total carbon (TC) and nitrogen (TN) concentrations were determined by using a N/C Soil Analyzer (Flash EA 11121 Series; Thermo Finnigan, Milan, Italy) (Nie et al., 2009). Ammonium (NH_4^+) and nitrate (NO_3^-) were extracted from fresh soil with 2 M KCl at *in situ* temperature for 1 h and measured using a continuous flow analyzer (SAN++, Skalar, the Netherlands) (Deng et al., 2015; Lin and Lin, 2022). Soil organic matter content (SOM) was determined as loss on ignition at 550°C for 5 h (Zhang et al., 2019). Aboveground living plant tissues were collected by clipping the entire contents of three randomly positioned 25 × 25 cm quadrats in each plot, and roots were collected from the same quadrats using a PVC tube (corer of 15 cm diameter, 20 cm depth) (Wei et al., 2020). The roots were immediately washed in clean water to remove all soil, and then both the aboveground living plant tissues and roots were oven dried at 80°C to a constant weight.

Nitrification and Denitrification

The nitrification potential was measured according to a modified shaken soil-slurry method (Hart et al., 1994; Li et al., 2021b). In brief, 15 g of sieved fresh sediment samples was placed in a 250 mL Erlenmeyer flask. Then, 100 mL of 1.0 mM phosphate buffer (pH=7.2) containing 1.0 mM NH_4^+ was added to the Erlenmeyer flask and mixed well. The soil slurry was shaken on an orbital shaker at 200 rpm in the dark for 24 h, and aeration was maintained. After shaking began, 10 mL of the soil slurry was collected at 2, 4, 12, 22, and 24 h. The collected slurry samples were centrifuged at 8000 ×g for 8 min, and then the supernatant was filtered and stored at -20°C until analysis. Nitrite (NO_2^-) and NO_3^- concentrations were measured by continuous-flow injection analysis (Skalar Analytical SAN^{++}, the Netherlands). The calculation of potential rates of nitrification was based on a linear regression of (NO_2^-+NO_3^-) concentration over time.

The ^{15}N tracer technique was used to measure the potential rates of denitrification (Hou et al., 2013; Lin et al., 2017). Briefly, soil slurries were prepared by mixing fresh sediment and helium-purged tidal water (30 min) at a sediment: water ratio of 1:7 (w/w). Then, the resulting slurries were transferred into 12-mL glass vials (Exetainer; Labco, High Wycombe, Buckinghamshire, UK) and sealed with butyl rubber stoppers. A 36-h preincubation step at the prevailing *in situ* temperature (25°C for August) was performed to consume the residual oxygen, NO_3^- and NO_2^- (Hou et al., 2015; Lin et al., 2016). After the preincubation period was complete, 100 μL of helium-purged stock solutions of $^{15}NO_3^-$ (99% ^{15}N) at a concentration of 100 μmol L^{-1} was spiked into each vial. Then, one-half of the vials were injected with 200 μL of 50% $ZnCl_2$ solution and regarded as the initial samples. The remaining vials were regarded as the final samples, and these vials were again incubated for another 8 h and fixed with 200 μL of 50% $ZnCl_2$ solution at the end of the incubation period. The ^{15}N atom% (F_N) was calculated by considering ^{15}N atom% of stock solutions and any residual ambient NO_x^- (2.04–7.53 μM) as determined by difference, ranging from 0.92 to 0.99. The abundance of $^{29}N_2$ and $^{30}N_2$ in each vial was measured with membrane inlet mass spectrometry (MIMS) (Hou et al., 2013). The potential rates of denitrification and anammox were calculated using the following equation (Thamdrup and Dalsgaard, 2002):

$$P_{29} = A_{29} + D_{29} \quad (1)$$

Where P_{29} (nmol N $g^{-1}h^{-1}$) is the total $^{29}N_2$ production rate; A_{29} and D_{29} (nmol N $g^{-1}h^{-1}$) represent the rates of $^{29}N_2$ production from anammox and denitrification, respectively. $^{28}N_2$, $^{29}N_2$, and $^{30}N_2$ generated from denitrification following random isotope pairing, D_{29}, can be estimated by using equation (2):

$$D_{29} = P_{30} \times 2 \times \left(1 - F_N\right) \times F_N^{-1} \quad (2)$$

Where P_{30} (nmol N $g^{-1}h^{-1}$) denotes the total $^{30}N_2$ production rate, F_N (%) is the fraction of ^{15}N in the total NO_3^-, which can be calculated according to the concentrations of NO_3^- before and after the addition of $^{15}NO_3^-$ to the incubated slurry; Hence, denitrification and anammox were calculated using equations (3) and (4), respectively, as follows:

$$D_{total} = D_{29} + 2 \times D_{30} \quad (3)$$

$$A_{29} = P_{29} - D_{29} \quad (4)$$

where D_{total} is potential rate of denitrification, A_{29} (nmol N $g^{-1}h^{-1}$) denotes the potential rate of anammox.

DNA Isolation and Quantitative PCR

Soil DNA was extracted from 0.25 g of frozen soil using Powersoil™ DNA Isolation Kits according to the manufacturer's protocol (MOBIO, USA). The quality and quantity of the extracted DNA were checked with a NanoDrop spectrophotometer (NanoDrop Technologies, Wilmington, DE). The extracted soil DNA was stored at -20°C for further use. Gene abundances of nitrifiers (ammonia-oxidizing archaea (AOA) *amoA* and ammonia-oxidizing bacteria (AOB) *amoA*) and denitrifiers (*nirK* and *nirS*) were determined using real-time PCR (q-PCR). The extracted DNA samples were diluted 10-fold prior to q-PCR. All q-PCRs were performed in triplicate with an ABI 7500 Detection System (Applied Biosystems, Canada) using the SYBR Green method. The primers Arch-amoAF (STAATGGTCTGGCTTAGACG) and Arch-amoAR (GCGGCCATCCATCTGTATGT) were used to quantify the abundance of the AOA *amoA* gene (Gao et al., 2018), the primers amoA-1F (GGGGTTTCTACTGGTGGT) and amoA-2R (CCCCTCKGSAAAGCCTTCTTC) were used to quantify the abundance of the AOB *amoA* gene (Rotthauwe et al., 1997), the primers F1aCu (ATCATGGTSCTGCCGCG) and R3Cu (GCCTCGATCAGRTTGTGGTT) were used to quantify the abundance of the *nirK* gene (Hallin and Lindgren, 1999) and the primers cd3aF(GTSAACGTSAAGGARACSGG) and R3cd (GASTTCGGRTGSGTCTTGA) were used to quantify the abundance of the *nirS* gene (Throbäck et al., 2004). Details regarding the q-PCR conditions for these genes are provided in **Table S1**. In each amplification, the absence of DNA template was used as a negative control. The standard curves for these genes were created using a 10-fold dilution series (10^2–10^9 copies) of the standard plasmid DNA. Only results with efficiency and correlation coefficients above 95% and 98% were used. The abundances of the four genes were calculated based on the constructed standard curves.

Data Analyses and Statistical Tests

All data analysis in this research were done with SPSS Statistics version 19.0 (SPSS, Inc., Chicago, IL, USA) and RStudio software version 3.5.1 (RStudio, Inc., Boston, MA, USA). We used two-way ANOVA to determine the effects of grazing prohibition and marsh zone on plant community characteristics, soil physicochemical properties, the potential rates of nitrification and denitrification, and nitrifier and denitrifier gene abundances. Tukey's HSD test was used to determine the significance level ($p < 0.05$). Values were the mean ($n=6$) ± standard error (*SE*). Pearson correlation heatmaps were applied to analyze potential rates of nitrification and denitrification with soil physicochemical properties and abundances of key nitrogen removal communities. Stepwise multiple regression analyses were used to identify which factors can best explain the variations in potential rates of denitrification. All statistical analyses were performed with R software.

RESULTS

Effects of Grazing Prohibition on Nitrification and Denitrification

Potential rates of nitrification changed significantly with marsh zones and grazing prohibition time (**Table S2**, $p < 0.05$). Nitrification rates were higher in the high marsh than these in the middle marsh. In the high marsh, there was no significant difference in nitrification rates between short-term grazing prohibition and long-term grazing prohibition (**Figure 2**). In the middle marsh, the nitrification rates under long-term grazing prohibition were 25.70% higher than those under short-term grazing prohibition (**Figure 2A**).

Potential rates of denitrification were significantly affected by grazing prohibition time, but not affected by marsh zones (**Table S2**, $p < 0.05$). In both the middle marsh and the high

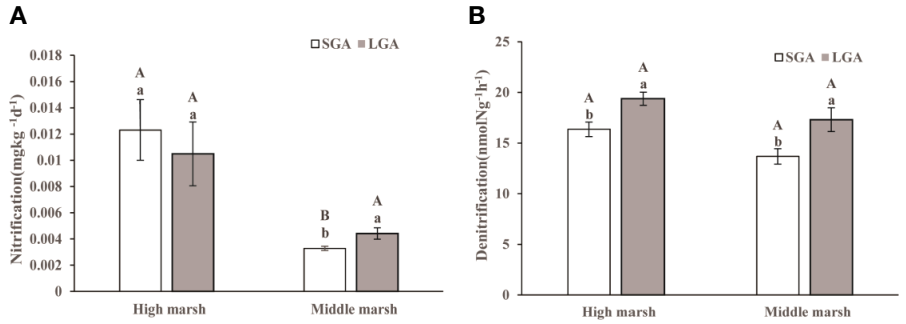

FIGURE 2 | Nitrification and denitrification under different treatments in the middle and high marsh. **(A)** Nitrification and **(B)** Denitrification. SGA, Short-term grazing prohibition; LGA, Long-term grazing prohibition. Error bars indicate standard errors. Different uppercase letters indicate significant differences ($p < 0.05$) between elevations under the same treatment, and different lowercase letters indicate significant differences ($p < 0.05$) between different treatments.

marsh, long-term grazing prohibition dramatically increased the denitrification rate compared with that under short-term grazing prohibition (**Figure 2B**). Compared with that in the short-term grazing prohibition treatment, long-term grazing prohibition increased the denitrification rates in the high marsh and middle marsh by 15.56% and 21.00%, respectively (**Figure 2B**).

Effects of Grazing Prohibition on the Abundances of Nitrifiers and Denitrifiers

Grazing prohibition significantly influenced the abundances of nitrifiers. The abundances of the AOA *amoA* gene and AOB *amoA* gene under long-term grazing prohibition were 47.53% and 76.34% higher than those under short-term grazing prohibition, respectively (**Figures 3A, B**). There were no significant differences in the abundances of the *nirK* gene among the different grazing prohibition treatments (**Figure 3C**). However, compared with that under short-term grazing prohibition, the abundances of the *nirS* gene under long-term grazing prohibition in the high marsh and middle marsh increased by 51.12% and 73.13%, respectively (**Figure 3D**). In addition, marsh zones also had great influences on the abundances of the AOA *amoA* gene and *nirK* gene (**Figure 3** and **Table S3**).

Effects of Grazing Prohibition on Plant Community Characteristics and Soil Physicochemical Properties

Plant community characteristics was significantly affected by grazing prohibition time, but not affected by marsh zone (**Table S4**). Compared with that under short-term grazing prohibition, long-term grazing prohibition increased the aboveground and belowground biomass and plant community height, decreased the plant community density, changed the plant community composition, and caused *Phragmites australis* to become the single dominant species (**Table 1**).

Soil physicochemical properties changed significantly with marsh zones and grazing prohibition time (**Table 2** and **Table S5**). Temperature, soil moisture, bulk density, SOC, TN and TC in the high marsh were higher than these in the middle marsh. In the high marsh, compared with that under short-term grazing prohibition, long-term grazing prohibition reduced the soil bulk density and temperature and significantly increased the soil Eh, salinity, soil organic

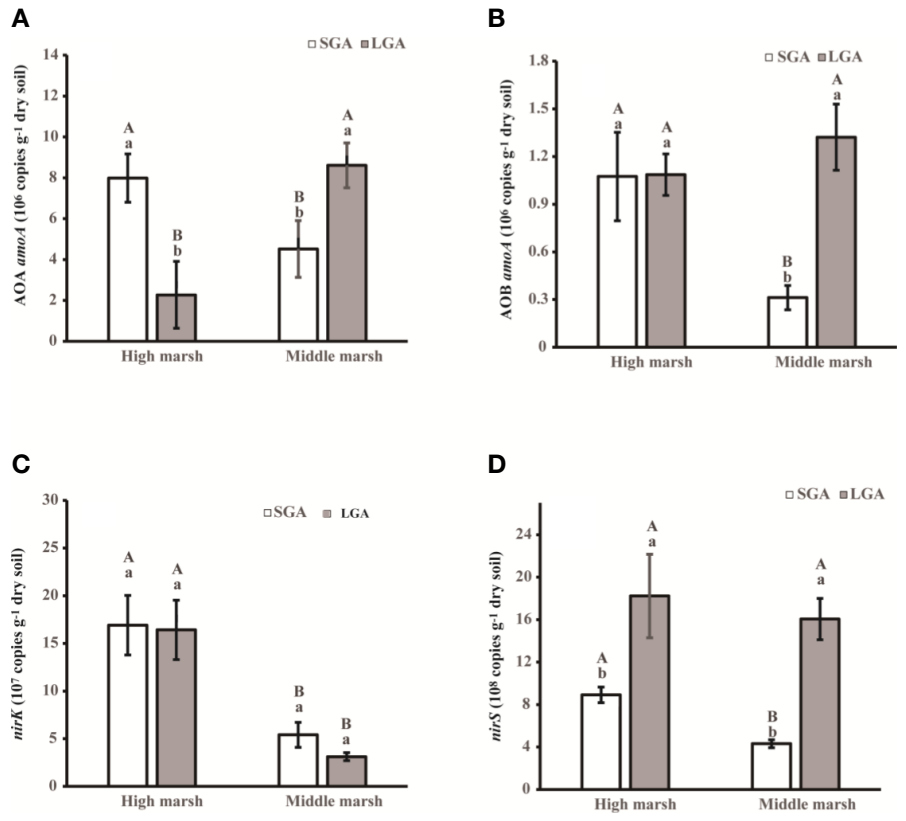

FIGURE 3 | Abundance of *amoA* sequences from AOA and AOB and *nirK* and *nirS* sequences from soil in the different treatments. SGA, Short-term grazing prohibition; LGA, Long-term grazing prohibition. Error bars indicate standard errors. Different uppercase letters indicate significant differences ($p < 0.05$) between elevations under the same treatment, and different lowercase letters indicate significant differences ($p < 0.05$) between different treatments.

TABLE 1 | Influence of grazing abandonment on plant averaged height, averaged density, biomass and community compositions (Mean ± SE).

Marsh zone	Plant properties	SGA	LGA
High marsh	Plant height (cm)	93.92 ± 6.20b	298.63 ± 11.98a
	Plant density	52.40 ± 6.20a	14.53 ± 1.34b
	Aboveground biomass (g·m^{-2})	815.94 ± 119.58b	1611.92 ± 109.53a
	Belowground biomass (g·m^{-2})	506.21 ± 37.89b	1158.26 ± 201.60a
	Dominant species	*Phragmites australis* *Carex scabrifolia*	*Phragmites australis*
Middle marsh	Plant height (cm)	81.01 ± 4.75b	338.27 ± 5.34a
	Plant density	57.37 ± 13.27a	11.00 ± 0.57b
	Aboveground biomass (g·m^{-2})	907.42 ± 105.10b	1594.96 ± 27.78a
	Belowground biomass (g·m^{-2})	423.84 ± 23.44b	770.82 ± 69.86a
	Dominant species	*Phragmites australis* *Carex scabrifolia* *Imperata cylindrica* *Scirpus mariqueter*	*Phragmites australis*

LGA, Long-term grazing abandonment, SGA, Short-term grazing abandonment; different letters (a and b) indicate significant differences ($p< 0.05$) between LGA and SGA.

carbon (SOC), NH_4^+, NO_3^-, TC, TN and moisture ($p< 0.05$) (**Table 2**). In the middle marsh, long-term grazing significantly increased the soil salinity, SOC, NH_4^+, NO_3^-, TN, and moisture ($p< 0.05$) (**Table 2**).

Factors Controlling Nitrification and Denitrification

Pearson correlation heatmap shown that potential rates of nitrification and denitrification in the middle marsh were significantly positive related to AOA *amoA* gene abundance and *nirS* gene abundance, respectively (**Figure 4A**). Whereas, in the high marsh, potential rates of nitrification and denitrification were affected not only by the abundance of functional microorganisms, but also by SOC and TN contents, respectively (**Figure 4B**).

For different marsh zones, we executed multiple linear regression analysis to point out which linear combination of independent variables best to explain changes of nitrification and denitrification after grazing prohibition in salt marsh (**Table 3**). In the high marsh, the main factors affecting nitrification were belowground biomass and NH_4^+, while the main factor affecting denitrification was soil moisture. In the middle marsh, nitrification was mainly affected by SOC, while denitrification was largely explained by the *nirS* gene abundance (**Table S6**). The denitrification rate was also affected by soil salinity, temperature, clay content and *nirK* gene abundance.

DISCUSSION

Understanding the changes in nitrification and denitrification after grazing prohibition in salt marshes is of vital importance to assess the consequences of conversion measures for salt marsh ecosystem functions. In this study, we quantified grazing prohibition-induced changes in the potential microbial activities driving soil nitrogen dynamics in high and middle marshes. Our results show that long-term grazing prohibition increased nitrification and denitrification compared with those processes under short-term grazing prohibition, which indicates that the nitrogen removal ability of salt marshes improved after grazing prohibition after a certain time (**Figure 5**). Our results were consistent with previous findings in other systems (Song et al., 2019; Pan et al., 2015; Walker

TABLE 2 | Effects of grazing prohibition on soil physicochemical properties.

Physicochemical properties	High marsh		Middle marsh	
	SGA	LGA	SGA	LGA
Eh (mV)	**81.32 ± 5.31b**	**78.95 ± 20.41a**	35.53 ± 36.29a	60.11 ± 29.33a
Temperature (°C)	**31.70 ± 0.29a**	**27.39 ± 0.03b**	28.55 ± 0.37a	27.85 ± 0.18a
pH	7.52 ± 0.05a	7.54 ± 0.02a	7.55 ± 0.04a	7.57 ± 0.02a
Salinity (mg kg^{-1})	**0.89 ± 0.17b**	**2.00 ± 0.26a**	**0.87 ± 0.06b**	**1.58 ± 0.15a**
Soil moisture (mg kg^{-1})	**0.31 ± 0.01b**	**0.42 ± 0.02a**	**0.25 ± 0.00b**	**0.27 ± 0.00a**
Bulk density (g cm^{-3})	**1.20 ± 0.03a**	**0.95 ± 0.03b**	**1.26 ± 0.05a**	**1.23 ± 0.04a**
NH_4^+-N (g kg^{-1})	4.05 ± 0.21a	5.20 ± 0.19a	3.47 ± 0.19a	4.04 ± 0.12a
NO_3^-N (g kg^{-1})	**0.34 ± 0.03b**	**3.71 ± 0.54a**	**0.61 ± 0.07b**	**1.16 ± 0.07a**
SOC (%)	**6.67 ± 0.51b**	**10.93 ± 0.86a**	**5.98 ± 0.07b**	**7.23 ± 0.39a**
TN (%)	**0.09 ± 0.01b**	**0.15 ± 0.01a**	**0.06 ± 0.00b**	**0.10 ± 0.00a**
TC (%)	**1.71 ± 0.04b**	**2.19 ± 0.04a**	**1.46 ± 0.03b**	**1.74 ± 0.02a**

Mean ± standard error, n=6; SGA, Short-term grazing prohibition; LGA, Long-term grazing prohibition. Different letters indicate significant differences ($p< 0.05$) in soil physicochemical properties between short-term grazing prohibition and long-term grazing prohibition. Bold font indicates a significant effect.

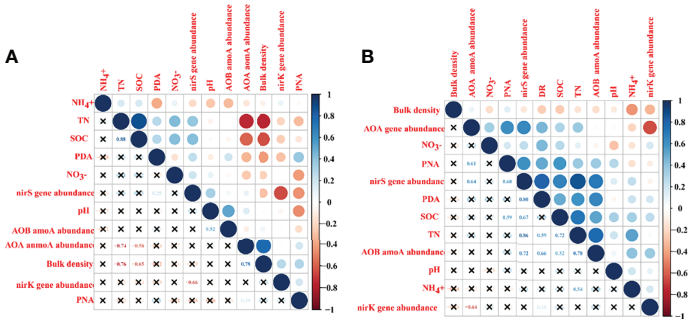

FIGURE 4 | Pearson correlation heatmap of potential rates of nitrification and denitrification with soil physicochemical properties and abundances of key nitrogen removal communities. **(A)** in the middle marsh; **(B)** in the high marsh. The colors show in the figure represent the correlation between two variables. The darker the blue, the stronger the positive correlation, and the deeper the red, the stronger the negative correlation. The larger the circle, the greater the absolute value of the correlation coefficient, the cross in the figure indicates that there is no correlation between the two variables. PNA, potential rates of nitrification; PDA, potential rates of denitrification.

et al., 2009). Compared to other ecosystems around the world, salt marshes have a similar ability to recover soil N cycling processes after grazing prohibition. For example, a research conducted by Olofsson et al. (2006) found that excluding rabbits less than four years had no significant effect on N mineralization, whereas N mineralization level increased after herbivore exclusion for a long time. The report by Walker et al. (2009) showed that cattle exclusion increased N trace gas fluxes and denitrification rates in a restored riparian zone in the southern Appalachians. Song et al. (2019) found that potential rates of microbial N turnover is facilitated by grazing prohibition in a semiarid area in China.

In the high marsh, belowground biomass and NH_4^+ were key factors influencing nitrification. Previous studies have shown that grazing prohibition could reduce nutrient and have significantly impact on vegetation index, belowground biomass, and soil nutrients (Anderson et al., 2007; Chen et al., 2012; Li et al., 2022). Our results showed that belowground biomass increased with grazing prohibition time, which mainly due to the absence of eating and trampling by herbivores (Liu et al., 2019). Growing vegetation intercepts more inorganic nitrogen but also improves the absorption of NH_4^+ in the sediment with grazing prohibition time (Martin and Reddy, 1977; Berg et al., 1997). Moreover, nutrients from cattle manure and urine entering the soil were gradually diluted as the grazing prohibition time increased (Paul et al., 2013), which resulted in no difference in NH_4^+ between short- and long-term grazing prohibition. NH_4^+ provides a substrate for nitrification (McGilloway et al., 2003; Huang et al., 2022), which resulted in no changes in nitrification between the short- and long-term grazing prohibition treatments (**Figure 2A**). Soil moisture was a key factor influencing denitrification. There was no trampling by herbivores after grazing prohibition was implemented, the soil gradually became looser, the soil bulk density gradually decreased, and the soil porosity gradually increased. Therefore, the ability of water to penetrate and accumulate was improved, and the migration of NO_3^- from tidal water to the soil and its subsequent transformation were accelerated, which was conducive to the occurrence of denitrification (Reddy et al., 1989).

In the middle marsh, SOC and *nirS* gene abundance were the most important factors affecting nitrification and denitrification, respectively. As grazing prohibition proceeds, the vegetation community gradually recovers (Su et al., 2005), aboveground biomass significantly increases, and a large amount of litter is returned to the sediment (Belsky, 1992; Liu et al., 2019). The higher plant biomass caused nutrient accumulation, including the accumulation of SOC, NH_4^+ and NO_3^- (**Table 2**), which can provide energy and substrates for nitrifying and denitrifying bacteria (Pinay et al., 2003; Navada et al., 2020). Our study showed that in comparison with that under short-term grazing prohibition, the SOC content and the abundance of the *nirS* gene significantly increased after long-term grazing prohibition in the middle marsh (**Table 2**), which resulted in an increase in nitrification and denitrification under long-term grazing prohibition when compared to that under short-term grazing prohibition.

TABLE 3 | Multiple linear regression equations reported for nitrification or denitrification versus several environmental factors and abundances of key nitrogen removal communities.

Marsh zone	Best model	R^2	P
High marsh	PNA = 0.692 + 1.374Belowground biomass + 0.261 NH_4^+	0.053	0.003
	PDA = 8.517 + 25.726Soil moisture	0.634	0.006
Middle marsh	PNA = -0.001 + 0.001SOC	0.505	<0.001
	PDA = 78.979 + 1.438*nirS* gene abundance + 0.709Temperature - 0.760Salinity + 0.509Clay + 0.182*nirK* gene abundance	0.998	<0.001

PNA, potential rates of nitrification; PDA, potential rates of denitrification. R^2 is the overall explanation rate of the model to the dependent variable, and P represents the significance level.

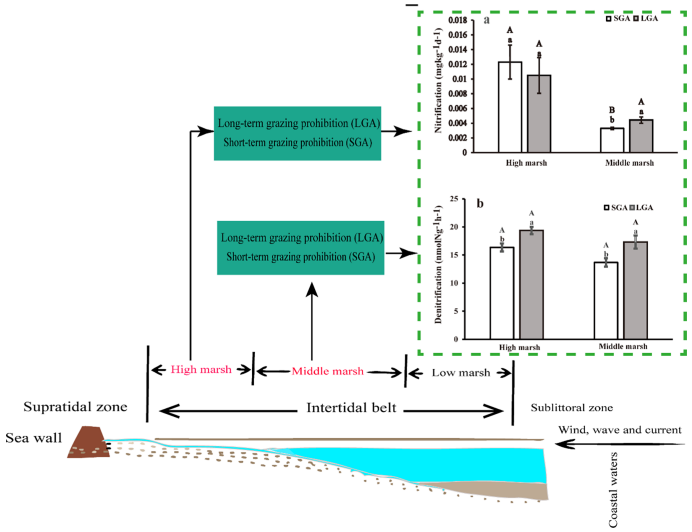

FIGURE 5 | Graphical abstract of grazing prohibition on nitrification and denitrification in the different marsh zones in salt marshes.

For the first time, we explored the effects of grazing prohibition on the nitrogen removal ability of salt marsh ecosystems. Our results show that grazing prohibition could improve the nitrogen removal ability of salt marshes, indicating that the ecosystem service ability of salt marshes was improved during the restoration process. The improvement of the nitrogen removal capacity of salt marshes after grazing prohibition helps to alleviate the environmental pressure exerted by excessive terrestrial N inputs on marine ecosystems.

Nitrogen removal capacity potential is facilitated by grazing prohibition, probably through enhanced biomass production *via* increases in nutrient and carbon sources into the soil. In addition, previous studies on the ecosystem multifunctionality of salt marshes have mainly focused on the variables related to the operating rates of ecosystems but often ignored variables related to ecosystem services (Jing et al., 2015; Zhang et al., 2021). Therefore, it is necessary to integrate indicators related to ecosystem function and ecosystem services when conducting research on salt marsh ecosystem multifunctionality.

CONCLUSIONS

Nitrogen removal is a vital ecosystem service provided by coastal salt marshes. Based on the findings of this study, we established that the nitrogen removal ability of salt marshes was significantly improved after grazing prohibition for a certain period in salt marshes. Nitrification and denitrification under long-term grazing prohibition were higher than those under short-term grazing prohibition, and this information is beneficial to better assess the ecosystem services provided by salt marshes after restoration, especially in terms of their nitrogen removal capacity. Changes in soil N cycling mechanisms following restoration of the salt marshes were primarily driven by nutrient and carbon sources into the soil due to the recovery of plant communities. Nevertheless, this study analyzed only the dynamic changes in nitrification and denitrification after the restoration of salt marshes over a certain period time. The restoration of the ecosystem functions of salt marshes after disturbance may occur different situations over time. Therefore, to provide more evidence for a comprehensive scientific assessment of grazing prohibition, continued monitoring should be carried out over a long-time scale in the future. In general, our findings are important for assessing the effects of grazing prohibition on the key nitrogen removal processes occurring in salt marshes.

DATA AVAILABILITY STATEMENT

The original contributions presented in the study are included in the article/**Supplementary Material**. Further inquiries can be directed to the corresponding author.

AUTHOR CONTRIBUTIONS

NL, methodology, investigation, software, formal analysis, and writing original draft. MN and MW, conceptualization, writing-review and editing, and funding acquisition. JW, conceptualization, resources, methodology, supervision, project administration, writing-review and editing, and funding acquisition. All authors contributed to the article and approved the submitted version.

FUNDING

This research was supported by the NSFC funding (32030067) and the Shanghai Science and Technology Committee (20DZ1204702).

ACKNOWLEDGMENTS

We thank J. Chai for help in field sampling. JW and NL designed the study. NL conducted the work and analyzed the data, and all authors wrote the manuscript.

SUPPLEMENTARY MATERIAL

The Supplementary Material for this article can be found online at: https://www.frontiersin.org/articles/10.3389/fmars.2022.958803/full#supplementary-material

REFERENCES

Anderson, T. M., Ritchie, M. E. and McNaughton, S. (2007). Rainfall and Soils Modify Plant Community Response to Grazing in Serengeti National Park. *Ecology* 88, 1191–1201. doi: 10.1890/06-0399

Belsky, A. J. (1992). Effects of Grazing, Competition, Disturbance and Fire on Species Composition and Diversity in Grassland Communities. *J. Veg. Sci.* 3, 187–200. doi: 10.2307/3235679

Berg, W. A., Bradford, J. A. and Sims, P. L. (1997). Long-Term Soil Nitrogen and Vegetation Change on Sandhill Rangeland. *J. Range Manage.* 50, 482–486. doi: 10.2307/4003702

Cheng, J., Jing, G., Wei, L. and Jing, Z. (2016). Long-Term Grazing Exclusion Effects on Vegetation Characteristics, Soil Properties and Bacterial Communities in the Semi-Arid Grasslands of China. *Ecol. Eng.* 97, 170–178. doi: 10.1016/j.ecoleng.2016.09.003

Chen, Y., Li, Y., Zhao, X., Awada, T., Shang, W. and Han, J. (2012). Effects of Grazing Exclusion on Soil Properties and on Ecosystem Carbon and Nitrogen Storage in a Sandy Rangeland of Inner Mongolia, Northern China. *Environ. Manage.* 50, 622–632. doi: 10.1007/s00267-012-9919-1

Chen, J., Zhou, X., Wang, J., Hruska, T., Shi, W., Cao, J., et al. (2016). Grazing Exclusion Reduced Soil Respiration But Increased its Temperature Sensitivity in a Meadow Grassland on the Tibetan Plateau. *Ecol. Evol.* 6, 675–687. doi: 10.1002/ece3.1867

Che, R., Qin, J., Tahmasbian, I., Wang, F., Zhou, S., Xu, Z., et al. (2018). Litter Amendment Rather Than Phosphorus can Dramatically Change Inorganic Nitrogen Pools in a Degraded Grassland Soil by Affecting Nitrogen-Cycling Microbes. *Soil Biol. Biochem.* 120, 145–152. doi: 10.1016/j.soilbio.2018.02.006

Costanza, R., D'Arge, R., de Groot, R., Farber, S., Grasso, M., Hannon, B., et al. (1997). The Value of the World's Ecosystem Services and Natural Capital. *Nature.* 387, 253–260. doi: 10.1038/387253a0

Cui, J., Chen, X., Nie, M., Fang, S., Tang, B., Quan, Z., et al. (2017). Effects of Spartina Alterniflora Invasion on the Abundance, Diversity, and Community Structure of Sulfate Reducing Bacteria Along a Successional Gradient of Coastal Salt Marshes in China. *Wetlands* 37, 221–232. doi: 10.1007/s13157-016-0860-6

Deng, F., Hou, L., Liu, M., Zheng, Y., Yin, G., Li, X., et al. (2015). Dissimilatory Nitrate Reduction Processes and Associated Contribution to Nitrogen Removal in Sediments of the Yangtze Estuary. *J. Geophys. Res. Biogeosci.* 120, 1521–1531. doi: 10.1002/2015JG003007

Eldridge, D. J. and Delgado-Baquerizo, M. (2017). Continental-Scale Impacts of Livestock Grazing on Ecosystem Supporting and Regulating Services. *L. Degrad. Dev.* 28, 1473–1481. doi: 10.1002/ldr.2668

Eriksson, P. G., Svensson, J. M. and Carrer, G. M. (2003). Temporal Changes and Spatial Variation of Soil Oxygen Consumption, Nitrification and Denitrification Rates in a Tidal Salt Marsh of the Lagoon of Venice, Italy. *Estuar. Coast. Shelf. Sci.* 58, 861–871. doi: 10.1016/j.ecss.2003.07.002

Gao, J., Hou, L., Zheng, Y., Liu, M., Yin, G., Yu, C., et al. (2018). Shifts in the Community Dynamics and Activity of Ammonia-Oxidizing Prokaryotes Along the Yangtze Estuarine Salinity Gradient. *J. Geophys. Res. Biogeosci.* 123, 3458–3469. doi: 10.1029/2017JG004182

Hallin, S. and Lindgren, P. E. (1999). PCR Detection of Genes Encoding Nitrite Reductase in Denitrifying Bacteria. *Appl. Environ. Microbiol.* 65, 1652–1657. doi: 10.1128/AEM.65.4.1652-1657.1999

Hart, S. C., Stark, J. M., Davidson, E. A. and Firestone, M. K. (1994). "Nitrogen Mineralization, Immobilization, and Nitrification," In: Weaver RW (ed) Methods of Soil Analysis: Microbiological and Biochemical Properties, 3rd edn. Soil Science Society of America, Madison, pp 985 –1018

Hou, L., Zheng, Y., Liu, M., Gong, J., Zhang, X., Yin, G., et al. (2013). Anaerobic Ammonium Oxidation (Anammox) Bacterial Diversity, Abundance, and Activity in Marsh Sediments of the Yangtze Estuary. *J. Geophys. Res. Biogeosci.* 118, 1237–1246. doi: 10.1002/jgrg.20108

Hou, L., Zheng, Y., Liu, M., Li, X., Lin, X., Yin, G., et al. (2015). Anaerobic Ammonium Oxidation and its Contribution to Nitrogen Removal in China's Coastal Wetlands. *Sci. Rep.* 5, 1–11. doi: 10.1038/srep15621

Huang, F., Lin, X., Hu, W., Zeng, F., He, L. and Yin, K. (2021). Nitrogen Cycling Processes in Sediments of the Pearl River Estuary: Spatial Variations, Controlling Factors, and Environmental Implications. *Catena.* 206, 105545. doi: 10.1016/j.catena.2021.105545

Huang, F., Lin, X. and Yin, K. (2022). Effects of Marine Produced Organic Matter on the Potential Estuarine Capacity of NOx– Removal. *Sci. Total Environ.* 812, 151471. doi: 10.1016/j.scitotenv.2021.151471

Huang, Q., Shen, H., Wang, Z., Liu, X. and Fu, R. (2006). Influences of Natural and Anthropogenic Processes on the Nitrogen and Phosphorus Fluxes of the Yangtze Estuary, China. *Reg. Environ. Change* 6, 125–131. doi: 10.1007/s10113-005-0001-x

Hu, Z., Li, S., Guo, Q., Niu, S., He, N., Li, L., et al. (2016). A Synthesis of the Effect of Grazing Exclusion on Carbon Dynamics in Grasslands in China. *Glob. Chang Biol.* 22, 1385–1393. doi: 10.1111/gcb.13133

Jing, X., Sanders, N. J., Yu, S., Chu, H., Classen, A. T., Zhao, K., et al. (2015). The Links Between Ecosystem Multifunctionality and Above-and Belowground Biodiversity are Mediated by Climate. *Nat. Commun.* 6, 8159. doi: 10.1038/ncomms9159

Law, A., Jones, K. C. and Willby, N. J. (2014). Medium vs. Short Term Effects of Herbivory by Eurasian Beaver on Aquatic Vegetation. *Aquat. Bot.* 116, 27–34. doi: 10.1016/j.aquabot.2014.01.004

Liao, L. R., Wang, J., Zhang, C., Liu, G. B. and Song, Z. L. (2019). Effects of Grazing Exclusion on the Abundance of Functional Genes Involved in Soil Nitrogen Cycling and Nitrogen Storage in Semiarid Grassland. *J. Appl. Ecol.* 30, 3473–3481. doi :10.13287/j.1001-9332.201910.002

Li, W., Cao, W., Wang, J., Li, X., Xu, C. and Shi, S. (2017). Effects of Grazing Regime on Vegetation Structure, Productivity, Soil Quality, Carbon and Nitrogen Storage of Alpine Meadow on the Qinghai-Tibetan Plateau. *Ecol. Eng.* 98, 123–133. doi: 10.1016/j.ecoleng.2016.10.026

Li, B., Liao, C., Zhang, X., Chen, H., Wang, Q., Chen, Z., et al. (2009). Spartina Alterniflora Invasions in the Yangtze River Estuary, China: An Overview of Current Status and Ecosystem Effects. *Ecol. Eng.* 35, 511–520. doi: 10.1016/j.ecoleng.2008.05.013

Li, N., Li, B., Nie, M. and Wu, J. (2020). Effects of Exotic Spartina Alterniflora on Saltmarsh Nitrogen Removal in the Yangtze River Estuary, China. *J. Clean. Prod.* 271, 122557. doi: 10.1016/j.jclepro.2020.122557

Lin, X., Hou, L., Liu, M., Li, X., Zheng, Y., Yin, G., et al. (2016). Nitrogen Mineralization and Immobilization in Sediments of the East China Sea: Spatiotemporal Variations and Environmental Implications. *J. Geophys. Res. Biogeosci.* 121, 2842–2855. doi: 10.1002/2016JG003499

Li, N., Nie, M., Li, B., Wu, J. and Zhao, J. (2021b). Contrasting Effects of the Aboveground Litter of Native Phragmites Australis and Invasive Spartina Alterniflora on Nitrification and Denitrification. *Sci. Total Environ.* 764, 144283. doi: 10.1016/j.scitotenv.2020.144283

Lin, X., Li, X., Gao, D., Liu, M. and Cheng, L. (2017). Ammonium Production and Removal in the Sediments of Shanghai River Networks: Spatiotemporal Variations, Controlling Factors, and Environmental Implications. *J. Geophys. Res. Biogeosci.* 122, 2461–2478. doi: 10.1002/2017JG003769

Lin, G. and Lin, X. (2022). Bait Input Altered Microbial Community Structure and Increased Greenhouse Gases Production in Coastal Wetland Sediment. *Water Res.* 218, 118520. doi: 10.1016/j.watres.2022.118520

Liu, J., Bian, Z., Zhang, K., Ahmad, B. and Khan, A. (2019). Effects of Different Fencing Regimes on Community Structure of Degraded Desert Grasslands on Mu Us Desert, China. *Ecol. Evol.* 9, 3367–3377. doi: 10.1002/ece3.4958

Li, M., Wang, L., Li, J., Peng, Z., Wang, L., Zhang, X., et al. (2022). Grazing Exclusion had Greater Effects Than Nitrogen Addition on Soil and Plant Community in a Desert Steppe, Northwest of China. *BMC Plant Biol.* 22, 60. doi: 10.1186/s12870-021-03400-z

Li, J., Zhao, Y., Zhang, A., Song, B. and Hill, R. L. (2021a). Effect of Grazing Exclusion on Nitrous Oxide Emissions During Freeze-Thaw Cycles in a Typical Steppe of Inner Mongolia. *Agric. Ecosyst. Environ.* 307, 107217. doi: 10.1016/j.agee.2020.107217

Martin, J. F. and Reddy, K. R. (1997). Interaction and Spatial Distribution of Wetland Nitrogen Processes. *Ecol. Modell.* 105, 1–21. doi: 10.1016/S0304-3800(97)00122-1

McGilloway, R. L., Weaver, R. W., Ming, D. W. and Gruener, J. E. (2003). Nitrification in a Zeoponic Substrate. *Plant Soil.* 256, 371–378. doi: 10.1023/A:1026174026995

Mitsch, W. J., Day, J. W., Gilliam, J. W., Groffman, P. M., Hey, D. L., Randall, G. W., et al. (2001). Reducing Nitrogen Loading to the Gulf of Mexico From the Mississippi River Basin: Strategies to Counter a Persistent Ecological Problem. *Bioscience.* 51, 373–388. doi: 10.1641/0006-3568(2001)051[0373:RNLTTG]2.0.CO;2

Moradi, M., Jorfi, M. R., Basiri, R., Yusef Naanaei, S. and Heydari, M. (2021). Beneficial Effects of Livestock Exclusion on Tree Regeneration, Understory Plant Diversity, and Soil Properties in Semiarid Forests in Iran. *Land Degrad. Dev.* 33, 324–332. doi: 10.1002/ldr.4154

Navada, S., Knutsen, M. F., Bakke, I. and Vadstein, O. (2020). Nitrifying Biofilms Deprived of Organic Carbon Show Higher Functional Resilience to Increases in Carbon Supply. *Sci. Rep.* 10, 1–11. doi: 10.1038/s41598-020-64027-y

Nie, M., Zhang, X. D., Wang, J. Q., Jiang, L. F., Yang, J., Quan, Z. X., et al. (2009). Rhizosphere Effects on Soil Bacterial Abundance and Diversity in the Yellow River Deltaic Ecosystem as Influenced by Petroleum Contamination and Soil Salinization. *Soil Biol. Biochem.* 41, 2535–2542. doi: 10.1016/j.soilbio.2009.09.012

Olofsson, J., Mazancourt, C. D. and Crawley, M. J. (2006). Contrasting Effects of Rabbit Exclusion on Nutrient Availability and Primary Production in Grasslands at Different Time Scales. *Oecologia.* 150, 582–589. doi: 10.1007/s00442-006-0555-4

Pagès, J. F., Jenkins, S. R., Bouma, T. J., Sharps, E. and Skov, M. W. (2019). Opposing Indirect Effects of Domestic Herbivores on Saltmarsh Erosion. *Ecosystems.* 22, 1055–1068. doi: 10.1007/s10021-018-0322-5

Pan, H., Li, Y., Guan, X., Li, J., Xu, X., Liu, J., et al. (2015). Management Practices Have a Major Impact on Nitrifier and Denitrifier Communities in a Semiarid Grassland Ecosystem. *J. Soils Sediments.* 16, 896–908. doi: 10.1007/s11368-015-1321-1

Pan, H., Li, Y., Guan, X., Li, J., Xu, X., Liu, J., et al. (2016). Management Practices Have a Major Impact on Nitrifier and Denitrifier Communities in a Semiarid Grassland Ecosystem. *J. Soils Sediments.* 16, 896–908.

Paul, S., Meer, H. V., Onduru, D., Ebanyat, P., Zake, J., Wouters, B., et al. (2013). Effects of Cattle and Manure Management on the Nutrient Economy of Mixed Farms in East Africa: A Scenario Study. *Afr. J. Agric. Res.* 8, 5129–5148. doi: 10.5897/AJAR10.009

Pinay, G., O'Keefe, T., Edwards, R. and Naiman, R. J. (2003). Potential Denitrification Activity in the Landscape of a Western Alaska Drainage Basin. *Ecosystems.* 6, 336–343. doi: 10.1007/s10021-002-0169-6

Reddy, K. R., Patrick, W. H. and Lindau, C. W. (1989). Nitrification-Denitrification at the Plant Root-Sediment Interface in Wetlands. *Limnol. Oceanogr.* 34, 1004–1013. doi: 10.4319/LO.1989.34.6.1004

Rotthauwe, J. H., Witzel, K. P. and Liesack, W. (1997). The Ammonia Monooxygenase Structural Gene Amoa as a Functional Marker: Molecular Fine-Scale Analysis of Natural Ammonia-Oxidizing Populations. *Appl. Environ. Microbiol.* 63, 4704–4712. doi: 10.1128/aem.63.12.4704-4712.1997

Song, Z., Wang, J., Liu, G. and Zhang, C. (2019). Changes in Nitrogen Functional Genes in Soil Profiles of Grassland Under Long-Term Grazing Prohibition in a Semiarid Area. *Sci. Total Environ.* 673, 92–101. doi: 10.1016/j.scitotenv.2019.04.026

Su, Y. Z., Li, Y. L., Cui, J. Y. and Zhao, W. Z. (2005). Influences of Continuous Grazing and Livestock Exclusion on Soil Properties in a Degraded Sandy Grassland, Inner Mongolia, Northern China. *Catena.* 59, 267–278. doi: 10.1016/j.catena.2004.09.001

Tang, H., Nolte, S., Jensen, K., Yang, Z., Wu, J. and Mueller, P. (2020). Grazing Mediates Soil Microbial Activity and Litter Decomposition in Salt Marshes. *Sci. Total Environ.* 720, 137559. doi: 10.1016/j.scitotenv.2020.137559

Thamdrup, B. and Dalsgaard, T. (2002). Production of N2 Through Anaerobic Ammonium Oxidation Coupled to Nitrate Reduction in Marine Sediments. *Appl. Environ. Microbiol.* 68, 1312–1318. doi: 10.1128/AEM.68.3.1312-1318.2002

Throbäck, I. N., Enwall, K., Jarvis, Å. and Hallin, S. (2004). Reassessing PCR Primers Targeting Nirs, nirK and nosZ Genes for Community Surveys of Denitrifying Bacteria With DGGE. *FEMS Microbiol. Ecol.* 49, 401–417. doi: 10.1016/j.femsec.2004.04.011

Väisänen, M., Tuomi, M. W., Bailey, H. L. and Welker, J. M. (2021). Plant and Soil Nitrogen in Oligotrophic Boreal Forest Habitats With Varying Moss Depths: Does Exclusion of Large Grazers Matter? *Oecologia.* 196, 839–849. doi: 10.1007/s00442-021-04957-0

Valiela, I. and Cole, M. L. (2002). Comparative Evidence That Salt Marshes and Mangroves may Protect Seagrass Meadows From Land-Derived Nitrogen Loads. *Ecosystems.* 5, 92–102. doi: 10.1007/s10021-001-0058-4

Valiela, I. and Teal, J. M. (1979). The Nitrogen Budget of a Salt Marsh Ecosystem. *Nature.* 280, 652–656. doi: 10.1038/280652a0

Walker, J. T., Vose, J. M., Knoepp, J. and Geron, C. D. (2009). Recovery of Nitrogen Pools and Processes in Degraded Riparian Zones in the Southern Appalachians. *J. Environ. Qual.* 38, 1391–1399. doi: 10.2134/jeq2008.0259

Wang, C., Han, X. and Xing, X. (2010). Effects of Grazing Exclusion on Soil Net Nitrogen Mineralization and Nitrogen Availability in a Temperate Steppe in Northern China. *J. Arid. Environ.* 74, 1287–1293. doi: 10.1016/j.jaridenv.2010.05.024

Wei, H., Gao, D., Liu, Y. and Lin, X. (2020). Sediment Nitrate Reduction Processes in Response to Environmental Gradients Along an Urban River-Estuary-Sea Continuum. *Sci. Total Environ.* 718, 137185. doi: 10.1016/j.scitotenv.2020.137185

Yang, Z., Nolte, S. and Wu, J. (2017). Tidal Flooding Diminishes the Effects of Livestock Grazing on Soil Micro-Food Webs in a Coastal Saltmarsh. *Agric. Ecosyst. Environ.* 236, 177–186. doi: 10.1016/j.agee.2016.12.006

Yang, W. H., Traut, B. H. and Silver, W. L. (2015). Microbially Mediated Nitrogen Retention and Loss in a Salt Marsh Soil. *Ecosphere.* 6, 1–15. doi: 10.1890/ES14-00179.1

Yin, Y., Wang, Y., Li, S., Liu, Y., Zhao, W., Ma, Y., et al. (2019). Soil Microbial Character Response to Plant Community Variation After Grazing Prohibition for 10 Years in a Qinghai-Tibetan Alpine Meadow. *Plant Soil.* 458, 175–189. doi: 10.1007/s11104-019-04044-7

Zhang, Y., Pennings, S. C., Li, B. and Wu, J. (2019). Biotic Homogenization of Wetland Nematode Communities by Exotic Spartina Alterniflora in China. *Ecology.* 100, 1–11. doi: 10.1002/ecy.2596

Zhang, P., Yang, Z. and Wu, J. (2021). Livestock Grazing Promotes Ecosystem Multifunctionality of a Coastal Salt Marsh. *J. Appl. Ecol.* 58, 2124–2134. doi: 10.1111/1365-2664.13957

Conflict of Interest: The authors declare that the research was conducted in the absence of any commercial or financial relationships that could be construed as a potential conflict of interest.

Publisher's Note: All claims expressed in this article are solely those of the authors and do not necessarily represent those of their affiliated organizations, or those of the publisher, the editors and the reviewers. Any product that may be evaluated in this article, or claim that may be made by its manufacturer, is not guaranteed or endorsed by the publisher.

frontiers | Frontiers in Marine Science

TYPE Original Research
PUBLISHED 25 July 2022
DOI 10.3389/fmars.2022.959144

OPEN ACCESS

EDITED BY
Xianbiao Lin,
Ocean University of China, China

REVIEWED BY
Weifang Hu,
Guangdong Academy of Agricultural Sciences, China
Genmei Lin,
School of Marine Sciences,
Sun Yat-sen University, China

*CORRESPONDENCE
Lu Xia
lulu8668@yeah.net
Shuqing An
anshq@nju.edu.cn

‡These authors have contributed equally to this work

SPECIALTY SECTION
This article was submitted to Marine Biogeochemistry, a section of the journal Frontiers in Marine Science

RECEIVED 01 June 2022
ACCEPTED 04 July 2022
PUBLISHED 25 July 2022

CITATION
Qin G, Feng H, Zhao H, Xia L, Yang W, Zhao Y, Jeelani N and An S (2022) Seasonal soil-plant nitrogen dynamics of a cordgrass salt marsh in response to coastal embankments in Eastern China.
Front. Mar. Sci. 9:959144.
doi: 10.3389/fmars.2022.959144

Seasonal soil-plant nitrogen dynamics of a cordgrass salt marsh in response to coastal embankments in Eastern China

Ge Qin[1,2‡], Hongyu Feng[1,2‡], Hui Zhao[2], Lu Xia[1,2*], Wen Yang[3], Yongqiang Zhao[4], Nasreen Jeelani[1,2] and Shuqing An[1,2*]

[1]School of Life Science and Institute of Wetland Ecology, Nanjing University, Nanjing, China, [2]Nanjing University Ecology Research Institute of Changshu, Changshu, China, [3]College of Life Sciences, Shaanxi Normal University, Xi'an, China, [4]Yancheng Wetland Natural Reserve for Rare Birds, Yancheng, China

The effects of coastal embankments on nitrogen (N) cycling in the *Spartina alterniflora* salt marsh have been extensively reported. However, it remains unclear effects of the embankment on the sizes of diverse N subpools in the plant-soil subsystems year-round. This study examined seasonal changes in various N subpools of plant subsystems; soil subsystems [e.g., soil organic N (SON), recalcitrant organic N (RON), labile organic N (LON), dissolved organic N (DON), ammonium N(NH+4 N), and nitrate N(NO3-N)]; N mineralization [e.g., soil net ammonification (R_A) and nitrification (R_N) rate]; and immobilization [e.g., microbial biomass N (MBN)] in embanked and adjacent *S. alterniflora* natural salt marshes on the coast of Eastern China. The embankment significantly reduced the litter N storage by 62.7–71.8% over the four seasons and decreased the root N storage by 53.0% during winter. The SON, LON, RON, and N H +4 N concentrations declined significantly by 43.0–60.2%, 35.8–64.8%, 44.9–59.0%, and 20.8–42.2%, respectively, over the four seasons following the embankment construction. Furthermore, the embankment dramatically reduced the DON concentrations by 21.9% in spring, 14.6% in summer, and 10.4% in winter, while notably diminishing the NO3 N concentrations by 33.4% in autumn and 44.9% in winter, and the R_A and R_N in spring and summer. However, the embankment clearly increased the MBN concentrations during summer and autumn, the NO3 N concentrations in spring, and the R_A and R_N in winter at different levels. Due to the decreased soil N inputs from plants, the embankment decreased the organic and inorganic N subpools every season to varying degrees, except for the NO3 N concentration in spring. We suggest that the decreased soil salinity following embankment establishment might increase the uptake of ions by microbes, while stimulating the production of MBN. Ultimately, the NO3 N and DON were two vital N sources for *S. alterniflora*, and plants absorbed N from the soil to promote their biomass, as well as N concentration and storage. This study is conducive toward understanding the mechanisms behind the effects of coastal

embankments on the N transfer among various N subpools in the plant and soil systems.

KEYWORDS

coastal reclamation, soil nitrogen subpool, nitrogen cycling, plant nitrogen subpool, soil microbial biomass

Introduction

Coastal embankments function to hold seawater back from salt marshes. Many countries spanning Europe, North America, and East Asia have established coastal embankments to promote regional economic development (Iost et al., 2007; Kirwan and Megonigal, 2013), satisfy local demands for farming and housing (Barbier et al., 2011), and control invasive plants (An et al., 2007). More than 60% of coastline is enclosed by embankments in China (Ma et al., 2014), which has led to significant alterations in local biogeochemical cycles (e.g., nitrogen (N) cycling) (Yang et al., 2016; van de Broek et al., 2019; Zhou and Bi, 2020; Feng et al., 2022). Biogeochemical cycling is complex and can be influenced by myriad factors (Purvaja et al., 2008; Aufdenkampe et al., 2011; Lin and Lin, 2022). Although the impacts of coastal embankments on biogeochemical cycling have been extensively reported (Yang et al., 2016; van de Broek et al., 2019; Feng et al., 2022), few investigation has explored the seasonal dynamics of N pools following the establishment of embankments in salt marshes.

Seasonality may directly affect N cycling *via* soil moisture and temperature, or indirectly through modified plant productivity and the seasonal patterns of organic matter release (Wuest, 2015; Zhao et al., 2016; Evangelou et al., 2021). For instance, the accumulation of soil organic N is generally positively related to seasonal variations in soil moisture, which influences soil oxygen levels that affect the rate at which debris is decomposed by microorganisms (Huang et al., 2013; Zhao et al., 2016). However, higher salinity levels can inhibit the activities of soil microorganisms during N cycling (Gao et al., 2012; Zhao et al., 2016). Moreover, seasonal SON in coastal ecosystems has positive correlations with the quality and quantity of plant residues (e.g., plant litter biomass), which exhibit seasonal variations (Ake-Castillo et al., 2006; Elsey-Quirk et al., 2011). Generally, the decomposition rates of plant residues are positively correlated with the average annual temperature, precipitation, etc. (Ake-Castillo et al., 2006; Battle and Golladay, 2007; Abu Hena et al., 2015), which also ultimately impact the seasonal SON. Several earlier studies also have demonstrated that higher net N mineralization rates in the soil and the N uptake of plants always occur in warmer environments, which has combined effects on the magnitudes of soil inorganic N pools (Augustine et al., 2014; Hu et al., 2015; Sanders-DeMott et al., 2018). Similarly, soil-residing inorganic N pools can be affected by the minimal activities of plants and microorganisms during autumn and/or winter (Urakawa et al., 2014; Sanders-DeMott et al., 2018). Soil microbial biomass N (MBN) comprises the mass of the living components of soil organic N, wherein soil microorganisms absorb both dissolved organic N (DON) and inorganic N (e.g., ammonium (NH_4^+) and nitrate (NO_3^-)) and transform them to MBN (Wang et al., 2019; Evangelou et al., 2021). As recently reported that the highest concentrations of MBN are observed during the warmer season (e.g., spring and/or autumn) in coastal ecosystems (Liu et al., 2019; Chen et al., 2022). Therefore, the seasonality has important effects on the plant-soil N dynamics in temperate coastal regions (Urakawa et al., 2014; Sanders-DeMott et al., 2018; Wang et al., 2018) through dynamic N fixation (Dovrat and Sheffer, 2019), plant uptake (Socci and Templer, 2011), and N mineralization (Hu et al., 2015; Huang et al., 2021); and determining effects of coastal embankments on various N pools in different seasons may improve our understanding of how these embankments impact N pools or N cycling in salt marshes.

Jiangsu Province is home to the largest coastal wetland area (4570 km^2) and longest stretches of coastal embankments (954 km) in China (Zhang et al., 2006; Zhang et al., 2013; Cui et al., 2018). The exotic *Spartina alterniflora* Loisel (*S. alterniflora*) is the dominant plant along Chinese coasts, which was introduced from North America in 1979 (Xu and Zhuo,

Abbreviations: ALB, Aboveground living biomass; ANC, Aboveground living N concentration; ANS, Aboveground living N storage; ANOVA, Analysis of variance; BPlant, biomass per centiare; C_NPlant, N concentration; DON, Dissolved organic N; ESA, Embanked *Spartina alterniflora* salt marshes; LB, Litter biomass; LNC, Litter N concentration; LNS, Litter N storage; LON, Labile organic N; MBC, Microbial biomass carbon; MBN, Microbial biomass N; N, Nitrogen; NH_4^+ – N, Ammonium N; NMDS, Non-metric Multi-Dimensional Scaling; NO_3^- – N, Nitrate N; NO_2^- – N, Nitrite N; NSA Natural *Spartina alterniflora* salt marshes; PE, Polyethylene; R_A Soil net, ammonification rate; RB, Root biomass; R_N Soil net, nitrification rate; RNC, Root N concentration; RNS, Root N storage; RMSEA, Root-mean-square error of approximation; RON, Recalcitrant organic N; S_N Plant, N storage; SON Total; soil organic N; SEM, Structural equation modelling.

1985; An et al., 2007) and over the last few decades has expanded rapidly across salt marshes (An et al., 2007; Wan et al., 2009). A growing number of studies have focused on the ecological management of *S. alterniflora* (An et al., 2007; Patten et al., 2017), with coastal embankments being one of the more common approaches at present (An et al., 2007; Ma et al., 2014).

Our previous studies revealed that embankments significantly decreased the biomass and N storage capacities of plants, soil N pools, and soil microbial diversity, and altered the compositions of soil microbial communities in *S. alterniflora* salt marshes during the growing season (Yang et al., 2016; Feng et al., 2017; Feng et al., 2022). However, to the best of our knowledge, there exists very limited knowledge regarding the seasonal dynamics of N pools in natural salt marshes and those with embankments. Furthermore, seasonal variations in salt marshes following the development of coastal embankments should not be disregarded, as they may have additional deleterious effects on soil N dynamics.

Consequently, we hypothesized that embankments may reduce variant N subpools in the soil and plant subsystems in *S. alterniflora* salt marshes year-round. For this study, to verify our hypothesis, we compared various soil N subpools, plant N subpools, microorganismal growth (e.g., microbial biomass carbon (MBC) and MBN), soil N transformation rates (e.g., N immobilization and mineralization), and physiochemical soil properties in both embanked and adjoining natural *S. alterniflora*-dominated salt marshes in April, July, October 2017, and January 2018. The primary objectives of this study were to quantify and identify the (1) effects of the embankment on the sizes of various N subpools in the *S. alterniflora* salt marsh in four seasons, and (2) how the embankment influenced the N transfer among various N subpools in plant and soil subsystems in plant and soil subsystems. Ultimately, this study sought to provide a theoretical basis for the control and rational utilization of *S. alterniflora*, particularly in the coastal ecosystem where the primary productivity is conventionally thought to be limited by N (Vitousek et al., 1997).

Materials and methods

Site description

The field work for this study was conducted in the core region of the Dafeng Milu National Nature Reserve (32°59′N-33°03′N, 120°47′E-120°53′E), on the Yellow Sea coast of Jiangsu Province, China (Figure 1). This Reserve was established in 1986 and is listed as part of the World Natural Heritage in 2019, as it plays a significant role in international biodiversity conservation. It is situated such that it encompasses the transition of warm temperate and northern subtropical zones, which are primarily impacted by oceanic and continental climates (Cui et al., 2018). According to the report of China Meteorological Administration, the mean monthly temperatures were 13.1°C in April, 26.7°C in July, 16.5°C in October, and 1.6°C in January; the mean monthly precipitations were 55.2 mm in April, 251.3 mm in July, 54.1 mm in October, and 33.9 mm in January; the radiations per unit area were 135 kw·m^{-2} in April, 150 kw·m^{-2} in July, 98 kw·m^{-2} in October, and 70 kw·m^{-2} in January. A regular semidiurnal tide occurs along the coastal area, with an annual average tidal range of about 3 m (Ren, 1986; Li et al., 2018).

The coastal embankments of this region were established in 2011, with a typical length, thickness, and height of 2400 m, 2 m, and 2 m, respectively. Thus, both seawater and river water are prevented from entering the embanked range. The natural and embanked ranges have not been subjected to anthropogenic activities or other disturbances (Yang et al., 2016).

Field sample collection

In spring (April 2017), summer (July 2017), autumn (October 2017), and winter (January 2018), four parallel transects (40 × 40 m) were established in the natural and embanked *S. alterniflora* salt marshes (Figure 1), and three plots (2 × 2 m) in each transect were randomly selected. Three soil core samples (0-10 cm, 10-20 cm, and 20-30 cm depths) were randomly extracted from each plot, whereafter core samples from the same depths and plots were evenly mixed as the final soil samples.

Briefly, 96 soil samples (four replicates × three depths × two treatments × four seasons) were obtained. Following the removal of all belowground plant components, the soil samples were transferred to the laboratory and divided into three subsamples. The first subsample was employed to measure the soil moisture, whereas the second was air-dried and sifted through a 1-mm sieve, which was used to determine the soil pH, salinity, SOC, and SON. The third fresh subsample was sifted through a 2-mm sieve and stored at 4°C, which was used to quantify the DON, MBC, MBN, NH_4^+ – N and NO_3^- – N concentrations.

The soil net ammonification (R_A) and nitrification (R_N) rate were quantified using the closed-top PE (polyethylene) tube incubation technique, which was based on the sequential soil coring of the undisturbed soil and *in situ* exposure (Raison et al., 1987). Eight PE pipes (Ø5 cm x 30 cm long) per sample were vertically inserted into the soil at random, after which they were carefully extracted. Four PE pipes were transferred to the laboratory for the quantification of the NH_4^+ – N and NO_3^- – N concentrations. The other four were buried *in situ* for cultivation to determine the NH_4^+ – N and NO_3^- – N concentrations after 30 days, where their tops and bottoms were wrapped with plastic film and gauze, respectively. Furthermore, four quadrats (50 × 50 cm) were established in each transect for the acquisition of plant tissues, including leaves, stems, litter, and roots.

Laboratory analyses

The leaves, stems, and litter were separated, whereas the roots were collected by sifting through a 100-mm sieve, which

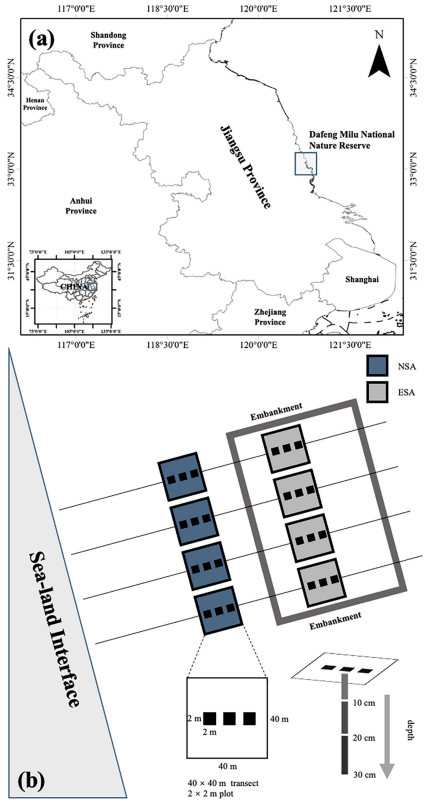

FIGURE 1
(A) Location of the study site and **(B)** schematic diagram of the study area in Dafeng Milu National Nature Reserve, Yancheng, Jiangsu Province, China. NSA, natural *Spartina alterniflora* salt marsh; ESA, embanked *S. alterniflora* salt marsh.

was used to remove any clods and stones. All *S. alterniflora* tissues were thoroughly rinsed under running water (Yang et al., 2016). Each type of tissue biomass was oven-dried at 65°C, and the N concentration was determined using an Elementar Vario Micro CHNS analyzer (Elementar Analysen system GmbH, Germany). The tissue N storage for each plant was computed using the following formula:

$$S_N = C_N \times B \quad (1)$$

where S_N is the plant N storage, C_N is the plant N concentration, and B is the plant biomass per centiare.

The first fresh soil subsample was used to determine the soil bulk density (BD), pH, salinity, and moisture according to methods that reported by Slavich and Petterson (1990) and Yang et al. (2016).

The recalcitrant organic N (RON) was processed using the acid hydrolysis method (Rovira and Vallejo, 2002; Yang et al., 2016). The concentrations of SON and RON were measured using an Elementar Vario Micro CHNS analyser (Elementar Analysen system GmbH, Germany), whereas the labile organic N (LON) was computed using the following formula.

$$\mathrm{LON} = \mathrm{SON} - \mathrm{RON} \quad (2)$$

Additionally, DON was determined following the procedure of Jones et al. (2004). The MBC and MBN concentrations were determined following the chloroform fumigation-extraction method (Brookes et al., 1985).

A mixture of 2.5 g of fresh soil samples and 25 mL of 2 M KCl (1:10 w/v soil:solution) were placed into 50 mL PP (polypropylene) bottles and shaken at 200 rpm for 60 min using a reciprocating shaker. Subsequently, the supernatant was employed to quantify the concentrations of $NH_4^+ - N$, $NO_2^- - N$ and $NO_3^- - N$ with an AQ2+ Automated Discrete Analyser (SEAL, Britain, shown after the determination of R_A and R_N:

$$R_A = \frac{(\mathrm{NH}_4^+ - \mathrm{N}_{i+1}) - (\mathrm{NH}_4^+ - \mathrm{N}_i)}{t_{i+1} - t_i} \quad (3)$$

$$R_N = \frac{(\mathrm{NO}_3^- - \mathrm{N}_{i+1} + \mathrm{NO}_2 - \mathrm{N}_{i+1})\,(\mathrm{NO}_3^- - \mathrm{N}_{i+1} + \mathrm{NO}_2 - \mathrm{N}_{i+1})}{t_{i+1} - t_i} \quad (4)$$

Where t_i and $t_{i+1}$are the incubation start and end times (d), respectively; $NH_4^+ - N_i$ and $NH_4^+ - N_{i+1}$ are the soil $NH_4^+ - N$ concentrations (mg/kg) at the onset and conclusion of incubation, respectively; NO_2-N_i and NO_2-N_{i+1} are the soil NO_2-N concentrations (mg/kg) at the start and end of incubation, respectively; $NO_3^- - N_i$ and $NO_3^- - N_{i+1}$ are the soil $NO_3^- - N$ concentrations (mg/kg) at the beginning and end of incubation, respectively.

Statistical analyses

We employed one-way analysis of variance (ANOVA) to (1) verify the impacts of the embankment on the concentrations of SON, DON, LON, RON, $NH_4^+ - N$, $NO_3^- - N$, MBC, MBN, R_A, and R_N, as well as the biomass of aboveground living (ALB), litter (LB), and root (RB) tissues and N storage of aboveground living (ALNS), litter (LNS), and root (RNS) tissues for the different seasons; (2) confirmed the seasonal variations in these indices for the natural and embanked salt marshes; (3) seasonal plant and soil N subpools were studied with a NMDS (Non-metric Multi-Dimensional Scaling); (4) interactions of SON with LNS and RNS in the natural and embanked salt marshes were test by using linear models. Besides, Multi-way ANOVA was employed to examine the impacts of embankment and season, as well as their interactive effects on the various N subpools in plant and soil subsystems. All above analyses were performed using R software (R Studio Inc., Massachusetts, USA).

We analyzed the relationships between plant biomass and N storage, various soil N fractions, MBC, MBN, and assorted mineralization rates for both natural and embanked *S. alterniflora* by using Pearson's correlation analysis (Figure S1). Furthermore, structural equation modelling (SEM) was utilized to test the multivariate relationships between the direct effects of the coastal embankment and indirect impacts of parameters during the different seasons related to soil organic and inorganic N, MBC, MBN, R_A, and R_N, which was based on a conceptual *a priori* model (Figure S2). Using the maximum likelihood for parameter estimation (Boldea and Magnus, 2009), the best fitting model was selected through the sequential removal of nonsignificant coefficients ($p < 0.05$). We employed a chi-squared test (χ^2) and the root-mean-square error of approximation (RMSEA; Schermelleh-Engel et al., 2003) for evaluating the model. The SEM analysis was implemented using AMOS 22.0 software (IBM, SPSS, New York).

Results

Plant biomass and N allocation

The embankment significantly decreased the ALB, LB, ALNS, and LNS of *S. alterniflora* throughout the year, ranging from 47.9% to 70.3%, 66.5% to 76.4%, 52.7% to 69.5%, and 62.7% to 71.8%, respectively ($p < 0.05$; Figure 2). Further, they reduced the RB by 57.9% and 67.7% in autumn and winter, respectively, as well as the RNS by 53.0% in winter ($p < 0.05$; Figure 2). Conversely, the embankment increased the ALNC remarkably by 24.8% in spring and the LNC by 20.2% in autumn, as well as the RNC by 49.7% and 80.8% in summer and autumn, respectively ($p < 0.05$; Figure 2). Additionally, the maximum values of RB, RNS, and ALNC occurred in spring, and the peaks of AB and ANS appeared in autumn for both the natural and embanked salt marshes ($p < 0.05$; Figure 2). The values of LNS and LB in spring and winter were remarkably higher than those in summer and autumn for both the natural and embanked salt marshes ($p < 0.05$). The LNC values in both the natural and embanked salt marshes were the lowest during winter, with the lowest RNC value in the natural salt marsh appearing in autumn ($p < 0.05$). However, there were no significant differences in the RNC value in the embanked salt marsh across all seasons ($p \geq 0.05$, Figure 2).

Soil N subpools

In the soil organic N subpool, there were significant decreases in the concentrations of SON, LON, and RON in the embanked salt marsh, which ranged from 43.0% to 60.2%, 35.8% to 64.8%, and 44.9% to 59.0%, respectively, over the four seasons ($p < 0.001$; Figure 3). In contrast to those in the natural salt marsh, the concentrations of DON in the embanked salt marsh decreased significantly by 21.9%, 14.6%, and 10.4% in spring, summer, and winter, respectively ($p < 0.05$; Figure 3).

Negligible seasonal variations in the SON concentration values were observed in the natural salt marsh ($p \geq 0.05$; Figure 3), with the exception of the highest being observed in spring for the embanked salt marsh ($p < 0.05$; Figure 3). The maximum LON concentrations were observed in spring for both the natural and embanked salt marshes ($p < 0.05$), but there is no difference in the LON concentrations between spring and winter in the natural salt marshes ($p \geq 0.05$; Figure 3). The minimum concentration of RON was seen in spring for the natural salt marsh ($p < 0.05$; Figure 3), while there were no significant seasonal changes in the RON concentrations in the embanked salt marsh ($p \geq 0.05$; Figure 3). The lowest DON concentrations were observed in autumn for both the natural and embanked salt marshes (Figure 3).

For the soil inorganic N subpool, the effects of the embankment significantly influenced the soil $NH_4^+ - N$ (Table 1). The embankment significantly decreased the soil $NH_4^+ - N$ concentrations (20.8 – 42.2%) through spring, summer, autumn, and winter ($p < 0.05$; Figure 3). The embankment also reduced the soil $NO_3^- - N$ concentrations in autumn and winter by 33.4% and 44.9%, respectively, while they significantly increased the soil $NO_3^- - N$ concentration by 132.6% in spring ($p < 0.05$;

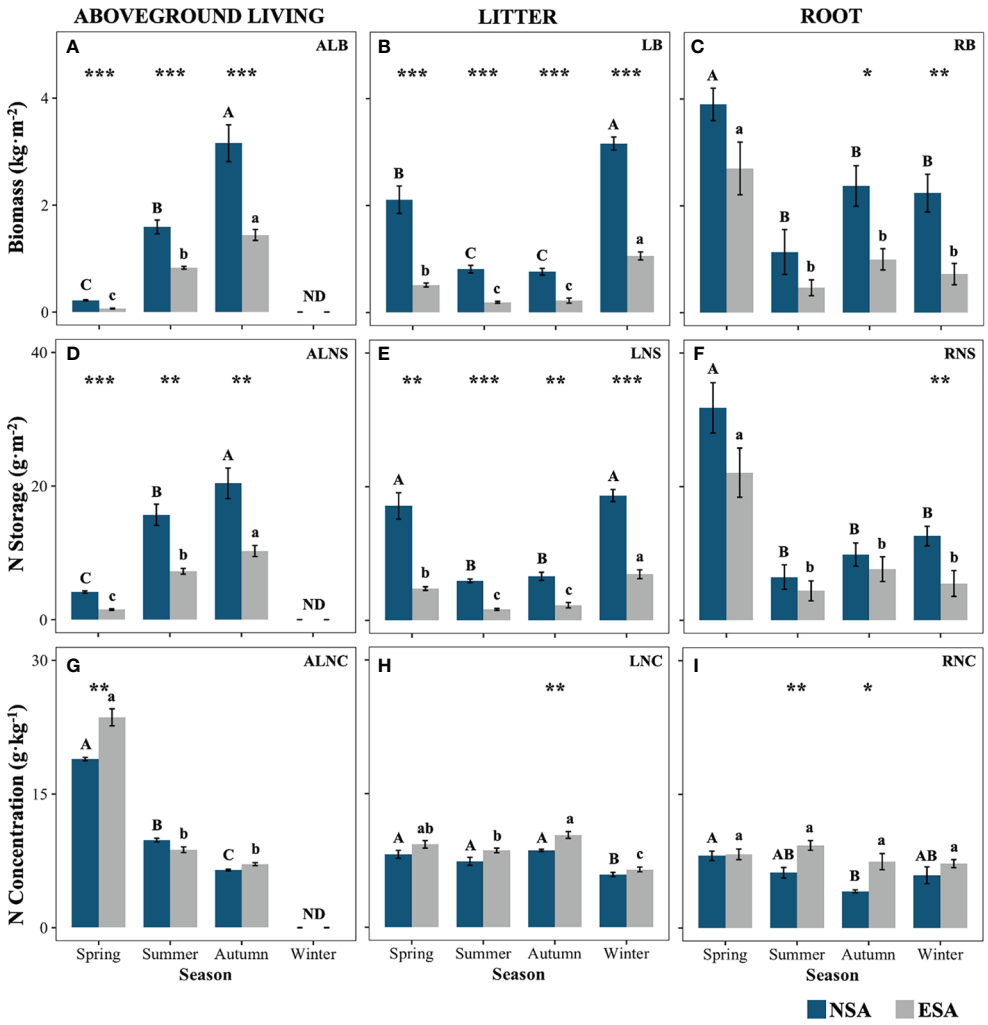

FIGURE 2
Values of **(A–C)** biomass, and nitrogen **(D–F)** storages and **(G–I)** concentrations of various *Spartina alterniflora* tissues in natural (NSA) and embanked (ESA) salt marshes in spring, summer, autumn, and winter. ALB, aboveground living biomass; ALNS, aboveground living nitrogen storage; ALNC, aboveground living nitrogen concentration; LB, litter biomass; LNS, litter nitrogen storage; LNC, litter nitrogen concentration; RB, root biomass; RNS, root nitrogen storage; RNC, root nitrogen concentration. The averages and standard errors of four replicates are shown. Bars labelled with different uppercase and lowercase letters denote significant differences ($p < 0.05$) between seasons in NSA and ESA, respectively. The differences between NSA and ESA were significant at ***$p < 0.001$, **$p < 0.01$ and *$p < 0.05$, and blanks indicate no significance at $p \geq 0.05$.

Figure 3). Moreover, the peak concentrations of soil NH_4^+ – N and NO_3^- – N were observed in autumn for both the natural and embanked salt marshes (Figure 3).

Growth, N immobilization, and mineralization of microorganisms

The soil MBC concentration was significantly reduced by 52.1% in winter with the embankment, whereas on the contrary the soil MBN concentration significantly increased in summer and autumn by 189.2% and 200.8%, respectively ($p < 0.05$; Figure 4). The peak values of both the soil MBC and MBN concentrations were observed in winter for the natural salt marsh, whereas there were insignificant seasonal variations in the MBC and MBN following the establishment of the embankment ($p < 0.05$; Figure 4).

Furthermore, both the R_A and R_N were remarkably reduced in spring and summer, while they were significantly increased in autumn following embankment development ($p < 0.01$; Figure 4). The lowest R_A values (< 0 mg·kg^{-1}·d^{-1}) were observed in autumn, while they peaked in summer for both the natural and embanked salt marshes (Figure 4). The highest and lowest R_N values ($p < 0.05$) were observed in spring and autumn, respectively, in the natural salt marsh, while the highest and lowest R_N values were

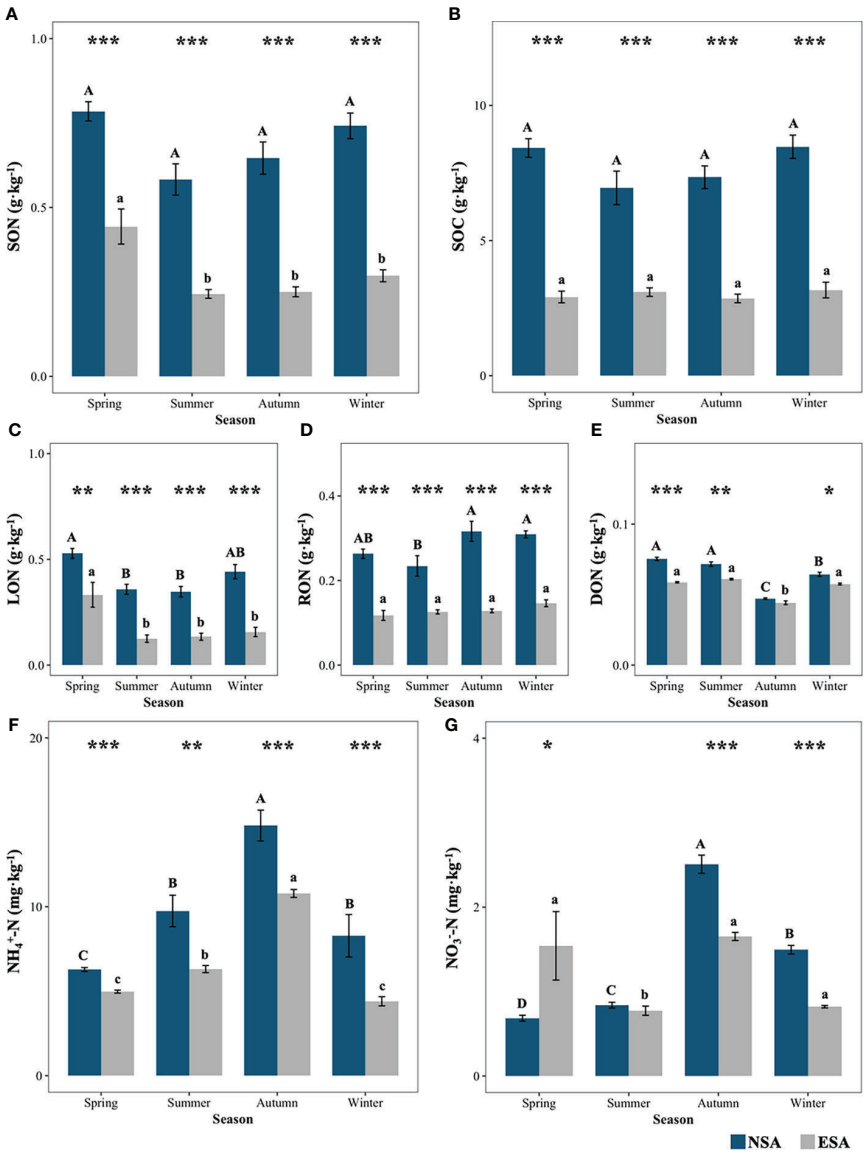

FIGURE 3
Values of **(A)** total soil organic nitrogen (SON), **(B)** total soil organic carbon (SOC), **(C)** labile organic nitrogen (LON), **(D)** recalcitrant organic nitrogen (RON), **(E)** dissolved organic nitrogen (DON), **(F)** ammonia nitrogen (NH+4 N), and **(G)** nitrite nitrogen (NO3 N) in natural (NSA) and embanked (ESA) *Spartina alterniflora* salt marshes in spring, summer, autumn, and winter. The averages and standard errors of four replicates are shown. Bars labelled with different uppercase and lowercase letters denote significant differences ($p < 0.05$) between seasons in NSA and ESA, respectively. The differences between NSA and ESA were significant at ***$p < 0.001$, **$p < 0.01$ and *$p < 0.05$, and blanks indicate no significance at $p \geq 0.05$.

observed in autumn and spring, respectively, in the embanked salt marsh (Figure 4).

Physicochemical soil properties

The soil moisture and salinity values in the embanked salt marsh were significantly lower than those in the natural salt marsh for every season ($p < 0.001$) (Figure S3). The soil pH and BD values in the embanked salt marsh were significantly higher than those in the natural salt marsh in every season ($p < 0.001$) (Figure S3). However, no significant seasonal differences in the soil moisture, salinity, pH and BD were found in both the natural and embanked salt marshes ($p \geq 0.05$) (Figure S3).

10.3389/fmars.2022.959144

TABLE 1 Statistical significance of the effects of the embankment, seasons, and their interactions on (a) biomasses, N concentrations and storages of litter and roots, (b) soil organic N subpools, and (c) soil inorganic N subpools, R_A and R_N according to multi-way ANOVA.

(a)	LB ($kg \cdot m^{-2}$)	LNC ($g \cdot kg^{-1}$)	LNS ($g \cdot m^{-2}$)	RB ($kg \cdot m^{-2}$)	RNC ($g \cdot kg^{-1}$)	RNS ($g \cdot m^{-2}$)
Embankment	871.233***	83.822***	674.409***	93.928***	70.259***	35.725***
Season	352.875***	123.775***	208.441***	74.352***	21.704***	122.311***
Embankment × Season	85.788***	3.609*	50.940***	2.278	10.255***	4.602**
(b)	SON ($g \cdot kg^{-1}$)	LON ($g \cdot kg^{-1}$)	RON ($g \cdot kg^{-1}$)	DON ($g \cdot kg^{-1}$)	MBN ($mg \cdot kg^{-1}$)	
Embankment	109.285***	70.403***	158.889***	38.990***	6.982*	
Season	5.949***	10.374***	3.811*	45.073***	4.419**	
Embankment × Season	0.48	0.49	1.93	3.877*	4.244**	
(c)	NH_4^+ – N ($mg \cdot kg^{-1}$)	NO_3^- – N ($mg \cdot kg^{-1}$)	R_A ($mg \cdot kg^{-1} \cdot d^{-1}$)	R_N ($mg \cdot kg^{-1} \cdot d^{-1}$)		
Embankment	75.854***	3.37	22.937***	0.15		
Season	78.912***	29.813***	34.532***	4.989**		
Embankment × Season	3.017*	14.690***	19.34	20.30		

LB, litter biomass; LNC, litter nitrogen concentration; LNS, litter nitrogen storage; RB, root biomass; RNC, root nitrogen concentration; RNS, root nitrogen storage; SON, soil total organic nitrogen; LON, soil labile organic nitrogen; RON, soil recalcitrant organic nitrogen; DON, soil dissolved organic nitrogen; MBN, microbial biomass nitrogen; R_A, soil net ammonification rate; R_N, soil net nitrification rate. Asterisks indicate statistically significant at ***p < 0.0001, **p < 0.001, *p < 0.05, and blanks indicate no significance at p ≥ 0.05.

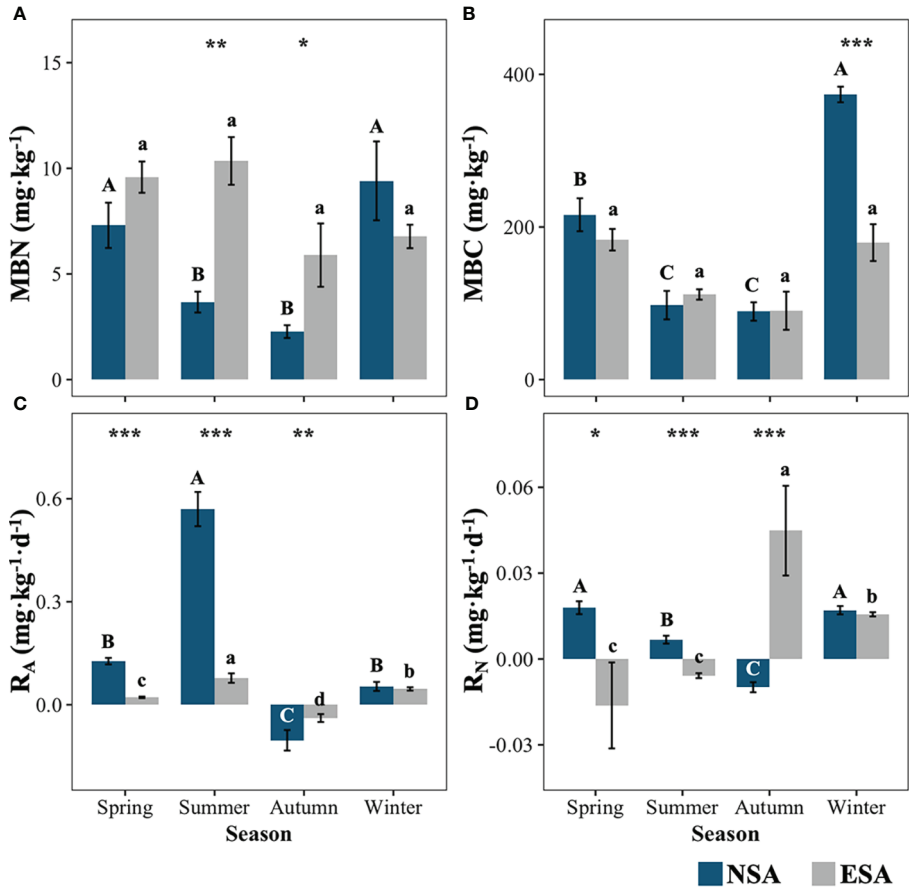

FIGURE 4
Values of the soil microbial biomass **(A)** nitrogen (MBN) and **(B)** carbon (MBC), and net soil **(C)** ammonification (R_A) and **(D)** nitrification (R_N) rate in natural (NSA) and embanked (ESA) *Spartina alterniflora* salt marshes in spring, summer, autumn, and winter. The averages and standard errors of four replicates are shown. Bars labelled with different uppercase and lowercase letters denote significant differences ($p < 0.05$) between seasons in NSA and ESA, respectively. The differences between NSA and ESA were significant at ***$p < 0.001$, **$p < 0.01$ and *$p < 0.05$, and blanks indicate no significance at $p \geq 0.05$.

Correlation analysis

The NMDS revealed that the soil N pool compositions in the embanked salt marsh were clustered and distinct from those in the natural salt marsh in every season (Stress < 0.001; Figure 5). Besides, the SON amounts highly correlated with the LNS values in natural salt marsh (p = 0.025; Figure 6), whereas the relationship between the SON amounts and the LNS values in embanked salt marsh was insignificant ((p = 0.1415; Figure 6).

The results of SEM analyses are shown in Figure 7. It indicated a highly positive correlation between the N storage of each plant tissue and the biomass of the corresponding tissues in both the natural and embanked salt marshes. A remarkable positive correlation was found between the LON, RON, and LNS amounts in the natural salt marsh; a significantly positive relationship was observed between the DON and LNS amounts in the embanked salt marsh. The DON concentration was significantly and positively associated with the RNS value in the natural salt marsh; the LON concentration was dramatically positive correlation with the RNS value in the embanked salt marsh. The NH_4^+ – N concentrations in both the natural and embanked salt marshes were significantly and negatively associated with the DON concentrations. The NO_3^- – N concentrations were significantly positively associated with those of NH_4^+ – N, but observably negative with the RNC values in both the natural and embanked salt marshes.

Discussion

The N storages in the plant subsystem

The storage of N in plants is a vital component of ecosystem N pools (Liu et al., 2017). A recent study has reported that coastal embankments can alter the N storage of plants by influencing their growth (Feng et al., 2022). In this study, the embankment was observed to significantly reduce the N storage and biomass of aboveground living tissue year-round (Figure 2). SEM analysis indicated that low soil salinity induced low aboveground living biomass in the embanked *S. alterniflora*

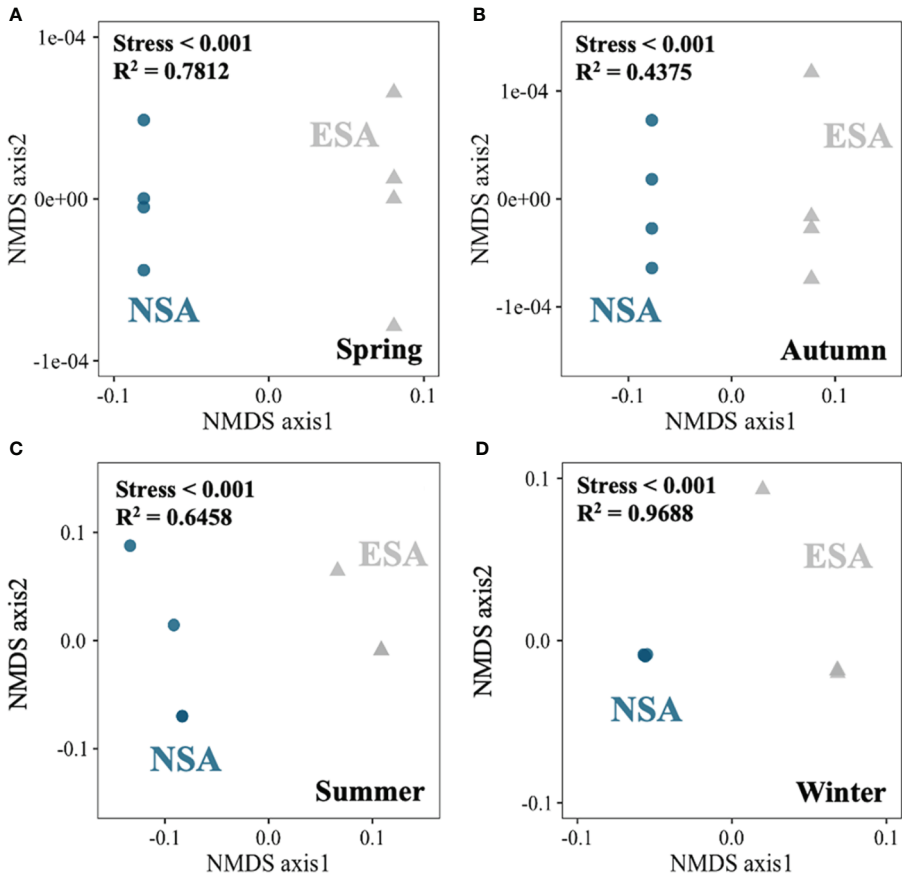

FIGURE 5
Non-metric multidimensional scaling (NMDS) plot of dissimilarity of the edaphic N pools between the natural (NSA) and embanked (ESA) *Spartina alterniflora* salt marshes in **(A)** spring, **(B)** summer, **(C)** autumn, and **(D)** winter.

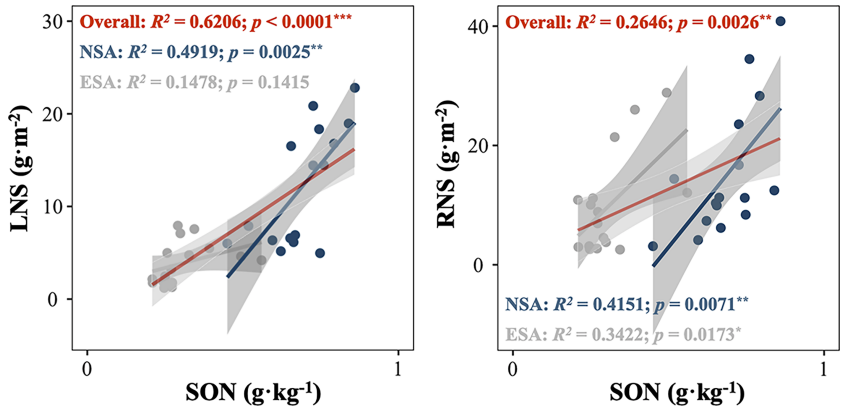

FIGURE 6
(A) Total soil organic nitrogen (SON) in relation to litter nitrogen storage (LNS) of *Spartina alterniflora*; **(B)** total soil organic nitrogen (SON) in relation to root nitrogen storage (RNS) of *S. alterniflora* in the natural (NSA) and embanked (ESA) salt marshes. Asterisks indicate statistically significant at ***p < 0.0001, **p < 0.001, and blanks indicate no significance at p ≥ 0.05.

salt marsh (Figure 7), which was supported by our recent study (Feng et al., 2022). This might have been attributed to the chlorophyll content and net *S. alterniflora* assimilation rate that are reduced under low-salinity conditions, which decreases the generation of photosynthetic products and ultimately decreases the biomass (Ma et al., 2011). The decreased biomass of aboveground living tissues reduced their N storage (Figure 5). Furthermore, the decreased biomass and N

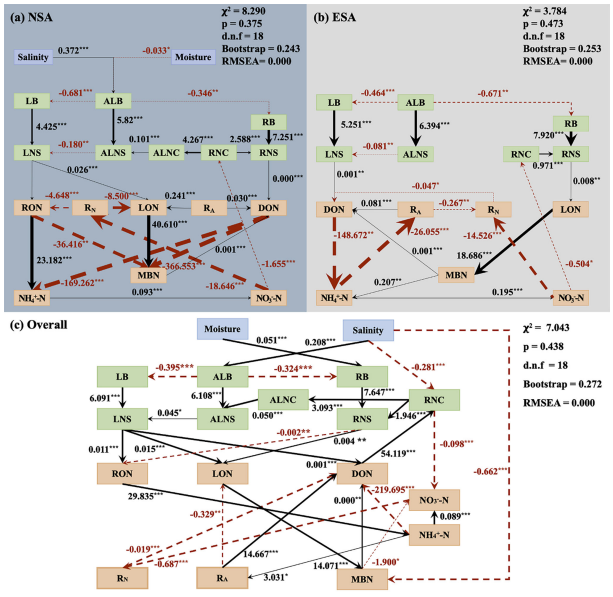

FIGURE 7
Nitrogen turnover among various nitrogen subpools in plant and soil subsystems in the **(A)** natural (NSA), and **(B)** embanked (ESA) salt marshes, as well as **(C)** their combine was examined by structural equation modelling (SEM). Solid and dashed arrows indicate positive and negative relationships, respectively. Numbers adjacent to arrows are the path coefficients (***p < 0.001, **p < 0.01 and *p < 0.05). ALB, aboveground living biomass; ALNS, aboveground living nitrogen storage; ALNC, aboveground living nitrogen concentration; LB, litter biomass; LNS, litter nitrogen storage; LNC, litter nitrogen concentration; RB, root biomass; RNS, root nitrogen storage; RNC, root nitrogen concentration; SON, total soil organic nitrogen; DON, dissolved organic nitrogen; LON, labile organic nitrogen; RON, recalcitrant organic nitrogen; NH+4 N, ammonia nitrogen; NO3 N, nitrite nitrogen; MBC, soil microbial biomass nitrogen; MBN, soil microbial biomass nitrogen; R_A, soil net ammonification rate; R_N, soil net nitrification rate.

storage of aboveground living tissues lowered the biomass and N storage of aboveground dead tissues (i.e., litter) in the embanked *S. alterniflora* salt marsh (Figure 7) (Jiang et al., 2009; Ma et al., 2011; Ge et al., 2015).

The embankment reduced the N storage of roots year-round, although it was insignificant in spring, summer, and autumn (Figure 2). SEM analysis suggested that low soil moisture could limit *S. alterniflora* root growth in the embanked salt marsh (Figure 7). This could be explained by *S. alterniflora* investing more nutrients for root growth when water resources were adequate, which enabled it to occupy more habitats (He et al., 2009). Further, this might reduce the tiller number and resource consumption by limiting the root growth when water was scarce (He et al., 2009). Thus, the decreased root biomass caused its N storage to be depressed (Figure 7). Besides, the temperature is generally considered as a vital factor which determines the plant growth (Elsey-Quirk et al., 2011). However, the root biomasses did not corelated with the temperature any more in the embanked salt marsh, which indicated that the embankment altered the seasonal variation of the root growth (Figure S4). This may be because the embankment altered the physiological process of *S. alterniflora* by changing the soil physicochemical properties, which affected its response to the temperature (Shi and Bao, 2007). In summary, since soil salinity and moisture are two critical drivers that influence plant growth in salt marshes, the coastal embankment reduced the N storage of *S. alterniflora* by restricting plant growth through decreased soil salinity and moisture (Figure 7).

The organic N subpool in the soil subsystem

The embankment drastically shrunk the size and modified compositions of the soil N pool in *S. alterniflora* salt marsh in every season (Figures 3, 5). The organic N subpool is an essential element of ecosystem N pools (Feyissa et al., 2020), while it regulates net plant primary production in most ecosystems and typically sensitive to changes in plant N storage (Jones et al., 2004; Chen et al., 2017; Feng et al., 2017). This is because soil organic matter was derived from the biodegradation of plant debris and dead roots (Figure 7; Zhou et al., 2015; Li et al., 2018). Thus, the embankment remarkably decreased the N storage of *S. alterniflora* litter and roots, which further reduced the size of the organic N subpools (e.g., SON, LON, RON, and DON) for every season (Figures 2, 3, 6).

The embankment also changed the N turnover from the plant subsystem to the soil subsystem in the *S. alterniflora* salt marsh, for example, the plant litter N storage (i.e., LNS) did not make the contribution to the size of the soil organic N subpool (i.e., SON) due to the embankment (Figures 6, 7). RON is generally composed of organics that are recalcitrant to decomposition (Lin et al., 2016; Xi et al., 2020; Xi et al., 2021). According to SEM analysis, the RON in the natural salt marsh was primarily derived from organic litter inputs (Figure 7). This was because lignin and lignocellulosic are rich in *S. alterniflora* litter, where the roots may not contain abundant refractory materials (Zeng et al., 2020; Feng et al., 2022). However, the effects of the litter N storages on the RON amount were negligible in the embanked salt marsh, which was possibly due to the litter N storage observably decreased due to the embankment (Figures 3, 7).

LON comprises the active component of the soil organic N subpools (Lin et al., 2016; Xi et al., 2020; Xi et al., 2021). The embankment also changed the source of LON, and the organic N inputs was from the litter in the natural salt marsh to the roots in the embanked salt marsh (Figure 7). This was probably also because the dramatically decreased litter and root N storage due to the embankment (Figure 2). However, the embankment did not alter the seasonal variation of LON (Figure 3). Generally, LON was more responsive to changes in plant N inputs compared to RON (Feyissa et al., 2020). On the coast of Jiangsu, the ALB of *S. alterniflora* attained a maximum in summer and autumn (Zhao et al., 2005; Zhang et al., 2010). Thus, the limited death of the aboveground *S. alterniflora* tissues led to a low LB in summer and autumn (Zhao et al., 2005; Zhang et al., 2010). Furthermore, the roots of *S. alterniflora* are nutrients storage tissues (Lawrence et al., 2013; Zhao et al., 2016). During the growing season, nutrients stored by roots were transported to support aboveground plant growth, thus the LB was low (Lytle and Hull, 1980; Lana et al., 1991; Chen et al., 2014). Therefore, lower LB and RB led to low LNS, RNS, and LON during summer and autumn for both natural and embanked *S. alterniflora* salt marshes (Figures 2, 3). In spring and winter, the aboveground living organs of *S. alterniflora* died and were transformed to litter; thus, high values of LB were observed (Figures 2, 3, 7) (Chen and Xu, 2006; Zhou et al., 2015). Additionally, *S. alterniflora* rapidly occupied habitats through the vegetative reproduction of its roots at the beginning of the growth season, and as a result the highest level of RB was observed in spring (Figure 2). Therefore, the elevated LB and RB resulted in the high LNS, RNS, and LON in spring and winter for both the natural and embanked *S. alterniflora* salt marshes (Figures 2, 3).

DON is the most active portion of the soil organic N subpool (Rentsch et al., 2007; Cott et al., 2020), which includes low-molecular weight compounds (e.g., amino acids, polypeptides, and purines) and high-molecular weight compounds (e.g., proteins and chlorophyll) (Quan et al., 2022). In this study, we found that the organic N inputs from roots was the primary source of DON in the natural salt marsh (Figure 7). This was possibly because the living roots could exude various low-molecular weight compounds (e.g., organic acids and sugar), meanwhile the decomposition of the death roots also promoted the accumulation of DON (Chen and Xu, 2006; Zhou et al., 2015). However, the DON in the embanked salt marsh mainly

came from the organic N inputs from litter, which was explained by the passive leaching of soluble organic matter from litter in the soil (Figure 7; Chen and Xu, 2006; Zhou et al., 2015). Further, according to the SEM analysis, MBN was an additional important source of DON in the natural and embanked *S. alterniflora* salt marsh (Figure 7). This might be due to DON having the capacity to be released into the soil after microbial death (Isobe et al., 2018; Evangelou et al., 2021; Heinzle et al., 2021).

The inorganic N subpool in the soil subsystem

The embankment not only changed the process of the organic N inputs from the plant subsystem to the soil subsystem, but also altered the N turnover from the organic N subpools into the inorganic N subpools in the soil subsystem (Figure 7). Generally, the generation of inorganic N in soil is regulated by its organic N content (Cartaxana et al., 1999; Cott et al., 2020). SEM analysis indicated that the major contributor of the soil NH_4^+ – N was RON in the natural salt marsh (Figure 7). Prior studies reported that bacteria and fungi, which can degrade high-molecular weight substances (e.g., RON), were rich in the *S. alterniflora* sediment (Yang et al., 2021; Feng et al., 2022). However, there was lack of contribution of RON to the soil NH_4^+ – N in the embanked salt marsh, because there was inappreciable organic N input form the litter or roots to the soil RON (Figure 7). Additionally, according to the SEM analysis, an increased soil NH_4^+ – N content can lead to decreased DON in the natural and embanked salt marshes (Figure 7). Since DON is rich in a variety of amino acids it can be mineralized to release NH_4^+ – N through the microbial generation of extracellular enzymes (Berman and Bronk, 2003; Schimel and Bennett, 2004; Geisseler et al., 2009; Xing et al., 2010). Therefore, we speculated that DON is also a non-negligible source of NH_4^+ – N in the soil of *S. alterniflora* salt marshes, where lower DON may lead to reduced NH_4^+ – N in the soil following the establishment of the embankment. In summary, microorganisms may produce NH_4^+ –N by decomposing the organic N; thus, the embankment significantly diminished the quantities of NH_4^+ – N by shrinking the size of the organic N (e.g., RON, and DON) year-round (Figures 3, 7; Feng et al., 2022).

NO_3^- – N is another primary inorganic form of N that is intimately related to NH_4^+ – N due to soil nitrification (Figure 7) (Ueda et al., 2013; Augustine et al., 2014; Nguyen et al., 2017). Thus, the concentrations of NO_3^- – N decreased under lower NH_4^+ – N concentrations in summer, autumn, and winter after the establishment of the embankment (Figure 7). Nevertheless, the NO_3^- – N concentration increased significantly in spring following embankment development (Figure 3). Thus, we speculated that, (1) nitrification might continue in spring, even when the soil NH_4^+ – N concentration was low (Augustine et al., 2014; Schütt et al., 2014; Heinzle et al., 2021); (2) the rapid decrease in NO_3^- – N utilization by plants at the onset of plant growth occurred in spring due to the dramatically decreased plant biomass following the establishment of the embankment (Augustine et al., 2014; Che et al., 2018; Heinzle et al., 2021).

Microbial N mineralization and immobilization

Organic soil N is converted to inorganic N *via* N mineralization, which is influenced by multiple factors (Zhou et al., 2015; Nguyen et al., 2017). In this study, R_A in the embanked salt marsh decreased significantly in spring and summer but rapidly increased in autumn (Figure 4). Previous studies have reported that the soil N mineralization rate was determined by microbial activities, which are always highly associated with the temperatures (Augustine et al., 2014; Lozano-García et al., 2016; Heinzle et al., 2021). For example, higher temperatures can stimulate microbial activities, which directly expedite the soil N turnover rate (Lozano-García et al., 2016). In the study, we found R_A was positive correlation with temperatures in the natural salt marsh, whereas the association between R_A and temperatures was not observed in the embanked salt marsh (Figure S4). This result indicated that the embankment probably dramatically modified the microbial responses to the temperature changes, which ultimately altered the seasonal variation of R_A (Figure 4). Simultaneously, the maximum and minimum R_A values were observed in summer and autumn, respectively, in both the natural and embanked salt marshes (Figure 4). Organic soil N, particularly DON, serves as a vital mineralization substrate that drives the rate of soil N mineralization (Figure 7; Montano et al., 2007; Näsholm et al., 2009). In fact, previous studies have reported that soluble organic matter can provide energy for heterotrophic microorganisms, which is favored for higher levels of N mineralization (Montano et al., 2007; Näsholm et al., 2009). This was supported by the SEM analysis of this study (Figure 7). The highest and lowest DON amounts were observed in summer and autumn, respectively; thus, the seasonal variations in R_A may be contributed to by those of the DON content (Figures 3, 4). Besides, enhanced microbial activities and accelerated soil N turnover rates under increased temperatures stimulated R_A in summer and autumn either (Figures 3, 7; Augustine et al., 2014; Lozano-García et al., 2016; Heinzle et al., 2021).

Furthermore, the R_N decreased significantly in spring and summer, while it increased to a considerable degree in autumn following the establishment of the embankment (Figure 4). These changes were consistent with the variations in R_A following embankment development, as organic matter initially mineralized to NH_4^+ – N. Subsequently, NO_3^- – N was derived from the nitrification of NH_4^+ – N (Figure 4; Khalsa et al., 2020).

Microbial immobilization is also a crucial process in the soil N cycle, as organic and inorganic N can be assimilated by microbes and rapidly converted to MBN (Fahey et al., 2011; Nguyen et al., 2017). In this study, high LON concentrations promoted the accumulation of MBN in the natural and embanked salt marshes according to the SEM analysis, which suggested that soil LON was a vital N source for microorganisms (Figure 7). Nevertheless, the embankment observably decreased the soil LON, but it dramatically elevated the MBN amount in summer and autumn (Figures 3, 4). Besides, earlier studies reported that MBN was closely and positively correlated with MBC, SOC, and SON in general. Whereas in this study, MBC concentrations did not increase significantly, and concentrations of SOC and SON prominently decreased in summer or autumn (Figures 3, 4; Manirakiza et al., 2019). Therefore, the increased MBN content was not caused by lower concentrations of LON, MBC, SOC, or SON. SEM analysis revealed that the decreased soil salinity following embankment establishment raised the concentration of MBN (Figure 7). Salinity is a vital factor that drives the growth of microbes in coastal wetlands due to its being the determinant of the osmotic potential of the soil (Gao et al., 2012). Consequently, the decreased soil salinity induced an increased solution osmotic potential, which ultimately enhanced the uptake of ions (e.g., NO_3^- – N) by microbes and stimulated the production of MBN in the embanked *S. alterniflora* salt marsh (Figure 7) (Mavi and Marschner, 2013).

Plants N absorption

The soil N pool is not only the N sink but also the N source for plants in salt marshes (Geisseler et al., 2009). Soil inorganic N is the primarily source of N for plants (Jones et al., 2004; Jones et al., 2005). Based on SEM analysis, increased RNC led to decreased soil NO_3^- – N but had little impact on soil NH_4^+ – N (Figure 7). This indicated that *S. alterniflora* possessed a greater capacity to take up NO_3^- – N rather than NH_4^+ – N from soil (Jones et al., 2005). This was possibly due to NO_3^- – N not being easily adsorbed by soil particles with negative charges, and its easy leaching into the soil for take up by plants (Jones et al., 2005). Besides, according to the SEM analysis, increased soil DON stimulated RNC, which indicated that DON is another essential available source of N supplies for plant uptake (Figure 7; Kerley and Read, 1995; Alexandre et al., 2015; Cott et al., 2020). Earlier studies revealed that plants can acquire a wide variety of low molecular weight N compounds from DON as the N source, *via* roots when they grow rapidly (e.g., amino acids, amino sugars, and peptides) (Kerley and Read, 1995; Alexandre et al., 2015; Cott et al., 2020). Soil N (e.g., NO_3^- – N and DON) can be absorbed by roots, which promoted the growth and N storage of roots (i.e., RB and RNS). Moreover, the N absorbed by roots can be transferred from root tissues to aboveground living tissues, which promote their N storage (i.e., ALNS) in the natural salt marsh (Figure 7). However, the embankment seems stop the N transfer from root tissues to aboveground living tissues (Figure 7). Therefore, the embankment also converted N absorption of plants (Figure 7).

Conclusion

The coastal embankment dramatically reduced the plant N storage and the soil N pool in the *S. alterniflora* salt marsh year-round, and modified the N transfer processes in the plant subsystem and soil subsystem. Firstly, the litter and root biomass of *S. alterniflora* were significantly decreased due to the lower soil salinity and moisture in the embanked salt marsh, compared to those in the natural salt marsh for every season. Further, the decreased litter and root biomass of *S. alterniflora* translated to the remarkable reduction of N storage in the embanked salt marsh year-round. Secondly, due to the decreased N inputs from plants, the soil organic N subpool (e.g., SON, RON, LON, DON) was observably reduced during every season to varying degrees. Thirdly, the embankment also significantly diminished most of the soil inorganic N subpool (i.e., NH_4^+ – N and NO_3^- – N) which was regulated by the diminution of the organic N content (e.g., RON and DON). Fourthly, although the sizes of the soil organic and inorganic N subpools were reduced, the soil MBN concentrations increased in spring, summer, and winter at different levels due to the embankment. We suggest that the decreased soil salinity following the development of the embankment induced a higher osmotic potential, which ultimately increased the uptake of ions (e.g., NO_3^- – N) by microbes, while stimulating the production of MBN. Ultimately, the soil NO_3^- – N and DON were two vital N sources for *S. alterniflora*, and plants absorbed N from the soil and promote their biomass, N concentrations, and storage (e.g., RB, RNC, RNS, ALB, ALNS). Our study is conducive toward further understanding the mechanisms behind the effects of coastal embankments on the seasonal variations in plant-soil N pools.

Data availability statement

The original contributions presented in the study are included in the article/Supplementary Material. Further inquiries can be directed to the corresponding authors.

Author contributions

GQ: writing – original draft. HF: conceptualization, software, formal analysis, data curation, and writing – original draft. HZ: methodology and investigation. LX:

conceptualization, methodology, software, formal analysis, data curation, writing – original draft, writing – review and editing, and visualization. WY: conceptualization and methodology. YZ: methodology, resources, and investigation. NJ: writing – review and editing. SA: conceptualization, resources, writing – review and editing, project administration, and funding acquisition. All authors contributed to the article and approved the submitted version.

Funding

This study was supported by the National Program on Key Basic Research Project (973 Program) [grant No. 2013CB430405].

Acknowledgments

The authors thank the Dafeng Milu National Nature Reserve and Yancheng National Nature Reserve for their assistants in the field investigation.

Conflict of interest

The authors declare that the research was conducted in the absence of any commercial or financial relationships that could be construed as a potential conflict of interest.

Publisher's note

Supplementary material

The Supplementary Material for this article can be found online at: https://www.frontiersin.org/articles/10.3389/fmars.2022.959144/full#supplementary-material.

References

Abu Hena, M. K., Sidik, B. J., Idris, M. H., Nesarul, M. H., Aysha, A., Islam, M. S., et al. (2015). Forest structure and litter production of naturally re-generated white mangrove *Avicennia marina* in sub-tropical estuarine coast. *J. Environ. Biol.* 36, 1199–1204.

Ake-Castillo, J. A., Vazquez, G., and Lopez-Portillo, J. (2006). Litterfall and decomposition of *Rhizophora mangle* l. in a coastal lagoon in the southern gulf of Mexico. *Hydrobiologia* 559, 101–111. doi: 10.1007/s10750-005-0959-x

Alexandre, A., Hill, P. W., Jones, D. L., and Santos, R. (2015). Dissolved organic nitrogen: A relevant, complementary source of nitrogen for the seagrass *Zostera marina*. *Limnol. Oceanogr.* 6, 1477–1483. doi: 10.1002/lno.10084

An, S. Q., Gu, B. H., Zhou, C. F., Wang, Z. S., Deng, Z. F., Zhi, Y. B., et al. (2007). *Spartina invasion* in China: Implications for invasive species management and future research. *Weed Res.* 47, 183–191. doi: 10.1111/j.1365-3180.2007.00559.x

Aufdenkampe, A. K., Mayorga, E., Raymond, P. A., Melack, J. M., Doney, S. C., Alin, S. R., et al. (2011). Riverine coupling of biogeochemical cycles between land, oceans, and atmosphere. *Front. Ecol. Environ.* 9, 53–60. doi: 10.1890/100014

Augustine, D. J., Brewer, P., Blumenthal, D. M., Derner, J. D., and Fischer, J. C. (2014). Prescribed fire, soil inorganic nitrogen dynamics, and plant responses in a semiarid grassland. *J. Arid Environ.* 104, 59–66. doi: 10.1016/j.jaridenv.2014.01.022

Barbier, E. B., Hacker, S. D., Kennedy, C., Koch, E. W., Stier, A. C., and Silliman, B. R. (2011). The value of estuarine and coastal ecosystem services. *Ecol. Monogr.* 81, 169–193. doi: 10.1890/10-1510.1

Battle, J. M., and Golladay, S. W. (2007). How hydrology, habitat type, and litter quality affect leaf breakdown in wetlands on the gulf coastal plain of Georgia. *Wetlands* 27, 251–260. doi: 10.1672/0277-5212(2007)27[251:HHHTAL]2.0.CO;2

Berman, T., and Bronk, D. A. (2003). Dissolved organic nitrogen: A dynamic participant in aquatic ecosystems. *Aquat. Microb. Ecol.* 31, 279–305. doi: 10.3354/ame031279

Boldea, O., and Magnus, J. R. (2009). Maximum likelihood estimation of the multivariate normal mixture model. *J. Am. Stat. Assoc.* 104, 1539–1549. doi: 10.1198/jasa.2009.tm08273

Brookes, P. C., Landman, A., Pruden, G., and Jenkinson, D. S. (1985). Chloroform fumigation and the release of soil-nitrogen - a rapid direct extraction method to measure microbial biomass nitrogen in soil. *Soil Biol. Biochem.* 17, 837–842. doi: 10.1016/0038-0717(85)90144-0

Cartaxana, P., Cacador, I., Vale, C., Falcao, M., and Catarino, F. (1999). Seasonal variation of inorganic nitrogen and net mineralization in a salt marsh ecosystem. *Mangrove Salt Marshes* 3, 127–134. doi: 10.1023/A:1009941219215

Chen, G. Z., Lu, Q. Q., Bai, J. H., Wen, L. X., Zhang, G. L., Wang, W., et al. (2022). Organic sulfur mineralization in surface soils from coastal wetlands with different flooding periods affected by the flow-sediment regulation in the yellow river delta, China. *Catena* 215, 106343. doi: 10.1016/j.catena.2022.106343

Chen, C. R., and Xu, Z. H. (2006). On the nature and ecological functions of soil soluble organic nitrogen (SON) in forest ecosystems.s. *J. Soil Sediment* 6, 63–66. doi: 10.1065/jss2006.06.159

Chen, S. Y., Yoshitake, S., Iimura, Y., Asai, C., and Ohtsuka, T. (2017). Dissolved organic carbon (DOC) input to the soil: DOC fluxes and their partitions during the growing season in a cool-temperate broad-leaved deciduous forest, central Japan. *Ecol. Res.* 32, 713–724. doi: 10.1007/s11284-017-1488-6

Chen, Y., Zeng, Z. H., Qin, X. J., and Yang, G. (2014). Monthly variation of asexual reproduction of *Spartina alterniflora* (Loisel). *J. Biosaf.* 23, 173–177. doi: 10.3969/j.issn.2095-1787.2014.03.006

Che, R. X., Qin, J. L., Tahmasbian, I., Wang, F., Zhou, S. T., Xu, Z. H., et al. (2018). Litter amendment rather than phosphorus can dramatically change inorganic nitrogen pools in a degraded grassland soil by affecting nitrogen-cycling microbes. *Soil Biol. Biochem.* 120, 145–152. doi: 10.1016/j.soilbio.2018.02.006

Cott, G. M., Jansen, M. A., and Megonigal, J. P. (2020). Uptake of organic nitrogen by coastal wetland plants under elevated CO_2. *Plant Soil* 450, 521–535. doi: 10.1007/s11104-020-04504-5

Cui, L. L., Li, G. S., Ouyang, N. L., Mu, F. Y., Yan, F., Zhang, Y. T., et al. (2018). Analyzing coastal wetland degradation and its key restoration technologies in the coastal area of jiangsu, China. *Wetlands* 38, 525–537. doi: 10.1007/s13157-018-0997-6

Dovrat, G., and Sheffer, E. (2019). Symbiotic dinitrogen fixation is seasonal and strongly regulated in water-limited environments. *N. Phytol.* 221, 1866–1877. doi: 10.1111/nph.15526

Elsey-Quirk, T., Seliskar, D. M., and Gallagher, J. L. (2011). Nitrogen pools of macrophyte species in a coastal lagoon salt marsh: implications for seasonal storage and dispersal. *Estuar. Coast.* 34, 470–482. doi: 10.1007/s12237-011-9379-5

Evangelou, E., Tsadilas, C., and Giourga, C. (2021). Seasonal variation of soil microbial biomass carbon and nitrogen as affected by land use in a Mediterranean agro- ecosystem. *Commun. Soil Sci. Plan.* 52, 222–234. doi: 10.1080/00103624.2020.1854298

Fahey, T. J., Yavitt, J. B., Sherman, R. E., Groffman, P. M., Fisk, M. C., and Maerz, J. C. (2011). Transport of carbon and nitrogen between litter and soil organic matter in a northern hardwood forest. *Ecosystems* 14, 326–340. doi: 10.1007/s10021-011-9414-1

Feng, H. Y., Zhao, H., Xia, L., Yang, W., Zhao, Y. Q., Jeelani, N., et al. (2022). Nitrogen cycling in plant and soil subsystems is driven by changes in soil salinity following coastal embankment in typical coastal saltmarsh ecosystems of Eastern China. *Ecol. Eng.* 174, 106467. doi: 10.1016/j.ecoleng.2021.106467

Feng, J. X., Zhou, J., Wang, L. M., Cui, X. W., Ning, C. X., Wu, H., et al. (2017). Effects of short-term invasion of *Spartina alterniflora* and the subsequent restoration of native mangroves on the soil organic carbon, nitrogen and phosphorus stock. *Chemosphere* 184, 774–783. doi: 10.1016/j.chemosphere.2017.06.060

Feyissa, A., Yang, F., Feng, J., Wu, J. J., Chen, Q., and Cheng, X. L. (2020). Soil labile and recalcitrant carbon and nitrogen dynamics in relation to functional vegetation groups along precipitation gradients in secondary grasslands of south China. *Environ. Sci. Pollut. Res.* 27, 10528–10540. doi: 10.1007/s11356-019-07583-9

Gao, H. F., Bai, J. H., Xiao, R., Yan, D. H., Huang, L. B., and Huang, C. (2012). Soil net nitrogen mineralization in salt marshes with different flooding periods in the yellow river delta, China. *Clean Soil Air Water* 40, 1111–1117. doi: 10.1002/clen.201200031

Ge, Z. M., Guo, H. Q., Zhao, B., and Zhang, L. Q. (2015). Plant invasion impacts on the gross and net primary production of the salt marsh on eastern coast of China: Insights from leaf to ecosystem. *J. Geophys Res.-Biogeo.* 120, 169–186. doi: 10.1002/2014JG002736

Geisseler, D., Horwath, W. R., and Doane, T. A. (2009). Significance of organic nitrogen uptake from plant residues by soil microorganisms as affected by carbon and nitrogen availability. *Soil Biol. Biochem.* 41, 1281–1288. doi: 10.1016/j.soilbio.2009.03.014

Heinzle, J., Wanek, W., Tian, Y., Kengdo, S. K., Borken, W., Schindlbacher, A., et al. (2021). No effect of long-term soil warming on diffusive soil inorganic and organic nitrogen fluxes in a temperate forest soil. *Soil Biol. Biochem.* 158, 108261. doi: 10.1016/j.soilbio.2021.108261

He, J., Zhao, C. J., Qing, H., Gan, L., and An, S. Q. (2009). Effect of soil-water condition on morphological plasticity of clonal plant *Spartina alterniflora*. *Acta Ecol. Sin.* 29, 3518–3524. doi: 10.3321/j.issn:1000-0933.2009.07.009

Huang, L. B., Bai, J. H., Gao, H. F., Xiao, R., Liu, P. P., and Chen, B. (2013). Soil organic carbon content and storage of raised field wetlands in different functional zones of a typical shallow freshwater lake, China. *Soil Res.* 50, 664–671. doi: 10.1071/SR12236

Huang, F., Lin, X., Hu, W., Zeng, F., He, L., and Yin, K. (2021). Nitrogen cycling processes in sediments of the pearl river estuary: Spatial variations, controlling factors, and environmental implications. *Catena* 206, 105545. doi: 10.1016/j.catena.2021.105545

Hu, R., Wang, X. P., Pan, Y. X., Zhang, Y. F., Zhang, Y. F., Zhang, H., et al. (2015). Seasonal variation of net n mineralization under different biological soil crusts in tengger desert, north China. *Catena* 127, 9–16. doi: 10.1016/j.catena.2014.12.012

Iost, S., Landgraf, D., and Makeschin, F. (2007). Chemical soil properties of reclaimed marsh soil from zhejiang province PR China. *Geoderma* 142, 245–250. doi: 10.1016/j.geoderma.2007.08.001

Isobe, K., Oka, H., Watanabe, T., Tateno, R., Urakawa, R., Liang, C., et al. (2018). High soil microbial activity in the winter season enhances nitrogen cycling in a cool-temperate deciduous forest. *Soil Biol. Biochem.* 124, 90–100. doi: 10.1016/j.soilbio.2018.05.028

Jiang, L. F., Luo, Y. Q., Chen, J. K., and Li, B. (2009). Ecophysiological characteristics of invasive spartina alterniflora and native species in salt marshes of Yangtze river estuary, China. *Estuar. Coast. Shelf Sci.* 81, 74–82. doi: 10.1016/j.ecss.2008.09.018

Jones, D. L., Healey, J. R., Willett, V. B., Farrar, J. F., and Hodge, A. (2005). Dissolved organic nitrogen uptake by plants - An important n uptake pathway. *Soil Biol. Biochem.* 37, 413–423. doi: 10.1016/j.soilbio.2004.08.008

Jones, D. L., Shannon, D., Murphy, D. V., and Farrar, J. (2004). Role of dissolved organic nitrogen (DON) in soil n cycling in grassland soils. *Soil Biol. Biochem.* 36, 749–756. doi: 10.1016/j.soilbio.2004.01.003

Kerley, S. J., and Read, D. J. (1995). The biology of mycorrhizal in the ericaceae. XVIII. chitin degradation by *Hymenoscyphus ericae* and transfer of chitin-nitrogen to the host plant. *N. Phytol.* 131, 369–375. doi: 10.1111/j.1469-8137.1995.tb03073.x

Khalsa, S. D. S., Smart, D. R., Muhammad, S., Armstrong, C. M., Sanden, B. L., Houlton, B. Z., et al. (2020). Intensive fertilizer use increases orchard n cycling and lowers net global warming potential. *Sci. Total Environ.* 722, 137889. doi: 10.1016/j.scitotenv.2020.137889

Kirwan, M. L., and Megonigal, J. P. (2013). Tidal wetland stability in the face of human impacts and sea-level rise. *Nature* 504, 53–60. doi: 10.1038/nature12856

Lana, P. C., Guiss, C., and Disaró, S. T. (1991). Seasonal-variation of biomass and production dynamics for aboveground and belowground components of a spartina alterniflora marsh in the euhaline sector of paranaguá bay. *Estuar. Coast. Shelf Sci.* 32, 231–241. doi: 10.1016/0272-7714(91)90017-6

Lawrence, B. A., Fahey, T. J., and Zedler, J. B. (2013). Root dynamics of *Carex* stricta-dominated tussock meadows. *Plant Soil* 364, 325–339. doi: 10.1007/s11104-012-1360-y

Lin, G., and Lin, X. (2022). Bait input altered microbial community structure and increased greenhouse gases production in coastal wetland sediment. *Water Res.* 218, 118520. doi: 10.1016/j.watres.2022.118520

Lin, W., Ma, H., Pei, G. T., Gao, R., Yin, Y. F., and Lin, Y. Y. (2016). Effects of nitrogen addition on soil carbon and nitrogen pools in mid-subtropical forest. *Res. Environ. Sci.* 29, 67–76. doi: 10.13198/j.issn.1001-6929.2016.01.09

Liu, S., Luo, D., Liu, Q. L., Zhang, L., Yang, H. G., and Shi, Z. M. (2017). Carbon and nitrogen storage and distribution in different forest ecosystems in the subalpine of western sichuan. *Acta Ecol. Sin.* 37, 1074–1083. doi: 10.5846/stxb201604150688

Liu, P., Qiu, Y., Wang, Y. T., Wei, Z. P., Fan, J. G., and Cao, B. H. (2019). Seasonal dynamics of soil microbial biomass in typical shelterbelts on the bohai muddy coast. *Acta Ecol. Sin.* 39, 363–370. doi: 10.5846/stxb201711021961

Li, R. X., Yu, Q., Wang, Y. W., Wang, Z. B., Gao, S., and Flemming, B. (2018). The relationship between inundation duration and *Spartina alterniflora* growth along the jiangsu coast, China. *Estuar. Coast. Shelf Sci.* 213, 305–313. doi: 10.1016/j.ecss.2018.08.027

Lozano-García, B., Parras-Alcántara, L., and Brevik, E. C. (2016). Impact of topographic aspect and vegetation (native and reforested areas) on soil organic carbon and nitrogen budgets in Mediterranean natural areas. *Sci. Total Environ.* 544, 963–970. doi: 10.1016/j.scitotenv.2015.12.022

Lytle, R. W., and Hull, R. J. (1980). Photoassimilate distribution in *Spartina alterniflora* loisel. II. autumn and winter storage and spring regrowth. *Agron. J.* 72, 933–938. doi: 10.2134/agronj1980.00021962007200060017x

Ma, J. A., Chai, M. W., and Shi, F. C. (2011). Effects of long-term salinity on the growth of the halophyte *Spartina alterniflora* loisel. *Afr. J. Biotechnol.* 10, 17962–17968. doi: 10.5897/AJB11.2300

Ma, Z., Melville, D. S., Liu, J., Chen, Y., Yang, H., Ren, W., et al. (2014). Rethinking China's new great wall. *Science* 346, 912–914. doi: 10.1126/science.1257258

Manirakiza, E., Ziadi, N., St Luce, M., Hamel, C., Antoun, H., and Karam, A. (2019). Nitrogen mineralization and microbial biomass carbon and nitrogen in response to co-application of biochar and paper mill biosolids. *Appl. Soil Ecol.* 142, 90–98. doi: 10.1016/j.apsoil.2019.04.025

Mavi, M. S., and Marschner, P. (2013). Salinity affects the response of soil microbial activity and biomass to addition of carbon and nitrogen. *Soil Res.* 1, 68–75. doi: 10.1071/SR12191

Montano, N. M., García-Oliva, F., and Jaramillo, V. J. (2007). Dissolved organic carbon affects soil microbial activity and nitrogen dynamics in a Mexican tropical deciduous forest. *Plant Soil* 295, 265–277. doi: 10.1007/s11104-007-9281-x

Näsholm, T., Kielland, K., and Ganeteg, U. (2009). Uptake of organic nitrogen by plants. *N. Phytol.* 182, 31–48. doi: 10.1111/j.1469-8137.2008.02751.x

Nguyen, T. T. N., Xu, C. Y., Tahmasbian, I., Che, R. X., Xu, Z. H., Zhou, X. H., et al. (2017). Effects of biochar on soil available inorganic nitrogen: A review and meta-analysis. *Geoderma* 288, 79–96. doi: 10.1016/j.geoderma.2016.11.004

Patten, K., O'Casey, C., and Metzger, C. (2017). Large-Scale chemical control of smooth cordgrass (*Spartina alterniflora*) in willapa bay, WA: Towards eradication and ecological restoration. *Invas. Plant Sci. Mana.* 10, 284–292. doi: 10.1017/inp.2017.25

Purvaja, R., Ramesh, R., Ray, A. K., and Rixen, T. (2008). Nitrogen cycling: A review of the processes, transformations and fluxes in coastal ecosystems. *Curr. Sci.* 94, 1419–1438.

Quan, Z., Liu, X. A., and Liu, D. (2022). Research progress on soil soluble organic nitrogen. *Chin. J. Appl. Ecol.* 33, 277–288. doi: 10.13287/j.1001-9332.202201.010

Raison, R. J., Connell, M. J., and Khanna, P. K. (1987). Methodology for studying fluxes of soil mineral-n *in-situ*. *Soil Biol. Biochem.* 19, 521–530. doi: 10.1016/0038-0717(87)90094-0

Ren, M. E. (1986). *Comprehensive investigation of the coastal zone and tidal land resources of jiangsu province* (Beijing: Ocean Press).

Rentsch, D., Schmidt, S., and Tegeder, M. (2007). Transporters for uptake and allocation of organic nitrogen compounds in plants. *FEBS Lett.* 581, 2281–2289. doi: 10.1016/j.febslet.2007.04.013

Rovira, P., and Vallejo, V. R. (2002). Labile and recalcitrant pools of carbon and nitrogen inorganic matter decomposing at different depths in soil: An acid hydrolysis approach. *Geoderma* 107, 109–141. doi: 10.1016/S0016-7061(01)00143-4

Sanders-DeMott, R., Sorensen, P. O., Reinmann, A. B., and Templer, P. H. (2018). Growing season warming and winter freeze–thaw cycles reduce root

nitrogen uptake capacity and increase soil solution nitrogen in a northern forest ecosystem. *Biogeochemistry* 137, 337–349. doi: 10.1007/s10533-018-0422-5

Schermelleh-Engel, K., Moosbrugger, H., and Müller, H. (2003). Evaluating the fit of structural equation models: tests of significance and descriptive goodness-of -fit measures. *Methods Psychol. Res. Online* 8, 23–74. doi: 10.13287/j.1001-9332.202201.010

Schimel, J. P., and Bennett, J. (2004). Nitrogen mineralization: Challenges of a changing paradigm. *Ecology* 85, 591–602. doi: 10.1890/03-8002

Schütt, M., Borken, W., Spott, O., Stange, C. F., and Matzner, E. (2014). Temperature sensitivity of c and n mineralization in temperate forest soils at low temperatures. *Soil Biol. Biochem.* 69, 320–327. doi: 10.1016/j.soilbio.2013.11.014

Shi, F. C., and Bao, F. (2007). Effects of salt and temperature stress on ecophysiological characteristics of exotic cordgrass, *Spartina alterniflora*. *Acta Ecol. Sin.* 27, 2733–2741. doi: 10.1016/S1872-2032(07)60061-4

Slavich, P. G., and Petterson, G. H. (1990). Estimating average rootzone salinity from electromagnetic induction (EM-38) measurements. *Aust. J. Soil Res.* 28, 453–463. doi: 10.1071/SR9900453

Socci, A. M., and Templer, P. H. (2011). Temporal patterns of inorganic nitrogen uptake by mature sugar maple (*Acer saccharum* marsh.) and red spruce (*Picea rubens* sarg.) trees using two common approaches. *Plant Ecol. Divers.* 4, 141–152. doi: 10.1080/17550874.2011.624557

Ueda, M. U., Muller, O., Nakamura, M., Nakaji, T., and Hiura, T. (2013). Soil warming decreases inorganic and dissolved organic nitrogen pools by preventing the soil from freezing in a cool temperate forest. *Soil Biol. Biochem.* 61, 105–108. doi: 10.1016/j.soilbio.2013.02.016

Urakawa, R., Shibata, H., Kuroiwa, M., Inagaki, Y., Tateno, R., Hishi, T., et al. (2014). Effects of freeze–thaw cycles resulting from winter climate change on soil nitrogen cycling in ten temperate forest ecosystems throughout the Japanese archipelago. *Soil Biol. Biochem.* 74, 82–94. doi: 10.1016/j.soilbio.2014.02.022

van de Broek, M., Baert, L., Temmerman, S., and Govers, G. (2019). Soil organic carbon stocks in a tidal marsh landscape are dominated by human marsh embankment and subsequent marsh progradation. *Eur. J. Soil Sci.* 70, 338–349. doi: 10.1111/ejss.12739

Vitousek, P. M., Aber, J. D., Howarth, R. W., Likens, G. E., Matson, P. A., Schindler, D. W., et al. (1997). Human alteration of the global nitrogen cycle: Sources and consequences. *Ecol. Appl.* 7, 737–750. doi: 10.1890/1051-0761(1997)007[0737:HAOTGN]2.0.CO;2

Wang, Z. X., Chen, Q. M., Huang, Y. Y., Deng, H. N., Shen, X., Tang, S. Y., et al. (2019). Response of soil respiration and microbial biomass carbon and nitrogen to nitrogen application in subalpine forests of western sichuan. *Acta Ecol. Sin.* 39, 7197–7207. doi: 10.5846/stxb201805271164

Wang, T., Wang, K., and Jiang, X. (2018). Transportation of nitrogen between water column and surficial sediments in simulate wetting season. *Fresen. Environ. Bull.* 27, 6460–6468.

Wan, S. W., Qin, P., Liu, J. N., and Zhou, H. X. (2009). The positive and negative effects of exotic *Spartina alterniflora* in China. *Ecol. Eng.* 35, 444–452. doi: 10.1016/j.ecoleng.2008.05.020

Wuest, S. B. (2015). Seasonal variation in soil bulk density, organic nitrogen, available phosphorus, and pH. *Soil Sci. Soc Am. J.* 79, 1188–1197. doi: 10.2136/sssaj2015.02.0066

Xing, S. H., Chen, C. R., Zhou, B. Q., Zhang, H., Nang, Z. M., and Xu, Z. H. (2010). Soil soluble organic nitrogen and active microbial characteristics under adjacent coniferous and broadleaf plantation forests. *J. Soil Sediment* 10, 748–757. doi: 10.1007/s11368-009-0159-9

Xi, D., Weng, H. D., Hu, Y. L., and Wu, J. P. (2021). Effects of canopy nitrogen addition and understory removal on soil organic carbon fractions in a Chinese fir plantation. *Acta Ecol. Sin.* 41, 8525–8534. doi: 10.5846/stxb202008162130

Xi, D., Yu, Z. P., Xiong, Y., Liu, X. Y., and Liu, J. (2020). Altitudinal changes of soil organic carbon fractions of evergreen broadleaved forests in guanshan mountain, Jiangxi, China. *Chin. J. Appl. Ecol.* 31, 3349–3356. doi: 10.13287/j.1001-9332.202010.009

Xu, G., and Zhuo, R. (1985). Preliminary studies of introduced *Spartina alterniflora* loisel in China. *J. Nanjing Univ.* 1, 212–225.

Yang, W., Jeelani, N., Cai, A. D., Cheng, X. L. , and An, S. Q. (2021). Coastal reclamation alters soil microbial communities following different land use patterns in the Eastern coastal zone of China. *Sci. Rep.* 11, 7265. doi: 10.1038/s41598-021-86758-2

Yang, W., Li, N., Leng, X., Qiao, Y. J., Cheng, X. L., and An, S. Q. (2016). The impact of sea embankment reclamation on soil organic carbon and nitrogen pools in invasive *Spartina alterniflora* and native *Suaeda salsa* salt marshes in eastern China. *Ecol. Eng.* 97, 582–592. doi: 10.1016/j.ecoleng.2016.10.064

Zeng, A., Hu, W. F., Zeng, C. S., Sun, Z. G., and Gao, D. Z. (2020). Litter decomposition and nutrient dynamics of native species (*Cyperus malaccensis*) and alien invasive species (*Spartina alterniflora*) in a typical subtropical estuary (Min river) in China. *Estuar. Coast.* 43, 1873–1883. doi: 10.1007/s12237-020-00744-x

Zhang, X. Q., Wang, G. X., and Wang, Y. (2006). The changes of erosion or progradation of tidal flat and retreat or extension of wetland vegetation of the yancheng coast, jiangsu. *Mar. Sci.* 30, 35–39. doi: 10.3969/j.issn.1000-3096.2006.06.007

Zhang, X., Yan, C., Xu, P., Dai, Y., Yan, W., Ding, X., et al. (2013). Historical evolution of tidal flat reclamation in the jiangsu coastal areas. *Acta Geogra. Sinca* 68, 1549–1558. doi: 10.11821/dlxb201311010

Zhang, Y. H., Zhang, F. C., Li, Y. X., Xie, X. J., Zhou, X. D., Li, Q., et al. (2010). Influence of exogenous n import on growth and leaf character of *Spartina alterniflora*. *Ecol. Environ. Sci.* 19, 2297–2301. doi: 10.1016/S1872-5813(11)60001-7

Zhao, Q. Q., Bai, J. H., Liu, Q., Lu, Q. Q., Gao, Z. Q., and Wang, J. J. (2016). Spatial and seasonal variations of soil carbon and nitrogen content and stock in a tidal salt marsh with *Tamarix chinensis*, China. *Wetlands* 36, 145–152. doi: 10.1007/s13157-015-0647-1

Zhao, G. Q., Zhang, L. Q., and Liang, X. (2005). A comparison of photosynthetic characteristics between an invasive plant spartina alterniflora and an indigenous plant *Phragmites australis*. *Acta Ecol. Sin.* 25, 1604–1611. doi: 10.3321/j.issn:1000-0933.2005.07.011

Zhou, S. W., and Bi, X. L. (2020). Seawall effects in a coastal wetland landscape: spatial changes in soil carbon and nitrogen pools. *J. Coast. Conserv.* 24, 1–11. doi: 10.1007/s11852-019-00718-7

Zhou, W. J., Sha, L. Q., Schaefer, D. A., Zhang, Y. P., Song, Q. H., Tan, Z. H., et al. (2015). Direct effects of litter decomposition on soil dissolved organic carbon and nitrogen in a tropical rainforest. *Soil Biol. Biochem.* 81, 255–258. doi: 10.1016/j.soilbio.2014.11.019

frontiers | Frontiers in Marine Science

TYPE Original Research
PUBLISHED 18 August 2022
DOI 10.3389/fmars.2022.961560

OPEN ACCESS

EDITED BY
Xianbiao Lin,
Ocean University of China, China

REVIEWED BY
Fangjuan Huang,
Sun Yat-sen University, China
Hongming Yao,
Shenzhen Institutes of Advanced Technology (CAS), China

*CORRESPONDENCE
Jibiao Zhang
zhangjb@gdou.edu.cn

SPECIALTY SECTION
This article was submitted to Marine Biogeochemistry, a section of the journal Frontiers in Marine Science

RECEIVED 04 June 2022
ACCEPTED 27 July 2022
PUBLISHED 18 August 2022

CITATION
Zhang P, Luo W, Fu M, Zhang J, Cheng M and Xie J (2022) Effects of tidal variations on total nitrogen concentration, speciation, and exchange flux in the Shuidong Bay coastal water, South China Sea. *Front. Mar. Sci.* 9:961560. doi: 10.3389/fmars.2022.961560

Effects of tidal variations on total nitrogen concentration, speciation, and exchange flux in the Shuidong Bay coastal water, South China Sea

Peng Zhang, Weisheng Luo, Miaojian Fu, Jibiao Zhang*, Mingyue Cheng and Jiale Xie

College of Chemistry and Environmental Science, Guangdong Ocean University, Zhanjiang, China

Nitrogen (N) plays an important role in marine ecosystems as a biogenic element for phytoplankton. The tidal cycle had major influence on various biogeochemical parameters of the bay and changed nutrients input with the ebb and flow of the tide. In this study, we collected samples from Shuidong Bay (SDB) in China, in August 2021, to explore the periodic variations in coastal waters during spring and neap tides. The effects of spring and neap tides on different speciation of nitrogen in the SDB and the exchange fluxes between the SDB and the South China Sea (SCS) were investigated. The results indicated that the concentrations of particulate nitrogen (PN) and N-NO_2^- were significantly different between the spring and neap tides ($P < 0.05$). The total nitrogen (TN) concentrations in SDB during the spring and neap tides were 258.12 ± 89.49 μmol/L and 231.77 ± 56.86 μmol/L. During the spring and neap tides, total dissolved nitrogen (TDN) accounted for 54.1% and 52.2% of TN, respectively. In addition, dissolved organic nitrogen (DON) accounted for 81.4% and 69.9% of the TDN during the spring and neap tides, respectively. Furthermore, the net exchange fluxes of different speciation of nitrogen showed that the net exchange fluxes of TN were transported from SDB to SCS during the spring and neap tide, with the net exchange fluxes of 37.7 t and 8.8 t, respectively. The net exchange flux of TN during spring tide was 4.3 times higher than that of neap tide. In addition, a significant negative correlation was observed between dissolved inorganic nitrogen (DIN) and salinity in SDB during the spring and neap tides ($P < 0.001$), indicated that DIN was mainly influenced by terrestrial sources inputs. A significant positive correlation ($P < 0.01$) was observed between PN and Chlorophyll-*a* in SDB during the spring and neap tides, implied that the assimilation of a large number of planktonic organisms promoted PN formation. The present results revealed that tidal variation played an important role in regulating N speciation and exchange flux in coastal waters, which had great implications for N biogeochemistry and water quality improvement in SDB.

KEYWORDS

total nitrogen, speciation, exchange flux, tidal variation, Shuidong Bay

1 Introduction

Nitrogen is an essential nutrient for the growth and reproduction of marine organisms (Tian, 1990; Dittmar and Lara, 2001; Xia et al., 2007; Fang et al., 2008; Gao et al., 2009; Cheng et al., 2020). Nitrogen is the basis of marine primary productivity and food chain and play an important role in marine biogeochemistry, which affects the biomass of marine ecosystems and community structure, causing the eutrophication of water bodies (Loh, 2000; Berman et al., 2003; Han et al., 2003; Zhou et al., 2003; Xin et al., 2010; Lin et al., 2013; Sui et al., 2016). The nitrogen cycle is a crucial part of biogeochemical processes that control the availability of nitrogenous nutrients and productivity levels of organisms in marine ecosystems (Galloway, 2005; Zhong and Li, 2014; Huang, et al., 2021; Lin and Lin, 2022). The major sources of nitrogen in the ocean are terrestrial runoff, surface water and groundwater input, sewage discharge, atmospheric deposition, and nitrogen fixation (Watson et al., 1993; Howarth, 2008; White et al., 2013; Guo et al., 2019; Du et al., 2020). Extremely high nutrient content caused the eutrophication of water bodies and even disasters, such as red tides (Sun et al., 2005; Zheng, 2010; Carey et al., 2011; Liu et at., 2011; Fatemi et al., 2012; Guo et al., 2012; Zhang et al., 2020c). In contrast, extremely low nutrient content may cause dysfunctional nutrient structures, preventing the normal growth of phytoplankton, and affecting the stability of marine ecosystems (Bricker et al., 2003; Geeraert et al., 2021; Niu et al., 2016; Xu et al., 2020; Zhou, 2021). In the water column, nitrogen is characterized by variable speciation. DIN is involved in the speciation of $N\text{-}NO_3^-$, $N\text{-}NO_2^-$, and $N\text{-}NH_4^+$. The changes in DIN speciation affecting the primary production, changing competitiveness among species, and altering biodiversity in water column (Collos, 1998; Feng et al., 2012; Tang et al., 2013 Kang et al., 2020; Li et al., 2020). Phytoplankton constitutes an indispensable link in the aquatic food chain, and they grow by absorbing nutrients from the water column in a certain proportion (Eppley and Peterson, 1979; Falkowski, 1997; Joseph et al., 2008; Li et al., 2008; Liu et al., 2011; Li et al., 2017; Xiu et al., 2019). DIN is taken up by phytoplankton and then released in the DON forms, which primarily contains humic substances, urea, free amino acids, amides, and vitamins. Particulate organic nitrogen included organic nitrogen debris, bacteria, and phytoplankton components (Yang et al., 1990; Moneta et al., 2014; Kanuri et al., 2018; Xiu et al., 2019). PN is an important speciation of nitrogen in the ocean and plays an important role in the transport of various elements of the ocean and in the supply of nutrients and biogeochemical processes. Changes in the ratio and concentration of PN plays an important role in the maintenance of primary productivity in the offshore (Fernandes, 2011; Yu et al., 2012; Zhou et al., 2019). The multiple species of nitrogen make its circulation in the marine environment relatively complex.

The tidal cycle has major influence on various physicochemical parameters of the bay and changes nutrients and organic matter input with the ebb and flow of the tide. The coastal zone is a key area for marine biogeochemical reactions, and the physical processes has a significant impact on biogeochemical reactions (Yin and Harrison, 2000; Qu et al., 2007; Fang et al., 2012; Li, 2021). Tidal forces are important factors controlling water–sediment dynamics in estuarine and coastal systems, including regulated water stratification and influenced the transport of freshwater and sediment from rivers into estuaries, further affecting the dynamics of organic and inorganic components (Tian, 1990; Dittmar and Lara, 2001; Xia et al., 2007; Fang et al., 2008; Gao et al., 2009; Cheng et al., 2020). The high intensity human activities had caused the ecological degradation of the bay, which were unique nearshore weak exchange hydrodynamic environments, were among most eutrophic water environments in the ocean under the influence of high-intensity human activities (Bricker et al., 2003; Daniel et al., 2009; Liu et al., 2011; Wang, 2019; Cui et al., 2020; Li et al., 2020). In recent years, nutrients in bay water have been influenced primarily by anthropogenic activities, resulting in the increase of terrestrial nutrients into coastal water (Zhang 2007b; Santos et al., 2008; Li et al., 2013; Amato et al., 2020). The distribution of nitrogen in coastal waters was influenced by tides, winds, convective diffusion, biological activities, and water-sediment interface exchange (Li, 2021; Liu et al., 2017; Zhang et al., 2016; Zhang et al., 2022). Therefore, nutrients had different biogeochemical processes and showed different spatial patterns under the influence of tidal variations, which further affect primary production and thus the nitrogen cycle in coastal waters (Zhou et al., 2003; Sun, 2008; Guo et al., 2014; Yuan et al., 2016).

Shuidong Bay (SDB) is a semi-enclosed bay, formed by the recent slight rise in the Earth's crust (Li et al., 2015). The bay is slightly curved, with its wide mouth facing south, and surrounded by a large sand dam. The tides in SDB were characterized by semi-diurnal tidal variations (Qin et al., 2014; Li et al., 2015; Feng et al., 2017). Semi-diurnal tidal variations may have a considerable influence on the dynamics of nutrients in SDB (Peng, 1987; Yang et al., 2011; Qin et al., 2014; Li et al., 2015; Feng et al., 2017). In addition, the input and output of nutrients and hydrological conditions of coastal bays determined the residence time of nutrients, and the combined influence of adjacent waters further complicates the biogeochemical processes of the nutrients involved (Hopkins et al., 1993; Li, 2021). As different speciation of nitrogen flow between SDB and SCS with seawater, some nutrients may be consumed or produced during transport. That would result in high or low nutrient concentrations during tidal changes (Li, 2021). However, with the rapid development of mariculture in recent years, it had caused a decrease in the exchange capacity of SDB waters and an increase in water eutrophication (Qin et al., 2014; Li et al., 2015; Li et al., 2016; Feng et al., 2017). At present, studies had focused on the mechanisms of tides and their effects on hydrodynamics (Song et al., 2011; Wu et al., 2011; Cheng et al., 2020) and distribution patterns of nutrients in estuarine bays (Guo, 2020; Lu et al., 2020; Liu et al., 2021; Zhang et al., 2021; Ke

et al., 2022). However, previous studies on SDB had primarily focused on the natural environment and dynamic conditions; previous studies lack real-time observations, particularly the simultaneous changes in nutrients during the spring and neap tidal cycles. In addition, most previous studies had focused on DIN for nitrogen speciation (Wang et al., 2016; Jiang et al., 2019; Yang et al., 2020; Zhang et al., 2020; Zhang et al., 2020b). However, the effects of tidal cycling on nitrogen species variations, particularly on PN and DON, were still scarce.

Therefore, to better understand the tidal effects on nitrogen speciation, we analyzed continuous observation data from four stations (S1, S2, S3, S4) in SDB to reveal the effects of tidal cycles on the concentrations of different nitrogen species and to analyze the causes of tidal variations affecting them. Thus, the main research objectives of this study were to explore (1) the effects of spring and neap tides on different nitrogen species, (2) exchange fluxes between SDB and SCS, and (3) caused of tidal variations in different nitrogen species. In this study, the effects of spring and neap tides on nitrogen speciation in SDB were assessed for the first time. Our results provided new insights into the analysis of the distribution and transport of different nitrogen species in coastal waters, which had great implications for nitrogen biogeochemical and water quality improvement in eutrophic SDB.

2 Materials and methods

2.1 Study areas

SDB is a semi-enclosed bay (Figure 1). It is connected to the SCS through a tidal channel that is 12.7 km long, 500–800 m wide, and 5–15 m deep (Li et al., 2015). The surface area of SDB is approximately 32 km^2 narrow at the mouth. SDB had a wide range of water, topography of the seafloor in SDB was complex, distribution of deep troughs was remarkable, and mudflat area was large (Feng et al., 2017). The rivers flowing into SDB include the Xijian, Danchang, Zaitou, and Nanhai rivers (Li et al., 2015). The marine dynamic environment of SDB was dominated by tidal action, and the tidal type was irregular semi-diurnal tide, with a maximum average flow velocity of 0.3–0.5 m/s and maximum flow velocity of 1.0 m/s in the tidal channel (Qin et al., 2014). The development of coastal aquaculture and increasing terrestrial pollutants in SDB had recently caused the gradual shrinking of the water area in SDB and deterioration of water quality conditions, even directly changing the tidal pattern in SDB (Qin et al., 2014; Li et al., 2015; Feng et al., 2017). Therefore, in this study, we collected data on spring and neap tides from four stations in SDB, and water sampling was conducted according to the tidal characteristics and hydrology of SDB. The coastal water monitoring stations in SDB were selected according to the method specified in the Specification of Oceanographic Survey (General Administration of Quality Supervision, Inspection, and Quarantine of the People's Republic of China).

2.2 Field sampling and pre-treatment

The current state of SDB environmental quality were surveyed and monitored under the hydrodynamic conditions of spring tide (August 22-23, 2021) and neap tide (August 29-30, 2021) in the summer. Four hydrodynamic monitoring stations and water quality monitoring stations (S1, S2, S3, S4) were deployed at sea on this simultaneous survey cruise for 24-h continuous monitoring, with hydrodynamic conditions monitored every 1 h and surface seawater sampling performed every 3 h. T1 was a tide gauge station for monitoring the tidal

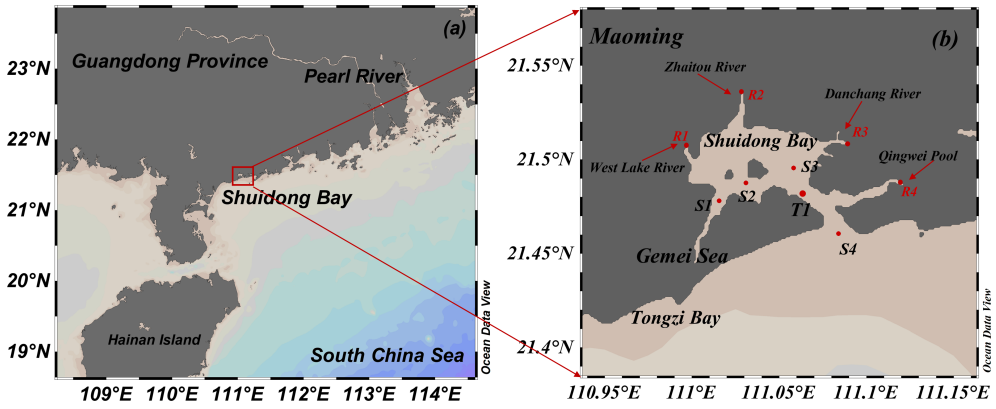

FIGURE 1
Geographic location of SDB **(A)** and field seawater monitoring stations in the SDB **(B)**.

height at different times. Considering the shallow the coastal water in the SDB, samples were collected from the depth of 0.5m in the surface layer. All samples were collected, processed, and preserved until analysis, according to the methods specified in the Marine Monitoring Code (GB17378-2007). Seawater samples were collected through a CTD-Rosette system using Teflon-coated bottles (10 L, Sea Bird Inc., USA) equipped with temperature, salinity, and fluorescence sensors. The collected water samples were packed in 100 ml acid-washed HDPE bottles and stored at -20°C. Approximately 1 L of seawater was filtered through pre-acid-washed and pre-assembled (held at 450°C for 4 h) 45 mm diameter Whatman GF/F glass fibre filters. Filtrate samples for TDN, $N\text{-}NH_4^+$, $N\text{-}NO_3^-$, and $N\text{-}NO_2^-$ determination were collected in acid-washed HDPE bottles and stored at -20°C until laboratory analysis. Water environmental factors (temperature, salinity, and pH) were determined *in situ* using a multiparameter water quality tester (Aquaprobe AP-7000).

2.3 Chemical analysis in the laboratory

Owing to the complexity of DON and PN, it was difficult to perform single component determination. Therefore, in this experiment, we used the potassium persulfate oxidation method to determine the concentration of TN and TDN in water bodies; the detection limit of this method was 2.64 μmol/L. The DON and PN concentrations were then calculated. The DON concentration was determined as the difference between TDN and DIN, and PN concentration was determined as the difference between TN and TDN. DIN was the sum of the $N\text{-}NO_3^-$, $N\text{-}NH_4^+$, and $N\text{-}NO_2^-$ concentrations. The $N\text{-}NH_4^+$, $N\text{-}NO_3^-$, and $N\text{-}NO_2^-$ concentrations in the water samples were determined *via* the hypobromite oxidation, zinc–cadmium reduction, and diazo–azo methods, respectively, and the detection limits were 0.03 μmol/L, 0.05 μmol/L, and 0.02 μmol/L, respectively. All of the above methods were measured at 543 nm using a UV-visible spectrophotometer (Shimadzu UV2600i). Suspended particulate matter (SPM) was measured by weight method. Chlorophyll-*a* was determined by spectrophotometric method. The relative standard deviation of the above methods was <5% for repeatability, reproducibility and precision. All samples were collected, pretreated, and analyzed in strict accordance with the Marine Monitoring Code (GB17378-2007), and full monitoring quality control was implemented (AQSIQ, 2007a).

2.4 Net exchange flux of nitrogen calculation during tidal cycle

The fluxes of different nitrogen species exchanged between the SCS and SDB in the positive direction of the designated flow to SDB were estimated using the method described next.

SDB was connected to the SCS by only a narrow bay channel, and sites S1, S2, and S3 were away from the bay mouth. Therefore, the fluxes of different nitrogen species from the bay mouth of SDB to the SCS were estimated from the S4 site of SDB, which represented the fluxes of different nitrogen species from the bay mouth of SDB. The flow velocity and direction of seawater in the surface layer of S4 were measured continuously with an electromagnetic current meter (AME-USB, JFE, Japan). When the flow direction was 45°-225° it showed the flow from SDB to SCS. When the flow direction was 225°-360° and 0°-45° it showed the flow from SCS to SDB. Calculated the flux of water through S4 at different times by equation (1). Then, the net exchange flux of different nitrogen species between SDB and SCS was estimated by multiplying the water flux by the concentrations of different nitrogen species in the net coastal inflow water column by equation (2). The net exchange fluxes of different speciation of nitrogen between SDB and SCS at other moments were estimated on the transects of both sides of the bay according to the temporal variation of the flow velocity, and then the net exchange fluxes of different speciation of nitrogen between SDB and SCS in one day were calculated.

$$Q = W \times D \times V \quad (1)$$

Where Q was the net water flux at the mouth of SDB per unit time (L/h) in the vector, W was the width of S4 (m), D was the depth of S4 (m), V was the flow velocity at different times of S4 (cm/s).

$$F_N = C_N \times Q \times 10^{-6} \times M_N \quad (2)$$

Where F_N was the net exchange of different nitrogen species at the mouth of SDB (t/h), C_N was the concentration of different nitrogen species flowing through the mouth of SDB per second (μmol/L), and M_N was the relative atomic mass of nitrogen.

2.5 Statistical analysis

Student's t test was used to test the normality of the concentrations of different speciation of nitrogen during spring and neap tides, but the data did not show a normal distribution. Then a non-parametric Mann-Whitney U test was used for analysis to find significant differences between different speciation of nitrogen during spring and neap tides (Sánchez-Carrillo et al., 2009). Spearman correlation analysis was used to determine the correlation between the variables by environmental factors and the concentration of different speciation of nitrogen (Zhang et al., 2020). In addition, a linear regression analysis was performed to analyze the relationship between fluxes and flow velocity of different speciaton of nitrogen in spring and neap tides. If $P < 0.05$, it indicates a significant difference between the variables.

TABLE 1 Mean values of environmental factors for each station of SDB.

Environmental Factors	*S1*		*S2*		*S3*		*S4*	
	Spring tide	*Neap tide*	*Spring tide*	*Neap tide*	*Spring tide*	*Neap tide*	*Spring tide*	*Neap tide*
Temperature (°C)	*32.38 ± 0.72*	*30.60* ± 0.52	*32.15* ± 0.65	*30.45* ± 0.45	*32.00* ± 0.63	*30.43* ± 0.39	*31.49* ± 0.44	*29.72* ± 0.34
Salinity (‰)	*24.78 ± 0.55*	*23.24* ± 0.41	*25.09* ± 2.08	*24.39* ± 1.80	*26.69* ± 0.87	*27.37* ± 1.19	*27.91* ± 0.49	*30.51* ± 0.80
pH	*8.04 ± 0.11*	*7.49* ± 0.09	*7.99* ± 0.12	*7.83* ± 0.21	*8.05* ± 0.09	*7.81* ± 0.07	*8.17* ± 0.04	*7.88* ± 0.07
SPM (mg/L)	*23.82 ± 9.85*	*5.38* ± 3.27	*18.49* ± 8.60	*7.05* ± 3.52	*21.49* ± 4.64	*5.11* ± 2.43	*24.27* ± 10.66	*8.49* ± 4.42
Flow velocity *(cm/s)*	*12.75 ± 12.72*	*5.23* ± 1.93	*29.35* ± 18.52	*15.43* ± 8.70	*42.22* ± 24.64	*25.38* ± 12.07	*37.68* ± 17.31	*25.30* ± 9.36

3 Results

3.1 Hydrographic conditions in SDB

The environmental factors for the different stations of the SDB were presented in Table 1. SDB was an irregular semi-diurnal tide, with two high tides and two low tides in one day. During the SDB spring tide, two high tides occurred at 10:00 and 23:00, with tide heights of 382 cm and 254 cm respectively and two low tides occurred at 17:00 and 4:00, with tide heights of 47 cm and 130 cm respectively, and the tidal difference during the spring tide was 335 cm. During the neap tide in SDB, two high tides occurred at 14:00 and 3:00, with tide heights of 230 cm and 280 cm, and two low tides occurred at 20:00 and 9:00, with tide heights of 140 cm and 153 cm, respectively, and the tidal difference during the neap tide was 140 cm. During the spring and neap tides, the average flow velocity of all four stations in SDB were S3 > S4 > S2 > S1. During the spring and neap tides, the maximum flow velocity of S3 was 42.22 ± 24.64 cm/s and 25.38 ± 12.07 cm/s, respectively. Furthermore, the average *salinity* of all four stations in SDB were S4 > S3 > S2 > S1 during the spring and neap tides. The salinity of S4 was maximum during spring and neap tides with 27.91 ± 0.49‰ and 30.51 ± 0.80‰, respectively. During the SDB spring tide, the maximum tidal exchange from the SDB to the SCS occurred at 15:00 with a tidal exchange of 1.0×10^{10} t/h. The maximum tidal exchange from the SCS to the SDB occurred at 22:00 with a tidal exchange of 8.2×10^{9} t/h. During the SDB neap tide, the maximum tidal exchange from the SDB to the SCS occurred at 16:00 with a tidal exchange of 6.1×10^{9} t/h. The maximum tidal exchange from SCS to SDB occurred at 22:00, with a tidal exchange of 5.9×10^{9} t/h. During the SDB spring and neap tides, the net tidal exchange was from SCS to SDB, the net tidal exchange is 4.4×10^{9} t and 2.3×10^{9} t respectively.

3.2 Dynamics of TN in SDB during the spring and neap tides

3.2.1 Dynamics of TN in SDB during the spring and neap tides

The TN concentrations did not differ between the spring and neap tides ($P > 0.05$), but the PN concentrations differed between the spring and neap tides ($P > 0.05$). The concentrations of different nitrogen species were presented in Table 2. The range of the TN concentration during the spring (Figure 2A) and neap tides (Figure 2B) was 77.79–421.79 μmol/L and 113.62–350.55 μmol/L, respectively, with averages of 258.12 ± 89.49 μmol/L and 231.77 ± 56.86 μmol/L, respectively; thus, the range of the average concentration during the spring and neap tides was small. The maximum value of the TN concentration occurred at 23:00 in S1, and the minimum value occurred at 23:00 in S4 during the spring tide. The averages of TN during the spring and neap tides in SDB indicated that S1 >S2 >S3 >S4 and S4 >S3 >S2 >S1, respectively; these results indicated that the TN concentration in SDB was influenced by the tide. The TN concentration in SDB during the spring tide was higher than that in the bay mouth, whereas the opposite was true during the neap tide. The TN concentrations of S1, S2, and S3 during the spring tide were higher than those during the neap tide; however, the TN concentration of S4 during the spring tide was lower than that during the neap tide. TDN accounted for 54.1% and 52.2% of TN during the spring and neap tides, respectively. This indicated that TDN was the dominant species of TN. The range of the PN concentration during the spring and neap tides was 8.51–304.66 μmol/L and 12.76–246.71 μmol/L, respectively, and the average concentrations were 118.51 ± 84.57 μmol/L and 110.74 ± 63.18 μmol/L, respectively; the average PN concentration of S1 was higher during the spring tide than during the neap tide, and the average PN concentration of S4 was lower during the spring tide than during the neap tide.

3.2.2 Dynamics of TDN in SDB during the spring and neap tides

The TDN concentrations did not differ between the spring and neap tides ($P > 0.05$). The range of the TDN concentration during the spring (Figure 2C) and neap tides (Figure 2D) was 31.53–356.93 μmol/L and 27.81–204.86 μmol/L, respectively, and the average concentrations were 139.61 ± 66.09 μmol/L and 121.03 ± 41.77 μmol/L, respectively. The average TDN concentration during the spring and neap tides changed little; however, the variations in the TDN concentration during the spring tide was more evident, and the maximum TDN concentration occurred at 20:00 in S1. In addition, DON accounted for 81.4% and 69.9% of the TDN during the spring and neap tides, respectively. This indicates that DON was the

TABLE 2 Mean values of nitrogen species concentrations at each station in SDB (μmol/L).

Nitrogen Species	S1		S2		S3		S4		All stations	
	Spring tide	Neap tide	Spring tide	Neap tide	Spring tide	Neap tide	Spring tide	Neap tide	Average of spring tide	Average of neap tide
TN	343.58 ± 50.71	198.07 ± 37.20	289.70 ± 50.33	216.50 ± 69.15	260.16 ± 54.01	251.30 ± 44.35	139.05 ± 39.13	261.22 ± 46.70	258.12 ± 89.49	231.77 ± 56.86
TDN	160.08 ± 74.42	118.79 ± 34.64	169.30 ± 62.66	115.24 ± 40.85	155.24 ± 45.77	158.19 ± 31.58	73.83 ± 6.49	91.91 ± 29.09	139.61 ± 66.09	121.03 ± 41.77
PN	183.49 ± 84.57	79.28 ± 39.81	120.40 ± 67.70	101.26 ± 65.18	104.92 ± 66.66	93.11 ± 50.33	65.22 ± 42.01	169.32 ± 52.71	118.51 ± 84.57	110.74 ± 63.18
DON	139.35 ± 74.98	56.85 ± 30.85	134.81 ± 71.90	74.40 ± 40.97	129.67 ± 43.42	131.53 ± 28.09	50.48 ± 11.33	75.39 ± 31.50	113.58 ± 67.38	84.54 ± 43.51
DIN	20.73 ± 9.56	61.94 ± 13.20	34.49 ± 27.83	40.84 ± 23.83	25.57 ± 16.26	26.66 ± 17.28	23.35 ± 11.44	16.52 ± 8.09	26.03 ± 18.49	36.49 ± 23.81
$N\text{-}NH_4^+$	4.76 ± 1.09	10.77 ± 0.35	4.93 ± 2.77	5.55 ± 2.63	4.53 ± 1.67	4.80 ± 2.66	4.09 ± 1.31	3.02 ± 1.09	4.58 ± 1.86	6.03 ± 3.48
$N\text{-}NO_3^-$	15.67 ± 8.89	49.39 ± 13.17	28.87 ± 25.43	34.47 ± 21.35	20.64 ± 16.31	21.19 ± 14.67	19.06 ± 10.93	13.33 ± 8.05	21.06 ± 17.37	29.60 ± 20.37
$N\text{-}NO_2^-$	0.30 ± 0.32	1.78 ± 0.12	0.69 ± 0.52	0.82 ± 0.74	0.40 ± 0.27	0.67 ± 0.29	0.20 ± 0.11	0.16 ± 0.11	0.40 ± 0.38	0.86 ± 0.71

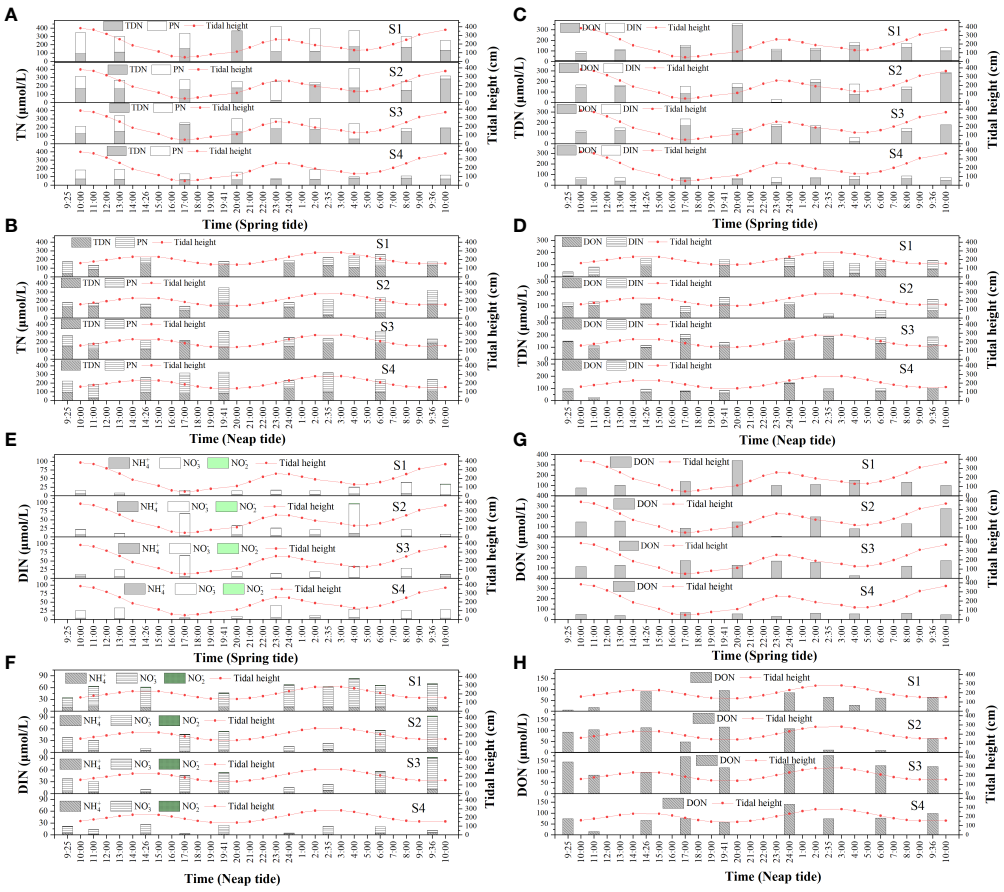

FIGURE 2
Dynamics of TN **(A),**, TDN **(C)**, DIN **(E)** and DON **(G)** during the spring tide in SDB and dynamics of TN **(B)**, TDN **(D)**, DIN **(F)** and DON **(H)** during the neap tide in SDB.

dominant species of TDN. The average concentrations of TDN in SDB during the spring and neap tides were S2>S1>S3>S4 and S3>S1>S2>S4, respectively. S4 was less affected by tide, and the TDN concentration in SDB was higher than that at the mouth of the bay.

3.3 Dynamics of DIN in SDB during the spring and neap tides

There were no significant differences in the concentrations of DIN, $N\text{-}NO_3^-$ and $N\text{-}NH_4^+$ during the spring and neap tides ($P > 0.05$), but the $N\text{-}NO_2^-$ concentrations were significantly different during the spring and neap tides ($P < 0.05$). The ranges of DIN during the spring (Figure 2E) and neap tides (Figure 2F) were 4.67–97.78 μmol/L and 3.68–92.70 μmol/L, respectively, with averages of 26.03 ± 18.49 μmol/L and 36.49 ± 23.81 μmol/L. The DIN concentration during the spring tide exceeded the seawater quality index category II standard, whereas the DIN concentration during the neap tide exceeded the seawater quality index category IV standard. Only S2 exceeded the second category of seawater quality index during the spring tide, while S1 and S2 exceeded the fifth category of seawater quality index during the neap tide, and the DIN concentration of S1 was considerably higher than that of S2. During spring tide, $N\text{-}NH_4^+$, $N\text{-}NO_3^-$, and $N\text{-}NO_2^-$ accounted for 17.6%, 80.9%, and 1.5% of DIN, respectively. During the neap tide, $N\text{-}NH_4^+$, $N\text{-}NO_3^-$, and $N\text{-}NO_2^-$ accounted for 16.5%, 81.1%, and 2.4% of DIN, respectively. DIN was primarily dominated by $N\text{-}NO_3^-$, followed by $N\text{-}NH_4^+$, and $N\text{-}NO_2^-$. The $N\text{-}NO_3^-$ concentration ranged from 2.38 to 84.93 μmol/L and from 1.00 to 78.95 μmol/L during the spring and neap tides, respectively, with averages of 21.06 ± 17.37 μmol/L and 29.60 ± 20.37 μmol/L, respectively, and the $N\text{-}NO_3^-$ concentrations were higher in the neap tide than in the spring tide. The $N\text{-}NO_3^-$ concentrations were lower during the S1 spring tide than during the neap tide, whereas the $N\text{-}NO_3^-$ concentrations were higher during the S4 spring tide than during the neap tide. The ranges of $N\text{-}NH_4^+$ concentrations during the spring and neap tides were 1.17–10.94 μmol/L and 1.95–11.65 μmol/L, respectively, with averages of 4.58 ± 1.86 μmol/L and 6.03 ± 3.48 μmol/L, respectively. The ranges of $N\text{-}NO_2^-$ concentrations during the spring and neap tides were 0.02–1.91 μmol/L and 0.02–2.25 μmol/L, respectively, with averages of 0.40 ± 0.38 μmol/L and 0.86 ± 0.71 μmol/L, respectively. Although $N\text{-}NH_4^+$ and $N\text{-}NO_2^-$ only accounted for a small part of DIN, the average concentration of $N\text{-}NH_4^+$ was still considerably larger than that of $N\text{-}NO_2^-$, and both $N\text{-}NH_4^+$ and $N\text{-}NO_2^-$ had higher concentrations in the neap tide than in the spring tide. The averages of DIN, $N\text{-}NO_3^-$, and $N\text{-}NH_4^+$ during the spring and neap tides in SDB were S2 >S1 >S3 >S4 and S1> S2> S3> S4, respectively. The average concentrations of $N\text{-}NO_2^-$ during the spring and neap tides in SDB were S2 >S3 >S1 >S4 and S1 >S2 >S3 >S4, respectively. The DIN concentrations (including N-NO3-, N-NO2-, and N-NH4+) all exhibited higher concentrations in the bay than at the mouth of the bay.

3.4 Dynamics of DON in SDB during the spring and neap tides

There were no significant differences in the concentrations of DON during the spring and neap tides ($P > 0.05$). The ranges of DON concentrations during the spring (Figure 2G) and neap tides (Figure 2H) were 5.08–342.37 μmol/L and 5.87–175.54 μmol/L, respectively, with averages of 113.58 ± 67.38 μmol/L and 84.54 ± 43.51 μmol/L, respectively. The concentration and range of DON at spring tide were higher than neap tide. The average DON concentrations in SDB during the spring and neap tides were S1 >S2 >S3 >S4 and S3 >S4 >S2 >S1, respectively, which indicated that the tide had a great influence on DON concentration. The DON concentration at stations S1 and S2 was higher during the spring tide than during the neap tide, and DON concentration at S3 and S4 was slightly lower during the spring tide than during the neap tide.

3.5 The net exchange TN flux with SCS during the spring and neap tides in SDB

During spring and neap tides, the net exchange fluxes between SDB and SCS were different. During the SDB spring tide (Figure 3A) and neap tide (Figure 3B), the daily net exchange fluxes of TN and PN flowed from SDB to SCS. However, the daily net exchange fluxes of TDN (including DIN and DON) flowed from SCS to SDB during the SDB spring tide (Figure 3C) and neap tide (Figure 3D). In addition, the daily net exchange fluxes of TN and PN during spring tide were 37.7 t and 44.3 t, respectively, and the daily net exchange fluxes of DIN and DON were 1.9 t and 4.7 t, respectively. Furthermore, the daily net exchange fluxes of TN and PN during neap tide in SDB were 8.8 t and 15.0 t, respectively, and the daily net exchange fluxes of DIN and DON were 0.8 t and 5.4 t, respectively. The net exchange flux of TN in spring tide was 4.3 times higher than that of neap tide. Therefore, SDB was a source of TN for SCS.

4 Discussion

4.1 Comparison of the TN levels in estuaries and coastal waters worldwide

A comparison of the nitrogen concentrations in SDB with other semi-enclosed bays in China and the world was presented in Table 3. SDB had the highest TN concentration, which was

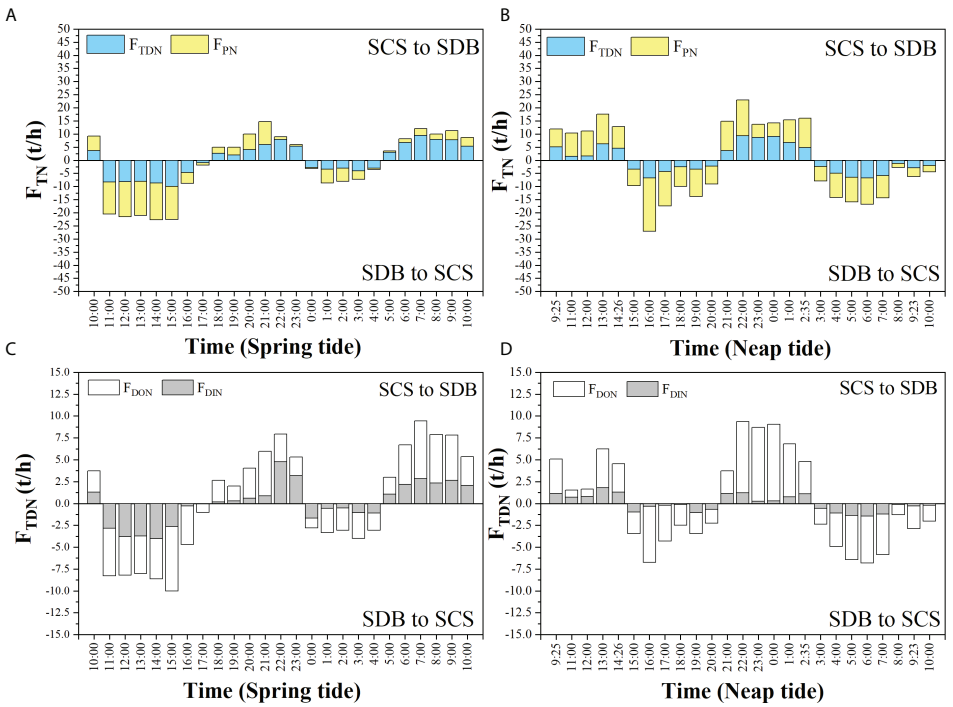

FIGURE 3
During the spring tide, TN **(A)** and TDN **(C)** in the exchange flux between SDB and SCS. During the neap tide, TN **(B)** and TDN **(D)** in the exchange flux between SDB and SCS.

higher than estuaries and bays with human influence such as Liusha Bay, Chesapeake Bay, Yangtze Estuary and Mississippi Estuary (Turner et al., 2007; Cao et al., 2011; Harding et al., 2016; Ge et al., 2021). In addition, TDN/TN in SDB was only 53.2%, which was considerably lower than the corresponding values in Daya bay and Yangtze Estuary (Zhou et al., 2019; Ge et al., 2021). The highest PN concentration was found in SDB, which was much higher than that in Daya Bay and Yangtze River Estuary (Zhou et al., 2019; Ge et al., 2021). By comparing the Chlorophyll-*a* of SDB with that of Jiaozhou Bay and Zhanjiang Bay (Li et al., 2005; Zhou et al., 2021), the highest Chlorophyll-*a* was found in SDB, indicated the high biomass of SDB. The high concentration of PN in SDB may be due to assimilation of DIN during the photosynthesis by phytoplankton. Furthermore, the DIN concentration in SDB was lower than that in Mississippi Estuary and Pearl River Estuary (Turner et al., 2007; Ke et al., 2022), but higher than that in Jiaozhou Bay, Persian Gulf and Daya Bay (Lu et al., 2016; Zhou et al., 2019; Maryam et al., 2021). The $N\text{-}NO_3^-$ content in SDB was second only to that in the Pearl River Estuary (Zhao et al., 2000; Wu, 2014; Zhou et al., 2019; Ge et al., 2021; Maryam et al., 2021; Ke et al., 2022), and $N\text{-}NO_3^-$ was the dominant component of DIN in SDB. With the increase of population and development of mariculture in SDB (Qin et al., 2014; Li et al., 2015; Li et al., 2016; Feng et al., 2017), containing higher concentrations of $N\text{-}NH_4^+$ was discharged into the SDB with the river and will be oxidized with the shoreline to $N\text{-}NO_3^-$ (Archana et al., 2018). The high nitrogen load in SDB may be caused by the untreated urban polluted wastewater and large amount of farming wastewater discharged into SDB. Furthermore, the TDN/TN ratios were 53.3%, 55.8%, 61.3% and 44.15% for S1, S2, S3 and S4 during the spring and neap tides in SDB, respectively. This indicated that TDN was the dominant component in S1, S2 and S3, but PN was the dominant component in S4. During spring and neap tides, the net exchange fluxes of different speciation of nitrogen in SDB showed that TN and PN flowed from SDB to SCS, while TDN (including DIN and DON) flowed from SCS to SDB, which resulted in larger TDN/TN ratios in S1, S2 and S3 than in S4.

4.2 Hydrodynamics induced by tidal variations on nitrogen species dynamics

The correlation between different nitrogen species and environmental factors during the spring and neap tides were shown in Figure 4A and Figure 4B, respectively. A significant positive correlation existed between PN and Chlorophyll-*a* during the spring and neap tides ($P < 0.01$), which was related to the strong biological action of particulate matter (Lin et al., 2013). The assimilation of a large number of planktonic organisms promoted PN formation. Moreover, the living

TABLE 3 Nitrogen species in SDB and its adjacent waters and bays around the world (μmol/L).

Latitude	Longitude	Region	Time	N-NO_2^-	N-NO_3^-	N-NH_4^+	DIN	DON	TDN	PN	TN	TDN/TN	References
25°50′-27°0′N	55°00′-57°00′E	Persian Gulf	2021	1.34 ±0.81	6.41±4.64	0.004 ±0.003	7.75 ±5.45	—	—	—	—	—	Maryam et al., 2021
30°59′-31°00′N	122°24′-123°11′E	Yangtze Estuary	2018	0.42 (0.05-0.80)	13.53 (0.46-32.62)	1.13 (ND-11.56)	13.97 (2.04-33.83)	13.97 (ND-44.08)	27.96 (8.26-63.57)	5.39 (0.75-27.42)	34.35 (3.42-90.86)	81.4%	Ge et al., 2021
21°80′-23°00′N	113°40′-114°00′E	Pearl River Estuary	2018	7.00 ±5.57	56.01 ±30.65	5.24 ±4.16	68.25 ±35.69	—	—	—	—	—	Ke et al., 2022
22°45′-22°85′N	114°45′-114°85′E	Daya Bay	2015-2016	0.90	6.11	4.60	11.29	12.29	24.50	8.20 ±4.75 (2.63-26.24)	32.7	74.9%	Zhou et al., 2019
36°00′-36°12′N	120°80′-120°20′E	Jiaozhou Bay	2012-2013	—	—	—	24.91 (12.69-60.14)	36.07 (17.70-59.21)	60.98	16.71 (4.69-28.58)	77.68 (48.74-139.60)	—	Lu et al., 2016
20°30′-21°28′N	108°15′-109°53′E	The northern part of the Beibu Gulf	2011	0.46 (0.03-4.45)	1.17 (ND-12.5)	0.91 (0.21-5.42)	2.54 (0.35-13.6)	—	—	—	16.8 (5.58-29.3)	—	Wu, 2014
20°22′-20°27′N	109°54′-109°59′E	Liusha Bay	2008	—	—	—	4.43 (2.64-13.79)	—	—	—	49.21 (22.93-72.64)	—	Cao et al., 2011
37°26′-37°38′N	121°24′-121°38′E	Forty Mile Bay	1997	1.58 (1.15-2.03)	1.66 (1.07-2.93)	3.37 (0.64-9.41)	6.61 (3.13-13.24)	—	—	—	—	—	Zhao et al., 2000
30°45′ N	91°23′E	Mississippi Estuary	1980-1993	61.43 ±2.86	—	—	99.6	—	—	—	127.14 ±3.79	—	Turner et al., 2007
36°50′-39°50′N	75°50′-77°50′E	Chesapeake Bay	1945-2012	—	—	—	—	—	—	—	118.57	—	Harding et al., 2016
21°45′-21°55′N	111°00′-111°15′E	SDB	2021	0.63 ±0.62 (0.02-2.25)	25.33± 19.41 (1.00-84.93)	5.31 ±2.88 (1.17-11.65)	31.26 ±21.95 (3.68-97.78)	99.06 ±58.54 (5.08-342.37)	130.32 ±56.06 (27.81-356.93)	114.63 ±71.84 (8.51-304.66)	244.95 ±76.12 (77.79-421.79)	53.2%	The study

() was the range of different speciation of nitrogen; "—" indicated not detected; ND indicated non-detected values.

fraction of PN influenced DIN by producing secretions (Chowdhury et al., 2016), detritus, and excretions (Belcher et al., 2016), whereas the non-living fractions buffer DIN *via* processes such as adsorption–desorption (Lebo et al., 1991). The quality and source of PN determines its impact on coastal water quality. DON can be microbially converted to DIN, which can adversely affect the water quality of the bay (Stedmon et al., 2007; Mesfioui et al., 2012; Seitzinger and Sanders, 1997). Coastal waters were mainly influenced by ocean currents, as SDB and SCS exchange tidal currents through the mouth of the bay, which facilitates the dilute mixing of SDB seawater (Bejaoui et al., 2016; Bancon-Montigny et al., 2019). When the flow velocity slowed down, the particulate organic matter being settled down will be decomposed by bacteria (Yin et al., 2000). Simultaneously, sediment resuspension caused strong changes in the chemical composition of the overlying water column, released nutrients that may be available to pelagic species (Bancon-Montigny et al., 2019). With the rapid development of mariculture in the SDB, had caused a large amount of pollutants containing DON to enter the SDB (Qin et al., 2014; Li et al., 2015; Feng et al., 2017). Since DON and PN were likely to be absorbed by microorganisms and converted into DIN, coupled with the rich microbial population in the bay, the impact of DON and PN on the water quality of the bay should be taken seriously (Lu et al., 2020).

During spring and neap tides, TDN and DON showed a significant positive correlation ($P < 0.001$), and DON, as the main substance of TDN, influenced the concentration of TDN through the migration transformation of DON. During SDB spring tide, DIN showed a significant negative correlation with tidal height ($P < 0.05$), indicating that DIN was tidally influenced during spring tide, with DIN concentration decreasing with high tide and increasing with low tide. However, there was a significant negative correlation between DIN and salinity during spring and neap tides ($P < 0.0001$). Nutrient was higher in waters with low salinity, which was consistent with the findings in Chongming Dongtan and Hongwan (Wang, 1999; Qu et al., 2007; Li et al., 2012; Fu et al., 2020; Zhou et al., 2022). This suggested that terrestrial input may be responsible for influencing the variation of DIN. In addition, a

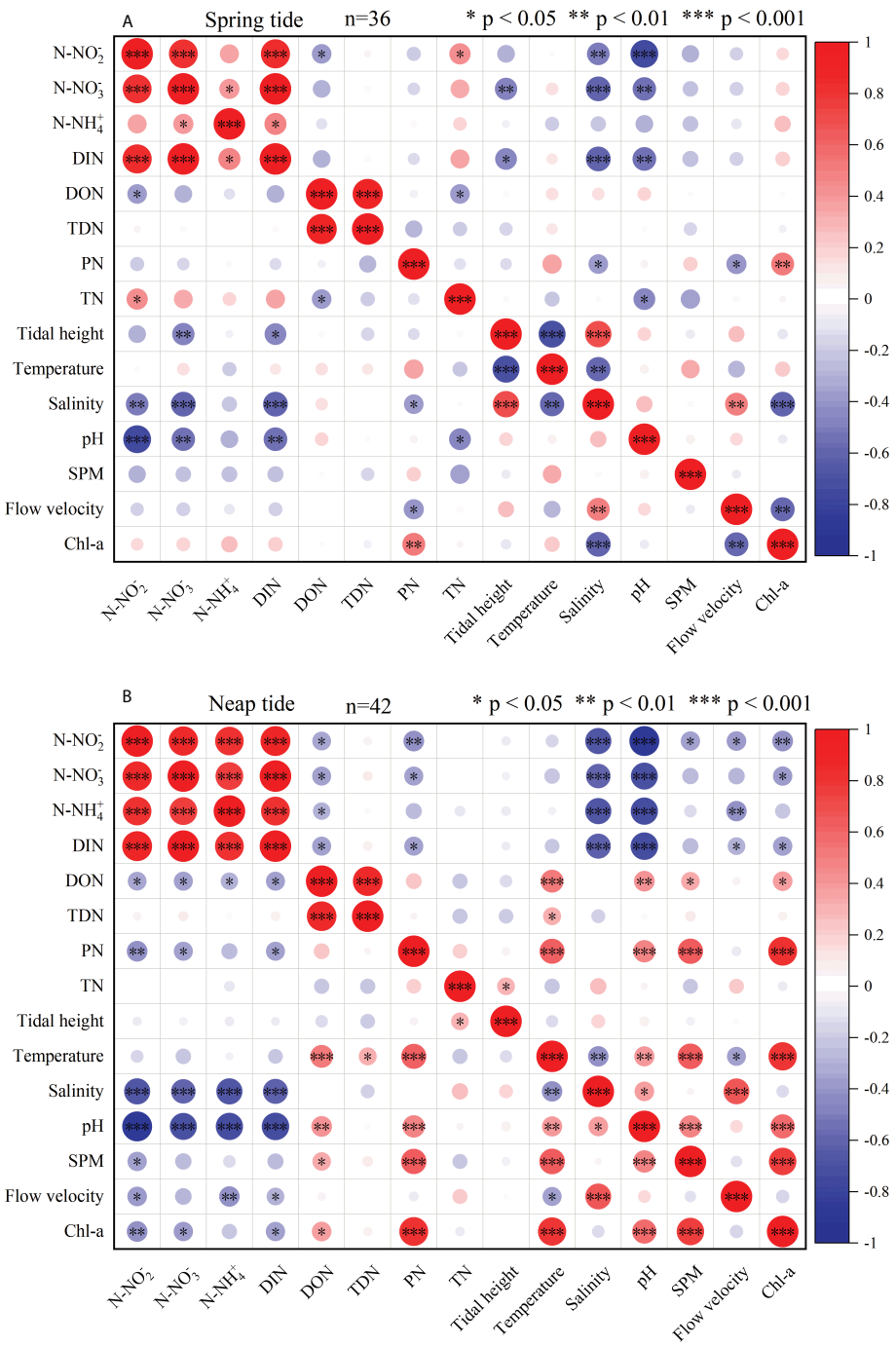

FIGURE 4
Correlation analysis of nitrogen species with environmental factors during spring tide **(A)** and neap tide **(B)** in SDB.

significant positive correlation ($P < 0.001$) existed between N-NO_3^-, the dominant species of DIN, and DIN during the spring and neap tides, indicating a similarity in the transformation and transport between N-NO_3^- and DIN. A significant negative correlation ($P < 0.01$) was found between N-NH_4^+ and salinity during neap tide, indicating that N-NH_4^+ was mainly influenced by terrestrial inputs, and with the development of terrestrial aquaculture in the SDB, effluents containing high concentrations of N-NH_4^+ was discharged into the SDB (Chen et al., 2011; Liu et al., 2011). Furthermore, there was a negative correlation between N-NH_4^+ and DON during neap tides ($P < 0.05$). This demonstrated that N-NH_4^+ and DON transformed their

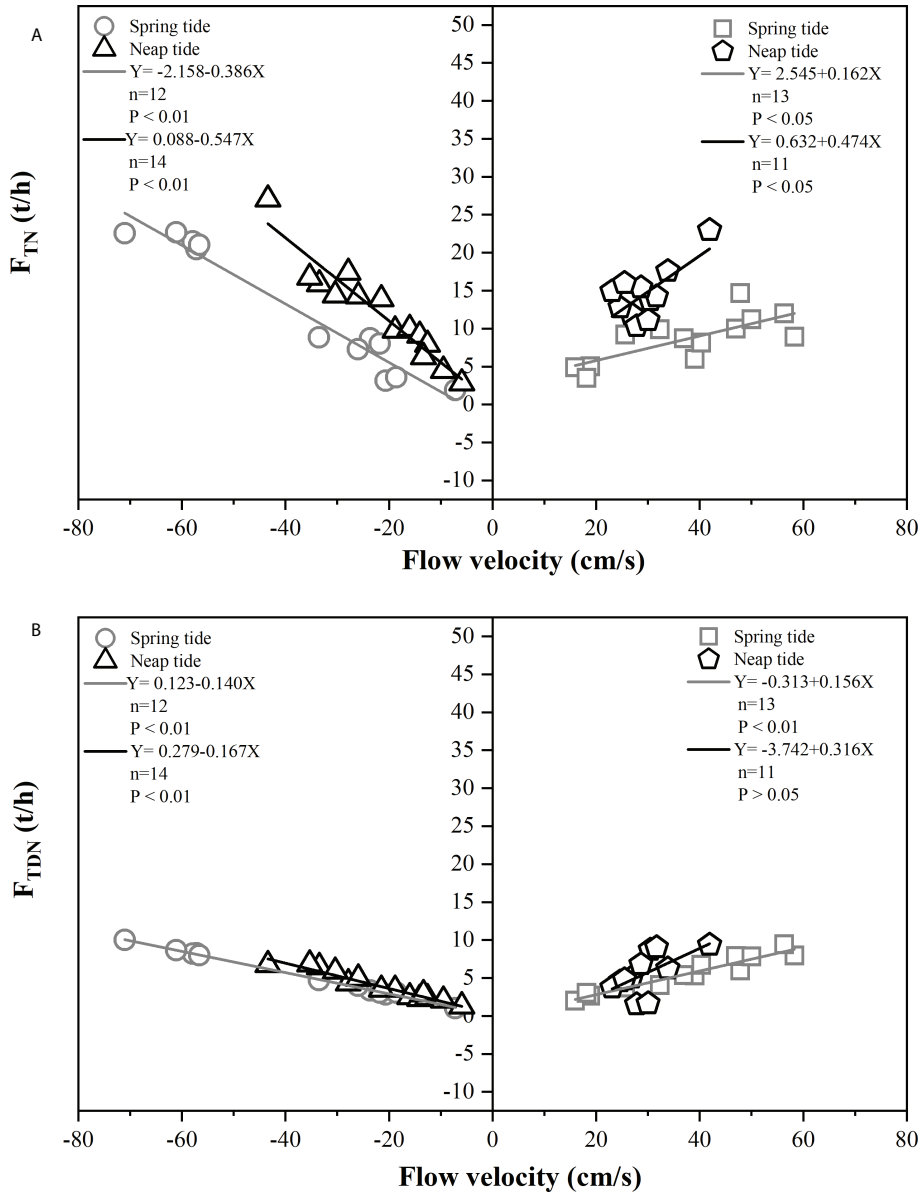

FIGURE 5
Linear regression analysis of FTN **(A)** and FTDN **(B)** with flow velocity.

concentrations through mutual migration. In addition, DON can be converted to N-NH_4^+ *via* microbial activity (Lu et al., 2016; Pisam, et al., 2017). Additionally, the respiratory activity of marine organisms was a key process in nutrient regeneration.

4.3 Impacts of the exchange of TN speciation flux between SDB and SCS

Figure 5A and Figure 5B showed the TN and TDN flux as a function of the flow velocity during the spring and neap tides, respectively. When the flow velocity was greater than 0, it indicated that the exchange flux flowed from SCS to SDB, and the flow velocity was less than 0 indicated that the exchange flux flowed from SDB to SCS. The results indicated that there were significant relationships between the flow velocity and nitrogen flux. During the spring tide and neap tide in SDB, F_{TN} was significantly negatively correlated ($P < 0.01$) with flow velocity when the net exchange flux of TN flowed from SDB to SCS. Furthermore, F_{TN} was significantly positively correlated with flow velocity, when the net exchange flux of TN flowed from SCS to SDB during the spring tide and neap tide in SDB ($P < 0.05$). The high TN in the SDB was

discharged from the terrestrial pollutants and flowed from the SDB to the SCS. The high flow velocity tended to greatly increase the exchange flux of different nitrogen species between SDB and SCS. Therefore, the hydrological conditions of the sea area predominated the transport of different species of nitrogen in coastal waters (Zhao et al., 1998; Passeri et al., 2015; Chen et al., 2019). Thus, the flow velocity of coastal water between the open ocean and bay was influenced by hydrodynamic conditions, resulting in the net exchange fluxes of different nitrogen species both into and out of SDB during the day.

4.4 Implications for the effective improvement of water quality in SDB

Under the implementation of the 14th Five-Year Plan for Marine Ecological Environment Protection in Guangdong Province and the programme of key engineering measures for marine ecological protection and restoration in SDB (Department of Ecological Environment in Guangdong Province, 2022), terrestrial pollutant inputs should be reduced based on the characteristics of SDB to improve water quality (Li et al., 2018; Zhang et al., 2019; Zhang et al., 2019b; Zhou et al., 2020). In this study, we revealed that terrestrial sources and hydrodynamics jointly dominated the nitrogen under tidal variations. On the one hand, SDB and SCS should be considered as a single system to prevent nitrogen pollution. Owing to the high intensity of anthropogenic activities during the past decades, land reclamation decreasing seawater area, resulting in a sharp decline in water exchange and purification capacity (Feng, 2017). However, to achieve accurate terrestrial source reduction in SDB, there should be a shift from only control DIN to control TN in water. The discharge of land-source pollutants should be reduced based on environmental capacity, considering local urban sewage, industrial wastewater, and sewage from livestock breeding and aquaculture. However, there were inconsistencies in the current monitoring nitrogen indicators of river (TN) and coastal water quality (DIN). The total control of land-source pollution in polluted areas and management of river nutrient discharges into the sea should be strengthened (Strokal et al., 2017; Zhang et al., 2020), and the future coastal seawater quality should be linked to the management of the flux control of TN (Zhang et al., 2020). In addition, mangrove systems should be restored to reduce terrestrial nitrogen sources in SDB, particularly in marine aquaculture. Therefore, the long-term monitoring of nitrogen continued in SDB and SCS, as it will help us improve our understanding of the influence of tidal variations on the different nitrogen species in SDB. The establishment of a land–ocean space can effectively control and manage the water quality conditions of SDB.

5 Conclusions

In this study, we investigated the variations in nitrogen species in SDB during the spring and neap tides. The results indicated that the concentrations of PN and N-NO_2^- were significantly different between the spring and neap tides ($P < 0.05$). The TN concentrations in SDB during the spring and neap tides were 258.12 ± 89.49 μmol/L and 231.77 ± 56.86 μmol/L, respectively. During the spring and neap tides, TDN accounted for 54.1% and 52.2% of TN, respectively. DIN and DON exhibited semi-diurnal cyclic variation, indicating a period of high concentration at low tide and relatively low concentration in hight tide. In addition, the contribution of DON to TDN was the largest. A significant negative correlation was observed between the concentration of DIN and salinity ($P < 0.001$), and a significant positive correlation was observed between PN and Chlorophyll-*a* in SDB during the spring and neap tides ($P < 0.01$). This indicated that the concentration of different nitrogen species in SDB was not only controlled by tidal variations but also by the terrestrial source input. Moreover, the net exchange fluxes of different speciation of nitrogen between SDB and SCS showed that the TN were transported from SDB to SCS during the spring and neap tide, with the daily net exchange fluxes of 37.7 t and 8.8 t, respectively. The net exchange flux of TN in spring tide was 4.3 times higher than that of neap tide. Thus, SDB was a source of TN for SCS. Semi-diurnal tidal variations may drive the changes in the concentrations of different nitrogen species, thereby affecting the transport flux, biogeochemical behavior of nitrogen, and primary production. The present results provided scientific basis and key parameters for studying the tidal behaviors of different nitrogen species.

Data availability statement

The original contributions presented in the study are included in the article/supplementary material. Further inquiries can be directed to the corresponding author.

Author contributions

Conceptualization, PZ. Methodology, PZ and JZ. Software, WL, MF, MC, and JX. Validation, WL, MF, MC, and JX. Formal analysis, WL, MF, MC, and JX. Writing-original draft preparation, PZ and WL. Writing-review and editing, PZ and WL. Visualization, PZ and JZ. Supervision, PZ and JZ. Project management, PZ and JZ. Funding acquisition, PZ and JZ. All listed authors made substantial, direct, and intellectual contributions to the work and are approved for publication.

Funding

This research was financially supported by Research and Development Projects in Key Areas of Guangdong Province (2020B1111020004), Guangdong Basic and Applied Basic

Research Foundation (2020A1515110483), Research on hydrodynamic changes and environmental remediation plan of Gemei Sea dike diversion (B21137). Guangdong Ocean University Fund Project (R18021), Science and Technology Special Project of Zhanjiang City (2019B01081), First-class Special Fund (231419018), Innovation Strong School Project (230420021) of Guangdong Ocean University.

Acknowledgments

The authors are grateful for the anonymous reviewers' careful review and valuable suggestions to improve the manuscript.

Conflict of interest

The authors declare that the research was conducted in the absence of any commercial or financial relationships that could be construed as a potential conflict of interest.

Publisher's note

All claims expressed in this article are solely those of the authors and do not necessarily represent those of their affiliated organizations, or those of the publisher, the editors and the reviewers. Any product that may be evaluated in this article, or claim that may be made by its manufacturer, is not guaranteed or endorsed by the publisher.

References

Amato, H. K., Wong, N. M., and Pelc, C. (2020). Effects of concentrated poultry operations and cropland manure application on anti- biotic resistant escherichia coli and nutrient pollution in Chesapeake bay watersheds. *Sci. Total. Environ.* 735 (15), 1–11. doi: 10.1016/j.scitotenv.2020.139401

Archana, A., Thibodeau, B., Geeraert, N., Xu, M. N., Kao, S. J., and Baker, D. M. (2018). Nitrogen sources and cycling revealed by dual isotopes of nitrate in a complex urbanized environment. *Water Res.* 142 (oct.1), 459–470. doi: 10.1016/j.watres.2018.06.004

AQSIQ (2007a) *Specifications for oceanographic surey-part 4: Survey of chemical parameters in sea water (GB/T 12764.4-2-7).* (Beijing: Standards Press of China)

AQSIQ (2007b) *The specification for marine monitoring-part 4: Seawater analysis (GB 17378.4-2007).* (Beijing: Standards Press of China)

Bancon-Montigny, C., Gonzalez, C., Delpoux, S., Avenzac, M., Spinelli, S., Mhadhbi, T., et al. (2019). Seasonal changes of chemical contamination in coastal waters during sediment resuspension. *CHEMOSPHERE.* 235, 651–661. doi: 10.1016/j.chemosphere.2019.06.213

Béjaoui, B. C. S., Harzallah, A., Chevalier, C., Chapelle, A., Zaaboub, N., and Aleya, L. 3D modeling of phytoplankton seasonal variation and nutrient budget in a southern Mediterranean lagoon. *Mar. pollut. Bull.* 114 (2), 962-976. doi: 10.1016/j.marpolbul.2016.11.001.

Belcher, A., Iversen, M., and Manno, C. (2016). The role of particle associated microbes in remineralization offecal pellets in the upper mesopelagic of the Scotia Sea, Antarctica. *Limnol. Oceanogr.* 61, 1049–1064. doi: 10.1002/lno.10269

Berman, T., and Bronk, D. A. (2003). Dissolved organic nitrogen: a dynamic participant in aquatic ecosystems. *Aquat. Microb. Ecol.* 31, 279–305. doi: 10.3354/ame031279

Bricker, S. B., Ferreira, J. G., and Simas, T. (2003). An integrated methodology for assessment of estuarine trophic status. *Ecol. Model.* 169 (1), 39–60. doi: 10.1016/S0304-3800(03)00199-6

Cao, Z. W., and Wang, D. P. (2011). Investigation and evaluation of water quality conditions in ganxi liushawan and yingpan pearl culture areas. *Trans. Oceanology Limnology* 4, 31–38. doi: CNKI:SUN:GXSC.0.2010-04-013

Carey, R. O., Migliaccio, K. W., and Brown, M. T. (2011). Nutrient discharges to Biscayne bay, Florida: trends, loads, and a pollutant index. *Sci. Total. Environ.* 409 (3), 530–539. doi: 10.1016/j.scitotenv.2010.10.029

Cheng, P., Yu, F., Chen, N., and Wang, A. (2020). Observational study of tidal mixing asymmetry and eddy viscosity-shear covariance-induced residual flow in the jiulong river estuary. *Cont. Shelf. Res.* 193, 104035. doi: 10.1016/j.csr.2019.104035

Chen, H. M., Sun, C. X., and Wu, Y. Q. (2011). Analysis of trend of nutrient structure and influencing factors in changjiang estuary and its adjacent sea during 23 years. *Mar. Environ. Sci.* 30 (04), 551–553+563. doi: 10.3969/j.issn.1007-6336.2011.04.022

Chen, B., Xu, Z. X., Ya, H. Z., Chen, X. Y., and Xu, M. B. (2019). Impact of the water input from the eastern qiongzhou strait to the beibu gulf on guangxi coastal circulation. *Acta Oceanol. Sin.* 38 (9), 1–11. doi: 10.1007/s13131-019-1472-2

Chowdhury, C., Majumder, N., and Jana, T. K. (2016). Seasonal distribution and correlates of transparentexopolymer particles (TEP) in the waters surrounding mangroves in the sundarbans. *J. Sea. Res.* 112, 65–74. doi: 10.1016/j.seares.2016.01.004

Collos, Y. (1998). Nitrate uptake, nitrite release and uptake, and new production estimates. *Mar. Ecol. Prog. Ser.* 171, 293–301. doi: 10.3354/meps171293

Cui, X., Huang, C., Wu, J., Liu, X., and Hong, Y. (2020). Temporal and spatial variations of net anthropogenic nitrogen inputs (NANI) in the pearl river basin of China from 1986 to 2015. *PloS One* 15 (2), 0228683. doi: 10.1371/journal.pone.0228683

D'Croz, L., and O'Dea, A. (2007). Variability in upwelling along the pacific shelf of Panama and implications for the distribution of nutrients and chlorophyll. *Estuar. Coast. Shelf.* S. 73 (1–2), 325–340. doi: 10.1016/j.ecss.2007.01.013

Daniel, J. C., Hans, W. P., and Rober, W. H. (2009). Controlling eutrophication: nitrogen and phosphorus. *SCIENCE.* 323, 1014–1015. doi: 10.1126/science.1167755

Dan, S. F., Liu, S. M., Udoh, E. C., and Ding, S. (2019). Nutrient biogeochemistry in the cross river estuary system and adjacent gulf of Guinea, south East Nigeria (West Africa). *Cont. Shelf. Res.* 179, 1–17. doi: 10.1016/j.csr.2019.04.001

Department of Ecological Environment in Guangdong Province (2022). In *"14th five year plan" for marine ecological environment protection in guangdong province.* (Guangdong Province: Department of ecological environment), 1–40.

Dittmar, T., and Lara, R. J. (2001). Driving forces behind nutrient and organic matter dynamics in a mangrove tidal creek in north Brazil. *Estuar. Coast. Shelf.* S, 52(2). doi: 10.1006/ecss.2000.0743

Du, E., Terrer, C., Pellegrini, A. F. A., Ahlström, A., Lissa, C. J., Zhao, X., et al. (2020). Global patterns of terrestrial nitrogen and phosphorus limitation. *Nat. Geosci.* 13 (3), 221–226. doi: 10.1038/s41561-019-0530-4

Eppley, R. W., and Peterson, B. J. (1979). Particulate or-ganic-matter flux and planktonic new production in the deep ocean. *NATURE*, 282. doi: 10.1038/282677a0

Falkowski, P. G. (1997). Evolution of the nitrogen cycle and its influence on the biological sequestration of CO_2 in the ocean. *Nature.: Int. weekly. J. Sci.* 387, 272–275. doi: 10.1038/387272a0

Fang, T., Feng, Z. H., and Gao, L. (2012). Tidal cycle variation of nutrient salts and chlorophyll a in the south branch waters of the Yangtze river estuary. *Trans. Oceanology. Limnology.* 03), 58–65.

Fang, T., Li, D. J., Kong, D. J., Yu, L. H., Li, Y., Gao, L., et al. (2008). Distribution of n and p nutrients and their tidal variations in the Yangtze river estuary and adjacent waters in summer and autumn. *Mar. Environ. Sci.* 05), 437–442.

Fatemi, S. M. R., Nabavi, S. M. B., and Vosoghi, G. (2012). The relation between environmental parameters of hormuzgan coastline in Persian gulf and occurrence of the first harmful algal bloom of cochlodinium polykrikoides (Gymnodiniaceae). *Iran. J. Fish. Sci.* 11 (3), 475–489.

Feng, S. J. (2017). Characterization and 3D numerical simulation of tidal currents in shuidong bay. *J. Appl. Oceanogr.* 36 (03), 333–340.

Feng, L. L., Li, Z. K., and Zhou, T. (2012). Temporal and spatial distributions of phytoplankton and various forms of inorganic nitrogen in lake taihu. *J. Lake. Sci.* 24 (5), 739–745.

Fernandes, L. (2011). Origin and biochemical cycling of particulate nitrogen in the mandovi estuary. *Estuar. Coast. Shelf.* S. 94, 291–298. doi: 10.1016/j.ecss.2011.07.007

Fu, D., Zhong, Y., Chen, F., Yu, G., and Zhang, X. (2020). Analysis of dissolved oxygen and nutrients in zhanjiang bay and the adjacent sea area in spring. *Sustainability-Basel.* 12 (3), 899. doi: 10.3390/su12030889

Galloway, J. N. (2005). The global nitrogen cycle: past, present and future. *Sci. China. Ser. C. Life Sci.* S2), 669–677. doi: 10.1007/BF03187108

Gao, L., Li, D. J., and Ding, P. X. (2009). Quasi-simultaneous observation of currents, salinity and nutrients in the changjiang (Yangtze river) plume on the tidal timescale. *J. Mar. Systems.: J. Mar. Sci. Tech-Japan.* 75 (1-2), 265–279. doi: 10.1016/j.jmarsys.2008.10.006.

Geeraert, N., Archana, A., Xu, M. N., Kao, S. J., Baker, D. M., and Thibodeau, B. (2021). Investigating the link between pearl river-induced eutrophication and hypoxia in Hong Kong shallow coastal waters. *Sci. Total. Environ.* 772, 145007. doi: 10.1016/j.scitotenv.2021.145007

Ge, T. T., Wang, X. Y., Tan, L. J., and Li, T. (2021). Influence of water stratification and tidal action on the transport of particulate nitrogen and phosphorus in the Yangtze estuary in summer. *Mar. Sci.* 45 (08), 1–9.

Guo, J. (2020). *Nitrogen biogeochemical processes and nutrient deposition records in the nearshore waters of beibu gulf, guangxi* (Nanning: Guangxi University).

Guo, J., Wang, Y., Lai, J., Pan, C., Wang, S., Fu, H., et al. (2019). Spatiotemporal distribution of nitrogen biogeochemical processes in the coastal regions of northern beibu gulf, south China Sea. *CHEMOSPHERE* 239, 124803. doi: 10.1016/j.chemosphere.2019.124803

Guo, Z. H., Wang, C., Yan, L., and Wang, J. K. (2012). Spatial and temporal variation characteristics of major pollutants in the jiulong river estuary. *China Environ. Sci.* 32 (04), 679–686. doi: 10.3969/j.issn.1000-6923.2012.04.017

Guo, W. D., Yang, L. Y., Zhai, W. D., Chen, W. Z., Osburn, C. L., Huang, X., et al. (2014). Runoff-mediated seasonal oscillation in the dynamics of dissolved organic matter in different branches of a large bifurcated estuary–the changjiang estuary. *J. Geophys. Res.* 119 (5). doi: 10.1002/2013JG002540

Han, X. Y., Wang, X. L., Sun, X., Shi, X. Y., Zhu, C. J., Zhang, C. S., et al. (2003). Nutrient distribution and its relationship with occurrence of red tide in coastal area of East China Sea. *J. Appl. Ecol.* 14 (7), 1097–1101.

Harding, L. W., Gallegos, C. L., Perry, E. S., Miller, W. D., Adolf, J. E., Mallonee, M. E., et al. (2016). Long-term trends of nutrients and phytoplankton in chesapeake bay. *Estuaries. Coasts.* 39 (3), 664–681. doi: 10.1007/s12237-015-0023-7

Herbeck, L. S., Unger, D., Wu, Y., and Jennerjahn, T. C. (2013). Effluent, nutrient and organic matter export from shrimp and fish ponds causing eutrophication in coastal and back-reef waters of NE hainan, tropical China. *Cont. Shelf. Res.* 57, 92–104. doi: 10.1016/j.csr.2012.05.006

Hopkins, J. S., Hamilton, R. D.II, Sandifer, P. A., Browdy, C. L., and Stokes, A. D. (1993). Effect of water exchange rate on production, water quality, effluent characteristics and nitrogen budgets of intensive shrimp ponds. *J. World Aquacult. Soc* 24, 304–320. doi: 10.1111/j.1749-7345.1993.tb00162.x

Howarth, R. W. (2008). Coastal nitrogen pollution: A review of sources and trends globally and regionally. *Harmful. Algae.* 8 (1), 0–20. doi: 10.1016/j.hal.2008.08.015

Huang, F. J., Lin, X. B., and Yin, K. D. (2021). Effects of marine produced organic matter on the potential estuarine capacity of NOx(-) removal. *Sci. Total. Environ.* 812, 151471. doi: 10.1016/j.scitotenv.2021.151471

Jiang, S., Müller, M., Jin, J., Wu, Y., Zhu, K., Zhang, G. S., et al. (2019). Dissolved inorganic nitrogen in a tropical estuary in Malaysia: transport and transformation. *BIOGEOSCIENCES.* 16, 2821–2836. doi: 10.5194/bg-16-2821-2019

Joseph, N., Boyer, C. R., Kelble, P. B., and David, T. R. (2008). Phytoplankton bloom status: Chl-a biomass as an indicator of water quality condition in the southern estuaries of Florida. *U.S.A. Ecol. Indic.* 9 (6). doi: 10.1016/j.ecolind.2008.11.013

Kang, J. H., Lin, Y. L., Wang, Y., and Lan, W. L. (2020). Evaluation of the eutrophication level of marine environment in qinzhou bay and its effect on phytoplankton chlorophyll a. *Ocean. Dev. Management.* 37 (11), 67–74.

Kanuri, V. V., Muduli, P. R., Robin, R. S., Charan, K. B., Lova, R. A., Sivaji, P., et al. (2018). Bioavailable dis- solved organic matter and its spatio-temporal variation in a river dominated tropical brackish water lagoon, India. *Mar. Pollut. Bull.* 131, 460–467. doi: 10.1016/j.marpolbul.2018.04.059

Ke, S., Zhang, P., Ou, S. J., Zhang, J. X., Chen, J. Y., and Zhang, J. B. (2022). Spatiotemporal nutrient patterns, composition, and implications for eutrophication mitigation in the pearl river estuary, China. *Estuarine. Estuar. Coast. Shelf. S.* 226, 107749. doi: 10.1016/j.ecss.2022.107749

Lebo, M. E. (1991). Particle-bound phosphorus along an urbanized coastal plain estuary. *Mar. Chem.* 34, 225–246. doi: 10.1016/0304-4203(91)90005-H

Li, J. C. (2021). Influence of tidal action, typhoon and human activities on the circulation of biogenic elements in zhanjiang bay. (Zhanjiang: Master's dissertation Guangdong Ocean University.).

Li, K. Q., He, J., Li, J. L., Guo, Q., Liang, S. K., Li, Y. B., et al. (2018). Linking water quality with the total pollutant load control management for nitrogen in jiaozhou bay. *China. Ecol. Indicat.* 85, 57–66. doi: 10.1016/j.ecolind.2017.10.019

Li, S., Huang, Z. R., and Chen, Z. Z. (2015). Structural characteristics of phytoplankton communities in spring and autumn in shuidong bay. *South. Aquat. Science.* 11 (04), 27–33. doi: 10.3969/j.issn.2095-0780.2015.04.004

Li, Y., Li, D. J., Fang, T., and Wang, Y. M. (2008). Sunday Variation of chlorophyll a concentration in the Yangtze river estuary. *Mar. Bull.* 05), 30–34. doi: CNKI:SUN:HUTB.0.2008-05-007

Li, B. S., Li, C. X., Jin, Y. X., Ji, P., Zhao, X. L., and He, S. (2020). Evaluation of spatial and temporal distribution of nutrient salts and eutrophication in guanghai bay sea. *Mar. Environ. Sci.* 39 (05), 657–663.

Li, R. H., Liu, S. M., Zhang, G. L., Ren, J. L., and Zhang, J. (2013). Biogeochemistry of nutrients in an estuary affected by human activities: The wanquan river estuary, eastern hainan island. *China. Cont. Shelf. Res.* 57 (1), 18–3. doi: 10.1016/j.csr.2012.02.013

Li, K. Q., Ma, Y. P., Dai, A. Q., and Wang, X. L. (2017). Degradation dynamics and bioavailability of land-based dissolved organic nitrogen in the bohai Sea: Linking experiment with modeling. *Mar. Pollut. Bull.* 124 (2). doi: 10.1016/j.marpolbul.2017.02.033

Li, G. J., Ma, Y. L., Wei, Li, Wang, J. L., and Wei, H. (2012). Evaluation of nutrient distribution and potential eutrophication in bohai bay during spring. *J. Tianjin. Univ. Sci. Technology.* 27 (05), 22–27. doi: CNKI:SUN:TQYX.0.2012-05-006

Lin, P., Guo, L. D., and Chen, M. (2013). Distribution, partitioning and mixingbehavior of phosphorus species in the jiulong river estuary. *Mar. Chem.* 157, 93–105. doi: 10.1016/j.marchem.2013.09.002

Lin, G. M., and Lin, X. B. (2022). Bait input altered microbial community structure and increased greenhouse gases production in coastal wetland sediment. *Water Res.* 218, 118520. doi: 10.1016/j.watres.2022.118520

Liu, S. (2011). Diatom to dinoflagellate shift in the summer phytoplankton community in a bay impacted by nuclear power plant thermal effluent. *Mar. Ecol. Prog. Ser.* 424, 75–85. doi: 10.3354/meps08974

Liu, X. F., Duan, X. Y., Tian, Y., Cao, K., Gao, F., Yin, P., et al. (2021). Nutrient changes in the water column of sanmen bay and its response to human activities. *Front. Mar. Geol.* 37 (05), 46–56. doi: 10.16028/j.1009-2722.2020.052

Liu, Y. L., Gao, L., Chen, W. Q., Wang, T., and Li, D. J. (2017). Dynamics of nutrients in the northeastern east China sea in summer. *Oceanol. Limnol. Sin.* 48, 734–744.

Liu, F., Li, X. Q., Dong, G. C., Qin, Y. G., Chen, Y. G., Wang, Z. Z., et al. (2011). Study of water quality pollutants in coastal wetlands of the yellow river estuary. *China Environ. Sci.* 31 (10), 1705–1710.

Liu, S. M., Li, R. H., Zhang, G. L., Wang, D. R., Du, Z., Herbeck, L. S., et al. (2011). The impact of anthropogenic activities on nutrient dynamics in the tropical wenchanghe and wenjiaohe estuary and lagoon system in east hainan, China. *Mar. Chem.* 125 (1-4), 49–68. doi: 10.1016/j.marchem.2011.02.003

Li, C. L., Zhang, F., Shen, X., Yang, B., Shen, Z. L., and Sun, S. (2005). Concentration and distribution characteristics of chlorophyll in jiaozhou bay and its annual changes. *Ocean. Lake. Marsh.* 2005 (06), 21–28. doi: 10.3321/j.issn:0029-814X.2005.06.003

Li, J. L., Zheng, B. H., Zhang, S. Z., Jin, X. W., Hu, X. P., Liu, F., et al. (2016). Eutrophication characteristics and difference analysis of major estuarine bays in China. *China Environ. Sci.* 36 (02), 506–516. doi: 10.3969/j.issn.1000-6923.2016.02.030

Loh, A. N., and Bauer, J. E. (2000). Distribution, partitioning and fluxes of dissolved and particulate organic c, n and p in the eastern north pacific and southern oceans. *DEEP-SEA. Res. Pt. I.* 47 (12), 0–2316. doi: 10.1016/S0967-0637(00)00027-3

Lu, D. L., Kang, Z. J., Yang, B., Dan, S. F., Zhang, D., Zhang, P., et al. (2020). Compositions and spatio-temporal distributions of different nitrogen species and lability of dissolved organic nitrogen from the dafengjiang river to the sanniang bay. *China. Mar. Pollut. Bull.* 156, 111205. doi: 10.1016/j.marpolbul.2020.111205

Lu, D. L., Yang, N. N., Liang, S. K., Li, K. Q., and Wang, X. L. (2016). Comparison of land-based sources with ambient estuarine concentrations of total dissolved nitrogen in jiaozhou bay (China). *Estuar. Coast. Shelf. Sci.* 180, 82–90. doi: 10.1016/j.ecss.2016.06.032

Maryam, G., Behrooz, A., and Sara, G. (2021). Spatial distribution of nutrients and chlorophyll a across the Persian gulf and the gulf of Oman. *Ocean. Coast. Manage.*, 201, 105476. doi: 10.1016/j.ocecoaman.2020.105476.

Mesfioui, R., Love, N. G., Bronk, D. A., Mulholland, M. R., and Hatcher, P. G. (2012). Reactivit and chemical characterization of effluent organic nitrogen from

wastewater treatment plants determined by Fourier transform ion cyclotron resonance mass spec-trometry. *Water Res.* 46, 622–634. doi: 10.1016/j.watres.2011.11.022

Moneta, A., Veuger, B., Van Rijswijk, P., Meysman, F. J. R., Soetaert, K., and Middelburg, J. J. (2014). Dissolved inorganic and organic nitrogen uptake in the coastal north Sea: A seasonal study. *Eestuar. Coast. Shelf.* S. 147, 78–86. doi: 10.1016/j.ecss.2014.05.022

Niu, L. X., Gelder, P.H.A.J.M., Zhang, C. K., Guan, Y. Q., and Vrijling, J. K. (2016). Physical control of phytoplankton bloom development in the coastal waters of jiangsu (China). *Ecol. Model.* 321, 75–83. doi: 10.1016/j.ecolmodel.2015.10.008

Passeri, D. L., Hagen, S. C., Medeiros, S. C., and Bilskie, M. V. (2015). Impacts of historic morphology and sea level rise on tidal hydrodynamics in a microtidal estuary (Grand bay, Mississippi). *CONT. SHELF. Res.* 111, 150–158. doi: 10.1016/j.csr.2015.08.001

Peng, B. J. (1987). Asymmetry of flow velocity in the tidal channel of the eastern part of the western guangdong water and analysis of flow simulation. *Mar. Sci.* 06), 17–22.

Pisam, O., Boyer, J. N., Podgorski, D. C., Thomas, C. R., Coley, T., and Jaffeet, R. (2017). Molecular composition and bioavailability of dissolved organic nitrogen in a lake flow-influenced river in south Florida, USA. *Aquatic. Sci.* 79, 891–908. doi: 10.1007/s00027-017-0540-5

Qi, X. H., Liu, M. S., Zhang, J., Ren, J. L., and Zhang, G. L. (2011). Cycling of phosphorus in the jiaozhou bay. *Acta Oceanologica. Sinica.* 30 (2), 62–74. doi: 10.1007/s13131-011-0106-7

Qin, F. S., Yang, Z. G., Yao, S. S., and Li, S. (2014). Simulation study on the effect of comprehensive improvement project on water and sand dynamics in shuidong bay of maoming city. *China Harbour. Engineering.* 3, 51–56. doi: 10.7640/zggwjs201403010

Qu, F., Liu, M., Hou, L. J., Xu, S. Y., Liu, Q. M., and Ou, D. N. (2007). Changes of overlying water environmental factors and nitrogen nutrients under the influence of tidal cycle and their correlation. *Resour. Environ. Yangtze. Basin.* 3, 345–350. doi: 10.3969/j.issn.1004-8227.2007.03.016

Rabalais, N. N., Turner, R. E., JustiĆ, D., Quay, D., William J, W., and Sen Gupta, B. K. (1996). Nutrient changes in the Mississippi river and system responses on the adjacent continental shelf. *Estuaries.* 19 (2), 386–407. doi: 10.2307/1352458

Sánchez-Carrillo, S., Sánchez-Andrés, R., Alatorre, L. C., Angeler, D. G., M Álvarez-Cobelas, J. A., and Arreola-Lizárraga, (2009). Nutrient fluxes in a semi-arid microtidal mangrove wetland in the gulf of california. *Estuar. Coast. Shelf. S.* . 82 (4), 654–662. doi: 10.1016/j.ecss.2009.03.002

Santos, I. R. S., Burnett, W. C., and Chanton, J. (2008). Nutrient biogeochemistry in a gulf of Mexico subterranean estuary and groundwater - derived fluxes to the coastal ocean. *Limnol. Oceanogr.* 53 (2), 705–718. doi: 10.4319/lo.2008.53.2.0705

Seitzinger, S. P., and Sanders, R. W. (1997). Contribution of dissolved organic nitrogen from rivers to estuarine eutrophication. *Mar. Ecol. Prog. Ser.* 159, 1–12. doi: 10.3354/meps159001

Shi, Y. Z., Zhang, C. X., Zhang, J. B., Chen, C. L., Zhao, L. R., and Sun, S. L. (2017). Characteristics of tidal distribution of phytoplankton and its relationship with environmental factors in the sea of shuidong bay. *J. Ecol.* 37 (18), 5981–5992. doi: 10.5846/stxb201606291286

Song, D. H., Wang, X. H., Andrew, E., and Bao, X. W. (2011). The contribution to tidal asymmetry by different combinations of tidal constituents. *J. Geophys. Res-Oceans.* 116 (C12), C12007. doi: 10.1029/2011JC007270

Stedmon, C. A., Markager, S., Tranvik, L., Kronberg, L., TSlätis, T., and Martinsen, W. (2007). Photochemical production of ammonium and transformation of dissolved organic matter in the Baltic Sea. *Mar. Chem.* 104, 227–240. doi: 10.1016/j.marchem.2006.11.005

Strokal, M., Kroeze, C., Wang, M., and Ma, L. (2017). Reducing future river export of nutrients to coastal waters of China in optimistic scenarios. *Sci. Total. Environ.* 579, 517–528. doi: 10.1016/j.scitotenv.2016.11.065

Sui, Q., Xia, B., Xie, H. B., Cui, Y., Chen, B. J., Cui, Z. G., et al. (2016). Study on temporal and spatial variation of nutrients and evaluation on eutrophication in the seawater of the bohai Sea in winter and spring of 2014. *Prog. Fishery. Sci.* 37 (02), 10–15. doi: 10.11758/yykxjz.20150309002

Sun, S. (2008). Distribution of nutrients and exchange fluxes at the sediment-water interface in the East and yellow seas. *China Ocean. Univ*. doi: 10.7666/d.y1338095

Sun, P. X., Wang, Z. L., Zhan, R., Xia, B., and Wang, X. Q. (2005). Distribution and eutrophication of inorganic nitrogen in the seawater of jiaozhou bay. *Adv. Mar. Sci.* 04), 466–471.

Tang, S. M., Yan, Y., and Chen, B. (2013). Effects of warm water drainage from daya bay nuclear power plant on the structure of marine phytoplankton community in spring and summer. *J. Oceanogr.* 32 (03), 373–382. doi: 10.3969/J.ISSN.2095-4972.2013.03.010

Tian, X. P. (1990). The role of jet diffusion of outflow water from tidal channels on the formation of barrage sand. *J. Zhongshan. University. Nat. Sci. Ed.* 03), 177–182. doi: CNKI:SUN:ZSDZ.0.1990-03-028

Turner, R. E., Rabalais, N. N., Alexander, R. B., Mcisaac, G., and Howarth, R. W. (2007). Characterization of nutrient, organic carbon, and sediment loads and concentrations from the Mississippi river into the northern gulf of Mexico. *Estuar. Coast.* 30 (5), 773–790. doi: 10.1007/BF02841333

Wang, C. Y. (2019). Investigation of water quality conditions in the main bays of zhangzhou city and evaluation of eutrophication. *Fish. Res.* 41 (06), 526–531. doi: 10.14012/j.cnki.fjsc.2019.06.010

Wang, X. P., Jia, X. P., Lin, Q., Li, C. H., Gan, J. L., Cai, W. G., et al. (1999). Characteristics and interrelationships of dissolved oxygen, pH, salinity and nutrient distribution in honghai bay. *Mar. Bull.* 5, 35–40. doi: 10.3969/j.issn.1001-6392.1999.05.005

Wang, J. N., Li, X. Y., Yan, W. J., Chen, L., and Zhang, Z. (2016). Nitrogen balance and dissolved inorganic nitrogen fluxes in the Yangtze river basin based on MEA scenarios: Integrated watershed-estuary/bay nitrogen management. *J. Environ. Sci.* 36 (01), 38–46. doi: 10.13671/j.hjkxxb.2015.0449

Watson, P. G., Frickers, P. E., and Howland, R. J. M. (1993). Benthic fluxes of nutrients and some trace metals in the Tamar estuary, SW England. *Neth. J. Aquat. Ecol.* 27, 135–146. doi: 10.1007/BF02334776

White, A. E., Foster, R. A., Benitez-Nelson, C. R., Masqué, P., Verdeny, E., Popp, B. N., et al. (2013). Nitrogen fixation in the gulf of California and the Eastern tropical north pacific. *Prog. Oceanogr.* 109, 1–17. doi: 10.1016/j.pocean.2012.09.002

Wu, M. L. (2014). *Study on the distribution characteristics of nutrient salts and its impact on the ecosystem in the northern part of beibu bay* (Xiamen: Xiamen Ocean University).

Wu, H., Zhu, J. R., Shen, J., and Wang, H. (2011). Tidal modulation on the changjiang river plume in summer. *J. Geophys. Res-Oceans.* 116 (8), C08017. doi: 10.1029/2011JC007209

Xia, H. Y., Lin, D. Y., and Niu, Z. W. (2007). Prediction of effects of tidal and reclamation on the seabed erodion-accretions in the zhanjiang bay. *Mar. Sci. Bull.* 1, 61–66. doi: 10.3969/j.issn.1001-6392.2007.01.010

Xin, M., Wang, B. D., Sun, X., and Xie, L. P. (2010). The distribution characteristics and seasonal variation of nutrients in guangxi coastal area. *Mar. Sci.* 34 (9), 5–9.

Xiu, B., Liang, S. K., He, X. L., Wang, X. K., Cui, Z. G., and Jiang, Z. J. (2019). Bioavailability of dissolved organic nitrogen and its uptake by ulva prolifera: Implications in the outbreak of a green bloom off the coast of qingdao, China. *Mar. Pollut. Bull.* 140, 563–572. doi: 10.1016/j.marpolbul.2019.01.057

Xu, H. Y., Wang, B. D., Xin, M., Sun, X., Wang, Z. X., Chen, C., et al. (2020). Long-term changes of nutrient salinity in jiaozhou bay and its ecological effects. *Adv. Mar. Science.* 38 (02), 276–286. doi: 10.3969/j.issn.1671-6647.2020.02.008

Yang, B., Gao, X., Zhao, J., Lu, Y., and Gao, T.. (2020). Biogeochemistry of dissolved inorganic nutrients in an oligotrophic coastal mariculture region of the northern Shandong peninsula, north yellow Sea. *Mar. Pollut. Bull.* 50, 110693. doi: 10.1016/j.marpolbul.2019.110693

Yang, L. Z., Liu, H. K., Ren, J., and Yu, F. H. (2011). Preliminary study on two-way jet system in the near-shore waters of shuidong bay. *Acta Scientiarum. Naturalium. Universitatis. Sunyatseni.* 50 (02), 116–119.

Yang, X. L., and Zhu, M. Y. (1990). New progress of phytoplankton nutrient metabolism research. *Adv. Mar. Science.* 03), 65–74.

Yin, K. D., and Harrison, P. (2000). Influences of flood and ebb tides on nutrient fluxes and chlorophyll on an intertidal flat. *Mar. Ecol. Prog. Ser.* 196 (3), 75–85. doi: 10.3354/meps196075

Yuan, Q., Xu, Z. Y., Peng, H. Q., Lu, J. M., Huang, L. C., Liang, X. J., et al. (2016). Study on the trends of nitrogen and phosphorus in seawater in zhanjiang bay and its nearby waters in the past 5 years. *J. Green Sci. Technology.* 24), 41–45. doi: CNKI:SUN:LVKJ.0.2016-24-016

Yu, Y., Song, J. M., Li, X. G., Yan, H. M., and Li, N. (2012). Distribution, sources and budgets of particulate phosphorus and nitrogen in the East China Sea. *Cont. Shelf. Res.* 43, 142–155. doi: 10.1016/j.csr.2012.05.018

Zhang, P., Chen, Y., Peng, C. H., Dai, P. D., Lai, J. Y., Zhao, L. R., et al. (2020b). Spatiotemporal variation, composition of DIN and its contribution to eutrophication in coastal waters adjacent to hainan island, China. *Reg. Stud. Mar. Sci.* 37, 101332. doi: 10.1016/j.rsma.2020.101332

Zhang, P., Dai, P. D., Zhang, J. B., Li, J. X., Zhao, H., and Song, Z. G. (2021). Spatiotemporal variation, speciation, and transport flux of TDP in leizhou peninsula coastal waters, south China Sea. *Mar. Pollut. Bull.*, 167. doi: 10.1016/j.marpolbul.2021.112284

Zhang, P., Peng, C., Zhang, J., Zhang, J., Chen, J., and Zhao, H. (2022). Long-term harmful algal blooms and nutrients patterns affected by climate change and anthropogenic pressures in the zhanjiang bay, China. *Front. Mar. Sci.* 9, 849819. doi: 10.3389/fmars.2022.849819

Zhang, P., Wei, L. R., Lai, J. Y., Dai, P. D., Chen, Y., and Zhang, J. B. (2019b). Concentration, composition and fluxes of land-based nitrogen and phosphorus source pollutants input into zhanjiang bay in summer. *J. Guangdong. Ocean. U.* 39 (4), 46–55. doi: 10.3969/j.issn.1673-9159.2019.04.000

Zhang, P., Xu, J. L., Zhang, J. B., Li, J. X., Zhang, Y. C., Li, Y., et al. (2020c). Spatiotemporal dissolved silicate variation, sources, and behavior in the eutrophic zhanjiang bay, China. *Water-Sui.* 12 (12), 3586–3586. doi: 10.3390/w12123586

Zhang, J. B., Zhang, P., Dai, P. D., Lai, J. Y., and Chen, Y. (2019). Spatial and temporal distribution of dissolved inorganic phosphorus and eutrophication in the nearshore waters of hainan island. *J. Environ. Sci-china.* 39 (06), 2541–2548. doi: CNKI:SUN:ZGHJ.0.2019-06-041

Zhang, Y. Y., Zhang, J., Wu, Y., and Zhu, Z. Y. (2007b). Characteristics of dissolved oxygen and its affecting factors in the Yangtze estuary. *Environ. Sci.* 28 (8), 1649–1654. doi: 10.3321/j.issn:0250-3301.2007.08.001

Zhang, J. B., Zhang, Y. C., Zhang, P., Li, Y., Li, J. X., Luo, X. Q., et al. (2020). Seasonal phosphorus variation in coastal water affected by the land-based sources input in the eutrophic zhanjiang bay, China. *Estuar. Coast. Shelf.* S, 252. doi: 10.1016/J.ECSS.2021.107277

Zhang, Y. J., Zhao, R. D., Hu, Y. C., Liang, S. K., and Wang, X. L. (2016). The influence of typhoon- induced precipitation on biogenic element supplementary and distribution of jiaozhou bay. *China. J. Ocean. U. China* 46 (4), 79–88.

Zhao, W. H., Jiao, N. Z., and Zhao, Z. X. (2000). Distribution and dynamics of nutrient salts in the cultured waters of yantai shiliwan. *Mar. Sci.* 4, 31–34. doi: CNKI:SUN:HYKX.0.2000-04-010

Zhao, X. D., Zhu, C. J., and Shi, Z. L. (1998). The forms and distributions of nitrogen of seawater in eastern jiaozhou bay. *Mar. Sci.* 01), 40–44. doi: CNKI:SUN:HYKX.0.1998-01-016

Zheng, X. H. (2010). Changes in nitrogen and phosphate and eutrophication character in minjiang estuary. *J. Oceanogr. Taiwan. Strait.* 29 (1), 42–46. doi: 10.1080/09500340.2010.529951

Zhong, H. G., and Li, P. (2014). Study on the dynamics of total nitrogen and total phosphorus in coastal waters of sanya bay, dadonghai and yalong bay. *Hebei. Fishery.* 05), 12–14+26. doi: 10.3969/j.issn.1004-6755.2014.05.005

Zhou, M. (2021). Study on the spatial and temporal distribution of chlorophyll a and nutrient salts and potential eutrophication in Zhanjiang Bay sea surface in autumn 2017-2020. *Guangdong. Ocean. Univ.* doi: 10.27788/d.cnki.ggdhy.2021.000178

Zhou, W. H., Huo, W. Y., Yuan, X. C., and Yin, K. D. (2003). Distribution features of chlorophyll a and primary productivity in high frequency area of red tide in East China Sea during spring. *J. Appl. Ecol.* 14 (7), 1055–1059.

Zhou, Y., Wang, L. L., Zhou, Y. Y., and Mao, X. Z. (2020). Eutrophication control strategies for highly anthropogenic influenced coastal waters. *Sci. Total. Environ.* 705, 135760. doi: 10.1016/j.scitotenv.2019.135760

Zhou, C. F., Yuan, G. W., Peng, M., and Zhang, P. (2022). Characteristics, composition and nutrient level evaluation of nitrogen and phosphorus nutrient distribution in the sea adjacent to qidong, jiangsu. *Environ. pollut. Control.* 44 (01), 104–110. doi: 10.15985/j.cnki.1001-3865.2022.01.018

Zhou, C. H., Zhang, J. P., Huang, X. P., Zhao, C. Y., and Wu, Y. C. (2019). Spatial and temporal distribution, key influencing factors and potential ecological significance of particulate nitrogen and phosphorus in daya bay. *Mar. Environ. Sci.* 38 (05), 696–702+711. doi: CNKI:SUN:HYHJ.0.2019-05-008

Zhou, M., and Zhao, H. (2021). Characteristics of spatial and temporal distribution of chlorophyll a concentration in zhanjiang bay in autumn and its correlation with environmental factors. *J. Guangdong. Ocean. Univer.* 41 (06), 25–35.

frontiers | Frontiers in Marine Science

TYPE Original Research
PUBLISHED 02 September 2022
DOI 10.3389/fmars.2022.982051

OPEN ACCESS

EDITED BY
Jing Wei,
Sun Yat-sen University, China

REVIEWED BY
Anirban Chakraborty,
Idaho State University, United States
Alberto Sánchez-González,
Instituto Politécnico Nacional (IPN), Mexico

*CORRESPONDENCE
Hong-Chun Li
hcli1960@ntu.edu.tw

†These authors have contributed equally to this work

SPECIALTY SECTION
This article was submitted to Marine Biogeochemistry, a section of the journal Frontiers in Marine Science

RECEIVED 30 June 2022
ACCEPTED 10 August 2022
PUBLISHED 02 September 2022

CITATION
Xu H, Li D-W, Li H-C, Zhao M, Berelson WM, Jin G'e, Li L and Misra S (2022) Local and remote forcing on the interannual variations of the sedimentary $\delta^{15}N$ in Santa Barbara Basin during the past 80 years. *Front. Mar. Sci.* 9:982051. doi: 10.3389/fmars.2022.982051

Local and remote forcing on the interannual variations of the sedimentary $\delta^{15}N$ in Santa Barbara Basin during the past 80 years

Hanyue Xu[1,2†], Da-Wei Li[1,2†], Hong-Chun Li[1,3*], Meixun Zhao[1,2], William M. Berelson[4], Gui'e Jin[1], Li Li[1] and Satabdi Misra[3]

[1]Frontiers Science Center for Deep Ocean Multispheres and Earth System, and Key Laboratory of Marine Chemistry Theory and Technology, Ministry of Education, Ocean University of China, Qingdao, China, [2]Laboratory for Marine Ecology and Environmental Science, Qingdao National Laboratory for Marine Science and Technology, Qingdao, China, [3]Department of Geosciences, National Taiwan University, Taipei, Taiwan, [4]Department of Earth Sciences, University of Southern California, Los Angeles, CA, United States

Sedimentary nitrogen isotope ($\delta^{15}N_{sed}$) in Santa Barbara Basin (SBB) has been mostly interpreted as the record of the eastern tropical North Pacific (ETNP) intermediate water denitrification process. Nevertheless, debate remains regarding sources and control mechanisms of $\delta^{15}N_{sed}$ signal in SBB. Multi-proxy analyses including $\delta^{15}N_{sed}$, total organic carbon (TOC), total nitrogen (TN), C/N ratio, and marine biomarkers were performed on a 46-cm sediment core (SBB-190629) collected from SBB in 2019. The core was dated with varve counting and ^{210}Pb dating method, showing a depositional history of 1938–2019 CE with a sedimentation rate of 0.564 cm/year. The findings show that the $\delta^{15}N_{sed}$ record (at ~0.25-year resolution) ranges from 6.24‰ to 7.43‰, which was affected by both local and remote forcing. The long-term variations of the SBB $\delta^{15}N_{sed}$ signature show a general decreasing trend from 1940 to the late 1980s, low values during 1980~2000, and an increase afterward, which is thought to reflect changes in ETNP denitrification induced by the strength of tropical trade winds. Our results also reveal a series of abrupt annual to multiannual changes, superimposed on the long-term variation mentioned above. The SBB local $\delta^{15}N$ signal ($\Delta\delta^{15}N_{SBB}$) is accessed by using the deviation from the mean $\delta^{15}N$ ($\Delta\delta^{15}N$) of SBB-190629 to subtract the $\Delta\delta^{15}N$ of the ETNP. The $\Delta\delta^{15}N_{SBB}$ record compares well with redox-sensitive proxies (Re/Mo ratio and C_{29} stanol/stenol ratio) from the SBB bottom water and with the OC_{marine} content calculated based on the C/N ratio mixing model, indicating that the $\Delta\delta^{15}N_{SBB}$ is mainly controlled by bottom water denitrification, which was induced by the change of upwelling intensity and marine productivity. Since

various climatic factors (e.g., El Niño–Southern Oscillation (ENSO), Pacific Decadal Oscillation (PDO), and North Pacific Gyre Oscillation (NPGO)) have different impacts on the upwelling intensity (hence the marine productivity and denitrification) in SBB on different timescales, the influence of combined climatic factors on SBB denitrification is time dependent.

KEYWORDS

$\delta^{15}N_{sed}$ variation, denitrification, Santa Barbara Basin, climatic forcing, Eastern Tropical Northern Pacific ventilation

1 Introduction

In a marine system under oxygen-deficient conditions, e.g., eastern tropical North Pacific (ETNP), microbial activity converts bioavailable nitrate (NO_3^-) to nitrogen (N_2) *via* the denitrification process. The intensity of the oxygen-deficient zone (ODZ) controls water column denitrification, as nitrate becomes the favorable electron acceptor after dissolved O_2 is exhausted during microbially regulated organic carbon (OC) remineralization (Altabet et al., 1999; Ward, 2011; Horak et al., 2016; Margolskee et al., 2019). During the denitrification process, ^{14}N is preferentially removed from the water column, and ^{15}N is progressively enriched in the remaining nitrate pool (Altabet, 2006; Davis et al., 2019; Wang et al., 2019). Therefore, with a stronger ODZ, the water column denitrification is stronger, which creates a more positive $\delta^{15}N$ of the water column. The $\delta^{15}N_{nitrate}$-enriched water from the ODZ is upwelled into the photic zone and incorporated into phytoplankton. After the death of the phytoplankton, the organic matter with a high $\delta^{15}N$ signal *via* sinking particles is preserved in the marine sediment (Rayner et al., 2003; Wang et al., 2019). Under the circumstance of complete nitrate utilization (biological fractionation effects are negligible) and the absence of sedimentary diagenesis, such changes can be recorded in marine sedimentary $\delta^{15}N$ ($\delta^{15}N_{sed}$) (Altabet et al., 1999; Emmer and Thunell, 2000; Thunell and Kepple, 2004; Ward, 2011; Horak et al., 2016; Davis et al., 2019; Margolskee et al., 2019; Wang et al., 2019; Sánchez et al., 2022). Hence, in regions where these conditions are met, $\delta^{15}N_{sed}$ is accepted as a proxy for the integrated rates of denitrification and the volume of the ODZ: when the ODZ is expanded and the water column denitrification is intensified, the $\delta^{15}N_{sed}$ increases (Emmer and Thunell, 2000; Tems et al., 2015; Horak et al., 2016; Davis et al., 2019; Wang et al., 2019; Sánchez et al., 2022).

Santa Barbara Basin (SBB; Figure 1A) is located between the California Coast to the north and the Channel Islands to the south, particularly in the Southern California Bight (Emmer and Thunell, 2000; Hendy et al., 2015; Osborne et al., 2016; Davis et al., 2019; Wang et al., 2019). It is a shallow nearshore basin with a maximum depth of ~600 m. The basin is bordered with narrow sills to the west (~475-m depth) and east (~230-m depth), which further reduces ventilation combined with the re-mineralization of organic matter, creating an anoxic water environment (dissolved oxygen<0.1 ml/L) below the sills (Emmer and Thunell, 2000; Bograd et al., 2002; Goericke et al., 2015). The high sedimentation rate and anoxic depositional environment minimize bioturbation, creating high-resolution and low sedimentary diagenesis records in SBB (Hendy et al., 2015; Sarno et al., 2020). A minimal (<1‰) offset between the sediment trap $\delta^{15}N$ time series and down core $\delta^{15}N_{sed}$ records in SBB provides further support that diagenetic isotopic alteration on $\delta^{15}N_{sed}$ is negligible (Altabet et al., 1999; Emmer and Thunell, 2000; Davis et al., 2019; Wang et al., 2019). Furthermore, previous studies show that nitrogen utilization is complete in SBB surface waters throughout the year except in spring. During the spring, a large amount of nutrients is brought by upwelling, which may affect nitrogen utilization in the surface water. However, all of the upwelled nitrate is completely utilized on interannual scales (Emmer and Thunell, 2000; Davis et al., 2019). Therefore, $\delta^{15}N_{sed}$ from the SBB records the variation of $\delta^{15}N$ in the water column and is a good potential indicator of changes in ODZs and water column denitrification on longer than annual scales in the past.

The $\delta^{15}N$ (and $\delta^{15}N_{sed}$) value of the water column (sediment) in SBB is affected by several factors. In near-surface circulation (upper 100 m) of SBB, the interaction between the cold southward flowing California Current (CC) and relatively warm northward flowing countercurrents (Davidson current) creates a semi-permanent cyclonic gyre. Annual variations in the strength of the two surface currents under climatic forcing such as El Niño/La Niña and Pacific Decadal Oscillation (PDO) strongly affect the degree of upwelling, thermocline depth, and biological productivity within the basin and in turn influence water column denitrification and $\delta^{15}N$ value (Liu and Kaplan, 1989; Tems et al., 2015; Davis et al., 2019; Wang et al., 2019). Between depths of 100 and 400 m, the highly saline, anoxic, and $\delta^{15}N$-enriched waters originating from the ETNP zone are deflected to SBB through the California Undercurrent (CUC)

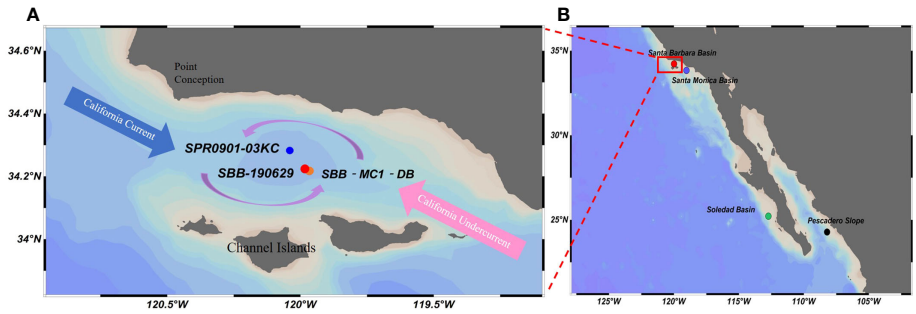

FIGURE 1
(A) Map of Santa Barbara Basin and the surrounding region, showing sampled and referred core locations in Santa Barbara Basin (SBB). Red circle (●), core SBB-190629 (this study); blue circle (●), core SPR0901-03KC from Wang et al. (2019); orange circle (●), core SBB-MC1-DB from Davis et al. (2019). Major currents are mentioned in the text. **(B)** Locations of core sites along the North American margin are referred to in this study. Red circle (●), Santa Barbara Basin core location in this study. Purple circle (●), Santa Monica Basin core location from Davis et al. (2019). Green circle (●), Soledad Basin core location from Deutsch et al. (2014). Black circle, Pescadero Slope core location from Deutsch et al. (2014). Red box indicates SBB region and is enlarged in panel A.

(Figure 1A). The ETNP has the largest volume of low-O_2 waters of all ODZs along the equator to mid-latitude in the northeastern Pacific (Horak et al., 2016); fluctuations of the intensity of denitrification in the ETNP are reflected on water $\delta^{15}N$ and advected to SBB. Compared with the denitrified water from ETNP, CC input with lower $\delta^{15}N$ is considered a relatively stable end-member on decadal scales in the nitrogen isotopic mass balance of the SBB input water. Therefore, in this study, the ETNP $\delta^{15}N$ variation represents the distal signal (or remote forcing) in SBB $\delta^{15}N$ budget. Finally, the SBB bottom waters (>475 m) are derived from North Pacific Intermediate Water (NPIW), which periodically flows over the deepest sill and further complicates the water column oxygen content and denitrification in SBB.

Previous studies have focused on the SBB $\delta^{15}N_{sed}$ records as the distal signal of ETNP denitrification. However, some studies show that variation of $\delta^{15}N_{sed}$ in SBB is associated not only with the change of ETNP ODZ but also with oxygen loss along the California Margin (Liu and Kaplan, 1989; Emmer and Thunell, 2000; Deutsch et al., 2014; Tems et al., 2015; Davis et al., 2019). In the study of Davis et al. (2019), the $\delta^{15}N_{sed}$ record of core SBB-MC1-DB (Figure 1A) covering a sedimentary history of 1892–2017 CE was used to examine the decadal-scale variability (via Walker Circulation) and long-term anthropogenic forcing to $\delta^{15}N$ signals; the difference of $\delta^{15}N_{sed}$ between ETNP and SBB was the result of anthropogenic forced changes; however, factors of regional oceanography may be a candidate but ignored. Wang et al. (2019) combined $\delta^{15}N_{sed}$ records (SPR0901-03KC in Figure 1A) of the SBB with additional productivity proxies to assess local and remote forcing of denitrification in the Northeast Pacific for the last 2,000 years. They suggest that wind curl upwelling (local signal) contributes to Southern California's primary productivity and denitrification process, especially during weak coastal upwelling intervals. However, the resolution and chronological coverage of the core SPR0901-03KC $\delta^{15}N_{sed}$ record was not able to compare with instrumental climatic records. Furthermore, recent studies have identified an increase in water column denitrification in the bottom waters of SBB (Goericke et al., 2015; White et al., 2019), and the $\delta^{15}N$ signal could be transported into the upper water column *via* eddy diffusion and upwelling. Hence, understanding of $\delta^{15}N$ variation on annual-to-decadal timescales and its influencing factors in SBB requires further investigation.

The present study aims to detect the local $\delta^{15}N$ signal from the $\delta^{15}N_{sed}$ record and understand the role of climatic fluctuations and oceanic upwelling on interannual $\delta^{15}N$ variations in SBB. To do this, a 46-cm-long sediment core spanning 80 years of depositional history was sampled at a high resolution (every ~0.25 years) and analyzed for nitrogen isotopic signature. The local $\delta^{15}N$ signals are separated from the bulk $\delta^{15}N_{sed}$ throughout the comparison with the distal $\delta^{15}N$ signals of the ETNP denitrification records published in the previous literature. Then, the variation of the SBB local $\Delta\delta^{15}N$ ($\Delta\delta^{15}N_{SBB}$) signals is compared with several geochemical parameters {$(Re/Mo)_{EF}$, C_{29} stanol/stenol ratio, marine OC, marine biomarkers} to understand changes in redox condition, O_2 content, and productivity in SBB. The role of climatic indices such as PDO, North Pacific Gyre Oscillation (NPGO), and El Niño–Southern Oscillation (ENSO) as influencing factors in shaping $\delta^{15}N_{sed}$ signatures of the SBB is comprehensively discussed.

2 Methods

2.1 Core SBB-190629 and sampling

Core SBB-190629 (34°13.4′N, 119°58.99′W; 583-m depth) was collected on board the *RV Oceanus* by a multi-core device

from SBB on 29 June 2019. The core was 46 cm long and contained clear laminations (Figure 2A). It was split in half and kept in a cold room at 4°C in the Department of Earth Sciences at the University of Southern California (USC). Half of the core was transported to the Department of Geosciences at the National Taiwan University (NTU) in February 2020. During the transportation, the sediments were contracted from 46 to 35 cm. Therefore, sampling depths were calibrated back to the original depths (Figure 2B). In Figure 2A, the depth scale of the core was the original depth. In Figure 2B, the depth scale of the core was the depth of the core at sampling time. The original depth of the core changed from 46 to 35 cm after the contraction. However, the main features of the color changes in the core sediments remained. Therefore, the depth correlations were able to be established (see the dashed lines in Figures 2A, B). With the correlated controlling depths, the relationship between sampling depth (D_1) and original depth (D_0) was $D_1 = 0.1408 + 0.6193 \times D_0 + 0.0037 \times D_0^2$ ($R^2 = 1.00$).

The half core was subsampled at a 1-cm interval for ^{210}Pb dating and biomarker analysis and then subsampled at a 2–3-mm interval (roughly four samples within 1 cm) for fine-resolution total organic carbon (TOC), total nitrogen (TN), and δ^{15}N analyses. A total of 160 subsamples had been obtained. All sediment samples were freeze-dried by a freeze vacuum dryer (model EYELA FDU-1200), then ground, and mixed well. All dried samples were stored in a refrigerator at 8°C until analysis.

2.2 ^{210}Pb dating

A total of 22 horizons of the core were analyzed for ^{210}Pb dating through a high-resolution ORTEC GEM-FX8530P4 gamma spectrometer with a 10-cm-thick low-background lead shield in the NTUAMS Lab at NTU. The energy of ^{210}Pb, ^{226}Ra, ^{214}Pb, and ^{214}Bi peaks in the gamma spectrometer was at 46, 186, 351, and 610 keV, respectively. Each dry sample (weighing ranging from 5 to 10 g) in a plastic sample container was placed on top of the detector. Counting efficiency, geometry, and density effects of the detector were calibrated by various standards. Supported ^{210}Pb activity was determined by either the ^{226}Ra activity or activity of (^{214}Pb + ^{214}Bi)/2 in the sample measurements (Li et al., 2019). The excess ^{210}Pb equals total ^{210}Pb activity minus either ^{226}Ra activity or activity of (^{214}Pb + ^{214}Bi)/2. The results are shown in Figure 2C and listed in Supplementary Table S1.

2.3 Total organic carbon, total nitrogen, and δ^{15}N analysis

Sediment samples were taken at 2–3-mm intervals for TOC, TN, and δ^{15}N analyses. The samples were treated with 0.5 mol/L of HCl for removal of carbonates and subsequently rinsed with Milli-Q water repeatedly until a pH of 7 was reached. After that, the samples were centrifuged to remove water and then oven-dried at 50°C for 48 h. Then, a small amount (approximately 5–10 mg) of

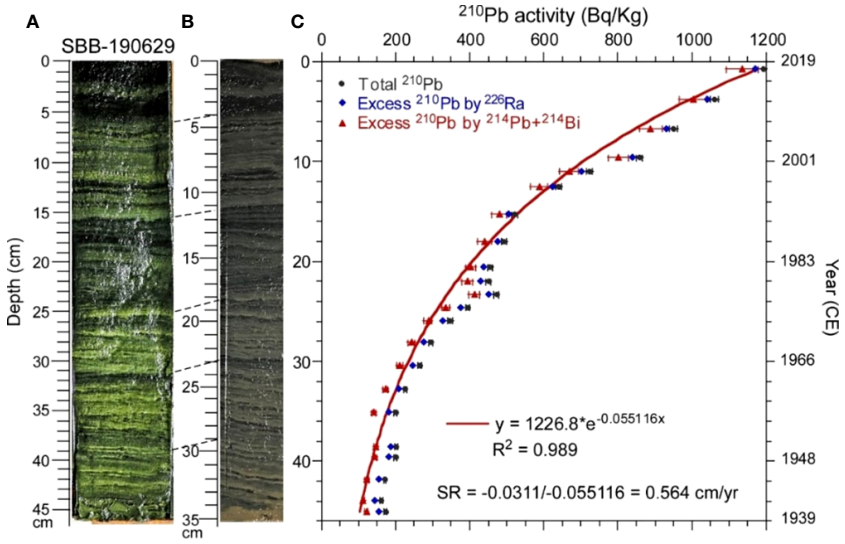

FIGURE 2
Photos and ^{210}Pb profile of core SBB-190629. **(A)** Photo of the core before transportation to National Taiwan University (NTU). **(B)** Photo of the core after transportation to NTU. **(C)** ^{210}Pb profile. The constructed ages are shown on the right-hand side of the plot. Red line represents the fitting curve.

samples were taken and placed in a tinfoil boat and analyzed for TOC and TN contents with an Elemental Analyzer FLASH 2000 at Ocean University of China (OUC) with a standard deviation of ±0.02 wt.% (n = 6), determined by replicate analysis of atropine (Thermo Fisher Scientific, Breda, Netherlands) and a low organic content soil (Elemental Microanalysis Ltd., Okehampton, UK). Other 0.5~1 mg samples were placed in a tinfoil boat and analyzed for $\delta^{15}N$ on EA-IRMS (FLASH EA 1112 series coupled with Thermo Fisher Delta V continuous flow isotopic ratio mass spectrometer) at OUC. Measured $\delta^{15}N$ values were calibrated against nitrogen isotope standards N-1 ($\delta^{15}N$ = 0.40‰) and USGS-40 ($\delta^{15}N$ = −4.52‰).

$$\delta^{15}N = \left[\left({}^{15}N/{}^{14}N_{sample}\right)/\left({}^{15}N/{}^{14}N_{standard}\right) - 1\right] \times 1{,}000 \quad (1)$$

The precision of the $\delta^{15}N$ measurements is reflected by the standard deviation of the duplicated N-1 and USGS-40 measurements, which is less than ±0.10‰ (n = 6). The results of TOC, TN, and $\delta^{15}N$ are shown in Figure 3 and listed in Supplementary Table S2.

2.4 Biomarker analysis

Total lipids were extracted from freeze-dried sediment samples (0.15–0.25 g) by using a dichloromethane and methanol (3:1 v/v) mixture utilizing ultrasonication (15 min). After that, an internal standard mixture containing C_{19} *n*-alkanol and *n*-$C_{24}D_{50}$ was added to the samples. The total lipid extracts were extracted by centrifuge. The extracts were then hydrolyzed with 6% KOH in MeOH. The non-polar lipid fractions were eluted with 8 ml of hexane using silica gel chromatography and then subsequently dried under a gentle N_2 stream. The alcohol lipid fractions (containing marine phytoplankton biomarkers) were further eluted with 12 ml of

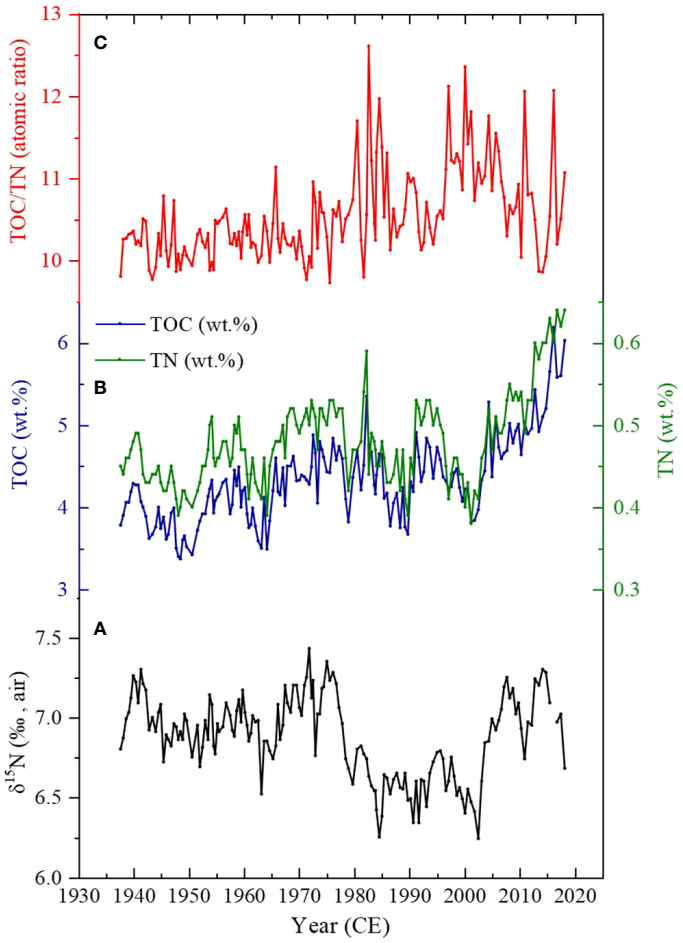

FIGURE 3
TOC, TN, and $\delta^{15}N$ variation of the core SBB-20190629. **(A)** $\delta^{15}N$ variation in core SBB-190629. **(B)** Total organic carbon (TOC, wt.%) and total nitrogen (TN, wt.%) records from SBB-20190629. **(C)** C/N atomic ratio (atom ratio of TOC/TN).

dichloromethane and methanol (95:5, v/v), dried under a gentle N_2 stream, and derivatized using *N*,*O*-bis(trimethylsilyl)-trifluoroacetamide (BSTFA) at 70°C for 1 h before instrumental measurements. Biomarker quantification was performed on an Agilent 6890N GC with a flame ionization detector (FID) (Li et al., 2014). The biomarker contents were plotted in Figure 4A and listed in Supplementary Table S3.

2.5 Data processing and sources

Ancillary hydrologic data over the period 1953–2018 CE were collected from the California Cooperative Oceanic Fisheries Investigations program (CalCOFI) as described at http://calcofi.org. Determinations as to the phase and state of PDO were available at http://jisao.washington.edu/pdo/PDO. The climate indices of ENSO represented by the Niño 3.4 region (5°N–5°S, 170°W–120°W) are available at https://www.esrl.noaa.gov/psd/gcos_wgsp/Timeseries/. The NPGO index by Di Lorenzo et al. (2008) is available at http://www.o3d.org/npgo/.

2.6 Statistics

The temporal changes of TOC, TN, and $\delta^{15}N$ over time were assessed using the sequential *t*-test analysis of regime shifts (STARs) (Rodionov, 2004; Rodionov and Overland, 2005; Howard et al., 2007; www.BeringClimate.noaa.gov). The STARs use a *t*-test analysis to determine whether sequential records in a time series represent statistically significant departures from mean values observed during the preceding period of a predetermined duration. The cutoff length (l) is set to 30 years, and the probability level to $\alpha = 0.1$.

The Adjacent-Averaging filter smooth was used to remove noise from signals by OriginPro8.0 software; for example, the measured $\delta^{15}N$ and marine OC have smoothed 5 points of window. Geochemical data were interpolated to obtain evenly spaced time series using OriginPro8.0 software prior to statistical analyses. The rule of interpolation is according to the resolution of data; as the result of the different resolutions of this study to others, all records are interpolated to annual resolution. When all of the data were adjusted to the same resolution, IBM SPSS Statistics software was further used for correlation analysis.

3 Results

3.1 Chronology of the core

The chronology of core SBB-190629 was determined by ^{210}Pb dating through a gamma spectrometer. In the ^{238}U–^{206}Pb decay series, ^{226}Ra ($T_{1/2}$ = 1,600 years), ^{214}Pb ($T_{1/2}$ = 26.8 min), and ^{214}Bi ($T_{1/2}$ = 19.9 min) are the parents of ^{210}Pb ($T_{1/2}$ = 22.3 years). If sample material is formed more than 200 years ago, its ^{226}Ra and ^{210}Pb activities reach secular equilibrium (i.e., the activities

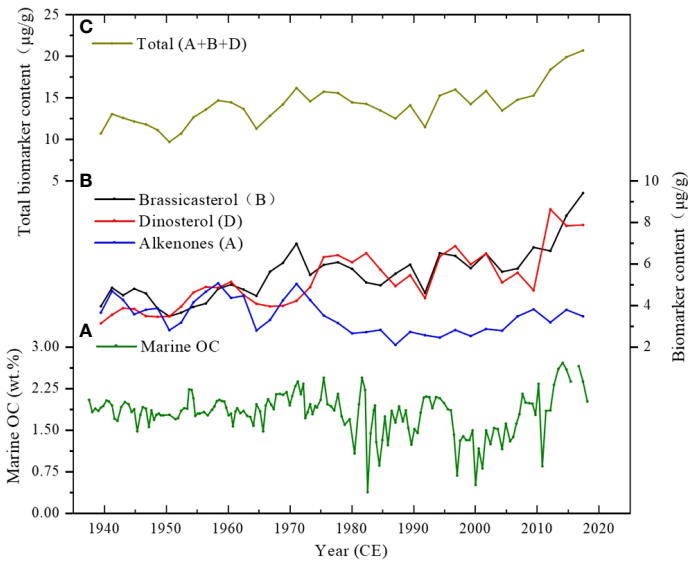

FIGURE 4
(A) Variation of marine organic carbon (OC) calculated by C/N atom ratio in core SBB-190629. Content of marine biomarkers was expressed in μg per g dry sediment (μg/g). **(B)** Total marine biomarkers calculated by A + B + D. **(C)** Variation of individual marine biomarkers: Brassicasterol (B), Dinosterol (D), and Alkenones (A).

are equal). Similarly, after the sample formation is more than 1 day, its ^{214}Pb, ^{214}Bi, and ^{210}Pb reach secular equilibrium. Therefore, we can use ^{226}Ra, ^{214}Pb, and ^{214}Bi to obtain the supported ^{210}Pb. Excess ^{210}Pb comes from ^{222}Rn ($T_{1/2}$ = 3.8 days) decay in the atmosphere and precipitates on Earth through wet and dry fallouts. As excess ^{210}Pb deposits on the Earth"s surface, its decay timer starts to count. Therefore, excess ^{210}Pb in a sediment sequence exponentially decreases with time (or depth) (Li et al., 2019):

$$^{210}Pb = {}^{210}Pb_0 \times e^{-\lambda t} = {}^{210}Pb_0 \times e^{-\lambda D/SR} \quad (2)$$

where D and SR represent depth and sedimentation rate, respectively. The slope of the Ln ^{210}Pb-D plot should yield a linear sedimentation rate (SR) (Appleby and Oldfield, 1992). Figure 2C shows the excess ^{210}Pb decay trend with the core depth. Because the excess ^{210}Pb activity is much higher than the supported ^{210}Pb activity, the decay trends of excess ^{210}Pb and total ^{210}Pb are very similar. With the use of ^{226}Ra or (^{214}Pb + ^{214}Bi)/2 as supported ^{210}Pb for calculation of excess ^{210}Pb, the fitting results are similar. Considering ^{214}Pb and ^{214}Bi can quickly reach secular equilibrium with ^{210}Pb, we choose to use the excess ^{210}Pb calculated from the total ^{210}Pb minus (^{214}Pb + ^{214}Bi)/2. An equation of $y = 1226.8 \times e^{-0.055116x}$ is obtained by using exponential fitting of the excess ^{210}Pb with depth. The estimated SR in SBB-190629 is 0.564 cm/year (Figure 2C). Based on this SR, the 46-cm-long core would cover about 80 years of depositional history. With the use of the SR of 0.564 cm/year, the age of each depth can be calculated assuming the age of the top sediment was 2019 CE.

3.2 δ^{15}N, total organic carbon, and total nitrogen variation of core SBB-190629

The $\delta^{15}N_{sed}$ in core SBB-190629 varies from 6.24‰ to 7.43‰ (Figure 3A). The variation of $\delta^{15}N_{sed}$ fluctuated between 6.70‰ and 7.20‰ from the late 1930s to the 1960s and then became higher during the 1970s with an average of 7.14‰. After that, a decline in $\delta^{15}N_{sed}$ of ~1‰ was evident from the mid-1980s to the mid-2000s. After that, the $\delta^{15}N_{sed}$ value increased sharply in the mid-2000s and reached 7.30‰ in 2015–2016.

The TOC of the samples varies from 3.37 to 6.19 wt.% (Figure 3B, blue). A decrease to approximately 2 wt.% occurred between the late-1930s and mid-1980s. The TOC further decreased with an average of 4.28 wt.% between the mid-1980s and mid-2000s. A sharp increase in TOC with a maximum at 6.19 wt.% was evident since the mid-2000s.

Sedimentary TN consists of organic nitrogen (ON) and inorganic nitrogen (IN). The TN of sediments in core SBB-190629 fluctuates between 0.38 and 0.64 wt.% (Figure 3B, green). The variation trend of TN is similar to that of TOC.

According to the results of STARs analysis, the regime shifts of TOC, TN, and δ^{15}N approximately appear at the same time: 1965~1970, 1978~1985, and 2005~2010 (Figure S1). In general, the variation of TOC, TN, and δ^{15}N roughly displayed similar temporal trends.

3.3 Marine organic carbon calculated by C/N and marine biomarkers

The C/N ratios (atom ratio of TOC/TN) in core SBB-190629 vary from 9.73 to 12.61, with an average of 10.53 (Figure 3C). Although both marine and terrigenous origins of organic matters could contribute to the sediments in the coring site, the good correlation between TOC and TN (Figure 3) suggests that the majority of the organic matters in the sediments came from the similar source. For the linear equation of TN = 0.092 * TOC + 0.081 (R^2 = 0.81, p< 0.01) (Figure S2), the intercept represents the average 0.081 wt.% of IN in the TN, which may be from terrestrial clay-bound N (Müller, 1977; Schubert and Calvert, 2001; Hu et al., 2013; Hendy et al., 2015; Wang et al., 2019). Compared to the average TN of 0.48 wt.% in SBB sediments, the IN accounts for about 16.9% of TN, so its interference is minor.

The C/N ratio has been utilized for assessing the source of organic matter. Generally, the C/N ratio of algae ranges from 4 to 10 (Thornton and McManus, 1994; Lamb et al., 2006), while the C/N ratio of approximately 20 indicates terrestrial vascular plant input (Meyers, 1997; Schubert and Calvert, 2001). A two-end-member mixing model was employed to estimate the relative contributions of OC from marine and river in the SBB sediments.

$$(C/N)_{sample} = f_{terrestrial} \times (C/N)_{terrestrial} + f_{marine} \times (C/N)_{marine} \quad (3)$$

$$f_{terrestrial} + f_{marine} = 1 \quad (4)$$

The terrestrial end-member is based on the mean values of the particular matter samples collected near Santa Clara River ($C/N_{terrestrial}$ = 13.07), which is the main terrestrial source of the SBB sediments (Masiello and Druffel, 2001; Komada et al., 2004). The average C/N ratio of phytoplankton is 7 for the marine end-member (Lamb et al., 2006). The OC_{marine} is calculated by multiplying the sediment proportion of marine by TOC; the trends are shown in Figure 4A. According to this calculation, the average values of OC_{marine} content and f_{marine} are 1.83 wt.% (ranging from 0.39 to 2.76 wt.%) and 41% (ranging from 12% to 55%), respectively. Compared with the average TOC content of 4.31 wt.%, the OC_{marine} proportion in the TOC is generally less than the $OC_{terrestrial}$, agreeing with the previous studies (Thunell, 1998; Hendy et al., 2015).

Brassicasterol (B) and Dinosterol (D) are major marine sediment biomarkers in SBB derived predominantly from cell membrane components of diatom and dinoflagellate among phytoplankton, which further reflect the corresponding

phytoplankton biomass in the euphotic layer (Volkman, 1986; Volkman et al., 1998; Xing et al., 2016). Alkenones (A) are another major lipid component that originated from haptophytes. Hence, the sum of Brassicasterol, Dinosterol, and Alkenones (B + D + A) can be successfully utilized for evaluating primary productivity (Schubert et al., 1998; Xing et al., 2016). The biomarker contents of the three lipid biomarkers are depicted in Figure 4B. Brassicasterol and Dinosterol contents gradually increased before the 1970s, slightly decreased after the 1980s, and increased again from the 2000s, consistent with TOC and OC_{marine} variations. Alkenone content decreased gradually over the last 80 years, despite a slightly high value in the late 1950s and early 1970s. The sum of the three biomarkers shows decadal variations and a strongly increasing trend from 2010 onward (Figure 4C).

4 Discussions

4.1 The influence of $\delta^{15}N$ signals transported from the eastern tropical North Pacific on Santa Barbara Basin

As mentioned above, surface water inputs to SBB have different $\delta^{15}N$ with heavier $\delta^{15}N$ of CUC originating from ETNP and lighter $\delta^{15}N$ of CC. In order to provide evidence of high $\delta^{15}N$ waters from ETNP that could be advected to Southern California *via* CUC to influence the water $\delta^{15}N$ along the Southern California Coast, we collected integrated $\delta^{15}N$ of nitrate (Sigman et al., 2003; Sigman et al., 2005) and salinity data sets of water samples within 100–400 m from the California Coast to the southern tip of Baja California (Van Geen, 2001). Figure S3 shows a strong positive correlation ($R^2 = 0.97$) between $\delta^{15}N$ and salinity, and the highest $\delta^{15}N$ and salinity in the southern tip of Baja California decreased to the lowest $\delta^{15}N$ and salinity near SBB. The conservative behavior of $\delta^{15}N$ with respect to salinity demonstrates the ETNP influence on the water along the California Coast. Although the CUC is the strongest in fall, Liu and Kaplan (1989) found a similar correlation between $\delta^{15}N$ and salinity along the California Coast water in the summer. In addition, as already noted, $\delta^{15}N_{sed}$ from the SBB records the variation of $\delta^{15}N$ in the water column; therefore, a positive correlation between $\delta^{15}N$ from an SBB box core (SPR0901-04BC, Figure 1A) and measured salinity at the core of CUC ($\sigma\theta$ = 26.4–26.5) from the CalCOFI during the last 50 years was verified by Wang et al. (2019) to support the influence of ETNP high $\delta^{15}N$ on SBB. Thus, ETNP water is an important source of enriched $\delta^{15}N_{nitrate}$ transported to SBB with the CUC.

Another test to demonstrate the ETNP $\delta^{15}N$ influence on the $\delta^{15}N$ signal in SBB is to use $\delta^{15}N_{sed}$ in ETNP to compare with the SBB $\delta^{15}N_{sed}$. The $\delta^{15}N_{sed}$ record of core SBB-190629 is compared with the $\delta^{15}N_{sed}$ records at three sites along the North American margin (Figure 5). The Pescadero Slope and Soledad Basin sites (Figure 1B) are within the anoxic zone in the ETNP (Deutsch et al., 2014). Adjacent to SBB, the third site in Santa Monica Basin (SMB, Figure 1B) is >1,000 km north of the anoxic zone but physically connected *via* the coastal undercurrent (Deutsch et al., 2014). Basically, the $\delta^{15}N_{sed}$ records at the Pescadero Slope and Soledad Basin sites reflect the strongest influence of the ETNP $\delta^{15}N$ (or the distal $\delta^{15}N$ signal), whereas the SBB and SMB sites are farther away from the ETNP influence. Despite the four cores having their own chronologies, the comparisons shown in Figure 5 reveal that 1) $\delta^{15}N_{sed}$ records (except the SBB $\delta^{15}N_{sed}$) showed a general decreasing trend from the late 1930s to ~1980. All four records showed relatively low values during 1980~2000 and then increasing trends after 2000. 2) The $\delta^{15}N_{sed}$ values became lower from the south site to the north site, indicating that the mixture from the ETNP $\delta^{15}N$ becomes weaker with increasing distance from ETNP. The latitudinal and chronological comparisons of the $\delta^{15}N_{sed}$ records at the four sites along the Eastern Pacific margin exhibit that the $\delta^{15}N_{sed}$ have recorded primarily large-scale oceanographic changes originating in the water column, and the water with the ETNP $\delta^{15}N$ signal can reach as far as the SBB, implying that the distal $\delta^{15}N$ signal should be distinguished from the local $\delta^{15}N$ signal in the SBB $\delta^{15}N_{sed}$. The visible dissimilarities on short timescales between the SBB $\delta^{15}N_{sed}$ record and other $\delta^{15}N_{sed}$ records further validate the local $\delta^{15}N$ signal interference. Below, we discuss the determination of the local $\delta^{15}N$ signal in the SBB $\delta^{15}N_{sed}$.

4.2 Estimation of the local $\delta^{15}N$ signal in Santa Barbara Basin

To distinguish the local $\delta^{15}N$ signal in SBB, the $\delta^{15}N_{sed}$ of Pescadero Slope and Soledad Basin belonging to the anoxic zone of ETNP were treated to represent the ETNP $\delta^{15}N$ variability (Deutsch et al., 2014). These two records from 1935 to 2010 were selected to keep the same timescale for this study. The $\delta^{15}N$ anomalies ($\Delta\delta^{15}N$) of ETNP were calculated by the individual $\delta^{15}N_{sed}$ value by subtracting the mean $\delta^{15}N$ value over 1935~2007 of each site and then averaging them. Figure 6A shows the ETNP $\Delta\delta^{15}N$ record (blue curve with shaded error area) during 1935~2007. In order to confirm the representative of the ETNP $\delta^{15}N$ signal, we compared the simulated changes in $\delta^{15}N$ (Figure 6A, green curve) using an ocean general circulation model (GCM) by Deutsch (2014) with our result. The modeled $\delta^{15}N$ record was based on numerical simulations of the cycle of N and its isotope cycle in the ETNP anoxic zone (125°W to coast, 5°N to 25°N) during 1959~2005. The result shows that decadal variations in the model predicted $\delta^{15}N$ of particulate organic N sinking into the anoxic zone, which closely matches the sediment proxy data in both amplitude and timing. The reliability of the calculated ETNP $\delta^{15}N$ signal is verified.

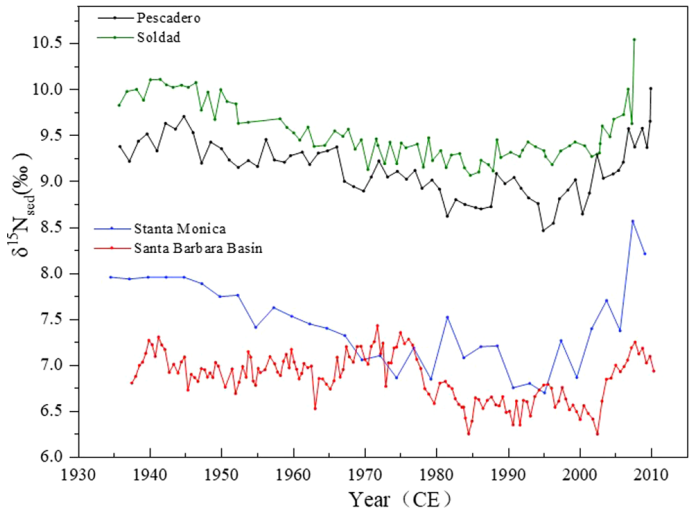

FIGURE 5
Bulk organic $\delta^{15}N$ from four sediment core sites along the North American margin: Soledad (Deutsch et al., 2014), Pescadero (Deutsch et al., 2014), Santa Monica Basin (Davis et al., 2019), and Santa Barbara Basin (this study). Locations of core sites are showing in Figure 1B.

Similarly, the $\Delta\delta^{15}N$ ($\delta^{15}N$ anomaly, deviation from the mean $\delta^{15}N$ of 1935~2007) record for the SBB $\delta^{15}N_{sed}$ record was obtained. By subtracting the ETNP $\Delta\delta^{15}N$ from the SBB $\Delta\delta^{15}N$, the local $\Delta\delta^{15}N$ in SBB ($\Delta\delta^{15}N_{SBB}$) was produced, shown in Figure 6B (red curve). Note that the local anomaly signals are only accessible from 1938 to 2007 owing to the lack of availability of the ETNP $\Delta\delta^{15}N$ since 2007. In Figure 6B, the $\Delta\delta^{15}N_{SBB}$ record ranges from −0.5 to 0.6, and the difference between the maximum and minimum value is 1.1, roughly equal to the change of bulk $\Delta\delta^{15}N$ (1.2); therefore, the local effect of $\delta^{15}N_{sed}$ is not insignificant. In addition, there are differences in the trend of $\Delta\delta^{15}N_{SBB}$ and bulk $\Delta\delta^{15}N$; the $\Delta\delta^{15}N_{SBB}$ appeared in decadal variations with a general increasing trend from 1945 to the late 1970s and a decreasing trend afterward. The outstanding peak of the $\Delta\delta^{15}N_{SBB}$ is during 1965~1978. In the following sections, we will discuss the causes of the variations in the $\Delta\delta^{15}N_{SBB}$.

4.3 Forcing factors on local $\Delta\delta^{15}N$ signal variation in Santa Barbara Basin on interannual timescales

4.3.1 Changes in the strength of bottom water denitrification in Santa Barbara Basin

The main influencing factors for the $\Delta\delta^{15}N_{SBB}$ fluctuations are i) incomplete nitrate utilization, ii) terrestrial input, and iii) bottom water denitrification. First of all, in Section 3.3, we have demonstrated that the IN accounted for 16.9% of the TN on average in the sediments. This IN mainly from terrestrial clay-bound N (Hendy et al., 2015; Wang et al., 2019) has little influence on the SBB $\delta^{15}N_{sed}$. How the influence of terrestrial input of organic N is compared with TN from the water column in SBB remains unclear. Secondly, the additionally isotopic variability arising from incomplete surface nutrient utilization is insignificant in magnitude and also confined to seasonal timescales (Emmer and Thunell, 2000; Davis et al., 2019). Therefore, Factors i) and ii) may have minor impacts on the $\Delta\delta^{15}N_{SBB}$ fluctuations on interannual timescales. In this present work, bottom water denitrification is thought to majorly impact local $\delta^{15}N$ variability. Denitrification in the anoxic waters and sediments in a semi-closed environment of SBB has been well documented in historic and modern records (Emmer and Thunell, 2000; Bograd et al., 2002; Goericke et al., 2015; Davis et al., 2019). SBB is influenced by Southern California eddy, which through strong vertical advection enhances water mixing (Chenillat et al., 2018). Chung (1973) reported a ^{222}Rn-based estimate of 3.9 cm^2/s for vertical eddy diffusivity in SBB, which yields a rough mixing time of 0.6–0.8 years for the basin water, implying significant and rapid water exchange across the bottom water and the overlying water (Sigman et al., 2003). In addition, tight correlations were observed between our $\Delta\delta^{15}N_{SBB}$ record and local redox proxies (Re/Mo ratio and C_{29} stanol/stenol ratio), which document SBB bottom water O_2 condition (see the detailed discussion as follows), providing evidence that SBB local denitrification process affects sediment $\delta^{15}N$ signal.

Molybdenum (Mo) and rhenium (Re) are redox-sensitive elements and can be accumulated in marine sediments beneath O_2-depleted waters. However, authigenic Mo precipitation

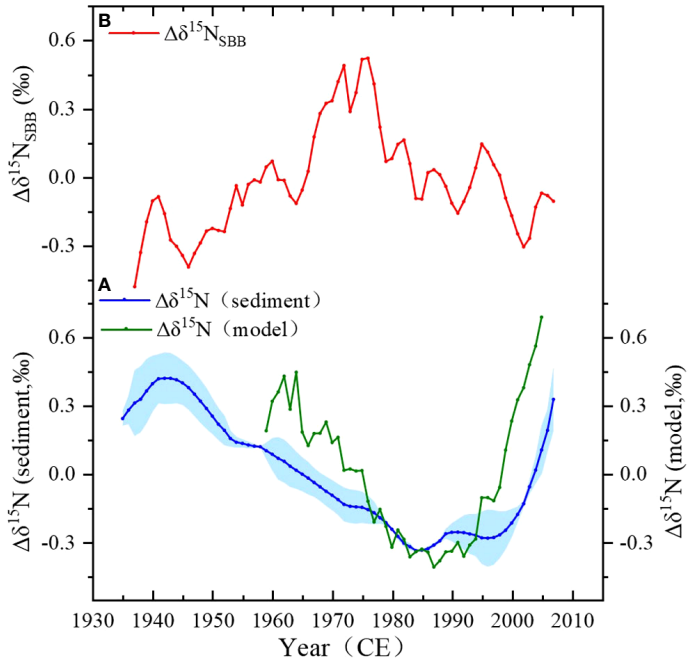

FIGURE 6
Calculation of ETNP $\Delta\delta^{15}N$ and $\Delta\delta^{15}N_{SBB}$. **(A)** Construction of the eastern tropical North Pacific (ETNP) $\Delta\delta^{15}N$ signal, the blue curve shows the result of the average $\Delta\delta^{15}N$ from Soledad and Pescadero sites, and the green curve shows the result of the model. **(B)** The calculated $\Delta\delta^{15}N_{SBB}$ (red curve).

only proceeds in the presence of free HS^- water, which is considered a more reducing environment compared with authigenic Re precipitation (Crusius et al., 1996). Thus, a decrease in sedimentary Re/Mo indicates the pore water shift from slightly to strongly reducing sulfidic environments (Crusius et al., 1996; Wang et al., 2017). In anoxic marine environments such as SBB, Re/Mo ratio in marine sediments is used to indicate changing redox conditions at the time of sediment deposition, with a higher Re/Mo ratio reflecting lower redox potential, or enhanced ODZ and denitrification degree and vice versa (Wang et al., 2017). Wang et al. (2017) measured total Mo and Re concentrations in the sediments and calculated enrichment factors for Re/Mo {$(Re/Mo)_{EF}$; 3-year resolution)} in SBB from 1759 to 2008. In order to compare with this record, a linear extrapolation was used to obtain annual resolution by using Origin software. The $\Delta\delta^{15}N_{SBB}$ record of core SBB-190629 was compared with the $(Re/Mo)_{EF}$ record (Figure 7B) of core SPR0901-04BC, showing a strong negative correlation ($r = -0.49$, $p < 0.05$) which demonstrates that the $\Delta\delta^{15}N_{SBB}$ was controlled by redox conditions.

Another redox-sensitive proxy in SBB is the C_{29} stanol/stenol ratio, as the 5α(H)-stanol/Δ5-stenol ratios increase through microbial conversion under anoxic conditions by the reduction of sterol Δ5 double bonds to 5α(H)-stanols (Rosenfeld and Hellmann, 1971; Eyssen et al., 1973). Thus, the C_{29} stanol/stenol ratio is used as an indicator of redox conditions related to oxygen availability in the sediments and bottom waters of the SBB, with a higher C_{29} stanol/stenol ratio reflecting lower redox potential, stronger anoxia, and denitrification and vice versa (Alfken et al., 2020). Alfken et al. (2021) used a matrix-assisted laser desorption/ionization coupled to Fourier transform-ion cyclotron resonance–mass spectrometry (MALDI-FT-ICR-MS) to measure C_{29} stanol/stenol from 1900 to 2009 (Figure 7C). We take the part of 1935–2009 for the comparison. In Figure 7, a general positive correlation between the C_{29} stanol/stenol ratio and $\Delta\delta^{15}N_{SBB}$ records further suggests that the change of $\Delta\delta^{15}N_{SBB}$ represents SBB bottom water denitrification. Note that the C_{29} stanol/stenol record was a few years ahead of the $\Delta\delta^{15}N_{SBB}$ record, which might be caused by chronological uncertainties or other unknown reasons. After the C_{29} stanol/stenol record was moved 5 years later, the positive correlation between the two records reaches the highest ($r = 0.61$, $p < 0.01$).

In summary, Figure 7 illustrates that the variations of the $\Delta\delta^{15}N_{SBB}$ record reflect changes in bottom water denitrification in SBB, with an increased $\Delta\delta^{15}N_{SBB}$ indicating reduced oxygen content and enhanced denitrification. According to the $\Delta\delta^{15}N_{SBB}$ record, the bottom water denitrification increased generally from 1945 to the late 1970s and then decreased at around 2000. The mechanisms controlling denitrification in SBB are discussed in detail as follows.

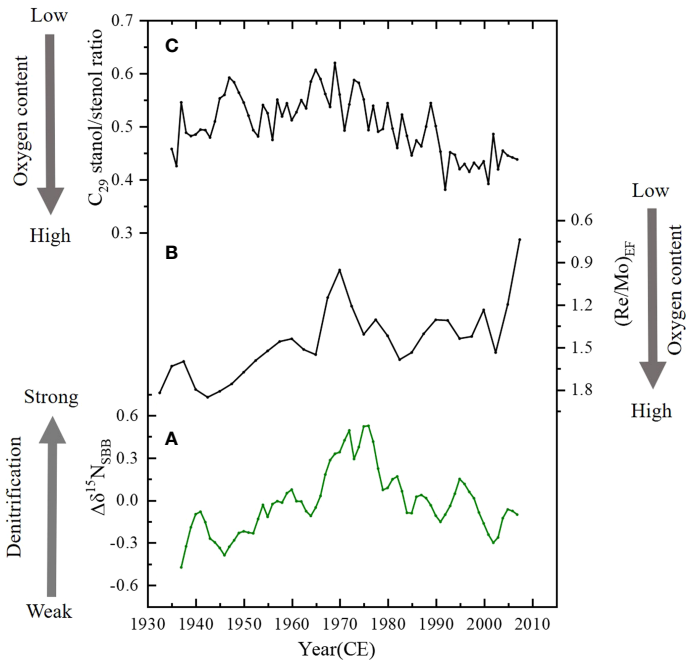

FIGURE 7
Comparisons of the **(A)** $\Delta\delta^{15}N_{SBB}$ with redox proxies: **(B)** $(Re/Mo)_{EF}$ record (Wang et al., 2017) and **(C)** C_{29} stanol/stenol ratio record (Alfken et al., 2021). Note that the scale of $(Re/Mo)_{EF}$ record is reversed.

4.3.2 The effect of upwelling and marine productivity on the variation of Santa Barbara Basin local $\delta^{15}N$ signal

As mentioned earlier, denitrification in SBB bottom water can be affected by 1) oxygen consumption of OC, which is related to marine productivity, and 2) O_2 input by flushing water from north of Point Conception, which are tightly connected with the local upwelling process. Variability of the upwelling north of Point Conception has been monitored since 1946 and can be described by the Pacific Fisheries Upwelling Index (PFEL) at 36°N (Davis et al., 2019). Upwelling provides nutrients to support phytoplankton growth in SBB (Checkley and Barth, 2009); stronger upwelling will cause higher productivity and result in higher marine OC (Wang et al., 2019). The general trend of marine OC (Figure 4) shows significant variability on a decadal timescale. The averages and standard deviations during 1937~1966, 1966~1982, 1982~2007, and 2007~2010 were 1.87 ± 0.16 (n = 61), 2.03 ± 0.27 (n = 23), 1.53 ± 0.42 (n = 47), and 2.10 ± 0.50 (n = 19) wt.%, respectively. The average and standard deviation during 1937~1966 indicate that the OC_{marine} had a small variation and was close to the average (1.83 wt.%) of the entire record. High contents prevailed during 1966~1982, and low OC_{marine} contents occurred during 1982~2007. However, the OC_{marine} record may involve a diagenetic effect. Marine biomarkers are considered an effective proxy for their resistance to sedimentary diagenesis and stable preservation in geological time, thus providing an independent measure of export productivity in the SBB water column. Figure 8 compares the $\Delta\delta^{15}N_{SBB}$ record (Figure 8A), the OC_{marine} record (Figure 8B), total marine biomarker (B + D + A) record (Figure 8C), and annual average upwelling index (Figure 8D). The comparisons showed good correlations among the four curves, indicating that higher OC_{marine} and total marine biomarker contents that resulted from higher productivity under stronger upwelling caused stronger denitrification in the SBB bottom water. According to the positive relationship between the $\Delta\delta^{15}N_{SBB}$ record and primary productivity records ($\Delta\delta^{15}N_{SBB}$ and OC_{marine}: $r = 0.40$, $p < 0.01$; $\Delta\delta^{15}N_{SBB}$ and marine biomarkers: $r = 0.61$, $p < 0.01$), enhanced productivity caused by upwelling (upwelling index and marine biomarkers $r = 0.63$, $p < 0.01$) should be more important than the O_2 brought by flushing events from north of Point Conception to the denitrification in the bottom water of the SBB. This probably means that 1) the O_2 amount brought by flushing events may be small, 2) the duration of the flushing events is short, and 3) the low O_2 but high nutrient upwelled water is dominant so that the annual hypoxia condition of SBB would not be affected significantly by the flushing O_2 amount. Therefore, upwelling and productivity seem to be the major factors to influence the $\delta^{15}N$ in SBB.

Several studies have also found that local upwelling-induced productivity may cause the sediment $\delta^{15}N$ changes in SBB,

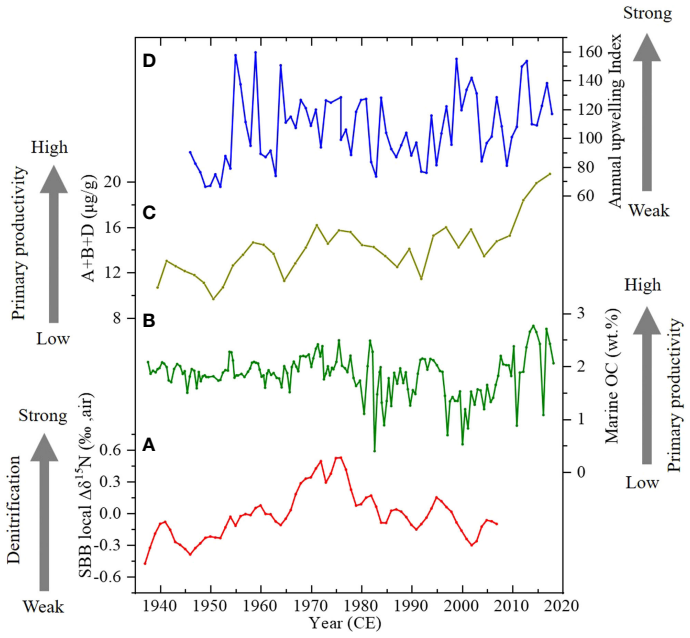

FIGURE 8
Comparisons of **(A)** the $\Delta\delta^{15}N_{SBB}$, **(B)** OC_{marine} (wt.%), and **(C)** total biomarker content in core SBB-190629 with **(D)** annual average upwelling index in 36°N at the north of Point Conception (Davis et al., 2019).

supporting our finding above (Wang et al., 2019; Sánchez et al., 2022). Wang et al. (2019) also proposed that nutrient-rich, higher $\delta^{15}N$ subarctic water, which was caused by incomplete nitrate utilization in the subarctic region when the Aleutian low is strong, might have been transported into the SBB and was recorded by sediment $\delta^{15}N$ during the Little Ice Age period. Indeed, a high-value state was found between 1965 and 1980 in our SBB $\delta^{15}N_{sed}$ when PDO was in the negative phase. Considering the phase relationship of negative PDO vs weak Aleutian Low (Chavez et al., 2003; Hendy et al., 2015), the southward transport mechanism could not explain the high SBB $\delta^{15}N_{sed}$ signal during 1965~1980, whereas the marine biomarkers, marine OC, and local redox proxies all support higher productivity and strengthened local denitrification in SBB during this time interval. Therefore, we suggest that the high value between 1965 and 1980 is more likely to be the result of local denitrification.

4.4 Local and remote forcing on $\delta^{15}N$ variations in Santa Barbara Basin

There have been many studies focusing on the climate effect on the bulk SBB $\delta^{15}N_{sed}$ (Emmer and Thunell, 2000; Tems et al., 2015; Horak et al., 2016; Davis et al., 2019; Wang et al., 2019); however, studies specifically about the separate signals are limited. Since the variability of upwelling strength in the California Coast system on annual-to-decadal timescales is linked with ENSO (e.g., Bograd and Lynn, 2001), PDO (e.g., Chhak and Di Lorenzo, 2007), and NPGO (e.g., Di Lorenzo et al., 2008; García-Reyes and Largier, 2010), here we discuss the influences of the climatic forcing on the upwelling, production, and denitrification in SBB. In Figure 9, the records of ENSO, PDO, and NPGO were compared with the records of upwelling, marine biomarkers, OC_{marine} (reflecting marine productivity), and the $\Delta\delta^{15}N_{SBB}$.

4.4.1 The role of tropical trade winds on $\delta^{15}N_{sed}$ signature as a remote influencing factor

The ETNP denitrification is controlled by the variations in wind intensity over the tropical Pacific by eventually regulating the ocean water upwelling, the zonal structure of the underlying thermocline, area of oxygen minimum zone (OMZ), and biological productivity (Canfield, 2006; Deutsch et al., 2014; Tems et al., 2015; Horak et al., 2016). Stronger tropical trade winds will generate stronger upwelling along the equator divergent zones and enhance primary productivity (Sydeman et al., 2014). Consequently, the area of OMZ and denitrification in ETNP will be intensified, thus elevating $\Delta\delta^{15}N$ of ETNP (Deutsch et al., 2014). The variations of $\delta^{15}N$ signals by ETNP denitrification are further transported northward by CUC and

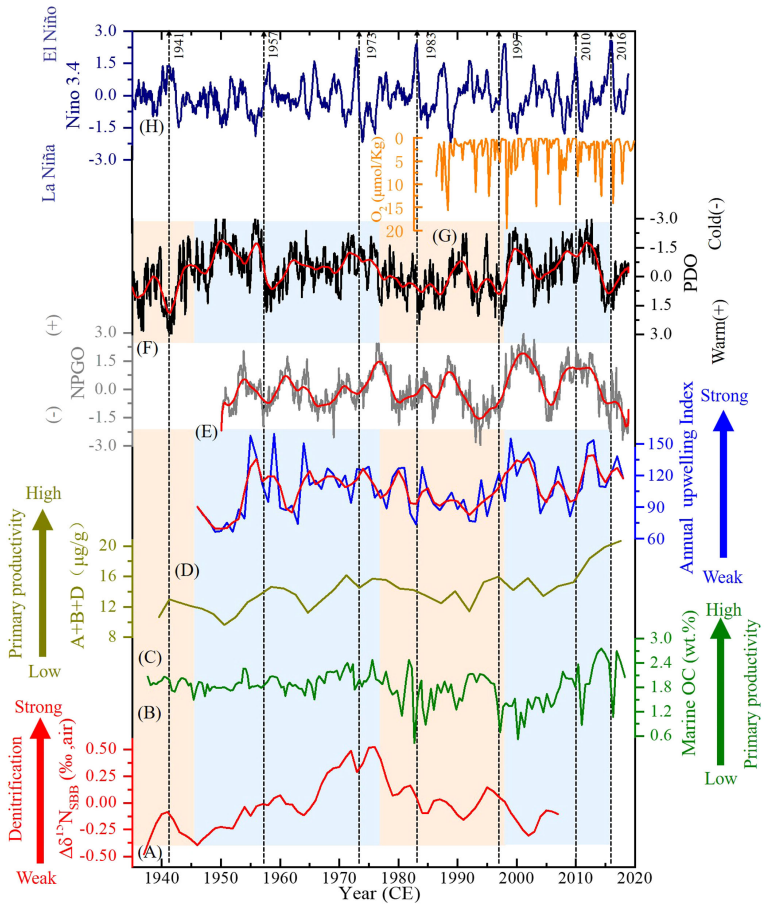

FIGURE 9
Comparisons of the Santa Barbara Basin (SBB) **(A)** local $\Delta\delta^{15}N$ (‰), **(B)** OC_{marine} (wt.%), **(C)** marine biomarkers (μg/g), **(D)** annual upwelling index, and **(G)** O_2 content (μmol/kg) records with **(E)** North Pacific Gyre Oscillation (NPGO) (http://www.o3d.org/npgo/). **(F)** Pacific Decadal Oscillation (PDO) (http://jisao.washington.edu/pdo/PDO), and **(H)** El Niño–Southern Oscillation (ENSO) (https://www.esrl.noaa.gov/psd/gcos_wgsp/Timeseries/) records. Strong El Niño events such as in 1941, 1957–1958, 1973, 1982–1983, 1997–1998, 2010, and 2016 are marked. Red lines in panels (**D–F**) represent the results of 3 years smoothed. Orange areas denote warm phase of PDO, whereas blue areas represent cold phase of PDO. Note that the scale of O_2 content and PDO is reversed.

finally recorded in SBB water and sediments. Therefore, tropical trade winds act as a remote influencing factor and control the general trend of SBB sedimentary $\delta^{15}N$ ($\delta^{15}N_{sed}$) signature. The general decreasing trends of the $\delta^{15}N_{sed}$ records shown in Figure 5 from 1940 to the late 1980s (except the SBB record) reflect reduced upwelling, productivity, and denitrification in the ETNP probably caused by the weakening of tropical trade wind (Deutsch et al., 2014; Tems et al., 2015). The strength of tropical trade wind remained low during 1980~2000 and then started to increase. Except for high values between 1965 and 1980, the SBB $\delta^{15}N_{sed}$ variation follows that of the ETNP, suggesting that tropical trade wind induced ETNP water column $\delta^{15}N$ change, which controlled the general trend of SBB $\delta^{15}N_{sed}$. After the removal of the distal $\delta^{15}N$ signature (the ETNP $\delta^{15}N$) from the SBB $\delta^{15}N_{sed}$ record, the local mechanism of the $\Delta\delta^{15}N_{SBB}$ trend needs an explanation.

4.4.2 The role of El Niño–Southern Oscillation, Pacific Decadal Oscillation, and North Pacific Gyre Oscillation on $\delta^{15}N_{sed}$ signature as a local controlling factor

The PDO is a long-term ocean fluctuation at the mid-latitudes of the Pacific Ocean and is controlled by the ocean–atmosphere climatic variability (Deser et al., 2004; Di Lorenzo et al., 2008). It is determined by the first dominant mode of variations in sea surface temperature (SST) and has triggered major environmental alterations in terms of physical and biological regime shifts along the western coast of North America (Di Lorenzo et al., 2008). The PDO shifts reflect changes in the strength and position of Aleutian low and concomitant changes in upwelling and SST, which have major environmental impacts in the area of SBB (Hendy et al., 2015). As shown in Figure 9, the positive (warm) PDO phase is

associated with depressed thermocline and weakened upwelling with shallow water depth and therefore induces a significant decline in marine productivity in SBB (Chavez et al., 2003; Venrick, 2012; Hendy et al., 2015; Wang et al., 2017). The decreased marine productivity of positive PDO reduces bottom water denitrification, further inducing a decline of $\Delta\delta^{15}N_{SBB}$. In contrast, the negative (cold) PDO phase is associated with higher productivity in SBB, which is attributed to intensified ocean water upwelling induced by the Aleutian low (Chavez et al., 2003; Di Lorenzo et al., 2008; Hendy et al., 2015), therefore increasing the $\Delta\delta^{15}N_{SBB}$ by enhancing bottom water denitrification in SBB. Hence, the PDO regime shift has a determining influence on the general trend of $\Delta\delta^{15}N_{SBB}$ on the decadal to centennial timescale.

The NPGO is a climate pattern that emerges as the second dominant mode of sea surface temperature variability in the Northeast Pacific and is driven by the atmosphere through the North Pacific Oscillation (Ceballos et al., 2009). The wind-driven upwelling and horizontal advection are the main driving factors of NPGO fluctuations, and their variations are correlated with salinity, nutrients, and chlorophyll of the central and eastern branches of the subtropical gyre (Di Lorenzo et al., 2008). However, the NPGO impact cannot be addressed before 1950 owing to the availability of NPGO indices only after 1950. According to the observation, positive correlations between the salinity, NO_3^- content, and Chl-*a* of CC and NPGO strength (Di Lorenzo et al., 2008) imply that stronger NPGO causes stronger upwelling in the south of 38°N areas. However, only a weak positive correlation between NPGO and upwelling ($r = 0.27$, $p < 0.05$) in SBB may be due to the alternating effects of the phase relationship between fluctuations of the PDO and NPGO modes. As the different dominant mode of SST in the Northeast Pacific, the NPGO index is plotted inversely for comparison with the PDO in general. In Figure 9, negative relationships between NPGO and PDO can be observed clearly after 1986; however, the relationships between the two were obscure before 1986. Therefore, the phase relationship between NPGO and PDO is complicated. For instance, during 1986~2015, the two parameters were strongly negatively correlated (in phase). In this period, the impacts of PDO and NPGO on the upwelling and productivity are in the same direction in SBB. Indeed, significant correlations are found between NPGO, PDO, and upwelling (NPGO and upwelling: $r = 0.48$, $p < 0.001$, PDO and upwelling: $r = -0.44$, $p < 0.001$). In contrast, during 1950~1985, the two parameters were out of phase. Under such circumstances, the effects of PDO and NPGO on upwelling and productivity would be opposite; thus, in this period, there is no direct correlativity between climate indexes, and upwelling can be found. In principle, the interaction of NPGO and PDO common controls the intensity of upwelling and primary productivity, further influencing denitrification in SBB on interannual timescales.

Previous studies have found increased SST and decreased upwelling in SBB, low O_2 content in the bottom water of SBB during El Niño events, and opposite situations during La Niña events (Goericke et al., 2015; Wang et al., 2017). The O_2 content in the bottom water of SBB from California Cooperative Oceanic Fisheries Investigations (CalCOFI) during 1987~2010 is compared with our records. Furthermore, the annual upwelling record and the Niño 3.4 record are also compared with our records (Figure 9). In Figure 9, several strong El Niño events such as in 1941, 1957–1958, 1973, 1982–1983, 1997–1998, 2010, and 2016 are marked. On the annual timescale, the relationships between ENSO phases and other parameters are inconsistent; however, the comparison does appear to indicate low upwelling (hence low productivity) and high O_2 content (due to low organic consumption) corresponding to strong El Niño events, and low OC_{marine} in the sediment record, e.g., 1983, 1997, and 2010, and vice versa during strong La Niña events, e.g., around 1989, 2000, and 2012. In contrast, not every equatorial El Niño affects SBB (Alfken et al., 2021). For instance, the broad OC_{marine} and $\Delta\delta^{15}N_{SBB}$ peaks centered at approximately 1941 and 1994 were matched with mainly El Niño conditions, and low upwelling, OC_{marine} content, and $\Delta\delta^{15}N_{SBB}$ at around 1950, 1964, and 1990 were matched with mainly La Niña conditions. In general, some strong ENSO events influence seasonal physical and biological fluctuations in SBB on the foundation of PDO and NPGO, but due to the chronology of core SBB-190629, it was used a linear sedimentation rate, and its uncertainty could be > ± 2 years in some sections. The comparison can only be valid on interannual-to-decadal timescales.

5 Conclusions

The high-resolution (~0.25-year) multi-proxy analyses including TOC, TN, biomarkers, and $\delta^{15}N$ of a 46-cm sediment core (SBB-190629) collected from the SBB reveal the role of local and remote influencing factors in controlling interannual $\delta^{15}N$ variations from 1938 to 2019 CE. The $\delta^{15}N_{sed}$ records from the ETNP anoxic zone (Pescadero Slope and Soledad Basin) are further evaluated to distinctly identify the transported ETNP $\delta^{15}N$ signature and local $\delta^{15}N$ signal variability. With the use of the deviation from the mean $\delta^{15}N$ ($\Delta\delta^{15}N$) of SBB-190629 to subtract the $\Delta\delta^{15}N$ of ETNP, $\Delta\delta^{15}N_{SBB}$ fluctuations have been generated. The $\Delta\delta^{15}N_{SBB}$ reflects the bottom water denitrification, which is mainly influenced by changes in oxygen content and productivity associated with oceanic water upwelling. The comparisons between the $\Delta\delta^{15}N_{SBB}$ record and redox-sensitive multi-proxies including the Re/Mo ratio, C_{29} stanol/stenol ratio, OC_{marine} content, and total marine biomarker concentration authenticate the $\Delta\delta^{15}N_{SBB}$ as an indicator of bottom water denitrification, which is proportional to marine productivity

and upwelling intensity in the SBB. In general, strong upwelling brings more nutrients and elevates marine productivity to lower O_2 content in the water column during La Niña and cold PDO conditions, resulting in high OC_{marine} and more denitrification (higher $\delta^{15}N$) and vice versa under El Niño and warm PDO. Such phenomena can be seen on annual timescales. However, the relationships of the SBB OC_{marine} and $\delta^{15}N$ records with ENSO and PDO records on longer-than-annual timescales are complicated because upwelling and O_2 content in the SBB can be influenced by PDO, NPGO, and ENSO. The combination of these climatic forcing factors has different impacts on the marine productivity in SBB at different timescales. Tropical trade winds act as a remote influencing factor and control the general trend of SBB sedimentary $\delta^{15}N$ ($\delta^{15}N_{sed}$) signature by transporting ETNP $\delta^{15}N$ signal to SBB. The general decreasing trend of the ETNP $\delta^{15}N$ from 1940 to the late 1980s probably reflected reduced upwelling, productivity, and denitrification caused by the weakening of tropical trade winds. The strength of tropical trade winds remained low during 1980~2000 and then started to increase afterward.

Data availability statement

The datasets presented in this study can be found in online repositories. The names of the repository/repositories and accession number(s) can be found in the article/Supplementary Material.

Author contributions

H-CL, D-WL, and HX designed the study and wrote the paper. H-CL provided accurate dating of core SBB-190629, and HX carried out measurements on total organic carbon, total nitrogen, biomarkers, and nitrogen isotopes. All co-authors provided intellectual input for data interpretation and writing of this manuscript. All authors contributed to the article and approved the submitted version.

Funding

This study was supported by the National Natural Science Foundation of China (Grant No. 41876076) to D-WL, the National Natural Science Foundation of China (Grant No. 41630966) to MZ, and grants from the Ministry of Science and Technology of Taiwan (MOST 107-2116-M-002-005, MOST 108-2116-M-002-012, MOST 109-2116-M-002-018 and MOST 110-2116-M-002-015) to H-CL.

Acknowledgments

We thank Dr. D. Burdige at Old Dominion University and Dr. T. Komada at San Francisco State University for their coring.

Conflict of interest

The authors declare that the research was conducted in the absence of any commercial or financial relationships that could be construed as a potential conflict of interest.

Publisher's note

Supplementary material

The Supplementary Material for this article can be found online at: https://www.frontiersin.org/articles/10.3389/fmars.2022.982051/full#supplementary-material

References

Alfken, S., Wörmer, L., Lipp, J. S., Napier, T., Elvert, M., Wendt, J., et al. (2021). Disrupted coherence between upwelling strength and redox conditions reflects source water change in Santa Barbara basin during the 20th century. *Paleoceanogr. Paleoclimatology* 36 (12), e2021PA004354. doi: 10.1029/2021PA004354

Alfken, S., Wörmer, L., Lipp, J. S., Wendt, J., Schimmelmann, A., and Hinrichs, K.-U. (2020). Mechanistic insights into molecular proxies through comparison of subannually resolved sedimentary records with instrumental water column data in the Santa Barbara basin, southern California. *Paleoceanogr. Paleoclimatol.* 35 (10), e2020PA004076. doi: 10.1029/2020PA004076

Altabet, M. A. (2006). "Isotopic tracers of the marine nitrogen cycle: present and past.", in *Marine organic matter: biomarkers, isotopes and DNA*. ed. J. K. Volkman (Berlin, Heidelberg: Springer), 251–293.

Altabet, M. A., Pilskaln, C., Thunell, R., Pride, C., Sigman, D., Chavez, F., et al. (1999). The nitrogen isotope biogeochemistry of sinking particles from the margin of the Eastern north pacific. *Deep-Sea Res. Part I-Oceanogr. Res. Pap.* 46, 655–679. doi: 10.1016/S0967-0637(98)00084-3

Bograd, S. J., and Lynn, R. J. (2001). Physical-biological coupling in the California current during the 1997–99 El niño-la niña cycle. *Geophys. Res. Lett.* 28 (2), 275–278. doi: 10.1029/2000GL012047

Bograd, S. J., Schwing, F. B., Castro, C. G., and Timothy, D. A. (2002). Bottom water renewal in the Santa Barbara basin. *Geophys. Res.-Oceans* 107, 9–1-9-9. doi: 10.1029/2001JC001291

Canfield, D. (2006). Models of oxic respiration, denitrification and sulfate reduction in zones of coastal upwelling. *Geochim. Cosmochim. Acta* 70, 5753–5765. doi: 10.1016/j.gca.2006.07.023

Ceballos, L. I., Di Lorenzo, E., Hoyos, C. D., Schneider, N., and Taguchi, B. (2009). North pacific gyre oscillation synchronizes climate fluctuations in the

Eastern and Western boundary systems. *J. Clim.* 22 (19), 5163–5174. doi: 10.1175/2009JCLI2848.1

Chavez, F. P., Ryan, J., Lluch-Cota, S. E., and Ñāiquen, C. M. (2003). From anchovies to sardines and back: Multidecadal change in the pacific ocean. *Science* 299 (5604), 217–221. doi: 10.1126/science.1075880

Checkley, J. D.M., and Barth, J. A. (2009). Patterns and processes in the California current system. *Prog. Oceanogr.* 83 (1-4), 49–64. doi: 10.1016/j.pocean.2009.07.028

Chenillat, F., Franks, P. J., Capet, X., Rivière, P., Grima, N., Blanke, B., et al. (2018). Eddy properties in the southern California current system. *Ocean Dyn.* 68 (7), 761–777. doi: 10.1007/s10236-018-1158-4

Chhak, K., and Di Lorenzo, E. (2007). Decadal variations in the California current upwelling cells. *Geophys. Res. Lett.* 34 (14), L14604. doi: 10.1029/2007GL030203

Chung, Y. C. (1973). Excess radon in the Santa Barbara basin. *Earth Planet. Sci. Lett.* 17 (2), 319–323. doi: 10.1016/0012-821X(73)90196-9

Crusius, J., Calvert, S., Pedersen, T., and Sage, D. (1996). Rhenium and molybdenum enrichments in sediments as indicators of oxic, suboxic and sulfidic conditions of deposition. *Earth Planet. Sci. Lett.* 145 (1-4), 65–78. doi: 10.1016/S0012-821X(96)00204-X

Davis, C. V., Ontiveros-Cuadras, J. F., Benitez-Nelson, C., Schmittner, A., Tappa, E. J., Osborne, E., et al. (2019). Ongoing increase in Eastern tropical north pacific denitrification as interpreted through the Santa Barbara basin sedimentary $\delta^{15}N$ record. *Paleoceanogr. Paleoclimatol.* 34, 1554–1567. doi: 10.1029/2019PA003578

Deser, C., Phillips, A. S., and Hurrell, J. W. (2004). Pacific interdecadal climate variability: Linkages between the tropics and the north pacific during boreal winter since 1900. *J. Clim.* 17 (16), 3109–3124. doi: 10.1175/1520-0442(2004)017<3109:PICVLB>2.0.CO;2

Deutsch, C., Berelson, W., Thunell, R., Weber, T., Tems, C., McManus, J., et al. (2014). Centennial changes in north pacific anoxia linked to tropical trade winds. *Science* 345, 665–668. doi: 10.1126/science.1252332

Di Lorenzo, E., Schneider, N., Cobb, K. M., Franks, P. J. S., Chhak, K., Miller, A. J., et al. (2008). North pacific gyre oscillation links ocean climate and ecosystem change. *Geophys. Res. Lett.* 35 (8), L08607. doi: 10.1029/2007GL032838

Emmer, E., and Thunell, R. C. (2000). Nitrogen isotope variations in Santa Barbara basin sediments: Implications for denitrification in the eastern tropical north pacific during the last 50,000 years. *Paleoceanogr. Paleoclimatol.* 15, 377–387. doi: 10.1029/1999PA000417

Eyssen, H. J., Parmentier, G. G., Compernolle, F. C., de Pauw, G., and Piessens-Denef, M. (1973). Biohydrogenation of sterols by eubacterium ATCC 21,408–Nova species. *Eur. J. Biochem.* 36 (2), 411–421. doi: 10.1111/j.1432-1033.1973.tb02926.x

García-Reyes, M., and Largier, J. (2010). Observations of increased wind-driven coastal upwelling off central California. *J. Geophys. Res.-Oceans* 115 (C4), C04011. doi: 10.1029/2009JC005576

Goericke, R., Bograd, S. J., and Grundle, D. S. (2015). Denitrification and flushing of the Santa Barbara basin bottom waters. *Deep-Sea Res. Part II-Top. Stud. Oceanogr.* 112, 53–60. doi: 10.1016/j.dsr2.2014.07.012

Hendy, I. L., Napier, T. J., and Schimmelmann, A. (2015). From extreme rainfall to drought: 250 years of annually resolved sediment deposition in Santa Barbara basin, California. *Quat. Int.* 387, 3–12. doi: 10.1016/j.quaint.2015.01.026

Horak, R. E., Ruef, W., Ward, B. B., and Devol, A. H. (2016). Expansion of denitrification and anoxia in the eastern tropical north pacific from 1972 to 2012. *Geophys. Res. Lett.* 43, 5252–5260. doi: 10.1002/2016GL068871

Howard, J. A. E., Jarre, A., Clark, A. E., and Moloney, C. L. (2007). Application of the sequential t-test algorithm for analysing regime shifts to the southern benguela ecosystem. *Afr. J. Mar. Sci.* 29, 437–451. doi: 10.2989/AJMS.2007.29.3.11.341

Hu, L., Shi, X., Guo, Z., Wang, H., and Yang, Z. (2013). Sources, dispersal and preservation of sedimentary organic matter in the yellow Sea: the importance of depositional hydrodynamic forcing. *Mar. Geol.* 335, 52–63. doi: 10.1016/j.margeo.2012.10.008

Komada, T., Druffel, E. R. M., and Trumbore, S. E. J. (2004). Oceanic export of relict carbon by small mountainous rivers. *Geophys. Res. Lett.* 2004, 31(7):L07504. doi: 10.1029/2004GL019512

Lamb, A. L., Wilson, G. P., and Leng, M. J. (2006). A review of coastal palaeoclimate and relative sea-level reconstructions using $\delta^{13}C$ and C/N ratios in organic material. *Earth-Sci. Rev.* 75 (1-4), 29–57. doi: 10.1016/j.earscirev.2005.10.003

Liu, K. K., and Kaplan, I. R. (1989). The eastern tropical pacific as a source of ^{15}N-enriched nitrate in seawater off southern California. *Limnology and Oceanography* 34 (5), 820–830. doi: 10.4319/lo.1989.34.5.0820

Li, H.-C., Wang, J., Sun, J.-J., Chou, C.-Y., Li, H.-K., Xia, Y.-Y., et al. (2019). Study of jinchuan mire in NE China I: AMS ^{14}C, ^{210}Pb and ^{137}Cs dating on peat cores. *Quat. Int.* 528, 9–17. doi: 10.1016/j.quaint.2019.07.020

Li, D., Zhao, M., and Chen, M. T. (2014). East Asian Winter monsoon controlling phytoplankton productivity and community structure changes in the southeastern south China Sea over the last 185 kyr. *Paleogeogr. Paleoclimatol. Paleoecol.* 414 (0), 233–242. doi: 10.1016/j.palaeo.2014.09.003

Margolskee, A., Frenzel, H., Emerson, S., and Deutsch, C. (2019). Ventilation pathways for the north pacific oxygen deficient zone. *Glob. Biogeochem. Cycle* 33, 875–890. doi: 10.1029/2018GB006149

Masiello, C. A., and Druffel, E. R. (2001). Carbon isotope geochemistry of the Santa Clara river. *Glob. Biogeochem. Cycle* 15, 407–416. doi: 10.1029/2000GB001290

Meyers, P. A. (1997). Organic geochemical proxies of paleoceanographic, paleolimnologic, and paleoclimatic processes. *Org. Geochem.* 27, 213–250. doi: 10.1016/S0146-6380(97)00049-1

Müller, P. J. (1977). CN ratios in pacific deep-sea sediments: Effect of inorganic ammonium and organic nitrogen compounds sorbed by clays. *Geochim. Cosmochim. Acta* 41 (6), 765–776. doi: 10.1016/0016-7037(77)90047-3

Osborne, E. B., Thunell, R. C., Marshall, B. J., Holm, J. A., Tappa, E. J., Benitez-Nelson, C., et al. (2016). Calcification of the planktonic foraminifera globigerina bulloides and carbonate ion concentration: Results from the Santa Barbara basin. *Paleoceanogr. Paleoclimatology* 31, 1083–1102. doi: 10.1002/2016PA002933

Rayner, N., Parker, D. E., Horton, E., Folland, C. K., Alexander, L. V., Rowell, D., et al. (2003). Global analyses of sea surface temperature, sea ice, and night marine air temperature since the late nineteenth century. *J. Geophys. Res.-Atmos.* 108 (D14), 4407. doi: 10.1029/2002JD002670

Rodionov, S. N. (2004). A sequential algorithm for testing climate regime shifts. *Geophys. Res. Lett.* 31 (9), L09204. doi: 10.1029/2004GL019448

Rodionov, S., and Overland, J. E. (2005). Application of a sequential regime shift detection method to the Bering Sea ecosystem. *ICES J. Mar. Sci.* 62, 328–332. doi: 10.1016/j.icesjms.2005.01.013

Rosenfeld, R. S., and Hellmann, L. (1971). Reduction and esterification of cholesterol and sitosterol by homogenates of feces. *J. Lipid Res.* 12 (2), 192–197. doi: 10.1016/S0022-2275(20)39529-8

Sánchez, A., Juárez, M., Ortiz-Hernández, M. C., and Domínguez-Samalea, Y. (2022). Variability of the oxygen minimum zone associated with primary productivity and hydrographic conditions in the Eastern north pacific during the last 1200 years. *Deep-Sea Res. Part I-Oceanogr. Res. Pap.* 186, 103810. doi: 10.1016/j.dsr.2022.103810

Sarno, C. T., Benitez-Nelson, C. R., Ziolkowski, L. A., Hendy, I. L., Davis, C. V., Tappa, E. J., et al. (2020). The impacts of flood, drought, and turbidites on organic carbon burial over the past 2,000 years in the Santa Barbara basin, california. *Paleoceanogr. Paleoclimatology* 35, e2020PA003849. doi: 10.1029/2020PA003849

Schubert, C. J., and Calvert, S. E. (2001). Nitrogen and carbon isotopic composition of marine and terrestrial organic matter in Arctic ocean sediments: implications for nutrient utilization and organic matter composition. *Deep-Sea Res. Part I-Oceanogr. Res. Pap.* 48, 789–810. doi: 10.1016/S0967-0637(00)00069-8

Schubert, C., Villanueva, J., Calvert, S., Cowie, G., Von Rad, U., Schulz, H., et al. (1998). Stable phytoplankton community structure in the Arabian Sea over the past 200,000 years. *Nature* 394 (6693), 563–566. doi: 10.1038/29047

Sigman, D. M., Granger, J., DiFiore, P. J., Lehmann, M. M., Ho, R., Cane, G., et al. (2005). Coupled nitrogen and oxygen isotope measurements of nitrate along the eastern north pacific margin. *Glob. Biogeochem. Cycle* 19 (4), GB4022. doi: 10.1029/2005GB002458

Sigman, D. M., Robinson, R., Knapp, A. N., van Geen, A., McCorkle, D. C., Brandes, J. A., et al. (2003). Distinguishing between water column and sedimentary denitrification in the Santa Barbara basin using the stable isotopes of nitrate. *Geochem. Geophys. Geosyst.* 4, 1–20. doi: 10.1029/2002GC000384

Sydeman, W., Garcia-Reyes, M., Schoeman, D., Rykaczewski, R., Thompson, S., Black, B., et al. (2014). Climate change and wind intensification in coastal upwelling ecosystems. *Science* 345, 77–80. doi: 10.1126/science.12516

Tems, C. E., Berelson, W. M., and Prokopenko, M. G. (2015). Particulate $\delta^{15}N$ in laminated marine sediments as a proxy for mixing between the California undercurrent and the California current: A proof of concept. *Geophys. Res. Lett.* 42, 419–427. doi: 10.1126/science.1251635

Thornton, S. F., and McManus, J. (1994). Application of organic carbon and nitrogen stable isotope and C/N ratios as source indicators of organic matter provenance in estuarine systems: evidence from the Tay estuary, Scotland. *Estuar. Coast. Shelf Sci.* 38 (3), 219–233. doi: 10.1006/ecss.1994.1015

Thunell, R. C. (1998). Particle fluxes in a coastal upwelling zone: sediment trap results from Santa Barbara basin, California. *Deep-Sea Res. Part II-Top. Stud. Oceanogr.* 45 (8-9), 1863–1884. doi: 10.1016/S0967-0645(98)80020-9

Thunell, R. C., and Kepple, A. B. (2004). Glacial-Holocene $\delta^{15}N$ record from the gulf of tehuantepec, Mexico: Implications for denitrification in the eastern equatorial pacific and changes in atmospheric N_2O. *Glob. Biogeochem. Cycle* 18, 1–12. doi: 10.1029/2002GB002028

Van Geen, A. (2001). Baja California Coring cruise OXMZ01MV: core descriptions and CTD/Rosette data: RV Melville, Lamont-Doherty Earth Observatory, Technical Report LDEO 2001-01.

Venrick, E. L. (2012). Phytoplankton in the California current system off southern California: Changes in a changing environment. *Prog. Oceanogr.* 104, 46–58. doi: 10.1016/j.pocean.2012.05.005

Volkman, J. K. (1986). A review of sterol markers for marine and terrigenous organic matter. *Org. Geochem.* 9 (2), 83–99. doi: 10.1016/0146-6380(86)90089-6

Volkman, J. K., Barrett, S. M., Blackburn, S. I., Mansour, M. P., Sikes, E. L., and Gelin, F. (1998). Microalgal biomarkers: a review of recent research developments. *Org. Geochem.* 29 (5-7), 1163–1179. doi: 10.1016/S0146-6380(98)00062-X

Wang, Y., Hendy, I., and Napier, T. J. (2017). Climate and anthropogenic controls of coastal deoxygenation on interannual to centennial timescales. *Geophys. Res. Lett.* 44, 11,528–511,536. doi: 10.1002/2017GL075443

Wang, Y., Hendy, I. L., and Thunell, R. (2019). Local and remote forcing of denitrification in the northeast pacific for the last 2,000 years. *Paleoceanogr. Paleoclimatol.* 34, 1517–1533. doi: 10.1029/2019PA003577

Ward, B. B. (2011). "Nitrification in the ocean.," in *Nitrification*, ed. B. B. Ward, D. J. Arp and M. G. Klotz (Washington, DC: American Society for Microbiology Press), 323–345.

White, M. E., Rafter, P. A., Stephens, B. M., Wankel, S. D., and Aluwihare, L. I. (2019). Recent increases in water column denitrification in the seasonally suboxic bottom waters of the Santa Barbara basin. *Geophys. Res. Lett.* 46, 6786–6795. doi: 10.1029/2019GL082075

Xing, L., Zhao, M., Zhang, T., Yu, M., Duan, S., Zhang, R., et al. (2016). Ecosystem responses to anthropogenic and natural forcing over the last 100 years in the coastal areas of the East China Sea. *Holocene* 26, 669–677. doi: 10.1177/0959683615618248

frontiers | Frontiers in Marine Science

TYPE Original Research
PUBLISHED 28 September 2022
DOI 10.3389/fmars.2022.1034145

OPEN ACCESS

EDITED BY
Xianbiao Lin,
Ocean University of China, China

REVIEWED BY
Min Luo,
Fuzhou University, China
Fenfang Wang,
Xiamen University, China

*CORRESPONDENCE
Xuexin Shao
shaoxuexin@126.com

SPECIALTY SECTION
This article was submitted to Marine Biogeochemistry, a section of the journal Frontiers in Marine Science

RECEIVED 01 September 2022
ACCEPTED 14 September 2022
PUBLISHED 28 September 2022

CITATION
Liu C, Li N, Shao X, Gao D, Xia J, Cui Q and Zhang D (2022) Effects of coastal marsh conversion to shrimp aquaculture ponds on sediment nitrogen fixation.
Front. Mar. Sci. 9:1034145.
doi: 10.3389/fmars.2022.1034145

Effects of coastal marsh conversion to shrimp aquaculture ponds on sediment nitrogen fixation

Cheng Liu[1], Niu Li[2], Xuexin Shao[2]*, Dengzhou Gao[3], Jiangbao Xia[1], Qian Cui[1] and Dongjie Zhang[1]

[1]Shandong Key Laboratory of Eco-Environmental Science for the Yellow River Delta, Binzhou University, Binzhou, China, [2]Wetland Ecosystem Research Station of Hangzhou Bay, Research Institute of Subtropical Forestry, Chinese Academy of Forestry, Hangzhou, China, [3]State Key Laboratory of Estuarine and Coastal Research, East China Normal University, Shanghai, China

As a common reclamation practice in global estuaries and coasts, conversion of natural wetlands to aquaculture ponds for food demand had significant effects on nitrogen (N) cycling processes. However, the response of sedimemt N fixation process on this conversion remains poorly understood. Here, slury incubation experiment combined with ^{15}N isotope tracing method and molecular analysis technique were used to investigate the influences of conversion of natural marshland to shrimp ponds on sediemt N fixation process. The results showed that conversion of natural marshland to shrimp ponds significantly promoted sediment N fixation rate. The increasing of sediment N fixation rate may be mainly attributed to the change of sediment EC, TOC and Fe^{2+}/Fe^{3+} rather than the change of N fixation gene abundance. In addition, there was no obvious difference in sediment N fixation rate between 5-year-old shrimp ponds and 18-year-old shrimp ponds, which may be ascribed to the increasing inhibiting effect of inorganic N concentration with reclamation time. Overall, our findings highlighted that conversion of natural wetlands to aquaculture ponds can affect the N budgets in estuarine and coastal regions by altering the sediment N fixation process.

KEYWORDS

N fixation, N cycling, agricultural reclamation, shrimp aquaculture, coastal wetland, environmental implication

Introduction

Coastal wetlands provide a variety of importance ecosystem services, including natural coastal protection, contaminant purification, bird habitat and nutrient cycle (Schuerch et al., 2018). Over the past few decades, reactive nitrogen (N) loadings in estuarine and coastal zones have increased significantly, causing a series of eco-environmental problems, such as eutrophication, algal bloom and hypoxia (Deegan et al., 2012; Damashek and Francis, 2018). Anthropogenic input of reactive N is regarded as the major reason for the overloaded N in this ecosystem (Capone et al., 2005; Fulweiler et al., 2015; Lin and Lin, 2022). However, microbial N fixation, the reduction of atmospheric dinitrogen gas (N_2) to available ammonia, may also be an important and internal source of reactive N in estuarine and coastal environments (Gardner et al., 2006). Thus, increasing attention to microbial N fixation process in estuarine and coastal ecosystems has been raised in recent years (Fulweiler et al., 2013; Lin et al., 2017; Hou et al., 2018).

Numerous studies have examined the spatio-temporal variability of the N fixation process across the estuarine and coastal ecosystems, and noted that the process rate is affected by temperature, pH, salinity, sulfide, carbon and N substrate availability to a certain extent (Fulweiler et al., 2013; Wang et al., 2018a; Li et al., 2021). For instance, Wang et al. (2018a) found that N fixation rates in the East China Sea were significantly related to temperature, salinity, sulfide, iron and C/N. While in the intertidal wetlands of Yangtze Estuary, the N fixation process was closely associated with salinity, pH, organic carbon and NH_4^+ (Hou et al., 2018). Saltmarsh plants can alter sediment physicochemical properties and further affect the N fixation process (Huang et al., 2016). In addition, a recent study reported that increased overlying NO_3^- contents can reduce microbial N fixation rates at different organic carbon concentrations (Li et al., 2021). Sediment microbial communities could also control the N fixation, with the abundance of *nifH* gene being indicative of N fixation activities in estuarine and coastal wetlands (Huang et al., 2016). Previous study found that the *nifH* gene abundance had similar spatial variation trend with the N fixation rate in the Yangtze Estuary, and a positive relationship was also observed for these two parameters (Hou et al., 2018). However, Wang et al. (2018a) reported that sediment physicochemical variables rather than functional microbes mediated the N fixation process rate in the East China Sea. Although a lot studies have been conducted to investigate N fixation process, the influencing factors and mechanisms controlling N fixation process in coastal wetlands remain largely uncertain due to the complexity of coupled biotic and abiotic conditions.

Reclamation of estuarine and coastal wetlands for agriculture is a common practice around the world and has resulted in a significant deterioration of wetland ecosystem functions (Sun et al., 2015; Murray et al., 2019). The aquaculture pond is one of the most common types of agricultural reclamation in estuarine and coastal wetlands, which can profoundly affect sediment element cycles due to the changed hydrology and management modes (Yang et al., 2017b). Generally, intensive aquaculture is maintained based on the daily addition of feeds, and the majority of feeds are accumulated in the sediments because only a small proportion of feeds is utilized by cultured animals (Chen et al., 2016). Therefore, aquaculture reclamation could dramatically increase sediment carbon and N contents (Murphy et al., 2016; Gao et al., 2018). In addition, remarkable changes of greenhouse gases emission were observed when natural saltmarsh conversion to aquaculture ponds (Yang et al., 2017a and Yang et al., 2019). Recently, some studies have explored the impacts of aquaculture on sediment nitrification, denitrification, anammox and dissimilatory nitrate reduction to ammonium (DNRA), and they noted that aquaculture can affect N budgets of aquatic ecosystems through changing microbial N transformation processes (Murphy et al., 2016; Gao et al., 2019b). In fact, sediment N fixation is also an important N source in estuarine and coastal ecosystems, but it is not clear how the N fixation process change after natural saltmarsh conversion to aquaculture ponds. Considering that China has the largest aquaculture industry in the world with a total area of 2.6×10^6 ha (Chen et al., 2016), we selected a typical shrimp aquaculture reclamation areas in the Min River estuary of southeastern China as study areas to reveal the influences of aquaculture reclamation on sediment N fixation process. The specific aims of this study were (1) to explore the changes in rate and associated functional gene abundance of sediment N fixation process after coastal saltmarsh conversion to shrimp aquaculture ponds, (2) to reveal the main environmental factors governing the sediment N fixation process, and (3) to assess the environmental implication changes of sediment N fixation process after the conversion of coastal saltmarsh to shrimp ponds.

Materials and methods

Study area and sample collection

The study was conducted in Shanyutan wetland (22°00′36″–26°03′42″N, 119°34′12″–119°41′40″E, Figure 1), the brackish-water tidal wetland in the Minjiang River estuary in Fujian Province, Southeast China (Tong et al., 2012). The study area is characterized by a subtropical monsoonal climate with hot and humid in summer and dry and cold in winter (Wang et al., 2018b). The mean annual temperature and precipitation were 19.6°C and 1350 mm, respectively (Tong et al., 2010). Shanyutan wetland is subjected to the formal semi-diurnal tide, with a tide range of 2.5 – 6 m (Zhang et al., 2015). The study area has a high

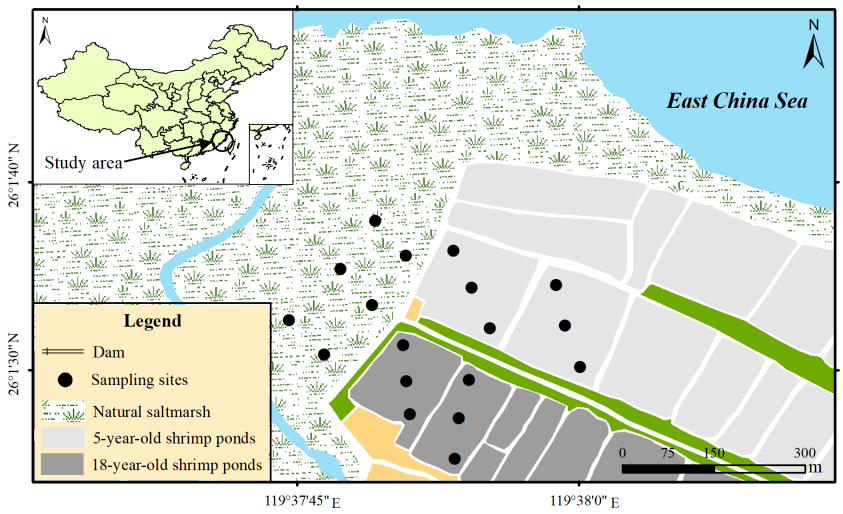

FIGURE 1
Study area and sampling sites (Figure 1 is quoted from our previous research (Gao et al., 2019b).

diversity of vegetation species, with native *Phragmite australis*, *Scirpus triqueter* and *Cyperus malaccensis* and exotic invasive *Spartina alterniflora* being the dominant vegetation species (Zhang et al., 2011).

In recent years, large-scale conversion of natural wetland was performed in Shanyutan, and almost all of the natural wetland was converted to aquaculture ponds to increase seafood demand (Yang et al., 2017a). Shrimp pond is one of the most important aquaculture ponds (Yang et al., 2019). The shrimp culture period usually starts in June and ends in November, with only harvest once a year (Yang et al., 2017a). Before breeding, saltwater from the adjacent estuary was injected into the shrimp pond using a submerged pump at once to retain the mean water depth of 1.4 m during the shrimp culture period (Yang et al., 2019). After harvest, the pond water was discharged into the adjacent estuary. During the shrimp culture period, feeding and aeration were operated twice and four times per day, respectively.

According to reclamation time, the shrimp ponds in Shanyutan could be mainly divided into two categories: shrimp ponds reclaimed in 1998 and 2011. To assess the impact of natural wetland conversion to shrimp culture pond on sediment N fixation process, sediment cores (5 cm deep) were retrieved twice in July and November 2016 in three typical sampling sites: natural saltmarsh, 5-year-old shrimp ponds (ponds reclaimed in 2011), and 18-year-old shrimp ponds (ponds reclaimed in 1998), each of which had six replicate locations. In this study, the sediment core was retrieved using an acrylic tube (7.0 cm diameter and 20 cm deep), which was installed into a surface-operated coring device equipped with a core cylinder and a one-way check valve (Gao et al., 2019b). After collection, the sediment cores were preserved in sterile bags and transported to the laboratory immediately. In the laboratory, sediment sample was mixed homogeneously and divided into two parts. One fresh part was used to determine the sediment N fixation rate and parameters. The other part was preserved at -80°C for analyses of molecular microbiology. In addition, 5 L overlying water was taken from each location for the determination of the sediment N fixation rate.

Analysis of sediment parameters

The *in situ* pH and electrical conductivity (EC) of sediment were measured using IQ150 pH meter (IQ Scientific Instruments, USA) and 2265FS EC meter (Spectrum Technologies Inc., USA), respectively. The water content was determined based on the weight loss of fresh sediment through oven drying (Hou et al., 2018). The TOC and TN of sediment were analyzed using Vario EL elemental analyzer (Elementar, Germany) as described by Gao et al. (2019a). Sediment NH_4^+ and NO_x^- were extracted using 1 M KCl and then measured by a continuous flow analyzer (Skalar Analytical SAN^{++}, Netherlands) (Hou et al., 2015). The Fe^{2+} and Fe^{3+} of sediment were extracted with 0.5 M HCl and then analyzed using the phenanthroline method (Lovley and Phillips, 1987).

Determination of sediment potential N fixation rate

In this study, sediment potential N fixation rates (NFR) was determined by using slurry incubation experiment in combination

with ^{15}N isotope tracing technique which was improved on the basis of the previous method described by Hou et al. (2018). Briefly, the slurry was prepared by mixing the overlying water and sediment at a ratio of 7:1. Then, the homogeneous slurry was purged with helium (He) for 30 min to remove background N_2 and transferred into 12 mL gas-tight vials (Exetainers, Labco, UK) in He-filled glove box. All vials were divided into two parts. One part was immediately injected with 0.2 mL saturated $ZnCl_2$ solution to inhibit microbial activity and designated as initial sample. The other part was injected with 0.5 mL 99 atom% ^{15}N-N_2 (Campro Scientific, Germany) and incubated in dark at near *in situ* temperature for about 24 h. These vials were preserved by adding 0.2 mL $ZnCl_2$ solution and designated as final samples. Then, all vials were purged with He for 30 min to remove N_2 and injected with hypobromite iodine solution to oxidize ^{15}N-labeled products generated by N fixation into N_2. The concentrations of $^{29}N_2$ and $^{30}N_2$ in all samples were determined by membrane inlet mass spectrometry (HPR-40, Hiden Analytical, UK). The differences of ^{15}N-labeled N_2 concentrations between final and initial samples were used to calculate NFR. This method is especially suitable for relative comparisons of different N transformation rates (Aoki and McGlathery, 2017). Nevertheless, because slurry mixing removed sediment biogeochemical gradients, the method may not reflect the actual N fixation rate *in situ* environment (Behrendt et al., 2013).

Sediment DNA extraction and quantitative polymerase chain reaction

We quantified the *nifH* encoding the key enzyme for N fixation to explore the potential impact of diazotrophs on N fixation process (Hou et al., 2018). According to the manufacturer's instruction, the sediment DNA was extracted with Powersoil™ DNA Isolation Kits (MO BIO, USA). The extracted sediment DNA was stored at -80°C before subsequent analysis. The *nifH* gene fragment was amplified using nifHfw (5'-GGH AAR GGH GGH ATH GGN AAR TC-3') and nifHrv (5'-GGC ATN GCR AAN CCV CCR CAN AC-3') primers (Wang et al., 2018a). Then, the abundance of *nifH* was quantified by q-PCR using an ABI 7500 Sequence Detection System (Applied Biosystems, Canada) and SYBR green method. The detailed information of q-PCR protocol was shown in Table S1. The relative abundance of *nifH* gene in sediment was calculated by the standard curve which was constructed by diluting a known amount of plasmid DNA including *nifH* fragment into six gradients (from 2.50×10^4 to 2.50×10^9 copies μL^{-1}). The amplification efficiency was above 96% in this study, and the correlation coefficient was higher than 0.99.

Statistical analysis

The data were checked for normal distribution and homogeneity of variance and transformed if necessary before statistical analysis (Täumer et al., 2020). Pearson's correlation analysis (SPSS 22.0) and Redundancy analysis (RDA) (Canoco 5) were performed to reveal relationships between sediment parameters, *nifH* abundance, and N fixation rate. Path analysis (AMOS 22.0) was used to futher explore the effects of shrimp aquaculture reclamation on N fixation process. Before path analysis, a conceptual model was constructed based on existing literature and ecological principles (Liu et al., 2018). Then, the model was improved in a stepwise manner. In present study, column and box charts were drawn using Origin 2021.

Results

Sediment physicochemical parameters

Measured sediment physicochemical parameters were shown in Figure 2 (This data was quoted from our previous studies (Gao et al., 2019b)). The water content of sediment was generally higher in 18-year-old ponds than in 5-year-old ponds and natural saltmarsh, but no obvious difference was observed between the latter two. Sediment pH ranged from 6.28 to 7.11 and 6.16 to 6.98 in summer and winter, respectively, with no significant difference among the natural saltmarsh, 5-year-old ponds and 18-year-old ponds. Summer EC in natural saltmarsh and 5-year-old ponds were significantly higher than that of 18-year-old ponds, while in winter, sediment EC was higher in natural saltmarsh than in 5-year-old ponds and 18-year-old ponds. Sediment TOC content varied from 16.03 to 33.24 g kg^{-1} and 16.01 to 35.40 g kg^{-1} in summer and winter, respectively, and the content was generally higher in shrimp ponds (5-year-old ponds and 18-year-old ponds) than in natural saltmarsh. The NH_4^+ and NO_x^- concentrations of sediment ranged from 15.78 to 98.31 mg kg^{-1} and 1.39 to 3.45 mg kg^{-1}, respectively, and their changes patterns were similar to TOC. There was no significant difference in TN content between the natural saltmarsh and shrimp ponds in summer, but the TN content in 18-year-old ponds was higher than that of the natural saltmarsh in winter. Sediment Fe^{2+}/Fe^{3+} in shrimp ponds (1.44 – 2.52) was generally higher than that of natural saltmarsh (0.64 – 0.91), although some difference was not significant.

Sediment potential N fixation rates and *nifH* gene abundance

Sediment potential N fixation rates ranged from 6.16 to 10.31 nmol g^{-1} h^{-1} and from 3.71 to 7.84 nmol g^{-1} h^{-1} in summer and winter, respectively, with higher N fixation rates in summer (Figure 3). Compared with natural saltmarsh, shrimp ponds had higher N fixation rates in both summer and winter (Figure 3). However, There was no obvious difference in N fixation rates between 5-year-old and 18-year-old shrimp ponds (Figures 3, 5).

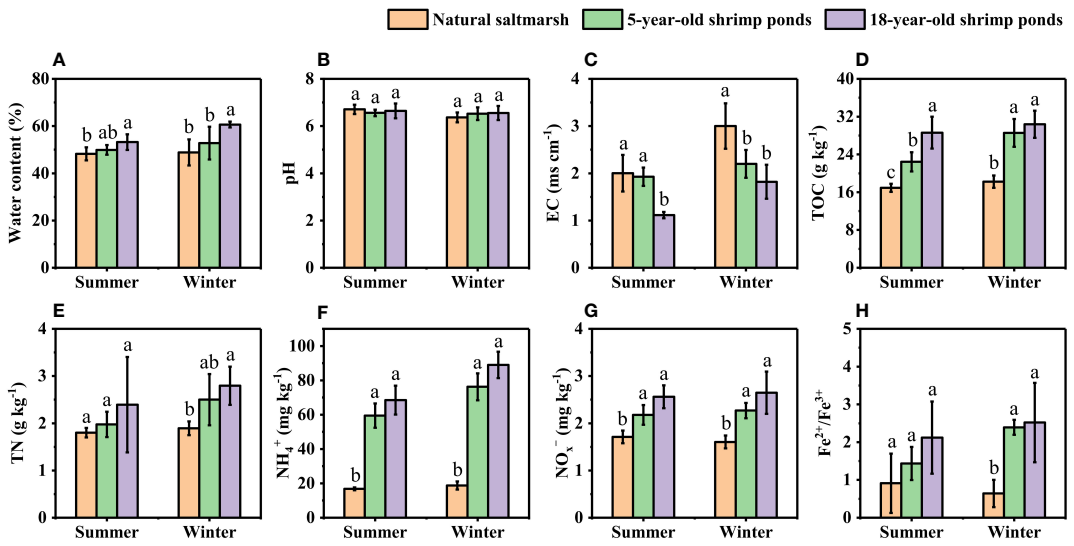

FIGURE 2
Sediment physicochemical properties of natural saltmarsh and shrimp ponds. Different lowercase letters indicate significant differences ($p < 0.05$) among natural saltmarsh and shrimp ponds in the same season. **(A)** Water content, **(B)** pH, **(C)** EC, **(D)** TOC, **(E)** TN, **(F)** NH4+, **(G)** NO_x-, **(H)** Fe^{2+}/Fe^{3+}.

Sediment *nifH* gene abundance varied from 1.26×10^8 to 1.26×10^8 copies g^{-1} and 7.33×10^7 to 1.04×10^8 copies g^{-1} in summer and winter, respectively, with no significant difference among the natural saltmarsh, 5-year-old and 18-year-old shrimp ponds (Figure 4). In addition, the mean abundance of *nifH* gene was also higher in summer than that in winter (Figure 4).

Influences of sediment parameters on N fixation rates

Potential N fixation rate was significantly related to sediment EC, TOC, NH_4^+, NO_x^- and Fe^{2+}/Fe^{3+} in summer and winter, respectively, and only significantly related to TN in winter

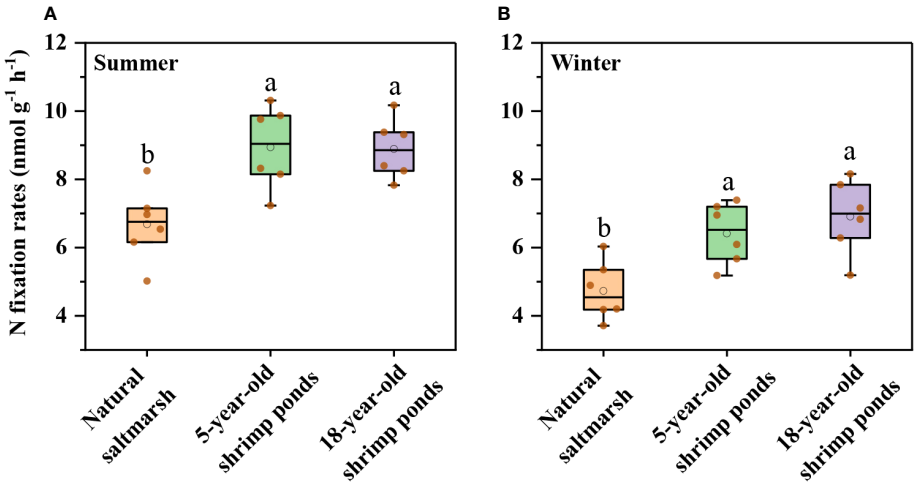

FIGURE 3
Sediment N fixations rates of natural saltmarsh and shrimp ponds in **(A)** Summer and **(B)** Winter. Different lowercase letters indicate significant differences ($p < 0.05$) among natural saltmarsh and shrimp ponds in the same season.

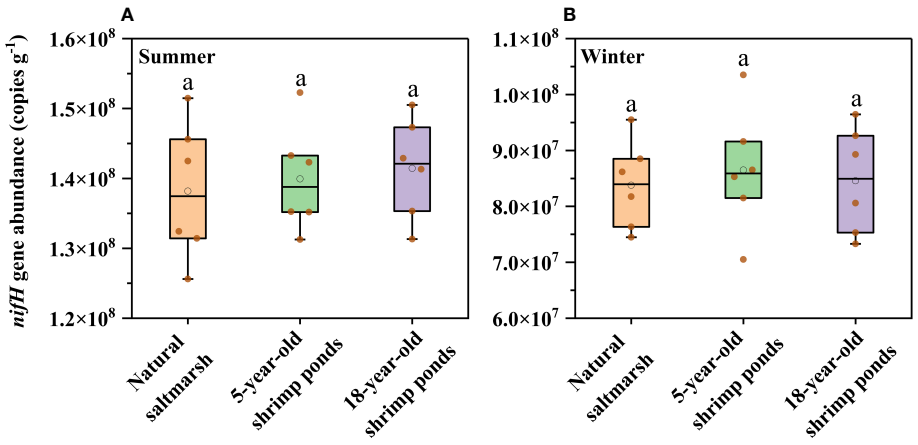

FIGURE 4
Sediment *nifH* gene abundance of natural saltmarsh and shrimp ponds in **(A)** Summer and **(B)** Winter. Different lowercase letters indicate significant differences ($p < 0.05$) among natural saltmarsh and shrimp ponds in the same season.

(Table 1). For bulked two-season data, the N fixation rate was significantly associated with sediment EC, NH_4^+, NO_x^- and *nifH* gene (Table 1). In addition, results from the RDA of sediment physicochemical parameters, *nifH* gene abundance and N fixation rate showed that sediment samples in natural saltmarsh were clearly separated from those in shrimp ponds along Axis 1 (Figure 5). The sum of Axis 1 and Axis 2 accounted for 60.4% and 55.3% of the variation in sediment parameters measured in summer and winter, respectively (Figure 5). Sediment N fixation rate, EC, TOC, NH_4^+, NO_3^- and Fe^{2+}/Fe^{3+} contributed significantly to the variation of Axis 1, while *nifH* gene abundance was minor importance in the variation of Axis 1 (Figure 5). Predicted path model further showed that reclamation time can influence N fixation rate by affecting sediment EC, NH_4^+ and *nifH* gene abundance (Figure 6).

TABLE 1 Pearson's correlation coefficients for relations between sediment parameters and N fixation rates.

Parameter	Pearson's correlation coefficients		
	Summer $n = 18$	winter $n = 18$	Summer + winter $n = 36$
Water content	0.25	0.36	0.02
pH	-0.08	0.10	0.20
EC	**-0.53***	**-0.72****	**-0.74****
TOC	**0.56***	**0.67****	0.30
TN	0.25	**0.54***	0.10
NH_4^+	**0.72****	**0.72****	**0.39***
NO_x^-	**0.56***	**0.74****	**0.49***
Fe^{2+}/Fe^{3+}	**0.48***	**0.49***	0.26
nifH gene	0.10	0.07	**0.61****

Bold values indicate significant correlation coefficients. Significance levels: *$p < 0.05$, **$p < 0.01$.

Discussion

Previous studies suggested that the conversion of natural saltmarsh to aquaculture ponds has a significant influence on nutrient element biogeochemical cycle (Murphy et al., 2016; Gao et al., 2019b). In present study, the sediment potential N fixation rates in shrimp ponds were significantly higher than those in natural saltmarsh (Figure 3), which verified previous studies (Gao et al., 2019b). RDA further indicated that the sediment potential N fixation rates in shrimp ponds were clearly separated from those in natural saltmarsh (Figure 5). This phenomenon could be explained by the changes of sediment physicochemical parameters.

Generally, low salinity was in favor of the metabolism of diazotrophic and N fixation process (Tel-or, 1980; Severin et al., 2012). Previous study shown that shrimp ponds water extracted from adjacent estuary could decrease sediment salinity of original natural saltmarsh (Yang et al., 2017b). In this study, the sediment EC of shrimp ponds were lower than those of natural saltmarsh, which was consistent with previous study (Figure 2C). Thus, decreased sediment EC provided a favorable environment for the N fixation process, which was supported by the significant negative correlation between sediment EC and N fixation rate (Table 1). TOC is another important factor in controlling N fixation process due to its supplement of energy for heterotrophic organisms (Gier et al., 2016; Moseman-Valtierra et al., 2016; Wang et al., 2018a). In present study, sediment TOC content increased significantly after the conversion of natural saltmarsh to shrimp ponds (Figure 2D), which could explain the increasing of the sediment potential N fixation rates. The significant positive correlatin between TOC content and N fixation rate further confirmed this explanation (Table 1). It has been noted that in

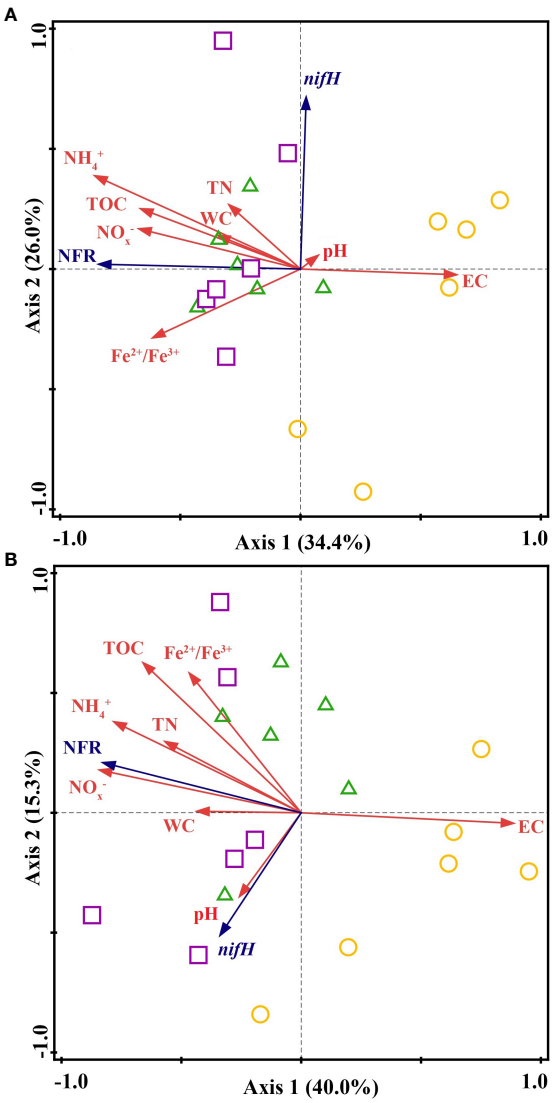

FIGURE 5
The redundancy analysis (RDA) of N fixation rates (NFR) and *nifH* gene abundance with sediment parameters. The yellow circles, green triangles and purple squares represent natural saltmarsh, 5-year-old shrimp ponds and 18-year-old shrimp ponds in **(A)** summer and **(B)** winter, respectively.

addition to the quantity of organic matter, the quality of organic matter may play a more important role in mediating the N fixation (Newell et al., 2016). However, we did not analyze the components of organic carbon and future studies will be conducted to explore the impact of different organic carbon fractions on N fixation process. Futhermore, we observed sediment Fe^{2+}/Fe^{3+} ratios in shrimp ponds were generally higher than those in natural saltmarsh (Figure 2H), indicating that shrimp ponds can stimulate the reduction of Fe^{3+} to Fe^{2+} (Gao et al., 2019b). The significant positive correlation of Fe^{2+}/Fe^{3+} ratio with N fixation rate was observed in present study (Table 1 and Figure 5). Previous studies have noted that iron-reducing bacteria may be also responsible for the N fixation process (Bertics et al., 2010; Gier et al., 2017). Thus, we hypothesize that the reduction of Fe^{3+} to Fe^{2+} can indirectly promote the process rates of N fixation.

In addition to environmental parameters, many works have noted that the N fixation process was influenced largely by relevant microorganisms, and *nifH* gene can be regarded as a critical indicator of N fixation process (Huang et al., 2016; Damashek and Francis, 2018; Hou et al., 2018). Despite the *nifH* gene abundance in shrimp ponds was higher than that in natural saltmarsh, there was no obvious correlation between *nifH* gene abundance and sediment potential N fixation rate

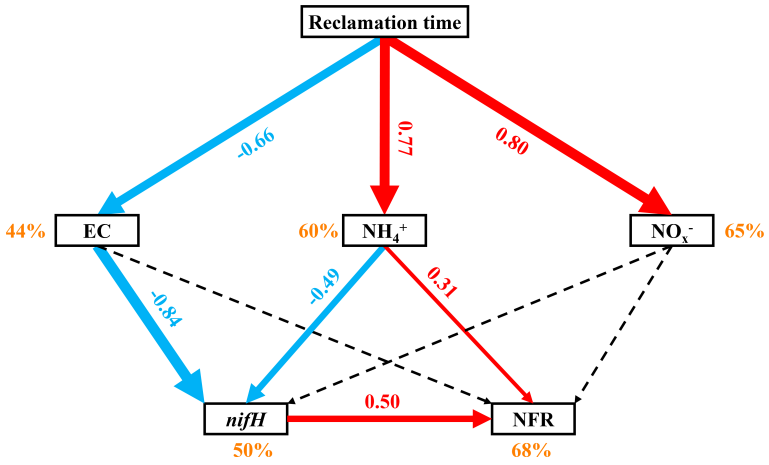

FIGURE 6
Predicted path models relating reclamation time to N fixation rates (NFR). Solid red lines indicate significant positive effects, solid blue lines indicate significantly negative effects, and black dashed lines indicate insignificant effects. Numbers adjacent to the lines are standardized path coefficients, also shown by the width of the lines. Percentages adjacent to the variables indicate their explained variance.

(Figure 4 and Figure 5), which indicated that compared with the change of sediment physicochemical factors, the change of *nifH* gene abundance may not be the main factor affecting the N fixation during the conversion of natural saltmarsh to shrimp ponds. In addition to functional gene abundance, the expression of functional gene and the structure and composition of microbial community may have significant impacts on microbial activitiy (Gao et al., 2017). Therefore, the role of microbe on N fixation should be further explored.

Compare with 5-year-old shrimp ponds, 18-year-old shrimp ponds had higher TOC contents and Fe^{2+}/Fe^{3+} ratios and lower sediment EC (Figure 2), which was expected to cause a higher N fixation rates in 18-year-old shrimp ponds than those in 5-year-old shrimp ponds. Unexpectedly, there was no significant difference in sediment potential N fixation rate between shrimp ponds with different reclamation time (Figure 3 and Figure 5). This phenomenon might be attributed to the inhibiting effect of inorganic N (Capone et al., 2005). Many previous studies found that high concentration of inorganic N, especially NH_4^+, may inhibit N fixation (Bertics et al., 2010; Moseman-Valtierra et al., 2016). Sediment NH_4^+ and NO_x^- in 18-year-old shrimp ponds were generally higher than those in 5-year-old shrimp ponds, which may be the important reason for this unexpected phenomenon. Predicted path model futher indicated that the increasing of reclamation time could promote the concentraions of NH_4^+, which could inhibit N fixation process (Figure 6).

It's noteworthy that natural saltmarsh and shrimp ponds had same seasonal dynamics of N fixation process with high N fixation rates in summer and low N fixation rates in winter (Figure 3). This phenomenon might be attributed to the temperature change. Previous studies have documented that temperature rising could directly promote N fixation rate in estuarine and coastal ecosystems (Hou et al., 2018). The temperature of the Min River Estuary was higher in July (31.2 – 33.9°C) than that in November (19.6 – 21.1°C) (Gao et al., 2019b), which caused that both natural saltmarsh and shrimp ponds in Min River Estuary had higher N fixation rates in summer than in winter. In addition to direct effect, temperature may regulate the N fixation process through its impact on relevant microorganisms (Huang et al., 2016; Damashek and Francis, 2018). Our result showed that *nifH* gene abundance in summer was significantly higher than that in winter, implying the functional gene may be an important factor in controlling the seasonal dynamics of N fixation process. For bulked two-season data, the N fixation rate were significantly associated with the *nifH* gene abundance, which also supported the aforesaid opinion (Table 1).

In last few decades, anthropogenic reactive N has continually increased due to intensive industrial and agricultural activities (Davidson, 2009). Since about 20–30% of reactive N has been delivered into estuarine and coastal ecosystems, the N transformation is important for the N balance in such ecosystems (Plummer et al., 2015; Huang et al., 2021). Reclamation is one of the main anthropogenic disturbances in coastal wetlands that could change the intrinsic N balance. Based on the measured N fixation rates and sediment densities, we estimated that the amounts of N fixation in natural marshland, 5-year-old and 18-year-old shrimp ponds were about 50.7, 68.3 and 70.2 g N m^{-2} $yr.^{-1}$, respectively. Previous study showed that the amounts of N loss in natural marshland, 5-year-old and 18-year-old shrimp ponds were about 88.9, 116.6 and 130.6 g N m^{-2} $yr.^{-1}$, respectively (Gao et al., 2019b). By comparing the amounts

of N fixation and N loss, we found that natural marshland, 5-year-old and 18-year-old shrimp ponds had same ratio of N fixation to N loss (about 55%), which suggested that although conversion of natural saltmarsh to shrimp ponds simultaneously promoted N fixation and loss, it had no obvious effects on the whole N cycling. Thus, when we evaluate the effects of reclamation on the N budgets in estuarine and coastal wetlands, comprehensive N cycling processes should be taken into full consideration.

Conclusion

This study elucidated the impacts of conversion of natural marshland to shrimp ponds on sediment N fixation process in estuarine and coastal areas. This conversion significantly promoted the process rate of sediment N fixation. However, different reclamation time of shrimp ponds had no significant effects on the sediment N fixation process. The variation of sediment EC, TOC, Fe^{2+}/Fe^{3+} and inorganic N driven by this conversion were key factors to control sediment N fixation. Futher, the conversion of natural marshland to shrimp ponds simultaneously facilitated sediment N fixation and N loss, highlighting the significance of considering comprehensive N cycling processes when evaluating the environmental implications of aquaculture reclamation on the N budgets in estuarine and coastal wetlands.

Data availability statement

The original contributions presented in the study are included in the article/Supplementary Material. Further inquiries can be directed to the corresponding author.

Author contributions

CL: Investigation, Formal analysis, Writing-original draft, Writing-review and editing. NL: Writing-review and editing. XS: Conceptualization, Funding acquisition, Methodology, Formal analysis, Writing-review and editing, Supervision. DG: Conceptualization, Funding acquisition, Project administration. JX, QC and DZ: Investigation. All authors contributed to the article and approved the submitted version.

Funding

This work was supported by the Natural Science Foundation of China (grant numbers: 31870597, 41901118 and 42101111). It was also funded by the Special fund for cooperation of Zhejiang Province and Chinese academy of forestry (2021SY03); the Youth Innovation Support Program of Shandong Universities [grant number 2021KJ081]; the Shandong Provincial Natural Science Foundation (grant number ZR2021QD101); grants from China Postdoctoral Science Foundation (2021M691020); Open Fund of Key Laboratory of Geographic Information Science (Ministry of Education), East China Normal University [grant number KLGIS2021A03]; the Fundamental Research Funds for the Central Universities; and the PhD research startup foundation of Binzhou University [grant numbers 2021Y14 and 2021Y36].

Acknowledgments

Thanks are given to the editor and anonymous reviewers for valuable comments on this manuscript.

Conflict of interest

The authors declare that the research was conducted in the absence of any commercial or financial relationships that could be construed as a potential conflict of interest.

Publisher's note

Supplementary material

The Supplementary Material for this article can be found online at: https://www.frontiersin.org/articles/10.3389/fmars.2022.1034145/full#supplementary-material

References

Aoki, L. R., and McGlathery, K. J. (2017). Push-pull incubation method reveals the importance of denitrification and dissimilatory nitrate reduction to ammonium in seagrass root zone. *Limnol. Oceanogr-Meth.* 15, 766–781. doi: 10.1002/lom3.10197

Behrendt, A., de Beer, D., and Stief, P. (2013). Vertical activity distribution of dissimilatory nitrate reduction in coastal marine sediments. *Biogeosciences.* 10, 7509–7523. doi: 10.5194/bgd-10-8065-2013

Bertics, V. J., Sohm, J. A., Treude, T., Chow, C. E. T., Capone, D. G., Fuhrman, J. A., et al. (2010). Burrowing deeper into benthic nitrogen cycling: the impact of bioturbation on nitrogen fixation coupled to sulfate reduction. *Mar. Ecol. Prog. Ser.* 409, 1–15. doi: 10.3354/meps08639

Capone, D. G., Burns, J. A., Montoya, J. P., Subramaniam, A., Mahaffey, C., Gunderson, T., et al. (2005). Nitrogen fixation by trichodesmium spp.: An important source of new nitrogen to the tropical and subtropical north Atlantic ocean. *Global. Biogeochem. Cy.* 19, GB2024. doi: 10.1029/2004gb002331

Chen, Y., Dong, S., Wang, F., Gao, Q., and Tian, X. (2016). Carbon dioxide and methane fluxes from feeding and no-feeding mariculture ponds. *Environ. pollut.* 212, 489–497. doi: 10.1016/j.envpol.2016.02.039

Damashek, J., and Francis, C. A. (2018). Microbial nitrogen cycling in estuaries: From genes to ecosystem processes. *Estuar. Coast.* 41, 626–660. doi: 10.1007/s12237-017-0306-2

Davidson, E. A. (2009). The contribution of manure and fertilizer nitrogen to atmospheric nitrous oxide since 1860. *Nat. Geosci.* 2, 659–662. doi: 10.1038/ngeo608

Deegan, L. A., Johnson, D. S., Warren, R. S., Peterson, B. J., Fleeger, J. W., Fagherazzi, S., et al. (2012). Coastal eutrophication as a driver of salt marsh loss. *Nature.* 490, 388–392. doi: 10.1038/nature11533

Fulweiler, R. W., Brown, S. M., Nixon, S. W., and Jenkins, B. D. (2013). Evidence and a conceptual model for the co-occurrence of nitrogen fixation and denitrification in heterotrophic marine sediments. *Mar. Ecol. Prog. Ser.* 482, 57–68. doi: 10.3354/meps10240

Fulweiler, R. W., Heiss, E. M., Rogener, M. K., Newell, S. E., LeCleir, G. R., Kortebein, S. M., et al. (2015). Examining the impact of acetylene on n-fixation and the active sediment microbial community. *Front. Microbiol.* 6. doi: 10.3389/fmicb.2015.00418

Gao, D. Z., Chen, G. X., Li, X. F., Lin, X. B., and Zeng, C. S. (2018). Reclamation culture alters sediment phosphorus speciation and ecological risk in coastal zone of southeastern China. *CLEAN-Soil. Air. Water.* 46, 1700495. doi: 10.1002/clen.201700495

Gao, D. Z., Hou, L. J., Li, X. F., Liu, M., Zheng, Y. L., Yin, G. Y., et al. (2019a). Exotic *Spartina alterniflora* invasion alters soil nitrous oxide emission dynamics in a coastal wetland of China. *Plant Soil.* 442, 233–246. doi: 10.1007/s11104-019-04179-7

Gao, D. Z., Li, X. F., Lin, X. B., Wu, D. M., Jin, B. S., Huang, Y. P., et al. (2017). Soil dissimilatory nitrate reduction processes in the spartina alterniflora invasion chronosequences of a coastal wetland of southeastern China: Dynamics and environmental implications. *Plant Soil.* 421, 383–399. doi: 10.1007/s11104-017-3464-x

Gao, D. Z., Liu, M., Hou, L. J., Lai, D. Y. F., Wang, W. Q., Li, X. F., et al. (2019b). Effects of shrimp-aquaculture reclamation on sediment nitrate dissimilatory reduction processes in a coastal wetland of southeastern China. *Environ. pollut.* 255, 113219. doi: 10.1016/j.envpol.2019.113219

Gardner, W. S., McCarthy, M. J., An, S., Sobolev, D., Sell, K. S., and Brock, D. (2006). Nitrogen fixation and dissimilatory nitrate reduction to ammonium (DNRA) support nitrogen dynamics in Texas estuaries. *Limnol. Oceanogr.* 51, 558–568. doi: 10.4319/lo.2006.51.1_part_2.0558

Gier, J., Löscher, C. R., Dale, A. W., Sommer, S., Lomnitz, U., and Treude, T. (2017). Benthic dinitrogen fixation traversing the oxygen minimum zone off Mauritania (NW Africa). *Front. Mar. Sci.* 4. doi: 10.3389/fmars.2017.00390

Gier, J., Sommer, S., Löscher, C. R., Dale, A. W., Schmitz, R. A., and Treude, T. (2016). Nitrogen fixation in sediments along a depth transect through the Peruvian oxygen minimum zone. *Biogeosciences.* 13, 4065–4080. doi: 10.5194/bg-13-4065-2016

Hou, L. J., Wang, R., Yin, G. Y., Liu, M., and Zheng, Y. L. (2018). Nitrogen fixation in the intertidal sediments of the Yangtze estuary: Occurrence and environmental implications. *J. Geophys. Res-Biogeo.* 123, 936–944. doi: 10.1002/2018jg004418

Hou, L. J., Zheng, Y. L., Liu, M., Li, X. F., Lin, X. B., Yin, G. Y., et al. (2015). Anaerobic ammonium oxidation and its contribution to nitrogen removal in china's coastal wetlands. *Sci. Rep-UK.* 5, 15621. doi: 10.1038/srep15621

Huang, F. J., Lin, X. B., Hu, W. F., Zeng, F., He, L., and Yin, K. D. (2021). Nitrogen cycling processes in sediments of the pearl river estuary: Spatial variations, controlling factors, and environmental implications. *Catena.* 206, 105545. doi: 10.1016/j.catena.2021.105545

Huang, J. X., Xu, X., Wang, M., Nie, M., Qiu, S. Y., Wang, Q., et al. (2016). Responses of soil nitrogen fixation to *Spartina alterniflora* invasion and nitrogen addition in a Chinese salt marsh. *Sci. Rep-UK.* 6, 20384. doi: 10.1038/srep20384

Lin, X. B., Li, X. F., Gao, D. Z., Liu, M., and Cheng, L. (2017). Ammonium production and removal in the sediments of shanghai river networks: Spatiotemporal variations, controlling factors, and environmental implications. *J. Geophys. Res-Biogeo.* 122, 2461–2478. doi: 10.1002/2017jg003769

Lin, G. M., and Lin, X. B. (2022). Bait input altered microbial community structure and increased greenhouse gases production in coastal wetland sediment. *Water. Res.* 218, 118520. doi: 10.1016/j.watres.2022.118520

Li, S., Twilley, R. R., and Hou, A. X. (2021). Heterotrophic nitrogen fixation in response to nitrate loading and sediment organic matter in an emerging coastal deltaic floodplain within the Mississippi river delta plain. *Limnol. Oceanogr.* 66, 1961–1978. doi: 10.1002/lno.11737

Liu, W. Z., Yao, L., Jiang, X. L., Guo, L. D., Cheng, X. L., and Liu, G. H. (2018). Sediment denitrification in Yangtze lakes is mainly influenced by environmental conditions but not biological communities. *Sci. Total. Environ.* 616–617, 978–987. doi: 10.1016/j.scitotenv.2017.10.221

Lovley, D. R., and Phillips, E. J. P. (1987). Rapid assay for microbially reducible ferric iron in aquatic sediments. *Appl. Microbiol. Biot.* 53, 1536–1540. doi: 10.1128/aem.53.7.1536-1540.1987

Moseman-Valtierra, S., Levin, L. A., and Martin, R. M. (2016). Anthropogenic impacts on nitrogen fixation rates between restored and natural Mediterranean salt marshes. *Mar. Ecol.* 37, 370–379. doi: 10.1111/maec.12289

Murphy, A. E., Anderson, I. C., Smyth, A. R., Song, B., and Luckenbach, M. W. (2016). Microbial nitrogen processing in hard clam (Mercenaria mercenaria) aquaculture sediments: The relative importance of denitrification and dissimilatory nitrate reduction to ammonium (DNRA). *Limnol. Oceanogr.* 61, 1589–1604. doi: 10.1002/lno.10305

Murray, N. J., Phinn, S. R., DeWitt, M., Ferrari, R., Johnston, R., Lyons, M. B., et al. (2019). The global distribution and trajectory of tidal flats. *Nature.* 565, 222–225. doi: 10.1038/s41586-018-0805-8

Newell, S. E., McCarthy, M. J., Gardner, W. S., and Fulweiler, R. W. (2016). Sediment nitrogen fixation: A call for re-evaluating coastal n budgets. *Estuar. Coast.* 39, 1626–1638. doi: 10.1007/s12237-016-0116-y

Plummer, P., Tobias, C., and Cady, D. (2015). Nitrogen reduction pathways in estuarine sediments: Influences of organic carbon and sulfide. *J. Geophys. Res-Biogeo.* 120, 1958–1972. doi: 10.1002/2015jg003057

Schuerch, M., Spencer, T., Temmerman, S., Kirwan, M. L., Wolff, C., and Lincke, D. (2018). Future response of global coastal wetlands to sea-level rise. *Nature.* 561, 231–234. doi: 10.1038/s41586-018-0476-5

Severin, I., Confurius-Guns, V., and Stal, L. J. (2012). Effect of salinity on nitrogenase activity and composition of the active diazotrophic community in intertidal microbial mats. *Arch. Microbiol.* 194, 483–491. doi: 10.1007/s00203-011-0787-5

Sun, Z. G., Sun, W. G., Tong, C., Zeng, C. S., Yu, X., and Mou, X. J. (2015). China's coastal wetlands: Conservation history, implementation efforts, existing issues and strategies for future improvement. *Environ. Int.* 79, 25–41. doi: 10.1016/j.envint.2015.02.017

Täumer, J., Kolb, S., Boeddinghaus, R. S., Wang, H. T., Schöning, I., Schrumpf, M., et al. (2020). Divergent drivers of the microbial methane sink in temperate forest and grassland soils. *Global. Change. Biol.* 27, 929–940. doi: 10.1111/gcb.15430

Tel-Or, E. (1980). Response of N_2-fixing cyanobacteria to salt. *Appl. Environ. Microb.* 40, 689–693. doi: 10.1128/aem.40.4.689-693.1980

Tong, C., Wang, W. Q., Huang, J. F., Gauci, V., Zhang, L. H., and Zeng, C. S. (2012). Invasive alien plants increase CH_4 emissions from a subtropical tidal estuarine wetland. *Biogeochemistry.* 111, 677–693. doi: 10.1007/s10533-012-9712-5

Tong, C., Wang, W. Q., Zeng, C. S., and Marrs, R. (2010). Methane emissions from a tidal marsh in the Min river estuary, southeast China. *J. Environ. Sci. Heal. A.* 45, 506–516. doi: 10.1080/10934520903542261

Wang, W. M., Hu, M. J., Ren, H. C., Li, J. B., Tong, C., and Musenze, R. S. (2018b). Seasonal variations of nitrous oxide fluxes and soil denitrification rates in subtropical freshwater and brackish tidal marshes of the Min river estuary. *Sci. Total. Environ.* 616–617, 1404–1413. doi: 10.1016/j.scitotenv.2017.10.175

Wang, R., Li, X. F., Hou, L. J., Liu, M., Zheng, Y. L., Yin, G. Y., et al. (2018a). Nitrogen fixation in surface sediments of the East China Sea: Occurrence and environmental implications. *Mar. pollut. Bull.* 137, 542–548. doi: 10.1016/j.marpolbul.2018.10.063

Yang, P., Bastviken, D., Lai, D. Y. F., Jin, B. S., Mou, X. J., Tong, C., et al. (2017a). Effects of coastal marsh conversion to shrimp aquaculture ponds on CH_4 and N_2O emissions. *Estuar. Coast. Shelf.* S. 199, 125–131. doi: 10.1016/j.ecss.2017.09.023

Yang, P., Lai, D. Y., Jin, B. S., Bastviken, D., Tan, L. S., and Tong, C. (2017b). Dynamics of dissolved nutrients in the aquaculture shrimp ponds of the Min river estuary, China: Concentrations, fluxes and environmental loads. *Sci. Total. Environ.* 603, 256–267. doi: 10.1016/j.scitotenv.2017.06.074

Yang, P., Zhang, Y., Yang, H., Zhang, Y. F., Xu, J., Tan, L. S., et al. (2019). Large Fine-scale spatiotemporal variations of CH_4 diffusive fluxes from shrimp aquaculture ponds affected by organic matter supply and aeration in southeast China. *Biogeosciences.* 124, 1290–1307. doi: 10.1029/2019jg005025

Zhang, W. L., Zeng, C. S., Tong, C., Zhai, S. J., Lin, X., and Gao, D. Z. (2015). Spatial distribution of phosphorus speciation in marsh sediments along a hydrologic gradient in a subtropical estuarine wetland, China. *Estuar. Coast. Shelf.* S. 154, 30–38. doi: 10.1016/j.ecss.2014.12.023

Zhang, W. L., Zeng, C. S., Tong, C., Zhang, Z. C., and Huang, J. F. (2011). Analysis of the expanding process of the *Spartina alterniflora* salt marsh in shanyutan wetland, minjiang river estuary by remote sensing. *Proc. Environ. Sci.* 10, 2472–2477. doi: 10.1016/j.proenv.2011.09.385

frontiers | Frontiers in Marine Science

TYPE Original Research
PUBLISHED 10 October 2022
DOI 10.3389/fmars.2022.1035095

OPEN ACCESS

EDITED BY
Xianbiao Lin,
Ocean University of China, China

REVIEWED BY
He Tao,
Jinan University, China
Yifei Zhang,
Northeast Institute of Geography and Agroecology (CAS), China

*CORRESPONDENCE
Yuehmin Chen
ymchen@fjnu.edu.cn
Linhai Zhang
mary12maryzhang@126.com

SPECIALTY SECTION
This article was submitted to Marine Biogeochemistry, a section of the journal Frontiers in Marine Science

RECEIVED 02 September 2022
ACCEPTED 26 September 2022
PUBLISHED 10 October 2022

CITATION
Hu W, Zeng C, Tong C, Li G, Lan X, Zhou J, Zhang M, Chen Y and Zhang L (2022) Nitrogen deposition may increase litter accumulative CO_2 release in a subtropical estuarine marsh.
Front. Mar. Sci. 9:1035095.
doi: 10.3389/fmars.2022.1035095

Nitrogen deposition may increase litter accumulative CO_2 release in a subtropical estuarine marsh

Weifang Hu[1,2,3], Congsheng Zeng[2,3], Chuan Tong[2,3], Guoliang Li[1], Xue Lan[4], Jiacong Zhou[2,3], Meiying Zhang[2,3], Yuehmin Chen[2,3]* and Linhai Zhang[2,3,5]*

[1]Institute of Agricultural Resources and Environment, Guangdong Academy of Agricultural Sciences, Guangzhou, China, [2]College of Geographical Science, Fujian Normal University, Fuzhou, China, [3]State Key Laboratory of Subtropical Mountain Ecology (Funded by Ministry of Science and Technology and Fujian Province), Fujian Normal University, Fuzhou, China, [4]College of Marine Sciences, South China Agricultural University, Guangzhou, China, [5]Fujian Provincial Key Laboratory for Plant Eco-physiology, Fujian Normal University, Fuzhou, China

Microbial evolution-mediated CO_2 from litter has aroused widespread concern, and knowing the factors controlling litter-derived CO_2 is important when considering the effects of accumulative CO_2 release from litter on the global greenhouse. We conducted a short-term N addition (6, 16, and 24 g N m^{-2} yr^{-1}) experiment in *Cyperus malaccensis* var. *brevifolius* (shichito matgrass) litter decomosition. Phospholipid fatty acid (PLFA) method and enzyme method were used to analysis litter microbial community composition and enzymatic activity. During a 220-day decomposition period, there was little effect of the N amendments on litter CO_2 evolution rates (9.97–307.54 μg C g^{-1} h^{-1}) with a notable exception regarding the increase of the high-N treatment at day 20. The accumulative CO_2 release significantly increased after N addition in the medium and late phases. The facilitation effect on accumulative CO_2 release by N amendments was more and more obvious over the decomposition time, especially for the low- and intermediate-N treatments. At the end of our experiment, compared with the control treatment, accumulative CO_2 release increased 69.75%, 76.62%, and 39.93% for low-, intermediate-, and high-N treatments, respectively. These observations highlight that N deposition could cause high losses of litter C as CO_2.

KEYWORDS

litter-derived CO_2, litter decomposition, nitrogen addition, estuarine marsh, accumulative CO_2 release

Introduction

Humans continue to transform the global nitrogen (N) cycle at a record pace, and serious N pollution could generate unacceptable environmental change (Galloway et al., 2008; Rockström et al., 2009). Significant fractions of this anthropogenic N enter coastal estuaries, and contributed to numerous eco-environmental problems, such as widespread eutrophication and accelerating greenhouse gasses emission (Simas and Ferreira, 2007; Lin et al., 2017; Lin and Lin, 2022). Previous studies have revealed that N deposition significantly promoted plant height and biomass, changed litter matrix, inhibited litter decomposition, and affected soil carbon (C) storage in the estuarine wetlands (Guan et al., 2019; Tao et al., 2019). To sequester more C in soil, we need to consider how to divert more litter into humus (Prescott, 2010), and to decrease fraction of litter C released as CO_2 to the atmosphere.

Despite growing research interest, uncertainties remain on the response of litter decomposition to the N amendments due to the different ecosystems, species, decomposition stages, and N thresholds (Knorr et al., 2005; Xu et al., 2016; Zhang et al., 2018; Ochoa-Hueso et al., 2019). Previous studies have demonstrated that N amendments may promote (Gerdol et al., 2007), inhibit (Tao et al., 2019) or no significant effect (Yu et al., 2019) on the litter decomposition rate in wetland. For decades, litter-derived CO_2 has aroused widespread concerns (Kuehn et al., 2000; Chambers et al., 2001; Kuehn et al., 2004; Zhang et al., 2014b; Hall et al., 2017; Mao et al., 2021). The fraction of litter C released as CO_2 to the atmosphere is nearly 30% of the total C (TC) (Rubino et al., 2010), that represents a substantial pathway of C input to the atmosphere (Day et al., 2018). Li et al. (2015) suggested that the combination of litter and N addition increased CO_2 release although N fertilization alone significantly inhibited CO_2 release rates. Simulated CO_2 emissions from soil fertilized with litter averaged across years were approximately 0.8 times higher than soil fertilized with NH_4NO_3 (Yang et al., 2019). Magill and Aber (2000) suggested that N inputs appear to affect the quantity of litter C consumed or released by increasing respiration (as measured by weight loss), rather than increasing litter-derived DOC release into the soil solution. In freshwater marshes, the N addition could significantly increase CO_2 emission (Hu et al., 2019a), however, the response of litter-derived CO_2 to N amendments remain poorly understood (Li et al., 2015). To better understand the C cycle in estuarine marshes, the fate of litter-derived CO_2 and its driving mechanism need to be identified.

Here, we asked a simple question: Does N deposition affect litter-derived CO_2 evolution rates and accumulative CO_2 release during litter decomposition? According to the results of previous research concerning an increase in litter-derived respiration (Magill and Aber, 2000) and an increase in litter input (Liu and Greaver, 2010; You et al., 2017), and a decrease in litter decomposition (Tu et al., 2011; Xu et al., 2016) after N fertilization, we hypothesized that, (1) N addition could increase litter-derived CO_2 evolution rates; and (2) consequently increase accumulative CO_2 release due to large amounts of remaining litter residue.

Materials and methods

Site description

Our study was conducted in a freshwater marsh, namely Tajiaozhou (25°56′48″ N; 119°22′1″ E), in the Min River Estuary (Figure 1). Located in the transition zone between the middle and southern subtropical zones, this area is exposed to an East Asian monsoon climate with annual mean temperature and precipitation of 19.7°C and 1200–1740 mm, respectively (Luo et al., 2019). Background N deposition of southeast China was

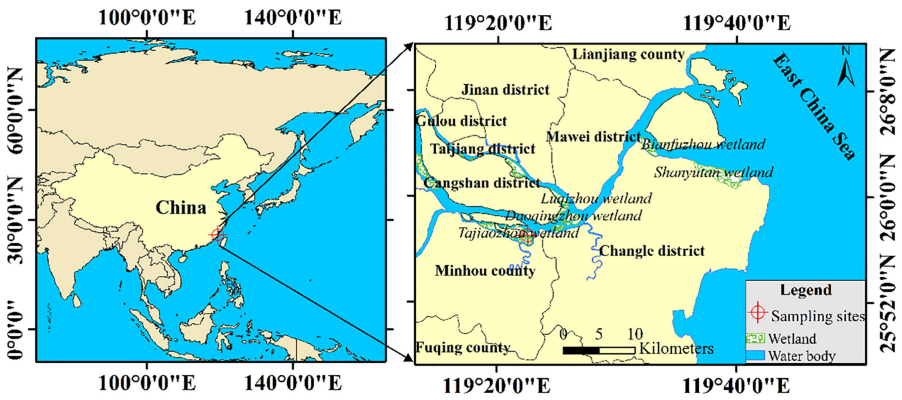

FIGURE 1
Study sites for the leaf-bag decomposition experiments.

estimated as 41.7 kg N ha^{-1} a^{-1} (Xu et al., 2015). This marsh experiences a semi-diurnal tide, and the inundation frequency at the measurement sites generally varied between 0 and 31.80%. The sediment is neutral or faintly acidic (~pH 6.11). *Cyperus malaccensis* var. *brevifolius* (shichito matgrass), a type of grass-like perennial, is a typical native species in this marsh.

Experimental design and treatments

We conducted a short-term N addition experiment during 220 days. To evaluate the effects of future elevated N-saturated conditions on litter-derived CO_2, the N levels applied in this study were in line with background N loading. N eutrophication symptoms in rivers discharging to oceans are mainly driven by nitrate (NO_3^-) in subtropical and temperate estuarine areas (Meybeck and Ragu, 2012), and thus additional reactive N was applied as $NaNO_3$ in this experiment. Three N treatments were designed with doses of 6 g N m^{-2} yr^{-1} (low N), 16 g N m^{-2} yr^{-1} (intermediate N), and 24 g N m^{-2} yr^{-1} (high N), and a control treatment was set up with no N added.

Two experimental blocks (I and II) were established at the sites with uniform vegetation, soil, and hydrological characteristics, which remained completely exposed during low or neap tide. In each block, there were four 0.6 m × 0.6 m plots (decomposition boxes, polyvinyl chloride) with 1-m buffers that were assigned to receive N treatments, giving a total of 12 treatment plots in each block. Additional N was added to *in situ* tidewaters (1 L) and supplied at neap tide twice a month, whereas control plots received additional and equivalent tidewater only. In block II, 12 porewater sample collectors were placed in each plot. Litter from block I was analyzed to determine the 2elemental composition of litter remains and litter properties. Litter from block II was used to determine CO_2 evolution rates and phospholipid fatty acid (PLFA) content of litter.

Standing dead litter of shichito matgrass stems were collected to serve as test material in March 2017. To unify the microbial levels of initial decomposition material, the collected litter was first washed with filtered stream water and then with deionized water in the laboratory. Litter material was cut into 5-cm long pieces, and then air-dried at approximately 18°C (mean daily temperature) for several weeks. A subsample of this air-dried material was weighed, oven-dried at 60°C, and reweighed to calculate the moisture correction factor for calculating the initial mass of the air-dried litter. Litter decay processes were investigated using the experimental leaf-bag technique (pre-dried litter enclosed in litterbags). For this, an aliquot of approximately 15 g (dry weight) was transferred to each litterbag (20 cm × 15 cm, prepared using 0.2-mm fiberglass mesh). Total 192 litterbags were placed in the experimental field (i.e., 2 blocks × 8 sampling time points × 4 treatments × 3 replicates). These litter-bags were tied to polypropylene canes that were buried in the ground to prevent their displacement by the tide (Zhang et al., 2014a). Based on the findings of Hu et al. (2019b) regarding shichito matgrass litter decay, and the litter decay phases described by Valiela et al. (1985), we set three retrieval phases. Litterbags were retrieved at 10-day intervals (early phase: days 10, 20, and 30), 30-day intervals (medium phase: days 60, 90, and 120), and 50-day intervals (late phase: days 170 and 220). In total, 24 litterbags were collected at each sampling interval. Litterbags were carefully retrieved and placed in sealed plastic bags in a portable cooler, and then immediately transported to the laboratory.

Litter properties

Litter remaining in the bags was washed gently and weighed after oven-drying to a consistent mass. The dried litter was then ground and passed through a 100-mesh (0.149-mm) sieve, and litter TC, total nitrogen (TN), and total sulfur (TS) concentrations were determined using a Vario EL Elemental Analyzer (Elementar Vario EL, Frankfurt, Germany). Litter-derived DOC was extracted from 0.5 g dry litter as described by Uselman et al. (2012), and analyzed using a total organic carbon analyzer (Shimadzu TOC-V_{CPH}, Kyoto, Japan)

Environmental parameters

The *in-situ* sediment pH was measured using an IQ150 instrument (IQ Scientific Instruments, Carlsbad, CA, USA), and electrical conductivity (EC) was measured using a 2265FS EC meter (Spectrum Technologies Inc., Aurora, CO, USA). TC and TN concentrations of the top 2 cm of sediment were determined using a Vario MAX CN element analyzer (Elementar). Porewater from the sample collectors was transferred into 50-mL plastic cups (polypropylene, acid washed) and filtered (0.45-μm membrane filters), and then analyzed for TN and dissolved inorganic N (DIN = $NH_4^+ + NO_3^- + NO_2^-$) using a continuous flow-injection analyzer (SKALAR San^{++}, Breda, the Netherlands) (Huang et al., 2021). The crab hole density, plant height, and plant density were measured within the plots (0.6 m × 0.6 m).

Litter CO_2 evolution rate assay

The assay we used for determining litter CO_2 evolution rates has been described previously (Zhang et al., 2014b). In brief, sterile tweezers were used to carefully remove visible debris and soil from fresh litter. Then the fresh litter samples (4 g fresh weight) were placed into sterile glass incubation jars (250 mL) containing sterile filter paper. An additional three jars containing a filter paper without plant material were used as controls. All jars were wetted until saturation with sterile

deionized water, placed in an incubator, pre-incubated for 2 h, and then sealed and incubated at 20°C (annual mean temperature). Gas samples were collected at 0, 4, and 8 h after the chamber was closed using a 20-mL syringe equipped with a three-way stopcock and were stored in gas sampling bags (Dalian Delin Gas Packing Co., Ltd., Dalian, China). The CO_2 concentrations were determined within 12 h of sampling using a gas chromatograph (GC-2010, Shimadzu).

Litter phospholipid fatty acid and enzyme assay

Litter PLFAs were extracted from 1 g of fresh litter according to Hassett and Zak (2005) and Rejmánková and Houdková (2006). Microbial biomass was calculated by summing total PLFAs (C_{14}–C_{20}), and PLFAs specific to fungi (18:2ω6,9c), gram-positive bacteria (i14:0, a16:0, i15:0, a15:0, i16:0, i17:0, and a17:0), and gram-negative bacteria (16:1ω7c, cy17:0, 18:1ω7c and cy19:0) were summarized separately (Feng and Simpson, 2009).

Fresh litter samples were assayed following published protocols for β-glucosidase and cellobiohydrolase using methyumbelliferyl-β-glucoside and methyumbelliferyl-cellobioside as substrates, respectively (Saiya-Cork et al., 2002; Sinsabaugh et al., 2005). Fluorescence was measured using a Multiscan Spectrum (Synergy H4, USA) calibrated for excitation at 365 nm, and with emissions set at 460 nm. All enzymatic activities were calculated as nmol h^{-1} g^{-1} OM.

Statistical calculation

We focused on CO_2 evolution from the residual mass of litter; thus, the litter residual mass (R, %) was calculated as follows:

$$R = W_t / W_0 \times 100\%$$

where W_0 (g) is the original dry mass, and W_t (g) is the dry mass at a time "t", and t (d) is decomposition time in days.

CO_2 evolution rates were calculated according to previous research as follows (Zhang et al., 2014b):

$$y_T = \frac{(dc/dt) \times (M \times V \times P \times T_0)}{(m \times V_0 \times P_0 \times T)}$$

where y_T is the CO_2 evolution rate (μg g^{-1} dry weight h^{-1}); dc/dt is the slope of the linear regression for gas concentration gradient through time (μL L^{-1} C h^{-1}); M is the atomic mass of C (12); V is the volume of the jar (L); P is the atmospheric pressure (MPa); m is the litter mass in jars (g); T is the absolute temperature during sampling (K); and V_0, P_0, and T_0 are the gas mole volume (L), atmospheric pressure (MPa), and absolute temperature (K) under standard conditions, respectively.

Accumulative CO_2 release (per initial dry weight per m^2) was calculated by integrating the area under the curve for all dates, based on the assumption that rates of CO_2 loss scaled linearly between time points (Jacobs et al., 2018) as follows:

$$y_t = x_t \times M_t \times 24 \times 10^{-3}$$

$$f(y) = ky + b$$

$$S_i = \int_t^{t+1} f(y)\ dt$$

$$AR_i = M_0 \times\ 10^{-3} \times \sum_{i=1}^{n} S_i$$

where AR_i is the accumulative CO_2 release per initial dry weight per m^2 at time i (g m^{-2}); x_t and y_T are the CO_2 evolution rates per hour (μg g^{-1} h^{-1}) and per day (mg), respectively; M_t is the residue mass of litter at time "t" (g); $f(y)$ is the accumulative CO_2 release during decomposition; S_i is accumulative CO_2 release at the interval between sampling times (mg g^{-1}); M_0 is the initial litter mass per m^2 (g m^{-2}), and the average yield of litter at control, low-N, intermediate-N, high-N treatments were 558.38 g m^{-2}, 1000.18 g m^{-2}, 723.67 g m^{-2}, and 633.52 g m^{-2}, respectively (unpublished data); n is the number of sampling time.

Data analysis

All datasets were tested for normality by the Shapiro-Wilk test, and homogeneity of variance by the Brown-Forsythe test. If these assumptions were not met, then the raw data were log transformed before further statistical analysis. One-way analysis of variance (ANOVA) and repeated measure analysis of covariance (ANCOVA) were used to assess differences among samples (SPSS 19.0, IBM, Armonk, NY, USA) with a significance level of $p < 0.05$.

Redundancy analysis (RDA) was used to partition the variation in CO_2 evolution rates and accumulative CO_2 release explained by environmental parameters, microbial biomass, and litter quality (Wang et al., 2015), and to interpret the extent and direction of compositional changes; these analyses were performed using Canoco 5.0.

Structural equation modeling (SEM) was performed to analyze the causal mechanisms underlying the response of litter accumulative CO_2 release to N addition using SPSS Amos 21.0 (IBM). The best-fit SEM was derived by maximum likelihood and the model fit was determined using chi-square tests (χ^2), p-values, goodness-of-fit index (GFI), root mean square errors of approximation (RMSEA), and Akaike information criteria (Zhu et al., 2018). The litter CO_2 evolution rates and accumulative release were generated using Origin 9.3 (OriginLab Corporation, Northampton, MA, USA),

and a conceptual framework was created using Microsoft Office Visio 2016 (Microsoft Corporation, Redmond, Washington, DC, USA).

Results

Litter quality, environmental, and microbial parameters

All N treatment in the medium phase and intermediate-N addition increased litter residual mass ($p < 0.05$), although N treatment had no impact on the litter residual mass in the early phase ($p > 0.05$, Table 1). Litter TC, TN, TS, litter-derived DOC contents, and the ratios of C/N were similar irrespective of the treatment with the exception of significantly low C/N ratio and TC and TS concentrations under low- and intermediate-N addition in the medium phase ($p < 0.05$, Table 1). The EC and pH of the sediment were similar irrespective of the treatment except for an increase in pH values after N addition in the early phase ($p < 0.05$, Table 2). Sediment TC and TN in the medium and TC in the late phase significantly decreased under the three N treatments ($p < 0.05$, Table 2). Most of the TN and DIN of the porewater were unchanged with the exception of the intermediate-N treatment in the early phase and the high-N treatment in the late phase (Table 2). Crab hole density tended to decrease after N addition in the early phase but increased in the medium phase and was unchanged in the late phase (Table 2). In addition, except a significantly low fungal biomass in high-N treatments and a relatively low cellobiohydrolase activities in low–N treatments, the biomass of gram-positive and gram-negative bacteria, fungi, total PLFA, β-glucosidase, and cellobiohydrolase did not change significantly after N addition (Table 3).

Response of litter CO_2 evolution rates and accumulative release to N addition

During decomposition, litter CO_2 evolution rates (9.97–307.54 μg C g^{-1} h^{-1}) significantly decreased over time ($p < 0.001$, Figure 2). In most decomposition times, there was no significant difference on litter CO_2 evolution rates with N treatment or interaction term [time × treatments] (Figure 2). Litter CO_2 evolution rates showed a similar temporal pattern among different N addition treatments, in that they peaked in the early phase, weakened in the medium phase, and maintained a low level into the late phase. A notable exception was day 20, when litter CO_2 evolution rates were significantly higher in the high-N treatment relative to those of the control. Another anomaly was that higher litter CO_2 evolution rates were observed with intermediate-N levels compared with those under high-N addition at days 30 and 120 ($p < 0.05$, Figure 2).

Accumulative CO_2 release significantly increased over time ($p < 0.001$), and there was a significant difference for the interaction term [time × treatments] ($p < 0.001$) but no significant difference for N treatment over time (Figure 3A). In the early phase, there was no significant difference in accumulative CO_2 release among different N amendments (Figure 3A). By moving into the medium phase, accumulative CO_2 release significantly increased under the low- and intermediate-N amendments relative to the control; and ultimately, all N treatment significantly increased accumulative CO_2 release ($p < 0.05$, Figure 3A). At the end of our experiment, compared with the control treatment, accumulative CO_2 release increased 69.75%, 76.62%, and 39.93% for low-, intermediate-, and high-N treatments, respectively. The facilitation effect on accumulative CO_2 release by N amendments was more and more obvious over the decomposition time, especially for the low- and intermediate-N treatments (Figure 3B).

Redundancy analysis and structural equation modeling analysis

RDA results showed that litter quality and environmental and microbial parameters could explain 95.46% of the variance in CO_2 evolution rates and accumulative CO_2 release (Figure 4). Litter TC contributed the most to changes, explaining 74.6% of the variance, and was significantly positively correlated with CO_2 evolution rates. Moreover, both litter residual mass (explaining 12.8% of the variance) and sediment TN (explaining 1.6% of the variance) were positively correlated with CO_2 evolution rates, but negatively correlated with accumulative CO_2 release (Figure 4). Litter TS (explaining 1.5% of the variance) was negatively correlated with CO_2 evolution rates, however, it was positively correlated with accumulative CO_2 release (Figure 4). In addition, CO_2 evolution rates were positively correlated with porewater DIN and crab hole density (Figure 4).

The SEM of the direct and indirect effects of both sediment and porewater TN on accumulative CO_2 release showed reasonable fits ($\chi^2 = 9.33$, $p = 0.87$, GFI = 0.95, RMSEA < 0.001), and the model accounted for 87% and 71% of the variance in litter CO_2 evolution rates and accumulative CO_2 release, respectively (Figure 5). We found negative relationships between both sediment and porewater TN and sediment pH, between sediment pH and gram-negative bacteria, and between gram-negative bacteria and both litter residual mass and litter-derived DOC (Figure 5). Conversely, we observed positive relationships between sediment TN and litter residual mass, between sediment pH and litter-derived DOC, between litter residual mass and CO_2 evolution rates, and between litter-derived DOC and CO_2 evolution rates (Figure 5). In addition, both litter CO_2 evolution rates and litter production were negatively correlated to accumulative CO_2 release, whereas gram-negative bacteria and litter residual mass were positively correlated to accumulative CO_2 release (Figure 5).

TABLE 1 Litter residual mass; total carbon (TC), total nitrogen (TN), and total sulfur (TS) concentrations; dissolved organic carbon (DOC); and the ratios of TC to TN (C/N) during the decomposition phase.

Indicators	Treatments	Early phase	Medium phase	Late phase
Litter residual mass (%)	Control	44.96	20.82	10.93
	Low N	48.67	**34.20***	13.99
	Intermediate N	56.73	**40.71***	**24.76***
	High N	48.47	**35.73***	23.02
TC (mg g^{-1})	Control	382.17	305.40	202.37
	Low N	394.70	**226.07***	154.17
	Intermediate N	366.83	**218.43***	148.43
	High N	394.40	263.20	144.40
TN (mg g^{-1})	Control	15.00	16.17	13.25
	Low N	15.27	13.10	9.00
	Intermediate N	14.67	13.33	9.03
	High N	15.43	18.28	8.57
TS (mg g^{-1})	Control	1.52	2.37	2.58
	Low N	1.69	**1.60***	1.53
	Intermediate N	**1.31***	**1.66***	1.50
	High N	1.47	2.14	1.39
C/N ratio	Control	25.55	18.93	15.62
	Low N	25.88	**17.20***	16.97
	Intermediate N	24.98	**16.42***	16.34
	High N	25.61	**17.28***	16.71
DOC (mg g^{-1})	Control	7.05	2.60	1.82
	Low N	5.04	2.74	1.70
	Intermediate N	7.00	3.05	1.70
	High N	6.89	2.83	1.61

Means in bold font followed by * indicate significant differences between the given parameter and the control treatment ($p < 0.05$, ANOVA).

Discussion

Litter CO_2 evolution rates

The results of this study show that litter CO_2 evolution rates of shichito matgrass were similar to those of standing-dead leaf blades (10–295 μg C g^{-1} h^{-1}) (Kuehn et al., 2004) but higher than those of culms litter (6.38–148.01 μg C g^{-1} h^{-1}) and lower than those of leaf litter (40.37–741.91 μg C g^{-1} h^{-1}) of *Phragmites australis* (Zhang et al., 2014b). During decomposition time, litter CO_2 evolution rates peaked in the early phase, weakened in medium phase, and maintained a low-level proceeding into the late phase (Figure 2), that was consistent with Li et al. (2015). The pattern of CO_2 evolution rates could be partly explained by C availability (Figures 4, 5), the variation in litter TC and DOC concentration were in line with the trend observed for CO_2 evolution rates (Table 1). Uselman et al. (2012) suggested that approximately 36% of the DOC was either respired or stored in the early phase. This labile pool was a source of microbial respiration rates (Day et al., 2018). The downtrend in CO_2 evolution rates did not mean that microbes would die or activity decline in a short time (Li et al., 2015), and this was further confirmed by the PLFA data (Table 3). Previous studies suggested that the increasing easily-available matter (especially labile C) would accelerate the turnover of microorganisms (r-strategists, mainly bacteria) in the early phase, and later replaced by k-strategists (mainly fungi) due to growth-limiting substrate concentrations (Fontaine et al., 2003; Dilly et al., 2004; McTee et al., 2017), however, our bacteria and fungi biomass data did not show this trend during decomposition process.

Response of litter CO_2 evolution rates to nitrogen addition

Our results do not support our first hypothesis that N addition did not change litter-derived CO_2 evolution rates in most decomposition times (Figure 2). On the one hand, crab may affect litter decomposition and respiration through consumption, an increase of soil drainage and soil oxidation-reduction potential (Bertness, 1985), colonization by bacteria and resulted in a rapid decline in the C/N ratio (Werry and Lee, 2005). Since some crabs may have a preference for ingesting high N and low C/N foods, N amendments may affect the crab burrows (Nordhaus and Wolff 2007), and the increase in crab hole density and decrease in litter C/N ratio in the medium phase (Tables 1, 2) were corroborating

TABLE 2 Environmental parameters (physicochemical properties of sediment and pore water, vegetation, and crab hole density) during the decomposition phase.

Indicators	Treatments	Early phase	Medium phase	Late phase
Sediment EC (mS cm^{-1})	Control	0.30	0.41	0.55
	Low N	0.24	0.43	0.57
	Intermediate N	0.24	0.53	0.41
	High N	0.20	0.59	0.47
Sediment pH	Control	6.42	5.93	6.51
	Low N	**6.70***	6.03	5.53
	Intermediate N	**6.84***	6.21	5.53
	High N	**6.70***	6.21	5.52
Sediment TC (mg g^{-1})	Control	23.25	23.39	17.14
	Low N	20.29	**19.19***	**15.89***
	Intermediate N	19.65	**19.40***	**15.39***
	High N	19.70	**19.94***	**15.16***
Sediment TN (mg g^{-1})	Control	1.76	1.90	1.46
	Low N	1.57	**1.64***	1.50
	Intermediate N	1.59	**1.70***	1.47
	High N	1.61	**1.63***	1.45
TN of pore water (mg L^{-1})	Control	0.33	0.85	1.55
	Low N	0.28	0.77	2.33
	Intermediate N	1.00	0.26	2.12
	High N	0.31	0.77	**2.83***
DIN of pore water (mg L^{-1})	Control	0.25	0.71	0.11
	Low N	0.26	0.67	0.13
	Intermediate N	**0.95***	0.22	0.15
	High N	0.22	0.68	0.14
Crab hole density (number m^{-2})	Control	81	35	72
	Low N	75	42	55
	Intermediate N	79	**61***	34
	High N	**43***	**73***	33

Means in bold font followed by * indicate significant differences between the given parameter and the control treatment ($p < 0.05$, ANOVA).

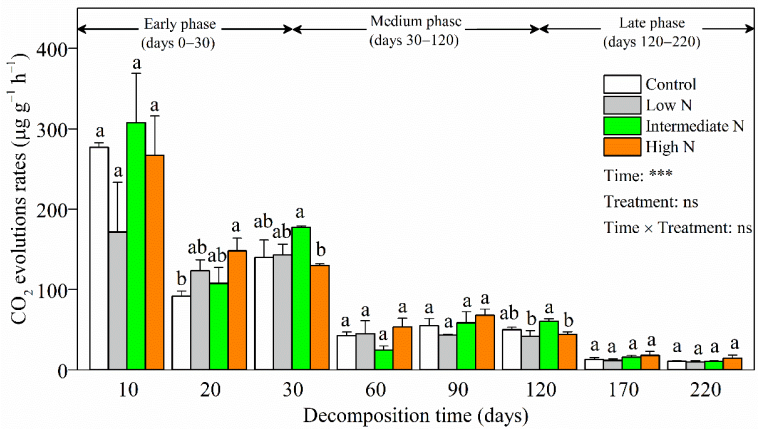

FIGURE 2
CO_2 evolution rates (mean ± SE) of C. malaccensis litter under different N addition treatments. Different letters above error bars indicate significant difference (ANOVA, $p > 0.05$). The results of repeated measure analysis of covariance are also noted and "Time × Treatment" is the combined effect of time and N treatment. *** significant at $p < 0.001$; ns, not significant.

TABLE 3 Litter phospholipid fatty acids (PLFA) and enzymes activities during the decomposition phase.

	Indicators	Treatments	Early phase	Medium phase	Late phase
PLFAs	Gram-positive bacteria biomass (nmol g^{-1})	Control	NA	89.10	99.36
		Low N	NA	95.71	112.28
		Intermediate N	36.59	100.51	86.49
		High N	40.41	104.80	94.15
	Gram-negative bacteria biomass (nmol g^{-1})	Control	NA	29.24	35.63
		Low N	NA	27.26	42.91
		Intermediate N	6.15	33.74	30.48
		High N	7.31	23.19	33.92
	Fungal biomass (nmol g^{-1})	Control	NA	8.02	8.63
		Low N	NA	8.03	10.10
		Intermediate N	2.31	8.90	9.03
		High N	2.53	**3.16***	6.54
	Total PLFA (nmol g^{-1})	Control	NA	186.35	201.99
		Low N	NA	174.18	230.65
		Intermediate N	83.55	210.73	178.81
		High N	97.22	196.15	201.76
Enzymes	β-glucosidase (nmol h^{-1} g^{-1})	Control	347.00	9.61	5.53
		Low N	288.42	8.65	10.53
		Intermediate N	366.80	12.50	4.39
		High N	351.79	15.59	14.02
	Cellobiohydrolase (nmol h^{-1} g^{-1})	Control	103.92	1.51	6.29
		Low N	**71.03***	0.65	12.21
		Intermediate N	129.04	0.69	7.20
		High N	104.10	0.71	11.63

NA, no data available.
Means in bold font followed by * indicate significant differences between the given parameter and the control treatment ($p < 0.05$, ANOVA).

these results. On the other hand, available C sources could facilitate microbial respiration initiated by high β-glucosidase activity (Badiane et al., 2001; Sinsabaugh et al., 2009; Turner and Wright, 2014). The studied N amendments had little effect on β-glucosidase, further led to a similar litter DOC for microbial respiration (Tables 1 and 3), although low litter TC and sediment TC were found after N addition in the medium phase. Eventually, although low litter TC and sediment TC may decrease litter-derived CO_2 evolution rates after N addition in the medium phase, these negative effects may offset by the positive effect of crab activity.

Interestingly, litter CO_2 evolution rates were significantly higher in the high-N treatment relative to the control in day 20 (Figure 2), this unexpected result indicated that high-N may be explained by sediment pH (Table 2 and Figure 5). In the early phase, litter leaching would increase in pH (Nykvist, 1963), consistent with our findings. In weak acidic or neutral environments (pH 6.19–7.13), acidobacteria subgroups 4 and 6 had higher sediment pH values (Jones et al., 2009; Keyport et al., 2019). These increases in relative pH may indirectly increase microbial respiration (Tables 2, 3 Figure 5).

By moving into the late phase, traditionally, litter remains were relatively refractory materials (i.e., lignin), and lignin-degradation rates regulated litter decomposition (Valiela et al., 1985; Berg and Matzner, 1997). The refractory lignin was decomposed by white-rot basidiomycetes and phenol oxidase, and they were greatly decreased by increased N availability (Dix and Webster, 1995; Carreiro et al., 2000; Gallo et al., 2005). Previous studies have suggested that N has a retarding effect on decomposition in the late phase when significant negative correlations were noted between N content in humus and respiration rate (Berg and Matzner, 1997). Our results challenge the traditional view that there was no significant difference in litter CO_2 evolution rates among the different N addition treatments in the late phase.

Response of litter accumulative CO_2 release to nitrogen addition

Our data supports hypothesis 2 based on the significant increase in accumulative CO_2 release in the medium and late phase, though this motivating effect was not observed in the early phases (Figure 3B). Rubino et al. (2010) reported the fraction of litter C released as CO_2 to the atmosphere to be nearly 30% of the total litter C loss. Based on this estimate, litter

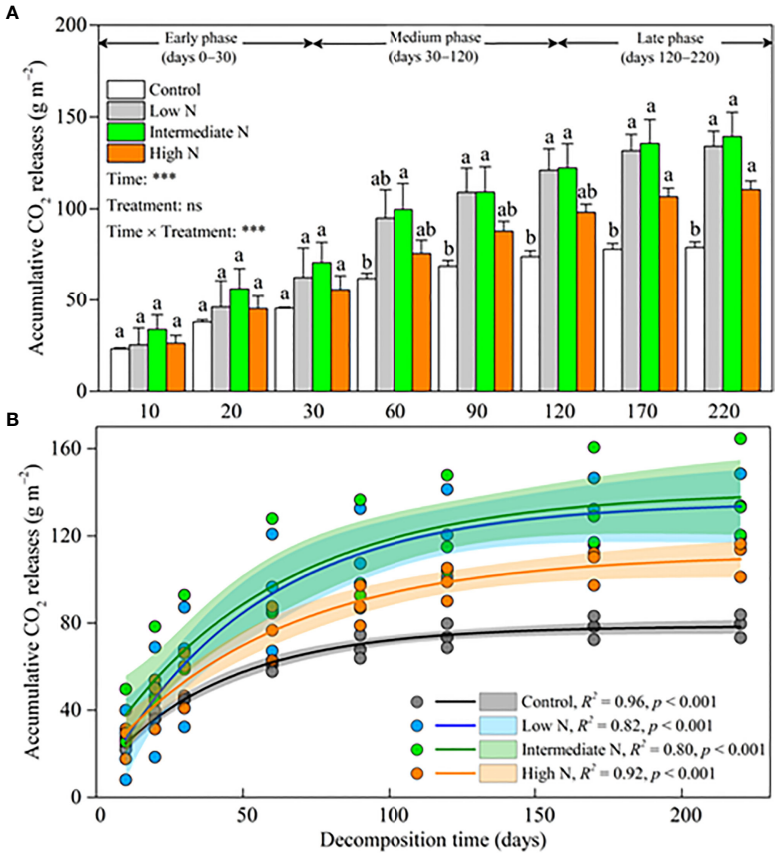

FIGURE 3
(A) Litter accumulative CO_2 release (mean ± SE) under different N addition treatments. Different letters above error bars indicate significant difference (ANOVA, $p > 0.05$). The results of repeated measure analysis of covariance are also noted, and "Time × Treatment" is the combined effect of time and N treatment. ** significant at $p < 0.01$; *** significant at $p < 0.001$; ns, not significant. **(B)** exponential regressions under different N addition treatments. The scatters are litter accumulative CO_2 release (three duplicates). The lines are asymptotic for exponential regressions. Shaded areas are 95% confidence intervals. R^2 and p values are from exponential regressions.

CO_2 release could reach 53% of the total litter C loss under intermediate-N deposition (16 g N m^{-2} yr^{-1}). The accumulative CO_2 released from litter was directly affected by litter CO_2 evolution rates, litter residual mass, and litter production (Figure 5). Because of no significant litter CO_2 evolution rates under different N treatments, we suggested that litter production and residual mass were the most important factors regulating accumulative CO_2 release.

Meta-analysis results indicated that N addition significantly increased aboveground biomass and litter input by 31% and 20%, respectively (Liu and Greaver, 2010; You et al., 2017). A similar relationship was found in our studies. Not only N fertilization increases litter production, but also ameliorates litter chemistry (Wedin and Tilman, 1996; Gerdol et al., 2007). Higher N availability increased plant lignin and protein, but decreased plant hemicellulose (Liu et al., 2016). On the other hand, litter residual mass increased after N addition in the medium and late phases. The retarding effect of increasing N on decomposition in the late phase has been demonstrated by previous studies, and there are four possible nonexclusive explanations: (i) decreasing sediment pH, further decreasing bacterial diversity (Geisseler and Scow, 2014); (ii) directly inhibiting the decay of lignin and cellulose (Tu et al., 2011); (iii) decreasing white-rot basidiomycetes and phenol oxidase, resulting in slow lignin decomposition (Dix and Webster, 1995; Carreiro et al., 2000; Gallo et al., 2005); (iv) causing more humus to be left, and the resulting lower levels of Mn further retards humus decomposition (Berg and Matzner, 1997). Ultimately, the combined effect of the increased litter input and the inhibiting effect of external N on litter decomposition increased accumulative CO_2 release (Figure 6).

Uncertainties and future study

To the best of our knowledge, our study was the first time to investigate the response of litter CO_2 evolution rates and

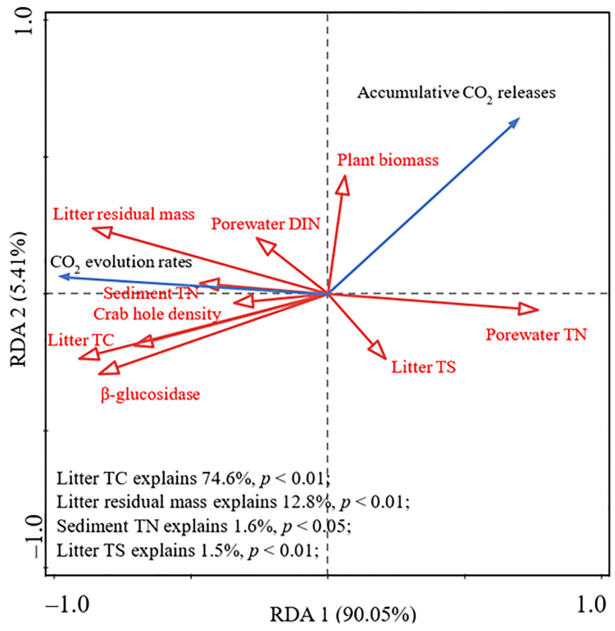

FIGURE 4
Redundancy analysis (RDA) ordination plots for the first two principal dimensions of the relationship among CO_2 evolution rate, accumulative CO_2 release, environmental parameters, microbial biomass, and litter matrix.

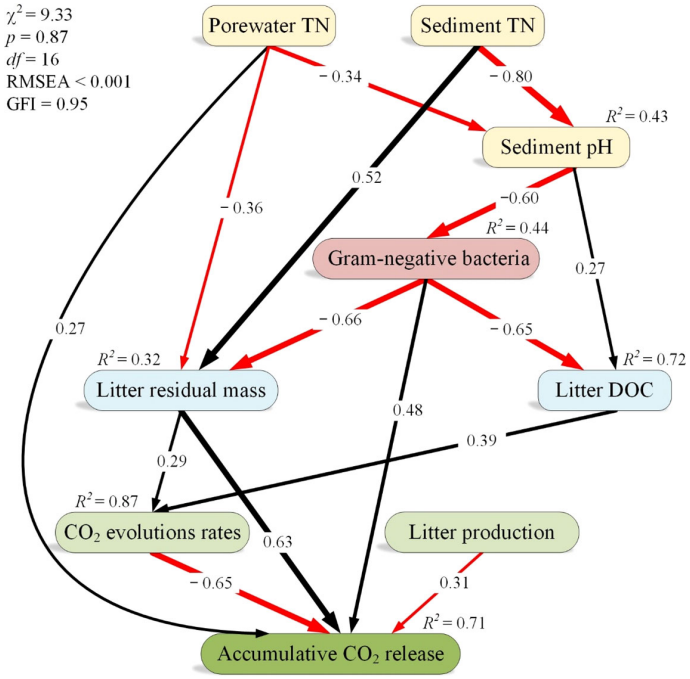

FIGURE 5
A structural equation model analysis of the effects of porewater total nitrogen (TN) on accumulative CO_2 release. The width of arrows indicates the strength of the standardized path coefficient. Black lines indicate positive path coefficients, while red lines indicate negative path coefficients ($p < 0.05$). R_2 values associated with response variables indicate the proportion of variation explained by relationships with other variables. GFI, goodness-of-fit index; RMSEA, root mean square errors of approximation; χ^2, chi-square tests.

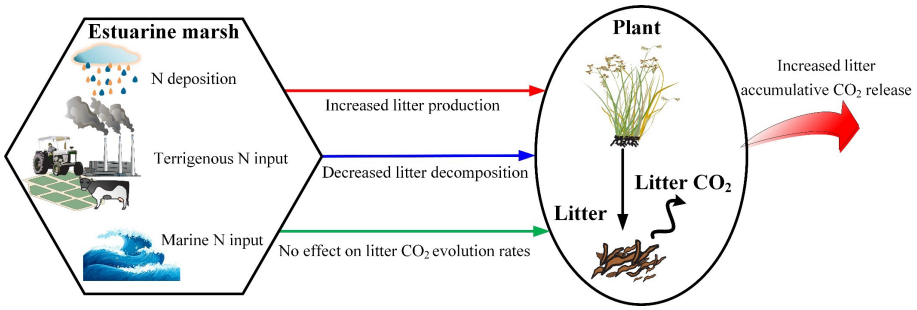

FIGURE 6
Conceptual schematic of the effect of N load on litter accumulative CO_2 release in estuarine marshes.

accumulative release to N addition in a subtropical estuarine marsh. Nevertheless, there remains a great deal of uncertainty in our results. Our data highlights the role of litter production and decomposition as important environmental factors influencing litter CO_2 production and emissions. The increase in litter input and inhibition of litter decomposition by N loading increased accumulative CO_2 release. This indicates that N input could greatly cause loss of litter C as CO_2 at the regional level and globally, particularly in tidal freshwater marshes. Previous studies have demonstrated that increases in sediment CO_2 emissions induced by N loads were counteracted by sea-level rise and the subsequent inhibition of the increase in N on C emissions (Hu et al., 2019a); to some extent, the litter CO_2 emissions played a similar role. Our findings provide a comprehensive perspective for understanding the underlying response of litter CO_2 release to N addition in an estuarine marsh, and thus, improve predictions and climate adaptation strategies.

Owing to the limitations of the study region, we selected litter of shichito matgrass for analysis. Nitrogen deposition is an ongoing process. Since litter quality, especially plants N matrix (i.e., C/N), is crucial for litter CO_2 evolution and decomposition (Chambers et al., 2001; Uselman et al., 2012; Zhang et al., 2014b; Day et al., 2018; Jacobs et al., 2018), the CO_2 evolution and release from litter of different vegetation types and the initial litter produced under different N deposition conditions are needed to investigate in further studies. In addition, the N added in the sample plots may be difficult to infiltrate or easily carried away by the tides. Therefore, it is necessary to carry out a microcosms experiment.

Conclusions

Our results, overall, provide a basis for developing guidelines for CO_2 emission predictions. Litter CO_2 evolution rates peaked in the early phase, weakened in the medium phase, and maintained a low-level proceeding into the late phase. Litter-derived CO_2 evolution rates were similar after N addition in most decomposition times. Although low litter TC and sediment TC may decrease litter-derived CO_2 evolution rates after N addition in the medium phase, these negative effects may offset by the positive effect of crab activity. Generally, the average accumulative CO_2 release increased after N addition, mainly driven by litter production and decomposition. Our results indicated that an increase in N load significantly increased the litter CO_2 release, and thus, improves predictions and provides key information for developing climate adaptation strategies.

Data availability statement

The original contributions presented in the study are included in the article/supplementary material. Further inquiries can be directed to the corresponding authors.

Author contributions

WH: Writing – Original Draft, Conceptualization, Software, Formal analysis, Data Curation. CZ, CT, and GL: Conceptualization, Methodology, Writing – Review & Editing. XL, JZ, and MZ: Methodology, Software, and Formal analysis. YC and LZ: Writing – Review & Editing, Project administration, Funding acquisition. All authors contributed to the article and approved the submitted version.

Funding

The project was supported by the Public Service Foundation of Science and Technology Department of Fujian Province (no. 2017R1034-6), the National Science Foundation of China (no. 41877335), and Program for Innovative Research Teams of Fujian Normal University (no. IRTL1205), and the Special fund for scientific innovation strategy-construction of high-level Academy of Agriculture Science (R2020YJ-YB3006). We are greatly grateful to the Wetland Ecosystem Research Station of

Minjiang Estuary, State Forestry and Grassland Administration, China, for logistical support and laboratory assistance.

Conflict of interest

The authors declare that the research was conducted in the absence of any commercial or financial relationships that could be construed as a potential conflict of interest.

Publisher's note

References

Badiane, N. N. Y., Chotte, J. L., Pate, E., Masse, D., and Rouland, C. (2001). Use of soil enzyme activities to monitor soil quality in natural and improved fallows in semi-arid tropical regions. *Appl. Soil Ecol.* 18 (3), 229–238. doi: 10.1016/S0929-1393(01)00159-7

Berg, B., and Matzner, E. (1997). Effect of n deposition on decomposition of plant litter and soil organic matter in forest systems. *Environ. Rev.* 5, 1–25. doi: 10.1139/er-5-1-1

Bertness, M. D. (1985). Fiddler crab regulation of *Spartina alterniflora* production on a new England salt marsh. *Ecology* 66 (3), 1042–1055. doi: 10.2307/1940564

Carreiro, M. M., Sinsabaugh, R. L., Repert, D. A., and Parkhurst, D. F. (2000). Microbial enzyme shifts explain litter decay responses to simulated nitrogen deposition. *Ecology* 81 (9), 2359–2365. doi: 10.1890/0012-9658(2000)081[2359:MESELD] 2.0.CO;2

Chambers, J. Q., Schimel, J. P., and Nobre, A. D. (2001). Respiration from coarse wood litter in central Amazon forests. *Biogeochemistry* 52, 115–131. doi: 10.1023/A:1006473530673

Day, T. A., Bliss, M. S., Tomes, A. R., Ruhland, C. T., and René, G. (2018). Desert leaf litter decay: coupling of microbial respiration, water-soluble fractions and photodegradation. *Global Change Biol.* 24 (11), 5454–5470. doi: 10.1111/gcb.14438

Dilly, O., Bloem, J., Vos, A., and Munch, J. C. (2004). Bacterial diversity in agricultural soils during litter decomposition. *Appl. Environ. Microb.* 70 (1), 468–474. doi: 10.1128/AEM.70.1

Dix, N. J., and Webster, J. (1995). *Fungal ecology*. (Dordrecht: Springer), 284–301.

Feng, X., and Simpson, M. J. (2009). Temperature and substrate controls on microbial phospholipid fatty acid composition during incubation of grassland soils contrasting in organic matter quality. *Soil Biol. Biochem.* 41 (4), 804–812. doi: 10.1016/j.soilbio.2009.01.020

Fontaine, S., Mariotti, A., and Abbadie, L. (2003). The priming effect of organic matter: a question of microbial competition? *Soil Biol. Biochem.* 35 (6), 837–843. doi: 10.1016/S0038-0717(03)00123-8

Gallo, M., Lauber, C., Waldrop, M., Sinsabaugh, R., and Zak, D. (2005). Soil organic matter and litter chemistry response to experimental n deposition in northern temperate deciduous forest ecosystems. *Global Change Biol.* 11 (9), 1514–1521. doi: 10.1111/j.1365-2486.2005.001001.x

Galloway, J., Townsend, A., Erisman, J., Bekunda, M., Cai, Z., Freney, J., et al. (2008). Transformation of the nitrogen cycle: Recent trends, questions, and potential solutions. *Science* 320 (5878), 889–892. doi: 10.1126/science.1136674

Geisseler, D., and Scow, K. M. (2014). Long-term effects of mineral fertilizers on soil microorganisms–a review. *Soil Biol. Biochem.* 75, 54–63. doi: 10.1016/j.soilbio.2014.03.023

Gerdol, R., Petraglia, A., Bragazza, L., Iacumin, P., and Brancaleoni, L. (2007). Nitrogen deposition interacts with climate in affecting production and decomposition rates in *Sphagnum* mosses. *Global Change Biol.* 13 (8), 1810–1821. doi: 10.1111/j.1365-2486.2007.01380.x

Guan, B., Xie, B., Yang, S., Hou, A., Chen, M., and Han, G. (2019). Effects of five years' nitrogen deposition on soil properties and plant growth in a salinized reed wetland of the yellow river delta. *Ecol. Eng.* 136, 160–166. doi: 10.1016/j.ecoleng.2019.06.016

Hall, S. J., Huang, W., and Hammel, K. E. (2017). An optical method for carbon dioxide isotopes and mole fractions in small gas samples: Tracing microbial respiration from soil, litter, and lignin. *Rapid Commu Mass Sp* 31 (22), 1938–1946. doi: 10.1002/rcm.7973

Hassett, J. E., and Zak, D. R. (2005). Aspen harvest intensity decreases microbial biomass, extracellular enzyme activity, and soil nitrogen cycling. *Soil Sci. Soc. Am. J.* 69 (1), 227–235. doi: 10.2136/sssaj2005.0227

Huang, F., Lin, X., Hu, W., Zeng, F., He, L., and Yin, K. (2021). Nitrogen cycling processes in sediments of the pearl river estuary: Spatial variations, controlling factors, and environmental implications. *Catena* 206, 105545. doi: 10.1016/j.catena.2021.105545

Hu, M., Peñuelas, J., Sardans, J., Huang, J., Li, D., and Tong, C. (2019a). Effects of nitrogen loading on emission of carbon gases from estuarine tidal marshes with varying salinity. *Sci. Tot. Environ.* 667, 648–657. doi: 10.1016/j.scitotenv.2019.02.429

Hu, W., Zhang, L., Lai, D. Y., Gao, J., Sun, Z., Tong, C., et al. (2019b). The difference of litter decay, litter- and sediment-associated hydrolytic enzymes between brackish and freshwater tidal marshes. *Estuar. Coast.* 42 (5), 1328–1341. doi: 10.1007/s12237-019-00565-7

Jacobs, L. M., Sulman, B. N., Brzostek, E. R., Feighery, J. J., and Phillips, R. P. (2018). Interactions among decaying leaf litter, root litter and soil organic matter vary with mycorrhizal type. *J. Ecol.* 106 (2), 502–513. doi: 10.1111/1365-2745.12921

Jones, R. T., Robeson, M. S., Lauber, C. L., Hamady, M., Knight, R., and Fierer, N. (2009). A comprehensive survey of soil acidobacterial diversity using pyrosequencing and clone library analyses. *ISME J.* 3 (4), 442–453. doi: 10.1038/ismej.2008.127

Keyport, S., Carson, B. D., Johnson, O., Lawrence, B. A., Lishawa, S. C., Tuchman, N. C., et al. (2019). Effects of experimental harvesting of an invasive *hybrid cattail* on wetland structure and function. *Restor. Ecol.* 27, 389–398. doi: 10.1111/rec.12859

Knorr, M., Frey, S. D., and Curtis, P. S. (2005). Nitrogen additions and litter decomposition: a meta-analysis. *Ecology* 86 (12), 3252–3257. doi: 10.1890/05-0150

Kuehn, K., Lemke, M., Suberkropp, K., and Wetzel, R. (2000). Microbial biomass and production associated with decaying leaf litter of the emergent macrophyte *Juncus effusus*. *Limnol Oceanogr* 45 (4), 862–870. doi: 10.4319/lo.2000.45.4.0862

Kuehn, K. A., Steiner, D., and Gessner, M. O. (2004). Diel mineralization patterns of standing-dead plant litter: implications for CO_2 flux from wetlands. *Ecology* 85 (9), 2504–2518. doi: 10.1890/03-4082

Li, H. C., Hu, Y. L., Rong, M., Zhao, Q., and Zeng, D. H. (2015). Effects of nitrogen addition on litter decomposition and CO_2 release: considering changes in litter quantity. *PloS One* 10 (12), e0144665. doi: 10.1371/journal.pone.0144665

Lin, G., and Lin, X. (2022). Bait input altered microbial community structure and increased greenhouse gases production in coastal wetland sediment 2022. *Water Res.* 218, 118520. doi: 10.1016/j.watres.2022.118520

Lin, X., Liu, M., Hou, L., Gao, D., Li, X., Lu, K., et al. (2017). Nitrogen losses in sediments of the East China Sea: Spatiotemporal variations, controlling factors and environmental implications. *J. Geophys. Res.: Biogeosci.* 122 (10), 2699–2715. doi: 10.1002/2017JG004036

Liu, L., and Greaver, T. L. (2010). A global perspective on belowground carbon dynamics under nitrogen enrichment. *Ecol. Lett.* 13, 819–828. doi: 10.1111/j.1461-0248.2010.01482.x

Liu, J., Wu, N., Wang, H., Sun, J., Peng, B., Jiang, P., et al. (2016). Nitrogen addition affects chemical compositions of plant tissues, litter and soil organic matter. *Ecology* 97 (7), 1796–1806. doi: 10.1890/15-1683.1

Luo, M., Zhu, W., Huang, J., Liu, Y., Duan, X., Wu, J., et al. (2019). Anaerobic organic carbon mineralization in tidal wetlands along a low-level salinity gradient of a subtropical estuary: Rates, pathways, and controls. *Geoderma* 337, 1245–1257. doi: 10.1016/j.geoderma.2018.07.030

Magill, A. H., and Aber, J. D. (2000). Dissolved organic carbon and nitrogen relationships in forest litter as affected by nitrogen deposition. *Soil Biol. Biochem.* 32 (5), 603–613. doi: 10.1016/S0038-0717(99)00187-X

Mao, R., Wu, P. P., Xu, J. W., Wan, S. Z., and Zhang, Y. (2021). Leaf litter decomposition in the air should not be ignored in subtropical plantations of China. *For. Ecol. Manag* 499, 119614. doi: 10.1016/j.foreco.2021.119614

McTee, M. R., Lekberg, Y., Mummey, D., Rummel, A., and Ramsey, P. W. (2017). Do invasive plants structure microbial communities to accelerate decomposition in intermountain grasslands? *Ecol. Evol.* 7 (24), 11227–11235. doi: 10.1002/ece3.3608

Meybeck, M., and Ragu, A. (2012). *GEMS-GLORI world river discharge database* (Paris: Laboratoire de Géologie Appliquée, Université Pierre et Marie Curie). doi: 10.1594/PANGAEA.804574

Nordhaus, I., and Wolff, M. (2007). Feeding ecology of the mangrove crab *Ucides cordatus* (Ocypodidae): food choice, food quality and assimilation efficiency. *Mar. Biol.* 151 (5), 1665–1681. doi: 10.1007/s00227-006-0597-5

Nykvist, N. (1963). Leaching and decomposition of water-soluble organic substancesfrom different types of leaf and needle litter. *Studia Forestalla Suecica*, 3, 1–29.

Ochoa-Hueso, R., Delgado-Baquerizo, M., King, P. T. A., Benham, M., Arca, V., and Power, S. A. (2019). Ecosystem type and resource quality are more important than global change drivers in regulating early stages of litter decomposition. *Soil Biol. Biochem.* 129, 144–152. doi: 10.1016/j.soilbio.2018.11.009

Prescott, C. E. (2010). Litter decomposition: what controls it and how can we alter it to sequester more carbon in forest soils? *Biogeochemistry* 101, 133–149. doi: 10.1007/s10533-010-9439-0

Rejmánková, E., and Houdková, K. (2006). Wetland plant decomposition under different nutrient conditions: what is more important, litter quality or site quality? *Biogeochemistry* 80 (3), 245–262. doi: 10.1007/s10533-006-9021-y

Rockström, J., Steffen, W., Noone, K., Persson, Å., Chapin, F. S.III, Lambin, E. F., et al. (2009). A safe operating space for humanity. *Nature* 461, 472. doi: 10.1038/461472a

Rubino, M., Dungait, J., Evershed, R., Bertolini, T., De Angelis, P., D'Onofrio, A., et al. (2010). Carbon input belowground is the major c flux contributing to leaf litter mass loss: Evidences from a ^{13}C labelled-leaf litter experiment. *Soil Biol. Biochem.* 42 (7), 1009–1016. doi: 10.1016/j.soilbio.2010.02.018

Saiya-Cork, K., Sinsabaugh, R., and Zak, D. (2002). The effects of long term nitrogen deposition on extracellular enzyme activity in an *Acer saccharum* forest soil. *Soil Biol. Biochem.* 34 (9), 1309–1315. doi: 10.1016/S0038-0717(02)00074-3

Simas, T. C., and Ferreira, J. G. (2007). Nutrient enrichment and the role of salt marshes in the tagus estuary (Portugal). *Estuar. Coast. Shelf S* 75 (3), 393–407. doi: 10.1016/j.ecss.2007.05.046

Sinsabaugh, R. L., Gallo, M. E., Lauber, C., Waldrop, M. P., and Zak, D. R. (2005). Extracellular enzyme activities and soil organic matter dynamics for northern hardwood forests receiving simulated nitrogen deposition. *Biogeochemistry* 75 (2), 201–215. doi: 10.1007/s10533-004-7112-1

Sinsabaugh, R. L., Hill, B. H., and Follstad Shah, J. J. (2009). Ecoenzymatic stoichiometry of microbial organic nutrient acquisition in soil and sediment. *Nature* 462 (7274), 795–798. doi: 10.1038/nature08632

Tao, B., Zhang, B., Dong, J., Liu, C., and Cui, Q. (2019). Antagonistic effect of nitrogen additions and warming on litter decomposition in the coastal wetland of the yellow river delta, China. *Ecol. Eng.* 131, 1–8. doi: 10.1016/j.ecoleng.2019.02.024

Tu, L., Hu, H., Hu, T., Zhang, J., Liu, L., Li, R., et al. (2011). Decomposition of different litter fractions in a subtropical bamboo ecosystem as affected by experimental nitrogen deposition. *Pedosphere* 21 (6), 685–695. doi: 10.1016/S1002-0160(11)60171-9

Turner, B. L., and Wright, S. J. (2014). The response of microbial biomass and hydrolytic enzymes to a decade of nitrogen, phosphorus, and potassium addition in a lowland tropical rain forest. *Biogeochemistry* 117 (1), 115–130. doi: 10.1007/s10533-013-9848-y

Uselman, S. M., Qualls, R. G., and Lilienfein, J. (2012). Quality of soluble organic c, n, and p produced by different types and species of litter: Root litter versus leaf litter. *Soil Biol. Biochem.* 54 (6), 57–67. doi: 10.1016/j.soilbio.2012.03.021

Valiela, I., Teal, J. M., Allen, S. D., Van Etten, R., Goehringer, D., and Volkmann, S. (1985). Decomposition in salt marsh ecosystems: the phases and major factors affecting disappearance of above-ground organic matter. *J. Exp. Mar. Biol. Ecol.* 89 (1), 29–54. doi: 10.1016/0022-0981(85)90080-2

Wang, Y., Yang, J., Liu, L., and Yu, Z. (2015). Quantifying the effects of geographical and environmental factors on distribution of stream bacterioplankton within nature reserves of fujian, China. *Environ. Sci. pollut. R* 22 (14), 11010–11021. doi: 10.1007/s11356-015-4308-y

Wedin, D. A., and Tilman, D. (1996). Influence of nitrogen loading and species composition on the carbon balance of grasslands. *Science* 274 (5293), 1720–1723. doi: 10.1126/science.274.5293.172

Werry, J., and Lee, S. (2005). Grapsid crabs mediate link between mangrove litter production and estuarine planktonic food chains. *Mar. Ecol. Prog. Ser.* 293, 165–176. doi: 10.3354/meps293165

Xu, Y., Fan, J., Ding, W., Bol, R., Chen, Z., Luo, J., et al. (2016). Stage-specific response of litter decomposition to n and s amendments in a subtropical forest soil. *Biol. Fert Soils* 52 (5), 711–724. doi: 10.1007/s00374-016-1115-7

Xu, W., Luo, X., Pan, Y., Zhang, L., Tang, A., Shen, J., et al. (2015). Quantifying atmospheric nitrogen deposition through a nationwide monitoring network across China. *Atmos Chem. Phys.* 15 (21), 12345–12360. doi: 10.5194/acp-15-12345-2015

Yang, W., Feng, G., Tewolde, H., and Li, P. (2019). CO_2 emission and soil carbon sequestration from spring-and fall-applied poultry litter in corn production as simulated with RZWQM2. *J. Clean Prod* 209, 1285–1293. doi: 10.1016/j.jclepro.2018.10.251

You, C., Wu, F., Gan, Y., Yang, W., Hu, Z., Xu, Z., et al. (2017). Grass and forbs respond differently to nitrogen addition: a meta-analysis of global grassland ecosystems. *Sci. Rep-UK* 7 (1), 1563–1573. doi: 10.1038/s41598-017-01728-x

Yu, X., Guo, J., Lu, X., Wang, G., Jiang, M., and Zou, Y. (2019). Comparative analyses of wetland plant biomass accumulation and litter decomposition subject to *in situ* warming and nitrogen addition. *Sci. Tot. Environ.* 691, 769–778. doi: 10.1016/j.scitotenv.2019.07.018

Zhang, T. A., Luo, Y., Chen, H. Y. H., and Ruan, H. (2018). Responses of litter decomposition and nutrient release to n addition: A meta-analysis of terrestrial ecosystems. *Appl. Soil Ecol.* 128, 35–42. doi: 10.1016/j.apsoil.2018.04.004

Zhang, X., Mao, R., Gong, C., Qiao, T., and Song, C. (2014b). CO_2 evolution from standing litter of the emergent macrophyte *Deyeuxia angustifolia* in the sanjiang plain, northeast China. *Ecol. Eng.* 63, 45–49. doi: 10.1016/j.ecoleng.2013.12.002

Zhang, L., Tong, C., Marrs, R., Wang, T., Zhang, W., and Zeng, C. (2014a). Comparing litter dynamics of *Phragmites australis* and *Spartina alterniflora* in a sub-tropical Chinese estuary: Contrasts in early and late decomposition. *Aquat Bot.* 117, 1–11. doi: 10.1016/j.aquabot.2014.03.003

Zhu, Z., Ge, T., Luo, Y., Liu, S., Xu, X., Tong, C., et al. (2018). Microbial stoichiometric flexibility regulates rice straw mineralization and its priming effect in paddy soil. *Soil Biol. Biochem.* 121, 67–76. doi: 10.1016/j.soilbio.2018.03.003

frontiers | Frontiers in Marine Science

TYPE Review
PUBLISHED 13 October 2022
DOI 10.3389/fmars.2022.1038400

OPEN ACCESS

EDITED BY
Jing Wei,
Sun Yat-sen University, China

REVIEWED BY
Xiaolong Yang,
Zhejiang Ocean University, China
Fanzhu Qu,
Ludong University, China

*CORRESPONDENCE
Chaobin Xu
xuchaobin@fjnu.edu.cn

SPECIALTY SECTION
This article was submitted to Marine Biogeochemistry, a section of the journal Frontiers in Marine Science

RECEIVED 07 September 2022
ACCEPTED 29 September 2022
PUBLISHED 13 October 2022

CITATION
Wei H, Wang M, Ya M and Xu C (2022) The denitrifying anaerobic methane oxidation process and microorganisms in the environments: A review. *Front. Mar. Sci.* 9:1038400. doi: 10.3389/fmars.2022.1038400

The denitrifying anaerobic methane oxidation process and microorganisms in the environments: A review

Hengchen Wei[1], Mengxin Wang[1], Miaolei Ya[2] and Chaobin Xu[3]*

[1]School of Environmental Science and Engineering, Nanjing Tech University, Nanjing, China, [2]State Key Laboratory of Estuarine and Coastal Research, East China Normal University, Shanghai, China, [3]Fujian Provincial Key Laboratory for Plant Eco-Physiology, School of Geographical Sciences, School of Carbon Neutrality Future Technology, Fujian Normal University, Fuzhou, China

Methane (CH_4) is an important greenhouse gas with a global warming potential 28 – 34 times that of CO_2 over the 100-year horizon. Denitrifying anaerobic methane oxidation (DAMO) is a recently discovered process that potentially represents an important CH_4 sink globally. This process involves two possible pathways: the nitrite-dependent DAMO mediated by NC10 bacteria and the nitrate-dependent DAMO by ANME-2d archaea. Both are widely detected in freshwater and coastal habitats using molecular tools. However, the distributions of these two processes and the functional microorganisms and their interactions with other N cycling pathways are far from clear. In this review, we conducted a scientometric analysis on a co-citation network consisting of 835 references derived from 354 citing articles closely related to the distribution of DAMO in the environment. Through this analysis, we found that current studies focus more on freshwater systems than coastal systems, and ANME-2d archaea are generally under-studied compared to NC10 bacteria. The emerging research topics in this area include AMO processes coupled to alternative electron acceptors and their role as CH_4 sinks. We further reviewed papers focusing on DAMO distribution in freshwater and coastal environments guided by the result of the scientometric analysis. Finally, we identified several areas that require further research and proposed future research including comparisons of DAMO with other N cycling pathways and environmental conditions in the context of the river-estuary-sea continuum.

KEYWORDS

DAMO, scientometric analysis, M. oxyfera, M. nitroreducens, review, CiteSpace

1 Introduction

Methane (CH_4) is an important greenhouse gas with a 100-year global warming potential 28-34 times that of CO_2 (Dean et al., 2018). CH_4 is estimated to be responsible for 0.5°C of increase in global average temperature during 2010-2019 compared to 1850-1900, contributing to 16% of global warming (IPCC, 2021). Therefore, controlling CH_4 emissions is the key to mitigating the global greenhouse effect and global warming. In ecosystems, the microbe-mediated CH_4 oxidizing processes are important sinks for global CH_4 emission. Anaerobic methane oxidation (AMO) has long been discovered in marine sediments, which is typically coupled with sulfate reduction, removing 90% of marine CH_4 emissions before they leave the sea (Knittel and Boetius, 2009). This process plays a critical role in controlling atmospheric CH_4 concentrations globally. In recent years, a related process, denitrifying anaerobic methane oxidation (DAMO), has been observed, drawing great attention as a novel CH_4 cycling pathway. DAMO is an anaerobic process that couples anaerobic CH_4 oxidation with NO_3^- and NO_2^- reduction, making it one of the linkages between C and N cycles, and can potentially remove CH_4 and reactive N. Therefore, a better understanding of the DAMO processes in natural and engineered ecosystems can help us reduce greenhouse gas emissions and mitigate eutrophication in aquatic environments.

DAMO was first observed in an enrichment culture after long-term incubation retrieved from eutrophic freshwater sediments in Netherland (Raghoebarsing et al., 2006). Since then, many studies have focused on DAMO in freshwater systems, including sediments of lakes (Deutzmann and Schink, 2011; Kojima et al., 2012), reservoirs (Han and Gu, 2013), paddy fields (Hu et al., 2014; Vaksmaa et al., 2016), and wetlands (Hu et al., 2014; Shen et al., 2015b). Their distributions in coastal marine environments, such as coastal rivers, estuaries, and adjacent seas, however, have not been examined as much. Scientometric reviews based on the statistical analysis of the bibliometric records of a research field can help understand the intellectual structures of the underlying field and identify emerging directions in the research. This process is increasingly facilitated by available science mapping tools such as CiteSpace (Chen, 2006), VosViewers (van Eck and Waltman 2010), etc. They have been widely used in scientometric reviews in areas such as medicine (Chen et al., 2014?), greenhouse emission (Wang et al., 2021), ecosystem health (Yang et al., 2019), etc. However, a scientometric analysis of the vast body of DAMO literature has not been reported to the best of our knowledge.

In light of this, we reviewed studies focusing on DAMO distributions and their affecting factors in freshwater and coastal marine ecosystems, compared the abundance and dominating microorganisms in these two types of systems, identified knowledge gaps, and provided an outlook for this area. This review intends to give a comprehensive overview of the current research on DAMO and to provide insights into factors that help shape the distribution of DAMO processes in freshwater and coastal marine ecosystems, and their potential in removing CH_4 emission and reactive N in these systems.

The specific objectives of this review were to (1) provide a brief overview of the DAMO processes, (2) identify influential references and emerging hot topics, (3) review the DAMO processes in freshwater and coastal systems in depth, and (4) point out limitations and propose future research directions. These objectives were addressed in each of the following sections of this review.

2 The DAMO processes

Scientists have long discovered that CH_4 oxidation could be coupled to sulfate reduction under anoxic conditions (Barnes and Goldberg, 1976). This pathway has been recognized to remove more than 90% of CH_4 emission from the ocean (Knittel and Boetius, 2009), which makes the ocean a minor contributor to global CH_4 emission (6 – 2 Tg CH_4 yr^{-1}, accounting for 1 – 2% of the global emission), despite that it covers 70% of the Earth's surface (Weber et al., 2019; Wallenius et al., 2021). The sulfate-dependent AMO uses SO_2^- as the electron (e^-) acceptor and prevails in the open ocean, considering the mean sulfate concentration of 28 mmol/L in seawater (Jørgensen et al., 2019). However, the concentrations of other potential e^- acceptors (e.g., NO_3^- and NO_2^-) can be much higher in coastal and freshwater systems compared to the open ocean, and in theory, they can drive several different AMO pathways (Table 1). Because of anthropogenic activities, especially the use of synthetic fertilizers and fossil fuel combustion, large amounts of reactive N are delivered to freshwater and coastal environments. As a result, AMO coupled with NO_3^- or NO_2^- reduction, also known as the DAMO process, has drawn much attention. DAMO microorganisms were first enriched in the laboratory after 16 months' incubation of highly eutrophic freshwater sediments (Raghoebarsing et al., 2006). The enriched culture contained bacteria and archaea, which performed AMO while using both NO_3^- and NO_2^- as e^- acceptors. Ettwig et al. (2008); Ettwig et al. (2010) further enriched the DAMO bacteria Candidatus Methylomirabilis oxyfera (M. oxyfera), which are nitrite-dependent and belong to the NC10 clade. M. oxyfera can catalyze the nitrite-dependent DAMO process, which reduces NO_2^- to N_2 while oxidizing CH_4 to CO_2 (Eqn. 3, Table 1). From the methane perspective, the nitrite-dependent DAMO by M.oxyfera follows the classical aerobic methane oxidation pathway, where methane is converted into methanol catalyzed by the particulate Methane monooxygenase (pMMO) enzyme (Wu et al., 2011). The produced methanol is further oxidized into formaldehyde, formate, and CO_2 catalyzed by the methanol

TABLE 1 AMO reactions driven by different e^- acceptors and their Gibbs free energy.

AMO reactions with different e^- acceptors	Gibbs Free Energy ΔG^{θ}(kJ/mol)
(1) $CH4 + SO_4^{2-} \rightarrow HCO_3^- + HS- + H2O$	-34
(2) $CH4 + 4NO_3^- + 4H+ \rightarrow CO2 + 4NO_2^- + 2H2O$	-503
(3) $3CH4 + 8NO_2^- + 8H+ \rightarrow 3CO2 + 4N2 + 10H2O$	-928
(4) $CH4 + 8Fe3+ + 3H2O \rightarrow HCO3- + 8Fe2+ + 9H+$	-435
(5) $5CH4 + 8MnO4- \rightarrow 5HCO_3^- + 8Mn2+ + 17H2O$	-1008

dehydrogenase, formaldehyde dehydrogenase, and formate dehydrogenase enzymes. The end-product CO_2 is assimilated into the organism *via* the Calvin Benson Bassham cycle. On the nitrite side, the nitrite-dependent DAMO follows a novel denitrification pathway, where NO_2^- is metabolized into O_2 and N_2 *via* NO, catalyzed by enzymes including nitrite reductase and a postulated putative NO dismutase (Ettwig et al., 2010; Wu et al., 2012) (Figure 1A). This pathway is different from the canonical denitrification pathway, in that NO is not reduced to N_2O as in the canonical pathway, catalyzed by the nitric oxide reductase enzyme (Ettwig et al., 2009). Rather, M.oxyfera lacks the genes responsible for N_2O reduction to N_2, but only a trace-amount of N_2O was detected in nitrite-dependent DAMO by M.oxyfera (Ettwig et al., 2009; Ettwig et al., 2010; Reimann et al., 2015). To solve this apparent paradox, a unique dismutation reaction was proposed to convert NO into N_2 and O_2, catalyzed by the putative nitric oxide dismutase (NOD) enzyme (Ettwig et al., 2012). Through this pathway, 75% of the produced O_2 is then used to oxidize CH_4 through the classical aerobic methane oxidation pathway as described earlier (Ettwig et al., 2010; Wu et al., 2011). Because the source of the O_2 is from the NC10 bacteria themselves, this aerobic methane oxidation process is obligate anaerobic and is also called an "intra-aerobic" (Wu et al., 2011). More research is required to thoroughly understand the proposed intra-aerobic pathway.

After the enrichment of DAMO bacteria, DAMO archaea were also enriched in 2013, after incubating in an anaerobic bioreactor fed with NO_3^-, NH_4^+, and CH_4 for 350 days (Haroon et al., 2013). The enriched archaea, which was named Methanoperedens nitroreducens (M. nitroreducens) belonging to ANME-2d, performed AMO through the reverse methanogenesis pathway using NO_3^- as the terminal e^- acceptor (Figure 1B). The ANME-2d contains all required functional genes for a complete reverse methanogenesis pathway (Haroon et al., 2013; Leu et al., 2020). The first step of this pathway is catalyzed by the methyl-coenzyme M reductase (MCR) enzymes. This step requires energy and has drawn great research interest since it is considered the rate-limiting step of the reverse methanogenesis pathway; however, the kinetic properties of the MCR enzyme remain largely unknown (Cai et al., 2021). The rest of the reverse methanogenesis pathway involves another 6 steps, each catalyzed by a specific enzyme, which has been reviewed in Timmers et al., 2017. This reverse methanogenesis process is coupled to NO_3^- reduction to NO_2^-, catalyzed by the nitrate reductase subunit NarG (Haroon et al., 2013). ANME-2d cannot further reduce NO_2^- to N_2; this process was finished by the syntrophic partner, anammox bacteria in the enriched co-culture (Haroon et al., 2013). Unlike M. oxyfera, ANME-2d reportedly can use multiple e^- acceptors other than NO_3^-, including Fe (Cai et al., 2018) and Mn (Leu et al., 2020).

Recently, the development of molecular tools, such as polymerase chain reaction (PCR), denaturing gradient gel electrophoresis (DGGE), and fluorescence *in situ* hybridization (FISH), enables relatively rapid detection of both M. oxyfera-like bacteria and ANME-2d archaea in the environment. PCR is the most used tool. A large group of PCR primers targeting 16s rRNA has been developed for the detection of M. oxyfera-like bacteria in the environment. In addition, the M. oxyfera-like bacteria use particular methane monooxygenase (pMMO) for CH_4 oxidation (Figure 1A). This allows scientists to use

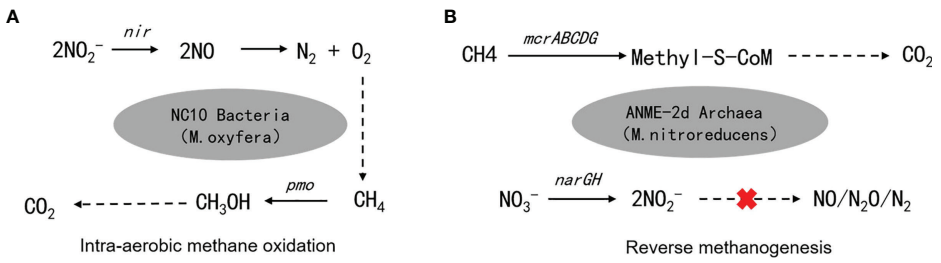

FIGURE 1
Metabolic pathways of **(A)** nitrite-dependent DAMO mediated by NC10 bacteria M. oxyfera and **(B)** nitrate-dependent DAMO mediated by ANME-2d archaea M.nitroreducens.

functional gene pmoA as biomarkers for the detection of M. oxyfera-like bacteria (Luesken et al., 2011). To date, a number of primers have been developed, and they have been summarized comprehensively in (Shen et al., 2015a), including the sequences and the PCR thermal profiles. Compared to M. oxyfera bacteria, the development of primers for DAMO archaea M. nitroreducens started later. In 2015, Ding and colleagues designed 16s rRNA primers for DAMO archaea in samples from several freshwater sediments and paddy soils (Ding et al., 2015), which marks the first PCR primers designed for DAMO archaea. The ANME-2d archaea possess the mcrA gene, which encodes the alpha-submit of the MCR enzyme, making it a popular functional gene for the environmental detection of ANME-2d (Vaksmaa et al., 2017a). Although primers targeting functional genes pmoA and mcrA have high specificity, Shen and colleagues (Shen et al., 2017; Shen et al., 2019a) also pointed out that clone library analysis based on 16s rRNA combined with high throughput sequencing can increase sequencing depths and result in more operational taxonomic units (OTUs), which helps with community diversity analysis. In addition to the PCR approach, early studies also employed the FISH methods to identify M. oxyfera in cultures, such as in (Raghoebarsing et al., 2006; Ettwig et al., 2008; Ettwig et al., 2009). The catalyzed reporter deposition-FISH method was used to detect NC10 bacteria in the sediments of Lake Biwa, which marks the first application of the FISH method in environmental samples. However, for the purpose of environmental detection, the FISH method is considered less sensitive compared with the PCR approach and could be limited if the abundance of the target microorganism is low in the environment (Chen et al., 2016).

Molecular evidence for DAMO bacteria and archaea is often complemented by potential rates measured using isotope tracing methods combined with slurry incubations. In general, ^{13}C tracers are usually added with e^- acceptors such as NO_3^- and NO_2^- to the incubated samples and are compared with the control treatments. The rates can be inferred from the production of $^{13}CO_2$, measured by GC-IRMS. Measured this way, the original structure and gradients of the sediment is likely destroyed because of the homogenization of the slurry, and samples are fertilized with substrates such as CH_4 and NO_3^- and NO_2^- during the incubation. Therefore, the rate should not be considered the true rate in the field, but rather, represents the potential rate of the measured process under the incubation conditions. Despite these limitations, ^{13}C tracing combined with slurry incubation is widely used for measuring the potential DAMO rates in sediment samples (Hu et al., 2014; Shen et al., 2016; Zhang et al., 2018; Li et al., 2020). Techniques combining isotope tracing and sequencing, such as stable carbon isotope probing can result in a more nuanced understanding of the DAMO process and the role each specific microorganism plays in the process (Sharp et al., 2012; Rasigraf et al., 2014).

3 Scientometric analysis of the DAMO research

Scientometric is a branch of informatics focusing on quantitative analysis of research papers and journals to understand the development and mechanisms of science. Co-citation is a common measurement used in quantitative studies, as a group of scientific papers frequently being co-cited by citing documents that represent key knowledge, methods, or concepts in a research field. The co-citation patterns could be used to map out the relationships between key references, authors, or keywords, to reveal the knowledge structure behind a research field. In fact, science mapping represents an important research topic in the field of bibliometrics (Cobo et al., 2011).

In the field of DAMO research, since the prediction of the DAMO process and the successful enrichment of DAMO organisms in 2006 (Raghoebarsing et al., 2006), the number of publications has grown rapidly. To understand where we stand in the domain of DAMO, particularly the distributions of DAMO in the environment, we conducted a co-citation network analysis on a literature database collected from the Web of Science Core Collection. The goals of this section are to (1) reveal the structure of the co-citation network in this field, (2) identify influential references that shape the development of the field, and (3) detect the emerging hot topics and areas of DAMO research based on co-citation analysis on the references of the literature database.

The co-citation analysis and visualization were implemented using CiteSpace 6.1 R3. CiteSpace is a science mapping tool capable of exploring the literature co-citation network and visualizing the knowledge structure of a field. The foundation and application of CiteSpace in exploring and visualizing a research field have been demonstrated in a series of publications (Chen, 2004; Chen, 2006; Chen et al., 2012; Chen and Song, 2019; Chen, 2020), and it has been used to summarize research in ecology (Yang et al., 2019; Hu et al., 2019). For the current review work, we used CiteSpace to analyze the co-citation network with emphasis on three key aspects: (1) the structure and the timeline view of the co-citation network, (2) references with citation bursts (i.e., an abrupt change in citation counts), and (3) keywords with citation bursts. By focusing on these three aspects, we hope to achieve the three goals of this section as stated earlier. Several key concepts in CiteSpace that we will focus on include citation burst, clustering, and labeling. Briefly, a burst refers to a surge of frequencies of certain types of events, including the citation count, keyword appearance, or noun phrases in the titles, abstracts, or other parts of the publication. CiteSpace adopts the algorithm from Kleinberg 2002 to determine such burst events. CiteSpace also partitions the co-citation network into mutually-exclusive clusters such that references were tightly associated with each other but

loosely connected with references outside the cluster using the spectral clustering algorithm formulated as an optimization problem (Chen et al., 2010). The technical details are described in (Shi and Malik, 2000; Ng et al., 2002; Chen et al., 2010). After the clusters are defined, they are automatically labeled by noun phrases extracted from the titles, abstracts, and indexed keywords of the citing publications and ranked using the log-likelihood ratio (LLR) test (Dunning 1993).

For the current review, we built the citing article dataset focused on DAMO in the environment. We collect data from the Web of Science Core Collection using keywords "anaerobic oxidation of methane", "anaerobic methane oxidation", "nitrate-dependent anaerobic methane oxidation", "nitrite-dependent anaerobic methane oxidation", "denitrifying anaerobic methane oxidation", "n-damo", "damo", "M. oxyfera", "M. nitroreducens", "NC10", "ANME-2d". The resulting literature was further refined using keywords including "river", "lake", "reservoir", "estuary", "sea", "marine", "sediment", "soil", and "wetland" to limit the search to studies on those environments. The resulting literature dataset contained 354 publications, including 316 research articles, 35 reviews, and 2 editorials, ranging from 2000 to 2022.

The literature database was then analyzed by CiteSpace for the 2000 – 2022 period, with configurations suggested by the developer (Chen et al., 2012). The CiteSpace project files and model configurations were available in Mendeley Data (10.17632/mwrkrmp3jn.2). A co-citation network of 835 nodes was derived from the citing article database. In terms of countries, China contributed the most, accounting for 34% of all references, followed by Germany and the USA, each contributing 13%, and Netherland ranked the 4th, which contributed 12% (Figure 2). The network was divided into 17 clusters such that the references were closely related to each other within a cluster and references were loosely connected between clusters (Figure 2). The top 8 largest clusters were listed in Table 2. They each have >20 member references, which can represent the sub-research area reasonably well. Their silhouette values were close to 1, suggesting a good homogeneity within each cluster (Table 2, Chen et al., 2012).

Clusters 0 and 2 were the two clusters with the most citation bursts. Cluster 0 was labeled n-damo based on the indexed keywords of the citing articles using the LLR test (Chen et al., 2012). This was the largest cluster containing 103 member references, and the representative references were focused on the distribution of DAMO and other AMO pathways in the environment. For example, in a series of works by Shen and colleagues, they demonstrated that nitrite-dependent DAMO and M.oxyfera were more active and abundant in freshwater marshes in East China (Shen et al., 2017). Later, in Shen et al., 2019a, AMO processes driven by different e^- acceptors (including nitrate, nitrite, sulfate, and iron) across different riverbeds in England were compared, with nitrate- and nitrite-

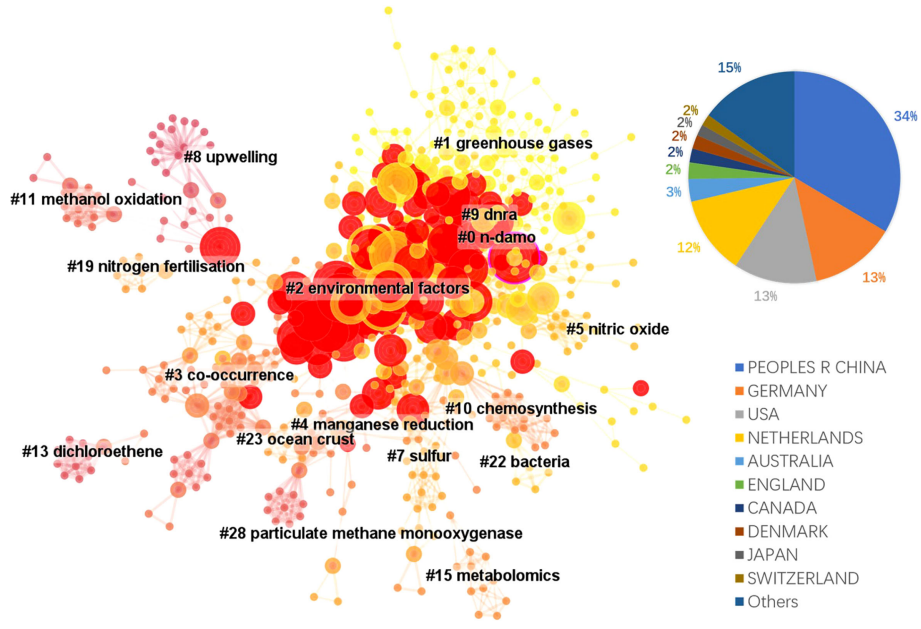

FIGURE 2
The landscape view of the reference co-citation network (total 835 nodes) derived from the 354 citing references from 2000 to 2022 and the country contributions of the citing references. Red circles represent references with citation bursts; the size of the circles reflects citation counts; links between nodes suggest that they were co-cited by citing references.

TABLE 2 Major clusters of the co-cited references.

Cluster ID	Size	Silhouette	Mean Cite Year	Label (LLR)*
0	103	0.834	2018	n-damo
1	87	0.868	2020	greenhouse gases
2	82	0.841	2014	environmental factors
3	62	0.966	2010	co-occurance
4	46	0.951	2011	manganese reduction
5	34	0.982	2017	nitric oxide
7	29	0.983	2015	sulfur
8	27	0.919	2006	upwelling

*Labels selected based on indexed keywords using log-likelihood ratio test method (LLR).

dependent AMO being the most active pathways. Moreover, the nitrite-dependent AMO activity was higher than the nitrate-dependent pathway, consistent with their findings for the freshwater marshes (Shen et al., 2017). These two papers were co-cited later by authors other than the Shen group focusing on similar topics, such as by Chen et al. (2021), who compared nitrite-/nitrate-dependent DAMO in estuaries and intertidal wetlands in the Yangtze Estuary.

The second largest cluster, cluster 2 was labeled as environmental factors based on the indexed keywords of the citing articles. Their co-cited reference network contained several fundamental references in this area, such as the series of research by Ettwig et al. (2008); Ettwig et al. (2009); Ettwig et al. (2010), where the bacteria community performing nitrite-dependent DAMO was enriched and the metabolic pathways were investigated. Cluster 2 also contained the milestone paper by Haroon et al. (2013), where the ANME-2d archaea N. nitroreducens capable of nitrate-dependent DAMO was enriched. We demonstrated some of the most representative articles (with citation bursts) of the two largest clusters in the area. The complete list of all cluster members and their citation data (including burstiness and citation counts) is available as the open data associated with this manuscript in Mendeley Data (10.17632/mwrkrmp3jn.2). This cluster also contained many representative papers reporting the DAMO community in various natural environments. For example, Shen and colleagues investigated the nitrite-dependent DAMO distributions in the sediments of the Jiaojiang Estuary (Shen et al., 2014b), Xiazhuhu wetland (Shen et al., 2015b) in China, and 7 permeable riverbeds in England (Shen et al., 2019a), and explored the effects of different environmental conditions on their distribution in these systems. A more detailed discussion on DAMO distributions in freshwater and coastal systems is presented in Section 4.

Taking a timeline view, cluster 8 first emerged around 2007 (Figure 3). The most cited paper (and with citation burst) in this cluster was the landmark reference Raghoebarsing et al., 2006, which reported the first enriched culture performing DAMO in the laboratory. Cluster 2 contained the most high-profile references (i.e., references with strong citation bursts, indicated by the large red rings), as discussed earlier for the landscape view of the co-citation network (Figure 2). The timeline view further revealed that these high-profile references emerged in two periods; first started around 2007 – 2010, which was featured by the series of research by Ettwig and colleagues, co-cited with the Raghoebarsing et al., 2006 reference (Figure 3). These references were focused on the metabolic pathways of the nitrite-dependent DAMO. The second cluster was around the famous Haroon et al., 2013 paper, where the enrichment of N. nitroreducens was reported. High-profile reference groups were also formed after 2013 in cluster 0, as highlighted in Figure 3. They include a highly cited review on nitrite- and nitrate-dependent DAMO by Welte et al. (2016), and studies on primer designs for DAMO archaea (Ding et al., 2015), DAMO bacteria and archaea distributions in paddy field (Vaksmaa et al., 2016; Ding et al., 2016), freshwater rivers (Long et al., 2017b; Shen et al., 2019b), reservoirs (Long et al., 2017a), marshes (Shen et al., 2017), and in coastal systems (Zhang et al., 2018). These references will be discussed in more depth in the later sections of the review. In addition to these two major clusters, cluster 1 was a notably new one, as the mean citing year was 2018 (Table 2). This recently formed cluster featured only a few high-profile references, which were focused on novel e^- acceptors such as humic substances (Valenzuela et al., 2019; Bai et al., 2019) and metals (He et al., 2018). These novel processes are associated with ANME archaea. For example, recently, AMO processes coupled to Fe(III) and Mn(IV) were reported after long-term incubation. They were performed by novel species belonging to ANME-2d, which were named Candidatus Methanoperedens ferrireducens (Cai et al., 2018)and Candidatus Methanoperedens manganicus (Leu et al., 2020), respectively. The metal reduction was hypothesized to be conducted through the direct interspecies e^- transfer (DIET) pathway catalyzed by the multi-heme c-type cytochrome (MHCs), similar to other common metal-reducing organisms (Shi et al., 2016; Cai et al., 2018; Leu et al., 2020). Other novel e^- acceptors include As(V) (Shi et al., 2020) and humic acids (Bai et al., 2019) can also fuel AMO, supposedly through the MHC-dependent DIET process. This

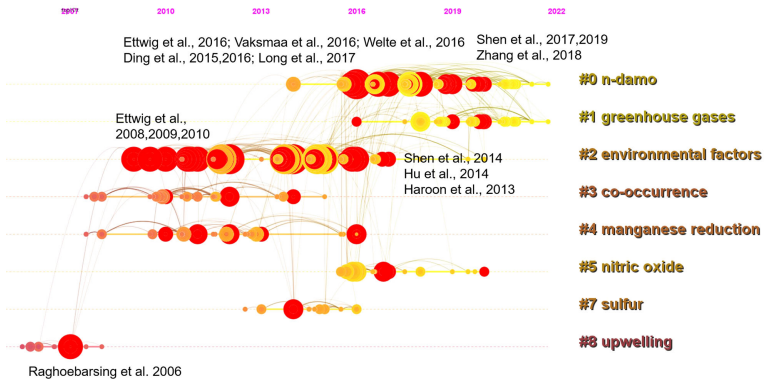

FIGURE 3
A timeline view of the co-citation network with the 8 largest clusters. Red circles represent references with citation bursts; the size of the circles reflects citation counts; links between nodes suggest that they were co-cited by citing references.

cluster represents one of the frontiers in the research of AMO processes, as the role of different e^- acceptors and their interactions with DAMO can have important implications for the CH_4 sink/source behaviors of a system.

The emerging trends of the DAMO research were further investigated through the co-occurrence analysis of reference keywords. Before the successful enrichment and the naming of the DAMO bacteria M.oxyfera, "methane production" was the keyword with a long burst duration (2000 – 2011, Figure 4), as the scientific community had a strong interest in understanding CH_4 emission in various types of ecosystems, such as rice paddies and peatlands (e.g., Chidthaisong and Conrad, 2000; Liesack et al., 2000 in our citing article database). "M.oxyfera" and "denitrifying methanotrophic bacteria" were the two keywords refer to the DAMO bacteria, with the latter term bursting for a shorter period from 2012 – 2016 (Figure 4). The term "enrichment" became popular in 2013-2016, reflecting the research effort to investigate the DAMO bacteria and archaea through enriched cultures (e.g., Ettwig et al., 2010; Ettwig et al., 2016). Later on, keywords about natural ecosystems started to experience citation bursts, including "lake", "freshwater lake", and "wetland". The most recent keywords were "sink" and "removal", which referred to DAMO as N and CH_4 sinks in ecosystems including wetlands (Xie et al., 2020; Yang et al., 2022; Wang et al., 2022) and aquatic systems (Shen et al., 2020; Li et al., 2020). These new trends suggest that the distribution of DAMO in the environment and the potential contributions to CH_4 and N sinks are becoming the current focus of research and like to continue in the future. Comparing freshwater and coastal systems, keywords contained "freshwater", "lake", "river", "reservoir", and "paddy" resulted in a total of 100 occurrences, whereas keywords contained "coastal", "coast", "estuary", "bay", "marine", "ocean", and "sea" resulted in 41 occurrences. Keywords related to M.oxyfera also occurred more frequently than the keywords related to ANME-2d archaea. The keywords and their occurrence frequencies were available together with other CiteSpace documents in Mendeley Data as stated earlier. This result suggests that freshwater systems are currently more studied than coastal systems, and DAMO bacteria is more studied than their archaeal counterparts.

In summary, the co-citation analysis of the literature database helped us identify the important areas in the field of DAMO in the environment. We identified a number of key references with abrupt increases in citation counts over the 2000 – 2022 period, which were focused on DAMO metabolic pathways, laboratory enrichment, and environmental distributions in environments including wetlands, rice paddies, and freshwater and coastal systems. The timeline view also revealed the evolution of research in this area, from studies on enriched cultures to their distributions in the environment. The latest trends include the role of DAMO as N and CH_4 sinks and alternative e^- acceptors of AMO, such as humic substances and metals. In the next sections, we will be focused on DAMO distribution in freshwater and coastal environments, and analyze the relevant literature in more depth guided by the results of the co-citation analysis.

4 DAMO in freshwater and coastal systems

4.1 Freshwater systems

As revealed by the co-citation analysis, in early studies, DAMO was often investigated in the laboratory with enriched cultures. However, as molecular tools evolved and primers for DAMO bacteria and archaea were designed, their distribution and activities in the fields have been studied more. To date, DAMO microorganisms and activities have been reported in a wide range of

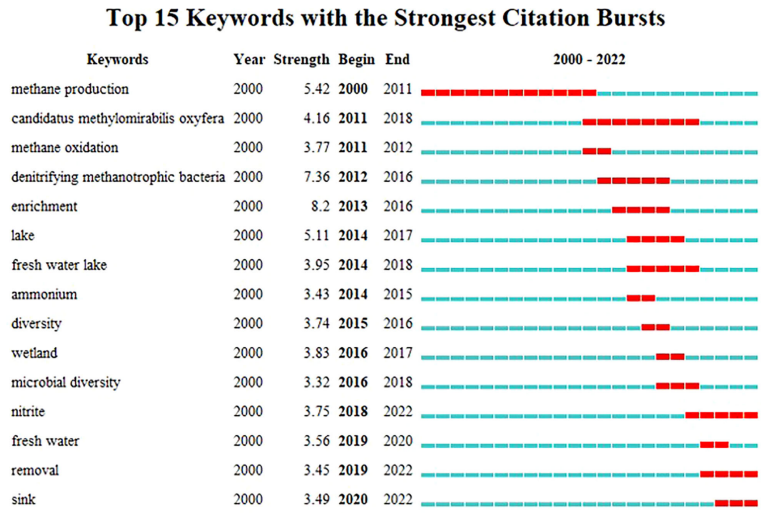

FIGURE 4
Keywords with strong citation bursts from 2000 – 2022.

natural and engineered habitats (Table 3). For freshwater systems, Hu et al. (2014) estimated that in freshwater wetlands, the potential rates of nitrite-dependent DAMO can reach 4.1 – 6.1 Tg CH_4 m^{-2} yr^{-1}, accounting for 2 – 6% of CH_4 emission by global wetlands, suggesting that DAMO could be an important but overlooked CH_4 sink. Zhu et al. (2015) compared 91 soil samples from 24 different wetlands in China and proved that M. oxyfera-like bacteria are widely distributed in freshwater wetlands. These results show that M. oxyfera-like bacteria are widely distributed in freshwater environments. Common environmental factors in freshwater systems affecting the distribution of DAMO bacteria include oxygen levels, CH_4 concentrations, and nutrient and organic matter conditions. For example, Shen et al. (2015b) studied DAMO bacteria and the corresponding nitrite-dependent DAMO rates in soils of Xiazhuhu wetland, China, and found that DAMO bacteria abundance and activities were higher in deep soil layers, where the oxygen levels were low and CH_4 concentrations were high. As described in Section 2, the M.oxyfera employs an intra-aerobic pathway, and thus, detrimental effects from the external supply of O_2 can be expected. Evidence supporting this idea comes from laboratory experiments with M. oxyfera cultures, where DO concentrations of 1 or 4 mg/L suppressed the CH_4 and NO_2^- metabolism (Luesken et al., 2012). However, exposed at lower oxygen levels, increases in both CH_4 and NO_2^- consumption rates were observed (Kampman et al., 2018), suggesting that micro-oxygenic environments might stimulate the M. oxyfera metabolism. Dissolved CH_4 concentrations represent another major factor that can regulate the metabolism of DAMO. The NC10 bacteria typically have higher CH_4 affinity than ANME-2d archaea, as the CH_4 affinity constant can be 1 – 2 orders of magnitudes lower for the NC10 bacteria than their archaeal counterparts (He et al., 2013; Lu et al., 2019). Long et al. (2017b) compared DAMO bacteria abundance and community structures in Dongjiang and its tributaries from May to August and identified that NO_2^-, NH_4^+, and C/N affected the community structure. In addition, Long et al. (2017a) also examined the vertical and horizontal distributions of DAMO bacteria in reservoir sediments and pointed to NO_2^-, total organic C, P, and N as key factors contributing to the variations in DAMO bacteria abundance and rates.

Compared with DAMO bacteria, DAMO archaea are in general less studied for their environmental distributions (Table 3). As the conditions for nitrate- and nitrite-dependent DAMO processes to occur are similar, and NO_3^- is more prevalent in natural environments, ANME-2d and M. oxyfera-like bacteria are likely to co-exist in natural habitats. According to the reaction kinetics, compared to NO_3^-, NO_2^- as the e^- acceptor produces more energy (Table 1), and some studies do show that DAMO bacteria have high abundance as well as potential rates than archaea, such as in wetlands (Shen et al., 2017) and reservoirs (Shen et al., 2020). However, opposite results also exist, such as in a Tibetan alpine wetland (Xie et al., 2020). Oxygen levels may be one of the factors that cause niche differentiation between DAMO bacteria and archaea, as M. oxyfera bacteria are hypothesized to better tolerate oxygen (Wallenius et al., 2021). In their study, the interaction of M. oxyfera with other N cycling microorganisms was found to be affected by multiple factors, including temperature, N, and P contents, whereas the interaction of M. nitroreducens with other microorganisms was solely affected by N compounds (Xie et al., 2020). These results suggest that multiple mechanisms may play a role in shaping distributions of DAMO bacteria and archaea, requiring further studies.

TABLE 3 Nitrite- and nitrate-dependent DAMO rates and microorganisms in freshwater habitats.

Habitat	e^- acceptor	DAMO rate	Microorganism	Reference
Lake Constance	NO_3^-/NO_2^-	1.8–3.6*	NC10	(Deutzmann and Schink, 2011)
Lake Biwa	NO_3^-/NO_2^-	NR**	NC10	(Kojima et al., 2012)
Qiantang River	NO_2^-	NR	NC10	(Shen et al., 2014a)
Lakes in Yunnan, China	NO_2^-	NR	NC10	(Liu et al., 2015)
Aquifer	NO_3^-	NR	ANME-2d	(Flynn et al., 2013)
Dongjiang River	NO_2^-	NR	NC10	(Long et al., 2017b)
Yellow River Estuary	NO_2^--	NR	NC10	(Yan et al., 2015)
Inland rivers in England	NO_2^-	0.4–61	NC10	(Shen et al., 2019b)
	NO_3^-	0.5–20	ANME-2d	
	SO4	0.6–4.4	ANME-2d	
	Fe	1.5–8.1	ANME-2d	
Dongchang Lakes	NO_2^-	NR	NC10	(Wang et al., 2017b)
Three Gorges Dam reservoir	NO_2^-	NR	NC10	(Wang et al., 2016)
Xinfengjiang reservoir	NO_2^-	NR	NC10	(Long et al., 2017a)
Jiulonghu reservoir-	NO_2^-	4.7–14.1	NC10	(Shen et al., 2020)
	NO_3^-	0.8–2.6	ANME-2d	
A river in Suzhou	NO_3^-	NR	ANME-2d	(Ding et al., 2015)
Taihu Lake	NO_3^-	NR	ANME-2d	
Chaohu Lake	NO_3^-	NR	ANME-2d	
Xiazhuhu wetland	NO_2^-	0.2–14.5	NC10	(Shen et al., 2015b)
Xixi wetland	NO_2^-	0.68–4.92	NC10	(Hu et al., 2014)
Green Bay wetland	NO_2^-	2.1–5.1	NC10	(Shen et al., 2017)
	NO_3^-	0.4–1.2	ANME-2d	
Tibetan alpine wetland	NO_2^-	0.4–5.1	NC10	(Xie et al., 2020)
	NO_3^-	0.7–9.5	ANME-2d	
Rice paddies in China	NO_2^-	0.2–2.1	NC10	(Hu et al., 2014)
Rice paddies in Italy	NO_2^-	55 (max.)	NC10	(Vaksmaa et al., 2017b)
	NO_3^-	57 (max.)	ANME-2d	
	Fe	56 (max.)	ANME-2d	

DAMO rates are in nmol g^{-1} $d^{-1.}$
*DAMO rates in nmol ml^{-1} $d^{-1.}$
**NR represents not reported.

Overall, using molecular tools, researchers found that DAMO and the functional microorganisms are widely distributed in natural habitats, especially in freshwater systems, including paddy soils. However, M. oxyfera and nitrite-dependent DAMO are generally more reported than ANME-2d and nitrate-dependent DAMO, and factors and mechanisms controlling their distribution patterns, relative abundance, and niche separation are far from clear.

4.2 Coastal systems

Lying between the land-ocean interface, coastal systems, including river networks, estuaries, and adjacent seas are routinely submerged in water and due to the terrestrial input of nutrient and organic matter, often have high NO_3^- and NO_2^- availabilities, making them preferable habitats for DAMO processes to occur (Kraft et al., 2014; Lin and Lin, 2022). However, DAMO in these coastal systems is far under-studied than in freshwater systems, as suggested by the keywords frequencies from the scientometric analysis. Currently, studies on coastal systems are focused on tidal flats and mangroves. For example, Zhang et al. (2018) measured nitrite-dependent DAMO ranging from 26 – 704 nmol CH_4 g^{-1} d^{-1} in the mangrove sediments of Zhangjiang Estuaries, even higher than some rice paddies (Table 3). The DAMO bacteria abundances and activities were higher in the surface layer not deeper, contrary to the reported freshwater wetland and lake systems (Kojima et al., 2012; Hu et al., 2014; Xie et al., 2020). The opposite observation was explained by the micro-oxygen environments in the surface layer of the mangrove system, as trace-level oxygen can be beneficial to M. oxyfera (Luesken et al., 2012). The detail of this mechanism and how it is different from the freshwater systems need further investigation. Wang et al.

(2017a) compared the spatial and temporal distribution of nitrite-dependent DAMO process in low, median, high tidal flats, and compared DAMO to CH_4 removal, and pointed out that bacterial DAMO can be important sinks for CH_4 and reactive N in tidal flat systems. Compared with M. oxyfera, studies that also considered ANME-2d are fewer for coastal systems (Table 4). The limited studies considered both DAMO processes show that their relative abundances and activities can vary from different habitats even within the same system. For example, Chen et al. (2021) sampled multiple locations along the salinity gradient of the Yangtze Estuary and studied the distributions of both nitrate- and nitrite-dependent DAMO. Their results show that intertidal wetlands can be hotspots for DAMO, where both M. oxyfera-like bacteria and ANME-2d archaea exist, but bacteria dominated the microorganism community. As a result, nitrite-dependent DAMO contributed more to CH_4 removal, and total DAMO rates decreased along the gradient, significantly correlated with pH, total organic C, Fe (II), and Fe(III). On the other hand, in a parallel study (Zheng et al., 2020) on the intertidal marshes on an island of the Yangtze Estuary, results show that NC10 bacteria and ANME-2d archaea had similar abundances with comparable potential rates, suggesting that both processes can be important in intertidal marshes of the Yangtze Estuary. Affected by oxygen levels, NC10 bacteria and nitrite-dependent DAMO were higher in the water-sediment interface, whereas ANME-2d and nitrate-dependent DAMO occupied deeper layers. An interesting observation was that in the layers where ANME-2d abundance was high, NO_3^- concentrations were actually low, which leaves open the possibility of ANME-2d exploiting alternative e^- acceptors such as Fe(III) and SO_4^{2-}, requiring further investigation (Zheng et al., 2020).

Compared to the organic-rich tidal flats and mangroves, the sediments of coastal rivers, estuaries, and adjacent seas may contain lower levels of nutrients and organic matter, and the DAMO microorganism abundance and rates may be lower. For example, Shen et al. (2016) studied nitrite-dependent DAMO and M. oxyfera bacteria in Hangzhou Bay and found DAMO rates ranged from 0.2 – 1.3 nmol CH_4 g^{-1} dry soil d^{-1}, accounting for 2 – 9.4% of CH_4 oxidation. This rate is ~1 – 2 orders of magnitudes lower than in the coastal wetlands (Table 4), but considering the vast area of an estuary, the role of estuary sediments as potential CH_4 sink should not be overlooked.

In summary, DAMO in coastal systems is generally understudied compared to freshwater systems. However, existing research shows that in some coastal wetlands, DAMO rates can be even higher than in some highly eutrophic freshwater systems, such as rice paddies. The highly dynamic environments and the existence of salinity gradients in coastal systems can result in different distribution patterns compared to freshwater systems. The mechanisms controlling niche differentiation and interactions between NC10 bacteria and AMNE-2d archaea still require further study.

5 Limitation and outlook

Studies on the DAMO process and microorganisms have been expanding over the past years. However, research focusing on DAMO in coastal environments is still very limited. In this review, we attempted to identify several areas in studies on coastal DAMO that require more research efforts. First, existing research mainly focuses on M. oxyfera and nitrite-dependent DAMO process, whereas the relative abundance and activities of ANME-2d archaea and nitrate-dependent DAMO in coastal

TABLE 4 Nitrite- and nitrate-dependent DAMO rates and microorganisms in coastal habitats.

Habitat	e^- acceptor	DAMO rate	Microorganism	Reference
Zhangjiang Estuary	NO_2^-	26–704	NC10	(Zhang et al., 2018)
Yangtze Estuary sediment	NO_2^-	NR*	NC10	(Li et al., 2020)
Yangtze Estuary sediment	NO_3^-/NO_2^-	0.07–0.28	NR	(Li et al., 2019)
Chongming Island intertidal flat	NO_2^-	1.3–39.9	NC10	(Chen, 2020)
	NO_3^-	0.6–46.7	ANME-2d	
Tidal flow constructed wetland	NO_2^-	8.5–23.5	NC10	(Zhang et al., 2020)
Chongming Island intertidal flat	NO_2^-	0.1–3.8	NC10	(Zheng et al., 2020)
	NO_3^-	0.1–4.1	ANME-2d	
Yangtze estuary intertidal wetland	NO_2^-	0.2–84.3	NC10	(Chen et al., 2021)
	NO_3^-	0.4–32.6	ANME-2d	
Hangzhou Bay sediment	NO_2^-	0.2–1.3	NC10	(Shen et al., 2016)
East China Sea intertidal zone	NO_2^-	0.52–5.7	NC10	(Wang et al., 2017a)
Jiaojiang Estuary	NO_2^-	NR	NC10	(Shen et al., 2014b)
Mai Po wetland	NO_2^-	NR	NC10	(Chen et al., 2015)

DAMO rates are in nmol g^{-1} d^{-1}.
*NR represents not reported.

systems are largely overlooked. More field- and laboratory-based studies are needed to understand the environmental factors and mechanisms controlling the distributions and interactions between DAMO bacteria and archaea (Wallenius et al., 2021). Second, ANME-2d archaea have the potential to use multiple e^- acceptors, such as Fe, Mn, and sulfate. In certain coastal habitats, their contents can be higher than NO_3^-. AMO driven by different e^- acceptors and their relative contributions to CH_4 removal remains unclear for coastal systems. We can improve our understanding of ANME-2d in coastal environments by comparing their AMO activities driven by different e^- acceptors.

Lastly, the coastal environments are not isolated sections, but rather hydraulically connected continua along which physical and biological factors evolve. Current research focuses more on DAMO distribution in a specific coastal habitat, such as a wetland, or an estuary, whereas comparisons among different types of habitats along the river-estuary-sea continuum are quite limited. Direct comparisons of DAMO community and activities among different habitats along the river-estuary-sea continuum are rarely reported. However, such comparisons are necessary to understand how DAMO microorganisms and processes vary along the continuum as a whole to make comprehensive management decisions. In fact, some studies have shown that factors including oxygen levels, nutrient conditions, organic matter contents, pH, Fe, and sulfate, as well as N cycling processes, can change dramatically along the river-estuary-sea continuum (Lin et al., 2016; Lin et al., 2017b; Lin et al. 2017a; Wei et al., 2020; Wei and Lin, 2021), most of which are also sensitive factors for DAMO as we reviewed.

In light of this, we call for more research comparing DAMO microorganisms, activities, and interactions with other N cycling processes, among different types of habitats along the river-estuary-sea continuum to better understand the environmental factors shaping their distributions in coastal systems, and their contributions to CH_4 and reactive N removal (Figure 5). Specifically, we propose for direct comparisons of DAMO community composition and activity using consistent methods among hydraulically connected representative habitats (e.g., tidal freshwater rivers, estuaries, and adjacent seas). We also propose to compare the DAMO processes with other N cycling pathways, such as denitrification, anaerobic ammonium oxidation, and dissimilatory nitrate reduction to ammonium, and with AMO processes coupled to other e^- acceptors, such as the metal- and humic acid-dependent AMO.

6 Conclusion

In this study, we reviewed the existing research on environmental distributions of DAMO microorganisms and activities. Through the co-citation analysis, we identified the active areas, key references, and emerging topics in the study of DAMO. Under the guidance of the co-citation analysis, we further reviewed the literature on DAMO in freshwater and coastal environments in more depth. Current studies show that DAMO bacteria and archaea can be widely distributed in freshwater and coastal systems, including rivers, lakes, reservoirs, wetlands, tidal flats, mangroves, and estuarine and sea sediments. However, compared to freshwater systems, fewer studies focus on coastal systems. NC10 bacteria and nitrite-dependent DAMO are more studied than ANME-2d and nitrate-dependent DAMO. In general, environmental factors and mechanisms that control the distributions of nitrite- and nitrate-DAMO in freshwater and coastal systems are far from clear. We identified several areas that require further research and called for more research focusing on direct comparisons of DAMO community and activity in the context of the river-estuary-sea continuum. These kinds of information can improve

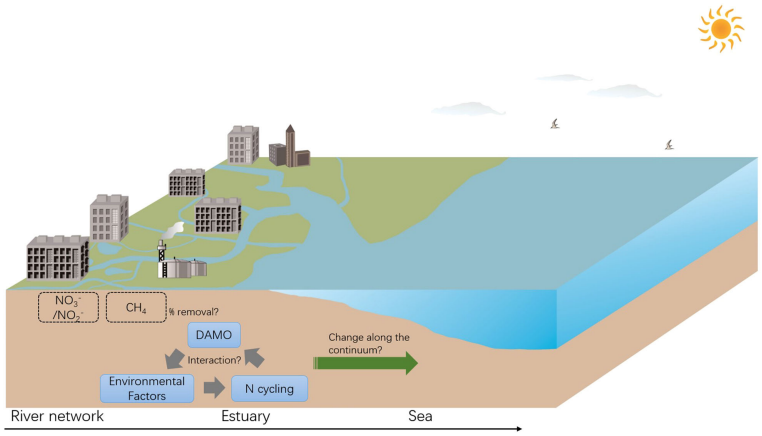

FIGURE 5
Proposed studies focusing on the interactions between DAMO, other N cycling processes, and environmental factors, and their changes along the river-estuary-sea continuum, with implications for CH_4 and reactive N removal.

our understanding of DAMO distributions in the coastal zones and help us make more comprehensive management decisions.

Author contributions

HW conducted the scientometric analysis, reviewed the literature, and wrote the manuscript. MW and MY conducted the scientometric analysis. CX conducted the scientometric analysis and reviewed the literature. All authors contributed to the article and approved the submitted version.

Funding

This work is supported by the following funding sources, the National Science Foundation of China (41601008), the General Program of Natural Science Foundation of Fujian Province of China (2018J01737), the project of Fujian Forestry Bureau (2021FKJ29), Natural Science Foundation of Jiangsu Province (BK20190483), and the Natural Science Foundation of the Jiangsu Higher Education Institutions of China (22KJB170013).

Acknowledgments

We would like thank Zhichao Wang and Yalan Zhao for their help with CiteSpace and suggestions throughout this work.

Conflict of interest

The authors declare that the research was conducted in the absence of any commercial or financial relationships that could be construed as a potential conflict of interest.

Publisher's note

References

Bai, Y., Wang, X., Wu, J., Lu, Y., Fu, L., Zhang, F., et al. (2019). Humic substances as electron acceptors for anaerobic oxidation of methane driven by ANME-2d. *Water Res.* 164, 114935. doi: 10.1016/j.watres.2019.114935

Barnes, R. O., and Goldberg, E. D. (1976). Methane production and consumption in anoxic marine sediments. *Geology* 4, 297. doi: 10.1130/0091-7613(1976)4<297:MPACIA>2.0.CO;2

Cai, C., Leu, A. O., Xie, G.-J., Guo, J., Feng, Y., Zhao, J.-X., et al. (2018). A methanotrophic archaeon couples anaerobic oxidation of methane to Fe(III) reduction. *ISME J.* 12, 1929–1939. doi: 10.1038/s41396-018-0109-x

Cai, C., Zhang, X., Wu, M., Liu, T., Lai, C. Y., Frank, J., et al. (2021). Roles and opportunities for microbial anaerobic oxidation of methane in natural and engineered systems. *Energy Environ. Sci.* 14, 4803–4830. doi: 10.1039/d1ee00708d

Chen, C. (2004). Searching for intellectual turning points: Progressive knowledge domain visualization. *Proc. Natl. Acad. Sci.* 101, 5303–5310. doi: 10.1073/pnas.0307513100

Chen, C. (2006). CiteSpace II: Detecting and visualizing emerging trends and transient patterns in scientific literature. *J. Am. Soc. Inf. Sci. Technol.* 57, 359–377. doi: 10.1002/asi.20317

Chen, J., Dick, R., Lin, J. G., and Gu, J. D. (2016). Current advances in molecular methods for detection of nitrite-dependent anaerobic methane oxidizing bacteria in natural environments. *Appl. Microbiol. Biotechnol.* 100, 9845–9860. doi: 10.1007/s00253-016-7853-5

Chen, C., Dubin, R., and Kim, M. C. (2014). Emerging trends and new developments in regenerative medicine: A scientometric updat-2014). *Expert Opin. Biol. Ther.* 14, 1295–1317. doi: 10.1517/14712598.2014.920813

Chen, C., Ibekwe-SanJuan, F., and Hou, J. (2010). The structure and dynamics of cocitation clusters: A multiple-perspective cocitation analysis. *J. Am. Soc. Inf. Sci. Technol.* 61, 1386–1409. doi: 10.1002/asi.21309

Chen, C. (2020). A glimpse of the first eight months of the COVID-19 literature on Microsoft academic graph: Themes, citation contexts, and uncertainties. *Front. Res. Metr. Anal.* 5. doi: 10.3389/frma.2020.607286

Chen, C., Hu, Z., Liu, S., and Tseng, H. (2012). Emerging trends in regenerative medicine: a scientometric analysis in *CiteSpace*. *Expert Opin. Biol. Ther.* 12, 593–608. doi: 10.1517/14712598.2012.674507

Chen, C., and Song, M. (2019). Visualizing a field of research: A methodology of systematic scientometric reviews. *PloS One* 14, e0223994. doi: 10.1371/journal.pone.0223994

Chen, F., Zheng, Y., Hou, L., et al. (2020). Denitrifying anaerobic methane oxidation in marsh sediments of chongming eastern intertidal flat. *Mar. pollut. Bull.* 150, 110681. doi: 10.1016/j.marpolbul.2019.110681

Chen, F., Zheng, Y., Hou, L., Niu, Y., Gao, D., An, Z., et al. (2021). Microbial abundance and activity of nitrite/nitrate-dependent anaerobic methane oxidizers in estuarine and intertidal wetlands: Heterogeneity and driving factors. *Water Res.* 190, 116737. doi: 10.1016/j.watres.2020.116737

Chen, J., Zhou, Z., and Gu, J. D. (2015). Complex community of nitrite-dependent anaerobic methane oxidation bacteria in coastal sediments of the mai po wetland by PCR amplification of both 16S rRNA and pmoA genes. *Appl. Microbiol. Biotechnol.* 99, 1463–1473. doi: 10.1007/s00253-014-6051-6

Chidthaisong, A., and Conrad, R. (2000). Turnover of glucose and acetate coupled to reduction of nitrate, ferric iron and sulfate and to methanogenesis in anoxic rice field soil. *FEMS Microbiol. Ecol.* 31, 73–86. doi: 10.1111/j.1574-6941.2000.tb00673.x

Cobo, M. J., López-Herrera, A. G., Herrera-Viedma, E., and Herrera, F. (2011). Science mapping software tools: Review, analysis, and cooperative study among tools. *J. Am. Soc. Inf. Sci. Technol.* 62, 1382–1402. doi: 10.1002/asi.21525

Dean, J. F., Middelburg, J. J., Röckmann, T., Aerts, R., Blauw, L. G., Egger, M., et al. (2018). Methane Feedbacks to the Global Climate System in a Warmer World. *Rev. Geophysics* 56, 207–250. doi: 10.1002/2017RG000559

Deutzmann, J. S., and Schink, B. (2011). Anaerobic oxidation of methane in sediments of lake constance, an oligotrophic freshwater lake. *Appl. Environ. Microbiol.* 77, 4429–4436. doi: 10.1128/AEM.00340-11

Ding, J., Ding, Z. W., Fu, L., Lu, Y. Z., Cheng, S. H., Zeng, R. J., et al. (2015). New primers for detecting and quantifying denitrifying anaerobic methane oxidation archaea in different ecological niches. *Appl. Microbiol. Biotechnol.* 99, 9805–9812. doi: 10.1007/s00253-015-6893-6

Ding, J., Fu, L., Ding, Z., Lu, Y.-Z., Cheng, S. H., Zeng, R. J., et al. (2016). Environmental evaluation of coexistence of denitrifying anaerobic methane-oxidizing archaea and bacteria in a paddy field. *Appl. Microbiol. Biotechnol.* 100, 439–446. doi: 10.1007/s00253-015-6986-2

Dunning, T. (1993). Accurate methods for the Statistics of Surprise and Coincidence. *Comput. Linguistics* 19.

Ettwig, K. F., Butler, M. K., le Paslier, D., Pelletier, E., Mangenot, S., Kuypers, M. M.M., et al. (2010). Nitrite-driven anaerobic methane oxidation by oxygenic bacteria. *Nature* 464, 543–548. doi: 10.1038/nature08883

Ettwig, K. F., Shima, S., van de Pas-Schoonen, K. T., Kahnt, J., Medema, M. H., Op Den Camp, H. J.M., et al. (2008). Denitrifying bacteria anaerobically oxidize methane in the absence of archaea. *Environ. Microbiol.* 10, 3164–3173. doi: 10.1111/j.1462-2920.2008.01724.x

Ettwig, K. F., van Alen, T., van de Pas-Schoonen, K. T., Jetten, M. S.M., and Strous, M. (2009). Enrichment and molecular detection of denitrifying methanotrophic bacteria of the NC10 phylum. *Appl. Environ. Microbiol.* 75, 3656–3662. doi: 10.1128/AEM.00067-09

Ettwig, K. F., Speth, D. R., Reimann, J., Wu, M. L., Jetten, M. S. M., and Keltjens, J. T. (2012). Bacterial oxygen production in the dark. *Front. Microbiol.* 3. doi: 10.3389/fmicb.2012.00273

Ettwig, K. F., Zhu, B., Speth, D., Keltjens, J. T., Jetten, M. S.M., Kartal, B., et al. (2016). Archaea catalyze iron-dependent anaerobic oxidation of methane. *Proc. Natl. Acad. Sci.* 113, 12792–12796. doi: 10.1073/pnas.1609534113

Flynn, T. M., Sanford, R. A., Ryu, H., Bethke, C. M., Levine, A. D., Ashbolt, N. J., et al. (2013). Functional microbial diversity explains groundwater chemistry in a pristine aquifer. *BMC Microbiol.* 13, 146. doi: 10.1186/1471-2180-13-146

Han, P., and Gu, J. (2013). A newly designed degenerate PCR primer based on pmoA gene for detection of nitrite-dependent anaerobic methane-oxidizing bacteria from different ecological niches. *Appl. Microbiol. Biotechnol.* 97, 10155–10162. doi: 10.1007/s00253-013-5260-8

Haroon, M. F., Hu, S., Shi, Y., Imelfort, M., Keller, J., Hugenholtz, P., et al. (2013). Anaerobic oxidation of methane coupled to nitrate reduction in a novel archaeal lineage. *Nature* 500, 567–570. doi: 10.1038/nature12375

He, Z., Cai, C., Geng, S., Lou, L., Xu, X., Zheng, P., et al. (2013). Modelling a nitrite-dependent anaerobic methane oxidation process: Parameters identification and model evaluation. *Bioresour Technol.* 147, 315–320. doi: 10.1016/j.biortech.2013.08.001

He, Z., Zhang, Q., Feng, Y., Luo, H., Pan, X., Gadd, G. M., et al. (2018). Microbiological and environmental significance of metal-dependent anaerobic oxidation of methane. *Sci. Total Environ.* 610–611, 759–768. doi: 10.1016/j.scitotenv.2017.08.140

Hu, W., Li, C., Ye, C., Wang, J., Wei, W., Deng, Y., et al. (2019). Research progress on ecological models in the field of water eutrophication: CiteSpace analysis based on data from the ISI web of science database. *Ecol. Modell* 410, 108779. doi: 10.1016/j.ecolmodel.2019.108779

Hu, B., Shen, L., Lian, X., Zhu, Q., Liu, S., Huang, Q., et al. (2014). Evidence for nitrite-dependent anaerobic methane oxidation as a previously overlooked microbial methane sink in wetlands. *Proc. Natl. Acad. Sci.* 111, 4495–4500. doi: 10.1073/pnas.1318393111

IPCC (2021). "Summary for Policymakers," *IPCC: Climate change 2021: The physical science basis. Contribution of Working Group I to the Sixth Assessment Report of the Intergovernmental Panel on Climate Change*, eds. V. Masson-Delmotte, P. Zhai, A. Pirani, S. , L. Connors, C. Péan, et al eds. (Cambridge, United Kingdom and New York, NY, USA: Cambridge University Press) 3–32. doi: 10.1017/9781009157896.001

Jørgensen, B. B., Findlay, A. J., and Pellerin, A. (2019). The biogeochemical sulfur cycle of marine sediments. *Front. Microbiol.* 10. doi: 10.3389/fmicb.2019.00849

Kampman, C., Piai, L., Temmink, H., Hendrickx, T. L. G., Zeeman, G., and Buisman, C. J. N. (2018). Effect of low concentrations of dissolved oxygen on the activity of denitrifying methanotrophic bacteria. *Water Sci. Technol.* 77, 2589–2597. doi: 10.2166/wst.2018.219

Knittel, K., and Boetius, A. (2009). Anaerobic oxidation of methane: Progress with an unknown process. *Annu. Rev. Microbiol.* 63, 311–334. doi: 10.1146/annurev.micro.61.080706.093130

Kojima, H., Tsutsumi, M., Ishikawa, K., Iwata, T., Mußmann, M., Fukui, M., et al. (2012). Distribution of putative denitrifying methane oxidizing bacteria in sediment of a freshwater lake, lake biwa. *Syst. Appl. Microbiol.* 35, 233–238. doi: 10.1016/j.syapm.2012.03.005

Kraft, B., Tegetmeyer, H. E., Sharma, R., Klotz, M. G., Ferdelman, T. G., Hettich, R. L., et al. (2014). The environmental controls that govern the end product of bacterial nitrate respiration. *Science* 345, 676–679. doi: 10.1126/science.1254070

Leu, A. O., Cai, C., McIlroy, S. J., Southam, G., Orphan, V. J., Yuan, Z, et al. (2020). Anaerobic methane oxidation coupled to manganese reduction by members of the methanoperedenaceae. *ISME J.* 14, 1030–1041. doi: 10.1038/s41396-020-0590-x

Liesack, W., Schnell, S., and Revsbech, N. P. (2000). Microbiology of flooded rice paddies. *FEMS Microbiol. Rev.* 24, 625–645. doi: 10.1111/j.1574-6976.2000.tb00563.x

Li, X., Gao, D., and Liu, M. (2019). Composition, diversity and abundance of candidatus m. oxyfera-like bacteria in response to the estuary salinity gradient. *Biogeochemistry* 143, 1–14. doi: 10.1007/s10533-019-00545-w

Li, X., Lai, D., and Gao, D. (2020). Anaerobic oxidation of methane with denitrification in sediments of a subtropical estuary: Rates, controlling factors and environmental implications. *J. Environ. Manage* 273, 111151. doi: 10.1016/j.jenvman.2020.111151

Lin, X., Li, X., Gao, D., Liu, M., and Cheng, L. (2017a). Ammonium production and removal in the sediments of shanghai river networks: Spatiotemporal variations, controlling factors, and environmental implications. *J. Geophys. Res. Biogeosci.* 122, 2461–2478. doi: 10.1002/2017JG003769

Lin, G., and Lin, X. (2022). Bait input altered microbial community structure and increased greenhouse gases production in coastal wetland sediment. *Water Res.* 218, 118520. doi: 10.1016/j.watres.2022.118520

Lin, X., Liu, M., Hou, L., Gao, D., Li, X., Lu, K., et al. (2017b). Nitrogen losses in sediments of the East China Sea: Spatiotemporal variations, controlling factors, and environmental implications. *J. Geophys. Res. Biogeosci.* 122, 2699–2715. doi: 10.1002/2017JG004036

Lin, X., Liu, M., Li, X., Zheng, Y., Yin, G., Hou, L., et al. (2016). Nitrogen mineralization and immobilization in sediments of the East China Sea: Spatiotemporal variations and environmental implications. *J. Geophys. Res. Biogeosci.* 121, 2842–2855. doi: 10.1002/2016JG003499

Liu, Y., Zhang, J., Zhao, L., Li, Y., Yang, Y., Xie, S., et al. (2015). Aerobic and nitrite-dependent methane-oxidizing microorganisms in sediments of freshwater lakes on the yunnan plateau. *Appl. Microbiol. Biotechnol.* 99, 2371–2381. doi: 10.1007/s00253-014-6141-5

Long, Y., Guo, Q., Li, N., Li, B., Tong, T., Xie, S., et al. (2017a). Spatial change of reservoir nitrite-dependent methane-oxidizing microorganisms. *Ann. Microbiol.* 67, 165–174. doi: 10.1007/s13213-016-1247-x

Long, Y., Jiang, X., Guo, Q., Li, B., and Xie, S. (2017b). Sediment nitrite-dependent methane-oxidizing microorganisms temporally and spatially shift in the dongjiang river. *Appl. Microbiol. Biotechnol.* 101, 401–410. doi: 10.1007/s00253-016-7888-7

Lu, P., Liu, T., Ni, B.-J., Guo, J., Yuan, Z., and Hu, S. (2019). Growth kinetics of Candidatus 'Methanoperedens nitroreducens' enriched in a laboratory reactor. *Sci. Total Environ.* 659, 442–450. doi: 10.1016/j.scitotenv.2018.12.351

Luesken, F. A., van Alen, T. A., van der Biezen, E., Frijters, C., Toonen, G., Kampman, C., et al. (2011). Diversity and enrichment of nitrite-dependent anaerobic methane oxidizing bacteria from wastewater sludge. *Appl. Microbiol. Biotechnol.* 92, 845–854. doi: 10.1007/s00253-011-3361-9

Luesken, F. A., Wu, M. L., Op den Camp, H. J. M., Keltjens, J. T., Stunnenberg, H., Francoijs, K.-J., et al. (2012). Effect of oxygen on the anaerobic methanotroph 'Candidatus methylomirabilis oxyfera': kinetic and transcriptional analysis. *Environ. Microbiol.* 14, 1024–1034. doi: 10.1111/j.1462-2920.2011.02682.x

Ng, A. Y., Jordan, M. I., and Weiss, Y. (2002). On spectral clustering: Analysis and an algorithm. in. *Adv. Neural Inf. Process. Systems.*

Raghoebarsing, A. A., Pol, A., van de Pas-Schoonen, K. T., Smolders, A. J.P., Ettwig, K. F., Rijpstra, W. I. C., et al. (2006). A microbial consortium couples anaerobic methane oxidation to denitrification. *Nature* 440, 918–921. doi: 10.1038/nature04617

Rasigraf, O., Kool, D. M., Jetten, M. S. M., Sinninghe Damsté, J. S., and Ettwig, K. F. (2014). Autotrophic carbon dioxide fixation *via* the Calvin-Benson-Bassham cycle by the denitrifying methanotroph "Candidatus methylomirabilis oxyfera." *Appl. Environ. Microbiol.* 80, 2451–2460. doi: 10.1128/AEM.04199-13

Reimann, J., Jetten, M. S. M., and Keltjens, J. T. (2015). "Metal Enzymes in 'Impossible' Microorganisms Catalyzing the Anaerobic Oxidation of Ammonium and Methane," 257–313. doi: 10.1007/978-3-319-12415-5_7

Sharp, C. E., Stott, M. B., and Dunfield, P. F. (2012). Detection of autotrophic verrucomicrobial methanotrophs in a geothermal environment using stable isotope probing. *Front. Microbiol.* 3. doi: 10.3389/fmicb.2012.00303

Shen, L., He, Z., Wu, H., and Gao, Z. (2015a). Nitrite-dependent anaerobic methane-oxidising bacteria: unique microorganisms with special properties. *Curr. Microbiol.* 70, 562–570. doi: 10.1007/s00284-014-0762-x

Shen, L., Huang, Q., He, Z., Lian, X., Liu, S., He, Y., et al. (2015b). Vertical distribution of nitrite-dependent anaerobic methane-oxidising bacteria in natural freshwater wetland soils. *Appl. Microbiol. Biotechnol.* 99, 349–357. doi: 10.1007/s00253-014-6031-x

Shen, L., Hu, B., Liu, S., Chai, X., He, Z., Ren, H., et al. (2016). Anaerobic methane oxidation coupled to nitrite reduction can be a potential methane sink in coastal environments. *Appl. Microbiol. Biotechnol.* 100, 7171–7180. doi: 10.1007/s00253-016-7627-0

Shen, L., Liu, S., Zhu, Q., Li, X., Cai, C., Cheng, D., et al. (2014a). Distribution and diversity of nitrite-dependent anaerobic methane-oxidising bacteria in the sediments of the qiantang river. *Microb. Ecol.* 67, 341–349. doi: 10.1007/s00248-013-0330-0

Shen, L., Ouyang, L., Zhu, Y., and Trimmer, M. (2019a). Active pathways of anaerobic methane oxidation across contrasting riverbeds. *ISME J.* 13, 752–766. doi: 10.1038/s41396-018-0302-y

Shen, L., Ouyang, L., Zhu, Y., and Trimmer, M. (2019b). Spatial separation of anaerobic ammonium oxidation and nitrite-dependent anaerobic methane oxidation in permeable riverbeds. *Environ. Microbiol.* 21, 1185–1195. doi: 10.1111/1462-2920.14554

Shen, L., Tian, M., Cheng, H., Liu, X., Yang, Y., Liu, J., et al. (2020). Different responses of nitrite- and nitrate-dependent anaerobic methanotrophs to increasing nitrogen loading in a freshwater reservoir. *Environ. pollut.* 263, 114623. doi: 10.1016/j.envpol.2020.114623

Shen, L., Wu, H., Liu, X., and Li, J. (2017). Cooccurrence and potential role of nitrite- and nitrate-dependent methanotrophs in freshwater marsh sediments. *Water Res.* 123, 162–172. doi: 10.1016/j.watres.2017.06.075

Shen, L., Zhu, Q., Liu, S., Du, P., Zeng, J., Cheng, D., et al. (2014b). Molecular evidence for nitrite-dependent anaerobic methane-oxidising bacteria in the jiaojiang estuary of the East Sea (China). *Appl. Microbiol. Biotechnol.* 98, 5029–5038. doi: 10.1007/s00253-014-5556-3

Shi, L., Dong, H., Reguera, G., Beyenal, H., Lu, A., Liu, J., et al. (2016). Extracellular electron transfer mechanisms between microorganisms and minerals. *Nat. Rev. Microbiol.* 14, 651–662. doi: 10.1038/nrmicro.2016.93

Shi, L.-D., Guo, T., Lv, P.-L., Niu, Z.-F., Zhou, Y.-J., Tang, X.-J., et al. (2020). Coupled anaerobic methane oxidation and reductive arsenic mobilization in wetland soils. *Nat. Geosci* 13, 799–805. doi: 10.1038/s41561-020-00659-z

Shi, J., and Malik, J. (2000). Normalized cuts and image segmentation. *IEEE Trans. Pattern Anal. Mach. Intell.* 22, 888–905. doi: 10.1109/34.868688

Timmers, P. H. A., Welte, C. U., Koehorst, J. J., Plugge, C. M., Jetten, M. S. M., and Stams, A. J. M. (2017). Reverse Methanogenesis and Respiration in Methanotrophic Archaea. *Archaea* 2017, 1–22. doi: 10.1155/2017/1654237

Vaksmaa, A., Jetten, M. S. M., Ettwig, K. F., and Lüke, C. (2017a). McrA primers for the detection and quantification of the anaerobic archaeal methanotroph 'Candidatus methanoperedens nitroreducens. *Appl. Microbiol. Biotechnol.* 101, 1631–1641. doi: 10.1007/s00253-016-8065-8

Vaksmaa, A., Lüke, C., van Alen, T., Valè, G., Lupotto, E., Jetten, M. S.M., et al. (2016). Distribution and activity of the anaerobic methanotrophic community in a nitrogen-fertilized Italian paddy soil. *FEMS Microbiol. Ecol.* 92, 1–11. doi: 10.1093/femsec/fiw181

Vaksmaa, A., van Alen, T. A., Ettwig, K. F., Lupotto, E., Valè, G., Jetten, M. S.M., et al. (2017b). Stratification of diversity and activity of methanogenic and methanotrophic microorganisms in a nitrogen-fertilized Italian paddy soil. *Front. Microbiol.* 8. doi: 10.3389/fmicb.2017.02127

Valenzuela, E. I., Avendaño, K. A., Balagurusamy, N., Arriaga, S., Nieto-Delgado, C., Thalasso, F., et al. (2019). Electron shuttling mediated by humic substances fuels anaerobic methane oxidation and carbon burial in wetland sediments. *Sci. Total Environ.* 650, 2674–2684. doi: 10.1016/j.scitotenv.2018.09.388

van Eck, N. J., and Waltman, L. (2010). Software survey: VOSviewer, a computer program for bibliometric mapping. *Scientometrics* 84, 523–538. doi: 10.1007/s11192-009-0146-3

Wallenius, A. J., Dalcin Martins, P., Slomp, C. P., and Jetten, M. S. M. (2021). Anthropogenic and environmental constraints on the microbial methane cycle in coastal sediments. *Front. Microbiol.* 12. doi: 10.3389/fmicb.2021.631621

Wang, X., Bai, J., Xie, T., Wang, W., Zhang, G., Yin, S., et al. (2021). Effects of biological nitrification inhibitors on nitrogen use efficiency and greenhouse gas emissions in agricultural soils: A review. *Ecotoxicol Environ. Saf.* 220, 112338. doi: 10.1016/j.ecoenv.2021.112338

Wang, Y., Huang, P., Ye, F., Jiang, Y., Song, L., Op den Camp, H. J. M., et al. (2016). Nitrite-dependent anaerobic methane oxidizing bacteria along the water level fluctuation zone of the three gorges reservoir. *Appl. Microbiol. Biotechnol.* 100, 1977–1986. doi: 10.1007/s00253-015-7083-2

Wang, S., Liu, Y., Liu, G., Huang, Y., and Zhou, Y. (2017b). A new primer to amplify pmoa gene from NC10 bacteria in the sediments of dongchang lake and dongping lake. *Curr. Microbiol.* 74, 908–914. doi: 10.1007/s00284-017-1260-8

Wang, J., Shen, L., He, Z., Hu, J., Cai, Z., Zheng, P., et al. (2017a). Spatial and temporal distribution of nitrite-dependent anaerobic methane-oxidizing bacteria in an intertidal zone of the East China Sea. *Appl. Microbiol. Biotechnol.* 101, 8007–8014. doi: 10.1007/s00253-017-8521-0

Wang, J., Yao, X., Jia, Z., Zhu, L., Zheng, P., Kartal, B., et al. (2022). Nitrogen input promotes denitrifying methanotrophs' abundance and contribution to methane emission reduction in coastal wetland and paddy soil. *Environ. pollut.* 302, 119090. doi: 10.1016/j.envpol.2022.119090

Weber, T., Wiseman, N. A., and Kock, A. (2019). Global ocean methane emissions dominated by shallow coastal waters. *Nat. Commun.* 10, 4584. doi: 10.1038/s41467-019-12541-7

Wei, H., Gao, D., Liu, Y., and Lin, X. (2020). Sediment nitrate reduction processes in response to environmental gradients along an urban river-estuary-sea continuum. *Sci. Total Environ.* 718, 137185. doi: 10.1016/j.scitotenv.2020.137185

Wei, H., and Lin, X. (2021). Shifts in the relative abundance and potential rates of sediment ammonia-oxidizing archaea and bacteria along environmental gradients of an urban river–estuary–adjacent sea continuum. *Sci. Total Environ.* 771, 144824. doi: 10.1016/j.scitotenv.2020.144824

Welte, C. U., Rasigraf, O., Vaksmaa, A., Versantvoort, W., Arshad, A., Op den Camp, H. J. M., et al. (2016). Nitrate- and nitrite-dependent anaerobic oxidation of methane. *Environ. Microbiol. Rep.* 8, 941–955. doi: 10.1111/1758-2229.12487

Wu, M. L., Ettwig, K. F., Jetten, M. S. M., Strous, M., Keltjens, J. T., van Niftrik, L., et al. (2011). "A new intra-aerobic metabolism in the nitrite-dependent anaerobic methane-oxidizing bacterium *Candidatus 'Methylomirabilis oxyfera'*, in *Biochem. Soc. Trans.* 39, 243–248. doi: 10.1042/BST0390243

Wu, M. L., van Teeseling, M. C. F., Willems, M. J. R., van Donselaar, E. G., Klingl, A., Rachel, R., et al. (2012). Ultrastructure of the denitrifying methanotroph "Candidatus methylomirabilis oxyfera," a novel polygon-shaped bacterium. *J. Bacteriol.* 194, 284–291. doi: 10.1128/JB.05816-11

Xie, F., Ma, A., Zhou, H., Liang, Y., Yin, J., Ma, K., et al. (2020). Niche differentiation of denitrifying anaerobic methane oxidizing bacteria and archaea leads to effective methane filtration in a Tibetan alpine wetland. *Environ. Int.* 140, 105764. doi: 10.1016/j.envint.2020.105764

Yang, H., Chen, X., Zhang, C., Zhao, M., Zhao, X., Perry, D. C., et al. (2022). Nitrogen removal by eutrophic coastal wetlands accomplished with CH4 emission reduction. *J. Clean Prod.* 332, 130082. doi: 10.1016/j.jclepro.2021.130082

Yang, H., Shao, X., and Wu, M. (2019). A review on ecosystem health research: A visualization based on CiteSpace. *Sustainability* 11, 4908. doi: 10.3390/su11184908

Yan, P., Li, M., Wei, G., Li, H., and Gao, Z. (2015). Molecular fingerprint and dominant environmental factors of nitrite-dependent anaerobic methane-oxidizing bacteria in sediments from the yellow river estuary, China. *PloS One* 10, e0137996. doi: 10.1371/journal.pone.0137996

Zhang, M., Huang, J.-C., Sun, S., Rehman, M. M.U., and He, S. (2020). Depth-specific distribution and significance of nitrite-dependent anaerobic methane oxidation process in tidal flow constructed wetlands used for treating river water. *Sci. Total Environ.* 716, 137054. doi: 10.1016/j.scitotenv.2020.137054

Zhang, M., Luo, Y., Lin, L., Lin, X., Hetharua, B., Zhao, W., et al. (2018). Molecular and stable isotopic evidence for the occurrence of nitrite-dependent anaerobic methane-oxidizing bacteria in the mangrove sediment of zhangjiang estuary, China. *Appl. Microbiol. Biotechnol.* 102, 2441–2454. doi: 10.1007/s00253-017-8718-2

Zheng, Y., Hou, L., Chen, F., Zhou, J., Liu, M., Yin, G., et al. (2020). Denitrifying anaerobic methane oxidation in intertidal marsh soils: Occurrence and environmental significance. *Geoderma* 357, 113943. doi: 10.1016/j.geoderma.2019.113943

Zhu, G., Zhou, L., Wang, Y., Wang, S., Guo, J., Long, X.-E., et al. (2015). Biogeographical distribution of denitrifying anaerobic methane oxidizing bacteria in Chinese wetland ecosystems. *Environ. Microbiol. Rep.* 7, 128–138. doi: 10.1111/1758-2229.12214

frontiers | Frontiers in Marine Science

TYPE Original Research
PUBLISHED 01 December 2022
DOI 10.3389/fmars.2022.1078653

OPEN ACCESS

EDITED BY
Jing Wei,
Sun Yat-sen University, China

REVIEWED BY
Lan Lu,
Hunan University, China
Mingcong Li,
Shandong Agricultural University, China

*CORRESPONDENCE
Yu Zhen
zhenyu@ouc.edu.cn

SPECIALTY SECTION
This article was submitted to Marine Biogeochemistry, a section of the journal Frontiers in Marine Science

RECEIVED 24 October 2022
ACCEPTED 14 November 2022
PUBLISHED 01 December 2022

CITATION
Teng Z, Zhen Y, Yu Z, Mi T and Cai T (2022) Nitrogen-loss and associated microbial communities in sediments from the Yangtze Estuary and adjacent sea.
Front. Mar. Sci. 9:1078653.
doi: 10.3389/fmars.2022.1078653

Nitrogen-loss and associated microbial communities in sediments from the Yangtze Estuary and adjacent sea

Zhenzhen Teng[1,2,3], Yu Zhen[1,2,3]*, Zhigang Yu[2,4], Tiezhu Mi[1,2,3] and Tao Cai[5]

[1]Key Laboratory of Marine Environment and Ecology, Ministry of Education, Ocean University of China, Qingdao, China, [2]Laboratory for Marine Ecology and Environmental Science, Pilot National Laboratory for Marine Science and Technology (Qingdao), Qingdao, China, [3]College of Environmental Science and Engineering, Ocean University of China, Qingdao, China, [4]Frontiers Science Center for Deep Ocean Multispheres and Earth System, and Key Laboratory of Marine Chemistry Theory and Technology, Ministry of Education, Ocean University of China, Qingdao, China, [5]School of Resources & Environment and Safety Engineering, University of South China, Hengyang, China

Introduction: Denitrification and anammox play the crucial role for N removal processes in coastal ecosystems, but the ecological distribution of denitrifying and anammox microorganisms and their N removal rates in the Yangtze Estuary and its adjacent sea are required in-depth analysis.

Methods: Here, we utilized high-throughput sequencing, qPCR, and ^{15}N isotope to reveal the community structure and function of denitrifying and anammox microorganisms in the surface sediments from Yangtze Estuary and adjacent sea.

Results: The results suggested that the gene abundances of *nir*S and *nir*K for denitrifiers were higher than AMX 16S rRNA for anammox bacteria. The genera composition of *nir*S- and *nir*K-encoding denitrifiers communities showed different distribution patterns. Furthermore, *Candidatus* Anammoximicrobium dominated the anammox community, implying the anammox oxidation capacity of the other genera should be noted in marine sediments.

Discussion: Compared to anammox, denitrification was the dominant contributor of nitrogen removal process and contributed 73.5% on average. The sediment Chl*a* was the key factor to regulate denitrification and anammox rates, indicating the fresh organic matter was more labile and easier to be utilized by NO_x^- removal processes.

KEYWORDS

denitrification, anammox, *nir*S/*nir*K, AMX 16S rRNA, ^{15}N isotope

Introduction

Nitrogen is a necessary nutrient element for all kinds of life. However, due to the rapid expansion of various anthropogenic N input, numerous estuaries and adjacent seas have high nitrogen loading, causing serious environmental problems such as eutrophication globally (Howarth, 2008), increased harmful algal blooms (Gobler, 2020), biodiversity loss (Worm et al., 2006), and increasing nitrous oxide (N_2O) emission (Murray et al., 2015; Lin and Lin, 2022). Excess anthropogenic N inputs have severely affected N-balance in coastal ecosystems (Zhao et al., 2020b), thus, N pollution has been widely concerned in global.

Both denitrification and anammox are the critical pathways in microbially-mediated N removal processes, which can remove excess nitrogen in estuarine and coastal ecosystems. Under hypoxic or anaerobic conditions, denitrification convert nitrate (NO_3^-) to N_2O or N_2 into the atmosphere, while anammox can oxide ammonium (NH_4^+) with nitrite (NO_2^-) to N_2 (Thamdrup and Dalsgaard, 2002; Medhi et al., 2017). It has been reported that ~45% of reactive N can be removed by denitrification in estuarine sediments (Seitzinger et al., 2006), which was considered as the main N removal process in aquatic ecosystems before the discovery of anammox (Trimmer et al., 2003; Fernandes et al., 2012). In 1995, the anammox process was found in a wastewater treatment plant (Mulder et al., 1995). Additionally, it has also been detected in marine sediments, freshwater sediments, and anaerobic water column (Thamdrup and Dalsgaard, 2002; Trimmer and Nicholls, 2009; Lisa et al., 2014). Some studies showed that anammox was the main N removal process in the marine environments, contribution up to 67% of N_2 production (Dalsgaard and Thamdrup, 2002; Kuypers et al., 2003). Hou et al. (2015) reported that 20.7% of inorganic nitrogen can be removed by anammox in coastal wetland ecosystems in China, reflecting a non-negligible role of anammox to N removal in marine ecosystems. However, denitrification and anammox have varied in their contribution to N removal in marine ecosystems, low anammox rates and even lower denitrification rates were found in most sites, while high denitrification rates were detected in a few isolated places (Babbin et al., 2014). C/N ratio was the crucial environmental factor to regulate the balance between denitrification and anammox, resulting in the different ratios of denitrification to anammox (Babbin et al., 2014). In addition, the two nitrogen removal processes have different effects on N_2O emissions, as well on C mineralization (Ravishankara et al., 2009; Babbin et al., 2020). Therefore, further explorations about denitrification and anammox are critical for maintaining and conserving the health of coastal ecosystems.

Different molecular markers have been broadly utilized to understand and identify denitrifying and anammox microorganisms. Two nitrite reductases (cytochrome cd 1 and copper-containing nitrite reductases) catalyze NO_2^- to form a gaseous product NO, which are the key enzymes in the denitrification process (Beman, 2014). The genes (*nir*S or *nir*k) encoding nitrite reductase are widespread and efficient biomarker for precise and direct identification of denitrifying communities in numerous environments, such as the aquatic ecosystems and sediments (Abell et al., 2010; Mosier and Francis, 2010; Xie et al., 2020). The16S rRNA gene and the other functional genes (*hzo* and *hzs*) are both used to investigate and detect the community structure and abundances of anammox bacteria (Harhangi et al., 2012; Yang et al., 2020). Due to high specificity and good amplification efficiency, 16S rRNA gene was broadly employed to identify anammox bacteria in diverse environments and enrichment cultures (Li et al., 2010; Yang et al., 2020). In addition, the abundance, community composition and rates of denitrification and anammox can be regulated by multiple environmental parameters, for instance, salinity (Bernhard et al., 2005), pH (Nicol et al., 2008), nitrogen availability (Di et al., 2010), and sediment total organic carbon (TOC) (Zheng et al., 2019). Thus, it is essential to common research of the diversity, abundance, and activity of denitrification and anammox under different geographic environmental factors, to better understand the contribution and role of N removal *via* denitrification and anammox, and further reveal the niche of denitrifiers and anammox bacteria in coastal ecosystems.

The Yangtze Estuary and its adjacent sea, the East China Sea (ECS), was chosen as the research region to investigate the characteristics of denitrifiers and anammox bacteria. Yangtze River, the greatest river in Asian regions, can transport amounts of anthropogenic nitrogen *via* estuary region to adjacent ECS (Chen et al., 2016). Increasing nitrogen has resulted in significant eutrophication and the appearance of toxic algal blooms in coastal ecosystem (Smith and Schindler, 2009; Anderson et al., 2012). In addition, the Yangtze River also transports most terrestrial sediments through currents into the ECS (Lim et al., 2007). The benthic sediments serve as the significant sink for reactive nitrogen and play the vital role in the N biogeochemical cycle (Lin et al., 2017). Meanwhile, the complex benthic environment favors the growth and survival of microorganisms (Basha et al., 2018). Liu and Wang demonstrated that the diversity of nirK- gene-encoded encoding denitrifiers was lower than that of *nir*S-encoding denitrifiers by high-throughput sequencing within sediments from northern ECS (Liu et al., 2018; Wang et al., 2019). Lin et al. (2017) confirmed that denitrification rates were higher than anammox *via* ^{15}N isotope tracer incubation experiment in surface sediment from Yangtze Estuary and its adjacent sea. Currently, molecular detection is used to understand the microbial community, and ^{15}N isotope tracer is used to study the denitrification and anammox rates. However, few studies have focused on common research of the community structure, abundance, and activity of anammox and denitrifiers bacteria in coastal ecosystems, to better understand the role of denitrifiers and anammox bacteria in N removal processes.

Herein, we studied the characteristics of denitrifiers and anammox bacteria and environmental parameters in surface

sediments (0–5 cm) from the Yangtze Estuary and its adjacent sea. The community structures and abundances were analyzed using the high-throughput sequencing and qPCR, as well as the rates of denitrification and anammox were tested by ^{15}N isotope tracer technology. The main objective of this work is to reveal possible roles of denitrifiers and anammox bacteria in nitrogen removal processes as well as how these microorganisms respond to various environmental factors in coastal ecosystems.

Materials and methods

Sampling collection and environmental factor analysis

The bottom water and surface sediments have been gathered from 16 stations in the Yangtze Estuary and adjacent sea from 1 to 6 March 2022 (Figure 1). At each station, surface sediments (0–5 cm) was extracted from the box cores, mixed homogeneously, and placed into air-tight sterile plastics bags. The sediment samples were then subdivided into two parts for different analyses. One part immediately stored at 4°C for denitrification and anammox rates incubation. Another was stored on board (-20°C) and then transferred to laboratory storage (−80°C) for DNA extraction and molecular analysis. The bottom water was filtered through a filter (0.45 μm) and stored in polyethylene bottles (-20°C). The salinity was determined onsite by HQ40d Water Analyzer (Hach, Loveland, USA). The sediment water content was calculated using wet-dry weight method (Klute, 1986). The NH_4^+, NO_3^- and PO_4^{3-} in bottom water were analyzed using QuAAtro nutrient autoanalyzer (Seal Analytical, Germany). 2 M KCl was used to extract the exchangeable NH_4^+, NO_2^- and NO_3^- from the sediments and then determined by QuAAtro nutrient autoanalyzer (Seal Analytical, Germany). Sediment TN and TOC were detected by the elemental analyzer (Vario EL cube, Germany). A laser particle sizer analyzer (LS 13320, Beckman, USA) was used to measure sediment grain size (MΦ). The sediment Fe(II) and Fe(III) contents were measured by phenanthroline spectrophotometric method (Lovley and Phillips, 1987). Under the dark condition of 4°C for 24 hours, Sediment Chl*a* can be extracted with 80% (v/v) acetone. A UV-5200 visible spectrophotometer was used to measure the absorbance of Chl*a* after centrifuging these extracts at 2200 g for 10 min.

Measurement of denitrification and anammox rates

The potential denitrification and anammox rates were measured by ^{15}N isotope-tracing technique (Lin et al., 2017).

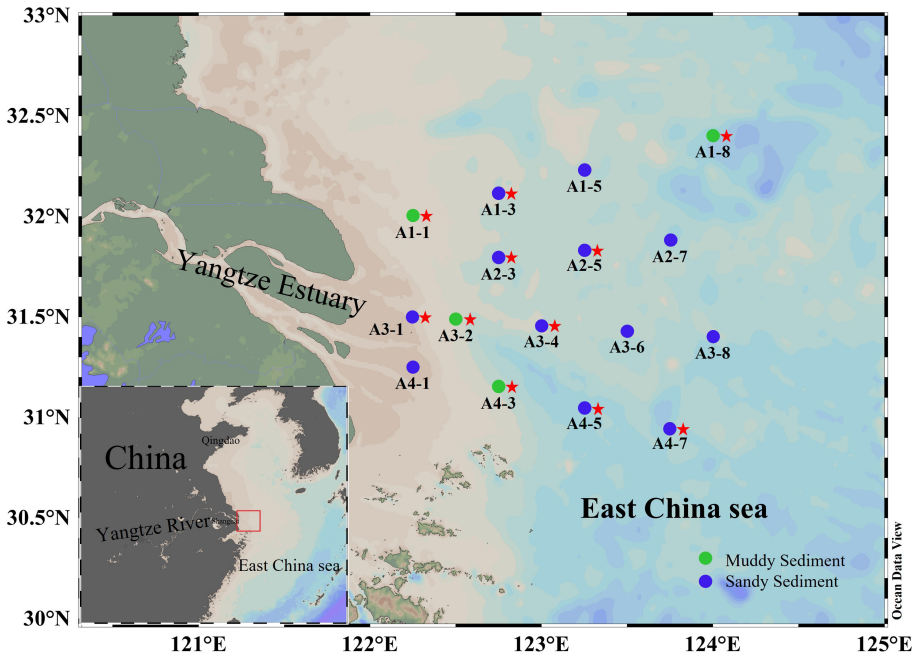

FIGURE 1
The map of sediment sampling stations. The dots represented sampling sites (green dots denoted muddy sediments and blue dots denoted sandy sediments). The red stars represent that the key functional genes were analyzed by high-throughput sequencing in these sampling sites.

Briefly, the laboratory slurry incubation experiments were made with the *in situ* benthic sterilized seawater and the sediments at a seawater/sediment mass ratio of 7:1, and the homogeneous mixture was fed with helium gas for 30 min before transferring into 12-mL vials (Labco Exetainers, UK). Subsequently, these 12-mL vials were in dark preincubated for 24 h to eliminate residual dissolved oxygen, nitrite, and nitrate. After the preincubation, three treatments were given to these vials as follows: (1) $^{15}NH_4^+$ (100 μmol N L^{-1}), (2) $^{15}NO_3^-$ (100 μmol N L^{-1}), and (3) $^{15}NH_4^+ + {}^{14}NO_3^-$ (100 μmol N L^{-1}). After 0 h and 8 h incubation, these vials were spiked with $ZnCl_2$ solution (200-μL 50%) to stop microbial activity. Produced $^{29}N_2$ and $^{30}N_2$ concentrations during incubation were determined by the membrane inlet mass spectrometry (MIMS, Hiden Analytical Ltd, UK), and denitrification and anammox rates were calculated according to previous methods (Thamdrup and Dalsgaard, 2002; Song et al., 2016).

DNA extraction and quantification for denitrifiers and anammox bacteria

Total DNA extraction was performed from 0.5 g of homogenized sediment samples by PowerSoil® DNA Isolation Kit (MoBio, USA). The obtained DNA was used as the template for real-time qPCR analysis with the primer pairs cad3Af/R3cd for the *nir*S gene, and FlaCu/R3Cu for *nir*K gene, and Amx-808-F/Amx-1040-R for Anammox 16S rRNA gene (Supplementary Table 1). Reactions were carried out using ABI PRISM®7500 Sequence Detection System (Applied Biosystems, Foster City, CA, USA). The 20-μL qPCR mixture reaction system contained FastStart Universal SYBR Green Master (ROX) (10 μL, Roche, Germany), ddH_2O (6.6 μL), each primer (0.6 μL, 10 μM), bovine serum albumin (0.2 μL, 20 mg·mL^{-1}), and template (2.0 μL). The qPCR reactions of *nir*S, *nir*K, and Anammox 16S rRNA gene were performed as the following: 50°C for 2 minutes, 95°C for 10 minutes, 45 cycles of 95°C for 30 seconds, and 58°C for 40 seconds, 72°C for 60 seconds (Throbäck et al., 2004; Hamersley et al., 2007). The significant linear relationships ($R^2 > 0.996$) were produced with a 10-fold dilution series (10^2–10^9 copies) of standard plasmids containing the key functional genes, and the qPCR efficiency was 84%, 110%, and 92%, respectively. The abundance of the key functional genes can be calculated by the standard curves. The melting curves contained a single peak, and non-specific amplification was not found by agarose gel electrophoresis, demonstrating amplification specificity.

High-throughput sequencing

11 sampling stations have been picked from 16 stations according to the class of muddy and sandy sediments (the value of median grain size (> 64 μm) was classified to sandy sediment). The PCR amplicons of key functional genes were from the same primer pairs with qPCR (cd3aF/R3cd and FlaCu/R3Cu for denitrifiers, and Amx-808-F/Amx-1040-R for anammox bacteria). The PCR conditions were as follows: initial denaturation was performed at 98°C for 2 min, followed by control at 98°C for 15 s, 55°C for 30 s and 72°C for 30 s (25-30 cycles), and finally extended at 72°C for 5 min. The Vazyme VAHTSTM DNA Clean Beads (Vazyme, Nanjing, China) and Quant-iT PicoGreen dsDNA Assay Kit (Invitrogen, Carlsbad, CA, USA) were used for the purification and quantification of PCR amplicons, respectively. The Illumina novaSeq PE250 platform (Shanghai, China) was used for the paired-ended sequenced of high-throughput sequencing of *nir*S/*nir*K and AMX 16S rRNA genes. The QIIME2 (2019.4) was used to incorporate, quality-filter, and dereplicate the sequences. High quality sequences with 97% similarity level were clustered into OTUs based on Vsearch (v2.13.4_linux_x86_64), and then representative OTUs were output. The raw sequences obtained in this study for *nir*S, *nir*K and AMX 16S rRNA was kept in NCBI under the accession numbers of PRJNA891470, PRJNA891480, and PRJNA891491.

Statistical analyses

The map of the sampling stations and the distribution of environmental parameters were drawn using Ocean Data View (ODV 5.2.1). The differences of *nir*S, *nir*K and AMX 16S rRNA gene abundances in the same station were studied using one-way analysis of variance (ANOVA). Correlation between the three microbial communities and environmental factors were identified with CCA/RDA analyses with Monte Carlo tests by Canoco 5 software. The Pearson and Spearman correlation analysis of denitrifiers and anammox bacteria with environmental parameters was created by IBM SPSS statistic 26 and R (version 4.2.1, R package corrplot) (Wei and Simko. 2021). MEGA11, TBtools and Origin 2022b software were used for graphics. Finally, the phylogenetic tree was visualized and beautified by Evolview online tool (http://www.evolgenius.info/evolview-v2/).

Results

Station characteristics

The physicochemical parameters of bottom water and surface sediments were given in Figure 2. The salinity ranged from 27.3 to 37.1 (Figure 2A). Bottom water NH_4^+ (0.1–3.15 μM), NO_3^- (3.55–23.93 μM), PO_4^{3-} (0.21–0.71 μM) values varied across different sampling sites (Figures 2B–D). The average concentrations of NH_4^+ and NO_3^- in the sediments varied from 0.32–1.20 μg N g^{-1}, 0.04–0.86 μg N g^{-1}, respectively

(Figure 2E, F). The sediment Fe(II)/Fe(III) ratios were in a range of 0.29–6.19 (Figure 2G). The contents of sediment TN and TOC ranged from 0.23 to 1.19 mg N g^{-1} with an average of 0.51 ± 0.25 mg N g^{-1} and from 1.05 to 6.97 mg C g^{-1} with an average of 2.62 ± 1.65 mg C g^{-1}, respectively (Figures 2H, I). The sediment median grain size showed a greater change. The sampling stations of A1-1, A1-8, A3-2, and A4-3 were muddy sediments (8.83–44.27 μm), while other stations were sandy sediments (93.32–333.41 μm) (Figure 2L). Meanwhile, the C/N ratios (TOC/TN) were higher in muddy sediments (A1-1, A1-8, A3-2, and A4-3) than in sandy sediments (Figure 2J). The average content of Chl*a* in sediment was in a range of 0.12–1.75 μg g^{-1}, with obvious spatial pattern (Figure 2K).

Abundances of denitrifiers and anammox bacteria and their influencing factors

The *nir*S/*nir*K gene and AMX 16S rRNA gene were utilized to quantify denitrifiers and anammox bacteria abundances in surface sediments, respectively. The abundances of *nir*S gene were ranging between 9.87×10^5 to 2.71×10^7 copies g^{-1} with the mean value of $(1.28 \pm 0.93) \times 10^7$ copies g^{-1} (Figure 3A, B). The *nir*S gene abundance had negative correlation with NO_3^- concentration in the bottom water (r = -0.576, p< 0.05) (Figure 4). The *nir*K gene abundances ranged from 4.64×10^5 to 1.26×10^7 copies g^{-1} with the mean value of $(4.52 \pm 3.34) \times 10^6$ copies g^{-1} (Figure 3A, B). Compared to *nir*S/*nir*K gene, the abundances of AMX 16S rRNA gene were obtained between 1.03×10^5 to 2.97×10^6 copies $g^{-1}$with the mean value of $(1.40 \pm 0.84) \times 10^6$ copies g^{-1} (Figure 3A, B). In all surface sediment samples, *nir*S abundances were the highest, followed by *nir*K abundances and then AMX 16S rRNA gene.

Potential rates of denitrification and anammox and their influencing factors

The potential rates of denitrification and anammox were analyzed in all sampling site of the surface sediments (n = 16), which varied considerably, ranging from 0–0.56 nmol N g^{-1} h^{-1} and 0–0.091 nmol N g^{-1} h^{-1}, respectively (Figure 3C, D). The highest denitrification rate was detected at A1-1, whereas the lowest denitrification rate was observed at A3-8. The potential denitrification rates had positive association with sediment water content, NH_4^+, TN, TOC, C/N, and Chl*a*, while negatively regulated by sediment NO_3^- and sediment grain size (Figure 4, Supplementary Table 5). Compared to denitrification rates, the highest anammox rate was detected at A2-3, whereas the lowest anammox rate was observed at A3-4. Anammox was positively correlated with NH_4^+ and Chl*a*, and negatively correlated with NO_3^- (Figure 4, Supplementary Table 5). Moreover, Pearson's correlation analyses showed that anammox was significantly related to denitrification (r = 0.710, p< 0.01) (Figure 4, Figure 5A; Supplementary Table 5). The contribution of denitrification to N removal (DEN%) was higher than anammox in most sampling sites except A3-4, A3-6, A3-8, and A4-1 (Figure 5B), with the contribution of 73.5% on average. In addition, DEN% was positively related to water content, NH_4^+, Fe(II)/Fe(III), TN, TOC, C/N, and Chl*a*, and negatively regulated by NO_2^-.

Community diversity and composition of *nir*S- and *nir*K-encoding denitrifiers

Totally, 1,219,102 filtered, high-quality *nir*S sequences were acquired from 11 surface sediments samples, ranging from 73,783–172,218 for each sample (Supplementary Table 2). The effective sequences were clustered into 7,536 OTUs based on the 97% similarity level. Additionally, Good's coverage (99.73–99.91%) indicated that most of the *nir*S-encoding denitrifiers had been obtained. The highest OTU numbers (1,186) and Chao1 richness estimators (1267.16) were observed in the samples A4-7. Higher Shannon diversity index and Simpson indices were found in samples A2-3, A4-5 and A4-7 (Supplementary Table 2). Moreover, the diversity of *nir*S gene decreased with the increasing the NH_4^+ concentration in the bottom water (Shannon: r = -0.732, p< 0.05; Simpson: r = -0.897, p< 0.01) (Supplementary Table 6). Compared to the *nir*S gene, 763,468 high-quality reads of *nir*K gene sequences were acquired and 3,151 OTUs were identified (Supplementary Table 3). The diversity and richness of *nir*K-encoding were lower than *nir*S-encoding denitrifiers in all samples. In additionally, the richness of *nir*K gene declined with the increasing NO_3^- concentrations in the bottom water (Chao1: r = -0.606, p< 0.05) and increased with the sediment total nitrogen concentration (Chao1: r = 0.603, p< 0.05) (Supplementary Table 6). The rarefaction curves showed that the majority of the *nir*S- and *nir*K-encoding denitrifiers was captured in the current study (Supplementary Figures 1A, B).

A total of 50 dominant OTUs of the *nir*S gene were phylogenetically classified into 10 different clusters (Figures 6A, B; Supplementary Figures 2, 3). Within these 10 clusters, only C9 belonged to α-proteobacteria and C5, C6, and C7 affiliated to β-Proteobacteria, whereas the other 6 clusters were belonged to γ-Proteobacteria. C3 only contained OTU01, which was existed exclusively in the A3-2 station, closely affiliating to *Pseudomonas* (Figures 6A, B, Supplementary Figure 3). C8 (belonging to *Marinobacter*), C9 (belonging to *Paracoccus*) and C10 (belonging to *Chromohalobacter*) were observed almost in muddy sediments (Figures 6A, B). According to a redundancy analysis (RDA) with the dominant OTUs, the first two axes (RDA1 and RDA2) explained 79.97% of the cumulative variance in the *nir*S-encoding denitrifiers communities (Figure 6C). The bottom water NH_4^+

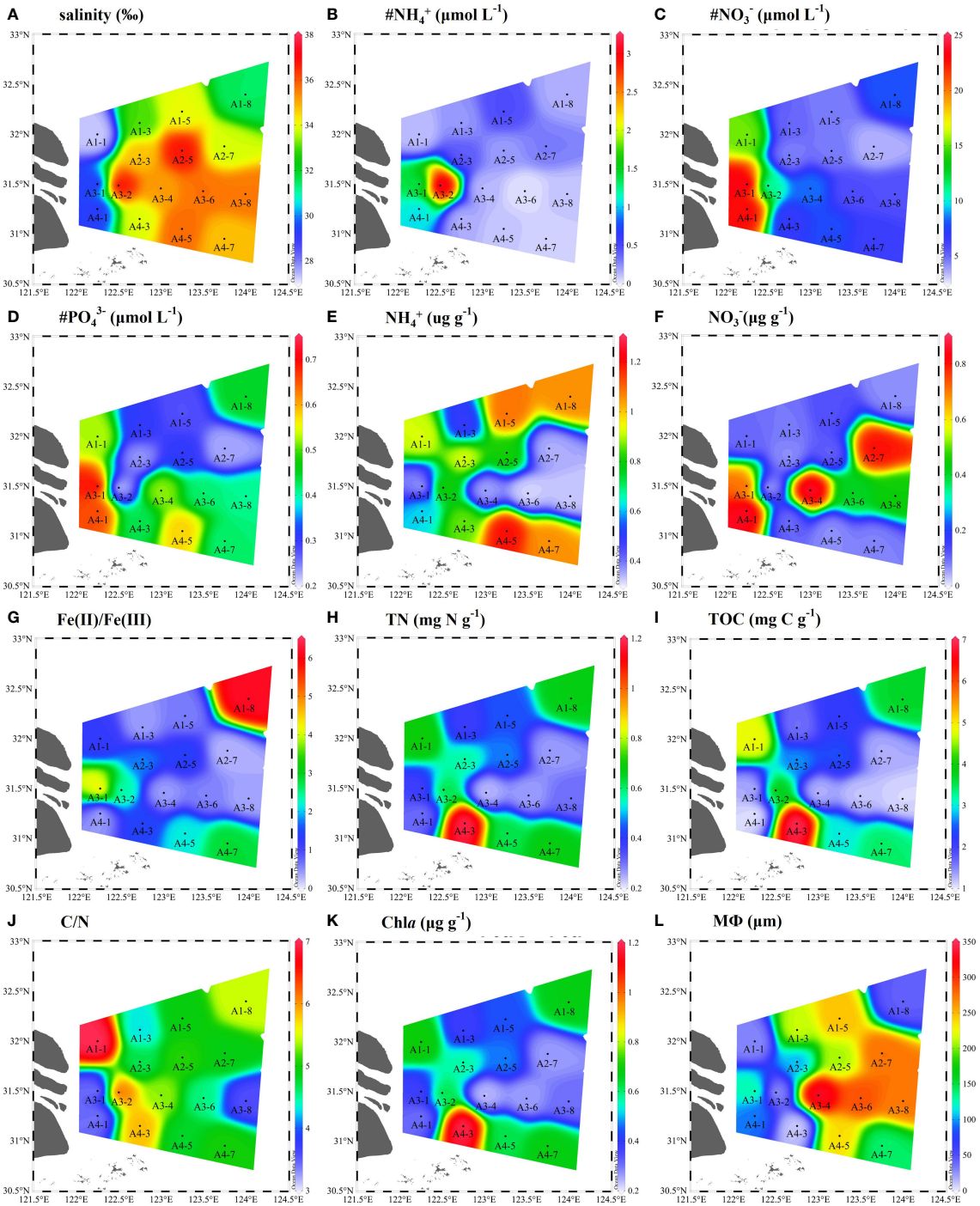

FIGURE 2
Spatial distributions of physicochemical parameters in bottom water and surface sediments of the Yangtze Estuary and East China Sea (ECS) **(A-L)**. # represents the bottom water properties (# NH_4^+, # NO_3^-, # PO_4^{3-}) and MΦ denote median grain size.

(pseudo-F = 3.1 and $p< 0.01$), NO_3^- (pseudo-F = 2.7 and $p< 0.01$), and C/N (pseudo-F = 2.6 and $p< 0.05$) were the major factors influencing the *nir*S gene community. At genus levels, *Pseudomonas* was dominant genera only in A3-2, while *Marinobacter* was dominant genera and observed in all sampling stations (Supplementary Figure 4B). Spearman's correlation analysis showed that *Pseudomonas* was positively related with in the bottom water ($p< 0.01$) (Supplementary Table 7), and

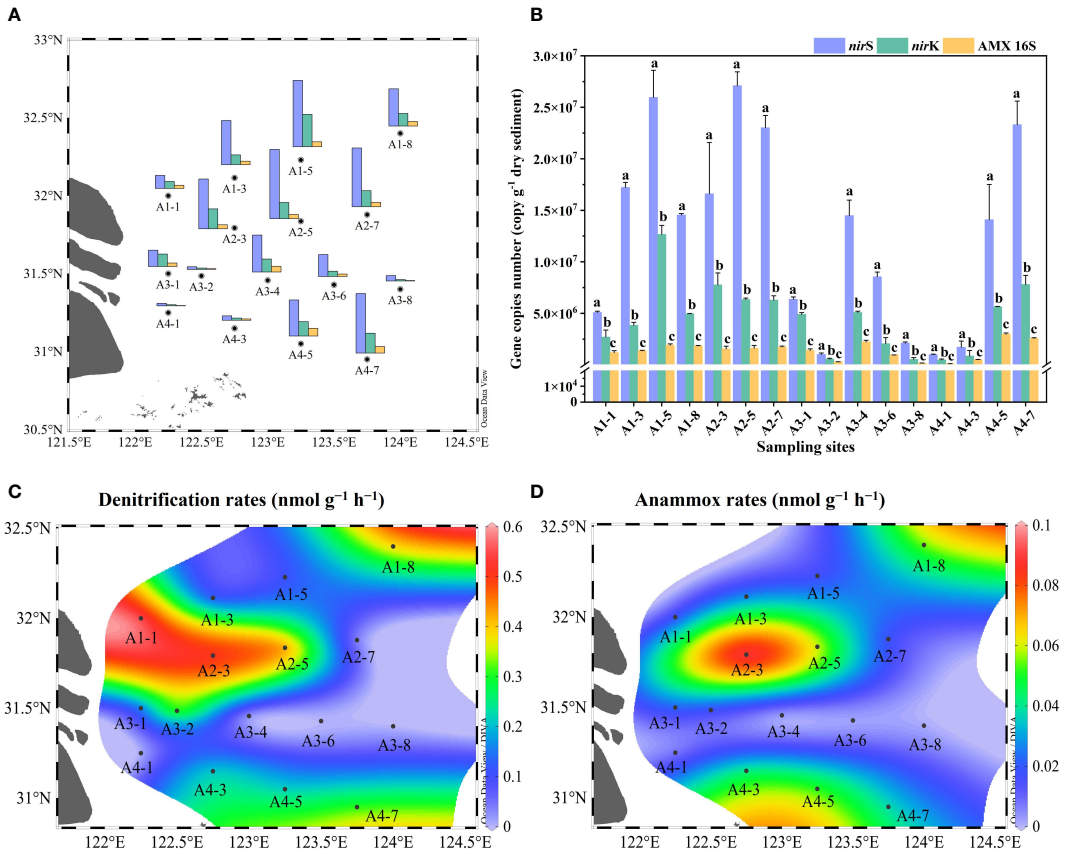

FIGURE 3
(A) Spatial distributions of gene abundances in the Yangtze Estuary and the adjacent sea; **(B)** Gene copies numbers of *nir*S, *nir*K and 16S rRNA. Error bars in the column represented the standard deviations of the triplicate qPCR reactions, and different letters indicated a significant difference between gene abundances in the same sampling sites ($p< 0.05$); **(C, D)** Denitrification and anammox rates.

Marinobacter was positively correlated with sediment NH_4^+ ($p< 0.05$).

Dominant OTUs (top 50 OTUs) of *nir*K gene were classified into 9 clusters, all belonging to the Proteobacteria (Figures 7A, B, Supplementary Figures 5, 6). Among the 9 clusters, C2, C5, and C7 belonged to the β-Proteobacteria, whereas the other 6 clusters were intimately related to the α-Proteobacteria (Figure 7B, Supplementary Figure 6). Moreover, C7 (with the lowest abundances of top 50 OTUs) only contained OTU32 which was detected in the A3-2 and A3-4 sample, showing some similarities with the sediment denitrifying microorganisms in the Yangtze lakes (Jiang et al., 2017). There were no obvious differences in the relative abundance of OTUs between muddy sediments and sandy sediments (Figure 7A). From the CCA (Figure 7C), the first two axes explained 36.10% of the cumulative variance, and NH_4^+ in the bottom water (pseudo-F = 2.0 and $p< 0.01$), PO_4^{3-} (pseudo-F = 2.1 and $p< 0.05$), sediment NO_3^- (pseudo-F = 2.2 and $p< 0.05$), and MΦ (pseudo-F = 2.0 and $p< 0.05$) had significant influences on the *nir*K-encoding denitrifiers community. At genus level, *Mesorhizobium* was the dominant genera in A2-5 and A3-1 sample with no other genera observed, however, *Bradyrhizobium* was detected in most sampling stations except A2-5 and A3-1 (Supplementary Figure 7B). Spearman's correlation analysis showed that *Mesorhizobium* was positively related with sediment **Fe(II)/Fe(III)** ($p< 0.05$) (Supplementary Table 7).

Community diversity and composition of anammox bacteria

For the anammox 16S rRNA gene (AMX 16S), a total of 479,390 high-quality reads were gained, which ranged from 40,134–47,445 for each sample (Supplementary Table 4). Based on the 0.03 genetic distance (97% as cutoff), 23,950 OTUs (2177 ± 440 OTUs per samples, n=11) were detected. The highest OTU numbers, Chao1 and Shannon index were found in station A4-7, showing the higher diversity and richness of the anammox 16S rRNA gene in surface sediment of station

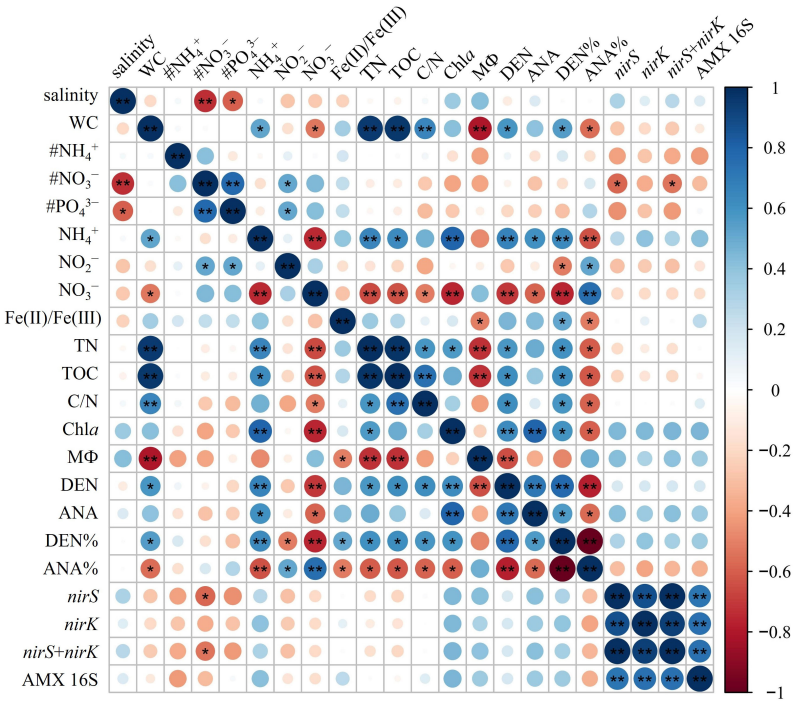

FIGURE 4
Pearson's correlations of environmental factors with the denitrification/anammox and related gene abundances. * significant at $p< 0.05$, ** significant at $p< 0.01$. # represents bottom water parameter (# NH_4^-, # PO_3^-, # PO_4^{3-}). WC, water content; Chl*a*, Chlorophyll a; DEN, denitrification rates; ANA, anammox rates; DEN%, the contribution of denitrification to N removal; ANA%, the contribution of anammox to N removal.

A4-7 than the other stations. In addition, Pielou's evenness (from 0.76 to 0.84) and Good's coverage values (from 98% to 99%) can be observed from each sample, demonstrating the dependability of the sequencing accuracy. The community diversity of the AMX 16S rRNA gene decreased with the increasing concentration in the bottom water (Chao1: r = -0.681, $p< 0.05$; Observed species: r = -0.710, $p< 0.05$), decreasing sediment NH_4^+ (Chao1: r = 0.677, $p< 0.05$; Observed species: r = 0.678, $p< 0.05$), and decreasing Chl*a* concentration (Chao1: r = 0.730, $p< 0.05$; Observed species: r =0.722, $p< 0.05$) (Supplementary Table 6). The rarefaction curves indicated that the majority of the anammox bacteria was captured in the current study (Supplementary Figure 1C).

The dominant OTUs (top 10 OTUs) of AMX 16S rRNA gene and their related sequences from the GenBank were phylogenetically analyzed to 4 clusters, including *Ca.* Anammoximicrobium moscowii and the other uncultured clusters (Figures 8A, B; Supplementary Figures 8, 9). The OTUs (OTU173, OTU159, and OTU65) were closely related to *Ca.* Anammoximicrobium moscowii, and the OTU abundances were higher in muddy sediment than those in sandy sediment. The other clusters were related to uncultured anammox bacteria, showing a very wide range and matched with marine habitats and activated sludge (Figure 8B). According to a redundancy analysis (RDA), the link between AMX 16S communities and environmental factors may be described by the first two axes (65.75% of the total variance) (Figure 8C). The sediment MΦ (pseudo-F = 6.1 and $p< 0.01$), Chl*a* (pseudo-F = 2.3 and $p< 0.05$), and bottom water NO_3^- (pseudo-F = 3.4 and $p< 0.05$), had huge impact on the anammox community. At genus level, *Candidatus* Anammoximicrobium was the dominant genera in all sampling stations except A3-2, while the dominant genera in A3-2 was *Rhodoplanes* (Supplementary Figure 10B). Spearman's correlation analysis revealed that *Candidatus* Anammoximicrobium was negatively related with sediment water content ($p< 0.05$), TOC ($p< 0.05$), and positively correlated with sediment grain size (Supplementary Table 7).

Discussion

Community characteristics of *nirS*/*nirK*-encoding denitrifiers

In coastal aquatic ecosystems, denitrification in sediments can reduce bioavailable nitrogen from anthropogenic and natural inputs, thus, sediments are recognized as hotspot

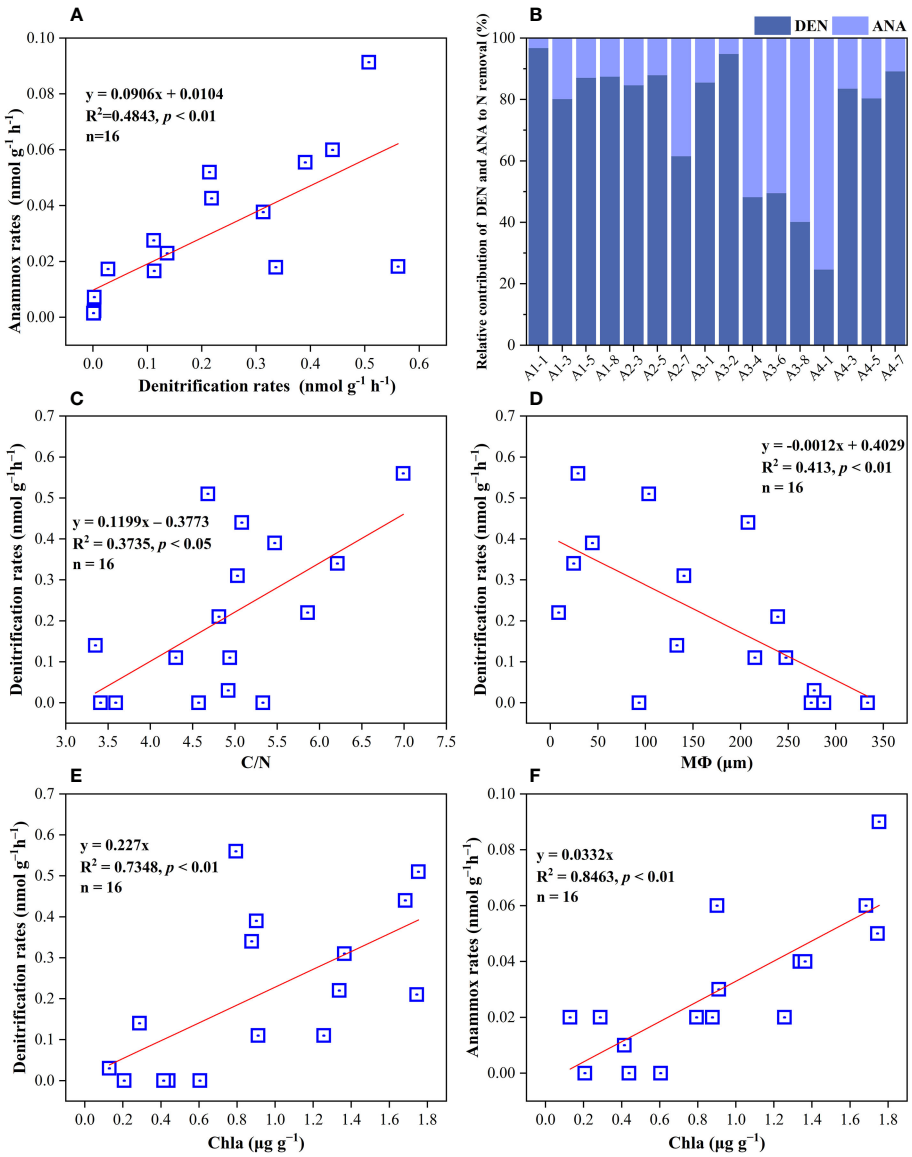

FIGURE 5
(A) Correlations analysis of anammox rates with denitrification rates in surface sediments. **(B)** The percentage of denitrification and anammox to NO_x^- removal in all sampling sites. **(C–F)** their regulating factors in sediments of the Yangtze Estuary and adjacent sea.

regions of N loss (Seitzinger et al., 2006). Lin et al. (2017) reported that the contribution of denitrification to N loss (2.2×10^6 t N yr^{-1}) was higher than anammox (4.6×10^5 t N yr^{-1}) in the surface sediments from the East China Sea. The biogeochemical cycle of nitrogen is driven by microorganisms, and the microbial communities are constantly changing to adapt to the complex coastal environments (Dang and Lovell, 2016; Hutchins and Fu, 2017). Thus, a further understanding of the microbial processes of N loss is still highly significant. Here, potential rates of denitrification and anammox, and their related gene abundances and community composition, along with influencing environmental factors were explored in the surface sediments from the Yangtze Estuary and the adjacent sea.

In the present study, the average abundance of *nir*S gene (1.28×10^7 copies g^{-1}) in the surface sediment was greater than that of *nir*K gene (4.52×10^6 copies g^{-1}), which were similar to the observations in the San Francisco Bay (1.50×10^7 copies g^{-1} for *nir*S and 3.20×10^6 copies g^{-1} for *nir*K) (Mosier and Francis, 2010). Some previous studies showed that the mRNA abundance of *nir*S was also higher compared with *nir*K, suggesting a main role in N removal processes of *nir*S-encoding denitrifiers (Graham et al., 2010; Liu et al., 2021). The differential abundance between *nir*S and *nir*K may be due to the

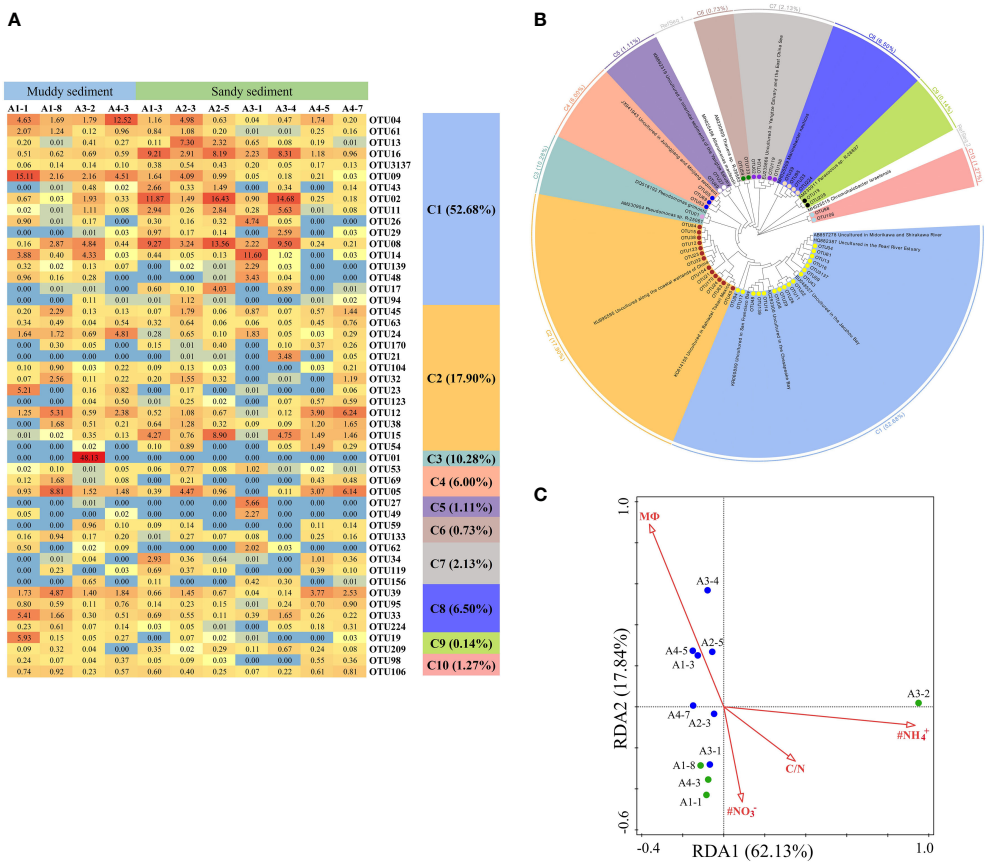

FIGURE 6
(A) The heat map of the dominant denitrification OTUs for the *nir*S gene (top 50 OTUs, 97% cutoff). **(B)** Reconstructed phylogenetic tree with neighbor-joining method of partial *nir*S-gene sequences (bootstrap 1000). **(C)** The redundancy analysis (RDA) for environmental factors and the *nir*S gene-encoded denitrifying communities.

competition for the substrates required by different enzyme synthesis (Huang et al., 2011). Moreover, compared to *nir*K-encoding denitrifiers, the variety of *nir*S-encoding denitrifiers was also greater, which is consistent with previous studies (Shi et al., 2019b; Ming et al., 2021). In general, *nir*S- and *nir*K-encoding denitrifiers had different respond to environmental parameters, and *nir*S denitrifiers had better adaptation to the coastal environments (Jones and Hallin, 2010; Likhitrattanapisal et al., 2021).

In consistent to our study (Figure 3), the abundance of *nir*S and *nir*K have the same change trends across the sampling sites (Zhang et al., 2019), which was affected by both the microbial interactions between *nir*S and *nir*K- denitrifiers, as well as the different preferences in structure components of corresponding nitrite reductases (Cutruzzolà et al., 2001). Nitrite reduction is the key step in denitrification, and both the *nir*S and *nir*K-encoded nitrite reductase are functionally identical while being evolutionarily distinct (Shrewsbury et al., 2016). The previous studies reported that both enzymes are often absent in the same bacterium, and the estimated number of denitrifiers in the soil sites was determined using the summation of *nir*S and *nir*K copy counts (Philippot et al., 2011; Zhang et al., 2019). However, *Pseudomonas* was found in *nir*S- and *nir*K-encoding denitrifiers at genus level in our study (Supplementary Figures 4B, 7B). Furthermore, there other different genera were detected in *nir*S- and *nir*K-encoding denitrifiers, which have capabilities of denitrification (Kim et al., 2008; Borrero-De Acuña et al., 2017; Gao et al., 2021). Thus, marker genes of *nir*S and *nir*K should be used to detect denitrifiers together. In addition, there are another four different genes involved in the denitrification pathway, nitric oxide reduction (*nor*B and *qnor*B), and nitrous oxide reduction (*nos*ZI and *nos*ZII). A single gene does not capture the entire denitrifying microbial community, due to several maker genes involved in denitrification pathway (Shrewsbury et al., 2016). Furthermore, Zhang et al. (2019) found that the contribution of denitrification to N removal was positively related to the relative abundance of *nosZ*/*nir*S, implying that marker genes from different denitrification steps should be considered simultaneously.

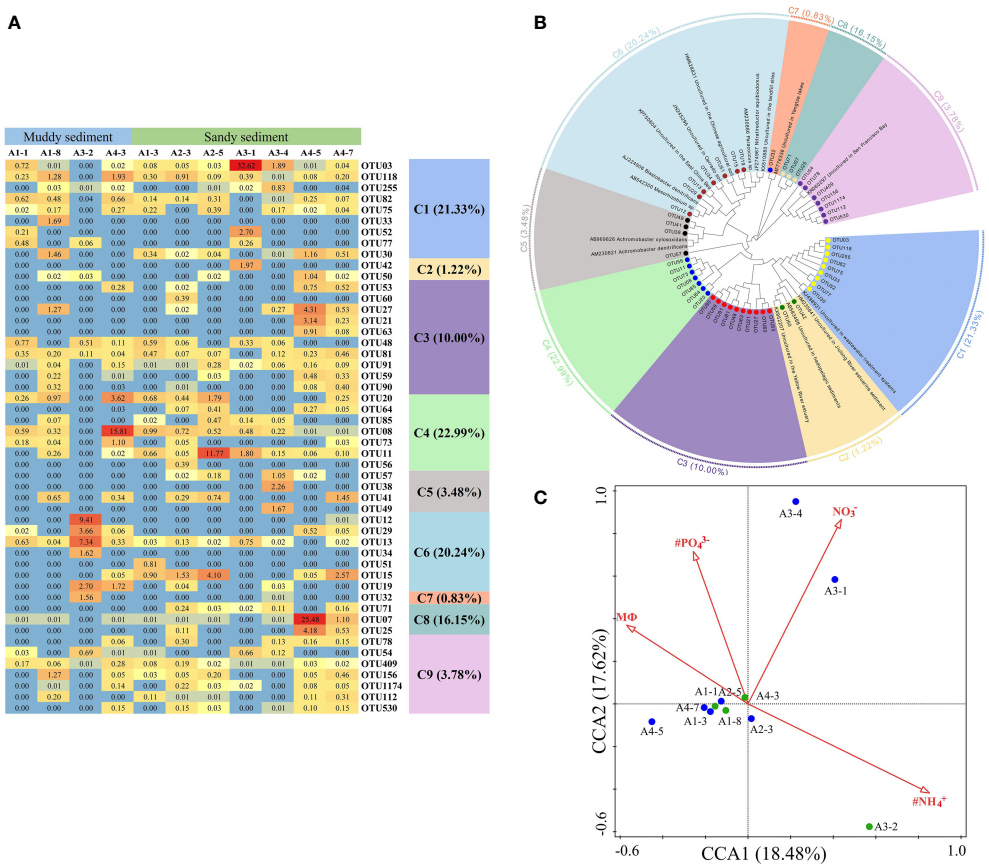

FIGURE 7
(A) The heat map of the dominant denitrification OTUs for the *nir*K gene (top 50 OTUs, 97% cutoff). **(B)** Reconstructed phylogenetic tree with neighbor-joining method of *nir*K-gene sequences (bootstrap 1000). **(C)** The canonical correspondence analysis (CCA) for environmental factors and the *nir*K gene-encoded denitrifying communities.

According to phylogenetic analysis, the dominant OTUs of *nir*S showed some similarities to multiple estuarine and marine sediments (Dang et al., 2008; Hong et al., 2014; Zheng et al., 2015; Gao et al., 2016). In contrast to *nir*S, the *nir*K-encoding denitrifiers were found to originate from several habitats, such as marine sediments, fresh sediments, agricultural soil, and wastewater treatment systems (Figure 7B, Supplementary Figure 6). Numerous studies have revealed that *nir*S and *nir*K-denitrifiers occupy different niches or have distinct habitat preferences in the environment (Smith and Ogram, 2008; Hallin et al., 2009; Knapp et al., 2009). The communities of *nir*S and *nir*K gene were observed to clearly separate in saline environments, and *nir*S-encoding denitrifiers predominated in marine environment (Jones and Hallin, 2010), in consistent with our study. Furthermore, *nir*K denitrifiers might exhibit more habitat selection, showing positive correlations with organic matter content (Smith and Ogram, 2008). In the present study, RDA/CCA demonstrated that C/N ratio and MΦ was the key factor affecting the community of *nir*S and *nir*K, respectively (Figure 6C, Figure 7C). High level of C/N ratio may promote the growth of denitrification bacteria, as previous studies showed that the denitrifiers OTUs and Shannon index decreased with decreasing organic matter and N contents (Chen et al., 2018; Wu et al., 2021). Meanwhile, the dominant OTUs of *nir*S- and *nir*K-encoding denitrifiers were affiliated with Proteobacteria (Figures 6B, 7B, Supplementary Figures 3, 6), which was consistent with previous reports (Kim et al., 2016; Xie et al., 2020). Furthermore, γ- Proteobacteria and α-Proteobacteria was the dominant class of *nir*S- and *nir*K-encoding denitrifiers, respectively. Some studies showed that denitrification can be performed by phylogenetically different microbes, and the most of denitrifiers early reported are belonging to subphyla of the Proteobacteria (Peralta et al., 2010; Wu et al., 2021). This phylum of Proteobacteria are widely distributed in aquatic environments because of high phylogenetic and phenotypic diversities (Liu et al., 2015; He and Zhang, 2016; Shi et al., 2019a). With the Proteobacteria community, *Pseudomonas* and *Mesorhizobium* were the

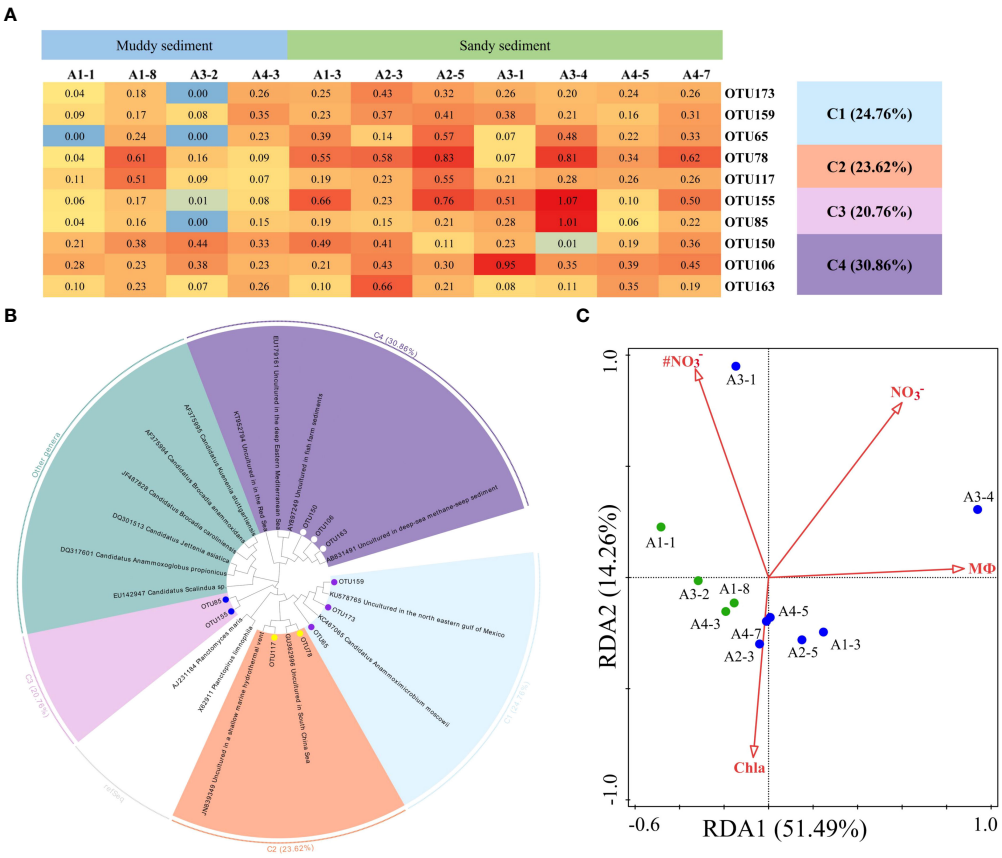

FIGURE 8
(A) The heat map of the dominant anammox OTUs for the 16S rRNA gene (top 10 OTUs, 97% cutoff). **(B)** Reconstructed phylogenetic tree with neighbor-joining method of 16S rRNA gene sequences (bootstrap 1000). **(C)** The redundancy analysis for environmental factors and the AMX 16S gene-encoded anammox bacterial communities.

dominant genera of *nir*S- and *nir*K-encoding denitrifiers, respectively. *Pseudomonas* stutzeri strain XL-2 and strain XL-2 were identified as the main denitrifiers which can remove 97.9% of nitrate (Dang and Lovell, 2016). In *nir*S bacterial community, *Pseudomonas* was mainly affected by NH_4^+ in the bottom water; while in *nir*K bacterial community, *Mesorhizobium* was significantly influenced by with sediment Fe(II)/Fe(III). In addition, it has been reported that the higher abundance of *Mesorhizobium* was observed in sandy soil (Li et al., 2019), in consistent to our study that *Mesorhizobium* was the dominant genera in A2-5 and A3-1 with high median grain size.

Community characteristics of anammox bacteria

In the present study, the abundance of AMX 16S rRNA gene was ranging from 1.03×10^5 to 2.97×10^6 copies g^{-1} (Figures 3A, B), which was lower than that of *nir*S and *nir*K gene in all sampling sites. The gene abundances of AMX 16S rRNA gene were like to the values in the Pearl River Estuary (Wu et al., 2020), but 1-2 orders magnitude lower than those in paddy soil (Zhu et al., 2011) and the coastal wetland sediments of China (Hou et al., 2015). Furthermore, anammox bacterial abundance was no obvious spatial heterogeneity at the sampling sites (Figure 3A).

The high-throughput sequencing of the 16S rRNA gene of anammox bacteria could provide adequate data, as compared to data from cloning libraries, to identify community changes and even recognize unusual bacteria with low relative abundance (Zhao et al., 2013; Shen et al., 2016). Based on the OTUs and the Shannon index, the AMX 16S genes in the surface sediment represented a very varied community of anammox bacteria (Supplementary Table 4). A wide variety of anammox bacteria was found in the surface sediment of Yangtze Estuary and the adjacent sea, in similarity to other estuarine sediments (Dale et al., 2009; Hong et al., 2014; Lisa et al., 2014). Salinity is a significant environmental factor that affects the diversity of anammox bacteria, according to earlier research (Schmid et al., 2007; Hamersley et al., 2009; Hu et al., 2012). However, in this

present study, the Chao1 had significantly correlated with NH_4^+ concentration in bottom water and sediment (Supplementary Table 6). These results implied that the substrates contents might be the main limiting factors for anammox bacteria.

In this study, the dominant OTUs were closely related to *Ca.* Anammoximicrobium moscowii and *Candidatus* Anammoximicrobium was the dominant genera at genus level (Supplementary Figures 9, 10B). In contrast to previous studies (Schmid et al., 2007; Fernandes et al., 2016; Fu et al., 2019; Wu et al., 2021), *Ca.* Scalindua are the dominant anammox bacteria in marine environments. Some studies reported that *Ca.* Scalindua has a relatively high tolerance for salinity and it can adapt to high hypersaline environment (Oshiki et al., 2017; Speth et al., 2017). Recently, the other genera have been found and *Ca.* Scalindua was not the only genus in the marine environments (Wu et al., 2019). *Ca.* Anammoximicrobium moscowii also can carry out anaerobic ammonium oxidation, which was firstly isolated in the Moscow region (Khramenkov et al., 2013), and the key role of this genus in N loss process cannot be ignored. Some studies reported that the different anammox bacteria lineages can become the dominant populations based on the slight change in the environment (Wang et al., 2021). In addition, the community composition study of anammox bacteria can be directly impacted by primer sets and sequencing depth. In the present study, considering the primer efficiency, Amx808F and Amx1040R was the appropriate choice for capturing anammox bacteria with good coverage, however, the specificity was not strong for *Ca.* Scalindua detection. From the RDA analysis, the MΦ and bottom water NO_3^- significantly affected anammox bacteria community. In addition, according to Spearman's correlation analysis, *Candidatus* Anammoximicrobium was negatively related by TOC.

Microbial processes for nitrogen loss and their environmental implications

For microbial mediated N transformation, the surface sediment are usually the most vibrant with greater potential N loss rates, particularly the denitrification rates; however, the potential rates of denitrification and anammox were lower than previous studies (Hou et al., 2015; Lin et al., 2017; Wu et al., 2021), denitrification and anammox can exhibit strongly spatiotemporal variabilities, and the rates might be affected by biotic and abiotic factors in sampling sites. The bulk of the samples belong to sandy sediments, with the low organic matter content and low N removal rates. In our study, denitrification was the main contributor of N loss, dominating the N loss process in surface sediment in most sampling sites (Figure 5B). These results were in accordance with those in the previous studies in estuarine and coastal habitats (Fernandes et al., 2012; Cao et al., 2017; Lin et al., 2017; Huang et al., 2021). Moreover, Huang et al. (2021) found that denitrification rates were substantially correlated with organics and median grain size (MΦ), implying that both MΦ and organic matter were the crucial factors regulating denitrification activities. High surface-to-volume ratios in fine-grained sediments typically result in greater organic matter absorption (Keil et al., 1994). Meanwhile, organic matter (as an electron donor) can directly or indirectly boost N removal processes by providing energy *via* the oxidation of organics (Devol, 2015). Additionally, we verified that denitrification rates were substantially correlated with MΦ and the C/N ratio (Figures 5C, D). Higher specific surface area in sediment with little grains was more suited to microbial colonization, and the required energy for the growth of heterotrophic denitrifiers were provided by organic matter Moreover, the contribution of anammox was higher than denitrification in few sampling stations with lower C/N ratio and higher median grain size, further implying that sediment texture can control the N loss rates *via* affecting the residence time of organic matter (Huang et al., 2021).

Anammox rates and denitrification rates have a positive correlation in this study (Figure 5A), suggesting that denitrification was probably the main source of NO_2^- for anammox. Coherent to many previous researches in the aquatic environment (Brin et al., 2017; Zhao et al., 2020a), anammox metabolism requires the substrates of NO_2^-, which are main supplied by denitrification rather than nitrification in these anaerobic environments. This coupling between anammox and denitrification may be mediated by an imbalance in NO_3^- and organic carbon needed for denitrification. Furthermore, in the present study, NO_2^- was negatively related to DEN%, but positively correlated to ANA%, implying the coupling of denitrification and anammox. However, there also studies showing that anammox coupled with nitrification rather than denitrification in estuarine sediments in winter (Hou et al., 2015; Lin et al., 2017). The uncertainties in the relationships between anammox and denitrification might be attributed to organic acids, and anammox bacteria can convert NO_3^- to NO_2^- in the presence of organic acids (Brin et al., 2014). Thus, coupled anammox and nitrification or denitrification play a vital role in N removal processes from the surface of marine sediments.

Previous studies have revealed that NH_4^+ and NO_3^- play the crucial and central role in N removal (Lin et al., 2017; Huang et al., 2021), which were as substrates in denitrification and anammox processes. In consistent to our study, NH_4^+ and NO_3^- were the key factors to influence denitrification and anammox rates. In the present study, Chl*a* was the key environmental regulator for denitrification rates ($p< 0.01$) (Figure 4, Figure 5E, Supplementary Table 5). The sediment Chl*a* is an indicator for the availability of labile organic matter which is obtained from phytoplankton deposited from upper waters, along as phytobenthos and benthic algal debris in the shallow marginal

system (Franco et al., 2007; Kitidis et al., 2017). The sediment organic matter correlates positively with Chl*a* in sediment and water column (Li et al., 2013), in similarity to our study (Figure 4, Supplementary Table 5). The growth of phytoplankton may be aided by light intensity and water temperature in March (Shi et al., 2019b), indicating that many phytoplankton cells might be destroyed to release labile DOC (Zhang et al., 2018), which could enhance denitrification by sinking down to anaerobic sediment layers. Meanwhile, anammox rates also positively correlated with Chl*a* ($p< 0.01$) (Figure 4, Figure 5F, Supplementary Table 5). The main reason for that was the substrates (NH_4^+ and NO_2^-) of anammox originated from the mineralization of organic matters (Zhang et al., 2018). Thus, both the quality and amount of organic matter in sediment are essential to manage estuarine N-cycling because fresh organics has a higher lability and simpler to be utilized by NO_x^- removal processes (Westrich and Berner, 1984; Henrichs and Doyle, 1986).

There were no significant correlations between N removal rates and related gene abundances in this study. The gene abundance obtained from the DNA levels has limitations. On the one hand, since DNA extracts include a wide variety of cells (e.g., active cells, inactive cells and dead cells) and its degraded or lysed extracellular DNA, gene abundance does not always indicate activity (Gaidos et al., 2011). On the other hand, the number of microbials just indicates potential microbial metabolism and has no direct impact on the activities of N transformation (Dai et al., 2008). It has been reported that the related functional gene transcript abundance is reflective of N transformation process potential, further revealing N transformation potential had a close relationship with active microbials (Li et al., 2022). Thus, to gain an insight into changes in denitrification and anammox potential, the functional transcript abundance combining with N removal rates are needed.

Conclusion

Taken as a whole, the current work described the distribution and diversity of denitrifiers and anammox bacteria in the Yangtze Estuary and the adjacent sea, and the potential rates of denitrification and anammox were measured together. We found the abundance and diversity of *nir*S-denitrifiers were higher than those of *nir*K-denitrifiers, and *nir*K-denitrifiers were more sensitive to the environments. For anammox bacteria, *Ca*. Anammoximicrobium moscowii has been found in surface sediment, and the other genera of anammox bacteria cannot be neglected in marine ecosystems. Compared to anammox, denitrification was the dominant contributor of N removal process and contributed 73.5% on average. Denitrification and anammox rates were regulated by multiple environmental factors, and the median grain size (MΦ), C/N ratio, and Chl*a* were the key factors.

Data availability statement

The datasets presented in this study can be found in online repositories. The names of the repository/repositories and accession number(s) can be found in the article/ Supplementary Material.

Author contributions

ZT: conceptualization,investigation, methodology, data curation, formal analysis, and writing-original draft. YZ: conceptualization, writing-review and editing, supervision, and funding acquisition. TM: writing-review and supervision. ZY: conceptualization, writing-review and editing, and supervision. TC: writing-review and editing. All authors contributed to the article and approved the submitted version.

Funding

This work was supported by the National Natural Science Foundation of China (No. 42130410, 41620104001, 41976133).

Acknowledgments

We thank Han Zhang and crew members on the R/V *Blue Sea 201* for the assistance provided in the collection of samples during the cruise.

Conflict of interest

The authors declare that the research was conducted in the absence of any commercial or financial relationships that could be construed as a potential conflict of interest.

Publisher's note

Supplementary material

The Supplementary Material for this article can be found online at: https://www.frontiersin.org/articles/10.3389/fmars.2022.1078653/full#supplementary-material

References

Abell, G. C. J., Revill, A. T., Smith, C., Bissett, A. P., Volkman, J. K., and Robert, S. S. (2010). Archaeal ammonia oxidizers and nirS-type denitrifiers dominate sediment nitrifying and denitrifying populations in a subtropical macrotidal estuary. *ISME J.* 4 (2), 286–300. doi: 10.1038/ismej.2009.105

Anderson, D. M., Cembella, A. D., and Hallegraeff, G. M. (2012). Progress in understanding harmful algal blooms: paradigm shifts and new technologies for research, monitoring, and management. *Annu. Rev. Mar. Sci.* 4, 143–176. doi: 10.1146/annurev-marine-120308-081121

Babbin, A. R., Buchwald, C., Morel, F. M. M., Wankel, S. D., and Ward, B. B. (2020). Nitrite oxidation exceeds reduction and fixed nitrogen loss in anoxic pacific waters. *Mar. Chem.* 224, 103814. doi: 10.1016/j.marchem.2020.103814

Babbin, A. R., Keil, R. G., Devol, A. H., and Ward, B. B. (2014). Organic matter stoichiometry, flux, and oxygen control nitrogen loss in the ocean. *Science* 344 (6182), 406–408. doi: 10.1126/science.1248364

Basha, S., Lingamgunta, L. K., Kannali, J., Gajula, S. K., Bandikari, R., Dasari, S., et al. (2018). Subsurface endospore-forming bacteria possess bio-sealant properties. *Sci. Rep.* 8 (1), 1–13. doi: 10.1038/s41598-018-24730-3

Beman, J.M. (2014). Activity, abundance, and diversity of nitrifying archaea and denitrifying bacteria in sediments of a subtropical estuary: Bahía del tóbari, Mexico. *Estuar. Coasts* 37 (6), 1343–1352. doi: 10.1007/s12237-013-9716-y

Bernhard, A. E., Donn, T., Giblin, A. E., and Stahl, D. A. (2005). Loss of diversity of ammonia-oxidizing bacteria correlates with increasing salinity in an estuary system. *Environ. Microbiol.* 7 (9), 1289–1297. doi: 10.1111/j.1462-2920.2005.00808.x

Borrero-De Acuña, J. M., Timmis, K. N., Jahn, M., and Jahn, D. (2017). Protein complex formation during denitrification by pseudomonas aeruginosa. *Microbial. Biotechnol.* 10 (6), 1523–1534. doi: 10.1111/1751-7915.12851

Brin, L. D., Giblin, A. E., and Rich, J. J. (2014). Environmental controls of anammox and denitrification in southern new England estuarine and shelf sediments. *Limnol. Oceanogr.* 59 (3), 851–860. doi: 10.4319/lo.2014.59.3.0851

Brin, L. D., Giblin, A. E., and Rich, J. J. (2017). Similar temperature responses suggest future climate warming will not alter partitioning between denitrification and anammox in temperate marine sediments. *Global Change Biol.* 23 (1), 331–340. doi: 10.1111/gcb.13370

Cao, W., Guan, Q., Li, Y., Wang, M., and Liu, B. (2017). The contribution of denitrification and anaerobic ammonium oxidation to N_2 production in mangrove sediments in southeast China. *J. Soils Sediments* 17 (6), 1767–1776. doi: 10.1007/s11368-017-1653-0

Chen, F., Hou, L., Liu, M., Zheng, Y., Yin, G., Lin, X., et al. (2016). Net anthropogenic nitrogen inputs (NANI) into the Yangtze river basin and the relationship with riverine nitrogen export. *J. Geophys. Res.: Biogeosci.* 121 (2), 451–465. doi: 10.1002/2015JG003186

Chen, S., Wang, F., Zhang, Y., Qin, S., Wei, S., Wang, S., et al. (2018). Organic carbon availability limiting microbial denitrification in the deep vadose zone. *Environ. Microbiol.* 20 (3), 980–992. doi: 10.1111/1462-2920.14027

Cutruzzolà, F., Brown, K., Wilson, E. K., Bellelli, A., Arese, M., Tegoni, M., et al. (2001). The nitrite reductase from pseudomonas aeruginosa: essential role of two active-site histidines in the catalytic and structural properties. *Proc. Natl. Acad. Sci.* 98 (5), 2232–2237. doi: 10.1073/pnas.041365298

Dai, M., Wang, L., Guo, X., Zhai, W., Li, Q., He, B., et al. (2008). Nitrification and inorganic nitrogen distribution in a large perturbed river/estuarine system: the pearl river estuary, China. *Biogeosciences* 5 (5), 1227–1244. doi: 10.5194/bg-5-1227-2008

Dale, O. R., Tobias, C. R., and Song, B. (2009). Biogeographical distribution of diverse anaerobic ammonium oxidizing (anammox) bacteria in cape fear river estuary. *Environ. Microbiol.* 11 (5), 1194–1207. doi: 10.1111/j.1462-2920.2008.01850.x

Dalsgaard, T., and Thamdrup, B. (2002). Factors controlling anaerobic ammonium oxidation with nitrite in marine sediments. *Appl. Environ. Microbiol.* 68 (8), 3802–3808. doi: 10.1128/AEM.68.8.3802-3808.2002

Dang, H., and Lovell, C. R. (2016). Microbial surface colonization and biofilm development in marine environments. *Microbiol. Mol. Biol. Rev.* 80 (1), 91–138. doi: 10.1128/MMBR.00037-15

Dang, H., Zhang, X., Sun, J., Li, T., Zhang, Z., and Yang, G. (2008). Diversity and spatial distribution of sediment ammonia-oxidizing crenarchaeota in response to estuarine and environmental gradients in the changjiang estuary and East China Sea. *Microbiology* 154 (7), 2084–2095. doi: 10.1099/mic.0.2007/013581-0

Devol, A. H. (2015). Denitrification, anammox, and N_2 production in marine sediments. *Annu. Rev. Mar. Sci.* 7, 403–423. doi: 10.1146/annurev-marine-010213-135040

Di, H. J., Cameron, K. C., Shen, J.-P., Winefield, C. S., O'callaghan, M., Bowatte, S., et al. (2010). Ammonia-oxidizing bacteria and archaea grow under contrasting soil nitrogen conditions. *FEMS Microbiol. Ecol.* 72 (3), 386–394. doi: 10.1111/j.1574-6941.2010.00861.x

Fernandes, S. O., Javanaud, C., Michotey, V. D., Guasco, S., Anschutz, P., and Bonin, P. (2016). Coupling of bacterial nitrification with denitrification and anammox supports n removal in intertidal sediments (Arcachon bay, France). *Estuar. Coast. Shelf Sci.* 179, 39–50. doi: 10.1016/j.ecss.2015.10.009

Fernandes, S. O., Michotey, V. D., Guasco, S., Bonin, P. C., and Bharathi, P. A. L. (2012). Denitrification prevails over anammox in tropical mangrove sediments (Goa, India). *Mar. Environ. Res.* 74, 9–19. doi: 10.1016/j.marenvres.2011.11.008

Franco, M. A., De Mesel, I., Diallo, M.D., van der Gucht, K., Van Gansbeke, D., Van Rijswijk, P., et al. (2007). Effect of phytoplankton bloom deposition on benthic bacterial communities in two contrasting sediments in the southern north Sea. *Aquat. Microbial. Ecol.* 48 (3), 241–254. doi: 10.3354/ame048241

Fu, L., Chen, Y., Li, S., He, H., Mi, T., Zhen, Y., et al. (2019). Shifts in the anammox bacterial community structure and abundance in sediments from the changjiang estuary and its adjacent area. *Syst. Appl. Microbiol.* 42 (3), 383–396. doi: 10.1016/j.syapm.2018.12.008

Gaidos, E., Rusch, A., and Ilardo, M. (2011). Ribosomal tag pyrosequencing of DNA and RNA from benthic coral reef microbiota: community spatial structure, rare members and nitrogen-cycling guilds. *Environ. Microbiol.* 13 (5), 1138–1152. doi: 10.1111/j.1462-2920.2010.02392.x

Gao, J., Hou, L., Zheng, Y., Liu, M., Yin, G., Li, X., et al. (2016). nirS-encoding denitrifier community composition, distribution, and abundance along the coastal wetlands of China. *Appl. Microbiol. Biotechnol.* 100 (19), 8573–8582. doi: 10.1007/s00253-016-7659-5

Gao, Y., Mania, D., Mousavi, S. A., Lycus, P., Arntzen, M. Ø., Woliy, K., et al. (2021). Competition for electrons favours N_2O reduction in denitrifying bradyrhizobium isolates. *Environ. Microbiol.* 23 (4), 2244–2259. doi: 10.1111/1462-2920.15404

Gobler, C. J. (2020). Climate change and harmful algal blooms: insights and perspective. *Harmful Algae* 91, 101731. doi: 10.1016/j.hal.2019.101731

Graham, D. W., Trippett, C., Dodds, W. K., O'brien, J. M., Banner, E. B. K., Head, I. M., et al. (2010). Correlations between *in situ* denitrification activity and nir-gene abundances in pristine and impacted prairie streams. *Environ. pollut.* 158 (10), 3225–3229. doi: 10.1016/j.envpol.2010.07.010

Hallin, S., Jones, C. M., Schloter, M., and Philippot, L. (2009). Relationship between n-cycling communities and ecosystem functioning in a 50-year-old fertilization experiment. *ISME J.* 3 (5), 597–605. doi: 10.1038/ismej.2008.128

Hamersley, M.R., Lavik, G., Woebken, D., Rattray, J. E., Lam, P., Hopmans, E. C., et al. (2007). Anaerobic ammonium oxidation in the Peruvian oxygen minimum zone. *Limnol. Oceanogr.* 52 (3), 923–933. doi: 10.4319/lo.2007.52.3.0923

Hamersley, M.R., Woebken, D., Boehrer, B., Schultze, M., Lavik, G., and Kuypers, M. M. M. (2009). Water column anammox and denitrification in a temperate permanently stratified lake (Lake rassnitzer, Germany). *Syst. Appl. Microbiol.* 32 (8), 571–582. doi: 10.1016/j.syapm.2009.07.009

Harhangi, H. R., Le Roy, M., Van Alen, T., Hu, B.-L., Groen, J., Kartal, B., et al. (2012). Hydrazine synthase, a unique phylomarker with which to study the presence and biodiversity of anammox bacteria. *Appl. Environ. Microbiol.* 78 (3), 752–758. doi: 10.1128/AEM.07113-11

Henrichs, S. M., and Doyle, A. P. (1986). Decomposition of 14C-labeled organic substances in marine sediments 1. *Limnol. Oceanogr.* 31 (4), 765–778. doi: 10.4319/lo.1986.31.4.0765

He, T., and Zhang, X. (2016). Characterization of bacterial communities in deep-sea hydrothermal vents from three oceanic regions. *Mar. Biotechnol.* 18 (2), 232–241. doi: 10.1007/s10126-015-9683-3

Hong, Y., Xu, X., Kan, J., and Chen, F. (2014). Linking seasonal inorganic nitrogen shift to the dynamics of microbial communities in the Chesapeake bay. *Appl. Microbiol. Biotechnol.* 98 (7), 3219–3229. doi: 10.1007/s00253-013-5337-4

Hou, L., Zheng, Y., Liu, M., Li, X., Lin, X., Yin, G., et al. (2015). Anaerobic ammonium oxidation and its contribution to nitrogen removal in china's coastal wetlands. *Sci. Rep.* 5 (1), 1–11. doi: 10.1038/srep15621

Howarth, R. W. (2008). Coastal nitrogen pollution: a review of sources and trends globally and regionally. *Harmful Algae* 8 (1), 14–20. doi: 10.1016/j.hal.2008.08.015

Huang, S., Chen, C., Wu, Y., Wu, Q., and Zhang, R. (2011). Characterization of depth-related bacterial communities and their relationships with the environmental factors in the river sediments. *World J. Microbiol. Biotechnol.* 27 (11), 2655–2664. doi: 10.1007/s11274-011-0739-x

Huang, F., Lin, X., Hu, W., Zeng, F., He, L., and Yin, K. (2021). Nitrogen cycling processes in sediments of the pearl river estuary: Spatial variations, controlling factors, and environmental implications. *Catena* 206, 105545. doi: 10.1016/j.catena.2021.105545

Hu, B.-L., Shen, L.-D., Zheng, P., Hu, A.-H., Chen, T.-T., Cai, C., et al. (2012). Distribution and diversity of anaerobic ammonium-oxidizing bacteria in the sediments of the qiantang river. *Environ. Microbiol. Rep.* 4 (5), 540–547. doi: 10.1111/j.1758-2229.2012.00360.x

Hutchins, D. A., and Fu, F. (2017). Microorganisms and ocean global change. *Nat. Microbiol.* 2 (6), 1–11. doi: 10.1038/nmicrobiol.2017.58

Jiang, X., Yao, L., Guo, L., Liu, G., and Liu, W. (2017). Multi-scale factors affecting composition, diversity, and abundance of sediment denitrifying microorganisms in Yangtze lakes. *Appl. Microbiol. Bbiotechnol.* 101 (21), 8015–8027. doi: 10.1007/s00253-017-8537-5

Jones, C. M., and Hallin, S. (2010). Ecological and evolutionary factors underlying global and local assembly of denitrifier communities. *ISME J.* 4 (5), 633–641. doi: 10.1038/ismej.2009.152

Keil, R. G., Montluçon, D. B., Prahl, F. G., and Hedges, J. I. (1994). Sorptive preservation of labile organic matter in marine sediments. *Nature* 370 (6490), 549–552. doi: 10.1038/370549a0

Khramenkov, S. V., Kozlov, M. N., Kevbrina, M. V., Dorofeev, A. G., Kazakova, E. A., Grachev, V. A., et al. (2013). A novel bacterium carrying out anaerobic ammonium oxidation in a reactor for biological treatment of the filtrate of wastewater fermented sludge. *Microbiology* 82 (5), 628–636. doi: 10.1134/S002626171305007X

Kim, H., Bae, H.-S., Reddy, K.R., and Ogram, A. (2016). Distributions, abundances and activities of microbes associated with the nitrogen cycle in riparian and stream sediments of a river tributary. *Water Res.* 106, 51–61. doi: 10.1016/j.watres.2016.09.048

Kim, M., Jeong, S.-Y., Yoon, S. J., Cho, S. J., Kim, Y. H., Kim, M. J., et al. (2008). Aerobic denitrification of pseudomonas putida AD-21 at different C/N ratios. *J. Biosci. Bioeng.* 106 (5), 498–502. doi: 10.1263/jbb.106.498

Kitidis, V., Tait, K., Nunes, J., Brown, I., Woodward, E. M. S., Harris, C., et al. (2017). Seasonal benthic nitrogen cycling in a temperate shelf sea: the celtic Sea. *Biogeochemistry* 135 (1), 103–119. doi: 10.1007/s10533-017-0311-3

Klute, A. (1986). Water retention: laboratory methods. *Methods Soil anal.: Part 1 Phys. Mineral. Methods* 5, 635–662. doi: 10.2136/sssabookser5.1.2ed.c26

Knapp, C. W., Dodds, W. K., Wilson, K. C., O'brien, J. M., and Graham, D. W. (2009). Spatial heterogeneity of denitrification genes in a highly homogenous urban stream. *Environ. Sci. Technol.* 43 (12), 4273–4279. doi: 10.1021/es9001407

Kuypers, M. M. M., Sliekers, A.O., Lavik, G., Schmid, M., Jørgensen, B. B., Kuenen, J.G., et al. (2003). Anaerobic ammonium oxidation by anammox bacteria in the black Sea. *Nature* 422 (6932), 608–611. doi: 10.1038/nature01472

Li, M., He, H., Mi, T., and Zhen, Y. (2022). Spatiotemporal dynamics of ammonia-oxidizing archaea and bacteria contributing to nitrification in sediments from bohai Sea and south yellow Sea, China. *Sci. Total Environ.* 825, 153972. doi: 10.1016/j.scitotenv.2022.153972

Li, M., Hong, Y., Cao, H., and Gu, J. (2013). Community structures and distribution of anaerobic ammonium oxidizing and nirS-encoding nitrite-reducing bacteria in surface sediments of the south China Sea. *Microbial. Ecol.* 66 (2), 281–296. doi: 10.1007/s00248-012-0175-y

Li, M., Hong, Y., Klotz, M. G., and Gu, J.-D. (2010). A comparison of primer sets for detecting 16S rRNA and hydrazine oxidoreductase genes of anaerobic ammonium-oxidizing bacteria in marine sediments. *Appl. Microbiol. Biotechnol.* 86 (2), 781–790. doi: 10.1007/s00253-009-2361-5

Likhitrattanapisal, S., Siriarchawatana, P., Seesang, M., Chunhametha, S., Boonsin, W., Phithakrotchanakoon, C., et al. (2021). Uncovering multi-faceted taxonomic and functional diversity of soil bacteriomes in tropical southeast Asian countries. *Sci. Rep.* 11 (1), 1–13. doi: 10.1038/s41598-020-79786-x

Lim, D. I., Choi, J. Y., Jung, H. S., Rho, K. C., and Ahn, K. S. (2007). Recent sediment accumulation and origin of shelf mud deposits in the yellow and East China seas. *Prog. Oceanogr.* 73 (2), 145–159. doi: 10.1016/j.pocean.2007.02.004

Lin, G., and Lin, X. (2022). Bait input altered microbial community structure and increased greenhouse gases production in coastal wetland sediment. *Water Res.* 218, 118520. doi: 10.1016/j.watres.2022.118520

Lin, X., Liu, M., Hou, L., Gao, D., Li, X., Lu, K., et al. (2017). Nitrogen losses in sediments of the East China Sea: spatiotemporal variations, controlling factors, and environmental implications. *J. Geophys. Res.: Biogeosci.* 122 (10), 2699–2715. doi: 10.1002/2017jg004036

Lisa, J. A., Song, B., Tobias, C. R., and Duernberger, K. A. (2014). Impacts of freshwater flushing on anammox community structure and activities in the new river estuary, USA. *Aquat. Microbial. Ecol.* 72 (1), 17–31. doi: 10.3354/ame01682

Liu, S., Chen, Y., and Xiao, L. (2021). Metagenomic insights into mixotrophic denitrification facilitated nitrogen removal in a full-scale A2/O wastewater treatment plant. *PloS One* 16 (4), e0250283. doi: 10.1371/journal.pone.0250283

Liu, X., Hu, H.-W., Liu, Y.-R., Xiao, K.-Q., Cheng, F.-S., Li, J., et al. (2015). Bacterial composition and spatiotemporal variation in sediments of jiaozhou bay, China. *J. Soils Sediments* 15 (3), 732–744. doi: 10.1007/s11368-014-1045-7

Liu, Y., Liu, J., Yao, P., Ge, T., Qiao, Y., Zhao, M., et al. (2018). Distribution patterns of ammonia-oxidizing archaea and bacteria in sediments of the eastern China marginal seas. *Syst. Appl. Microbiol.* 41 (6), 658–668. doi: 10.1016/j.syapm.2018.08.008

Li, H., Zhang, Y., Wang, T., Feng, S., Ren, Q., Cui, Z., et al. (2019). Responses of soil denitrifying bacterial communities carrying nirS, nirK, and nosZ genes to revegetation of moving sand dunes. *Ecol. Indic.* 107, 105541. doi: 10.1016/j.ecolind.2019.105541

Lovley, D. R., and Phillips, E. J. P. (1987). Rapid assay for microbially reducible ferric iron in aquatic sediments. *Appl. Environ. Microbiol.* 53 (7), 1536–1540. doi: 10.1128/aem.53.7.1536-1540.1987

Medhi, K., Singhal, A., Chauhan, D. K., and Thakur, I. S. (2017). Investigating the nitrification and denitrification kinetics under aerobic and anaerobic conditions by paracoccus denitrificans ISTOD1. *Biores. Technol.* 242, 334–343. doi: 10.1016/j.biortech.2017.03.084

Ming, H., Fan, J., Chen, Q., Su, J., Song, J., Yuan, J., et al. (2021). Diversity and abundance of denitrifying bacteria in the sediment of a eutrophic estuary. *Geomicrobiol. J.* 38 (3), 199–209. doi: 10.1080/01490451.2020.1822959

Mosier, A. C., and Francis, C. A. (2010). Denitrifier abundance and activity across the San Francisco bay estuary. *Environ. Microbiol. Rep.* 2 (5), 667–676. doi: 10.1111/j.1758-2229.2010.00156.x

Mulder, A., De Graaf, V., Astfid, A., Robertson, L. A., and Kuenen, J. G. (1995). Anaerobic ammonium oxidation discovered in a denitrifying fluidized bed reactor. *FEMS Microbiol. Ecol.* 16 (3), 177–183. doi: 10.1111/j.1574-6941.1995.tb00281.x

Murray, C. C., Agbayani, S., and Ban, N. C. (2015). Cumulative effects of planned industrial development and climate change on marine ecosystems. *Global Ecol. Conserv.* 4, 110–116. doi: 10.1016/j.gecco.2015.06.003

Nicol, G. W., Leininger, S., Schleper, C., and Prosser, J. I. (2008). The influence of soil pH on the diversity, abundance and transcriptional activity of ammonia oxidizing archaea and bacteria. *Environ. Microbiol.* 10 (11), 2966–2978. doi: 10.1111/j.1462-2920.2008.01701.x

Oshiki, M., Mizuto, K., Kimura, Z.-I., Kindaichi, T., Satoh, H., and Okabe, S. (2017). Genetic diversity of marine anaerobic ammonium-oxidizing bacteria as revealed by genomic and proteomic analyses of 'Candidatus scalindua japonica'. *Environ. Microbiol. Rep.* 9 (5), 550–561. doi: 10.1111/1758-2229.12586

Peralta, A. L., Matthews, J. W., and Kent, A. D. (2010). Microbial community structure and denitrification in a wetland mitigation bank. *Appl. Environ. Microbiol.* 76 (13), 4207–4215. doi: 10.1128/AEM.02977-09

Philippot, L., Andert, J., Jones, C. M., Bru, D., and Hallin, S. (2011). Importance of denitrifiers lacking the genes encoding the nitrous oxide reductase for N_2O emissions from soil. *Global Change Biol.* 17 (3), 1497–1504. doi: 10.1111/j.1365-2486.2010.02334.x

Ravishankara, A. R., Daniel, J. S., and Portmann, R. W. (2009). Nitrous oxide (N_2O): the dominant ozone-depleting substance emitted in the 21st century. *Science* 326 (5949), 123–125. doi: 10.1126/science.1176985

Schmid, M. C., Risgaard-Petersen, N., Van De Vossenberg, J., Kuypers, M. M. M., Lavik, G., Petersen, J., et al. (2007). Anaerobic ammonium-oxidizing bacteria in marine environments: widespread occurrence but low diversity. *Environ. Microbiol.* 9 (6), 1476–1484. doi: 10.1111/j.1462-2920.2007.01266.x

Seitzinger, S., Harrison, J. A., Böhlke, J. K., Bouwman, A. F., Lowrance, R., Peterson, B., et al. (2006). Denitrification across landscapes and waterscapes: a synthesis. *Ecol. Appl.* 16 (6), 2064–2090. doi: 10.1890/1051-0761(2006)016[2064:DALAWA]2.0.CO;2

Shen, L.-D., Zheng, P.-H., and Ma, S.-J. (2016). Nitrogen loss through anaerobic ammonium oxidation in agricultural drainage ditches. *Biol. Fertil. Soils* 52 (2), 127–136. doi: 10.1007/s00374-015-1058-4

Shi, R., Huang, H., Qi, Z., and Han, T. (2019a). Distribution patterns of nirS-encoding and nirK-encoding denitrifiers in the surface sediment of the pearl river estuary. *Russian J. Mar. Biol.* 45 (6), 453–463. doi: 10.1134s1063074019060099

Shi, R., Xu, S., Qi, Z., Huang, H., and Liang, Q. (2019b). Seasonal patterns and environmental drivers of nirS-and nirK-encoding denitrifiers in sediments of daya bay, China. *Oceanologia* 61 (3), 308–320. doi: 10.1016/j.oceano.2019.01.002

Shrewsbury, L. H., Smith, J. L., Huggins, D. R., Carpenter-Boggs, L., and Reardon, C. L. (2016). Denitrifier abundance has a greater influence on denitrification rates at larger landscape scales but is a lesser driver than environmental variables. *Soil Biol. Biochem.* 103, 221–231. doi: 10.1016/j.soilbio2016.08.016

Smith, J. M., and Ogram, A. (2008). Genetic and functional variation in denitrifier populations along a short-term restoration chronosequence. *Appl. Environ. Microbiol.* 74 (18), 5615–5620. doi: 10.1128/AEM.00349-08

Smith, V. H., and Schindler, D. W. (2009). Eutrophication science: where do we go from here? *Trends Ecol. Evol.* 24 (4), 201–207.

Song, G. D., Liu, S. M., Kuypers, M. M. M., and Lavik, G. (2016). Application of the isotope pairing technique in sediments where anammox, denitrification, and dissimilatory nitrate reduction to ammonium coexist. *Limnol. Oceanogr.: Methods* 14 (12), 801–815. doi: 10.1002/lom3.10127

Speth, D. R., Lagkouvardos, I., Wang, Y., Qian, P.-Y., Dutilh, B. E., and Jetten, M. S. M. (2017). Draft genome of scalindua rubra, obtained from the interface above the discovery deep brine in the red Sea, sheds light on potential salt adaptation strategies in anammox bacteria. *Microbial. Ecol.* 74 (1), 1–5. doi: 10.1007/s00248-017-0929-7

Thamdrup, B., and Dalsgaard, T. (2002). Production of N2 through anaerobic ammonium oxidation coupled to nitrate reduction in marine sediments. *Appl. Environ. Microbiol.* 68 (3), 1312–1318. doi: 10.1128/AEM.68.3.1312-1318.2002

Throbäck, I. N., Enwall, K., Jarvis, Å, and Hallin, S. (2004). Reassessing PCR primers targeting nirS, nirK and nosZ genes for community surveys of denitrifying bacteria with DGGE. *FEMS Microbiol. Ecol.* 49 (3), 401–417. doi: 10.1016/j.femsec.2004.04.011

Trimmer, M., and Nicholls, J. C. (2009). Production of nitrogen gas via anammox and denitrification in intact sediment cores along a continental shelf to slope transect in the north Atlantic. *Limnol. Oceanogr.* 54 (2), 577–589. doi: 10.4319/lo.2009.54.2.0577

Trimmer, M., Nicholls, J. C., and Deflandre, B. (2003). Anaerobic ammonium oxidation measured in sediments along the Thames estuary, united kingdom. *Appl. Environ. Microbiol.* 69 (11), 6447–6454. doi: 10.1128/AEM.69.11.6447-6454.2003

Wang, J., Kan, J., Qian, G., Chen, J., Xia, Z., Zhang, X., et al. (2019). Denitrification and anammox: Understanding nitrogen loss from Yangtze estuary to the east China sea (ECS). *Environ. pollut.* 252, 1659–1670. doi: 10.1016/j.envpol.2019.06.025

Wang, Q., Rogers, M. J., Ng, S., and He, J. (2021). Fixed nitrogen removal mechanisms associated with sulfur cycling in tropical wetlands. *Water Res.* 189, 116619. doi: 10.1016/j.watres.2020.116619

Westrich, J. T., and Berner, R. A. (1984). The role of sedimentary organic matter in bacterial sulfate reduction: The G model tested 1. *Limnol. Oceanogr.* 29 (2), 236–249. doi: 10.4319/lo.1984.29.2.0236

Worm, B., Barbier, E. B., Beaumont, N., Duffy, J.E., Folke, C., Halpern, B. S., et al. (2006). Impacts of biodiversity loss on ocean ecosystem services. *Science* 314 (5800), 787–790. doi: 10.1126/science.1132294

Wu, J., Hong, Y., Chang, X., Jiao, L., Li, Y., Liu, X., et al. (2019). Unexpectedly high diversity of anammox bacteria detected in deep-sea surface sediments of the south China Sea. *FEMS Microbiol. Ecol.* 95 (3), fiz013. doi: 10.1093/femsec/fiz013

Wu, J., Hong, Y., Liu, X., and Hu, Y. (2021). Variations in nitrogen removal rates and microbial communities over sediment depth in daya bay, China. *Environ. pollut.* 286, 117267. doi: 10.1016/j.envpol.2021.117267

Wu, J., Hong, Y., Wen, X., Li, Y., Wang, Y., and Chang, X. (2020). Activity, abundance, and community composition of anaerobic ammonia–oxidizing (anammox) bacteria in sediment cores of the pearl river estuary. *Estuar. Coasts* 43 (1), 73–85. doi: 10.1007/s12237-019-00668-1

Xie, H., Hong, Y., Liu, H., Jiao, L., Wu, J., and Wang, L. (2020). Spatio-temporal shifts in community structure and activity of nirS-type denitrifiers in the sediment cores of pearl river estuary. *PloS One* 15 (4), e0231271. doi: 10.1371/journal.pone.0231271

Yang, Y., Li, M., Li, H., Li, X.-Y., Lin, J.-G., Denecke, M., et al. (2020). Specific and effective detection of anammox bacteria using PCR primers targeting the 16S rRNA gene and functional genes. *Sci. Total Environ.* 734, 139387. doi: 10.1016/j.scitotenv.2020.139387

Zhang, Y., Ji, G., Wang, C., Zhang, X., and Xu, M. (2019). Importance of denitrification driven by the relative abundances of microbial communities in coastal wetlands. *Environ. pollut.* 244, 47–54. doi: 10.1016/j.envpol.2018.10.016

Zhang, X., Zhang, Q., Yang, A., Hou, L., Zheng, Y., Zhai, W., et al. (2018). Incorporation of microbial functional traits in biogeochemistry models provides better estimations of benthic denitrification and anammox rates in coastal oceans. *J. Geophys. Res.: Biogeosci.* 123 (10), 3331–3352. doi: 10.1029/2018jg004682

Zhao, Y., Chen, W., and Wen, D. (2020b). The effects of crude oil on microbial nitrogen cycling in coastal sediments. *Environ. Int.* 139, 105724. doi: 10.1016/j.envint.2020.105724

Zhao, R., Mogollón, J. M., Abby, S. S., Schleper, C., Biddle, J. F., Roerdink, D. L., et al. (2020a). Geochemical transition zone powering microbial growth in subsurface sediments. *Proc. Natl. Acad. Sci.* 117 (51), 32617–32626. doi: 10.1073/pnas.2005917117

Zhao, Y., Xia, Y., Kana, T. M., Wu, Y., Li, X., and Yan, X. (2013). Seasonal variation and controlling factors of anaerobic ammonium oxidation in freshwater river sediments in the taihu lake region of China. *Chemosphere* 93 (9), 2124–2131. doi: 10.1016/j.chemosphere.2013.07.063

Zheng, Y., Hou, L., Liu, M., Gao, J., Yin, G., Li, X., et al. (2015). Diversity, abundance, and distribution of nirS-harboring denitrifiers in intertidal sediments of the Yangtze estuary. *Microbial. Ecol.* 70 (1), 30–40. doi: 10.1007/s00248-015-0567-x

Zheng, Y., Hou, L., Liu, M., and Yin, G. (2019). Dynamics and environmental importance of anaerobic ammonium oxidation (anammox) bacteria in urban river networks. *Environ. pollut.* 254, 112998. doi: 10.1016/j.envpol.2019.112998

Zhu, G., Wang, S., Wang, Y., Wang, C., Risgaard-Petersen, N., Jetten, M. S. M., et al. (2011). Anaerobic ammonia oxidation in a fertilized paddy soil. *ISME J.* 5 (12), 1905–1912. doi: 10.1038/ismej.2011.63

frontiers | Frontiers in Marine Science

TYPE Original Research
PUBLISHED 02 December 2022
DOI 10.3389/fmars.2022.1063585

OPEN ACCESS

EDITED BY
Xiyang Dong,
Third Institute of Oceanography of the Ministry of Natural Resources, China

REVIEWED BY
Haikun Zhang,
Yantai Institute of Coastal Zone Research (CAS), China
Ling-Dong Shi,
University of California, Berkeley, United States

*CORRESPONDENCE
Hui He
hehui@ouc.edu.cn
Min Wang
mingwang@ouc.edu.cn

SPECIALTY SECTION
This article was submitted to Marine Biogeochemistry, a section of the journal Frontiers in Marine Science

RECEIVED 07 October 2022
ACCEPTED 11 November 2022
PUBLISHED 02 December 2022

CITATION
Zhao G, He H, Yue M, Wang H, Shao H and Wang M (2022) Differential responding patterns of the *nirK*-type and *nirS*-type denitrifying bacterial communities to an *Ulva prolifera* green tide in coastal Qingdao areas. *Front. Mar. Sci.* 9:1063585. doi: 10.3389/fmars.2022.1063585

Differential responding patterns of the *nirK*-type and *nirS*-type denitrifying bacterial communities to an *Ulva prolifera* green tide in coastal Qingdao areas

Guihua Zhao[1], Hui He[1]*, Ming Yue[2,3,4], Hualong Wang[1], Hongbing Shao[1] and Min Wang[1,5,6]*

[1]College of Marine Life Sciences, Institute of Evolution and Marine Biodiversity, Frontiers Science Center for Deep Ocean Multispheres and Earth System, Ocean University of China, Qingdao, China, [2]College of Environmental Science and Engineering, Ocean University of China, Qingdao, China, [3]Laboratory for Marine Ecology and Environmental Science, Pilot National Laboratory for Marine Science and Technology (Qingdao), Qingdao, China, [4]Key Laboratory of Marine Environment and Ecology, Ministry of Education, Ocean University of China, Qingdao, China, [5]OUC-UMT Joint Academic Centre for Marine Studies, Ocean University of China, Qingdao, China, [6]Department of Critical Care Medicine, the Affiliated Hospital of Qingdao University, Qingdao, China

Coastal eutrophication may be a vital inducement of green tide. Denitrification is an important nitrogen removal pathway that involves a series of enzymatic reactions. The rate-limiting step in the conversion of nitrite to nitric oxide is encoded by two functionally equivalent but structurally distinct genes, copper-containing nitrite reductase gene (*nirK*) and cytochrome cd1-containing nitrite reductase gene (*nirS*). Here, we used Illumina Miseq sequencing approach to examine the variations in denitrifying bacterial community characteristics and interactions during an *Ulva prolifera* green tide in coastal Qingdao areas. Our findings suggested that the variations in the denitrifying bacterial community structure during the green tide were closely related to the changes of chlorophyll *a* content, salinity and dissolved oxygen content. The *nirK*-type denitrifying bacteria were more sensitive to green tide than the *nirS*-type denitrifying bacteria. Additionally, the *nirK*-type denitrifying bacterial interactions were more stable and complex during the outbreak phase, while the *nirS*-type denitrifying bacterial interactions were more stable and complex during the decline phase. All of these characters demonstrated that the *nirK*-type and *nirS*-type denitrifying bacteria respond differently to the green tide, implying that they may occupy different niches during the green tide in coastal Qingdao areas.

KEYWORDS

Ulva profilera green tide, denitrifying bacteria, community structure, cooccurrence network, Illumina Miseq sequencing approach

Introduction

Green tide is a harmful algal bloom that occurs frequently in coastal areas. Since 2007, an annual green tide caused by *Ulva prolifera* has occurred in the Yellow Sea, which is thought to be the largest green tide ever (Liu et al., 2013; Zhang et al., 2019). In general, *U. prolifera* green tide appears along the Jiangsu coast from the middle of April to early May, migrates northward due to ocean currents and seasonal monsoons, reaches the coastal areas of the Shandong Peninsula in the middle of June, and then begins to decay in the middle of July (Zhang et al., 2019). During the migration period, *U. prolifera* multiplies rapidly and expands its coverage area, posing a major threat to coastal areas. It is reported that green tide alters not only the physicochemical factors of seawater, but also the microbial community in marine environments (van Alstyne et al., 2015; Lin et al., 2017; Qu et al., 2020). Qu et al. (2020), for example, stated that the outbreak of green tide reduced the abundance and diversity of bacterial community in Qingdao offshore areas. In turn, some microbial groups, such as *Cytophaga-Flexibacter-Bacteroides*, play a vital role in regulating the presence, development and decline of green tide (Marshall et al., 2006).

Green tide may be induced by coastal eutrophication caused by high nitrogen input (Li et al., 2017). Denitrification is regarded as the most effective nitrogen removal pathway, with the potential to minimize nitrogen pollution and eutrophication (Zumft, 1997; Falkowski et al., 2008; Guo et al., 2014). *U. prolifera* convert dissolved inorganic nitrogen (DIN) to dissolved organic nitrogen (DON) during the outbreak phase, and release quantities of DON and ammonium into seawater during the decline phase, as a result, *U. prolifera* green tide is regarded as a "nitrogen pump" and may have an impact on the denitrification process in coastal areas (Zhang et al., 2021a). Furthermore, *U. prolifera* competes for nitrate with denitrifying bacteria, which may affect the denitrification process and associated microbial activity (Christensen et al., 2000; Sun et al., 2020). Therefore, it is of importance to investigate variations in the denitrification process and associated microbial communities during the *U. prolifera* green tide.

As previously stated, denitrification is an important nitrogen removal pathway, accounting for 77% of total global nitrogen removal (Dalsgaard et al., 2012). According to reports, denitrification dominates the nitrogen removal in marine environments, rather than other processes such as anaerobic ammonium oxidation (Dalsgaard et al., 2005; Babbin et al., 2014). Denitrification is the process that contains a series of enzymatic reactions including nitrate reduction to nitrite, nitrite reduction to nitric oxide, nitric oxide reduction to nitrous oxide and nitrous oxide reduction to nitrogen, which are catalyzed sequentially by nitrate reductase (Nar), nitrite reductase (Nir), nitrogen oxide reductase (Nor) and nitrous oxide reductase (Nos) (Zumft, 1997). Due to the great phylogenetic diversity, studies on the denitrifying bacterial communities in natural environments should target the functional genes involved in the denitrification process (Lee and Francis, 2017).

The reduction of nitrite to nitric oxide is a rate-limiting step in the denitrification pathway, as well as the initial step in producing gaseous nitrogen products (Zumft, 1997). Copper-containing nitrite reductase gene (*nirK*) and cytochrome cd1-containing nitrite reductase gene (*nirS*) have been widely used as molecular markers to study the characteristics of denitrifying bacterial communities in a variety of habitats (Wolsing and Priemé, 2004; Santoro et al., 2006; Oakley et al., 2007; Francis et al., 2013; Liu et al., 2020). Though functionally equivalent, the *nirK* and *nirS* genes have distinct evolutionary histories and represent two ecologically separate groups of denitrifying bacteria (Jones and Hallin, 2010). Studies have shown that the community richness and abundance of the *nirS*-type denitrifying bacteria was greater than that of the *nirK*-type denitrifying bacteria in sediments of the San Francisco Bay (Mosier and Francis, 2010), whereas the *nirK*-type denitrifying bacterial community presented greater richness and more abundant in agricultural soils (Yoshida et al., 2009; Zhou et al., 2011; Yang et al., 2018). Bothe et al. (2000) pointed out that the *nirS*-type denitrifying bacteria has a more widely distribution than the *nirK*-type denitrifying bacteria. The *nirS*-type denitrifying bacteria is more susceptible to environmental changes than the *nirK*-type denitrifying bacteria (Yang et al., 2018). Overall, the *nirK*-type and *nirS*-type denitrifying bacteria may have different responses to environmental changes, implying that the two types of denitrifying bacteria may occupy different niches in the same environment (Yuan et al., 2012; Wei et al., 2015). However, it is unknown if the *nirK*-type and *nirS*-type denitrifying bacteria respond differently to the *U. prolifera* green tide.

In the present study, variations of the *nirK*-type and *nirS*-type denitrifying bacterial communities during an *U. prolifera* green tide in coastal Qingdao areas were studied using Illumina Miseq sequencing approach of the *nirK* and *nirS* genes. The prime goal of this study was to compare the responses of the *nirK*-type and *nirS*-type denitrifying bacteria to an *U. prolifera* green tide in coastal Qingdao areas. Furthermore, the possible critical physicochemical factors regulating variations of the *nirK*-type and *nirS*-type denitrifying bacterial communities during the green tide were also discussed in the present study.

Materials and methods

Sample collection and analysis of physicochemical factor

An *U. prolifera* green tide affected the coastal areas of the Yellow Sea from late April to early September 2019, according to Bulletin of China Marine Disaster, with a maximum distribution area and coverage area of 55699 km^2 and 508 km^2, respectively. The green tide arrived in the coastal areas of the Shandong

Peninsula in late May, began to decline around the end of July, and vanished in early September. In comparison to the previous green tide events, the green tide in 2019 vanished at the latest and had the second largest distribution areas, only second to the distribution areas of the green tide in 2016.

Three sampling stations in coastal Qingdao areas were chosen, and named XG (36.07°E, 120.30°N), ZQ (36.06°E, 120.31°N) and MD (36.05°E, 120.42°N) (Figure 1). Among the sampling stations, ZQ and MD were significantly influenced by the green tide, whereas XG was less likely to be influenced. Samples were taken between June and September 2019 (ten sampling time points). Twenty liters of seawater were filtered through an 800-mesh plankton net and a 0.22-μm pore-size polycarbonate membrane (Millipore, 47 mm in diameter), then the filters were stored at -80°C until DNA extraction. We also collected seawater samples to determine physicochemical factors, including temperature, salinity, dissolved oxygen (DO) content, pH, chlorophyll *a* (chl*a*) content, nitrate (NO_3^-) concentration, nitrite (NO_2^-) concentration, ammonium (NH_4^+) concentration and phosphate (PO_4^{3-}) concentration. The measurement methods of physicochemical factors have been previously described (Zhao et al., 2022), and results were displayed in Supplementary Figure 1. All samples were separated into two phases based on the chl*a* content: the outbreak phase (samples collected in 13 June, 27 June, 11 July, 18 July and 22 July) and the decline phase (samples collected in 6 August, 16 August, 23 August, 29 August and 5 September).

DNA extraction and quantitative PCR analysis

A FastDNA Spin kit for Soil (MP Biomedicals, OH, USA) was used to extract the genomic DNA. After being checked with agarose gel electrophoresis and spectrophotometer analysis, the eligible DNA was utilized to investigate the abundance of the *nirK*-type and *nirS*-type denitrifying bacterial communities during the green tide. The *nirK* and *nirS* genes were amplified separately using the primer pairs F1aCu (5'-ATC ATG GTS CTG CCG CG) and R3Cu (5'-GCC TCG ATC AGR TTG TGG TT), cd3aF (5'-GTS AAC GTS AAG GAR ACS GG) and R3cd (5'-GAS TTC GGR TGS GTC TTG A) (Hallin and Lindgren, 1999; Throbäck et al., 2004). The amplification started with a 10-minute activation at 95°C, followed by 40 cycles of 30 seconds at 95°C, 30 seconds at 55°C for the *nirK* gene (or 30 seconds at 53°C for the *nirS* gene) and 45 seconds at 72°C. The melting stage was added after amplification. The standard curve was generated by the quantification of the serially diluted standard plasmids containing the *nirK* or *nirS* gene. Each reaction was comprised of 10 μL FastStart Universal SYBR Green Master (ROX) (Roche, Germany), 0.3 μM forward primer, 0.3 μM reverse primer, 0.2 μg/μL bovine serum albumin (BSA) and 2.0 μL standard plasmid. All qPCR reactions were run in triplicate using SYBR Green I method on an ABI PRISM 7500 Sequence Detection System (Applied Biosystems, CA). The abundance of the *nirK* and *nirS* genes was examined under the above-mentioned procedures, and each reaction contained standard plasmids and negative controls to confirm an uncontaminated and stable amplification reaction.

Illumina Miseq sequencing analysis and sequence processing

The variations of the *nirK*-type and *nirS*-type denitrifying bacterial communities during the green tide were investigated by Illumina Miseq sequencing approach. The *nirK* and *nirS* genes were amplified with the specific primer pairs F1aCu/R3Cu and cd3aF/R3cd, respectively. Then, the amplicons were sequenced on an Illumina Miseq platform (Majorbio, Shanghai, China)

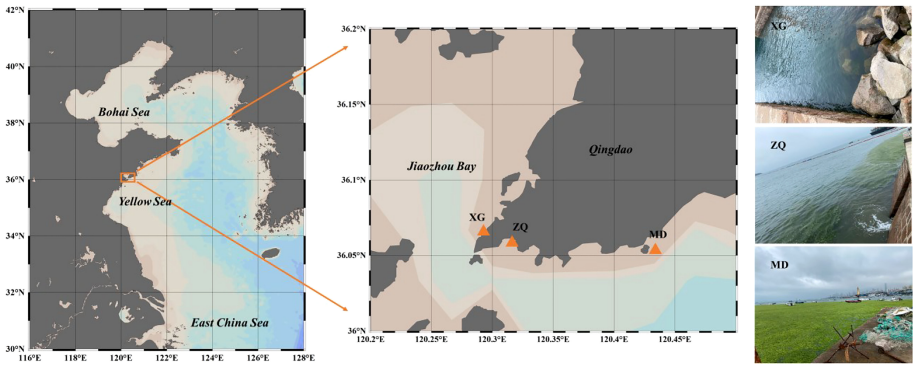

FIGURE 1
Locations of sampling stations chosen in coastal Qingdao areas during an *U. prolifera* green tide, and the right panel was the photos captured on 11 July, 2019 at three sampling stations.

after visualization, purification and quantification. Raw reads were submitted to the Sequence Read Archive (SRA) database of the National Center for Biotechnology Information (NCBI) under the accession numbers PRJNA781861 (*nirK* gene) and PRJNA781658 (*nirS* gene).

Raw reads were merged with Fast Length Adjustment of Short reads software (FLASH, version 1.2.11), and reads with overlap shorter than 10 bp and mismatch ratio less than 0.2 were removed (Magoč and Salzberg, 2011). Quantitative Insights into Microbial Ecology (QIIME, version 1.9.1) was used to screen the merged sequences (Caporaso et al., 2010). Operational taxonomic units (OTUs) were clustered using UPARSE software (version 7.0.1090) with a 97% sequence similarity cutoff, and chimeric sequences were examined and removed at the same time (Edgar, 2013). The most abundant sequence in each OTU was chosen as representative sequence, and then assigned by RDP classifier against the NCBI nr/nt database (ftp://ftp.ncbi.nih.gov/blast/db) to acquire the taxonomic information with a confidence level greater than 70%.

Statistical analysis

QIIME was used to calculate the Alpha-diversity of the *nirK*-type and *nirS*-type denitrifying bacterial communities, including Chao1 richness estimator, Shannon index and Good's coverage. The differences in the denitrifying bacterial community structure during the green tide were investigated with principal components analysis (PCA). Correlations of abundance, richness, diversity and relative abundance of dominant taxa with physicochemical factors was estimated with SPSS software (version 26). After variance inflation factor (VIF) analysis, distance-based redundancy analysis (db-RDA) was utilized to assess the influence of physicochemical factors on the denitrifying bacterial communities during the green tide. Variations of the denitrifying bacterial communities during the green tide, including abundance, richness, diversity and relative abundance of dominant taxa, were evaluated with one-way analysis of variance (ANOVA).

Six categories of co-occurrence network were established in this study, including (i) the denitrifying bacterial networks during the green tide, the outbreak phase and the decline phase; (ii) the denitrifying bacterial networks at station XG, ZQ and MD; (iii) the *nirK*-type denitrifying bacterial networks during the green tide, the outbreak phase and the decline phase; (iv) the *nirK*-type denitrifying bacterial networks at station XG, ZQ and MD; (v) the *nirS*-type denitrifying bacterial networks during the green tide, the outbreak phase and the decline phase; (vi) the *nirS*-type denitrifying bacterial networks at station XG, ZQ and MD. Only OTUs that occur in more than 25% of all samples were displayed. The OTUs that were statistically significant ($P < 0.01$ and $Q < 0.05$) and had a spearman's coefficient greater than |0.6| were subjected to further analysis using "fdrtool" and "igraph" packages of the R statistical software (version 4.0.4). The visualization of co-occurrence networks and the calculation of topological properties were generated with Gephi (version 0.9.2).

Results

Alpha-diversity of denitrifying bacterial communities

In total, we obtained 550946 and 641853 high-quality *nirK* and *nirS* gene sequences with average lengths of 425 bp and 371 bp, respectively. With a 97% sequence similarity cutoff, the high-quality sequences were clustered into 359 *nirK*-type denitrifying bacterial OTUs and 491 *nirS*-type denitrifying bacterial OTUs. Good's coverage of the *nirK*-type and *nirS*-type denitrifying bacterial communities across all samples was greater than 99.29%, indicating that this study covered the majority of *nirK*-type and *nirS*-type denitrifying bacteria in our studied areas.

Alpha-diversity of the *nirK*-type and *nirS*-type denitrifying bacterial communities was shown in Table 1. During the green tide, the Chao1 richness estimator of the *nirK*-type and *nirS*-type denitrifying bacterial communities ranged from 72.00 to 258.00 and 71.81 to 351.63, while the corresponding Shannon index ranged from 1.25 to 3.97 and 0.28 to 3.91, respectively. Overall, the richness of the *nirS*-type denitrifying bacterial community was significantly greater than that of the *nirK*-type denitrifying bacterial community during the green tide ($P < 0.01$); for the Shannon index, the average value of the *nirK*-type denitrifying bacterial community was greater, but not significantly ($P > 0.05$).

The Chao1 richness of the *nirK*-type and *nirS*-type denitrifying bacterial communities varied from 117.50 to 258.00 and 127.86 to 351.63 during the outbreak phase, and from 72.00 to 236.88 and 71.81 to 295.31 during the decline phase, respectively. During the outbreak phase, the Shannon diversity of the *nirK*-type and *nirS*-type denitrifying bacterial communities separately varied from 2.15 to 3.95 and 1.65 to 3.91, while during the decline phase, it ranged from 1.25 to 3.97 and 0.28 to 3.90, respectively. The Chao1 richness of the *nirK*-type and *nirS*-type denitrifying bacteria exhibited comparable tendencies during the green tide, with a greater community richness during the outbreak phase. Similar trends have also been observed on variations in community diversity of the *nirK*-type and *nirS*-type denitrifying bacteria. This finding revealed that the outbreak phase may be beneficial to increase the community richness and diversity of denitrifying bacteria.

The Chao1 richness of the *nirK*-type denitrifying bacterial community separately ranged from 115.43 to 236.88 at station

10.3389/fmars.2022.1063585

TABLE 1 Alpha-diversity of the *nirK*-type and *nirS*-type denitrifying bacterial communities during the green tide in Qingdao coastal areas.

	the *nirK*-type denitrifying bacteria			the *nirS*-type denitrifying bacteria		
	OTUs	Chao1	Shannon	OTUs	Chao1	Shannon
XG0613	131	145.44	3.10	177	204.35	2.70
XG0627	130	135.69	3.07	137	157.00	2.49
XG0711	112	128.24	2.41	178	200.04	2.56
XG0718	119	166.57	2.15	129	184.25	1.65
XG0722	144	194.17	2.42	176	212.67	2.24
XG0806	98	115.65	2.16	160	209.04	1.89
XG0816	191	236.88	3.52	205	249.72	2.28
XG0823	131	183.50	2.73	234	280.94	2.94
XG0829	137	205.33	2.65	235	294.00	3.44
XG0905	91	115.43	2.44	241	264.43	3.52
ZQ0613	158	165.50	3.67	155	161.60	3.56
ZQ0627	145	173.05	3.17	239	284.93	3.16
ZQ0711	170	205.04	3.48	298	351.63	3.84
ZQ0718	187	201.50	3.73	218	277.76	2.56
ZQ0722	216	258.00	3.95	244	301.12	3.42
ZQ0806	159	192.91	3.25	209	276.00	2.73
ZQ0816	76	142.43	1.93	146	197.04	1.72
ZQ0823	175	181.48	3.97	186	194.75	3.90
ZQ0829	122	157.05	1.25	262	276.27	3.61
ZQ0905	171	208.43	3.07	276	295.31	3.28
MD0613	137	141.77	3.21	197	206.00	3.64
MD0627	113	117.50	3.24	120	127.86	3.91
MD0711	149	196.25	3.44	170	177.43	3.37
MD0718	216	255.52	3.73	248	276.83	2.57
MD0722	199	221.97	3.68	243	250.92	3.90
MD0806	184	231.12	3.20	217	292.00	2.23
MD0823	53	72.00	1.34	75	80.63	0.99
MD0829	97	191.60	2.02	56	71.81	0.31
MD0905	108	147.18	2.20	58	132.38	0.28

XG, 142.43 to 258.00 at station ZQ, and 72.00 to 255.52 at station MD. The Shannon diversity of the *nirK*-type denitrifying bacterial community varied from 2.15 to 3.52 at station XG, 1.25 to 3.97 at station ZQ, and 1.34 to 3.73 at station MD, respectively. For the *nirS*-type denitrifying bacteria, the community richness separately ranged from 157.00 to 294.00 at station XG, 161.60 to 351.63 at station ZQ, and 71.81 to 292.00 at station MD; and the community diversity varied from 1.65 to 3.52 at station XG, 1.72 to 3.90 at station ZQ, and 0.28 to 3.91 at station MD, respectively. During the green tide, the *nirK*-type denitrifying bacteria had the lowest community Alpha-diversity at station XG and the highest at station ZQ, while the richness and diversity of the *nirS*-type denitrifying bacterial community exhibited the lowest average value at station MD and the highest average value at station ZQ. ANOVA analysis revealed that except for the community richness of the *nirS*-type denitrifying bacteria ($P < 0.05$), the community Alpha-diversity of the *nirK*-type denitrifying bacteria and the community diversity of the *nirS*-type denitrifying bacteria did not differ significantly among sampling stations ($P > 0.05$).

Composition and structure of denitrifying bacterial communities

Proteobacteria were the dominant phylum of the *nirK*-type and *nirS*-type denitrifying bacterial communities. *Alphaproteobacteria* and *Gammaproteobacteria* accounted for 59.28% and 34.98% of the total sequences in *Proteobacteria* for the *nirK*-type and *nirS*-type denitrifying bacteria, respectively. The compositions of the *nirK*-type and *nirS*-type denitrifying bacterial communities were studied at the family level in this study. The *nirK*-type denitrifying bacterial community was dominated by unclassified bacteria (9.28–90.55%), *Rhodobacteraceae* (0.99–46.69%), unclassified *Proteobacteria* (0.20–81.38%), unclassified *Alphaproteobacteria* (0.14–35.77%),

Pseudomonadaceae (0.00–28.16%), *Bradyrhizobiaceae* (0.00–1.44%) and unclassified *Rhizobiales* (0.00–1.81%) during the green tide (Figure 2A). *Rhodobacteraceae* ($P < 0.01$) and unclassified *Alphaproteobacteria* ($P > 0.05$) exhibited greater relative abundance during the outbreak phase, whereas unclassified bacteria ($P > 0.05$), unclassified *Proteobacteria* ($P < 0.05$) and *Pseudomonadaceae* ($P > 0.05$) were more abundant during the decline phase. Sampling stations may also have an effect on the *nirK*-type denitrifying bacterial community, and markedly influenced the relative abundance of unclassified bacteria ($P < 0.05$) and unclassified *Alphaproteobacteria* ($P < 0.01$) during the green tide.

The dominant *nirS*-type denitrifying bacterial community was comprised of unclassified *Proteobacteria* (1.68–86.92%), unclassified bacteria (2.89–97.86%), *Halomonadaceae* (0.00–55.00%), *Pseudomonadaceae* (0.02–55.41%), *Rhodobacteraceae* (0.08–36.06%) and unclassified *Gammaproteobacteria* (0.01–48.92%), and to a lesser extent, unclassified *Alphaproteobacteria* (0.00–2.04%), unclassified *Betaproteobacteria* (0.01–2.66%), *Rhodocyclaceae* (0.00–2.87%) and *Comamonadaceae* (0.00–1.46%, Figure 2B). Greater proportions of unclassified *Proteobacteria*, *Halomonadaceae*, *Pseudomonadaceae*, *Rhodobacteraceae*, unclassified *Betaproteobacteria* and *Comamonadaceae* were observed during the outbreak phase; in contrast, unclassified bacteria, unclassified *Gammaproteobacteria* and unclassified *Alphaproteobacteria* displayed greater average relative abundance during the decline phase. Only the relative abundance of unclassified bacteria differed significantly between the outbreak phase and the decline phase ($P < 0.05$). The sampling stations had a significant impact on the relative abundance of *Rhodobacteraceae* ($P < 0.01$) and unclassified *Alphaproteobacteria* ($P < 0.05$).

PCA was employed to examine the differences in denitrifying bacterial community structure during the green tide at the OTU level (Figure 3). Bloom phases had considerable impacts on both the *nirK*-type ($P < 0.01$, $R = 0.32$) and *nirS*-type ($P < 0.01$, $R = 0.16$) denitrifying bacterial communities, with the *nirK*-type denitrifying bacterial community having the most impact. Furthermore, sampling stations may influence both the *nirK*-type ($P < 0.05$, $R = 0.28$) and *nirS*-type ($P < 0.05$, $R = 0.25$) denitrifying bacterial communities, notably the *nirK*-type denitrifying bacterial community. Thus, it is possible to conclude that the *nirK*-type denitrifying bacteria may be more sensitive to the green tide.

Abundance of denitrifying bacterial communities

The abundance of the *nirK* and *nirS* genes ranged from 1.72×10^3 to 1.18×10^6 copies/L and 2.31×10^3 to 2.19×10^6 copies/L during the green tide, respectively (Figure 4). The *nirK* gene was more abundant during the outbreak phase than the decline

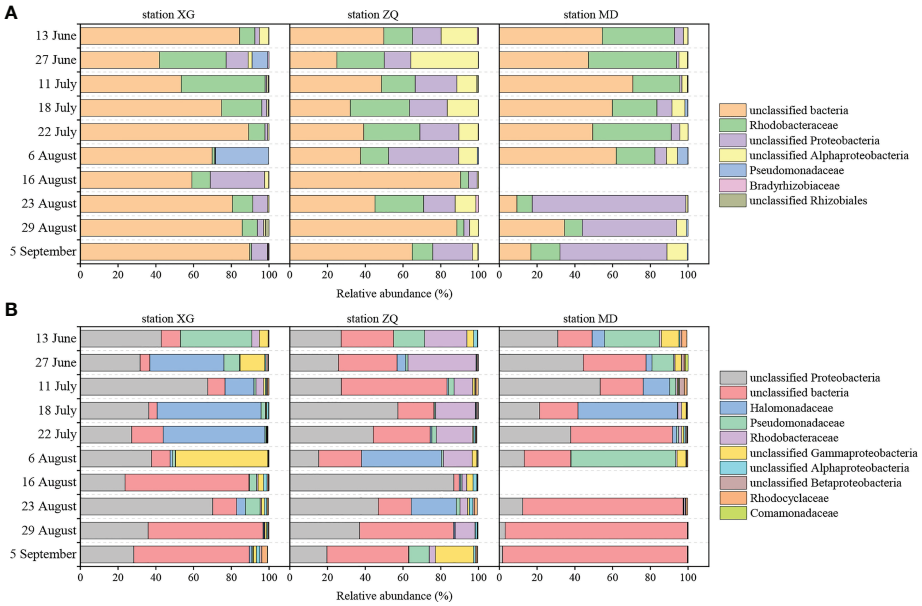

FIGURE 2
Relative abundance of the dominant *nirK*-type **(A)** and *nirS*-type **(B)** denitrifying bacteria (relative abundance greater than 1%) at the family level during the green tide in coastal Qingdao areas. Due to the failure of the *nirK* and *nirS* gene amplicon library construction on 16 August at station MD, the relevant community information was shown as blanks in the Figure.

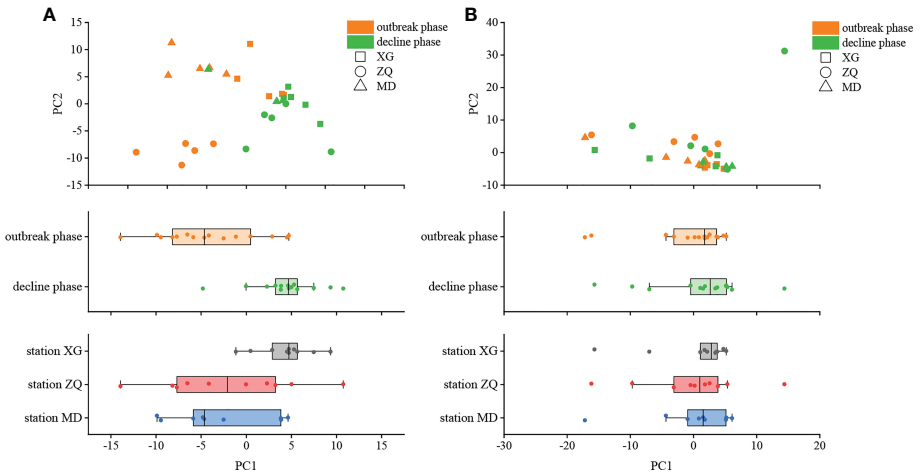

FIGURE 3
Principal component analysis (PCA) of the *nirK*-type **(A)** and *nirS*-type **(B)** denitrifying bacterial communities during the green tide in coastal Qingdao areas.

phase, while the *nirS* gene exhibited greater abundance during the decline phase, according to our data, but ANOVA analysis revealed no significant difference in the abundance of the *nirK* and *nirS* genes between the outbreak phase and the decline phase ($P > 0.05$). Meanwhile, we discovered that the abundance of the *nirK* and *nirS* genes followed a similar pattern across sampling stations, with lower abundance at station XG which was less likely to be influenced by the green tide, and greater abundance at station ZQ and MD which were significantly affected by the green tide. ANOVA analysis revealed that there were no obvious differences in the abundance of the *nirK* and *nirS* genes among sampling stations ($P > 0.05$).

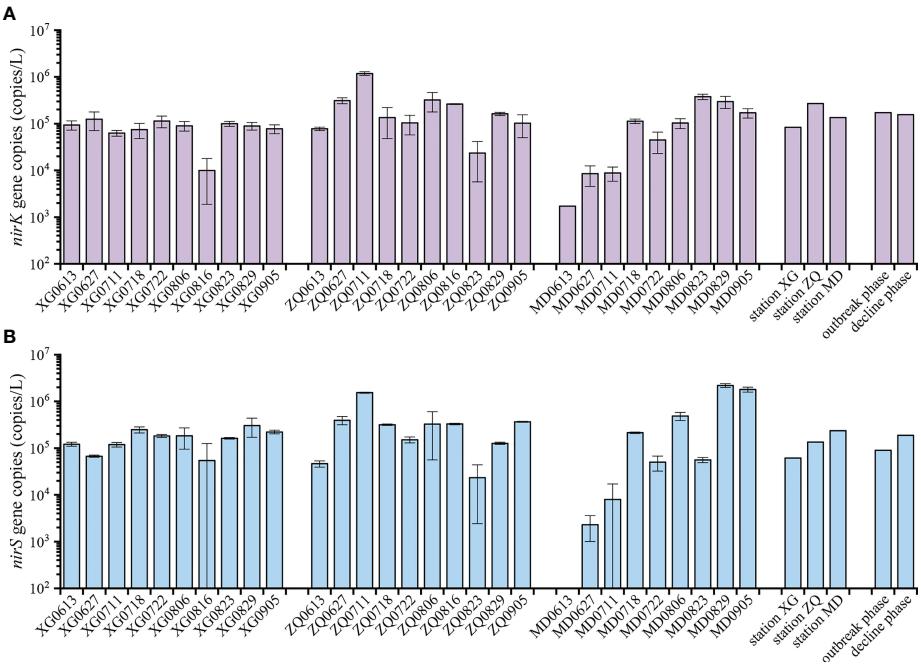

FIGURE 4
Quantitative analysis of the *nirK* **(A)** and *nirS* **(B)** genes during the green tide in coastal Qingdao areas.

Links between the denitrifying bacterial communities and physicochemical factors

Distance-based redundancy analysis (db-RDA) was used to illustrate the links between physicochemical factors and the denitrifying bacterial communities at the OTU level. The *nirK*-type denitrifying bacterial community structure was strongly related to chl*a* content (R^2 = 0.37, P < 0.01), salinity (R^2 = 0.30, P < 0.05) and DO content (R^2 = 0.25, P < 0.05), and the *nirS*-type denitrifying bacterial community structure was likewise clearly associated with salinity (R^2 = 0.32, P < 0.05), DO content (R^2 = 0.31, P < 0.05) and chl*a* content (R^2 = 0.28, P < 0.05) (Figure 5). Chl*a* content is an important indicator of phytoplankton biomass and eutrophication level. According to the results of Spearman correlation analysis, chl*a* content affected the denitrifying bacterial communities mostly through impacting the relative abundance of dominant taxa. For the *nirK*-type denitrifying bacterial community, chl*a* content had a substantial effect on the relative abundance of unclassified *Alphaproteobacteria* (R = 0.512, P < 0.05) during the green tide (Figure 6; Supplementary Figure 2). In regard to the *nirS*-type denitrifying bacterial community, chl*a* content correlated significantly with the relative abundance of *Rhodobacteraceae* (R = 0.532, P < 0.05) and unclassified *Gammaproteobacteria* (R = -0.556, P < 0.05) during the green tide, and was clearly related to the relative abundance of unclassified bacteria (R = 0.881, P < 0.01) and unclassified *Gammaproteobacteria* (R = -0.790, P < 0.05) during the outbreak phase (Figure 6; Supplementary Figure 3). Furthermore, chl*a* content may influence the Alpha-diversity of the denitrifying bacterial communities. In the current study, however, only the Chao1 richness of the *nirK*-type (R = 0.905, P < 0.01) and *nirS*-type (R = 0.857, P < 0.01) denitrifying bacterial communities during the outbreak phase was clearly linked with chl*a* content.

In addition, Spearman correlation analysis was also conducted to explore the associations of abundance, Alpha-diversity and relative abundance of dominant taxa with other physicochemical factors (Supplementary Figure 4). For the *nirK*-type denitrifying bacterial community during the green tide, *Rhodobacteraceae* was clearly correlated with temperature (R = -0.57, P < 0.01), NO_2^- concentration (R = -0.56, P < 0.01), NO_3^- concentration (R = -0.52, P < 0.01) and NO_x^- concentration (R = -0.52, P < 0.01); unclassified *Proteobacteria* and unclassified *Alphaproteobacteria* were positively related to DIN concentration (R = 0.41, P < 0.05) and salinity (R = 0.43, P < 0.05), respectively; unclassified *Rhizobiales* was negatively correlated with temperature (R = -0.44, P < 0.05). During the outbreak phase, temperature (R = 0.76, P < 0.01) was clearly associated with the Chao1 richness of the *nirK*-type denitrifying bacterial community, and the abundance of the *nirK* gene was negatively related to DO content (R = -0.71, P < 0.01). During the decline phase, the abundance of the *nirK* gene was clearly associated with NO_2^- concentration (R = -0.66, P < 0.01), NO_3^- concentration (R = -0.55, P < 0.05) and NO_x^- concentration (R = -0.55, P < 0.05); *Pseudomonadaceae*, *Bradyrhizobiaceae* and unclassified *Rhizobiales* were the major *nirK*-type denitrifying bacteria, and were strongly related to pH (R = -0.56, P < 0.05), NO_2^- concentration (R = 0.56, P < 0.05) and salinity (R = -0.69, P < 0.01), respectively. In regard to the *nirS*-type denitrifying bacterial community during the green tide, Shannon diversity was related to pH (R = 0.53, P < 0.01); *Pseudomonadaceae* (R = -0.52, P < 0.01), unclassified *Gammaproteobacteria* (R = -0.37, P < 0.05) and unclassified *Betaproteobacteria* (R = -0.37, P < 0.05) were negatively related to temperature; and *Rhodobacteraceae* was strongly related to salinity (R = 0.51, P < 0.01), NO_2^- concentration (R = -0.43, P < 0.05), NO_3^- concentration (R = -0.43, P < 0.05) and NO_x^- concentration (R = -0.43, P < 0.05). Numerous physicochemical factors had discernible effects on the abundance,

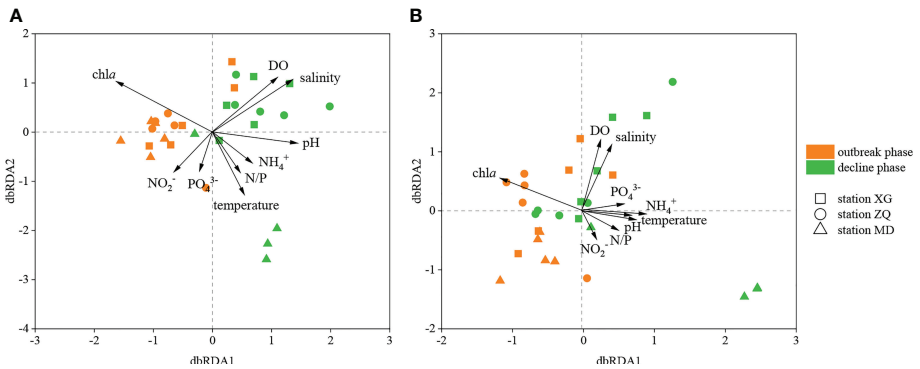

FIGURE 5
db-RDA analysis of the *nirK*-type **(A)** and *nirS*-type **(B)** denitrifying bacterial communities with physicochemical factors during the green tide in coastal Qingdao areas.

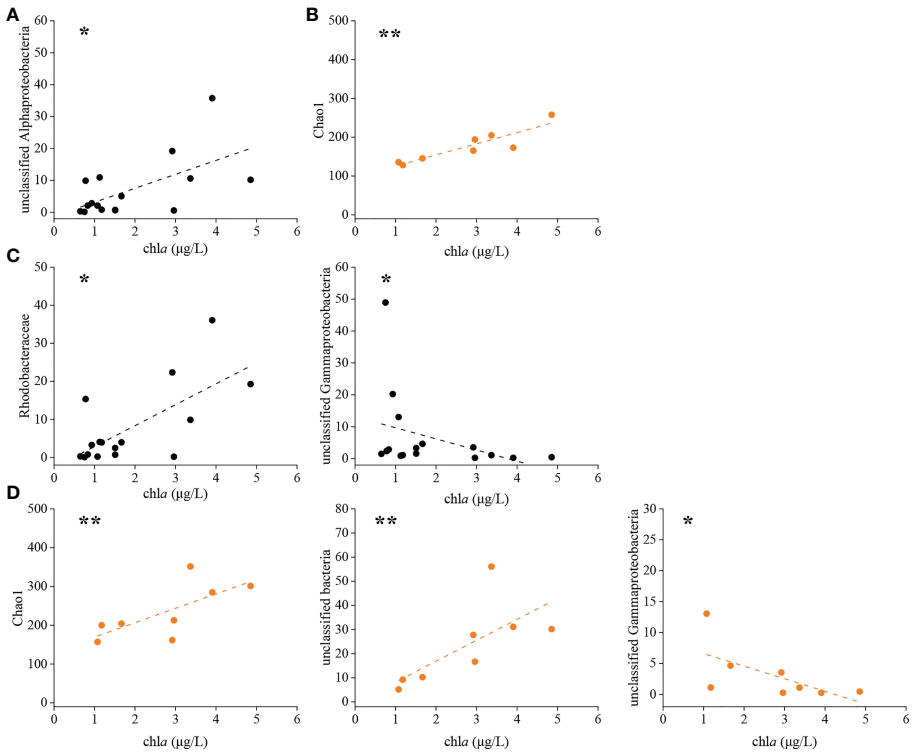

FIGURE 6
Significant relationships between chl*a* content and the *nirK*-type denitrifying bacterial community during the green tide **(A)** and the outbreak phase **(B)**, and the *nirS*-type denitrifying bacterial community during the green tide **(C)** and the outbreak phase **(D)**. *P < 0.05, **P < 0.01.

Alpha-diversity and dominant taxon of the *nirS*-type denitrifying bacterial community during the outbreak phase, for example, temperature (R = 0.59, P < 0.05) had a significant impact on the Chao1 richness, whereas pH (R = 0.64, P < 0.05), DO content (R = 0.58, P < 0.05) and NO_2^- concentration (R = -0.56, P < 0.05) were critical to the Shannon diversity; *Pseudomonadaceae* was significantly related to temperature (R = -0.73, P < 0.01), salinity (R = 0.78, P < 0.01) and pH (R = 0.60, P < 0.05); *Rhodocyclaceae* was markedly connected to NO_2^- concentration (R = -0.78, P < 0.01), NO_3^- concentration (R = -0.72, P < 0.01) and NO_x^- concentration (R = -0.73, P < 0.01). During the decline phase, unclassified *Proteobacteria* and unclassified *Gammaproteobacteria* were respectively shown to be negatively related to NH_4^+ concentration (R = -0.58, P < 0.05) and temperature (R = -0.54, P < 0.05), whereas unclassified bacteria was found to be significantly related to NH_4^+ concentration (R = 0.58, P < 0.05) and DIN concentration (R = 0.58, P < 0.05).

Co-occurrence network analysis of denitrifying bacteria

Networks were constructed to explore the co-occurrence patterns of denitrifying bacteria during the green tide, the outbreak phase and the decline phase. The majority of correlations in the networks were positive, indicating that mutualism may be the most important interaction among denitrifying bacteria during the green tide, as well as the outbreak phase and the decline phase (Figure 7). Meanwhile, we discovered that the nodes and edges in network of the outbreak phase (450 and 1702) were greater than those in network of the decline phase (436 and 1221), indicating a more complex denitrifying bacterial co-occurrence network during the outbreak phase (Figures 7B, C). The modularity of network was 0.517 and 0.710 during the outbreak phase and the decline phase, implying a more modular denitrifying bacterial network during the decline phase. Thus, a more complex and less modular denitrifying bacterial network was observed during the outbreak phase. Moreover, the nodes with greater relative abundance in each module were specific to a particular phase, for example, the majority of OTUs in module 6 had greater relative abundance during the outbreak phase, whereas most of OTUs in module 1 exhibited relatively greater abundance during the decline phase (Figure 7A).

The *nirK*-type denitrifying bacterial networks during the outbreak phase and the decline phase were separately built to discern the differences in microbial interactions between bloom phases, and the same analysis was also performed on the *nirS*-

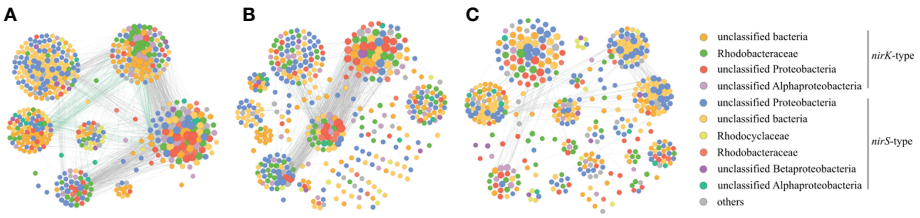

FIGURE 7
Co-occurrence networks of the denitrifying bacteria during the green tide **(A)**, the outbreak phase **(B)** and the decline phase **(C)** in coastal Qingdao areas.

denitrifying bacteria in the current study. For the *nirK*-type denitrifying bacteria, the nodes and edges in network of the outbreak phase (208 and 797) were greater than those in network of the decline phase (169 and 371), indicating that the *nirK*-type denitrifying bacterial network was more complex during the outbreak phase (Table 2; Figure 8). The modularity of the network was 0.524 and 0.682 during the outbreak phase and the decline phase, respectively, implying that a more modular *nirK*-type denitrifying bacterial network was observed during the decline phase. In comparison to the outbreak phase, the network of the decline phase had lower average degree (5.549 versus 3.643), lower graph density (0.037 versus 0.026), lower clustering coefficient (0.528 versus 0.440) and longer path length (4.771 versus 5.555), suggesting a more associated *nirK*-type denitrifying bacterial network during the outbreak phase. As a result, the *nirK*-type denitrifying bacterial community may be more complex, more associated and less modular during the outbreak phase than the decline phase.

The *nirS*-type denitrifying bacterial network contained 182 nodes and 337 edges during the outbreak phase, and 264 nodes and 908 edges during the decline phase (Table 2; Figure 8). In comparison to the decline phase, the network of the *nirS*-type denitrifying bacteria exhibited lower average degree (3.101 versus 5.688), longer path length (5.835 versus 4.929), lower graph density (0.020 versus 0.026), lower clustering coefficient (0.423 versus 0.455) and greater modularity (0.683 versus 0.618) during the outbreak phase. All of these characters manifested that the *nirS*-type denitrifying bacterial community was less complex, less associated and more modular during the outbreak phase than the decline phase. In comparison to the *nirK*-type denitrifying bacterial network, the *nirS*-type denitrifying bacterial network had more nodes (224 versus 261), more edges (1016 versus 1454), lower average degree (7.679 versus 5.049), lower clustering coefficient (0.514 versus 0.386) and longer path length (3.513 versus 3.687), indicating that *nirS*-type denitrifying bacterial network was more complex and associated than the *nirK*-type denitrifying bacterial network during the green tide. Taken together, it is hypothesized that the *nirK*-type and *nirS*-type denitrifying bacteria behave differently to the *U. prolifera* green tide, and may occupy different niches during the green tide in coastal Qingdao areas.

In addition, we also constructed the denitrifying bacterial networks, the *nirK*-type denitrifying bacterial networks and the *nirS*-type denitrifying bacterial networks at three sampling stations, respectively. The nodes and edges of the denitrifying bacterial network at station XG were less than those at two other stations, and the proportions of negative links at station XG were also less than those at two other stations, indicating that the

TABLE 2 Topological properties of the denitrifying bacterial co-occurrence networks during the green tide in coastal Qingdao areas.

	the *nirK*-type denitrifying bacteria		the *nirS*-type denitrifying bacteria	
	outbreak phase	**decline phase**	**outbreak phase**	**decline phase**
nodes	208	169	182	264
edges	797	371	337	908
average degree	5.549	3.643	3.101	5.688
network diameter	13	17	16	15
graph density	0.037	0.026	0.020	0.026
average clustering coefficient	0.528	0.440	0.423	0.455
average path length	4.771	5.555	5.835	4.927
modularity	0.524	0.682	0.696	0.618
modules	29	19	38	22

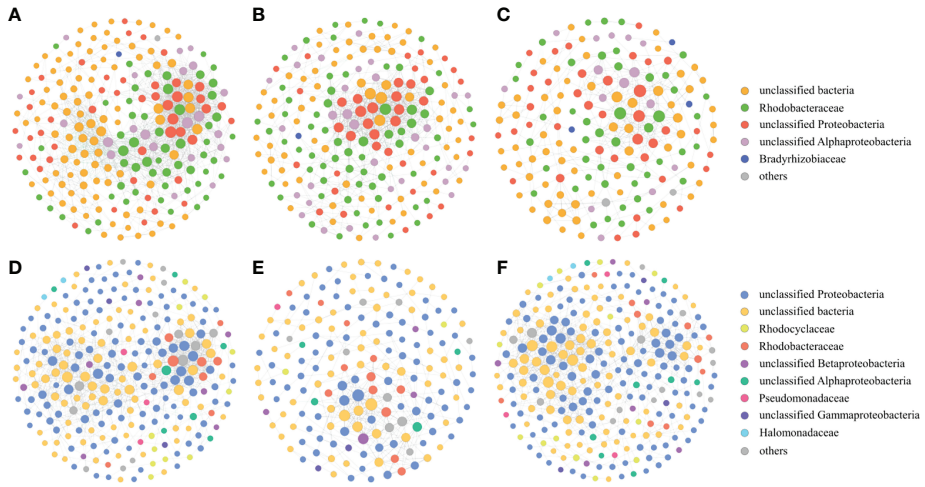

FIGURE 8
Co-occurrence networks of the *nirK*-type denitrifying bacteria during the green tide **(A)**, the outbreak phase **(B)** and the decline phase **(C)**, and co-occurrence networks of the *nirS*-type denitrifying bacteria during the green tide **(D)**, the outbreak phase **(E)** and the decline phase **(F)**.

denitrifying bacterial network was more complex and stable at station ZQ and MD which were greatly impacted by the green tide (Figures 9A–C). Both the *nirK*-type denitrifying bacterial networks and *nirS*-type denitrifying bacterial networks displayed a similar trend across sampling stations, with greater complexity and stability networks at station ZQ and MD (Figures 9D–I).

Discussion

Through Illumina Miseq sequencing, we explored variations of the *nirK*-type and *nirS*-type denitrifying bacterial communities during an *U. prolifera* green tide in coastal Qingdao areas. Chen et al. (2020) pointed out that a higher sequence similarity cutoff level may be preferable for obtaining more accurate and reliable information on community compositions and structures, so a 97% clustering level was used in the current study to investigate the community characteristics of denitrifying bacteria. According to our results, the structure and diversity of denitrifying bacterial communities, as well as the organization and structure of microbial co-occurrence networks, varied during an *U. prolifera* green tide in coastal Qingdao areas. Furthermore, we noticed that the *nirK*-type and *nirS*-type denitrifying bacteria respond differently to the green tide, implying that they may occupy different niches during the green tide in coastal Qingdao areas.

Salinity, DO content and chl*a* content were the most important factors influencing the structure of the *nirK*-type and *nirS*-type denitrifying bacterial communities during the green tide (Figure 5). Salinity strongly contributed to the *nirK*-type and *nirS*-type denitrifying bacterial communities during the green tide, which was consistent with previous reports on the dominant position of salinity in shaping the denitrifying bacterial community structure (Abell et al., 2010; Francis et al., 2013; Zheng et al., 2015). DO content has also been proven to be an important element in determining the structure of the denitrifying bacterial communities (Liu et al., 2003; Hanning et al., 2006). In the processes of green tide, rapid photosynthesis of *U. prolifera* during daytime could increase the DO content in seawater, whereas respiration of *U. prolifera* at night, as well as accumulation and decomposition of *U. prolifera*, could consume the DO content in seawater, resulting in the changes of DO content in seawater and further leading to the variations of the denitrifying bacterial community structure and abundance during the green tide. Variations of the denitrifying bacterial communities could also be explained by chl*a* content. Significant positive correlations between chl*a* content and denitrifying bacterial community structure were observed in the current study during the outbreak phase, probably because the high density of *U. prolifera* at this phase provides superior conditions for the growth and metabolism of denitrifying bacteria, which was consistent with the previous result conducted by Chen et al. (2016). In addition, other physicochemical factors, such as temperature, NO_2^- concentration and NO_3^- concentration, can influence the denitrifying bacterial communities. Temperature sensitivity differed among denitrifying bacterial taxa, indicating that temperature has a significant impact on the community structure of denitrifying bacteria, mostly through impacting their growth rate and metabolic activity. Temperature fluctuations may be one of the factors influencing the structure and diversity of the denitrifying bacterial communities in the

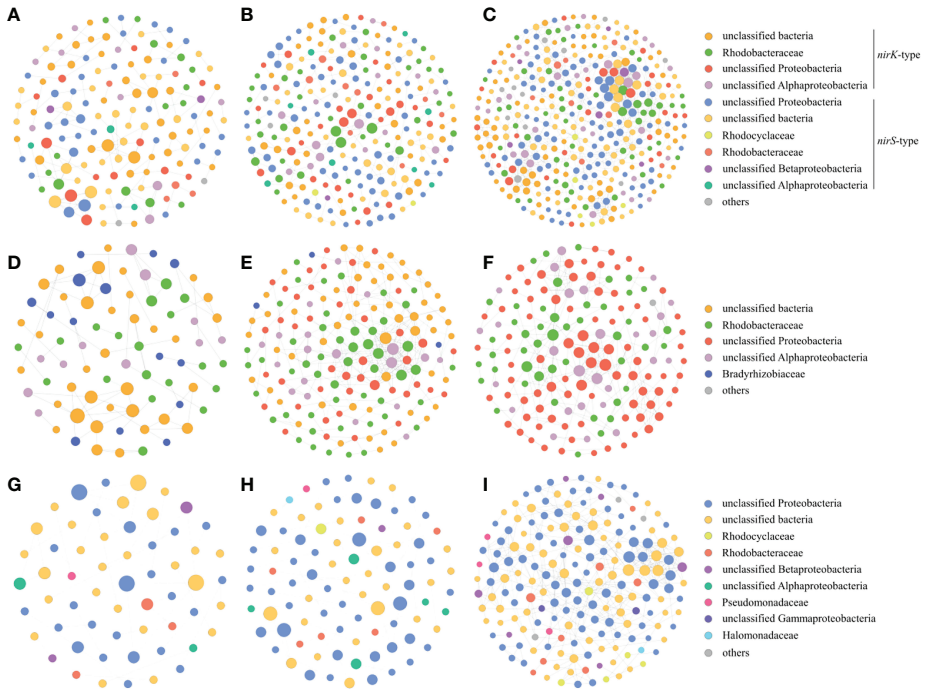

FIGURE 9
Co-occurrence networks of the denitrifying bacteria during the green tide **(A)**, the outbreak phase **(B)** and the decline phase **(C)**, co-occurrence networks of the *nirK*-type denitrifying bacteria during the green tide **(D)**, the outbreak phase **(E)** and the decline phase **(F)**, and co-occurrence networks of the *nirS*-type denitrifying bacteria during the green tide **(G)**, the outbreak phase **(H)** and the decline phase **(I)**.

current study (Supplementary Figure 4). As the substrate supply and electron acceptor of denitrification, NO_2^- and NO_3^- concentrations were regarded as critical factors influencing the denitrifying bacterial communities. In this study, we discovered that NO_2^- and NO_3^- concentrations have observable effects on the denitrifying bacterial communities, and comparable results have been seen in the pelagial of the central Baltic Sea and the San Francisco Bay (Hanning et al., 2006; Lee and Francis, 2017).

Three sampling stations were chosen in order to analyze how the impact degree of green tides influenced the denitrifying bacterial networks and community characteristics in different region of coastal Qingdao areas. The denitrifying bacteria's community richness, diversity and abundance, as well as their network complexity and stability, were greater at station ZQ and MD, suggesting that higher impact degree of green tide might result in higher community richness, community diversity, community abundance, and network complexity and stability of the denitrifying bacteria. Based on the relevant analysis of the *nirK*-type and *nirS*-type denitrifying bacteria, similar results were obtained in this study.

All of the denitrifying bacteria identified in the current study were *Proteobacteria*. *Alphaproteobacteria* and *Gammaproteobacteria* accounted for 59.28% and 34.98% of the total sequences in *Proteobacteria* for the *nirK*-type and *nirS*-type denitrifying bacteria, respectively. At the family level, unclassified bacteria, *Rhodobacteraceae*, unclassified *Proteobacteria* and unclassified *Alphaproteobacteria* dominated the *nirK*-type denitrifying bacterial community, and the dominant *nirS*-type denitrifying bacterial community was comprised of unclassified *Proteobacteria*, unclassified bacteria, *Halomonadaceae*, *Pseudomonadaceae* and *Rhodobacteraceae* (Figure 2). According to our findings, the outbreak phase may benefit the richness and diversity of denitrifying bacterial communities (Table 1). During the outbreak phase, the community richness of the *nirK*-type and *nirS*-type denitrifying bacteria was strongly positively related to chl*a* content which is an essential indicator of phytoplankton biomass ($P < 0.01$), according to the results of Spearman correlation analysis (Figure 6). The accumulation of *U. prolifera* may lead to a high nitrogen and low oxygen environment suitable for the growth of denitrifying bacteria, which may explain their greater community richness and diversity during the outbreak phase (Lin et al., 2017; Qu et al., 2020). The abundance of the *nirK* and *nirS* genes also displayed different patterns between the outbreak phase and the decline phase, with a higher abundance of the *nirK* gene during the outbreak phase but the *nirS* gene being more abundant during the decline phase (Figure 4). During the green tide, both bloom phases and sampling stations influenced the *nirK*-type and *nirS*-type denitrifying bacterial communities, but the effects varied.

Compared with the *nirS*-type denitrifying bacterial community, the *nirK*-type denitrifying bacterial community was well separated, both in terms of bloom phases and sampling stations, as validated by PCA analysis (Figure 3). These findings revealed that the *nirK*-type and *nirS*-type denitrifying bacteria behave differently to the green tide, and the *nirK*-type denitrifying bacteria may be more sensitive to the *U. prolifera* green tide in coastal Qingdao areas, which was consistent with previous reports (Jones et al., 2008; Yoshida et al., 2010).

For the denitrifying bacterial communities, the nodes and edges in network of the outbreak phase were greater than those in network of the decline phase (Figures 7B, C), which was consistent with the above result that a greater community richness and diversity was observed during the outbreak phase, indicating that the outbreak of green tide may increase not only the interactions among denitrifying bacteria, but also the complexity and stability of denitrifying bacterial networks. Moreover, greater proportions of negative links during the outbreak phase may enhance the stability of denitrifying bacterial communities under disturbances of the green tide, which was consistent with past observations that more negative interactions may mean more stable microbial networks and may help the microbial communities return to stability more quickly under disturbances (Coyte et al., 2015; de Vries et al., 2018).

Studies have shown that the topological properties of network can influence how microbial communities respond to environmental changes (de Vries et al., 2012; de Vries et al., 2018). The topological properties of the *nirK*-type denitrifying bacterial networks differed significantly between the outbreak phase and the decline phase, as did the *nirS*-type denitrifying bacterial networks (Table 2). Some topological properties of the *nirK*-type denitrifying bacterial networks, such as nodes, edges, average degree, average clustering coefficient and centrality, decreased from the outbreak phase to the decline phase, while others, such as average path length and modularity, increased. Topological properties of the *nirS*-type denitrifying bacterial networks, on the other hand, displayed the opposite trend from the outbreak phase to the decline phase when compared to the *nirK*-type denitrifying bacterial networks. As a result, the *nirK*-type denitrifying bacterial network possessed topological properties which indicated higher complexity, higher association and higher stability during the outbreak phase, whereas the *nirS*-type denitrifying bacterial network was more complex, more associated and more stable during the decline phase. In addition to the topological properties, the composition and structure of network also showed clear distinctions in both the *nirK*-type and *nirS*-type denitrifying bacteria during the green tide. Modules are clusters of closely connected microorganisms within communities, and more modules may be associated with stronger niche differentiation and greater community stability (Williams et al., 2014; Hou et al., 2018; Zhang et al., 2021b). The modules in the *nirK*-type denitrifying bacterial network were greater during the outbreak phase, whereas the modules of the *nirS*-type denitrifying bacterial network were greater during the decline phase (Table 2). Therefore, the *nirK*-type and *nirS*-type denitrifying bacteria displayed stronger niche differentiation and greater community stability during the outbreak phase and the decline phase, respectively. These results suggested that the *nirK*-type and *nirS*-type denitrifying bacteria respond differently to the green tide, and may display different environmental adaptation mechanisms during the green tide in coastal Qingdao areas. Some microorganisms with *nirK* and *nirS* genes, such as *Bradyrhizobium oligotrophicum* S58 (Sánchez and Minamisawa, 2018), have recently been discovered, and how these non-traditional denitrification pathways respond to the green tide warrants investigation. Meanwhile, N_2O is one of the important products in denitrification pathways, the impacts of green tide on N_2O emissions also need to be investigated further.

Conclusion

We studied the variations of the *nirK*-type and *nirS*-type denitrifying bacterial interactions and community characteristics during the green tide in coastal Qingdao areas in this study. According to our findings, the abundance, diversity and structure of the *nirK*-type and *nirS*-type denitrifying bacterial communities shifted during the green tide. The topological properties and organization of the *nirK*-type and *nirS*-type denitrifying bacterial networks have also changed during the green tide. During the outbreak phase, the *nirK*-type denitrifying bacteria displayed greater abundance, network complexity and network stability; whereas the *nirS*-type denitrifying bacteria exhibited greater abundance, network complexity and network stability during the decline phase. The *nirK*-type and *nirS*-type denitrifying bacteria respond differently to the green tide and may occupy different niches during the green tide in coastal Qingdao areas.

Data availability statement

The data presented in the study are deposited in the SRA repository, accession number PRJNA781861 and PRJNA781658.

Author contributions

GZ: investigation, methodology, data curation, formal analysis, and writing-original draft. HH: conceptualization, writing-review and editing, supervision, and funding acquisition. MY: methodology, and data curation. HW:

conceptualization, writing-review and editing, and supervision. HS: conceptualization, and supervision. MW: conceptualization, writing-review and editing, supervision, and funding acquisition. All authors contributed to the article and approved the submitted version.

Funding

This work was funded by the National Natural Science Foundation of China (Grant Nos. 41806131, 41976117, and 42120104006), and Fundamental Research Funds for the Central Universities (Grant No. 202172002).

Acknowledgments

We thanked Ding Zhang for the determination of physicochemical factors. We also appreciated the computing resources provided by IEMB-1, a high-performance computation cluster operated by the Institute of Evolution and Marine Biodiversity.

Conflict of interest

The authors declare that the research was conducted in the absence of any commercial or financial relationships that could be construed as a potential conflict of interest.

Publisher's note

Supplementary material

The Supplementary Material for this article can be found online at: https://www.frontiersin.org/articles/10.3389/fmars.2022.1063585/full#supplementary-material

References

Abell, G. C., Revill, A. T., Smith, C., Bissett, A. P., Volkman, J. K., and Robert, S. S. (2010). Archaeal ammonia oxidizers and nirS-type denitrifiers dominate sediment nitrifying and denitrifying populations in a subtropical macrotidal estuary. *ISME J.* 4, 286–300. doi: 10.1038/ismej.2009.105

Babbin, A. R., Keil, R. G., Devol, A. H., and Ward, B. B. (2014). Organic matter stoichiometry, flux, and oxygen control nitrogen loss in the ocean. *Science* 344, 406–408. doi: 10.1126/science.1248364

Bothe, H., Jost, G., Schloter, M., Ward, B. B., and Witzel, K. P. (2020). Molecular analysis of ammonia oxidation and denitrification in natural environments. *FEMS Microbiol. Rev.* 24 (5), 673-690. doi: 10.1111/j.1574-6976.2000.tb00566.x

Caporaso, J. G., Kuczynski, J., Stombaugh, J., Bittinger, K., Bushman, F. D., Costello, E. K., et al. (2010). QIIME allows analysis of high-throughput community sequence data. *Nat. Methods* 7 (5), 335–336. doi: 10.1038/nmeth.f.303

Chen, Q., Fan, J., Ming, H., Su, J., Wang, Y., and Wang, B. (2020). Effects of environmental factors on denitrifying bacteria and functional genes in sediments of bohai Sea, China. *Mar. Pollut. Bull.* 160, 111621. doi: 10.1016/j.marpolbul.2020.111621

Chen, X., Jiang, H., Sun, X., Zhu, Y., and Yang, L. (2016). Nitrification and denitrification by algae-attached and free-living microorganisms during a cyanobacterial bloom in lake taihu, a shallow eutrophic lake in China. *Biogeochemistry* 131, 135–146. doi: 10.1007/s10533-016-0271-z

Christensen, P. B., Rysgaard, S., Sloth, N. P., Dalsgaard, T., and Schwærter, S. (2000). Sediment mineralization, nutrient fluxes, denitrification and dissimilatory nitrate reduction to ammonium in an estuarine fjord with sea cage trout farms. *Aquat. Microb. Ecol.* 21, 73–84. doi: 10.3354/ame021073

Coyte, K. Z., Schluter, J., and Foster, K. R. (2015). The ecology of the microbiome: networks, competition, and stability. *Science* 350, 663–666. doi: 10.1126/science.aad2602

Dalsgaard, T., Thamdrup, B., and Canfield, D. E. (2005). Anaerobic ammonium oxidation (anammox) in the marine environment. *Res. Microbiol.* 156, 457–464. doi: 10.1016/j.resmic.2005.01.011

Dalsgaard, T., Thamdrup, B., Farias, L., and Revsbech, N. P. (2012). Anammox and denitrification in the oxygen minimum zone of the eastern south pacific. *Limnol. Oceanogr.* 57 (5), 1331–1346. doi: 10.4319/lo.2012.57.5.1331

de Vries, F. T., Griffiths, R. I., Bailey, M., Craig, H., Girlanda, M., Gweon, H. S., et al. (2018). Soil bacterial networks are less stable under drought than fungal networks. *Nat. Commun.* 9, 3033. doi: 10.1038/s41467-018-05516-7

de Vries, F. T., Liiri, M. E., Bjørnlund, L., Bowker, M. A., Christensen, S., Setälä, H. M., et al. (2012). Land use alters the resistance and resilience of soil food webs to drought. *Nat. Climate Change* 2, 276–280. doi: 10.1038/nclimate1368

Edgar, R. C. (2013). UPARSE: highly accurate OTU sequences from microbial amplicon reads. *Nat. Methods* 10, 996–998. doi: 10.1038/nmeth.2604

Falkowski, P. G., Fenchel, T., and Delong, E. F. (2008). The microbial engines that drive earth's biogeochemical cycles. *Science* 320, 1034–1039. doi: 10.1126/science.1153213

Francis, C. A., O'mullan, G. D., Cornwell, J. C., and Ward, B. B. (2013). Transitions in nirS-type denitrifier diversity, community composition, and biogeochemical activity along the Chesapeake bay estuary. *Front. Microbiol.* 4, 237. doi: 10.3389/fmicb.2013.00237

Guo, L., Hu, Z., Fang, F., Liu, T., Chuai, X., and Yang, L. (2014). Trophic status determines the nirS-denitrifier community in shallow freshwater lakes. *Ann. Microbiol.* 64, 999–1006. doi: 10.1007/s13213-013-0737-3

Hallin, S., and Lindgren, P. E. (1999). PCR detection of genes encoding nitrile reductase in denitrifying bacteria. *Appl. Environ. Microbiol.* 65 (4), 1652–1657. doi: 10.1128/AEM.65.4.1652-1657.1999

Hanning, M., Braker, G., Dippner, J., and Jürgens, K. (2006). Linking denitrifier community structure and prevalent biogeochemical parameters in the pelagial of the central Baltic proper (Baltic Sea). *FEMS Microbiol. Ecol.* 57 (2), 260–271. doi: 10.1111/j.1574-6941.2006.00116.x

Hou, L., Xie, X., Wan, X., Kao, S. J., Jiao, N., and Zhang, Y. (2018). Niche differentiation of ammonia and nitrite oxidizers along a salinity gradient from the pearl river estuary to the south China Sea. *Biogeosciences* 15, 5169–5187. doi: 10.5194/bg-15-5169-2018

Jones, C. M., and Hallin, S. (2010). Ecological and evolutionary factors underlying global and local assembly of denitrifier communities. *ISME J.* 4, 633–641. doi: 10.1038/ismej.2009.152

Jones, C. M., Stres, B., Rosenquist, M., and Hallin, S. (2008). Phylogenetic analysis of nitrite, nitric oxide, and nitrous oxide respiratory enzymes reveal a complex evolutionary history for denitrification. *Mol. Biol. Evol.* 25 (9), 1955–1966. doi: 10.1093/molbev/msn146

Lee, J. A., and Francis, C. A. (2017). Spatiotemporal characterization of San Francisco bay denitrifying communities: a comparison of nirK and nirS diversity and abundance. *Microbial Ecol.* 73, 271–284. doi: 10.1007/s00248-016-0865-y

Lin, G., Sun, F., Wang, C., Zhang, L., and Zhang, X. (2017). Assessment of the effect of enteromorpha prolifera on bacterial community structures in aquaculture environment. *PloS One* 12 (7), e0179792. doi: 10.1371/journal.pone.0179792

Liu, D., Keesing, J. K., He, P. M., Wang, Z. L., Shi, Y. J., and Wang, Y. J. (2013). The world's largest macroalgal bloom in the yellow Sea, China: formation and implications. *Estuar. Coast. Shelf Sci.* 129, 2–10. doi: 10.1016/j.ecss.2013.05.021

Liu, N., Liao, P., Zhang, J., Zhou, Y., Luo, L., Huang, H., et al. (2020). Characteristics of denitrification genes and relevant enzyme activities in heavy-metal polluted soils remediated by biochar and compost. *Sci. Total Environ.* 739, 139987. doi: 10.1016/j.scitotenv.2020.139987

Liu, X., Tiquia, S. M., Holguin, G., Wu, L., Nold, S. C., Devol, A. H., et al. (2003). Molecular diversity of denitrifying genes in continental margin sediments within the oxygen-deficient zone off the pacific coast of Mexico. *Appl. Environ. Microbiol.* 69 (6), 3549–3560. doi: 10.1128/AEM.69.6.3549-3560.2003

Li, H. M., Zhang, Y. Y., Tang, H. J., Shi, X. Y., Rivkin, R. B., and Legendre, L. (2017). Spatiotemporal variations of inorganic nutrients along the jiangsu coast, China, and the occurrence of macroalgal blooms (green tides) in the southern yellow Sea. *Harmful Algae* 63, 164–172. doi: 10.1016/j.hal.2017.02.006

Magoč, T., and Salzberg, S. L. (2011). FLASH: Fast length adjustment of short reads to improve genome assemblies. *Bioinformatics* 27, 2957–2963. doi: 10.1093/bioinformatics/btr507

Marshall, K., Joint, I., Callow, M. E., and Callow, J. A. (2006). Effect of marine bacterial isolates on the growth and morphology of axenic plantlets of the green alga ulva linza. *Microbial Ecol.* 52, 302–310. doi: 10.1007/s00248-006-9060-x

Mosier, A. C., and Francis, C. A. (2010). Denitrifier abundance and activity across the San Francisco bay estuary. *Environ. Microbiol. Rep.* 2 (5), 667–676. doi: 10.1111/j.1758-2229.2010.00156.x

Oakley, B. B., Francis, C. A., Roberts, K. J., Fuchsman, C. A., Srinivasan, S., and Staley, J. T. (2007). Analysis of nitrite reductase (nirK and nirS) genes and cultivation reveal depauperate community of denitrifying bacteria in the black Sea suboxic zone. *Environ. Microbiol.* 9 (1), 118–130. doi: 10.1111/j.1462-2920.2006.01121.x

Qu, T. F., Zhao, X. Y., Hao, Y., Zhong, Y., Guan, C., Hou, C. Z., et al. (2020). Ecological effects of ulva prolifera green tide on bacterial community structure in qingdao offshore environment. *Chemosphere* 244, 125477. doi: 10.1016/j.chemosphere.2019.125477

Sánchez, C., and Minamisawa, K. (2018). Redundant roles of bradyrhizobium oligotrophicum Cu-type (nirK) and cd1-type (nirS) nitrite reductase genes under denitrifying conditions. *FEMS Microbiol. Lett.* 365, fny015. doi: 10.1093/femsle/fny015

Santoro, A. E., Boehm, A. B., and Francis, C. A. (2006). Denitrifier community composition along a nitrate and salinity gradient in a coastal aquifer. *Appl. Environ. Microbiol.* 72 (3), 2102–2109. doi: 10.1128/AEM.72.3.2102-2109.2006

Sun, F., Wang, C., Chen, H., and Zheng, Z. (2020). Metagenomic analysis of the effect of enteromorpha prolifera bloom on microbial community and function in aquaculture environment. *Curr. Microbiol.* 77, 816–825. doi: 10.1007/s00284-019-01862-x

Throbäck, I. N., Enwall, K., Jarvis, A., and Hallin, S. (2004). Reassessing PCR primers targeting nirS, nirK and nosZ genes for community surveys of denitrifying bacteria with DGGE. *FEMS Microbiol. Ecol.* 49 (3), 401–417. doi: 10.1016/j.femsec.2004.04.011

van Alstyne, K. L., Nelson, T. A., and Ridgway, R. L. (2015). Environmental chemistry and chemical ecology of "green tide" seaweed blooms. *Integr. Comp. Biol.* 55 (3), 518–532. doi: 10.1093/icb/icv035

Wei, W., Isobe, K., Nishizawa, T., Zhu, L., Shiratori, Y., Ohte, N., et al. (2015). Higher diversity and abundance of denitrifying microorganisms in environments than considered previously. *ISME J.* 9, 1954–1956. doi: 10.1038/ismej.2015.9

Williams, R. J., Howe, A., and Hofmockel, K. S. (2014). Demonstrating microbial co-occurrence pattern analyses within and between ecosystems. *Front. Microbiol.* 5, 358. doi: 10.3389/fmicb.2014.00358

Wolsing, M., and Priemé, A. (2004). Observation of high seasonal variation in community structure of denitrifying bacteria in arable soil receiving artificial fertilizer and cattle manure by determining T-RFLP of nir gene fragments. *FEMS Microbiol. Ecol.* 48 (2), 261–271. doi: 10.1016/j.femsec.2004.02.002

Yang, Y. D., Hu, Y. G., Wang, Z. M., and Zeng, Z. H. (2018). Variations of the nirS-, nirK-, and nosZ-denitrifying bacterial communities in a northern Chinese soil as affected by different long-term irrigation regimes. *Environ. Sci. pollut. Res.* 25, 14057–14067. doi: 10.1007/s11356-018-1548-7

Yoshida, M., Ishiii, S., Otsuka, S., and Senoo, K. (2010). nirK-harboring denitrifiers are more responsive to denitrification-inducing conditions in rice paddy soil than nirS-harboring bacteria. *Microbes Environments* 25 (1), 45–48. doi: 10.1264/jsme2.ME09160

Yoshida, M., Ishii, S., Otsuka, S., and Senoo, K. (2009). Temporal shifts in diversity and quantity of nirS and nirK in a rice paddy field soil. *Soil Biol. Biochem.* 41 (10), 2044–2051. doi: 10.1016/j.soilbio.2009.07.012

Yuan, Q., Liu, P., and Lu, Y. (2012). Differential responses of nirK- and nirS-carrying bacteria to denitrifying conditions in the anoxic rice field soil. *Environ. Microbiol. Rep.* 4 (1), 113–122. doi: 10.1111/j.1758-2229.2011.00311.x

Zhang, Y. Y., He, P. M., Li, H. M., Li, G., Liu, J. H., Jiao, F. L., et al. (2019). Ulva prolifera green-tide outbreaks and their environmental impact in the yellow Sea, China. *Natl. Sci. Rev.* 6, 825–838. doi: 10.1093/nsr/nwz026

Zhang, C., Liu, Q., Li, X., Wang, M., Liu, X., Yang, J., et al. (2021b). Spatial patterns and co-occurrence networks of microbial communities related to environmental heterogeneity in deep-sea surface sediments around yap trench, Western pacific ocean. *Sci. Total Environ.* 759, 143799. doi: 10.1016/j.scitotenv.2020.143799

Zhang, P. Y., Xin, Y., Zhong, X. S., Yan, Z. W., Jin, Y. M., Yan, M. J., et al. (2021a). Integrated effects of ulva prolifera bloom and decay on nutrients inventory and cycling in marginal sea of China. *Chemosphere* 264, 128389. doi: 10.1016/j.chemosphere.2020.128389

Zhao, G., He, H., Wang, H., Liang, Y., Guo, C., Shao, H., et al. (2022). Variations in marine bacterial and archaeal communities during an ulva prolifera green tide in coastal qingdao areas. *Microorganisms* 10, 1204. doi: 10.3390/microorganisms10061204

Zheng, Y., Hou, L., Liu, M., Gao, J., Yin, G., Li, X., et al. (2015). Diversity, abundance, and distribution of nirS-harboring denitrifiers in intertidal sediments of the Yangtze estuary. *Microbial Ecol.* 70, 30–40. doi: 10.1007/s00248-015-0567-x

Zhou, Z. F., Zheng, Y. M., Shen, J. P., Zhang, L. M., and He, J. Z. (2011). Response of denitrification genes nirS, nirK, and nosZ to irrigation water quality in a Chinese agricultural soil. *Environ. Sci. pollut. Res. Int.* 18 (9), 1644–1652. doi: 10.1007/s11356-011-0482-8

Zumft, W. G. (1997). Cell biology and molecular basis of denitrification. *Microbiol. Mol. Biol. Rev.* 61 (4), 533–616. doi: 10.1128/mmbr.61.4.533-616.1997

frontiers | Frontiers in Marine Science

TYPE Original Research
PUBLISHED 08 December 2022
DOI 10.3389/fmars.2022.1082768

OPEN ACCESS

EDITED BY
Jing Wei,
Sun Yat-sen University, China

REVIEWED BY
Zucheng Wang,
Northeast Normal University, China
Lishan Tan,
The Chinese University of
Hong Kong, China

*CORRESPONDENCE
Jiafang Huang
wahugeo@fjnu.edu.cn

SPECIALTY SECTION
This article was submitted to
Marine Biogeochemistry,
a section of the journal
Frontiers in Marine Science

RECEIVED 28 October 2022
ACCEPTED 28 November 2022
PUBLISHED 08 December 2022

CITATION
Sun D, Huang J, Luo M, Chen C, Lan X and Hu W (2022) Dissimilatory nitrate reduction processes in surface sediments of shrimp ponds during the culture period.
Front. Mar. Sci. 9:1082768.
doi: 10.3389/fmars.2022.1082768

Dissimilatory nitrate reduction processes in surface sediments of shrimp ponds during the culture period

Dongyao Sun[1,2], Jiafang Huang[3]*, Min Luo[4], Cheng Chen[2], Xue Lan[5] and Weifang Hu[6]

[1]School of Geography Science and Geomatics Engineering, Suzhou University of Science and Technology, Suzhou, China, [2]Key Laboratory of Geographic Information Science (Ministry of Education), School of Geographic Sciences, East China Normal University, Shanghai, China, [3]School of Geographical Sciences, Fujian Normal University, Fuzhou, China, [4]Research Center of Geography and Ecological Environment, Fuzhou University, Fuzhou, China, [5]College of Marine Sciences, South China Agricultural University, Guangzhou, China, [6]Institute of Agricultural Resources and Environment, Guangdong Academy of Agricultural Sciences, Guangzhou, China

Intensive aquaculture in estuaries and coasts has resulted in several ecological and environmental problems. Among various nitrogen transformation pathway, dissimilatory nitrate (NO_3^-) reduction is considered to be highly important in regulating reactive nitrogen. However, there are relatively few studies on the processes and contribution of NO_x^- reduction in sediment during the shrimp pond culture period. Three sediment NO_3^- reduction processes, denitrification (DNF), anaerobic ammonium oxidation (ANA), and dissimilatory NO_3^- reduction to ammonium (DNRA), were surveyed in eight shrimp ponds across three subtropical estuaries using ^{15}N isotope tracing experiments. The rates of DNF, ANA and DNRA ranged from 2.87–18.11, 0.10–1.92, and 0.21–1.25 nmol N g^{-1} h^{-1}, respectively. DNF was responsible for 64.2–91.6% of the total NO_3^- reduction. Regarding environmental factors, C and N substrates, as well as salinity, significantly affected NO_3^- reduction. In general, the N losses were approximately 32.43–131.64 g N m^{-2} yr^{-1} for DNF and 2.38–15.85 g N m^{-2} yr^{-1} for ANA in this study, indicating that coastal reclamation is a nonnegligible way to remove nitrogen. Our results provide a scientific foundation for understanding the mechanism of nitrogen cycling in the artificial aquatic environment of shrimp ponds.

KEYWORDS

denitrification, anammox, DNRA, shrimp ponds, sediment

Introduction

With rapid economic development and the influence of human activities, large amounts of reactive nitrogen from upstream have been carried to estuarine and coastal systems by atmospheric transport and river runoff in recent years (Galloway et al., 2008; Canfield et al., 2010; Chen et al., 2016b). Reactive nitrogen mainly exists in the form of nitrate (NO_3^-), which has a significant influence on the ecology and functions of estuaries and coastal environments (Kennison and Fong, 2014; Macdonald et al., 2018). Such as eutrophication and algal blooms caused by increased NO_3^- concentrations, and even pose a potential threat to human heath (Birch and McCaskie, 1999; Wang et al., 2020). Thus, further understanding of the transformation processes in estuarine and coastal systems is required.

Dissimilatory NO_3^- reduction is an important pathway for removing reactive nitrogen and mainly includes three processes: denitrification (DNF), anaerobic ammonium oxidation (ANA), and dissimilatory NO_3^- reduction to ammonium (DNRA) (Thamdrup and Dalsgaard, 2002; Deng et al., 2015; Huang et al., 2021). Among these processes, DNF, which converts NO_3^-/NO_2^- to N_2 or N_2O, has long been considered the main pathway for NO_3^- removal progress (Seitzinger et al., 2006; Burgin and Hamilton, 2007). ANA oxidises ammonia (NH_4^+) into dinitrogen gas by reducing NO_3^-/NO_2^-, which has recently been thought to play an important role in the regulation of the sediment nitrogen cycle (Trimmer et al., 2003; Dale et al., 2009; Hou et al., 2015). While both DNF and ANA would remove NO_3^-/NO_2^- by conversion to gaseous nitrogen, DNRA converts NO_3^- to bioavailable NH_4^+, inducing the net retention of reactive N in the environment (Silver et al., 2005; Huygens et al., 2007; Dong et al., 2011). The contributions of the three NO_3^- reduction processes to nitrogen cycling differ depending on the type of ecosystem and sediment (Thamdrup and Dalsgaard, 2002; Laverman et al., 2007; Minick et al., 2016). Previous studies have shown that DNF was the main pathway of NO_3^- reduction processes in aquatic ecosystems (Deegan et al., 2012; Shan et al., 2016). However, studies have shown that DNRA plays an important role in mangrove systems (Cao et al., 2016). Studying the mechanism of NO_3^- reduction would help us to further understand the nitrogen transformation process in aquatic ecosystems.

As a key area of land-marine interaction, estuarine tidal flat wetlands are hotspots for the nitrogen cycle (Osburn et al., 2016; Hou et al., 2018). In recent years, because of the increasing demand for seafood products, large areas of tidal flat wetlands in China's coastal estuaries have been reclaimed as artificial aquaculture ponds (Chen et al., 2016a; Yang et al., 2017b). Owing to the addition of feed, aquaculture significantly increases carbon and nitrogen-based substances, changing carbon and nitrogen cycle processes, such as CH_4 and N_2O emissions (Yang et al., 2017a; Gao et al., 2018). According to previous research, the NO_3^- reduction route and proportion changed after the reclamation of estuarine tidal flat wetlands into aquaculture ponds (Gao et al., 2019). The process of NO_3^- reduction were closely related to environmental factors such as NO_3^-, TOC, and NH_4^+ (Deng et al., 2015; Cheng et al., 2016; Damashek and Francis, 2018). However, the detailed process of dissimilatory NO_3^- reduction in aquaculture ponds during the culture period remains unclear. With the continuous expansion of farming scale, it is necessary to develop the understanding of this special ecosystem.

This study selected shrimp ponds in three different regions of the subtropical estuarine and analysed the dissimilatory NO_3^- reduction process during the culture period using nitrogen isotopic techniques. In addition, the primary environmental factors influence DNF, ANA, and DNRA processes were studied. Furthermore, we compared the relative contributions of the three processes following the culture period in shrimp ponds. Our study provides a deeper understanding of nitrogen dynamics and the progress of aquaculture ponds in estuaries and coasts.

Materials and methods

Study area and samples collection

Three main estuaries in Fujian Province were selected as the study area: From north to south, the Min River, Mulan River, and Jiulong River. The three estuaries all have a subtropical monsoon climate, with an average annual rainfall of more than 1300 mm and an average annual temperature of 19.6 to 21.0°C (Zhang et al., 2011; Tong et al., 2012; Luo et al., 2019). In August 2017, eight sampling points were selected for shrimp culture ponds near the three estuaries, and surface sediments were collected underwater using a Plexiglas tube (Figure 1). The shrimp ponds at the sampling points were all reclaimed from estuary swamp wetlands, with similar land-use transformation years (7–9 years), and all were muddy pond slopes and pond bottoms. The shrimp ponds contained white shrimp (*Litopenaeus vannamei*). Shrimp seedlings are put in at the end of May every year, and farming ends after all the shrimps are harvested in mid- to late October. Shrimp farming ponds use local river water as a source of farming water. Each shrimp farming pond is equipped with two impeller aerators with a power of 1.5 kW, and the startup time is about 20:00 to 2:00 the next morning. The switch of the aerator during the day depends on the weather, the growth of fish and shrimp, and the water quality. The feed was provided twice a day at 7:00 and 17:00, and the feeding amount was in accordance with the conventional requirements. The basic features of shrimp ponds are listed in Table 1.

Analysis of sediment properties

Sediment density was measured using the syringe method (Percival and Lindsay, 1997), and the moisture content was dried

FIGURE 1
Study area and sampling sites.

using the weight loss method at 80°C to a constant weight. After removing sedimentary carbonate using 0.1 M HCl, the concentration of total organic carbon (TOC) and total nitrogen (TN) in the sediments were determined using a carbon-hydrogen-nitrogen elementary analyser (VVarioELIII, Elementary, Germany) and C N elemental analyser (Elementar Vario MAX CN, Germany), respectively (Lin et al., 2017; Hu et al., 2022). The sediment concentrations of NH_4^+ and NO_3^- were extracted with 2 M KCl solution and then determined using a continuous flow analyser (SAN Plus, Skalar Analytical B.V., The Netherlands) (Sun et al., 2022).

Determination of potential DNF, ANA, and DNRA rates

The potential DNF, ANA, and DNRA rates were measured using the nitrogen isotope tracing method (Yin et al., 2014; Deng et al., 2015; Gao et al., 2017). In brief, the slurry was prepared by mixing sediment into helium-purged water with a sediment/water volume ratio of 1:7 and then transferring to a helium-purged 12-mL vial (Labco Exetainers) (Hou et al., 2015). The vials were then pre-incubated for 36 h to remove surplus NO_3^-, NO_2^-, and O_2 at *in situ* temperatures. After pre-incubation,

TABLE 1 Environmental parameters in surface sediments of the shrimp ponds.

	MA	MB	MC	PG	PH	JD	JE	JF
Bulk density ($g\ cm^{-3}$)	1.29 ± 0.06	1.45 ± 0.02	1.59 ± 0.15	1.60 ± 0.06	1.63 ± 0.04	1.4 ± 0.02	1.5 ± 0.03	1.65 ± 0.76
Water content(%)	52.17 ± 3.03	48.68 ± 1.25	35.68 ± 0.98	39.57 ± 0.62	34.04 ± 2.89	55.62 ± 1.51	51.59 ± 2.65	36.62 ± 3.05
Salinity(ppt)	0.46 ± 0.01	0.91 ± 0.01	1.16 ± 0.05	0.07 ± 0.01	1.28 ± 0.05	1.60 ± 0.01	1.76 ± 0.03	1.93 ± 0.01
TN(%)	0.14 ± 0.01	0.15 ± 0.01	0.12 ± 0.01	0.14 ± 0.01	0.12 ± 0.01	0.11 ± 0.01	0.13 ± 0.01	0.08 ± 0.01
TOC(%)	1.76 ± 0.11	1.78 ± 0.11	1.24 ± 0.08	1.67 ± 0.07	0.92 ± 0.03	0.76 ± 0.04	0.62 ± 0.05	0.78 ± 0.08
TOC/TN	11.97 ± 0.78	11.66 ± 0.47	10.14 ± 0.09	11.53 ± 0.06	7.62 ± 0.13	6.86 ± 0.04	4.72 ± 0.18	10.47 ± 2.87
NH_4^+(mg N kg^{-1})	5.73 ± 0.11	7.06 ± 0.11	3.47 ± 0.13	7.86 ± 0.01	5.21 ± 0.04	3.72 ± 0.33	5.29 ± 0.11	2.88 ± 0.42
NO_3^-(mg N kg^{-1})	0.09 ± 0.02	0.13 ± 0.01	0.06 ± 0.01	0.07 ± 0.01	0.07 ± 0.01	0.06 ± 0.01	0.02 ± 0.01	0.09 ± 0.01

sterile anoxic solutions of $^{15}NO_3^-$ (^{15}N at 99%) was added to all vials *via* the septa, with the final content of ^{15}N being approximately 100 μM (Hou et al., 2013). Then, 200 μL of $ZnCl_2$ solution (50%) was added to half of the replicates (as initial samples). Then, half of the slurries were incubated for 8 h, and 200 μL of $ZnCl_2$ solution (50%) was added at the end of incubation to terminate the reaction (Lin et al., 2017). Both of the contents of $^{29}N_2$ and $^{30}N_2$ were measured by membrane inlet mass spectrometry (MIMS) during incubation, to calculate the DNF and ANA rates based on the difference in $^{29}N_2$ and $^{30}N_2$ produced among the final and initial results (Gao et al., 2019).

The DNF and ANA rates were approximated based on the accumulations of $^{29}N_2$ and $^{30}N_2$, respectively (Deng et al., 2015). The contributions of DNF and ANA to $^{29}N_2$ production were calculated using Equation (1).

$$P_{29} = A_{29} + D_{29} \quad (1)$$

Here, P_{29}, D_{29}, and A_{29} (nmol N g^{-1} h^{-1}) denote the total $^{29}N_2$ production rate and the production rate of $^{29}N_2$ from DNF and ANA during the slurry experiments, respectively. The ratio of ^{14}N and ^{15}N produced by $^{14}NO_3^-$ or $^{15}NO_3^-$ with random isotope pairing and D_{29} was calculated using equation (2) (Risgaard-Petersen et al., 2003).

$$D_{29} = P_{30} \times 2 \times (1 - F_N) \times F_N^{-1} \quad (2)$$

Here, P_{30} (nmol N g^{-1} h^{-1}) represents the production rate of total $^{30}N_2$, and F_N (%) denotes the proportion of ^{15}N in NO_3^-, which was estimated from the measured content of added $^{15}NO_3^-$ and surplus NO_3^- (Shan et al., 2016). Finally, the DNF potential rates were calculated using Equation (3), and the ANA was calculated using Equation (4).

$$D_{total} = D_{29} + 2 \times D_{30} \quad (3)$$

$$A_{29} = P_{29} - D_{29} \quad (4)$$

Here, D_{total} and A_{29} (nmol N g^{-1} h^{-1}) denote DNF and ANA rates, respectively.

The DNRA rate was calculated using the $^{15}NH_4^+$ oxidation and MIMS analysis (OX/MIMS) method (Yin et al., 2014). First, the sediment slurry was pre-incubated. After the preincubation, 100 μL of $^{15}NO_3$ (^{15}N at 99.6% and a final content of approximately 100 μM ^{15}N) was added to all the vials. Immediately, half of the slurry was saved (as initial sample) with 200 μL of $ZnCl_2$ solution (50%). The rest of the vials (as final samples) were further incubated 8 h before adding 200 μL of $ZnCl_2$ solution (50%). The potential rates of DNRA were calculated using Equation (5).

$$R_{DNRA} = \left[\left(^{15}N\ H_4^+\right)_{Final} - \left(^{15}N\ H_4^+\right)_{Initial}\right] \times V \times W^{-1} \times T^{-1} \quad (5)$$

Here, R_{DNRA} (nmol N g^{-1} h^{-1}) is the total potential rate of DNRA; $(^{15}NH_4^+)_{Final}$ and $(^{15}NH_4^+)_{Initial}$ (nmol N L^{-1}) are the content of $^{15}NH_4^+$ in the final and initial sample, respectively; and V (L), W (g), and T (h) denote the volume of the vial, dry weight of the sediment, and time, respectively (Gao et al., 2019).

Statistical analyses

The differences between the NO_3^- reduction rates among all points were analysed by one-way analysis of variance (ANOVA) (homogeneity of variance was tested by the LSD test, and Dunnett's T3 was used to test for heterogeneity of variance). The relationships between the environmental variables and DNF, ANA, and DNRA rates were revealed by Pearson correlation analyses. SPSS 22.0 was used for one-way ANOVA and pearson analysis. While Redundancy analysis (RDA) was used to evaluate variations in NO_3^- reduction rates with respect to environmental variables using software Canoco 4.5 (Sun et al., 2020). The significance level was set at 0.05.

Results

Physiochemical characteristics of the site

The physicochemical characteristics of each site are presented in Table 2. Sediment bulk density varied from 1.27 to 1.78 g·cm^{-3} in

TABLE 2 Basic characteristics of all shrimp ponds in the estuaries of Fujian Province.

Sampling Site	Name	Area (ha)	Average depth (m)	Unit product output(kg ha^{-1})	Food coefficient
MA	Shanyutan wetland of Min River estuary	0.753	1.3	9.77	1.38
MB	Bianfuzhou wetland of Min River estuary	0.982	1.9	12.3	1.90
MC	Culu Island of Min River estuary	0.521	1.4	10.2	1.77
PG	Dongxiang of Mulan River	1.113	2.1	12.1	1.76
PH	Zhe lang of Mulan River	1.255	2.8	13.0	1.86
JD	Changzhou of Jiu long River	0.226	1.6	10.3	1.82
JE	Junkennongchang of Jiu long River	0.749	1.7	11.2	1.64
JF	Xumaozhou of Jiu long River	0.739	1.6	10.6	1.56

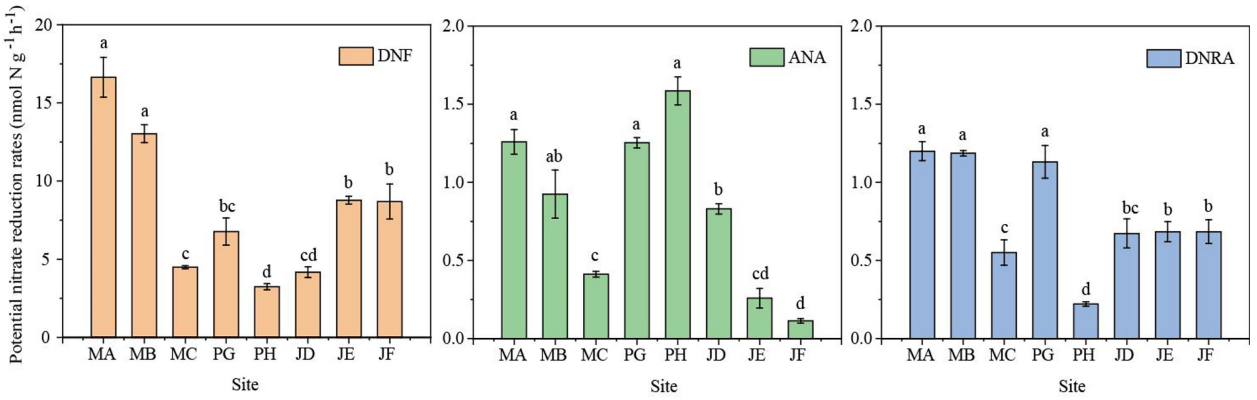

FIGURE 2
Sediment potential DNF, ANA and DNRA rates in the shrimp ponds. Different letters indicate significant differences ($p < 0.05$) among different sites. Error bars represent the standard deviation(n = 3).

the study area, and the water content in the sediment varied from 31 to 59%. The salinities of the shrimp ponds ranged from 0.06 to 1.93 ppt. The TOC, TN, and TOC/TN ratios in the sediment varied between 0.58 to 1.97%, 0.07 to 0.16%, and 4.51 to 13.75, respectively. The concentration of NH_4^+ and NO_3^- in sediments varied from 2.42 to 8.41 and 0.02 to 0.14 μmol·g^{-1}, respectively. In addition to the physicochemical characteristics of the sediments, the area and average depth of each shrimp pond were also different, and the largest area (1.113–1.255 ha) and average depth (2.1–2.8 m) of shrimp ponds were found in the Mulan estuary. The unit water output varied between 9.77–10.6 kg ha^{-1}, and the food coefficient ranged from 1.38–1.86 in the shrimp pond (Table 1).

Dissimilatory NO_3^- reduction processes

The sediment potential rates of DNF ranged from 2.87 to 18.11 nmol N g^{-1} h^{-1}, and there were significant differences between the all sites ($n = 24$, $p < 0.05$). The highest DNF rate was found at site MA, while the lowest DNF rate was at site PH (Figure 2). DNF contributed 64.2–91.5% of the total NO_3^- reduction rate (Figure 3). The rates of ANA varied from 0.10 to 1.92 nmol N g^{-1} h^{-1} in the study area, and a distinct spatial difference in the ANA rates was observed among sites ($n = 24$, $p < 0.05$). The highest ANA rate occurred at site PH, whereas the lowest ANA rate occurred at site JF. Compared to DNF, ANA

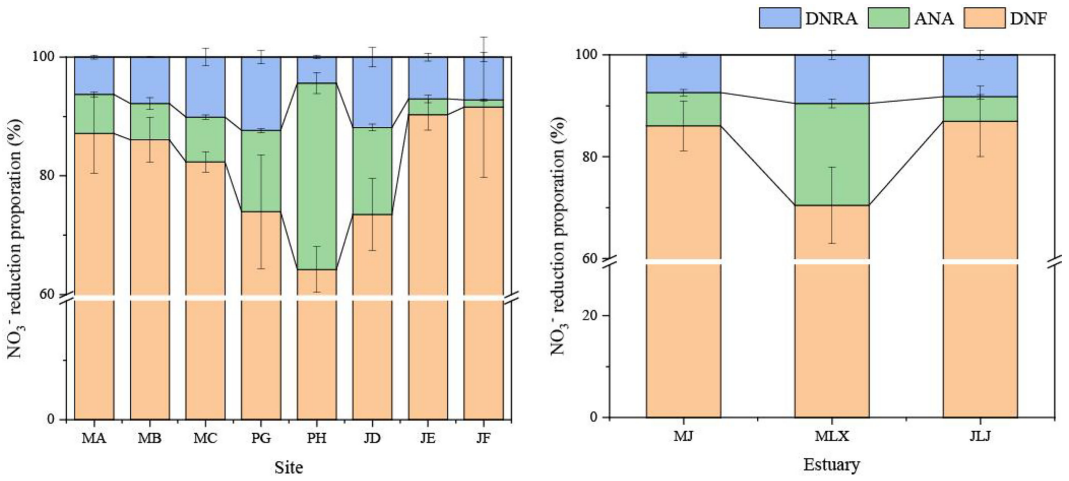

FIGURE 3
Relative contributions of DNF, ANA and DNRA to total NO_3^- reduction in the shrimp ponds. Error bars represent the standard deviation.

had less effect on NO_3^- reduction and contributed 1.2–31.4% to total nitrogen loss. Potential DNRA rates varied from 0.21 to 1.25 nmol N g^{-1} h^{-1}. Significant differences were observed among the sites in the study area (n = 24, $p < 0.05$). DNRA and DNF showed the same distribution, with the highest value appearing at the MA site and the lowest value appearing at the PH site. The contribution of DNRA accounted for 4.38–12.35% of the total NO_3^- reduction.

Influences of physiochemical characteristics on NO_3^- reduction rates

The RDA was implemented to evaluate variations in the NO_3^- reduction rate with respect to environmental variables. The first two RDA dimensions were found to account for 70.56% of the cumulative variance, and the first and second axes contributed 55.12 and 15.44%, respectively (Figure 4). The RDA results showed that salinity and TOC were significantly associated with various NO_3^- reduction process. The DNF rates were significantly and negatively correlated with bulk density (r = - 0.559, $p < 0.05$, n = 24) and positively correlated with water content (r = 0.464, $p < 0.05$, n =24), TOC (r = 0.590, $p < 0.01$, n = 24), TOC/TN (r = 0.495, $p < 0.05$, n = 24), and NO_3^- (r = 0.525, $p < 0.01$, n = 24) (Table 3). Of the detected environmental factors, salinity and the ANA rate showed a significant negative correlation (r = - 0.656, $p < 0.01$, n = 24), and there was a positive correlation with TN (r = 0.498, $p < 0.05$, n =24), TOC (r =0.506, $p < 0.05$, n = 24) and NH_4^+ (r = 0.577, $p < 0.05$, n = 24). The sediment potential rate of DNRA was negatively associated with bulk density (r = 0.441, $p < 0.05$, n = 24) and salinity (r = - 0.637, $p < 0.01$, n = 24) and positively related to water content (r = 0.472, $p < 0.05$, n = 24), TOC (r = 768, $p < 0.01$, n = 24), TN (r = 0.546, $p < 0.01$, n = 24), TOC/TN (r = 0.608, $p < 0.01$, n = 24), NH_4^+ (r = 0.604, $p < 0.05$, n = 24), and NO_3^- (r = 0.508, $p < 0.05$, n = 24) (Table 3). There are positive correlations of most of the dissimilatory NO_3^- reduction processes with TOC, TOC/TN, NH_4^+, and NO_3^- were found (Table 3).

Discussion

In coastal wetlands, reclaiming natural wetlands for aquaculture activities is a major anthropogenic disturbance that threatens intrinsic N balance. The addition of feed and the growth and excretion of shrimp during the breeding process increased C and N substrates in the sediment of shrimp ponds; at the same time, the rates of the dissimilatory NO_3^- reduction process were promoted (Wu et al., 2014; Chen et al., 2016b; Gao et al., 2019). The addition of bait to coastal wetlands can change

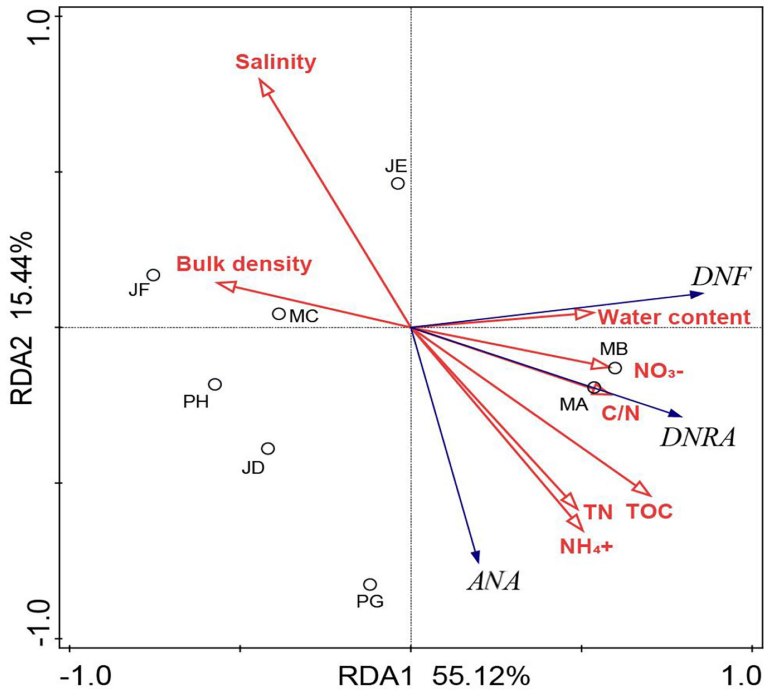

FIGURE 4
Ordination diagram showing the results of RDA of NO_3^- reduction processes and soil physicochemical characteristics. The hollow circles represent individual sediment samples from the eight shrimp ponds in the subtropics Estuary. The red arrows represent soil physicochemical characteristics, and blue arrows represent NO_3^- reduction processes.

TABLE 3 Person's correlations of sediment NO_3^- reduction rates with physico-chemical properties.

	DNF	ANA	DNRA
Bulk density	**-0.559** *	n.s.	**-0.441***
Water content	**0.464***	n.s.	**0.472***
Salinity	-0.339	**-0.656****	**-0.637****
TN	0.402	**0.498***	**0.546****
TOC	**0.590****	**0.506***	**0.768****
TOC/TN	**0.495***	0.355	**0.608****
NH_4^+	0.358	**0.577***	**0.604***
NO_3^-	**0.525****	0.304	**0.508***

* Significant at $p < 0.05$, ** Significant at $p < 0.01$, n = 24. The meaning of the bold values represent significant difference. The n.s. indicates a no statistical significance.

the microbial community structure in sediments and contribute to greenhouse gas (GHGs) emissions (Lin and Lin, 2022). DNF, ANA, and DNRA are the most crucial processes in dissimilar NO_3^- reduction processes in aquatic environments (Rysgaard et al., 2004; Song et al., 2013; Yang et al., 2022). We researched the distribution of dissimilatory NO_3^- reduction processes in shrimp ponds and analysed the main influencing factors controlling the process. In the present study, most of the dissimilatory NO_3^- reduction processes with TOC, TOC/TN, NH_4^+, and NO_3^- were showed a positive correlations. Therefore, the contribution of these environmental factors to NO_3^- reduction in shrimp ponds requires further elucidation.

NO_3^- reduction process and the influence of environmental factors

DNF rate were measured by ^{15}N tracer techniques according to the assumption of N_2, because of the ratio of N_2O to N_2 from DNF in aquatic ecosystems is very low (Dong et al., 2002). Salinity affected the DNF rate to some extent, although no statistically significant correlation was observed, and a decrease in denitrification activity associated with higher salinity was observed. RDA showed a negative correlation between salinity and DNF rate. Salinity may result in physiological stress on DNF, which in turn affects the DNF rate, which generally decreases with an increase in salinity (Rysgaard et al., 1999; Seo et al., 2008). In general, the DNF rate was positively related to the TOC content in previous studies, such as in lakes, rice fields, estuaries, and coastal environments (Vymazal, 2007; Deng et al., 2015; Yang et al., 2022). Our study showed that the DNF rate showed a positive relationship with the TOC content in the shrimp ponds, which is similar to previous research (Gao et al., 2019). Because shrimp ponds have been in a high organic carbon environment for a long time, they are beneficial for the growth of denitrifying-associated bacteria and promote the DNF rate (Canion et al., 2014; Plummer et al., 2015; Yang et al., 2017b). A remarkable relationship between the DNF rate and NO_3^- was observed in our study (Table 3), and it was confirmed that NO_3^- is a major driver of the rate of NO_3^- reduction in shrimp ponds. DNF microorganisms use NO_3^- as an electron acceptor and substrate, which is strongly dependent on the NO_3^- concentration (Giles et al., 2012; Shan et al., 2016; Palacin-Lizarbe et al., 2020).

Spatial variations in ANA rates have also been found, and numerous studies have reported that salinity is a crucial environmental factor affecting ANA (Wang et al., 2012; Hou et al., 2015). Salinity was significantly correlated with the ANA rate in this study, suggesting that high salinity might inhibit the rate of ANA activity. It has been reported that ANA activity is not directly caused by an energy source, but is influenced by C and N substrates in sediments (Hou et al., 2015). A strong correlation was found between ANA and the C and N substrates in our study; this C and N matrix mainly comes from the decomposition of a large amount of feed and manure residues in the culture period (Wu et al., 2014). Studies have shown that TOC and NH_4^+ concentrations at suitable concentrations can promote the ANA rate (Cheng et al., 2016; Damashek and Francis, 2018), as well as a significant positive correlation between TOC, NH_4^+, and ANA. However, it should be noted that high TOC concentrations may inhibit ANA activity (Bettazzi et al., 2010).

DNRA is often considered to be closely related to salinity, and previous studies have shown that increasing salinity accelerates the DNRA rate (Gardner et al., 2006; Giblin et al., 2010). However, some studies have found that the abundance of the *nrfA* gene associated with DNRA rates is not significantly affected by salinity (Yin et al., 2017). Interestingly, our results showed that DNRA and ANA rates declined significantly with increasing salinity, as both showed similar results (Table 3). RDA also showed a negative correlation between salinity and ANA, DNRA rates. TOC and NH_4^+ could be important factors influencing DNRA in sediments (Bu et al., 2017), which was also proven by the significant positive correlation between the rate of DNRA and TOC in our study. High TOC concentrations may provide adequate organic substrates for the growth of DNRA-associated microorganisms (Deng et al., 2015). DNRA can more efficiently utilise NO_3^- as an electron acceptor in a carbon-rich environment, thereby increasing the DNRA rate (Kraft et al., 2014; Cheng et al., 2016).

Relationship between different NO_3^- reduction processes

The DNF rate was compared with the ANA and DNRA rates to identify potential connections among them (Figure 5). These correlation analyses show that DNF is closely related to ANA and DNRA in the study area. During the interaction between ANA and DNF, DNF is a major source of NO_2^- for ANA in coastal wetland sediments (Meyer et al., 2005), and there was a significant relationship found between DNF and ANA rates in the shrimp

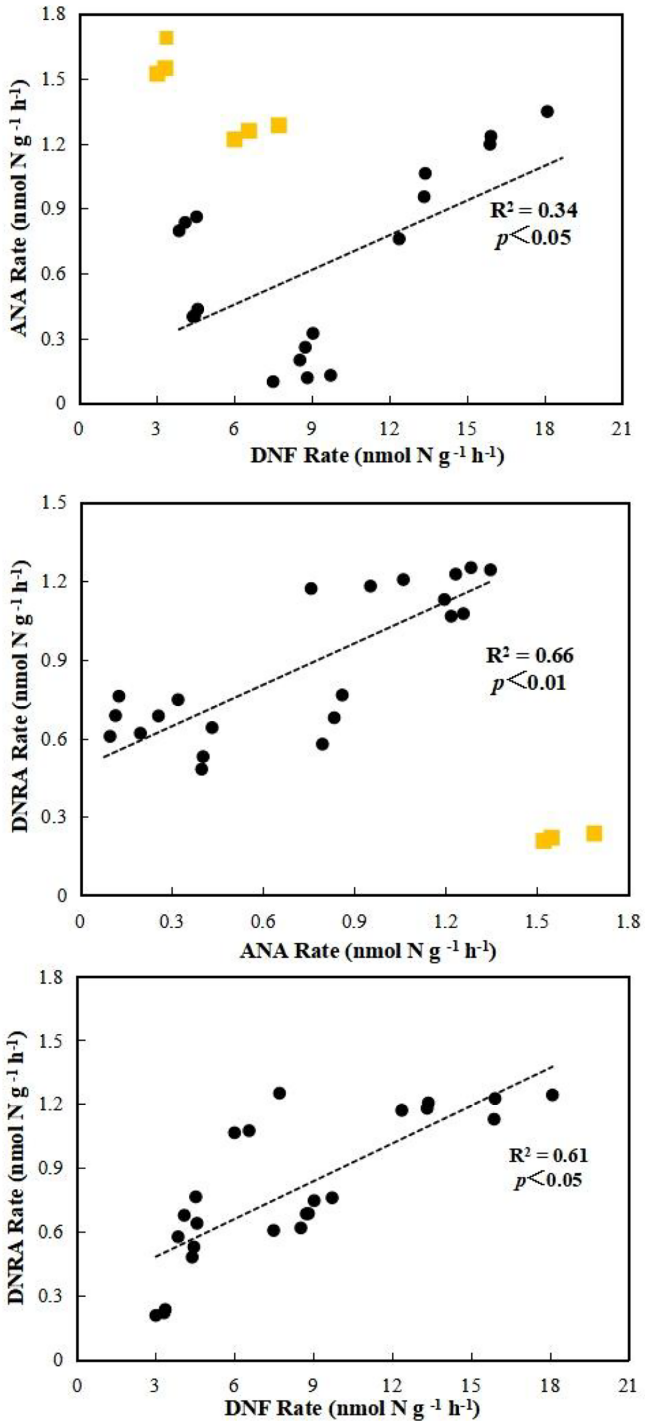

FIGURE 5
Correlations between DNF, ANA and DNRA rate. The linear regression is shown for the relation between DNF, ANA and DNRA rate. R^2 represents regression coefficient, and Yellow points represents not included in the statistics.The significance level was set at 0.05 and 0.01.

pond (R^2 = 0.34, $p < 0.05$). Studies have also found a coupling related process between ANA and DNF (Hou et al., 2015). The ANA rates were significantly associated with DNRA rates (R^2 = 0.66, $p < 0.01$), indicating that DNRA can produce NO_2^- as an intermediate product, which is an alternative substrate for ANA (Lam et al., 2009). DNF and DNRA compete for NO_3^- under hypoxic or anaerobic conditions. Our results showed that the DNF rates were significantly related with the DNRA rates in the sediment (R^2 = 0.61, $p < 0.05$) (Figure 5), indicating that the growth of NO_3^- substrate promoted both of them.

Competition among DNF, ANA, and DNRA can determine the fate of NO_3^- owing to their diverse roles in dissimilatory NO_3^- reduction. DNF was the dominant route contributing 64.2–91.6% (81.14%) of the total the dissimilatory NO_3^- reduction processes in the shrimp pond, while the contributions of ANA and DNRA were 1.2–31.4% (10.48%) and 4.34–12.4% (8.38%), respectively (Figure 6). According to several studies, DNF plays a major role in removing nitrogen from various aquatic systems, while the proportions of ANA and DNRA differ between ecosystems (Deng et al., 2015; Shan et al., 2016; Yang et al., 2022). Different aquatic environments contribute different amounts of dissimilatory NO_3^- reduction, as shown in Table 4. Studies have shown that the DNF, ANA, and DNRA rates in urban rivers and seas are higher than those in shrimp ponds (Song et al., 2013; Cheng et al., 2016). However, the rate of DNF in a paddy field was between 2.37 and 8.30 nmol N g^{-1} h^{-1}, and ANA and DNRA were also relatively low (Shan et al., 2016). The DNF rate in estuarine and lake regions ranges from 0.09 to 11.47 nmol N g^{-1} h^{-1}, which is lower than that in shrimp ponds (Deng et al., 2015; Yang et al., 2022). Compared with the estuary wetland, the dissimilation NO_3^- reduction rate increased after reclamation for shrimp ponds, showing an increasing trend with increasing reclamation years (Gao et al., 2019). It was found that the biggest difference between the shrimp ponds system and other systems may be more dependent on the difference caused by the high concentration of C and N matrix input. We found that the rate of DNF ranged from 3.24 to 16.64 nmol N g^{-1} h^{-1} in shrimp ponds, while the rate of ANA was slightly higher than that of DNRA (Figure 2). Further analysis showed that DNRA was higher than ANA in aquaculture ponds in the Min and Jiulong River estuaries, indicating that the contribution of DNRA to the total NO_3^- reduction was still higher than that of natural wetlands (Gao et al., 2019). ANA was found to be much higher than DNRA in the Mulan River estuary, especially the PH site at 31.4% (Figure 3). This may be related to the large size and depth of shrimp ponds in the estuary of the Mulan River, however, specific causes need to be identified.

If the average DNF and ANA rates were extrapolated to the study area, the N losses were approximately 32.43–131.64 g N m^{-2} yr^{-1} for DNF and 2.38–15.85 g N m^{-2} yr^{-1} for ANA. According to the area of aquaculture ponds in China's coastal wetland (2.6 $\times 10^6$ ha) (Chen et al., 2016a; Chen et al., 2016b), approximately 2.18 $\times$ 10^6 t N can be removed from shrimp ponds by this process annually, indicating that coastal reclamation is a considerable way to remove nitrogen. Recent results suggest that if natural wetlands are gradually converted into shrimp ponds, reactive nitrogen may be retained (Murphy et al., 2016). Shrimp ponds may be more important than nitrogen loss (Gao et al., 2019). Consequently, sediment N loads increase, resulting in decreased water quality and shrimp disease outbreaks (Castillo Soriano et al., 2013).

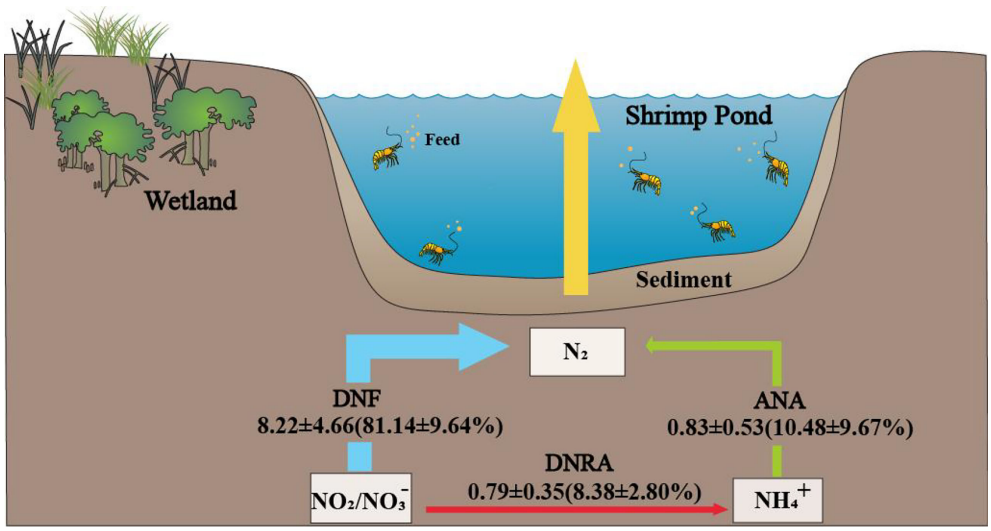

FIGURE 6
The conceptual map on NO_3^- reduction processes in the shrimp pond sediment. The unit of DNF, ANA, and DNRA rates were nmol N g^{-1} h^{-1}.

TABLE 4 Contributions of Denitrification, ANAMMOX, and DNRA to total nitrate reduction in our study and other aquatic ecosystems.

Aquatic system	DNF		ANA(%)		DNRA(%)		References
	Ratenmol N g^{-1} h^{-1}	Contribution (%)	Ratenmol N g^{-1} h^{-1}	Contribution (%)	Ratenmol N g^{-1} h^{-1}	Contribution (%)	
Paddy soil	2.37-8.30	76.8-92.5	0.15-0.77	4.5-9.2	0.03-0.54	0.5-17.6	(Shan et al., 2016)
Urban river	0.193-98.7	11.5-99.5	0.0387-23.7	0.343-81.6	0-10.3	0-52.3	(Cheng et al., 2016)
Urban lakes	3.54-11.47	58.87-63.89	0.07-1.60	3.72-8.86	1.10-4.18	29.38-35.28	(Yang et al., 2022)
East China Sea	0.6-20[a]	17-85 (65)	0.4-4[a]	8-66 (20)	2.6-9.7[a]	8-22 (15)	(Song et al., 2013)
Yangtze Estuary	0.09-4.52	66.2	0.01-0.52	8	0.03-0.89	25.8	(Deng et al., 2015)
Coastal wetlands	1.52-17.58	70-92.41	0.31-1.27	2.49-15.27	0.14-2.01	5.10-20.75	(Gao et al., 2017)
shrimp pond	2.5-14.3	57.2-82.2	0.6-2.1	10.3-17.3	1.6-3.8	7.5-27.4	(Gao et al., 2019)
Shrimp pond	2.87-18.11	64.2-91.6	0.10-1.92	1.2-31.4	0.21-1.25	4.4-12.4	This study

[a]means that the unit for nitrate reduction rates is nmol N cm^{-3} h^{-1}

Conclusion

This study investigated the process of NO_3^- dissimilation and reduction in shrimp pond sediments in a subtropical estuary area and identified the main factors influencing the process. Studies have shown that DNF is the main pathway, and that ANA and DNRA also play important roles. The feed added during the culture promoted the C and N matrices in the sediment, which in turn promoted the reduction of various NO_3^-. This process of nitrogen removal under intensive aquaculture in estuarine and coastal areas should receive more attention in future studies.

Data availability statement

The original contributions presented in the study are included in the article/supplementary material. Further inquiries can be directed to the corresponding author.

Author contributions

DS: Investigation, Formal analysis, Writing and editing. JH: Conceptualization, Methodology, Funding acquisition. ML: Methodology. XL, CC, WH: Formal analysis. All authors contributed to the article and approved the submitted version.

Funding

This work was supported by the Natural Science Foundation of China (grant numbers: 41601102 and 32071598). And Funded by Fujian Forestry Science and Technology Project (No. 2021FKJ30), Public Welfare Project of Fujian Science and Technology Department (No. 2022R1002007) and the Starting Research Program of Suzhou University of Science and Technology (No. 332214803).

Conflict of interest

The authors declare that the research was conducted in the absence of any commercial or financial relationships that could be construed as a potential conflict of interest.

Publisher's note

References

Bettazzi, E., Caffaz, S., Vannini, C., and Lubello, C. (2010). Nitrite inhibition and intermediates effects on anammox bacteria: A batch-scale experimental study. *Process Biochem.* 45, 573–580. doi: 10.1016/j.procbio.2009.12.003

Birch, S., and McCaskie, J. (1999). Shallow urban lakes: a challenge for lake management. *Hydrobiologia* 395–396, 365-378. doi: 10.1023/A:1017099030774

Burgin, A. J., and Hamilton, S. K. (2007). Have we overemphasized the role of denitrification in aquatic ecosystems? a review of nitrate removal pathways. *Front. Ecol. Environmen.* 5, 89–96. doi: 10.1890/1540-9295(2007)5[89:HWOTRO]2.0.CO;2

Bu, C., Wang, Y., Ge, C., Ahmad, H. A., Gao, B., and Ni, S.-Q. (2017). Dissimilatory nitrate reduction to ammonium in the yellow river estuary: Rates, abundance, and community diversity. *Sci. Rep.* 7, 6830–6811. doi: 10.1038/s41598-017-06404-8

Canfield, D. E., Giazer, A. N., and Falkowski, P. G. (2010). The evolution and future of earth's nitrogen cycle. *Science* 330, 192–196. doi: 10.1126/science.1186120

Canion, A., Overholt, W. A., Kostka, J. E., Huettel, M., Lavik, G., and Kuypers, M. M. M. (2014). Temperature response of denitrification and anaerobic ammonium oxidation rates and microbial community structure in Arctic fjord sediments: Temperature and n cycling in Arctic sediments. *Environ. Microbiol.* 16, 3331–3344. doi: 10.1111/1462-2920.12593

Cao, W., Yang, J., Li, Y., Liu, B., Wang, F., and Chang, C. (2016). Dissimilatory nitrate reduction to ammonium conserves nitrogen in anthropogenically affected subtropical mangrove sediments in southeast China. *Mar. pollut. Bull.* 110, 155–161. doi: 10.1016/j.marpolbul.2016.06.068

Castillo Soriano, F. A., Ibarra Junquera, V., Escalante Minakata, P., Mendoza Cano, O., Ornelas Paz, J., d., J., et al. (2013). Nitrogen dynamics model in zero water exchange, low salinity intensive ponds of white shrimp, litopenaeus vannamei, at colima, Mexico. *Latin Am. J. Aquat. Res.* 41, 68–79. doi: 10.3856/vol41-issue1-fulltext-5

Chen, Y., Dong, S., Wang, F., Gao, Q., and Tian, X. (2016b). Carbon dioxide and methane fluxes from feeding and no-feeding mariculture ponds. *Environ. pollut.* 212, 489–497. doi: 10.1016/j.envpol.2016.02.039

Cheng, L., Li, X., Lin, X., Hou, L., Liu, M., Li, Y., et al. (2016). Dissimilatory nitrate reduction processes in sediments of urban river networks: Spatiotemporal variations and environmental implications. *Environ. pollut.* 219, 545–554. doi: 10.1016/j.envpol.2016

Chen, F., Hou, L., Liu, M., Zheng, Y., Yin, G., Lin, X., et al. (2016a). Net anthropogenic nitrogen inputs (NANI) into the Yangtze river basin and the relationship with riverine nitrogen export. *J. geophysical Res. Biogeosciences* 121, 451–465. doi: 10.1002/2015JG003186

Dale, O. R., Tobias, C. R., and Song, B. (2009). Biogeographical distribution of diverse anaerobic ammonium oxidizing (anammox) bacteria in cape fear river estuary. *Environ. Microbiol.* 11, 1194–1207. doi: 10.1111/j.1462-2920.2008.01850.x

Damashek, J., and Francis, C. A. (2018). Microbial nitrogen cycling in estuaries: From genes to ecosystem processes. *Estuaries coasts* 41, 626–660. doi: 10.1007/s12237-017-0306-2

Deegan, L. A., Johnson, D. S., Warren, R. S., Peterson, B. J., Fleeger, J. W., Fagherazzi, S., et al. (2012). Coastal eutrophication as a driver of salt marsh loss. *Nature* 490, 388–392. doi: 10.1038/nature11533

Deng, F., Hou, L., Liu, M., Zheng, Y., Yin, G., Li, X., et al. (2015). Dissimilatory nitrate reduction processes and associated contribution to nitrogen removal in sediments of the Yangtze estuary. *J. geophysical Res. Biogeosci.* 120, 1521–1531. doi: 10.1002/2015JG003007

Dong, L. F., Nedwell, D. B., Underwood, G. J., Thornton, D. C., and Rusmana, I. (2002). Nitrous oxide formation in the colne estuary, England: the central role of nitrite. *Appl. Environ. Microbiol.* 68 (3), 1240e1249. doi: 10.1128/AEM.68.3.1240-1249.2002

Dong, L. F., Sobey, M. N., Smith, C. J., Rusmana, I., Phillips, W., Stott, A., et al. (2011). Dissimilatory reduction of nitrate to ammonium, not denitrification or anammox, dominates benthic nitrate reduction in tropical estuaries. *Limnology oceanogr.* 56, 279–291. doi: 10.4319/lo.2011.56.1.0279

Galloway, J. N., Townsend, A. R., Erisman, J. W., Bekunda, M., Cai, Z., Freney, J. R., et al. (2008). Transformation of the nitrogen cycle: Recent trends, questions, and potential solutions. *Science* 320, 889. doi: 10.1126/science.1136674

Gao, D., Chen, G., Li, X., Lin, X., and Zeng, C. (2018). 'Reclamation culture alters sediment phosphorus speciation and ecological risk in coastal zone of southeastern China. *Clean soil air Water* 46, 1700495–n/a. doi: 10.1002/clen.201700495

Gao, D., Li, X., Lin, X., Wu, D., Jin, B., Huang, Y., et al. (2017). Soil dissimilatory nitrate reduction processes in the spartina alterniflora invasion chronosequences of a coastal wetland of southeastern China: Dynamics and environmental implications. *Plant Soil.* 421, 383–399. doi: 10.1007/s11104-017-3464-x

Gao, D., Liu, M., Hou, L., Derrick, Y. F. L., Wang, W., Li, X., et al. (2019). Effects of shrimp-aquaculture reclamation on sediment nitrate dissimilatory reduction processes in a coastal wetland of southeastern China. *Environ. pollut.* 255, 113219–113219. doi: 10.1016/j.envpol.2019.113219

Gardner, W. S., McCarthy, M. J., An, S., Sobolev, D., Sell, K. S., and Brock, D. (2006). Nitrogen fixation and dissimilatory nitrate reduction to ammonium (DNRA) support nitrogen dynamics in Texas estuaries. *Limnology oceanogr.* 51, 558–568. doi: 10.4319/lo.2006.51.1_part_2.0558

Giblin, A. E., Weston, N. B., Banta, G. T., Tucker, J., and Hopkinson, C. S. (2010). The effects of salinity on nitrogen losses from an oligohaline estuarine sediment. *Estuaries coasts* 33, 1054–1068. doi: 10.1007/s12237-010-9280-7

Giles, M., Morley, N., Baggs, E. M., and Daniell, T. J. (2012). Soil nitrate reducing processes - drivers, mechanisms for spatial variation, and significance for nitrous oxide production. *Front. Microbiol.* 3. doi: 10.3389/fmicb.2012.00407

Hou, L., Wang, R., Yin, G., Liu, M., and Zheng, Y. (2018). Nitrogen fixation in the intertidal sediments of the Yangtze estuary: Occurrence and environmental implications. *J. geophysical Res. Biogeosciences* 123, 936–944. doi: 10.1002/2018JG004418

Hou, L., Zheng, Y., Liu, M., Gong, J., Zhang, X., Yin, G., et al. (2013). Anaerobic ammonium oxidation (anammox) bacterial diversity, abundance, and activity in marsh sediments of the Yangtze estuary. journal of geophysical research. *Biogeosciences* 118, 1237–1246. doi: 10.1002/JGRG.20108

Hou, L., Zheng, Y., Liu, M., Li, X., Lin, X., Yin, G., et al. (2015). Anaerobic ammonium oxidation and its contribution to nitrogen removal in china's coastal wetlands. *Sci. Rep.* 5, 15621. doi: 10.1038/srep15621

Huang, F., Lin, X., Hu, W., Zeng, F., He, L., and Yin, K. (2021). Nitrogen cycling processes in sediments of the pearl river estuary: Spatial variations, controlling factors, and environmental implications. *Catena* 206, 105545. doi: 10.1016/j.catena.2021.105545

Hu, M., Sardans, J., Le, Y., Yan, R., Zhong, Y., Huang, J., et al. (2022). Biogeochemical behavior of p in the soil and porewater of a low-salinity estuarine wetland: Availability, diffusion kinetics, and mobilization mechanism. *Water Res.* 219, 118617–118617. doi: 10.1016/j.watres.2022.118617

Huygens, D., Rütting, T., Boeckx, P., Van Cleemput, O., Godoy, R., and Müller, C. (2007). Soil nitrogen conservation mechanisms in a pristine south Chilean nothofagus forest ecosystem. *Soil Biol. Biochem.* 39, 2448–2458. doi: 10.1016/j.soilbio.2007.04.013

Kennison, R. L., and Fong, P. (2014). Extreme eutrophication in shallow estuaries and lagoons of California is driven by a unique combination of local watershed modifications that trump variability associated with wet and dry seasons. *Estuaries coasts* 37, S164–S179. doi: 10.1007/s12237-013-9687-z

Kraft, B., Tegetmeyer, H. E., Sharma, R., Klotz, M. G., Ferdelman, T. G., Hettich, R. L., et al. (2014). The environmental controls that govern the end product of bacterial nitrate respiration. *Science* 345, 676–679. doi: 10.1126/science.1254070

Lam, P., Lavik, G., Jensen, M. M., van de Vossenberg, J., Schmid, M., Woebken, D., et al. (2009). Revising the nitrogen cycle in the Peruvian oxygen minimum zone. *Proc. Natl. Acad. Sci.* 106, 4752–4757. doi: 10.1073/pnas.0812444106

Laverman, A. M., Canavan, R. W., Slomp, C. P., and Cappellen, P. V. (2007). Potential nitrate removal in a coastal freshwater sediment (Haringvliet lake, the Netherlands) and response to salinization. *Water Res.* 41, 3061–3068. doi: 10.1016/j.watres.2007.04.002

Lin, G., and Lin, X. (2022). Bait input altered microbial community structure and increased greenhouse gases production in coastal wetland sediment. *Water Res.* 218, 11850. doi: 10.1016/j.watres.2022.118520

Lin, X., Liu, M., Hou, L., Gao, D., Li, X., Lu, K., et al. (2017). Nitrogen losses in sediments of the East China Sea: Spatiotemporal variations, controlling factors, and environmental implications. *J. Geophysical Research: Biogeosci.* 122, 2699–2715. doi: 10.1002/2017JG004036

Luo, M., Zhu, W., Huang, J., Liu, Y., Duan, X., Wu, J., et al. (2019). Anaerobic organic carbon mineralization in tidal wetlands along a low-level salinity gradient of a subtropical estuary: Rates, pathways, and controls. *Geoderma* 337, 1245–1257. doi: 10.1016/j.geoderma.2018.07.030

Macdonald, D. M. J., Dixon, A. J., and Gooddy, D. C. (2018). Water and nitrate exchange between a managed river and peri-urban floodplain aquifer: Quantification and management implications. *Ecol. engineer.* 123, 226–237. doi: 10.1016/j.ecoleng.2018.09.005

Meyer, R. L., Risgaard-Petersen, N., and Allen, D. E. (2005). Correlation between anammox activity and microscale distribution of nitrite in a subtropical mangrove sediment. *Appl. Environ. Microbiol.* 71, 6142–6149. doi: 10.1128/AEM.71.10.6142-6149.2005

Minick, K. J., Pandey, C. B., Fox, T. R., and Subedi, S. (2016). Dissimilatory nitrate reduction to ammonium and N2O flux: effect of soil redox potential and n fertilization in loblolly pine forests. *Biol. fertility soils.* 52, 601–614. doi: 10.1007/s00374-016-1098-4

Murphy, A. E., Anderson, I. C., Smyth, A. R., Song, B., and Luckenbach, M. W. (2016). Microbial nitrogen processing in hard clam (Mercenaria mercenaria) aquaculture sediments: the relative importance of denitrification and dissimilatory nitrate reduction to ammonium (DNRA). *Limnology oceanogr.* 61, 1589–1604. doi: 10.1002/lno.10305

Osburn, C. L., Handsel, L. T., Peierls, B. L., and Paerl, H. W. (2016). Predicting sources of dissolved organic nitrogen to an estuary from an agro-urban coastal watershed. *Environ. Sci. tech.* 50, 8473–8484. doi: 10.1021/acs.est.6b00053

Palacin-Lizarbe, C., Camarero, L., Hallin, S., Jones, C. M., Catalan, J., and Sveriges, L. (2020). Denitrification rates in lake sediments of mountains affected by high atmospheric nitrogen deposition. *Sci. Rep.* 10, 3003–3003. doi: 10.1038/s41598-020-59759-w

Percival, J., and Lindsay, P. (1997). *Measurement of physical properties of sediments* (Boca Raton, Florida USA: CRC Press, Lewis Publishers), 287.

Plummer, P., Tobias, C., and Cady, D. (2015). Nitrogen reduction pathways in estuarine sediments: Influences of organic carbon and sulfide. *J. geophysical Res. Biogeosci.* 120, 1958–1972. doi: 10.1002/2015JG003057

Risgaard-Petersen, N., Nielsen, L. P., Rysgaard, S., Dalsgaard, T., and Meyer, R. L. (2003). Application of the isotope pairing technique in sediments where anammox and denitrification coexist. *Limnology oceanogr. Methods* 1, 63–73. doi: 10.1002/lom3.10127

Rysgaard, S., Glud, R. N., Risgaard-Petersen, N., and Dalsgaard, T. (2004). Denitrification and anammox activity in Arctic marine sediments. *Limnology Oceanogr.* 49, 1493–1502. doi: 10.4319/lo.2004.49.5.1493

Rysgaard, S., Thastum, P., Dalsgaard, T., Christensen, P. B., and Sloth, N. P. (1999). Effects of salinity on NH_4^+ adsorption capacity, nitrification, and denitrification in Danish estuarine sediments. *Estuaries* 22, 21–30. doi: 10.2307/1352923

Seitzinger, S., Harrison, J. A., Böhlke, J. K., Bouwman, A. F., Lowrance, R., Peterson, B., et al. (2006). Denitrification across landscapes and waterscapes: A synthesis. *Ecol. applications* 16, 2064–2090. doi: 10.1890/1051-0761(2006)016[2064:DALAWA]2.0.CO;2

Seo, D. C., Yu, K., and Delaune, R. D. (2008). Influence of salinity level on sediment denitrification in a Louisiana estuary receiving diverted Mississippi river water. *Archiv für Acker- und Pflanzenbau und Bodenkunde* 54, 249–257. doi: 10.1080/03650340701679075

Shan, J., Zhao, X., Sheng, R., Xia, Y., ti, C., Quan, X., et al. (2016). Dissimilatory nitrate reduction processes in typical Chinese paddy soils: Rates, relative contributions, and influencing factors. *Environ. Sci. Technol.* 50, 9972–9980. doi: 10.1021/acs.est.6b01765

Silver, W. L., Thompson, A. W., Reich, A., Ewel, J. J., and Firestone, M. K. (2005). Nitrogen cycling in tropical plantation forests: Potential controls on nitrogen retention. *Ecol. applications* 15, 1604–1614. doi: 10.1890/04-1322

Song, G. D., Liu, S. M., Marchant, H., Kuypers, M. M. M., and Lavik, G. (2013). Anammox, denitrification and dissimilatory nitrate reduction to ammonium in the East China Sea sediment. *Biogeosciences* 10, 6851–6864. doi: 10.5194/bg-10-6851-2013

Sun, D., Tang, X., Li, J., Liu, M., Hou, L., Yin, G., et al. (2022). Chlorate as a comammox *Nitrospira* specific inhibitor reveals nitrification and N_2O production activity in coastal wetland. *Soil Biol. Biochem.* 173, 108782. doi: 10.1016/j.soilbio.2022.108782

Sun, D., Tang, X., Zhao, M., Zhang, Z., Hou, L., Liu, M., et al. (2020). Distribution and diversity of comammox *Nitrospira* in coastal wetlands of China. *Front. Microbiol.* 11. doi: 10.3389/fmicb.2020.589268

Thamdrup, B., and Dalsgaard, T. (2002). Production of N_2 through anaerobic ammonium oxidation coupled to nitrate reduction in marine sediments. *Appl. Environ. Microbiol.* 68, 1312–1318. doi: 10.1128/AEM.68.3.1312-1318.2002

Tong, C., Wang, W.-Q., Huang, J.-F., Gauci, V., Zhang, L.-H., and Zeng, C.-S. (2012). Invasive alien plants increase CH_4 emissions from a subtropical tidal estuarine wetland. *Biogeochemistry* 111, 677–693. doi: 10.1007/s10533-012-9712-5

Trimmer, M., Nicholls, J. C., and Deflandre, B. (2003). Anaerobic ammonium oxidation measured in sediments along the Thames estuary, united kingdom. *Appl. Environ. Microbiol.* 69, 6447–6454. doi: 10.1128/AEM.69.11.6447-6454.2003

Vymazal, J. (2007). Removal of nutrients in various types of constructed wetlands. *Sci. total environ.* 380, 48–65. doi: 10.1016/j.scitotenv.2006.09.014

Wang, S., Pi, Y., Jiang, Y., Pan, H., Wang, X., Wang, X., et al. (2020). Nitrate reduction in the reed rhizosphere of a riparian zone: from functional genes to activity and contribution. *Environ. Res.* 180, 108867. doi: 10.1016/j.envres.2019.108867

Wang, S., Zhu, G., Peng, Y., Jetten, M. S. M., and Yin, C. (2012). Anammox bacterial abundance, activity, and contribution in riparian sediments of the pearl river estuary. *Environ. Sci. tech.* 46, 8834–8842. doi: 10.1021/es3017446

Wu, H., Peng, R., Yang, Y., He, L., Wang, W., Zheng, T., et al. (2014). Mariculture pond influence on mangrove areas in south China: Significantly larger nitrogen and phosphorus loadings from sediment wash-out than from tidal water exchange. *Aquaculture* 426-427, 204–212. doi: 10.1016/j.aquaculture.2014.02.009

Yang, P., Bastviken, D., Lai, D. Y. F., Jin, B. S., Mou, X. J., Tong, C., et al. (2017a). Effects of coastal marsh conversion to shrimp aquaculture ponds on CH_4 and N_2O emissions. *Estuarine Coast. shelf Sci.* 199, 125–131. doi: 10.1016/j.ecss.2017.09.023

Yang, P., Lai, D. Y. F., Jin, B., Bastviken, D., and Tan, L. (2017b). Dynamics of dissolved nutrients in the aquaculture shrimp ponds of the Min river estuary, China: Concentrations, fluxes and environmental loads. *Sci. total environ.* 603-604, 256–267. doi: 10.1016/j.scitotenv.2017.06.074

Yang, Z., Lu, L., Cheng, Z., Xian, J., Yang, Y., Liu, L., et al. (2022). Dissimilatory nitrate reduction in urban lake ecosystems: A comparison study between closed and open lakes in chengdu, China. *Water Res.* 214, 118218–118218. doi: 10.1016/j.watres.2022.118218

Yin, G., Hou, L., Liu, M., Liu, Z., and Gardner, W. S. (2014). A novel membrane inlet mass spectrometer method to measure $^{15}NH_4^+$ for isotope-enrichment experiments in aquatic ecosystems. *Environ. Sci. Technol.* 48, 9555–9562. doi: 10.1021/es501261s

Yin, G., Hou, L., Liu, M., Li, X., Zheng, Y., Gao, J., et al. (2017). DNRA in intertidal sediments of the Yangtze estuary. *J. geophysical Res. Biogeosci.* 122, 1988–1998. doi: 10.1002/2017JG003766

Zhang, Y., Yin, Y., Feng, L., Zhu, G., Shi, Z., Liu, X., et al. (2011). Characterizing chromophoric dissolved organic matter in lake tianmuhu and its catchment basin using excitation-emission matrix fluorescence and parallel factor analysis. *Water Res.* 45, 5110–5122. doi: 10.1016/j.watres.2011.07.014

frontiers | Frontiers in Marine Science

TYPE Original Research
PUBLISHED 12 December 2022
DOI 10.3389/fmars.2022.1040554

OPEN ACCESS

EDITED BY
Xianbiao Lin,
Ocean University of China, China

REVIEWED BY
Dengzhou Gao,
East China Normal University, China
Xiaoli Zhang,
Yantai Institute of Coastal Zone Research (CAS), China
Haiyan Jin,
Second Institute of Oceanography, Ministry of Natural Resources, China
Yanhong Lu,
Hong Kong University of Science and Technology, Hong Kong SAR, China
Lin Hui,
Ministry of Natural Resources, China

*CORRESPONDENCE
Min Nina Xu
minxu@hainanu.edu.cn
Shuh-Ji Kao
sjkao@xmu.edu.cn

†These authors have contributed equally to this work and share senior authorship

SPECIALTY SECTION
This article was submitted to Marine Biogeochemistry, a section of the journal Frontiers in Marine Science

RECEIVED 09 September 2022
ACCEPTED 21 November 2022
PUBLISHED 12 December 2022

CITATION
Tang J-M, Xu MN, Lin Y, Chen H, Jin H, Han L-L, Zou W and Kao S-J (2022) The biological transformation of ammonium and urea in a eutrophic estuarine system in Southern China. *Front. Mar. Sci.* 9:1040554. doi: 10.3389/fmars.2022.1040554

The biological transformation of ammonium and urea in a eutrophic estuarine system in Southern China

Jin-Ming Tang[1], Min Nina Xu[2*†], Yuxuan Lin[3], Huangxin Chen[1], Haoquan Jin[1], Li-Li Han[1], Wenbin Zou[1] and Shuh-Ji Kao[1,2*†]

[1]State Key Laboratory of Marine Environmental Science, College of Ocean and Earth Sciences, Xiamen University, Xiamen, China, [2]State Key Laboratory of Marine Resources Utilization in South China Sea, Hainan University, Haikou, China, [3]State Key Laboratory of Marine Environmental Science, College of Environment and Ecology, Xiamen University, Xiamen, China

Estuaries channel large amounts of anthropogenic nitrogen (N) from continents to the offshore where productivity is widely limited by N and phosphorus. Ammonium and urea, two reduced forms of anthropogenic N commonly observed, are the preferred substrates for various microorganisms (e.g., uptake by phytoplankton or bacteria and oxidation by nitrifier). Yet, it remains underexplored how they transform and their concentrations vary during transport in the estuary which may influence the offshore microbial community. We applied ^{15}N isotope tracer incubation techniques to determine the two main bio-consumption processes, i.e., uptake and oxidation, of ammonium and urea, in the dark for the Jiulong River Estuary, a eutrophic estuary in southeastern China. Results showed that light penetration depth ranged from 0.8-3.3 m leaving 76% of estuary water bodies to stay in dark situations throughout a day. Ammonia oxidation, which favors dark conditions, dominates the estuarine regenerated-N cycle, showing the rank: ammonia oxidation > ammonium uptake >> urea uptake ≈ urea oxidation. By compiling the reported case studies, we found the relatively low ratio of urea oxidation to ammonia oxidation was accompanied by a relatively high ammonium concentration. Microorganisms' high preference for ammonium over urea may lead to an inhibitory-like phenomenon. An analogous effect was evident by the increased urea uptake at downstream when ammonium was down to a few μM. The obstructed urea utilization resulted in 10 times longer lifetime for urea relative to ammonium (surface: 19 ± 9 days; bottom 12 ± 7 days). Such an inhibitory-like effect allows urea to be preserved in the estuary and allows urea to be transported farther offshore to stimulate microorganisms capable of utilizing urea, which may have significant impacts on offshore ecology.

KEYWORDS

urea oxidation, urea uptake, ammonia oxidation, ammonium uptake, Jiulong River Estuary, estuarine nitrogen cycle

1 Introduction

Nitrogen (N) is one of the most critical elemental species in the aquatic environment and is greatly influenced by human activities (Voss et al., 2011). Large quantities of fertilizer and N-containing sewage are discharged from continents into the ocean (Galloway, 2014). Acting as a bioreactor in the land-ocean interface, estuarine systems play a key role to host and transform multiple anthropogenic N species. The microbial modulation of anthropogenic reactive N during their transport inside the estuary may shift downstream ecological functioning, potentially leading to outbreaks of harmful algal bloom and hypoxia, threatening the ecological security of the coastal ocean (Glibert et al., 2016). Exploring the distribution and biogeochemical behavior of these reactive N species in estuaries is therefore crucial to our understanding of the human-influenced estuarine N cycle and fundamental to the development of future coastal zone management policies.

Ammonium and urea, the most direct products of man-made fertilizers, are considered to be the two most influential anthropogenic N and are classified as reduced-N (Glibert et al., 2016). Due to the lower energy utilization threshold, ammonium is often considered to be the most bioavailable inorganic N relative to nitrate and nitrite and can be directly taken up as a source of N by a wide variety of organisms including phytoplankton and bacteria to construct biomolecules represented by proteins (Mulholland and Lomas, 2008). In addition to being assimilated, ammonium can also be consumed *via* oxidation by chemoautotrophic organisms to provide energy (i.e., ammonia oxidation). Nitrification is recognized as the major biological source process of nitrite/nitrate (Ward, 2008), providing substrates for N removal processes like denitrification (Tan et al., 2020). Another representative estuarine anthropogenic N, urea, the small molecule of organic N closely associated with life activities, has received increasing attention (Glibert et al., 2006; Moschonas et al., 2017). In some estuaries, urea loaded from human activities has risen to several times higher (Glibert et al., 2006). Although its presence in organic form, urea can be easily accessed (i.e., low half saturation constant in the Michaelis-Menten equation) like ammonium in a previous study (Xu et al., 2019). Some reported urea uptake studies in the ocean and estuary show that rates of urea uptake can be comparable to that of some inorganic N uptake (Moschonas et al., 2017; Xu et al., 2019), but its biogeochemical behavior has been less studied compared to ammonium. Besides being uptaken, urea has recently shown the potential to act as an energy source for chemoautotrophs (Alonso-Saez et al., 2012; Kirchman, 2012), significantly improving our knowledge of urea's biological consumption pathway. However, only a few open-ocean (Xu et al., 2019; Shiozaki et al., 2021; Wan et al., 2021) and coastal studies (Tolar et al., 2017; Kitzinger et al., 2019) have reported on urea oxidation process. To our knowledge, there are currently no reports on urea oxidation rates in the estuarine environment to form a potential gap in estuarine N cycle research.

The four processes described above are difficult to trace by only measuring changes in substrate concentrations, especially when the rate magnitudes are small or when multiple processes occur simultaneously (Xu et al., 2017). The ^{15}N stable isotope tracing technique is a better approach (Glibert et al., 2019). We can obtain process rates by artificially adding ^{15}N-labelled substrates (e.g., ^{15}N-ammonium and ^{15}N-urea) and measuring these ^{15}N accumulations in product reservoirs (e.g., nitrate plus nitrite (NO_x^-) for the oxidation process; particulate organic N (PN) for the uptake process) after incubation. The highly sensitive isotope ratio mass spectrometry allows us to detect small changes in ^{15}N in the product pools and thus simultaneously traces the transformation rates from the substrate to different products (i.e., ammonia oxidation: ammonium to NO_x^-; urea oxidation: urea to NO_x^-; ammonium uptake: ammonium to PN; urea uptake: urea to PN).

The high turbidity in estuaries (e.g., Changjiang River Estuary, Pearl River Estuary, and Jiulong River Estuary in this study) makes dark conditions important for estuarine N cycling (Hsiao et al., 2014; Tseng et al., 2014; Xu et al., 2022). Darkness and low light periods exceed 1/2 of the day, additionally, light decays rapidly so that most estuarine water columns are in dark conditions even during the daytime (e.g., Figure 2D). Dark incubation was a common operation for nitrification incubation (Dai et al., 2008; Zheng et al., 2017; Peng et al., 2018). And for N uptake, many studies usually use only the rates under light conditions, but dark uptake can reach more than half of light uptake in some cases (especially for reduced-stated-N, such as ammonium), which is unignorable and scarcely studied (Mulholland and Lomas, 2008; Xu et al., 2019; Chen et al., 2020).

The Jiulong River Estuary (JRE), a typical subtropical macro-tide estuary (Lin et al., 2022) with a mean water discharge of 1.4×10^{10} m^3 yr^{-1} on the southeast coast of China, was selected to study the transformations of ammonium and urea along a salinity gradient specifically in the dark. In the past decades, JRE is heavily disturbed by anthropogenic activities like agriculture and pig/poultry farming, which have left footprints in nitrate isotopes (Wang et al., 2021). Dissolved inorganic nitrogen (DIN) flux in JRE is up to 34.8×10^3 t N yr^{-1} with a very high areal yield rate of DIN flux (2.3×10^3 kg N km^{-2} yr^{-1}) (Yan et al., 2012). The DIN discharge per unit area even exceeds many of the world's major rivers (e.g., Yangtze, Pearl River, Amazon River) (Wu et al., 2017). Previous studies of the JRE have focused on the fluxes (Yan et al., 2012), sources (Yan et al., 2019; Wang et al., 2021), and sinks (Tan et al., 2020) of N in the JRE, but little is known about the highly active internal turnover of ammonium and urea in the estuary.

In this study, we examined the ammonium and urea dynamics through the robust ^{15}N-pulse incubation technique, which enables us to obtain rates of N oxidation and uptake simultaneously. We aim to (1) explore the dominant pathways of reduced-N in the estuary; (2) provide fresh insights into urea's

role in the nutrient-rich estuary, especially for previously unreported estuarine urea oxidation; (3) explore the importance of dark N uptake compared to N oxidation; (4) examine the lifetime of ammonium and urea in the eutrophic JRE by taking all consumption processes (uptake and oxidation) into account simultaneously.

2 Materials and methods

2.1 Study site and sampling

The investigation along the JRE was conducted by using R/V *Ocean II* of Xiamen University on 3rd December 2018, when JRE was in the dry season with a monthly discharge of 4.17×10^8 m^3 (Figure S1) (data from http://slt.fujian.gov.cn/). Fourteen sampling stations were set up seaward along the main axis of the JRE (T1-T14; Figure 1) to collect samples of nitrogenous nutrients (DIN and urea), PN, Chlorophyll *a* (Chl *a*), and total suspended substances (TSS) from the 0.5 m surface water (Surface) and layer at 1 m above the bottom (Bottom), while onboard incubation was conducted simultaneously at these layers. At each station, salinity, temperature, pH, and light intensity were recorded by a Conductivity, Temperature, and Depth profiler (CTD, OCEAN SEVEN 316 Plus). Salinity for sampling layers was also measured onboard using a portable multiparameter water quality analyzer (WTW, Multi 3630 IDS Set F).

Water samples were collected in acid-washed 10 L bottles by a peristaltic pump system placed in parallel with the CTD. A portion was taken and filtered through a syringe polyethersulfone filter of 0.22 μm pore size to collect the filtrate for DIN concentration determination while approximately 50 mL of water was filtered by 0.7 μm GF/F membranes for urea measurement. 160-300 mL water samples were filtered through 25 mm pre-combusted (450°C for 4 hours) and pre-weighed GF/F membranes under a gentle vacuum pressure (< 200 mmHg) to collect the particulate samples for PN, TSS, and Chl *a* determination. In stations T1, T8, and T14, approximately 500 mL of water from the bottom layers was filtered in triplicate for qPCR analysis. All membrane samples were stored at -80°C while filtrate samples were stored at -20°C until analysis.

2.2 Analysis of chemical and biological parameters

2.2.1 DIN and urea analysis

Concentrations of nitrate and nitrite were measured using an AA3 Auto-Analyzer (Bran & Luebbe Co., Germany) (Dai et al., 2008), water samples pass through a copper-cadmium reduction column where the nitrate is reduced to nitrite, and nitrite is then reacted with sulfanilamide and N-1-naphthyl-ethylenediamine dihydrochloride (N-1-N/NEDD) to form a red dye for measurement of absorbance (Becker et al., 2020). Samples for ammonium were analyzed based on the indophenol blue spectrophotometric method (Pai et al., 2001), with correction for salinity/pH effect. Urea concentrations were measured using a five-centimeter cuvette based on the optimized colorimetric

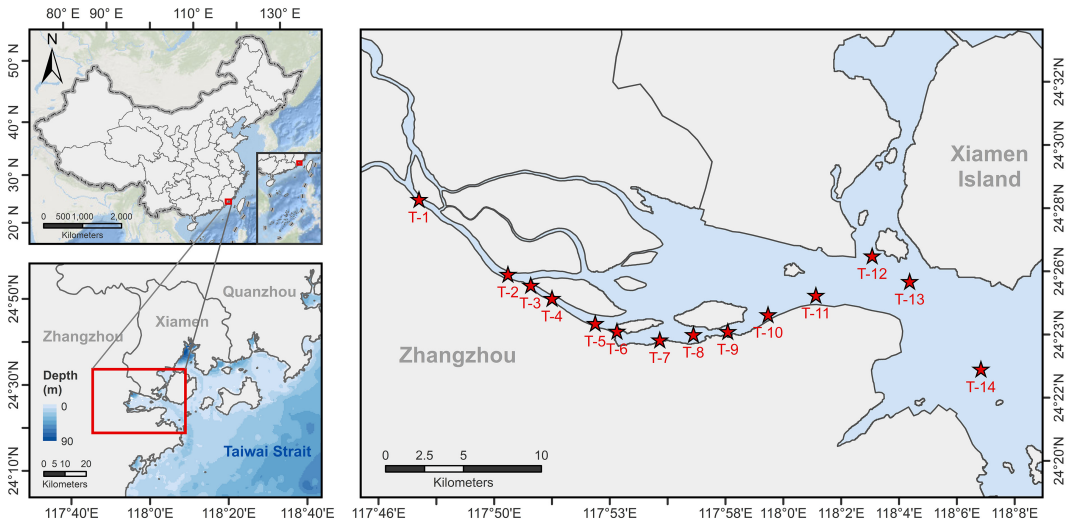

FIGURE 1
Station map for this study. The red stars show the 14 stations where incubation experiments were conducted and environmental parameters were collected during the study, with T1-T11 distributed along the main axis of the Jiulong River Estuary and T12-T14 representing the nearshore stations where surface salinity is above 24.

reaction with diacetyl monoxime (Chen et al., 2015). The detection limits for nitrate, nitrite, ammonium, and urea were 0.07, 0.02, 0.5, and 0.1 μM respectively.

2.2.2 Measurement of TSS, PN, and Chl *a*

After cold drying, the membrane was weighed again and the pre-filtration mass was deducted and divided by the filtration volume to obtain the TSS (mg/L). After the weighing, these GF/F filters were chemically oxidized using recrystallized potassium persulfate to turn PN into nitrate (Knapp et al., 2005; Xu et al., 2022) which was subsequently measured by NOx analyzer according to chemiluminescence method (Braman and Hendrix, 1989), with a detection limit of 0.05 μM.

We derived the total Chl *a* from the high-performance liquid chromatography procedure and details can be found in previous literature (Xiao et al., 2018; Ma et al., 2021).

2.2.3 *amoA* gene analysis

The determination of the copy numbers of the *amoA* gene for bacteria and archaea was performed *via* qPCR using a QuantStudio 7 pro instrument (ABI). Primer pairs and settings were based on previous reports, as follows: amoA-1F, amoA-2R (Rotthauwe et al., 1997) for bacterial *amoA* genes, and amoA-AF, amoA-AR (Francis et al., 2005) for archaeal *amoA* genes.

2.3 ^{15}N isotope tracer incubation method

2.3.1 Incubation onboard

Incubation experiments for N oxidation and uptake were conducted at all 14 stations along the salinity gradients of the estuary in both surface-bottom layers. Seawater for incubation was dispensed into 250 mL HDPE bottles within half an hour of collection. For each rate group, two biological replicates were set up. The ^{15}N tracer was added based on the historical nutrient data to achieve a final concentration of 1 μM and 0.5 μM for ammonium and urea, respectively, following the ^{15}N-tracer addition criterion of 10% or 20% of the ambient substrate concentrations (Raimbault and Garcia, 2008). The average final ^{15}N addition percentage was 13% and 22% for ammonium and urea, respectively (Table S1) on the basis of real measurement. And then all bottles were incubated for approximately 9 hours in the dark under *in situ* temperature in temperature-controlled incubators.

At the beginning (T_0) and end (T_1) of incubation, approximately 40 mL of water was taken for δ^{15}N-NO_x^- (nitrate plus nitrite) and 100-200 mL for δ^{15}N-PN for all groups, detailed collection and storage methods are described in section 2.1.

2.3.2 Analysis of ^{15}N isotopic composition

The isotopic composition of nitrate plus nitrite (δ^{15}N-NO_x^-) was determined by the bacterial method (Sigman et al., 2001). Briefly, ~20 nmol of nitrate plus nitrite in the water sample was quantitatively transformed into nitrous oxide gas in a 20 mL headspace bottle containing 3 mL of denitrifying bacteria (*Pseudomonas aureofaciens*, ATCC# 13985) that lack nitrous oxide reductase. And then the nitrous oxide gas was extracted and measured on a continuous flow Gasbench II-IRMS system (Yang et al., 2022). Three international isotopic references (IAEA-N3, δ^{15}N = 4.70‰; USGS-34, δ^{15}N = -1.80‰; USGS-32, δ^{15}N = 180.00‰) and a laboratory working standard (δ^{15}N = 13.8‰) were used to calibrate all δ^{15}N values of samples. The standard deviations of δ^{15}N were less than 0.2‰ based on standards measured in each batch and our previous results (Yang et al., 2022).

δ^{15}N-PN was measured indirectly by the potassium persulfate oxidation and bacterial method (Knapp et al., 2005; Xu et al., 2022). The nitrate is formed by the digestion of the PN, after which the oxidized nitrate is analyzed by the denitrifier method as described above.

2.3.3 Rate estimate

N transformation rates (ρ), including ammonia oxidation, ammonium uptake, urea oxidation, and urea uptake were determined from the increment of ^{15}N-composition in the product pool during the incubation, using the below equation, following Dugdale and Wilkerson (1986) and Zheng et al. (2017):

$$\rho = [P] \times \frac{r_1 - r_0}{T} \times \left(\frac{^{15}N + ^{14}N}{^{15}N}\right)_{substrate}$$

where [P] represents concentrations of product pool (NO_x^- for oxidation rates and PN for uptake rates); r_1 and r_0 represent the isotopic composition of the product at T_1 and T_0; T represents incubation intervals.

2.4 Statistical analysis

The nonparametric Spearman correlation and significance tests of environmental factors and N transformation rates (n = 14 for all parameters except for temperature which n = 13) in the surface and bottom layers were performed by *corrplot* package (Wei and Simko, 2021) in R Language (R-Core-Team, 2022). Redundancy analysis (RDA) was performed by Canoco 5 software (ter Braak and Smilauer, 2012).

3 Results

3.1 Environmental setting

The salinity in this study area ranged from 0 to 27.7 (Figure 2A). The T1 station, located upstream of JRE (Figure 1), has the lowest salinity (~0) on both surface and bottom layers. Both salinity increase with the

10.3389/fmars.2022.1040554

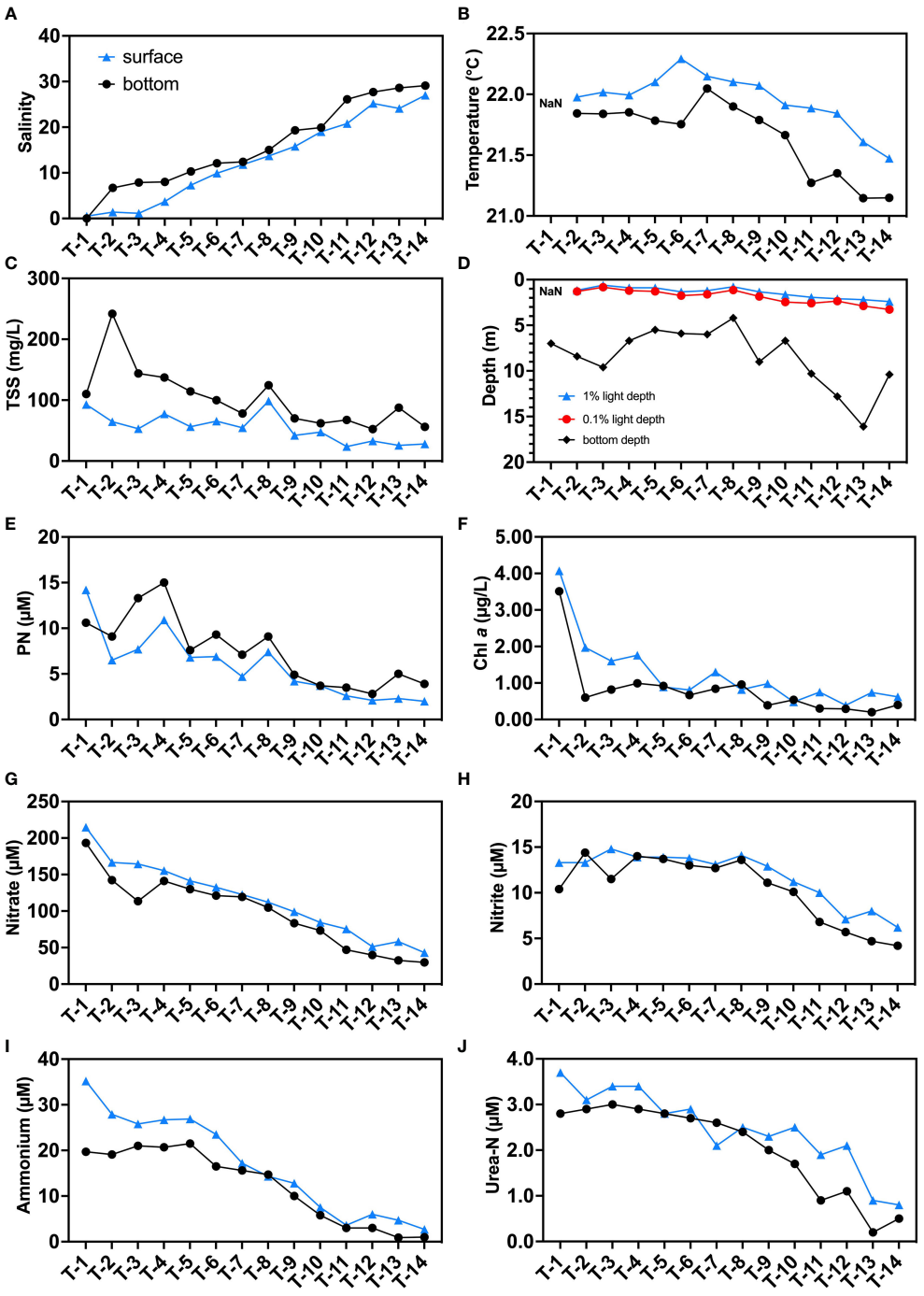

FIGURE 2
Distributions of environmental parameters in the sampling stations: **(A)** salinity; **(B)** temperature (°C); **(C)** total suspended substances (TSS, mg/L); **(D)** 1% surface light depth, 0.1% surface light depth, and bottom depth (m); **(E)** particulate N (PN, μM); **(F)** Chl *a* (μg/L); **(G)** nitrate (μM); **(H)** nitrite (μM); **(I)** ammonium (μM); and **(J)** urea-N (μM). Blue triangles indicate surface samples, black circles indicate bottom samples. "NaN" in subfigures **(B)** and **(D)** represent data that are not available.

main axis of the estuarine station towards the sea, reaching a maximum at station T14. The seawater intrusion was observed since higher salinity was found in bottom compared to surface layers in all stations. In this study, the range of water temperature was approximately between 21-22.5°C. And the high salinity stations were slightly cooler than upstream, possibly due to lower seawater temperatures (Figures 2B, S2A). In general, the surface layer was slightly warmer than the bottom layer in the vertical direction probably due to higher daytime temperatures and the heating of sunlight during the day.

The JRE is a turbid estuary where TSS can reach up to 272 mg/L upstream (T2) and over 50 mg/L at offshore stations (T12-T14) (Figures 2C, S2B). The bottom layers have higher TSS values (53-243 mg/L) than the surface layer (24-93 mg/L) which may be attributed to sediment resuspension. The high TSS resulted in a rapid weakening of light in the water column at the JRE. The 0.1% light intensity depths from the CTD data ranged from 0.8 m to 3.3 m, with an average of 76% (63%-91%) of depths in the sampled stations receiving no light even at noon (Figure 2D).

The PN shows a similar trend to the TSS, decreasing from upstream (~10 μM) to downstream (below 5 μM), and is higher at the bottom at most stations, suggesting a potential influence of sediment source (Figures 2E, S2C). Chl *a*, which is a representative of phytoplankton, had higher concentrations in the surface layer (0.39-4.07 μg/L) than in the bottom layer (0.20-3.51 μg/L), in contrast to the PN (Figures 2F, S2D).

All nitrogenous nutrients decrease in concentrations as salinity increases (Figures 2G–J, S2E–H). Nitrate dominates the DIN reservoirs in the JRE similar to previous studies (Yan et al., 2012). Nitrate concentrations fall below the conservative mixing line in upstream showing a slight deficit, and are conservative in the midstream and downstream (Figure S2E). The concentrations of nitrite (11.1 μM on average) were a magnitude lower than that of nitrate (average: 106.9 μM), and exhibit a significant addition pattern (Figure S2F). The ammonium and urea-N have their highest concentrations in upstream station T1's surface layer, which achieve 25.2 and 3.7 μM, respectively. The ammonium generally shows a removal pattern with data falling below the conservative mixing line while urea shows a slight addition pattern in midstream (Figures S2G, 2H). Urea-N accounts for approximately 13% of the total regenerated N reservoir (defined as ammonium plus urea-N here) on average.

3.2 N transformation rates

Oxidation and uptake pathways of both ammonium and urea in all 14 stations were measured simultaneously using the highly sensitive ^{15}N tracer technique (Figures 3, S3). Vertically, ammonia oxidation shows significantly higher rates in the bottom layers (43.7 nM/h on average) than that in the surface layers (21.6 nM/h on average) similar to previous research in Pearl River Estuary (Xu et al., 2022). The ammonia oxidation (Figure 3A) rate reaches the highest value for the surface (84.1 nM/h) and bottom (272.5 nM/h) rates at the upstream station T1. The surface rate gradually decreases from T1-T4, with little change from T4 to T14 (13.3 ± 3.6 nM/h, stands for mean value ± standard deviation of all data), while the bottom rate decreases from T1-T3, then slightly increases in T4 and T5, and reached stable in T6-T14 (16.9 ± 4.4 nM/h).

Ammonium uptake rates in the surface layers (16.0 nM/h) (Figure 3B), unlike ammonia oxidation, are generally greater than that in the bottom layers (11.6 nM/h). In the surface layers, ammonium uptake decreased from a maximum of 46.1 nM/h at station T1 to 19.4 nM/h at station T3 and then maintained a rate of ~20 nM/h at the four stations T3-T6, decreased to 5.5 nM/h (T11) seaward and finally slightly increased to ~10 nM/h at the offshore stations (T12-T14). In the bottom layers, T1 had the highest rate of 25.5 nM/h. After dropping to 8.3 nM/h at station T2, it was maintained at around 15 nM/h for the next 6 stations (T3-T8) before decreasing towards the sea end.

We report for the first time on urea oxidation and urea uptake in JRE. Similar to ammonium-related rates, vertically, urea-related rates show a bilayer structure, with urea oxidation in the surface layer (0.21 nM/h on average) being lower than the bottom layer (0.47 nM/h) and surface urea uptake (0.73 nM/h) higher than the bottom layer (0.24 nM/h) at most stations.

Urea oxidation rates (Figure 3C) in the bottom layers generally resemble the pattern of ammonia oxidation, while a slightly different pattern was found in the surface layers where urea oxidation rates peak in downstream station T12 (0.68 nM/h) which is near Xiamen Island and exhibit a high concentration of urea.

Unlike the above transformation processes, patterns of urea uptake were significantly different. Ammonia oxidation, ammonium uptake, and urea oxidation both had a negative correlation to salinity (Figures S3A–C), which may be due to the dilution of biomass (PN and Chl *a*, Figures S2C, D) and substrates (ammonium and urea, Figures S2G, H). Urea uptake (Figure 3D) is found to be active in the seaward, especially in the surface layers. The urea uptake rates in the seaward stations T11-T14 (1.60 ± 0.38 nM/h) were almost four times higher than that of other upstream stations (T1-T10: 0.38 ± 0.11 nM/h).

4 Discussion

4.1 Ammonia oxidation and its potentially influential factors

In the present study, we found ammonium-related rates were significantly higher than urea-related rates (Figures 4, S4). In particular, the ammonia oxidation rates were the highest of all

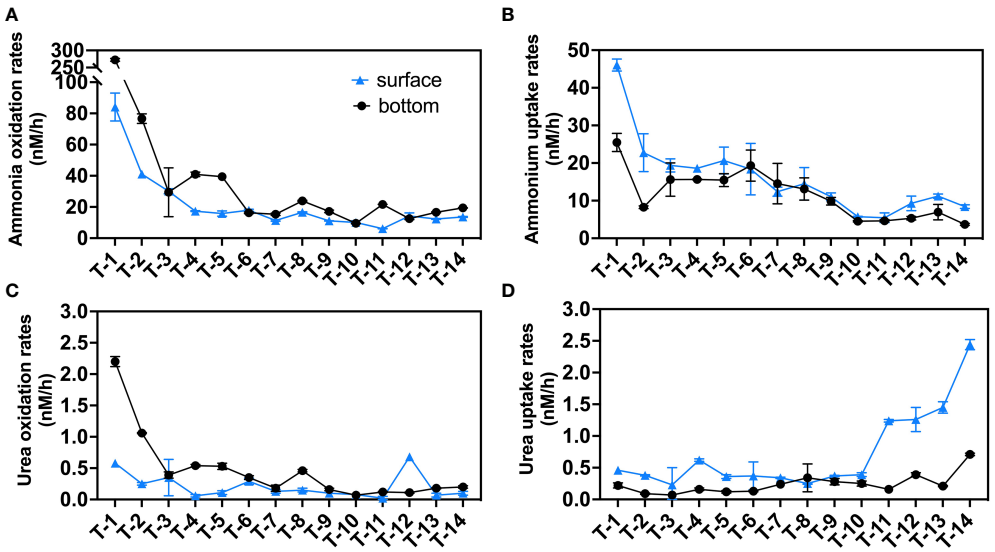

FIGURE 3
N transformation rates (nM/h) in the sampling stations: **(A)** ammonia oxidation rates; **(B)** ammonium uptake rates; **(C)** urea oxidation rates; **(D)** urea uptake rates. Blue triangles indicate surface rates, black circles indicate bottom rates and the error bars represent the standard deviation of the two biological replicates.

four N transformation rates, and only at a few stations the ammonium uptake rates in the surface layer could reach the order of magnitude of the ammonia oxidation rate.

Active ammonia oxidation in upstream stations is likely to cause nitrite accumulation in the JRE (Figure S2G) (Yan et al., 2019), which may further act as a substrate for denitrification and N uptake. The oxygen consumption that accompanies nitrification may also influence the biogeochemistry in the water column, with each molecule of ammonia oxidized being accompanied by 1.5 molecules of oxygen consumed to produce nitrite (Ward, 2008). Based on this ideal 1:1.5 stoichiometry, oxygen consumption due to nitrifiers (Figure S5) in winter averages 0.78 μM/day (0.2-3.3 μM/day) and 1.16 μM/day (0.5-9.8 μM/day) for the surface and bottom. Such consumption rates hardly affect the water column dissolved oxygen pool, especially in the case of short residence times in the estuary (days scale) (Wang et al., 2015). But in upstream (e.g., T1's bottom layer), the oxygen consumption due to nitrifiers can achieve a high value (9.8 μM/day), which even can be compared to community respiration 1.21-10.79 μM/day in the Changjiang River Estuary (Hsiao et al., 2014). This may partially contribute to the low oxygen condition in the bottom layer of JRE upstream which was found in previous research (Li et al., 2011).

During the winter in the JRE, rates of ammonia oxidation varied considerably from 6.1-272.5 nM/h (with a mean of 21.6 nM/h and 43.7 nM/h in the surface and bottom layers, respectively), significantly lower than the previous rate magnitude (5-850 nM/h, with a mean value of 145 nM/h) in the summer of the JRE (Yan et al., 2019). Such phenomenon also occurred in Pearl River Estuary (Dai et al., 2008), which may be related to the temperature preference of ammonia oxidation, as previous temperature manipulation experiments in the JRE showed that the optimum temperature for ammonia-oxidizing organisms under eutrophic conditions can even exceed 30°C (Zheng et al., 2020), suggesting that the present study (*in situ* temperatures between 21.0-22.5°C) should represent a lower limit for the rate of ammonia oxidation in the JRE.

TSS and light are two environmental factors that have opposite impacts on ammonia oxidation (Ward, 2008). In our study, ammonia oxidation rates of the surface layer were significantly lower than that of the bottom layer (Figures 3A, S3A). This pattern may attribute to significantly higher TSS (Figures 2C, S2B) and potentially higher attached nitrifier biomass in the bottom layer. TSS can provide a unique microenvironment with substrates and metals, which promotes the biomass of particle-attached nitrifiers and ammonia oxidation rate (Hsiao et al., 2014; Zheng et al., 2017). This effect may also influence the horizontal distribution of ammonia oxidation, as TSS and ammonia oxidation rates have a similar distribution pattern and are both significantly higher in upstream stations (Figures 2C, 3A). In contrast to TSS, light is a factor inhibiting the function of nitrifiers (Ward, 2008; Xu et al., 2019; Xu et al., 2022). In open ocean environments, light can affect the distribution of ammonia oxidation rates by influencing the *in situ* nitrifying biotas (Zakem et al., 2018). The weak light situation at the base of the euphotic zone may

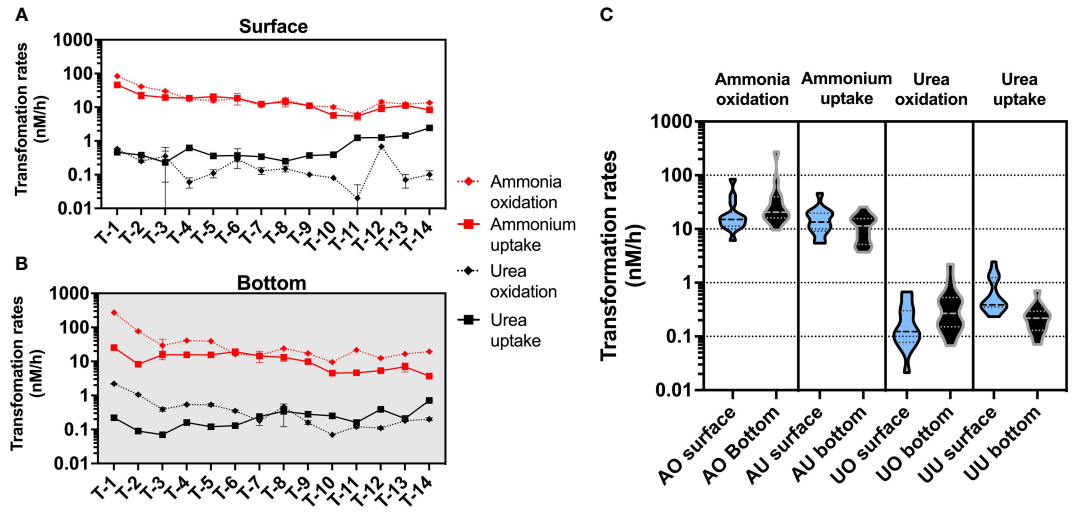

FIGURE 4
Magnitude distribution of different N transformation rates (nM/h) in the surface **(A)** and bottom **(B)** layers, with red and black representing ammonium and urea transformation rates, respectively. Subfigure **(C)** shows violin plots for different rates (AO, ammonia oxidation; AU, ammonium uptake; UO, urea oxidation; UU, urea uptake), with blue representing rates in the surface layer and black representing rates in the bottom layer.

shape the ecological niche in favor of nitrifying organisms. However, strong estuarine currents and seawater intrusion may introduce non-local biota and lead to shorter residence times of *in situ* communities which may greatly reduce the impact of the above-mentioned effect.

Besides the above-mentioned environmental factors, biomass may also significantly influence the spatial distribution of ammonia oxidation. In addition to being a facilitative factor in nitrification, TSS itself can be a nice indicator of nitrifiers biomass since a high proportion of nitrifiers is attached to large particles (Ma et al., 2019). We did not collect nitrifiers cell numbers. But we find that both TSS and PN in the bottom layer are significantly higher than that in the surface layer, while they are also significantly higher in the upstream than in the downstream, which is consistent with the distribution pattern of ammonia oxidation and suggests biomass difference largely shapes the spatial distribution of ammonia oxidation rates. Ammonium uptake may also be regulated by biomass. When we normalize ammonium uptake to Chl *a* (considered an indicator of phytoplankton biomass), the difference between upstream and downstream or surface and bottom becomes insignificant (Figure 5).

We also statistically analyzed the ammonia oxidation rate (and other N conversion rates) concerning environmental factors (Figure S8). But unfortunately, most of the environmental parameters are highly correlated with salinity distributions and each other, indicating the difficulties in separating single effects from multi-factors. Manipulation experiments for the mechanistic knowledge of the N cycle, need to be further implemented in future studies.

4.2 The potential inhibition-like effect of ammonium on urea utilization in eutrophic estuarine environments

Urea-N concentrations in this study were in a high range (0.25-3.73 μM, 2.25 μM on average), among the higher levels in aquatic environments worldwide (Figure 6A). This value falls within the concentration range of previous urea investigation in the winter of Xiamen sea area (0.50-3.09 μM in the surface and 0.36-3.23 μM in the bottom) (Wang et al., 2019) and comparable to those in the Pearl River estuary (0.16-8.24 μM) (Chen et al., 2015), another eutrophic estuary in southern China. Surprisingly, however, the rates of urea oxidation in JRE are of a much lower order than that of ammonia oxidation (which much higher than in the open ocean and some coastal systems, Figure 6E) and are only comparable to oligotrophic oceans where urea concentrations are only of the order of nM (e.g., western North Pacific, Figure 6D).

Both ammonia oxidation and urea oxidation can be carried out by ammonia-oxidizing microorganisms (AOM) (Alonso-Saez et al., 2012; Kitzinger et al., 2019; Shiozaki et al., 2021). In Earlier studies, ammonia-oxidizing archaea (AOA, e.g., *Thaumarchaeota*) are thought to be the primary performers of this process (Kirchman, 2012). But recent studies have shown that other microorganisms (including ammonia-oxidizing bacteria, AOB) may also be involved in the urea oxidation process (Shiozaki et al., 2021). Our qPCR results of *amoA* gene abundances suggest a switch of dominated AOM from AOB (freshwater, T1) to AOA (seaward, T14) (Figure S10). But such a switch in the nitrifiers community did not result in a significant

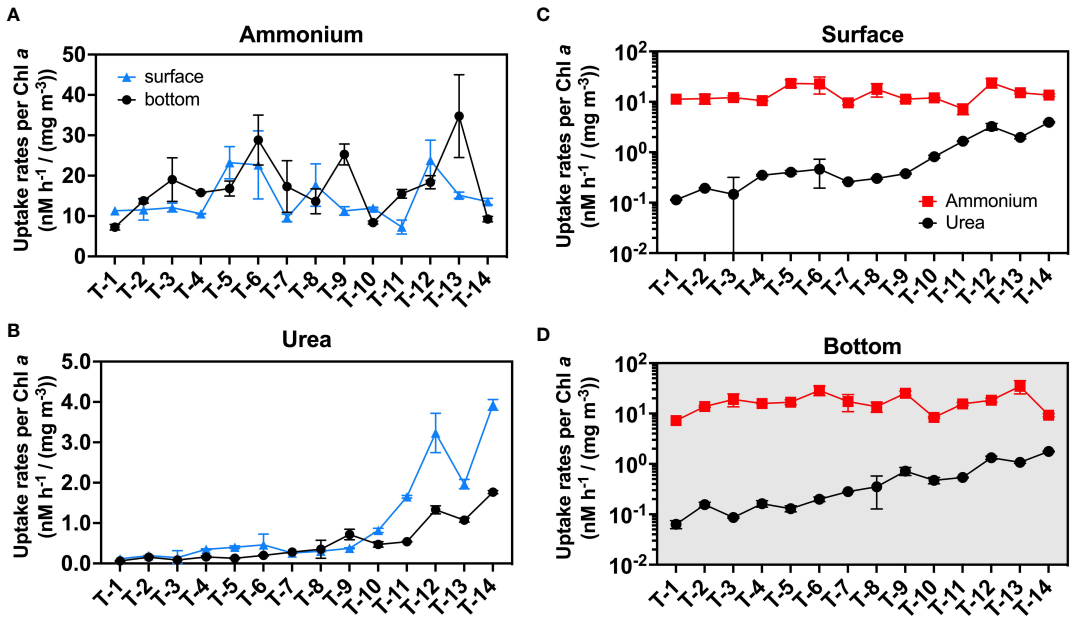

FIGURE 5
The uptake rate normalizes to Chl *a*. Subfigure **(A)** is plotted for the ammonium uptake rate while **(B)** is plotted for the urea uptake rate. Subfigures **(C)** and **(D)** are used for representing the magnitude of the rates in the surface **(C)** and bottom **(D)** layers. Blue triangles indicate surface rates, and black circles indicate bottom rates in subfigures **(A, B)**; red squares and black circles represent normalized ammonium and urea uptake rates, respectively in subfigures **(C, D)**. The error bars represent the standard deviation of the two biological replicates.

change in the urea oxidation to ammonia oxidation rate ratio (Figure 7) from upstream to downstream. This result implies that the nitrifiers community may not be the primary factor that results in the low urea oxidation rate. But, detailed knowledge of urea oxidizers is yet still lacking, and we cannot rule out the presence of other urea oxidizers other than AOM in the JRE.

We have summarized the data (including urea oxidation, ammonia oxidation, and their corresponding substrate concentrations; Figure 6) from this research and the literature covering various aquatic environments (Tolar et al., 2017; Kitzinger et al., 2019; Xu et al., 2019; Shiozaki et al., 2021; Wan et al., 2021) since the discovery of urea oxidation. A striking finding is the very low urea oxidation to ammonia oxidation ratio of the JRE (0.011 on average), which is significantly lower than open oceans such as the Northwest Pacific (0.29 on average) (Xu et al., 2019; Wan et al., 2021) and coastal regions (0.08-1.1) (Tolar et al., 2017).

Interestingly, the JRE has the highest ammonium concentration (Figure 6B) and the lowest urea-N/ammonium ratio (Figure 6C) among various aquatic environments, corresponding to the low ratio of urea oxidation/ammonia oxidation (Figure 6F). Ammonium is one of the most bioavailable forms of N and its preference by organisms may lead to a decrease in the transformation rates of other N species like nitrate, exhibiting an inhibition-like effect (Glibert et al., 2016). Urea oxidation and ammonia oxidation are both performed by nitrifiers and have similar physiological functions (provide energy). The presence of ammonium may lead to preferential use of it by microorganisms and less utilization of urea, which is requiring an additional step of hydrolysis. Yan et al. (2019) found that nitrate and nitrite uptake rates are inhibited when ammonium concentration is high, but once the ammonium is depleted, the uptakes rate greatly increases. Direct evidence about the influence of ammonium on urea oxidation has not been reported yet, but a strong inhibition of urea uptake by ammonium at a few μM was observed for a dinoflagellate species (*Alexandrium catenella*) (Jauzein et al., 2008). Thus, the very high concentration of ammonium in the JRE may have such effects on urea oxidation, resulting low urea oxidation to ammonia oxidation ratio, although urea is not scarce. Whereas for the open ocean, the extremely low concentration of ammonium (e.g., down to only a few nM) (Figure 6B) makes urea a potential option for nitrifying organisms and results in a higher urea oxidation ratio vs. ammonia oxidation (Figure 6F).

This may be supported by trends in urea uptake (Figures 3D, 5B, S9), which is high at stations T11-T14, where ammonium concentrations are low compared to upstream, and highest (2.5 nM/h) at the surface of station T14, where ammonium is at lowest. And a significant increase in urea uptake to ammonium uptake ratio also was observed in seaward sites (Figure 7) different from the constantly low urea oxidation to ammonia oxidation ratio.

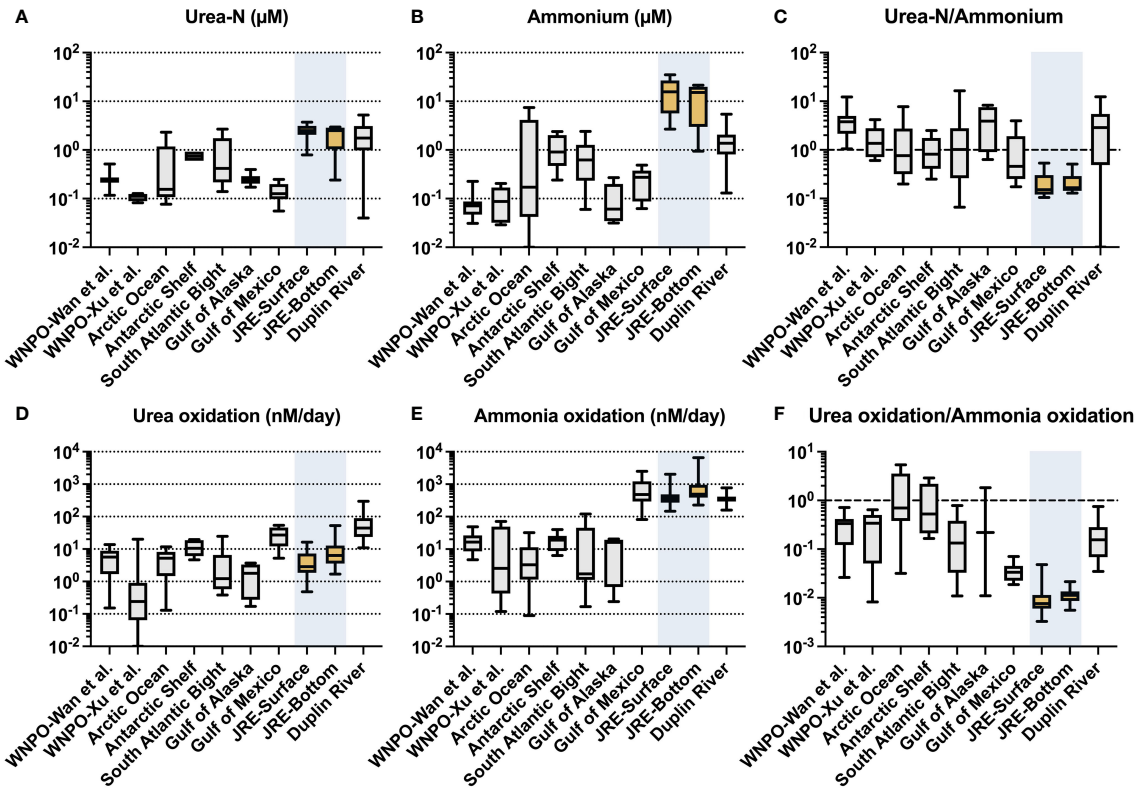

FIGURE 6
Urea-N concentration (μM), ammonium concentration (μM), ratio of urea-N to ammonium concentration; urea oxidation rates (nM/day), ammonia oxidation rates (nM/day), and urea oxidation to ammonia oxidation rates ratios collected from different literature: western North Pacific Ocean (WNPO) data was obtained from Wan et al. (2021) and Xu et al. (2019); Arctic Ocean data was obtained from Shiozaki et al. (2021); Antarctic Shelf, South Atlantic Bight, and Duplin River data were obtained from Tolar et al. (2017); Gulf of Mexico data was obtained from Kitzinger et al. (2019); Jiulong River Estuary (JRE) data was obtained from this study.

These trends may suggest that the inhibitory effect of ammonium on urea uptake is gradually released, and that urea oxidation may be more sensitive to ammonium than urea uptake and more easily be inhibited. Other factors like substrate concentration, biomass, and community structure can also influence the uptake process. But in seaward stations, urea concentrations at the sea end are much lower than upstream. The phenomenon of high values of urea uptake at the sea end did not disappear after normalization (normalize to PN as in Figure S9 and to Chl *a* as in Figure 5), but became more pronounced, showing that biomass is probably not the cause. Past studies have suggested that the phytoplankton of the JRE is dominated by diatoms (Xu et al., 2001; Xie et al., 2019). Fucoxanthin, a characteristic pigment of diatoms, was found to be almost dominant in the Xiamen Bay and JRE from upstream to downstream (Xu et al., 2001). Diatom has a high urea-utilizing capacity (Carpenter et al., 1972; Price and Harrison, 1988) and it is unlikely that the low urea uptake rates in upstream are caused by community reasons. Overall, it suggests that ammonium inhibition may play an important role in urea utilization in eutrophic environments.

4.3 Dark uptake, consumption, and the lifetime of ammonium and urea

Despite being in a dark condition, uptake shows considerable competitiveness relative to oxidation. In the surface layer, ammonium uptake could contribute to 44.8 ± 8.2% (Figure 8A) of total consumption rates on average, while that in the bottom layer was also able to reach an average proportion of 29.2 ± 13.2% (Figure 8B) of the ammonium consumption pathway. This proportion is even higher for urea in the surface (72.9 ± 18.9%, Figure 8C) and bottom layers (43.7 ± 26.4%, Figure 8D). These high proportions indicate that uptake is not negligible for sinks of ammonium and urea, even under dark conditions. Unlike the larger energy required for nitrate uptake, ammonium uptake is more energy-efficient, leading to a lower light-to-dark rate ratio in many aqueous environments relative to other oxidized N. In the Pearl River Estuary, the light-to-dark rate ratio for ammonium averages only about 2.45 (1.23-3.88), far below the mean value of 11.84 (1.05-28.37) for nitrate uptake (Xu et al., 2022). And in the western North Pacific, the light-to-dark ratio is less than 3 at most

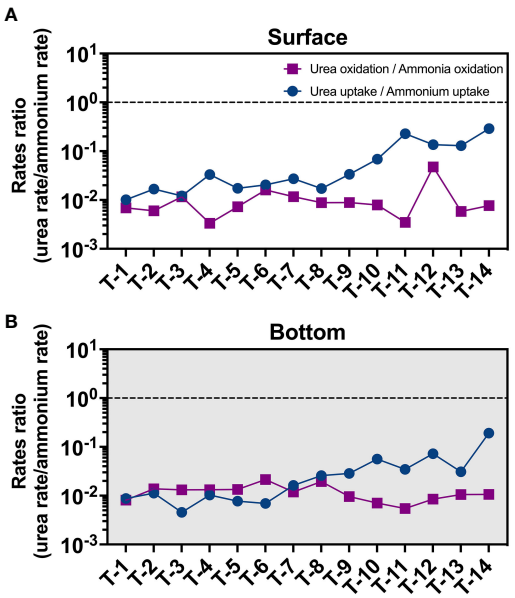

FIGURE 7
Distribution of urea oxidation to ammonia oxidation ratio (purple square) and urea uptake to ammonium uptake ratio (blue circle) in the surface **(A)** and bottom **(B)** layers.

stations with adequate substrates for both ammonium and urea uptake (Xu et al., 2019).

Combining the uptake and oxidation pathways, we were able to obtain the total consumption rate (Figures 8A–D) to explore the lifetime (defined as the reservoir divided by the consumption rate) of both ammonium and urea (Figures 8E, F). We found the lifetime of ammonium (surface: 19.3 ± 8.7 days; bottom 12.0 ± 7.2 days) was much less than that of urea (surface: 161.7 ± 87.6 days; bottom 148.0 ± 82.3 days), possibly due to the inhibition of urea-related rates by ammonium discussed in Section 4.2. Spatially, the upstream and offshore sites show shorter ammonium and urea lifetimes than the midstream; in the upstream, this may be due to relatively higher consumption rates of both reduced-state-N. While in the nearshore sites, for the ammonium case, it was due to lower concentrations relative to a conservative mixing line, while, for urea case, it may be that significantly higher urea uptake rates reduced urea lifetime to tens of days at these sites.

Although the above estimate of lifetimes may be an upper limit for the surface layer if the rate of N consumption in the surface layer is likely to be underestimated due to the lack of light incubation data, the high turbidity of the estuary results in a very shallow photic layer (1.36 m on average, Figure 2D). Since approximately 76 ± 8% of the water bodies experienced dark situations even in the daytime and the highly active estuarine circulation may bring surface organisms to the unlit layer, this estimate can still provide insights into dynamics of ammonium and urea in the estuary. In fact, this estimate is also consistent with our observed variation of the ammonium and urea reservoir with salinity, where we assume that the surface layer at the lowest salinity station T1 is the river end-member, and assume that nitrogenous nutrients have a concentration close to 0 at salinity 33, we can find that especially nearshore, ammonium shows a significant non-conservatism (deficit), which corresponds to the lifetime of ammonium at

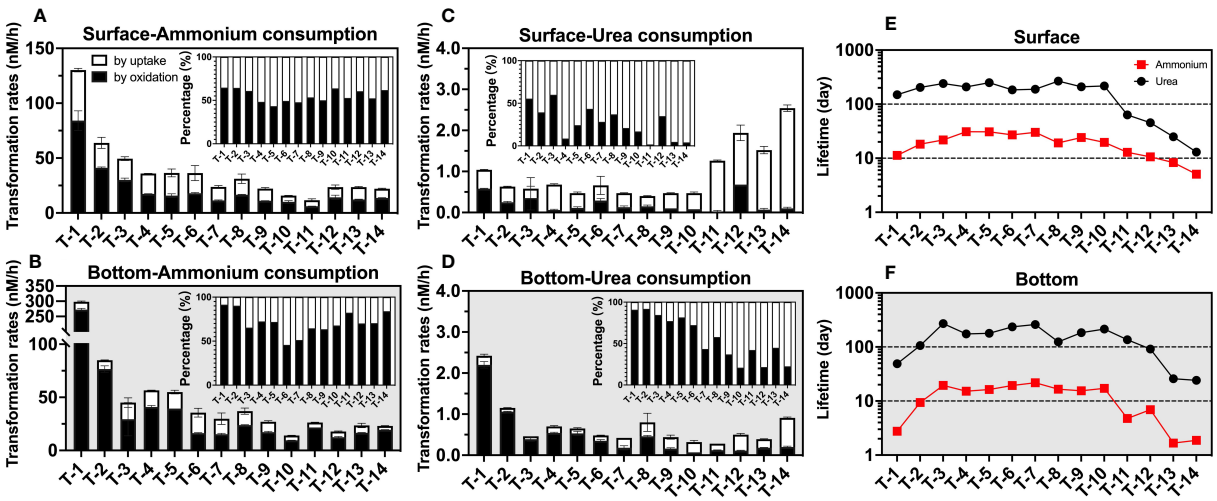

FIGURE 8
Consumption rates (nM/h) as well as lifetimes (day) of ammonium and urea. The graphs show the consumption rate of ammonium in the surface **(A)** and bottom **(B)** layers; the consumption rate of urea in the surface **(C)** and bottom **(D)** layers; and the lifetimes of urea and ammonium in the surface **(E)** and bottom **(F)** layers. In **(A–D)**, white represents consumption by uptake, black represents consumption by oxidation, the error bars represent the standard deviation of the two biological replicates, and the subplots indicate the percentage of different processes; in **(E, F)**, the red squares represent ammonium and the black circles represent urea.

offshore stations down to below 2 days (e.g., T13 bottom, 1.66 days), taking into account the estimate of 2.05 ± 0.95 days of flushing time in the winter derived from previous studies (Wang et al., 2015). In contrast, the trend of even near-addition of urea corresponds to its lifetime of hundreds of days, which may result from the ammonium's inhibition-like effect discussed above.

5 Conclusion

Overall, our observations provide new insights into estuarine ammonium and urea dynamics. Generally, ammonium-related processes (mainly ammonia oxidation) dominated the estuarine reduced-N cycle and found that dark uptake may also play an important role, showing a pattern that ammonia oxidation (32.6 ± 50.5 nM/h) > ammonium uptake (13.8 ± 8.7 nM/h) >> urea uptake (0.5 ± 0.5 nM/h) ≈ urea oxidation (0.3 ± 0.4 nM/h). Through the statistical analysis, we found that the salt-fresh water mixing of estuaries may dominate the distribution of all environmental factors as well as organisms and that the covariation of multiple factors influences the distribution of these rates, all of which make it difficult to separate the effects of single factors. From this perspective, more manipulation experiments still need to be performed to untangle the role of the specific environmental factors. By summarizing the available urea oxidation rates data, we found that high ammonium concentrations may have a significant inhibition-like effect on the urea process in the JRE, and our data imply that urea oxidation may be more sensitive to this effect than urea uptake. This effect suggests that high ammonium concentrations may further decrease the intensity of biogeochemical reactions of urea in the estuary, extend the lifetime of urea, and increase the urea delivering to offshore, which may have a significant impact on the coastal ecology.

Data availability statement

The original contributions presented in the study are included in the article/Supplementary Material. Further inquiries can be directed to the corresponding authors.

Author contributions

J-MT: Conceptualization, methodology, data curation, formal analysis, validation, software, visualization, writing - original draft, writing - review & editing. MNX: Conceptualization, formal analysis, validation, investigation, methodology, funding acquisition, resources, supervision, writing - original draft, writing - review & editing. YL: Data curation, formal analysis, visualization, writing - review & editing. HC: Methodology, writing - review & editing. HJ: Methodology, data curation, writing - review & editing. L-LH: Methodology, visualization, formal analysis, writing - review & editing. WZ: Investigation, methodology, project administration. S-JK: Conceptualization, funding acquisition, resources, supervision writing - review & editing. All authors contributed to the article and approved the submitted version.

Funding

This research was supported by the National Natural Science Foundation of China (91851209, 42106048, 41721005) and the Ph.D. Fellowship of the State Key Laboratory of Marine Environmental Science at Xiamen University.

Acknowledgments

We sincerely thank all crew members of RV *Ocean II* for their assistance. We thank valuable help from Yafei Xiao in the sampling and analysis of TSS, Chl *a*, and nutrients. We thank Li Tian for her help in project administration. We appreciate Xiaoqian Zhan for her help in collecting hydrological information. We are grateful to the Center for Major Equipment and Technology (COMET), State Key Laboratory of Marine Environmental Science, Xiamen University, for providing a platform for sharing instruments. We also thank Yuanzhi Li, Ruixiang Zhai, Jiaxin Sun, Yuxin Shen, and Zixiang Yang for their valuable advice about writing and thank the editor and five reviewers for their dedication to the peer review process to make this study better.

Conflict of interest

The authors declare that the research was conducted in the absence of any commercial or financial relationships that could be construed as a potential conflict of interest.

Publisher's note

Supplementary material

The Supplementary Material for this article can be found online at: https://www.frontiersin.org/articles/10.3389/fmars.2022.1040554/full#supplementary-material

References

Alonso-Saez, L., Waller, A. S., Mende, D. R., Bakker, K., Farnelid, H., Yager, P. L., et al. (2012). Role for urea in nitrification by polar marine archaea. *Proc. Natl. Acad. Sci. U.S.A.* 109 (44), 17989–17994. doi: 10.1073/pnas.1201914109

Becker, S., Aoyama, M., Woodward, E. M. S., Bakker, K., Coverly, S., Mahaffey, C., et al. (2020). GO-SHIP repeat hydrography nutrient manual: The precise and accurate determination of dissolved inorganic nutrients in seawater, using continuous flow analysis methods. *Front. Mar. Sci.* 7, 581790. doi: 10.3389/fmars.2020.581790

Braman, R. S., and Hendrix, S. A. (1989). Nanogram nitrite and nitrate determination in environmental and biological materials by vanadium(III) reduction with chemiluminescence detection. *Anal. Chem.* 61 (24), 2715–2718. doi: 10.1021/ac00199a007

Carpenter, E. J., Remsen, C. C., and Watson, S. W. (1972). Utilization of urea by some marine phytoplankters. *Limnol. Oceanogr.* 17 (2), 265–269. doi: 10.4319/lo.1972.17.2.0265

Chen, L., Ma, J., Huang, Y., Dai, M., and Li, X. (2015). Optimization of a colorimetric method to determine trace urea in seawater. *Limnol. Oceanogr.: Methods* 13 (6), 303–311. doi: 10.1002/lom3.10026

Chen, L., Zhang, X., He, B., Liu, J., Lu, Y., Liu, H., et al. (2020). Dark ammonium transformations in the pearl river estuary during summer. *J. Geophys. Res.: Biogeosci.* 125 (12), e2019JG005596. doi: 10.1029/2019jg005596

Dai, M., Wang, L., Guo, X., Zhai, W., Li, Q., He, B., et al. (2008). Nitrification and inorganic nitrogen distribution in a large perturbed river/estuarine system: the pearl river estuary, China. *Biogeosciences* 5 (5), 1227–1244. doi: 10.5194/bg-5-1227-2008

Dugdale, R. C., and Wilkerson, F. P. (1986). The use of ^{15}N to measure nitrogen uptake in eutrophic oceans; experimental considerations. *Limnol. Oceanogr.* 31 (4), 673–689. doi: 10.4319/lo.1986.31.4.0673

Francis, C. A., Roberts, K. J., Beman, J. M., Santoro, A. E., and Oakley, B. B. (2005). Ubiquity and diversity of ammonia-oxidizing archaea in water columns and sediments of the ocean. *Proc. Natl. Acad. Sci.* 102 (41), 14683–14688. doi: 10.1073/pnas.0506625102

Galloway, J. N. (2014). "10.12 - the global nitrogen cycle," in *Treatise on geochemistry*, *2nd ed.*, vol. 475-498 . Eds. H. D. Holland and K. K. Turekian (Oxford: Elsevier).

Glibert, P. M., Harrison, J., Heil, C., and Seitzinger, S. (2006). Escalating worldwide use of urea – a global change contributing to coastal eutrophication. *Biogeochemistry* 77 (3), 441–463. doi: 10.1007/s10533-005-3070-5

Glibert, P. M., Middelburg, J. J., McClelland, J. W., and Zanden, J. V. M. (2019). Stable isotope tracers: Enriching our perspectives and questions on sources, fates, rates, and pathways of major elements in aquatic systems. *Limnol. Oceanogr.* 64 (3), 950–981. doi: 10.1002/lno.11087

Glibert, P. M., Wilkerson, F. P., Dugdale, R. C., Raven, J. A., Dupont, C. L., Leavitt, P. R., et al. (2016). Pluses and minuses of ammonium and nitrate uptake and assimilation by phytoplankton and implications for productivity and community composition, with emphasis on nitrogen-enriched conditions. *Limnol. Oceanogr.* 61 (1), 165–197. doi: 10.1002/lno.10203

Hsiao, S. S. Y., Hsu, T. C., Liu, J.w., Xie, X., Zhang, Y., Lin, J., et al. (2014). Nitrification and its oxygen consumption along the turbid Chang jiang river plume. *Biogeosciences* 11 (7), 2083–2098. doi: 10.5194/bg-11-2083-2014

Jauzein, C., Loureiro, S., Garcés, E., and Collos, Y. (2008). Interactions between ammonium and urea uptake by five strains of *Alexandrium catenella* (Dinophyceae) in culture. *Aquat. Microb. Ecol.* 53 (3), 271–280. doi: 10.3354/ame01249

Kirchman, D. L. (2012). Marine archaea take a short cut in the nitrogen cycle. *Proc. Natl. Acad. Sci. U.S.A.* 109 (44), 17732–17733. doi: 10.1073/pnas.1215654109

Kitzinger, K., Padilla, C. C., Marchant, H. K., Hach, P. F., Herbold, C. W., Kidane, A. T., et al. (2019). Cyanate and urea are substrates for nitrification by thaumarchaeota in the marine environment. *Nat. Microbiol.* 4 (2), 234–243. doi: 10.1038/s41564-018-0316-2

Knapp, A. N., Sigman, D. M., and Lipschultz, F. (2005). N isotopic composition of dissolved organic nitrogen and nitrate at the Bermuda Atlantic time-series study site. *Global Biogeochem. Cycles* 19 (1), GB1018. doi: 10.1029/2004GB002320

Li, G., Gao, K., Yuan, D., Zheng, Y., and Yang, G. (2011). Relationship of photosynthetic carbon fixation with environmental changes in the jiulong river estuary of the south China Sea, with special reference to the effects of solar UV radiation. *Mar. pollut. Bull.* 62 (8), 1852–1858. doi: 10.1016/j.marpolbul.2011.02.050

Lin, J., Krom, M. D., Wang, F., Cheng, P., Yu, Q., and Chen, N. (2022). Simultaneous observations revealed the non-steady state effects of a tropical storm on the export of particles and inorganic nitrogen through a river-estuary continuum. *J. Hydrol.* 606, 127438. doi: 10.1016/j.jhydrol.2022.127438

Ma, L., Lin, H., Xie, X., Dai, M., and Zhang, Y. (2019). Major role of ammonia-oxidizing bacteria in N2O production in the pearl river estuary. *Biogeosciences* 16 (24), 4765–4781. doi: 10.5194/bg-16-4765-2019

Ma, L., Xiao, W., Laws, E. A., Bai, X., Chiang, K.-P., Liu, X., et al. (2021). Responses of phytoplankton communities to the effect of internal wave-powered upwelling. *Limnol. Oceanogr.* 66 (4), 1083–1098. doi: 10.1002/lno.11666

Moschonas, G., Gowen, R. J., Paterson, R. F., Mitchell, E., Stewart, B. M., McNeill, S., et al. (2017). Nitrogen dynamics and phytoplankton community structure: the role of organic nutrients. *Biogeochemistry* 134 (1), 125–145. doi: 10.1007/s10533-017-0351-8

Mulholland, M. R., and Lomas, M. W. (2008). "Chapter 7 - nitrogen uptake and assimilation," in *Nitrogen in the marine environment 2nd ed.* Eds. D. G. Capone, D. A. Bronk, M. R. Mulholland and E. J. Carpenter. (San Diego: Academic Press) 303–384

Pai, S.-C., Tsau, Y.-J., and Yang, T.-I. (2001). pH and buffering capacity problems involved in the determination of ammonia in saline water using the indophenol blue spectrophotometric method. *Anal. Chimica Acta* 434 (2), 209–216. doi: 10.1016/S0003-2670(01)00851-0

Peng, X., Fawcett, S. E., van Oostende, N., Wolf, M. J., Marconi, D., Sigman, D. M., et al. (2018). Nitrogen uptake and nitrification in the subarctic north Atlantic ocean. *Limnol. Oceanogr.* 63 (4), 1462–1487. doi: 10.1002/lno.10784

Price, N. M., and Harrison, P. J. (1988). Uptake of urea C and urea N by the coastal marine diatom *Thalassiosira pseudonana*. *Limnol. Oceanogr.* 33 (4), 528–537. doi: 10.4319/lo.1988.33.4.0528

Raimbault, P., and Garcia, N. (2008). Evidence for efficient regenerated production and dinitrogen fixation in nitrogen-deficient waters of the south pacific ocean: impact on new and export production estimates. *Biogeosciences* 5 (2), 323–338. doi: 10.5194/bg-5-323-2008

R-Core-Team (2022) *R: A language and environment for statistical computing* (Vienna, Austria: R Foundation for Statistical Computing). Available at: http://www.R-project.org/ (Accessed Septempter 17, 2022).

Rotthauwe, J. H., Witzel, K. P., and Liesack, W. (1997). The ammonia monooxygenase structural gene amoA as a functional marker: molecular fine-scale analysis of natural ammonia-oxidizing populations. *Appl. Environ. Microbiol.* 63 (12), 4704–4712. doi: 10.1128/aem.63.12.4704-4712.1997

Shiozaki, T., Hashihama, F., Endo, H., Ijichi, M., Takeda, N., Makabe, A., et al. (2021). Assimilation and oxidation of urea-derived nitrogen in the summer Arctic ocean. *Limnol. Oceanogr.* 66 (12), 4159–4170. doi: 10.1002/lno.11950

Sigman, D. M., Casciotti, K. L., Andreani, M., Barford, C., Galanter, M., and Böhlke, J. K. (2001). A bacterial method for the nitrogen isotopic analysis of nitrate in seawater and freshwater. *Anal. Chem.* 73 (17), 4145–4153. doi: 10.1021/ac010088e

Tan, E., Zou, W., Zheng, Z., Yan, X., Du, M., Hsu, T.-C., et al. (2020). Warming stimulates sediment denitrification at the expense of anaerobic ammonium oxidation. *Nat. Climate Change* 10 (4), 349–355. doi: 10.1038/s41558-020-0723-2

ter Braak, C. J. F., and Smilauer, P. (2012). *Canoco reference manual and user's guide: software for ordination, version 5.0* (Ithaca USA: Microcomputer Power).

Tolar, B. B., Wallsgrove, N. J., Popp, B. N., and Hollibaugh, J. T. (2017). Oxidation of urea-derived nitrogen by thaumarchaeota-dominated marine nitrifying communities. *Environ. Microbiol.* 19 (12), 4838–4850. doi: 10.1111/1462-2920.13457

Tseng, Y. F., Lin, J., Dai, M., and Kao, S. J. (2014). Joint effect of freshwater plume and coastal upwelling on phytoplankton growth off the changjiang river. *Biogeosciences* 11 (2), 409–423. doi: 10.5194/bg-11-409-2014

Voss, M., Wannicke, N., Deutsch, B., Bronk, D., Sipler, R., Purvaja, R., et al. (2011) "5.07 - internal cycling of nitrogen and nitrogen transformations," in *Treatise on estuarine and coastal science* Eds. E. Wolanski and D. McLusky (Waltham: Academic Press), 231–259.

Wang, K., Chen, B.-h., Luo, Y., Chen, W.-f., Wang, W.-l., and Lin, H. (2019). Spatial and temporal distribution of urea and its impacting factors in xiamen sea area (in Chinese). *J. Appl. Oceanogr.* 38 (2), 214–224.

Wang, G., Wang, Z., Zhai, W., Moore, W. S., Li, Q., Yan, X., et al. (2015). Net subterranean estuarine export fluxes of dissolved inorganic C, N, p, Si, and total alkalinity into the jiulong river estuary, China. *Geochimica Cosmochimica Acta* 149, 103–114. doi: 10.1016/j.gca.2014.11.001

Wang, X., Wu, X., Chen, M., Cheng, H., Chen, N., Yang, W., et al. (2021). Isotopic constraint on the sources and biogeochemical cycling of nitrate in the jiulong river estuary. *J. Geophys. Res.: Biogeosci.* 126 (3), e2020JG005850. doi: 10.1029/2020jg005850

Wan, X. S., Sheng, H. X., Dai, M., Church, M. J., Zou, W., Li, X., et al. (2021). Phytoplankton-nitrifier interactions control the geographic distribution of nitrite

in the upper ocean. *Global Biogeochem. Cycles* 35 (11), e2021GB007072. doi: 10.1029/2021gb007072

Ward, B. B. (2008). "Chapter 5 - nitrification in marine systems," in *Nitrogen in the marine environment*, *2nd ed.* Eds. D. G. Capone, D. A. Bronk, M. R. Mulholland and E. J. Carpenter (San Diego: Academic Press), 199–261

Wei, T., and Simko, S. (2021) *R package 'corrplot': Visualization of a correlation matrix (Version 0.92)*. Available at: https://github.com/taiyun/corrplot (Accessed September 17, 2022).

Wu, G., Cao, W., Huang, Z., Kao, C.-M., Chang, C.-T., Chiang, P.-C., et al. (2017). Decadal changes in nutrient fluxes and environmental effects in the jiulong river estuary. *Mar. pollut. Bull.* 124 (2), 871–877. doi: 10.1016/j.marpolbul.2017.01.071

Xiao, W., Wang, L., Laws, E., Xie, Y., Chen, J., Liu, X., et al. (2018). Realized niches explain spatial gradients in seasonal abundance of phytoplankton groups in the south China Sea. *Prog. Oceanogr.* 162, 223–239. doi: 10.1016/j.pocean.2018.03.008

Xie, Y., Wang, L., Liu, X., Li, X., Wang, Y., and Huang, B. (2019). Contrasting responses of intertidal microphytobenthos and phytoplankton biomass and taxonomic composition to the nutrient loads in the jiulong river estuary. *Phycol. Res.* 67 (2), 152–163. doi: 10.1111/pre.12363

Xu, L., Hong, H.-s., Wang, H.-l., and Chen, W.-q. (2001). The biogeochemistry of photosynthetic pigments in the jiulong river estuary and Western xiamen bay. *Chin. J. Oceanol. Limnol.* 19 (2), 164–171. doi: 10.1007/bf02863042

Xu, M. N., Li, X., Shi, D., Zhang, Y., Dai, M., Huang, T., et al. (2019). Coupled effect of substrate and light on assimilation and oxidation of regenerated nitrogen in the euphotic ocean. *Limnol. Oceanogr.* 64 (3), 1270–1283. doi: 10.1002/lno.11114

Xu, M. N., Wu, Y., Zhang, X., Tang, J.-M., Tan, E., Zheng, Z. Z., et al. (2022). Diel change in inorganic nitrogenous nutrient dynamics and associated oxygen stoichiometry along the pearl river estuary. *Water Res.* 222, 118954. doi: 10.1016/j.watres.2022.118954

Xu, M. N., Wu, Y., Zheng, L. W., Zheng, Z., Zhao, H., Laws, E. A., et al. (2017). Quantification of multiple simultaneously occurring nitrogen flows in the euphotic ocean. *Biogeosciences* 14 (4), 1021–1038. doi: 10.5194/bg-14-1021-2017

Yang, J.-Y. T., Tang, J.-M., Kang, S., Dai, M., Kao, S.-J., Yan, X., et al. (2022). Comparison of nitrate isotopes between the south China Sea and Western north pacific ocean: Insights into biogeochemical signals and water exchange. *J. Geophys. Res.: Oceans* 127 (5), e2021JC018304. doi: 10.1029/2021JC018304

Yan, X., Wan, X. S., Liu, L., Xu, M. N., Tan, E., Zheng, Z., et al. (2019). Biogeochemical dynamics in a eutrophic tidal estuary revealed by isotopic compositions of multiple nitrogen species. *J. Geophys. Res.: Biogeosci.* 124 (7), 1849–1864. doi: 10.1029/2018jg004959

Yan, X., Zhai, W., Hong, H., Li, Y., Guo, W., and Huang, X. (2012). Distribution, fluxes and decadal changes of nutrients in the jiulong river estuary, southwest Taiwan strait. *Chin. Sci. Bull.* 57 (18), 2307–2318. doi: 10.1007/s11434-012-5084-4

Zakem, E. J., Al-Haj, A., Church, M. J., van Dijken, G. L., Dutkiewicz, S., Foster, S. Q., et al. (2018). Ecological control of nitrite in the upper ocean. *Nat. Commun.* 9 (1), 1206. doi: 10.1038/s41467-018-03553-w

Zheng, Z.-Z., Wan, X., Xu, M. N., Hsiao, S. S.-Y., Zhang, Y., Zheng, L.-W., et al. (2017). Effects of temperature and particles on nitrification in a eutrophic coastal bay in southern China. *J. Geophys. Res.: Biogeosci.* 122 (9), 2325–2337. doi: 10.1002/2017JG003871

Zheng, Z.-Z., Zheng, L.-W., Xu, M. N., Tan, E., Hutchins, D. A., Deng, W., et al. (2020). Substrate regulation leads to differential responses of microbial ammonia-oxidizing communities to ocean warming. *Nat. Commun.* 11 (1), 3511. doi: 10.1038/s41467-020-17366-3

frontiers | Frontiers in Marine Science

TYPE Original Research
PUBLISHED 16 December 2022
DOI 10.3389/fmars.2022.1104135

OPEN ACCESS

EDITED BY
Xianbiao Lin,
Ocean University of China, China

REVIEWED BY
Yiguo Hong,
Guangzhou University, China
Guoyu Yin,
East China Normal University, China

*CORRESPONDENCE
Xiuli Yan
yanxl@stu.edu.cn
Shuh-Ji Kao
sjkao@xmu.edu.cn

SPECIALTY SECTION
This article was submitted to Marine Biogeochemistry, a section of the journal Frontiers in Marine Science

RECEIVED 21 November 2022
ACCEPTED 05 December 2022
PUBLISHED 16 December 2022

CITATION
Yan X, Yang J-YT, Xu MN, Tan E, Zheng Z, Zou W, Dai M and Kao S-J (2022) Isotope constraints on nitrogen dynamics in the upper water column of the South China Sea. *Front. Mar. Sci.* 9:1104135. doi: 10.3389/fmars.2022.1104135

Isotope constraints on nitrogen dynamics in the upper water column of the South China Sea

Xiuli Yan[1]*, Jin-Yu Terence Yang[2], Min Nina Xu[3], Ehui Tan[3], Zhenzhen Zheng[3], Wenbin Zou[2], Minhan Dai[2] and Shuh-Ji Kao[2,3]*

[1]Guangdong Provincial Key Laboratory of Marine Disaster Prediction and Prevention, Institute of Marine Sciences, Shantou University, Shantou, China, [2]State Key Laboratory of Marine Environmental Science, College of Ocean and Earth Sciences, Xiamen University, Xiamen, China, [3]State Key Laboratory of Marine Resource Utilization in South China Sea, Hainan University, Haikou, China

The supply of nitrogen (N) from various external and internal sources into the euphotic zone, e.g., atmospheric N deposition (AND), upwelling, lateral intrusion, and remineralization, modulates the biogeochemical and climatic roles of oligotrophic oceans and complicates N dynamics in the upper water column (≤200 m). However, our ability to resolve the mechanisms controlling upper-ocean N cycling is limited by the lack of high-resolution vertical observations. Here, we analyzed concentrations and dual isotopes of nitrate (NO_3^-) in the upper 200 m of the oligotrophic South China Sea. By examining dual isotopic signatures of NO_3^- ($\delta^{15}N_{NO3}$ and $\delta^{18}O_{NO3}$) and multiple associated parameters vertically throughout the upper water column, we resolved the dominant N sources and processes, including AND/N_2-fixation, assimilative fractionation, and nitrification, and quantitatively evaluated their contributions in the vertical distribution of NO_3^-, which can be separated into the $\Delta\delta^{18}O_{NO3}$-positive ($\delta^{18}O_{NO3-obs}-\delta^{18}O_{NO3-200m}>0$) and $\Delta\delta^{18}O_{NO3}$-negative layers ($\delta^{18}O_{NO3-obs}-\delta^{18}O_{NO3-200m}<0$) according to the deviation in $\delta^{18}O_{NO3}$ at a given depth ($\delta^{18}O_{NO3-obs}$) from that at 200 m ($\delta^{18}O_{NO3-200m}$). In the $\Delta\delta^{18}O_{NO3}$-positive layer, the NO_3^- assimilated by phytoplankton was largely sourced from nitrification (39 ± 11%) and AND/N_2 fixation (17-28%), whereas these two processes accounted for 17 ± 10% and 7 ± 6% of the total NO_3^- pool in the $\Delta\delta^{18}O_{NO3}$-negative layer. Considering a substantial contribution of the regenerated (nitrification-sourced) NO_3^- to the total NO_3^- pool especially in the $\Delta\delta^{18}O_{NO3}$-positive layer, caution should be taken that the new production assessed by the rates of NO_3^- uptake may be significantly overestimated in the SCS. These findings not only highlight the importance of these biogeochemical processes to NO_3^- dynamics in the upper water column of marginal seas, but also with important implications for the estimation of biological carbon pump and/or the *f*-ratio.

KEYWORDS

nitrogen dynamcis, South China Sea (SCS), nitrification, external nitrogen source, nitrogen isotope ($\delta^{15}N$), nitrogen uptake

1 Introduction

Nitrogen (N) supply limits productivity in the ocean (Moore et al., 2013), thereby connecting the N cycle with marine carbon sequestration (Falkowski, 1997; Buchanan et al., 2021). In oligotrophic regions, regenerated N is the main N source for phytoplankton growth in surface waters (<100 m), since inputs of subsurface (100-200 m) nitrate (NO_3^-) supply are generally limited by strong stratification (Yool et al., 2007; Van Oostende et al., 2017). However, in marginal seas, while diapycnal fluxes of N to the N-replete layer are sufficient to support the levels of export production, additional external sources of N from atmospheric N deposition/N_2 fixation (AND/N_2 fixation) can stimulate phytoplankton growth in the N-depleted layer (Kao et al., 2012; Du et al., 2017; Lu et al., 2019). In addition, lateral transport also influences N dynamics in the euphotic zone, as different water masses vary in their relative concentrations of N compounds and microbial communities that alter N dynamics physically and biologically (Du et al., 2013; Xu et al., 2018). Therefore, the co-influence of various external N sources and their differing magnitudes make N dynamics more complicated in the upper ocean of marginal seas (Kao et al., 2012; Liu et al., 2020).

The South China Sea (SCS) is one of the largest marginal seas in the world, with an area of 3.5×10^6 km^2. It is a typical stratified and oligotrophic oceanic regime, showing extremely low N:P ratios (0.4-4.4) in surface waters (<60 m), and thus low levels of biomass primarily due to N limitation (Chen et al., 2004; Du et al., 2017). Although many studies have found various N sources involved in biological production within the upper ocean, such as diapycnal transport, lateral transport, AND/N_2 fixation (Kao et al., 2012; Du et al., 2013; Yang et al., 2014; Du et al., 2017; Yang et al., 2017; Lu et al., 2019), it remains unclear how these sources and subsequent processes imprint on the N cycle of the upper water column of the SCS. These processes contribute to the complexity of N dynamics in the region over temporal and spatial scales. Seasonally, reactive N deposition to the SCS varies from 48 ± 34 μmol N/m^2/d in July to 99 ± 78 μmol N/m^2/d in September (Yang et al., 2014). Regionally, the depth-integrated N_2 fixation rates vary from 50 ± 10 μmol N/m^2/d in the basin to 463 ± 260 μmol N/m^2/d in the Kuroshio-affected region (Lu et al., 2019). In oligotrophic water column, the vertical diapycnal N flux is three orders of magnitude larger in the nutrient-replete layer relative to the nutrient-depleted layer (Du et al., 2017). This study aims to decipher the N dynamics of multiple external sources and internal processes by using a NO_3^- dual isotopic approach ($\delta^{15}N_{NO3}$ and $\delta^{18}O_{NO3}$), which serves as an integral tracer of the N pool in the upper water column of the SCS. These results contribute to our understanding of N dynamics in marginal seas, and benefit the development and parameterization of N-driven physical-biogeochemical models.

The $\delta^{15}N_{NO3}$ and $\delta^{18}O_{NO3}$ provide useful constraints on its source (Sigman et al., 2005; Rafter and Sigman, 2016; Yang et al., 2022) and can be used to explore relevant N cycling processes (Emeis et al., 2010; Fawcett et al., 2015; Buchanan et al., 2021). The first study to utilize a dual isotopic approach ($\delta^{15}N$ and $\delta^{13}C$) in the region focused on evaluating the role of N sources in zooplankton nutrition in the Vietnamese upwelling area (Loick et al., 2007). Additional work by Yang et al. (2017) examined N cycling using $\delta^{15}N$ in NO_3^- and particulate phases in the northern SCS. However, these two isotope studies had difficulty assessing the influence of nitrification (a common process in the euphotic zone) due to the lack of $\delta^{18}O_{NO3}$ measurements. Recently, two studies have illustrated the spatial variations of NO_3^- sources and N cycling in the SCS using both $\delta^{15}N_{NO3}$ and $\delta^{18}O_{NO3}$ (Chen et al., 2019; Yang et al., 2022); however, they mainly focused on the whole water column, with only 2-4 measurable isotope samples in the top 200 m. Thus, it is difficult to make a comprehensive assessment of NO_3^- dynamics within the upper ocean. In this study, we performed high-resolution vertical observation of the concentrations and dual isotopic composition of NO_3^-, in order to decipher the critical elements influencing NO_3^- dynamics in the upper water column of the SCS including the relative importance of external N sources and internal processes to NO_3^- uptake and assimilative fractionation.

2 Materials and methods

2.1 Study area

The circulation patterns in the SCS vary seasonally as a function of the East Asia monsoon (Figure 1A). In winter, the northeast monsoon pushes the SCS Warm Current southwestward and drives a basin-wide cyclonic gyre (Hu et al., 2000; Liu et al., 2016). In summer, the SCS Warm Current shifts northeastward and the basin-wide cyclonic gyre shifts eastward under the influence of southwesterly monsoon (Liu et al., 2016). The surface water mass in the SCS changes based on the extent of intrusion of the Kuroshio Current through the Luzon Strait, which varies both throughout the year and over decadal time scales (Hu et al., 2000; Yuan et al., 2006; Nan et al., 2015). Previous studies showed lateral Kuroshio intrusion influences not only the heat and salt of the SCS, but also N and carbon biogeochemical cycles due to high dissolved organic carbon and low nutrient concentrations in the Kuroshio waters (Du et al., 2013; Nan et al., 2015; Wu et al., 2015).

2.2 Field sample collections

Water samples were collected in the SCS onboard the R/V *Dongfanghong II* during March 2013, June 2014, May-June 2016, and onboard the R/V *TAN KAH KEE* during June 2017

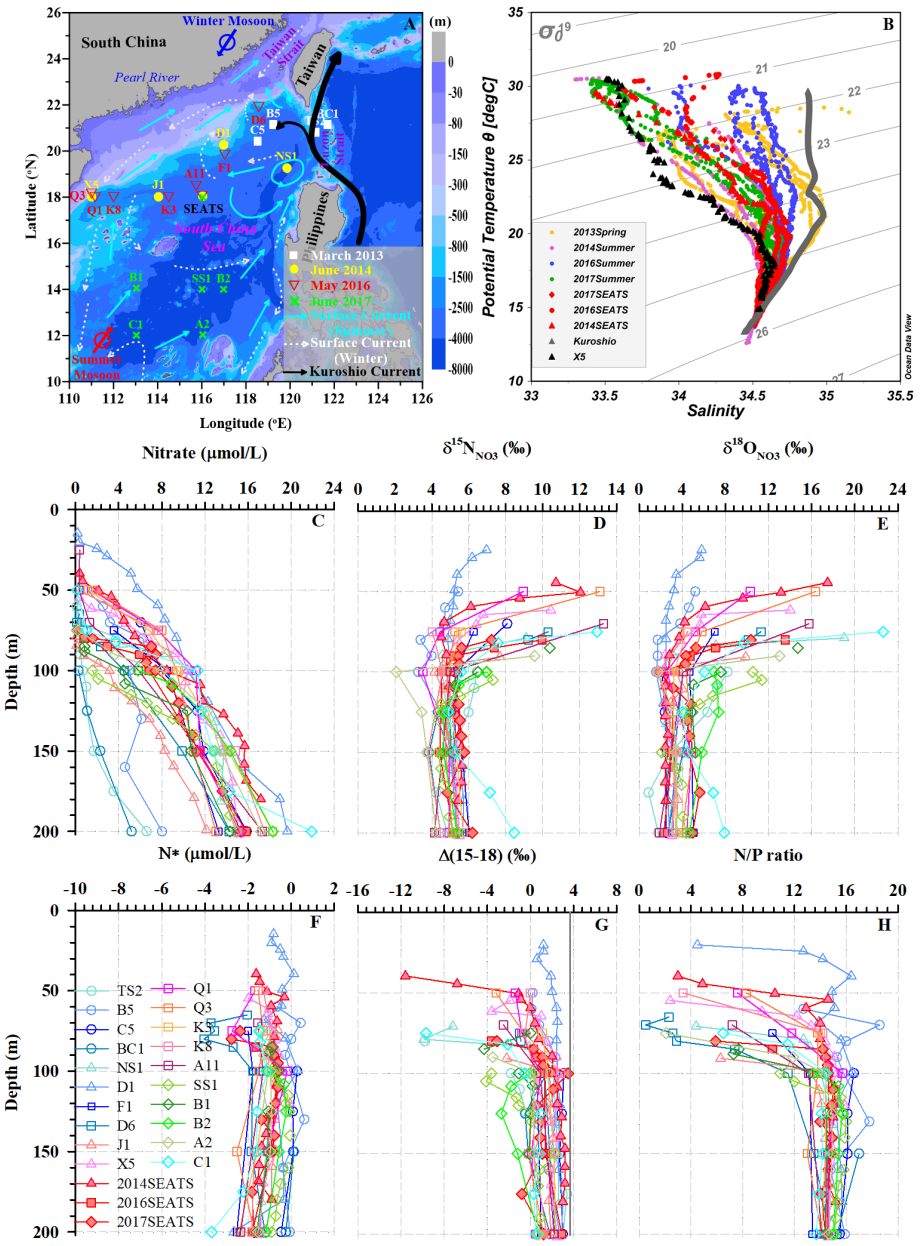

FIGURE 1
(A) Study area and sampling stations in the SCS. Surface circulation patterns are shown with arrows synthesized from previous studies (Yuan et al., 2006; Nan et al., 2015; Liu et al., 2016): summertime surface currents (cyan), wintertime surface currents (white dashed), and the Kuroshio Current (black). The color bar indicates water depth. **(B)** Potential temperature-salinity diagram for all stations. The red and black triangles indicate typical SCS water and coastal water, respectively. The gray triangles represent the Kuroshio Current. **(C–H)** Depth and isopycnal profiles for all samples with NO_3^- concentrations ≥0.5 μmol/L: NO_3^- concentrations **(C)**, $\delta^{15}N_{NO3}$ **(D)**, $\delta^{18}O_{NO3}$ **(E)**, N* **(F)**, Δ(15-18) **(G)**, and N/P ratio **(H)**.

(Figure 1A). Seawater was collected for analysis of the concentrations and isotopic composition of NO_3^- at 5-32 layers from the surface (5 m) to 200 m using 12 L Niskin bottles attached to a Seabird SBE-911 plus CTD-rosette sampling system. More details of the sampling layers/intervals in each station can be found in the Supplementary Table 1 and the datasets. Unfiltered seawater samples were collected in 125 mL acid-washed high-density polyethylene bottles that were

rinsed thoroughly with *in situ* seawater prior to filling. Water samples were immediately frozen on board at −20 °C until analysis.

2.3 Concentration and isotopic analysis of nitrate

The concentrations of NO_3^- and nitrite (NO_2^-) were measured using a Four-channel Continuous Flow Technicon AA3 Auto-Analyzer (Bran-Luebbe), with detection limits of 0.07 μmol/L for NO_3^- and 0.02 μmol/L for NO_2^- (Dai et al., 2008; Du et al., 2013).

The values of $\delta^{15}N_{NO3}$ and $\delta^{18}O_{NO3}$ (for samples with NO_3^- concentrations ≥ 0.5 μmol/L) were determined by the denitrifier method (Sigman et al., 2001; Casciott et al., 2002). Briefly, denitrifying bacteria lacking nitrous oxide (N_2O) reductase were used to quantitatively convert NO_3^- in samples to N_2O. Subsequently, the isotopic compositions of N_2O were measured *via* GasBench II-IRMS (Thermo Scientific DELTA V advantage) equipped with an on-line extraction and purification system. Four internationally recognized NO_3^- reference materials (International Atomic Energy Agency (IAEA)-NO_3^-: $\delta^{15}N$ = 4.7‰ and $\delta^{18}O$ = 25.6‰, U.S. Geological Survey (USGS)-34: $\delta^{15}N$ = −1.8‰ and $\delta^{18}O$ = −27.9‰, USGS-35: $\delta^{18}O$ = 57.5‰ and USGS-32: $\delta^{15}N$ = 180‰) were used for $\delta^{15}N$ and $\delta^{18}O$ calibration (Böhlke et al., 2003). One of the NO_3^- reference materials (IAEA-NO_3^-) was run in parallel to monitor bacterial conversion efficiency and mass spectrometer drift. In terms of sample replicates, the analytical precision of $\delta^{15}N_{NO3}$ and $\delta^{18}O_{NO3}$ measurements as better than ±0.2‰ and ±0.5‰, respectively (Yan et al., 2017; Yan et al., 2019). To avoid the influence of NO_2^- on $\delta^{15}N_{NO3}$ and $\delta^{18}O_{NO3}$ values, all samples were treated with sulfamic acid (Sigma, guaranteed reagent) to remove pre-existing NO_2^- following the procedure in Granger and Sigman (2009).

3 Results

3.1 Hydrological characteristics

From Figure 1B, we can see all potential temperature-salinity profiles merge at a salinity of 34.4 and temperature of 13 °C, suggesting the same subsurface water (~200 m) source among these stations. Generally, as the potential density anomaly (σ_Θ=σ−1000, unit: kg/m^3) decreased toward the surface (~5 m), the potential temperature rose while the salinity first increased and then decreased. However, distinct hydrological differences were found between offshore SCS water measured at the South-East Asian Time-series Study (SEATS) station, the Kuroshio Current and coastal water (station X5, σ_Θ<25.5). At the same isopycnal surface, the Kuroshio Current had the highest potential temperature and salinity, followed by SEATS, and the coastal water. The hydrological characteristics at most stations were controlled by the isopycnal mixing between the Kuroshio Current and the coastal water. Thus, due to greater influence from Kuroshio intrusion near the Luzon Strait, datapoints were more scattered and skewed toward the typical Kuroshio characteristics in spring relative to those in summer.

3.2 Vertical distributions of nitrate and its isotopic composition

The vertical profiles showed NO_3^- concentrations increased with increasing water depth (Figure 1C), with values ranging from 5.2 to 21.9 μmol/L. The lowest values (~0.1 μmol/L) were found mostly at depths of <50 m, while the highest values appeared at 200 m. Thus, the vertical gradients of NO_3^- differed among stations. For example, at stations TS2, B5 and BC1 near the Luzon Strait, which were more influenced by Kuroshio intrusion, NO_3^- concentrations were lower and varied within a narrow range of 0.1-8.0 μmol/L. However, at the southernmost station C1 where upwelling appeared, the NO_3^- concentration showed a steep gradient, changing from 0.2 μmol/L at 50 m depth to a maximum of 21.9 μmol/L at 200 m. Clearly, the vertical distributions of NO_3^- concentrations exhibited distinct north-to-south differences. By defining the nitracline depth as that where NO_3^- concentrations reached 2.0 μmol/L (Wilson and Coles, 2005), we found it ranged between 24-154 m, with a mean value of 77 ± 30 m (n=22, Table 1). The nitracline depths at stations near the Luzon Strait were the deepest due to the influence of warm, nutrient-depleted waters from Kuroshio intrusion.

The $\delta^{15}N_{NO3}$ values showed strong gradients above the nitracline (<125 m), but weaker gradients below the nitracline (Figure 1D). They generally fell within a narrow range of 3.4-5.7‰ below the nitracline; however, they became enriched upward toward the surface (6.4-13.3‰, ~20 m), accompanied by lower NO_3^- concentrations. For example, at station A11, $\delta^{15}N_{NO3}$ reached a maximum of 13.3‰ at 70 m. However, the site with the shallowest nitracline (station D1) had a weaker $\delta^{15}N_{NO3}$ gradient varying between 4.9-7.0‰ (Table 1). In addition, the $\delta^{15}N_{NO3}$ values at several stations (A2, Q1, B5 and C1) showed minima (2.1‰, 3.5‰, 3.3‰, and 4.9‰, respectively) at 75-125 m depths.

The $\delta^{18}O_{NO3}$ values were relatively constant below the nitracline but increased sharply from depths of 100-125 m toward ~20 m (Figure 1E), and $\delta^{18}O_{NO3}$ variability (5.2-22.5‰) was larger than that of $\delta^{15}N_{NO3}$ above the nitracline. The maximum values of $\delta^{18}O_{NO3}$ above the nitracline differed among stations. At stations NS1 and C1, $\delta^{18}O_{NO3}$ reached maximum values of 19.0‰ and 22.6‰, respectively, around a depth of 75 m. However, $\delta^{18}O_{NO3}$ maxima were observed at shallower depths (24-55 m) at stations D1 and B5, reaching only

TABLE 1 The isotope effect of NO_3^- assimilation estimated from the Rayleigh Model and the Open system Model at appropriate stations.

Station	Rayleigh Model				Open system Model				$^{18}\varepsilon$:$^{15}\varepsilon$	Nitracline depth (m)	Note
	Isotope effect ($^{15}\varepsilon$)	R^2 ($^{15}\varepsilon$)	Isotope effect ($^{18}\varepsilon$)	R^2 ($^{18}\varepsilon$)	Isotope effect ($^{15}\varepsilon$)	R^2 ($^{15}\varepsilon$)	Isotope effect ($^{18}\varepsilon$)	R^2 ($^{18}\varepsilon$)			
TS2	1.4 ± 0.2‰	0.95	4.7 ± 0.7‰	0.95	2.8 ± 0.4‰	0.93	8.9 ± 2.0‰	0.86	3.4	154	Rayleigh Model
NS1	3.7 ± 0.6‰	0.96	12.0 ± 4.0‰	0.81	6.2 ± 1.6‰	0.89	19.5 ± 8.8‰	0.71	3.2	74	Rayleigh Model
J1	1.8 ± 0.5‰	0.79	3.7 ± 0.7‰	0.90	3.3 ± 1.8‰	0.53	7.4 ± 2.9‰	0.69	2.0	95	*Rayleigh Model*
X5	3.0 ± 0.3‰	0.97	6.2 ± 0.9‰	0.94	6.0 ± 1.7‰	0.81	12.1 ± 3.9‰	0.76	2.0	62	Rayleigh Model
D1	1.3 ± 0.2‰	0.95	2.5 ± 0.3‰	0.96	2.4 ± 0.5‰	0.85	4.6 ± 0.7‰	0.92	1.9	24	Rayleigh Model
A11	3.7 ± 1.3‰	0.89	5.5 ± 1.6‰	0.92	8.3 ± 6.7‰	0.61	12.8 ± 9.1‰	0.66	1.5	73	Rayleigh Model
2016SEATS	2.5 ± 0.3‰	0.98	4.6 ± 0.4‰	0.99	6.1 ± 0.5‰	0.99	10.8 ± 2.3‰	0.92	1.8	83	Rayleigh Model
K3	n/a	n/a	1.7 ± 1.0‰	0.77	n/a	n/a	2.3 ± 1.6‰	0.68	n/a	53	*Rayleigh Model*
Q1	2.4 ± 0.5‰	0.92	3.2 ± 0.7‰	0.92	5.5 ± 1.8‰	0.82	7.6 ± 2.0‰	0.88	1.3	52	Rayleigh Model
Q3	4.3 ± 0.5‰	0.96	6.2 ± 0.5‰	0.98	9.9 ± 2.0‰	0.82	14.7 ± 3.1‰	0.88	1.4	51	Rayleigh Model
F1	n/a	n/a	1.7 ± 0.8‰	0.81	n/a	n/a	2.8 ± 2.0‰	0.65	n/a	66	Rayleigh Model
D6	2.0 ± 0.3‰	0.95	3.1 ± 0.4‰	0.97	5.3 ± 2.1‰	0.77	8.4 ± 3.0‰	0.80	1.6	83	Rayleigh Model
B1	2.3 ± 0.4‰	0.93	4.1 ± 0.9‰	0.91	5.4 ± 2.7‰	0.68	9.6 ± 5.2	0.63	1.8	92	Rayleigh Model
C1	3.1 ± 0.4‰	0.97	7.0 ± 1.2‰	0.97	7.1 ± 2.4‰	0.82	16.0 ± 6.0‰	0.78	2.3	78	Rayleigh Model
A2	5.6 ± 3.3‰	0.74	8.9 ± 4.5‰	0.80	8.8 ± 7.3‰	0.59	14.1 ± 10.3‰	0.65	1.6	86	Rayleigh Model
B2	2.7 ± 0.4‰	0.96	n/a	n/a	3.9 ± 1.0‰	0.90	n/a	n/a	n/a	89	Rayleigh Model
Mean	2.8 ± 1.2‰		5.0 ± 2.8‰						2.0 ± 0.6	76 ± 28	
B5	1.1 ± 0.2‰	0.91	2.0 ± 0.5‰	0.87	2.4 ± 0.2‰	0.99	4.4 ± 0.4‰	0.99	1.8	55	Open System Model
C5	5.3 ± 4.3‰	0.61	n/a	n/a	4.3 ± 2.9‰	0.69	n/a	n/a	n/a	<70	*Open System Model*
K8	n/a	n/a	1.7 ± 0.1‰	0.98	n/a	n/a	2.6 ± 0.1‰	0.99	n/a	55	Open System Model

(Continued)

TABLE 1 Continued

Station	Rayleigh Model				Open system Model				$^{18}\varepsilon$:$^{15}\varepsilon$	Nitracline depth (m)	Note
	Isotope effect ($^{15}\varepsilon$)	R^2 ($^{15}\varepsilon$)	Isotope effect ($^{18}\varepsilon$)	R^2 ($^{18}\varepsilon$)	Isotope effect ($^{15}\varepsilon$)	R^2 ($^{15}\varepsilon$)	Isotope effect ($^{18}\varepsilon$)	R^2 ($^{18}\varepsilon$)			
SS1	1.8 ± 0.3‰	0.93	4.2 ± 0.7‰	0.93	3.6 ± 0.4‰	0.96	8.6 ± 0.9‰	0.97	2.4	104	Open System Model
2017SEATS	1.1 ± 0.1‰	0.99	3.7 ± 0.4‰	0.99	2.3 ± 0.1‰	1.00	7.4 ± 0.6‰	0.99	3.2	80	Open System Model
Mean					3.2 ± 1.0‰		5.8 ± 2.7‰		2.5 ± 0.7	73 ± 20	
BC1	n/a	n/a	1.3 ± 0.2‰	0.99	n/a	n/a	2.6 ± 0.3‰	0.99	n/a	143	Mixing
2014SEATS	3.2 ± 1.1‰	0.64	6.7 ± 0.9‰	0.92	8.9 ± 2.3‰	0.74	17.5 ± 2.6‰	0.90	2.0	49	Mixing
Mean			4.7 ± 2.9‰		8.9 ± 2.3‰					96 ± 66	

The "R^2" is the coefficient of determination for the slopes derived from various models. The "n/a" indicates stations where the coefficient of determination is poor (<0.50) or the number of measurements is insufficient (<3) to yield a fractionation trend. The last column lists whether the isotope effect is best fit using the Rayleigh Model or Open system Model or Mixing. For those stations where isotope effect cannot be accurately quantified (R^2<0.80), the models are marked in italics in the last column.

5.8‰ and 5.2‰, respectively. Spatially, $\delta^{18}O_{NO3}$ values in the southern stations (SS1, B1, B2, A2 and C1) were mostly higher than that at stations further north, especially at depths from 90-150 m. Notably, the vertical distribution patterns of $\delta^{18}O_{NO3}$ did not with synchronous change of $\delta^{15}N_{NO3}$. The $\delta^{18}O_{NO3}$ values had an overall range of 0.9-22.6‰, which was twice the range of $\delta^{15}N_{NO3}$ (2.1-13.3‰). Moreover, the minimum $\delta^{18}O_{NO3}$ values did not occur in the subsurface waters (75-125 m) at stations A2, Q1 and B5.

4 Discussion

4.1 Significance of external N inputs revealed by N* and Δ(15-18)

In the subsurface near the nitracline where regeneration occurs intensively, NO_3^- was depleted in $\delta^{15}N$, with lower $\delta^{15}N_{NO3}$ (2.1-4.9‰) found at stations 2014SEATS, SS1, B5, Q1, J1, and C1 relative to other stations (Figure 1D). Such a negative shift in $\delta^{15}N_{NO3}$ near the nitracline suggests an external input of isotopically light N likely derived from AND/N_2 fixation. Here, a quasi-conservative tracer N* (N*=[NO_3^-]–16×[PO_4^{3-}]) (Gruber and Sarmiento, 1997; Deutsch et al., 2001), is used as an indicator to reflect external N inputs (i.e. AND/N_2 fixation) since the non-Redfieldian addition of external N can increase seawater N* (Sigman et al., 2005; Yoshikawa et al., 2015). Although N* is negative throughout the upper 200 m water column (Figure 1F), an upward increase in N* is evident from 1000 m toward the surface (<100 m) (Supplementary Figure 1A), providing evidence of the effects of external N inputs supplying excess N in the subsurface waters between 100-200 m (Kim et al., 2014; Yang et al., 2022).

The cumulative signal of AND/N_2 fixation on the subsurface NO_3^- pool (100-200 m) can also be elucidated by using a complementary tracer, Δ(15–18) (=$\delta^{15}N_{NO3}$ – $\delta^{18}O_{NO3}$) (Rafter et al., 2013; Yoshikawa et al., 2018). Our results show that Δ(15–18) values vary widely between –11.6‰ and 3.5‰, with larger variations above the nitracline (–0.9 ± 3.3‰, n=41) than below the nitracline (1.1 ± 1.7‰, n=142) (Figure 1G). These Δ(15–18) values are also consistent with previous reports from the SCS (–0.5~4.0‰; Yang et al., 2022) and the western subtropical gyre of North Pacific (0.9 ± 1.3‰; Yoshikawa et al., 2018). Overall, Δ(15–18) values remain nearly constant below the nitracline but decreased upward to ~20 m (Figure 1G and Supplementary Figure 1B). The decreasing trend is well explained by the accumulation of AND/N_2 fixation (Tuerena et al., 2021; Yang et al., 2022) since both featured negative $\delta^{15}N$ values mostly falling between –10‰ and 0‰ (Knapp et al., 2008; Yang et al., 2014; Shi et al., 2021). Isotopically light $\delta^{15}N_{NO3}$ relative to $\delta^{18}O_{NO3}$, which is influenced by $\delta^{18}O$ in H_2O and O_2 *via* nitrification, may thus cause a negative shift in Δ(15–18). Several independent lines of evidences have been reported to support the significance of external N inputs around the study area, with total AND rates of 50-90 mmol N/m^2/yr (Yang et al., 2014; Shi et al., 2021) and depth-integrated N_2 fixation rates of 18.2-169.0 mmol N/m^2/yr in the SCS (Lu et al., 2019). Accordingly, both AND and N_2 fixation potentially contribute to the negative shift in Δ(15–18) with the same order of magnitude. Alternatively, the negative shift in Δ(15–18) can also result from internal processes, such as the coupling of incomplete NO_3^- assimilation and remineralization of newly

fixed organic N and subsequent nitrification (Yoshikawa et al., 2018; Yang et al., 2022). Therefore, external N inputs from AND/N_2 fixation resulted in the upward increases in N* and decreases in Δ(15–18), confirming the significance of AND/N_2 fixation on modulating N dynamics in the upper water column of the SCS.

4.2 Nitrate isotopes reveal dominant N cycling processes

4.2.1 Nitrate assimilation and its isotope fractionation

NO_3^- assimilation is an important N cycling process in the euphotic zone, especially near the chlorophyll maximum (Rafter and Sigman, 2016; Wan et al., 2018; Tuerena et al., 2021). In our study area, NO_3^- uptake was evidenced by upward NO_3^- depletion and the synchronous elevation in $\delta^{15}N_{NO3}$ and $\delta^{18}O_{NO3}$ in the top 100 m (Figures 1C–1E) caused by the preferential uptake of ^{14}N and ^{16}O in the NO_3^- pool by phytoplankton (Granger et al., 2004; Sigman and Fripiat, 2018). This isotope shift was also supported by the highest NO_3^- uptake rates (56.8-132.7 nmol N/L/d) near nitracline at stations D1, 2014SEATS and NS1 (Wan et al., 2018, Tables 1, 2). The upward pattern of decreasing N/P ratios toward the surface (~20 m) further confirms NO_3^- assimilation by photosynthesis with removal of N and P at the Redfield ratio resulting in a decrease in the residual N/P ratios when N* was negative (Figures 1F, H, Supplementary Figure 1A) (Deutsch and Weber, 2012). Therefore, NO_3^- uptake was the dominant process modifying the vertical variations of $\delta^{15}N_{NO3}$ and $\delta^{18}O_{NO3}$ in the euphotic zone (Rafter and Sigman, 2016; Peng et al., 2018).

To evaluate the fractionation factor of NO_3^- assimilation, we plotted $\delta^{15}N_{NO3}$ or $\delta^{18}O_{NO3}$ against the natural logarithm of NO_3^- concentrations (Figures 2A, B). The isotope effect of NO_3^-

TABLE 2 Summary of nitrification rates, NO_3^- uptake rates, the contributions of nitrification to NO_3^- uptake (F_{nit}/F_{upt}), and the contributions of external N inputs to NO_3^- uptake ($F_{atm\text{-}fix}/F_{upt}$) in the $\Delta\delta^{18}O_{NO3}$-positive layer.

Station	Depth (m)	Nitrate (μmol/L)	$\delta^{15}N_{obs}$ (‰)	$\delta^{18}O_{obs}$ (‰)	$\delta^{15}N_{sub}$ (‰)	$\delta^{18}O_{sub}$ (‰)	Nitrification rate (nmol N/L/d)	Nitrate uptake rate (nmol N/L/d)	F_{Nit}/F_{upt} (%)	$F_{atm+fix}/F_{upt}$ (%)
NS1	79	3.7	9.1	19.0	4.6	2.5	2.58	56.78	5	>100
	84	4.4	7.1	7.1	4.6	2.5	5.46	11.21	49	/
	90	8.4	4.6	3.2	4.6	2.5	3.43	13.74	25	/
	Depth-integrated mean value								34	/
2014SEATS	44	0.7	10.7	17.5	4.9	2.4	9.15	44.00	21	>100
	51	2.2	12.0	13.2	4.9	2.4	11.28	90.91	12	43
	54	3.3	8.8	9.6	4.9	2.4	22.22	50.55	44	9
	59	3.8	6.1	6.1	4.9	2.4	9.08	21.09	43	/
	69	4.5	4.7	4.2	4.9	2.4	9.74	29.82	33	1
	79	5.5	4.5	3.7	4.9	2.4	5.36	5.45	98	/
	89	6.9	4.8	2.8	4.9	2.4	7.19	9.45	76	/
	100	8.5	4.8	2.7	4.9	2.4	3.14	/	/	/
	Depth-integrated mean value								53	28
D1	24	2.0	7.0	5.8	5.0	2.5	3.24	132.73	2	18
	29	2.9	6.2	5.6	5.0	2.5	7.65	54.18	14	16
	40	5.1	5.4	3.4	5.0	2.5	14.32	50.91	28	/
	49	5.7	5.2	3.2	5.0	2.5	11.28	28.36	40	/
	59	7.6	5.2	2.8	5.0	2.5	15.85	25.45	62	/
	Depth-integrated mean value								32	17

The nitrification rates and NO_3^- uptake rates were derived from Wan et al. (2018). $\delta^{15}N_{obs}$ and $\delta^{18}O_{obs}$ are the measured $\delta^{15}N_{NO3}$ and $\delta^{18}O_{NO3}$, $\delta^{15}N_{sub}$ and $\delta^{18}O_{sub}$ are the observed isotope values of subsurface waters (101 m at station NS1, 109 m at station 2014SEATS, 68 m at station D1).

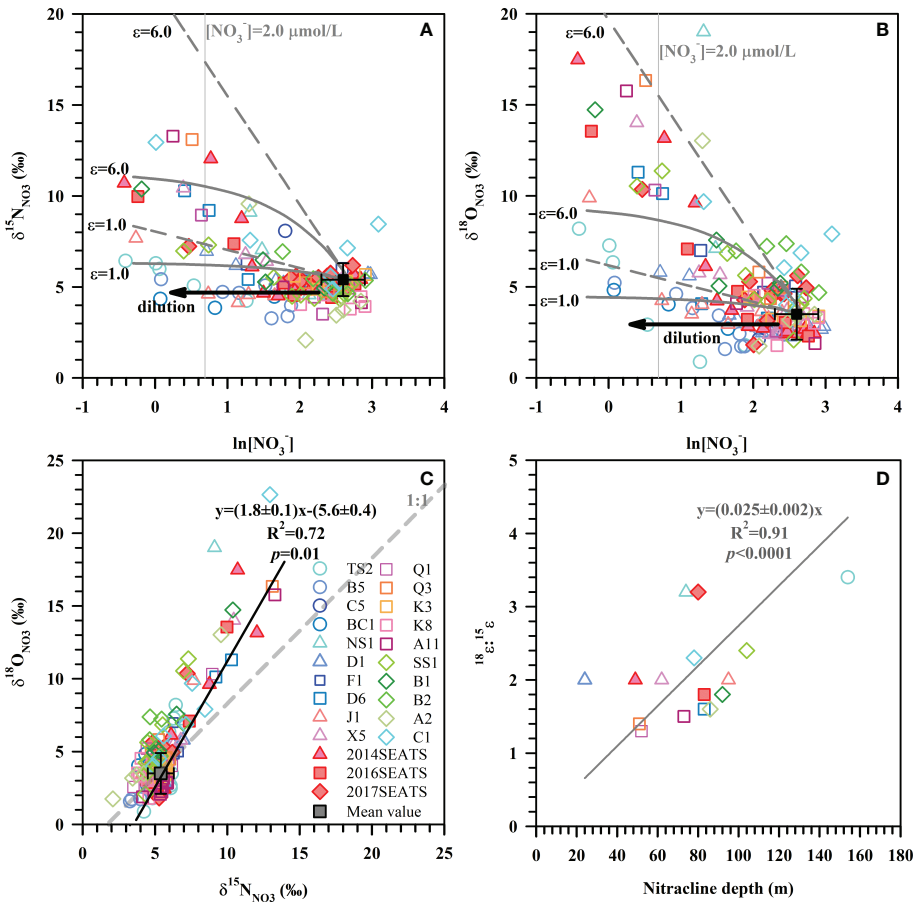

FIGURE 2
Values of $\delta^{15}N_{NO3}$ **(A)** and $\delta^{18}O_{NO3}$ **(B)** versus the natural logarithm of $[NO_3^-]$ for all stations. These data overlay models of NO_3^- uptake based on the average NO_3^- concentration and isotope at a depth of 200 m (black square, $[NO_3^-]$=14.8 ± 4.0 μmol/L, $\delta^{15}N_{NO3}$ = 5.4 ± 0.9‰, $\delta^{18}O_{NO3}$ = 3.5 ± 1.4‰, n=23). The straight dashed lines represent the Rayleigh model while the concave-down lines represent the Open system model. The black arrows represent the dilution effect of Kuroshio intrusion with low concentrations of NO_3^-. The gray vertical lines denote the nitracline of 2.0 μmol/L. **(C)** The relationship between $^{18}\epsilon$:$^{15}\epsilon$ ratios and the nitracline depth. **(D)** Scatter plot of $\delta^{18}O_{NO3}$ versus $\delta^{15}N_{NO3}$ for all stations. The solid line is the best fitting curve for all datapoints. The gray dashed line represents a 1:1 NO_3^- isotope assimilation trend.

assimilation generally follows Eq. (1) according to the Rayleigh model (closed-system) and follows Eq. (2) using an open-system model (Umezawa et al., 2014; Sigman and Fripiat, 2018).

$$\delta^{15}N_{NO3} = \text{initial}\delta^{15}N_{NO3} - \epsilon \times \ln(f) \quad , (1)$$

$$\delta^{15}N_{NO3} = \text{initial}\delta^{15}N_{NO3} + \epsilon \times (1 - f) \quad , (2)$$

where f is the residual fraction of NO_3^- in the water column from the initial NO_3^- concentration, and ϵ is the isotope effect (in ‰ units) for NO_3^- assimilation.

Our results show that samples enriched in $\delta^{15}N_{NO3}$ and $\delta^{18}O_{NO3}$ can be better explained by the combination of the Rayleigh model and the Open system model than solely by the Rayleigh model or the Open system model (Figures 2A, B). An isotope effect of 1.0-6.0‰ produced by the Rayleigh model can explain the majority of the increase in $\delta^{15}N_{NO3}$ and $\delta^{18}O_{NO3}$. Yet, for those stations near the Luzon Strait, the Open system model better predicts isotope behavior. Although the above estimated ranges were close to the typical isotope fractionation induced by phytoplankton in culture (1.4-21.0‰) (Waser et al., 1998; Needoba et al., 2003; Granger et al., 2004) and field studies (4-11.9‰) (DiFiore et al., 2010; Rohde et al., 2015; Rafter and Sigman, 2016), they exhibit large variations that are associated with ambient environmental conditions (e.g., light intensity) and phytoplankton species composition (Needoba and Harrison, 2004; DiFiore et al., 2010; Rohde et al., 2015). Below we estimate the isotope effect specifically for each station since they may have experienced different hydrological conditions and/or different plankton community structures (Rafter & Sigman, 2016).

Here, the isotope effect was estimated for stations with obvious NO_3^- drawdown and sufficient measurements (≥3) to

yield a fractionation trend. These calculations assumed that subsurface (~200 m) NO_3^- is the only NO_3^- source available for phytoplankton assimilation. The isotope effect yielded by the slope of the regression for the individual station is estimated (Table 1). Average isotope effects of 2.8 ± 1.2‰ (n=14) for $^{15}\epsilon$ and 5.0 ± 2.8‰ (n=15) for $^{18}\epsilon$ were obtained from 16 of the 23 stations using the Rayleigh model. The isotope effect was close to the mean isotope effect based on the Open system model (7 of the 23 stations), which yielded 3.2 ± 1.0‰ (n=4) for $^{15}\epsilon$ and 5.8 ± 2.7‰ (n=4) for $^{18}\epsilon$. These values fall well within the overall isotope effect estimates of 1.0-6.0‰ in Figures 2A, B and 2.2-6.2‰ derived from culture studies (Needoba et al., 2003). Noteworthy is the N and O isotope effect at stations near the Luzon Strait that yielded lower values of 1.1-3.1‰ and 1.3-4.7‰ (Table 1), respectively. This may be a consequence of NO_3^- depleted water supplied to the surface (<100 m) from Kuroshio Current. When NO_3^-depleted Kuroshio Current waters mixes with NO_3^-replete SCS waters, it reduces NO_3^- concentration of the remaining N pool (Du et al., 2013) without changing its isotopic composition (Deutsch et al., 2004). Similarly, the relatively low isotopic values ($\delta^{15}N_{NO3}$<5.4‰, $\delta^{18}O_{NO3}$<3.5‰) that failed to yield a fractionation trend can also be explained by the dilution effect from the Kuroshio Current.

4.2.2 Nitrification

The ratio of O:N isotope effects ($^{18}\epsilon$:$^{15}\epsilon$) was 2.0 ± 0.6 (n=13) derived from the Rayleigh model and 2.5 ± 0.7 (n=3) from the Open system model (Table 1), showing disproportionate change in $^{15}\epsilon$ and $^{18}\epsilon$. Such a high $^{18}\epsilon$:$^{15}\epsilon$ ratio differs from many field and culture studies that found a nearly equivalent isotope effect in N and O (Granger et al., 2008; Rohde et al., 2015; Rafter and Sigman, 2016). The input of newly fixed N from N_2 fixation can lower $^{15}\epsilon$ by introducing isotopically light N into the NO_3^- pool, which may partially explain the lower $^{15}\epsilon$ relative to $^{18}\epsilon$. Nevertheless, similarly high $^{18}\epsilon$:$^{15}\epsilon$ ratios have been reported for marine diatom *Thalassiosira weissflogii* ($^{18}\epsilon$:$^{15}\epsilon$=1.4), and as high as 2.0 for cultured heterotrophic α-proteobacterial strains (Granger et al., 2010; Karsh et al., 2014). Additionally, our findings compare well with the slope of 1.8 ± 0.1 (R^2 = 0.72, p=0.01) derived from the scatter plot of $\delta^{18}O_{NO3}$ versus $\delta^{15}N_{NO3}$ (Figure 2C). Such a positive shift in $\delta^{18}O_{NO3}$ relative to $\delta^{15}N_{NO3}$ can result from nitrification in recycled NO_3^- (Wankel et al., 2009), is consistent with the reported nitrification rates in the study area (Wan et al., 2018; Xu et al., 2018). Moreover, such positive deviations are more evident at stations where the nitracline was deeper (Table 1), as indicated by the positive correlation between $^{18}\epsilon$:$^{15}\epsilon$ ratios and nitracline depth (Figure 2D). This supports the idea that nitrification contributed to the high $^{18}\epsilon$:$^{15}\epsilon$ ratios since the influence of nitrification increased with increasing water depth and the lessening of photoinhibition for nitrifiers (Wan et al., 2018). However, nitrification still cannot explain the majority of the highest $\delta^{15}N_{NO3}$ and $\delta^{18}O_{NO3}$ values measured (Figure 2C), revealing that NO_3^- assimilation was the main process regulating N cycling in the upper ocean, followed by nitrification. Therefore, the isotope effect in this study was a conservative estimate since the influence of nitrification and N_2 fixation cannot be separated from NO_3^- uptake.

4.3 Relative importance of nitrification and external N inputs

The above discussion implies the importance of external N inputs from AND/N_2 fixation on the N pool in the upper ocean. Meanwhile, the relative importance of external N inputs and internal processes, which could be imprinted on NO_3^- isotope values, may differ vertically throughout the water column. However, the relative importance of these inputs is difficult to assess accurately without high-resolution sampling. Below we separated the water column of each station (those with high-resolution vertical sampling during 2014 and 2017 cruises) into a $\delta^{18}O_{NO3}$-based two-layer structure, according to the deviation in $\delta^{18}O_{NO3}$ at a given depth ($\delta^{18}O_{NO3\text{-}obs}$) from that at 200 m ($\delta^{18}O_{NO3\text{-}200m}$). Samples with a negative deviation ($\delta^{18}O_{NO3\text{-}obs<}$ $\delta^{18}O_{NO3\text{-}200m}$) were assigned to the $\Delta\delta^{18}O_{NO3}$-negative layer; otherwise, they were categorized as part of the $\Delta\delta^{18}O_{NO3}$-positive layer ($\delta^{18}O_{NO3\text{-}obs} > \delta^{18}O_{NO3\text{-}200m}$). Then the relative importance of various processes contributing to the isotope shifts in the $\Delta\delta^{18}O_{NO3}$-positive and $\Delta\delta^{18}O_{NO3}$-negative layers of those stations was assessed quantitatively.

4.3.1 The $\Delta\delta^{18}O_{NO3}$-positive layer

In the $\Delta\delta^{18}O_{NO3}$-positive layer where NO_3^- uptake dominated, the contribution of nitrification to NO_3^- uptake (F_{nit}/F_{upt}) was calculated directly from the reported nitrification to NO_3^- uptake rates at stations NS1, 2014SEATS and D1 (Wan et al., 2018). The results show that nitrification accounted for 2-98% of the NO_3^- uptake and its contribution increased with water depth in this layer (Table 2). To eliminate the influence of different sampling resolutions, F_{nit}/F_{upt} was first linearly interpolated at 1 m intervals, and then the mean depth-integrated value was calculated. Results show that the depth-integrated F_{nit}/F_{upt} was 34%, 53% and 32% for stations NS1, 2014SEATS and D1, respectively, with a mean of 39 ± 11% (n=3), confirming the importance of nitrification in supporting phytoplankton growth (Wan et al., 2018). Noteworthy, new production assessed by the NO_3^- uptake rates may be overestimated in this layer due to a substantial proportion of the NO_3^- assimilated by phytoplankton was produced from nitrification. The cumulative NO_3^- from nitrification should be considered as regenerated N rather new N (Dugdale and Goering, 1967). This finding has important implications for biological carbon pump and carbon cycling in the vast marginal seas.

To estimate the relative importance of AND/N_2 fixation to NO_3^- uptake ($F_{atm+fix}/F_{upt}$), a simplified one-dimensional model based on a N isotope mass balance (Bourbonnais et al., 2009)

was applied (Supplementary Figure 2). Details of the calculations are provided in the Supplementary Text 1. Results show that $F_{atm+fix}/F_{upt}$ was up to 100% at 79 m for station NS1 and at 44 m for station 2014SEATS (Table 2), suggesting the predominant role of external N inputs in supporting marine productivity at low-N depths. This is also consistent with the fact that extremely low diapycnal NO_3^- fluxes in the nutrient-depleted layer are observed in the SCS (Du et al., 2017). Combined with the very low F_{nit}/F_{upt} at these depths, our results also indicate that external N inputs from AND/N_2 fixation are rapidly consumed by phytoplankton without being remineralized. However, $F_{atm+fix}/F_{upt}$ decreased rapidly with depth at stations 2014SEATS and D1, along with the increasing contribution of nitrification. The mean depth-integrated of $F_{atm+fix}/F_{upt}$ was 28% and 17% at these two stations, respectively, which is lower than the proportion of nitrification (39 ± 11%). This suggests that nitrification and external N inputs make a significant contribution to NO_3^- uptake (~50%) in the upper water column (Bourbonnais et al., 2009; Yang et al., 2022).

4.3.2 The $\Delta\delta^{18}O_{NO3}$-negative layer

In the $\Delta\delta^{18}O_{NO3}$-negative layer, where NO_3^- uptake was limited by light and nitrification became more important, we estimated the proportion of regenerated NO_3^- ($f_{reg/tot}$) following the method mentioned by Granger et al. (2013) and Tuerena et al. (2021). Details of calculations are provided in the Supplementary Text 2. Results showed that $f_{reg/tot}$ ranged from 0-86% in the $\Delta\delta^{18}O_{NO3}$-negative layer (Table 3), with large vertical and spatial variability. The highest depth-integrated mean proportion of 34% was observed at station C1 while the lowest fractions of 2-4% occurred at stations 2014SEATS and B1. Overall, the depth-integrated $f_{reg/tot}$ was 17 ± 10% (n=10), revealing that on average ~17% of the NO_3^- pool was regenerated from nitrification in the $\Delta\delta^{18}O_{NO3}$-negative layer. This is consistent with many other field studies (15-27%, Wankel et al., 2007; Tuerena et al., 2021) and model results (~50%, Yool et al., 2007), indicating that nitrification plays a substantial role in the NO_3^- pool and its $\delta^{15}N_{NO3}$ and $\delta^{18}O_{NO3}$ signatures, as well as in oceanic productivity. Additionally, $f_{reg/tot}$ in the $\Delta\delta^{18}O_{NO3}$-negative layer varies greatly vertically, generally increasing then decreasing with depth, and peaking at 123 ± 21 m (n=9) (Table 3). This is consistent with reported nitrification rates that peaked at around 50-100 m (Wan et al., 2018; Xu et al., 2018), further confirming the significance of nitrification in regulating the size of the NO_3^- pool and its dynamics in the $\Delta\delta^{18}O_{NO3}$-negative layer, where low light intensity and abundant NO_3^- enhanced the success of nitrifiers (Wan et al., 2018; Marconia et al., 2019).

To assess the relative contributions of external N inputs to the NO_3^- pool ($f_{atm-fix/tot}$), a two-end-member mass and isotope balance was used following Yang et al. (2022). Details of the calculation are provided in the Supplementary Text 3. A vertically decreasing trend in $f_{atm-fix/tot}$ was observed at most stations (Table 3), consistent with observations in the Atlantic Ocean (Knapp et al., 2008). $f_{atm-fix/tot}$ also varied spatially, with higher proportions (8-33%) at southern stations (C1, A2) near the Nansha Island than northern stations (1-16%), implying a greater accumulation of external N in the south. The deeper nitracline in the southern SCS may hinder upwelling of subsurface (~200 m) NO_3^-, and thus favor the growth of diazotrophs, which would lead to higher $f_{atm-fix/tot}$. The depth-integrated mean value of $f_{atm-fix/tot}$ was 7 ± 6% (1-22%, n=10) in the $\Delta\delta^{18}O_{NO3}$-negative layer, slightly lower than in the $\Delta\delta^{18}O_{NO3}$-positive layer (17-28%) but comparable to the previously reported proportion of 1-22% (Wong et al., 2007; Lu et al., 2019; Yang et al., 2022). Taken together, the above results imply the importance of AND/N_2 fixation to the total NO_3^- pool in the upper ocean, although their average contribution is lower than that supplied by nitrification (Knapp et al., 2008; Bourbonnais et al., 2009; Tang et al., 2019).

By deducting the total NO_3^- contribution of nitrification (17 ± 10%) and external N inputs (7 ± 6%), we can obtain the average contribution of upwelled NO_3^- to the total NO_3^- pool as 76 ± 12% in the $\Delta\delta^{18}O_{NO3}$-negative layer. Therefore, $\delta^{15}N_{NO3}$ and $\delta^{18}O_{NO3}$ signature in the $\Delta\delta^{18}O_{NO3}$-negative layer were similar to that at 200 m (Figures 1D, 1E), but also under the co-influence of nitrification and external N inputs. This finding suggests the complicated of N dynamics in the upper ocean of marginal seas with variable contributions from various N sources and processes.

5 Conclusions

All information collected regarding NO_3^- dynamics, external sources and processes in the upper water column of the SCS was assembled into a conceptual diagram (Figure 3). Vertically, NO_3^- concentrations increased with depth while its $\delta^{15}N_{NO3}$ and $\delta^{18}O_{NO3}$ covaried becoming higher towards the surface (<20 m) due to phytoplankton assimilation. The isotope effect during NO_3^- uptake was 2.8 ± 1.2‰ (n=14) for N and 5.0 ± 2.8‰ (n=15) for O, deduced from the Rayleigh model, with a ratio of 2.0 ± 0.6 (O/N, n=13). This high O/N ratio was attributable to nitrification and/or N_2 fixation. At the depth of ~100 m at some stations, a negative shift in $\delta^{15}N_{NO3}$ deviated significantly from the vertical pattern of $\delta^{18}O_{NO3}$, suggesting an addition of isotopically light N. The relative contributions of external N sources and internal processes was assessed by taking advantage of high-resolution observations, revealing clear vertical variations in their contributions in the $\delta^{18}O_{NO3}$-based two-layer structure. In the $\Delta\delta^{18}O_{NO3}$-positive layer, the NO_3^- assimilated by phytoplankton were largely sourced from nitrification (39 ± 11%) and AND/N_2 fixation (17-28%). In the $\Delta\delta^{18}O_{NO3}$-negative layer, the proportions of regenerated NO_3^-

TABLE 3 Summary of the proportions of regenerated NO_3^- ($f_{reg/tot}$) and external N inputs from AND/N_2 fixation ($f_{atm\text{-}fix}$) in the $\Delta\delta^{18}O_{NO3}$-negative layer.

Station	Depth (m)	Nitrate (μmol/L)	$\delta^{15}N_{obs}$ (‰)	$\delta^{18}O_{obs}$ (‰)	$f_{reg/tot}$ (%)	$f_{atm+fix/tot}$ (%)	$\delta^{18}O_{exp}$ (‰)
NS1	101	10.7	4.6	2.5	17	11	2.7
	132	12.9	4.9	2.5	16	6	2.7
	151	13.8	5.1	2.5	18	4	2.7
	181	13.4	5.4	2.8	0	0	2.8
	Depth-integrated mean value				14	5	
J1	119	5.2	4.5	2.9	24	11	3.3
	130	6.9	4.7	2.9	28	8	3.3
	140	7.9	4.9	2.8	31	6	3.4
	150	8.3	5.1	3.6	/	4	3.4
	159	9.1	5.1	3.3	9	3	3.4
	179	11.0	5.3	3.6	/	1	3.4
	199	12.1	5.4	3.5	0	0	3.4
	Depth-integrated mean value				14	4	
X5	90	9.2	4.8	2.4	36	9	2.9
	100	10.4	4.9	2.3	40	8	2.9
	107	10.2	4.8	2.4	36	8	2.9
	120	9.9	5.0	2.4	37	6	3.0
	131	11.8	5.5	3.7	/	0	3.0
	140	13.4	5.5	3.1	/	0	3.0
	150	13.8	5.2	2.8	15	4	3.0
	169	14.5	5.3	3.4	/	2	3.0
	202	15.2	5.5	3.0	0	0	3.0
	Depth-integrated mean value				21	3	
2014SEATS	109	11.6	4.9	2.4	2	7	2.4
	119	11.8	5.1	2.5	/	5	2.4
	127	13.7	5.4	2.4	2	1	2.5
	139	15.1	5.5	2.7	/	/	/
	147	15.7	5.6	2.4	2	/	/
	158	15.6	5.6	2.5	0	/	/
	168	15.8	5.6	2.4	3	/	/
	180	17.2	5.4	2.5	0	0	2.5
	Depth-integrated mean value				2	1	
D1	68	8.3	5.0	2.5	23	9	2.7
	79	9.4	4.9	2.5	21	10	2.7
	100	10.4	5.0	2.5	21	9	2.7
	119	12.3	5.0	2.3	37	9	2.7
	160	15.6	5.6	2.9	/	2	2.8

(Continued)

TABLE 3 Continued

Station	Depth (m)	Nitrate (μmol/L)	$\delta^{15}N_{obs}$ (‰)	$\delta^{18}O_{obs}$ (‰)	$f_{reg/tot}$ (%)	$f_{atm+fix/tot}$ (%)	$\delta^{18}O_{exp}$ (‰)
	180	19.0	5.7	2.7	10	0	2.8
	200	19.6	5.7	2.8	0	0	2.8
	Depth-integrated mean value				21	6	
SS1	125	7.5	4.6	4.3	2	8	4.2
	130	9.0	4.4	4.2	4	10	4.1
	150	12.9	4.3	2.1	74	11	4.1
	160	13.1	4.5	3.6	26	9	4.1
	170	13.6	4.6	3.9	14	7	4.2
	190	14.3	5.0	4.1	10	2	4.3
	200	14.9	5.1	4.4	0	0	4.4
	Depth-integrated mean value				24	7	
2017 SEATS	90	7.5	5.4	4.3	17	9	4.7
	95	6.6	5.5	4.3	18	8	4.7
	100	7.4	5.3	1.8	86	11	4.6
	110	9.0	5.3	3.2	49	11	4.6
	120	9.6	5.5	4.8	4	9	4.7
	130	9.6	5.5	4.5	13	8	4.7
	140	10.8	5.6	4.7	8	7	4.7
	150	11.3	5.8	4.6	9	5	4.8
	175	13.6	4.8	5.6	/	16	4.5
	200	15.3	6.2	4.9	0	0	4.9
	Depth-integrated mean value				16	9	
B1	108	4.6	5.3	5.1	4	2	5.1
	125	10.4	4.9	4.9	7	0	5.2
	150	10.7	5.1	5.2	0	/	/
	Depth-integrated mean value				4	1	
C1	100	11.3	5.6	6.1	28	27	6.3
	125	11.7	4.9	4.0	59	33	5.9
	150	12.7	5.3	4.5	51	30	6.1
	175	14.3	7.1	6.9	16	12	7.2
	200	21.9	8.5	7.9	0	0	7.9
	Depth-integrated mean value				35	22	
A2	100	8.0	2.1	1.8	79	33	3.0
	125	12.2	3.5	3.2	15	12	3.3
	150	13.5	3.7	3.4	4	8	3.4
	200	17.2	4.2	3.5	0	0	3.5
	Depth-integrated mean value				16	10	

$\delta^{15}N_{obs}$ and $\delta^{18}O_{obs}$ are the measured $\delta^{15}N_{NO3}$ and $\delta^{18}O_{NO3}$, while $\delta^{18}O_{exp}$ represents the expected $\delta^{18}O_{NO3}$ calculating from mass balance (Supplementary Text 3).

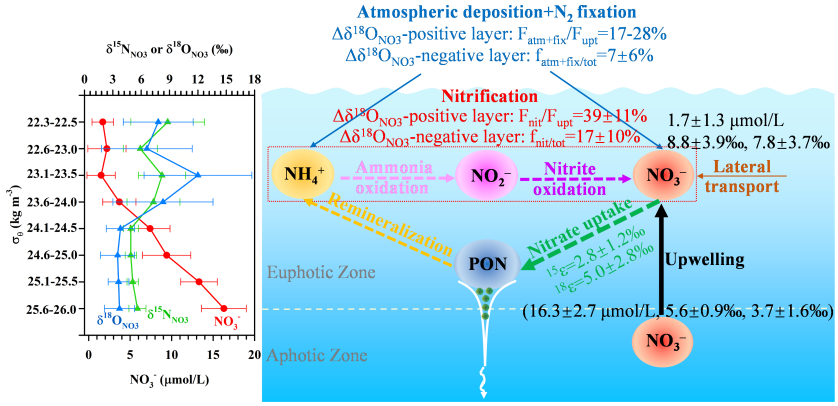

FIGURE 3
Conceptual diagram for NO_3^- dynamics in the upper water column of the SCS.

and external N inputs to the total NO_3^- pool were 17 ± 10% and 7 ± 6% (n=10), respectively. These findings suggests that in addition to upwelled NO_3^- from subsurface waters (~200 m), nitrification and external N sources (AND/N_2 fixation) also play an important role in modulating the NO_3^- pool, affecting its isotopic signatures and cycling dynamics in the upper water column of the SCS.

Data availability statement

The datasets presented in this study can be found in online repositories. The names of the repository/repositories and accession number(s) can be found below: the Zenodo deposit, https://www.zenodo.org/record/7219590 (Doi: 10.5281/zenodo.7219590).

Author contributions

S-JK and MD supervised and conceived this work. J-YY, MX, ET, ZZ and WZ contributed to the sample collection. XY conducted chemical and data analysis and wrote the manuscript. S-JK, XY and J-YY reviewed and edited the manuscript. All authors contributed to the article and approved the submitted version.

Funding

This research was supported by the National Natural Science Foundation of China (NSFC 42176046, 42106048, 41890802, 92058204, 41721005), the Basic and Applied Basic Research Foundation of Guangdong Province (2019A1515010611), the State Key Laboratory of Marine Resource Utilization in South China Sea (Hainan University; MRUKF2021017), and the Shantou University Scientific Research Foundation for Talents (NTF18013).

Acknowledgments

We are grateful to Lifang Wang, Tao Huang, Qiao Wu and Xianhui Wan for his assistance in sample collection and measurement during the cruise.

Conflict of interest

The authors declare that the research was conducted in the absence of any commercial or financial relationships that could be construed as a potential conflict of interest.

Publisher's note

Supplementary material

The Supplementary Material for this article can be found online at: https://www.frontiersin.org/articles/10.3389/fmars.2022.1104135/full#supplementary-material

References

Böhlke, J. K., Mroczkowski, S. J., and Coplen, T. B. (2003). Oxygen isotopes in nitrate: new reference materials for ^{18}O:^{17}O:^{16}O measurements and observations on nitrate-water equilibration. *Rapid Commun. Mass Spectrometry* 17 (16), 1835–1846. doi: 10.1002/rcm.1123

Bourbonnais, A., Lehmann, M. F., Waniek, J. J., and Schulz-Bull, D. E. (2009). Nitrate isotope anomalies reflect N_2 fixation in the Azores front region (subtropical NE Atlantic). *J. Geophysical Res.* 114 (C3), C03003. doi: 10.1029/2007jc004617

Buchanan, P. J., Aumont, O., Bopp, L., Mahaffey, C., and Tagliabue, A. (2021). Impact of intensifying nitrogen limitation on ocean net primary production is fingerprinted by nitrogen isotopes. *Nat. Communication* 12 (1), 6214. doi: 10.1038/s41467-021-26552-w

Casciott, K. L., Sigman, D. M., Hastings, M. G., Bohlke, J. K., and Hilkert, A. (2002). Measurement of the oxygen isotopic composition of nitrate in seawater and freshwater using the denitrifier method. *Analytical Chem.* 74 (19), 4905–4912. doi: 10.1021/ac020113w

Chen, Y.-l. L., Chen, H.-Y., Karl, D. M., and Takahashi, M. (2004). Nitrogen modulates phytoplankton growth in spring in the south China Sea. *Continental Shelf Res.* 24, 527–541. doi: 10.1016/j.csr.2003.12.006

Chen, F., Zhou, X., Lao, Q., Wang, S., Jin, G., Chen, C., et al. (2019). Dual isotopic evidence for nitrate sources and active biological transformation in the northern south China Sea in summer. *PLoS One* 14 (1), e0209287. doi: 10.1371/journal.pone.0209287

Dai, M., Wang, L., Guo, X., Zhai, W., He, B., and Kao, S. J. (2008). Nitrification and inorganic nitrogen distribution in a large perturbed river/estuarine system: the pearl river estuary, China. *Biogeosciences* 5, 1227–1244. doi: 10.5194/bg-5-1227-2008

Deutsch, C., Gruber, N., Key, R. M., Sarmiento, J. L., and Ganachaud, A. (2001). Denitrification and N_2 fixation in the pacific ocean. *Global Biogeochemical Cycles* 15 (2), 483–506. doi: 10.1029/2000gb001291

Deutsch, C., Sigman, D. M., Thunell, R. C., Meckler, A. N., and Haug, G. H. (2004). Isotopic constraints on glacial/interglacial changes in the oceanic nitrogen budget. *Global Biogeochemical Cycles* 18 (4), GB4012. doi: 10.1029/2003GB002189

Deutsch, C., and Weber, T. (2012). Nutrient ratios as a tracer and driver of ocean biogeochemistry. *Annu. Rev. Mar. Sci.* 4 (1), 113–141. doi: 10.1146/annurev-marine-120709-142821

DiFiore, P. J., Sigman, D. M., Karsh, K. L., Trull, T. W., Dunbar, R. B., and Robinson, R. S. (2010). Poleward decrease in the isotope effect of nitrate assimilation across the southern ocean. *Geophysical Res. Lett.* 37 (17), L17601. doi: 10.1029/2010GL044090

Dugdale, R., and Goering, J. (1967). Uptake of new and regenerated forms of nitrogen in marine production. *Limnology Oceanography* 12, 196–206. doi: 10.4319/lo.1967.12.2.0196

Du, C., Liu, Z., Dai, M., Kao, S. J., Cao, Z., Zhang, Y., et al. (2013). Impact of the kuroshio intrusion on the nutrient inventory in the upper northern south China Sea: insights from an isopycnal mixing model. *Biogeosciences* 10 (10), 6419–6432. doi: 10.5194/bg-10-6419-2013

Du, C., Liu, Z., Kao, S. J., and Dai, M. (2017). Diapycnal fluxes of nutrients in an oligotrophic oceanic regime: The south China Sea. *Geophysical Res. Lett.* 44 (11), 510–511, 518. doi: 10.1002/2017gl074921

Emeis, K.-C., Mara, P., Schlarbaum, T., Möbius, J., Dähnke, K., Struck, U., et al. (2010). External n inputs and internal n cycling traced by isotope ratios of nitrate, dissolved reduced nitrogen, and particulate nitrogen in the eastern Mediterranean Sea. *J. Geophysical Res.* 115 (G4), GB04041. doi: 10.1029/2009jg001214

Falkowski, P. (1997). Evolution of the nitrogen cycle and its influence on the biological sequestration of CO_2 in the ocean. *Nature* 387 (6630), 272–275. doi: 10.1038/387272a0

Fawcett, S. E., Ward, B. B., Lomas, M. W., and Sigman, D. M. (2015). Vertical decoupling of nitrate assimilation and nitrification in the Sargasso Sea. *Deep Sea Res. Part I: Oceanographic Res. Papers* 103, 64–72. doi: 10.1016/j.dsr.2015.05.004

Granger, J., Prokopenko, M. G., Mordy, C. W., and Sigman, D. M. (2013). The proportion of remineralized nitrate on the ice-covered eastern Bering Sea shelf evidenced from the oxygen isotope ratio of nitrate. *Global Biogeochemical Cycles* 27 (3), 962–971. doi: 10.1002/gbc.20075

Granger, J., and Sigman, D. M. (2009). Removal of nitrite with sulfamic acid for nitrate n and O isotope analysis with the denitrifier method. *Rapid Commun. Mass Spectrometry* 23 (23), 3753–3762. doi: 10.1002/rcm.4307

Granger, J., Sigman, D. M., Lehmann, M. F., and Tortell, P. (2008). Nitrogen and oxygen isotope fractionation during dissimilatory nitrate reduction by denitrifying bacteria. *Limnology Oceanography* 53 (6), 2533–2545. doi: 10.4319/lo.2008.53.6.2533

Granger, J., Sigman, D. M., Needoba, J. A., and Harrison, P. J. (2004). Coupled nitrogen and oxygen isotope fractionation of nitrate during assimilation by cultures of marine phytoplankton. *Limnology Oceanography* 49 (5), 1763–1773. doi: 10.4319/lo.2004.49.5.1763

Granger, J., Sigman, D. M., Rohde, M. M., Maldonado, M. T., and Tortell, P. D. (2010). N and O isotope effects during nitrate assimilation by unicellular prokaryotic and eukaryotic plankton cultures. *Geochimica Cosmochimica Acta* 74 (3), 1030–1040. doi: 10.1016/j.gca.2009.10.044

Gruber, N., and Sarmiento, J. L. (1997). Global patterns of marine nitrogen fixation and denitrification. *Global Biogeochemical Cycles* 11 (2), 235–266. doi: 10.1029/97GB00077

Hu, J., Kawamura, H., Hong, H., and Qi, Y. (2000). A review on the currents in the south China Sea: Seasonal circulation, south China Sea warm current and kuroshio intrusion. *J. Oceanography* 56 (6), 607–624. doi: 10.1023/a:1011117531252

Kao, S. J., Terence Yang, J. Y., Liu, K. K., Dai, M., Chou, W. C., Lin, H. L., et al. (2012). Isotope constraints on particulate nitrogen source and dynamics in the upper water column of the oligotrophic south China Sea. *Global Biogeochemical Cycles* 26 (2), GB2033. doi: 10.1029/2011GB004091

Karsh, K. L., Trull, T. W., Sigman, D. M., Thompson, P. A., and Granger, J. (2014). The contributions of nitrate uptake and efflux to isotope fractionation during algal nitrate assimilation. *Geochimica Cosmochimica Acta* 132, 391–412. doi: 10.1016/j.gca.2013.09.030

Kim, I.-N., Lee, K., Gruber, N., Karl, D. M., Bullister, J. L., Yang, S., et al. (2014). Increasing anthropogenic nitrogen in the north pacific ocean. *Science* 346 (6213), 1102–1106. doi: 10.1126/science.1258396

Knapp, A. N., DiFiore, P. J., Deutsch, C., Sigman, D. M., and Lipschultz, F. (2008). Nitrate isotopic composition between Bermuda and Puerto Rico: Implications for N_2 fixation in the Atlantic ocean. *Global Biogeochemical Cycles* 22 (3), GB3014. doi: 10.1029/2007GB003107

Liu, S. M., Ning, X., Dong, S., Song, G., Wang, L., Altabet, M. A., et al. (2020). Source versus recycling influences on the isotopic composition of nitrate and nitrite in the East China Sea. *J. Geophysical Research: Oceans* 125 (8), e2020JC016061. doi: 10.1029/2020jc016061

Liu, Z., Zhao, Y., Colin, C., Stattegger, K., Wiesner, M. G., Huh, C.-A., et al. (2016). Source-to-sink transport processes of fluvial sediments in the south China Sea. *Earth-Science Rev.* 153, 238–273. doi: 10.1016/j.earscirev.2015.08.005

Loick, N., Dippner, J., Doan, H. N., Liskow, I., and Voss, M. (2007). Pelagic nitrogen dynamics in the Vietnamese upwelling area according to stable nitrogen and carbon isotope data. *Deep Sea Res. Part I: Oceanographic Res. Papers* 54 (4), 596–607. doi: 10.1016/j.dsr.2006.12.009

Lu, Y., Wen, Z., Shi, D., Lin, W., Bonnet, S., Dai, M., et al. (2019). Biogeography of N_2 fixation influenced by the Western boundary current intrusion in the south China Sea. *J. Geophysical Research: Oceans* 124 (10), 6983–6996. doi: 10.1029/2018jc014781

Marconia, D., Weiganda, M. A., and Sigmana, D. M. (2019). Nitrate isotopic gradients in the north Atlantic ocean and the nitrogen isotopic composition of sinking organic matter. *Deep-Sea Res. Part I* 145, 109–124. doi: 10.1016/j.dsr.2019.01.010

Moore, C. M., Mills, M. M., Arrigo, K. R., Berman-Frank, I., Bopp, L., Boyd, P. W., et al. (2013). Processes and patterns of oceanic nutrient limitation. *Nat. Geosci.* 6 (9), 701–710. doi: 10.1038/ngeo176

Nan, F., Xue, H., and Yu, F. (2015). Kuroshio intrusion into the south China Sea: A review. *Prog. Oceanography* 137, 314–333. doi: 10.1016/j.pocean.2014.05.012

Needoba, J. A., and Harrison, P. J. (2004). Influence of low light and a light:dark cycle on NO_3^- uptake, intracellular NO_3^-, and nitrogen isotope fractionation by marine phytoplankton. *J. Phycology* 40 (3), 505–516. doi: 10.1111/j.1529-8817.2004.03171.x

Needoba, J. A., Waser, N. A., Harrison, P. J., and Calvert, S. (2003). Nitrogen isotope fractionation in 12 species of marine phytoplankton during growth on nitrate. *Mar. Ecol. Progresss Serises* 255, 81–91. doi: 10.3354/meps255081

Peng, X., Fawcett, S. E., van Oostende, N., Wolf, M. J., Marconi, D., Sigman, D. M., et al. (2018). Nitrogen uptake and nitrification in the subarctic north Atlantic ocean. *Limnology Oceanography* 63 (4), 1462–1487. doi: 10.1002/lno.10784

Rafter, P. A., DiFiore, P. J., and Sigman, D. M. (2013). Coupled nitrate nitrogen and oxygen isotopes and organic matter remineralization in the southern and pacific oceans. *J. Geophysical Research: Oceans* 118 (10), 4781–4794. doi: 10.1002/jgrc.20316

Rafter, P. A., and Sigman, D. M. (2016). Spatial distribution and temporal variation of nitrate nitrogen and oxygen isotopes in the upper equatorial pacific ocean. *Limnology Oceanography* 61 (1), 14–31. doi: 10.1002/lno.10152

Rohde, M. M., Granger, J., Sigman, D. M., and Lehmann, M. F. (2015). Coupled nitrate n and O stable isotope fractionation by a natural marine plankton consortium. *Front. Mar. Sci.* 2 (28). doi: 10.3389/fmars.2015.00028

Shi, G., Ma, H., Zhu, Z., Hu, Z., Chen, Z., Jiang, S., et al. (2021). Using stable isotopes to distinguish atmospheric nitrate production and its contribution to the surface ocean across hemispheres. *Earth Planetary Sci. Lett.* 564, 116914. doi: 10.1016/j.epsl.2021.116914

Sigman, D. M., Casciott, K. L., Andreani, M., Barford, C., Galanter, M., and Bohlke, J. K. (2001). A bacterial method for the nitrogen isotopic analysis of nitrate in seawater and freshwater. *Analytical Chem.* 73 (17), 4145–4153. doi: 10.1021/ac010088e

Sigman, D. M., and Fripiat, F. (2019). "Nitrogen isotopes in the ocean," in *Encyclopedia of ocean sciences*, *3rd ed.* Ed. J. K. Cochran, H. J. Bokuniewicz and P. L. Yager, (Oxford: Academic Press). 263–278. doi: 10.1016/b978-0-12-409548-9.11605-7

Sigman, D. M., Granger, J., DiFiore, P. J., Lehmann, M. M., Ho, R., Cane, G., et al. (2005). Coupled nitrogen and oxygen isotope measurements of nitrate along the eastern north pacific margin. *Global Biogeochemical Cycles* 19 (4), GB4022. doi: 10.1029/2005GB002458

Tang, W., Wang, S., Fonseca-Batista, D., Dehairs, F., Gifford, S., Gonzalez, A. G., et al. (2019). Revisiting the distribution of oceanic N_2 fixation and estimating diazotrophic contribution to marine production. *Nat. Communication* 10 (1), 831. doi: 10.1038/s41467-019-08640-0

Tuerena, R. E., Hopkins, J., Ganeshram, R. S., Norman, L., de la Vega, C., Jeffreys, R., et al. (2021). Nitrate assimilation and regeneration in the barents Sea: insights from nitrate isotopes. *Biogeosciences* 18 (2), 637–653. doi: 10.5194/bg-18-637-2021

Umezawa, Y., Yamaguchi, A., Ishizaka, J., Hasegawa, T., Yoshimizu, C., Tayasu, I., et al. (2014). Seasonal shifts in the contributions of the changjiang river and the kuroshio current to nitrate dynamics in the continental shelf of the northern East China Sea based on a nitrate dual isotopic composition approach. *Biogeosciences* 11 (4), 1297–1317. doi: 10.5194/bg-11-1297-2014

Van Oostende, N., Fawcett, S. E., Marconi, D., Lueders-Dumont, J., Sabadel, A. J. M., Woodward, E. M. S., et al. (2017). Variation of summer phytoplankton community composition and its relationship to nitrate and regenerated nitrogen assimilation across the north Atlantic ocean. *Deep Sea Res. Part I: Oceanographic Res. Papers* 121, 79–94. doi: 10.1016/j.dsr.2016.12.012

Wankel, S. D., Kendall, C., and Paytan, A. (2009). Using nitrate dual isotopic composition ($\delta^{15}N$ and $\delta^{18}O$) as a tool for exploring sources and cycling of nitrate in an estuarine system: Elkhorn Slough, California. *J. Geophysical Res.* 114 (G1), G01011. doi: 10.1029/2008jg000729

Wankel, S. D., Kendall, C., Pennington, J. T., Chavez, F. P., and Paytan, A. (2007). Nitrification in the euphotic zone as evidenced by nitrate dual isotopic composition: Observations from Monterey bay, California. *Global Biogeochemical Cycles* 21 (2), GB2009. doi: 10.1029/2006gb002723

Wan, X. S., Sheng, H. X., Dai, M., Zhang, Y., Shi, D., Trull, T. W., et al. (2018). Ambient nitrate switches the ammonium consumption pathway in the euphotic ocean. *Nat. Communication* 9 (1), 915. doi: 10.1038/s41467-018-03363-0

Waser, N., Harrison, P., Nielsen, B., Calvert, S., and Turpin, D. (1998). Nitrogen isotope fractionation during the uptake and assimilation of nitrate, nitrite, ammonium, and urea by a marine diatom. *Limnology Oceanography* 43 (2), 215–224. doi: 10.4319/lo.1998.43.2.0215

Wilson, C., and Coles, V. J. (2005). Global climatological relationships between satellite biological and physical observations and upper ocean properties. *J. Geophysical Res.* 110 (C10), C10001. doi: 10.1029/2004jc002724

Wong, G. T. F., Tseng, C.-M., Wen, L.-S., and Chung, S.-W. (2007). Nutrient dynamics and n-anomaly at the SEATS station. *Deep Sea Res. Part II: Topical Stud. Oceanography* 54 (14), 1528–1545. doi: 10.1016/j.dsr2.2007.05.011

Wu, K., Dai, M., Chen, J., Meng, F., Li, X., Liu, Z., et al. (2015). Dissolved organic carbon in the south China Sea and its exchange with the Western pacific ocean. *Deep Sea Res. Part II: Topical Stud. Oceanography* 122, 41–51. doi: 10.1016/j.dsr2.2015.06.013

Xu, M. N., Zhang, W., Zhu, Y., Liu, L., Zheng, Z., Wan, X. S., et al. (2018). Enhanced ammonia oxidation caused by lateral kuroshio intrusion in the boundary zone of the northern south China Sea. *Geophysical Res. Lett.* 45, 6585–6593. doi: 10.1029/2018GL077896

Yang, J.-Y., Hsu, S.-C., Dai, M., Hsiao, S.-Y., and Kao, S.-J. (2014). Isotopic composition of water-soluble nitrate in bulk atmospheric deposition at dongsha island: sources and implications of external n supply to the northern south China Sea. *Biogeosciences* 11 (7), 1833–1846. doi: 10.5194/bg-11-1833-2014

Yang, J.-Y. T., Kao, S.-J., Dai, M., Yan, X., and Lin, H.-L. (2017). Examining n cycling in the northern south China Sea from n isotopic signals in nitrate and particulate phases. *J. Geophysical Research: Biogeosciences* 122 (8), 2118–2136. doi: 10.1002/2016JG003618

Yang, J.-Y. T., Tang, J.-M., Kang, S., Dai, M., Kao, S.-J., Yan, X., et al. (2022). Comparison of nitrate isotopes between the south China Sea and Western north pacific ocean. *J. Geophysical Research: Oceans* 127, e2021JC018304. doi: 10.1029/2021JC018304

Yan, X., Wan, X. S., Liu, L., Xu, M. N., Tan, E., Zheng, Z., et al. (2019). Biogeochemical dynamics in a eutrophic tidal estuary revealed by isotopic compositions of multiple nitrogen species. *J. Geophysical Research: Biogeosciences* 124 (7), 1849–1864. doi: 10.1029/2018jg004959

Yan, X., Xu, M. N., Wan, X. S., Yang, J.-Y. T., Trull, T. W., Dai, M., et al. (2017). Dual isotope measurements reveal zoning of nitrate processing in the summer changjiang (Yangtze) river plume. *Geophysical Res. Lett.* 44 (24), 12289–12297. doi: 10.1002/2017GL075951

Yool, A., Martin, A. P., Fernandez, C., and Clark, D. R. (2007). The significance of nitrification for oceanic new production. *Nature* 447 (7147), 999–1002. doi: 10.1038/nature05885

Yoshikawa, C., Makabe, A., Matsui, Y., Nunoura, T., and Ohkouchi, N. (2018). Nitrate isotope distribution in the subarctic and subtropical north pacific. *Geochemistry Geophysics Geosystems* 19, 2212–2214. doi: 10.1029/2018GC007528

Yoshikawa, C., Makabe, A., Shiozaki, T., Toyoda, S., Yoshida, O., Furuya, K., et al. (2015). Nitrogen isotope ratios of nitrate and n* anomalies in the subtropical south pacific. *Geochemistry Geophysics Geosystems* 16 (5), 1439–1448. doi: 10.1002/2014gc005678

Yuan, D., Han, W., and Hu, D. (2006). Surface kuroshio path in the Luzon strait area derived from satellite remote sensing data. *J. Geophysical Res. Oceans* 111 (C11), C11007. doi: 10.1029/2005JC003412

frontiers | Frontiers in Marine Science

TYPE Original Research
PUBLISHED 16 December 2022
DOI 10.3389/fmars.2022.1100289

OPEN ACCESS

EDITED BY
Xianbiao Lin,
Ocean University of China, China

REVIEWED BY
Minjie Hu,
Fujian Normal University, China
Pengfei Zheng,
Ministry of Natural Resources, China

*CORRESPONDENCE
Xiangyu Wang
cyswangxiangyu@shandong.cn
Hongxia Zhang
hxzhang@sibs.ac.cn

SPECIALTY SECTION
This article was submitted to Marine Biogeochemistry, a section of the journal Frontiers in Marine Science

RECEIVED 16 November 2022
ACCEPTED 05 December 2022
PUBLISHED 16 December 2022

CITATION
Song Y, Ma L, Zhang H, Fu R, Liang X, Li J, Li J, Li M, Shan Y, Cheng J, Wang X and Zhang H (2022) The diversity and structure of diazotrophic communities in the rhizosphere of coastal saline plants is mainly affected by soil physicochemical factors but not host plant species.
Front. Mar. Sci. 9:1100289.
doi: 10.3389/fmars.2022.1100289

The diversity and structure of diazotrophic communities in the rhizosphere of coastal saline plants is mainly affected by soil physicochemical factors but not host plant species

Yanjing Song[1], Lan Ma[1], Haiyang Zhang[1], Rao Fu[1], Xiaoyan Liang[1], Junlin Li[1], Jiajia Li[1], Meng Li[1], Yan Shan[1], Jieshan Cheng[2,3], Xiangyu Wang[1]* and Hongxia Zhang[1,2,3]*

[1]Shandong Institute of Sericulture, Shandong Academy of Agricultural Sciences, Yantai, China, [2]The Engineering Research Institute of Agriculture and Forestry, Ludong University, Yantai, China, [3]Key Laboratory of Molecular Module-Based Breeding of High Yield and Abiotic Resistant Plants in Universities of Shandong (Ludong University), Ludong University, Yantai, China

The diversity and community structure of rhizospheric microbes are largely affected by soil physicochemical properties and plant species. In this work, high throughput sequencing and quantitative real-time PCR targeting *nifH* gene were used to assess the abundance and diversity of diazotrophic community in the coastal saline soils of Yellow River Delta (YRD). We demonstrated that the copy number of *nifH* gene encoding the Fe protein subunit of the nitrogenase in the nitrogen fixation process was significantly affected by soil physiochemical factors, and the abundance of diazotrophs in the rhizospheric soil samples collected from different locations was positively related with soil physicochemical properties. Soil salinity (P=0.003) and moisture (P=0.003) were significantly co-varied with the OTU-based community composition of diazotrophs. Taxonomic analysis showed that most diazotrophs belonged to the *Alphaproteobacteria*, *Gammaproteobacteria* and *Deltaproteobacteria*. Linear discriminant analysis (LDA) effect size (LEfSe) and canonical correspondence analysis (CCA) showed that diazotrophic community structure significantly varied with soil salinity, moisture, pH and total nitrogen, carbon, sulphur and nitrite (NO_2^-N) content. Our findings provide direct evidence toward the understanding of different effects of soil physicochemical properties and host plant traits such as halophytes types, life span and cotyledon type, on the community composition of diazotrophic populations in the rhizosphere of plants grown in coastal saline soils.

KEYWORDS

diazotroph, nifH gene, community structure, rhizosphere, halophyte

Introduction

Nitrogen (N) is one of the essential primary macronutrients for plant growth and production (Li et al., 2018). Through the reduction of atmospheric N_2 to biologically available ammonium, about 70% of total N is fixed (Galloway et al., 2004; Lin et al., 2016). An efficient way to introduce N_2 into the biosphere is N fixation, since plants cannot directly utilize gaseous N_2. In the rhizosphere of plants, a wide variety of diazotrophs, including free living bacteria, sulfate reducing bacteria and symbiotic diazotrophs, usually dominated by *Proteobacteria*, *Cyanobacteria* and *Firmicutes*, inhabited (Wang et al., 2016; Zhang et al., 2021). These diazotrophs shared the same operon in which the *nifH* gene encoding the Fe protein subunit of the nitrogenase in the nitrogen fixation process has been widely used for phylogenetic analyses (Ininbergs et al., 2011; Ospina-Betancourth et al., 2020; Dong et al., 2022). Plant diversity could affect the composition and function of microbial community, which in return, increased soil N supply to plants (Zak et al., 2003). Due to the high genetic diversity, rhizospheric diazotrophs could play multiple roles in plant growth and development (Vejan et al., 2016; Oliveira et al., 2017). Generally, diazotrophs provided readily available N sources to host plants, and in return, host plants supplied carbon sources to diazotrophs through photosynthesis (Gupta et al., 2006; Liu et al., 2019).

The diversity and composition of microbial communities in the rhizosphere of plants were affected by soil properties (Garbeva et al., 2008; Tkacz et al., 2015; Jiang et al., 2017; Li et al., 2021). In some studies, a greater impact of host plant species on microbial assemblage composition, than of abiotic parameters, has been observed, since the selection of microbial communities in rhizospheric soils was dependent on the root morphology, root exudation and nutrient competition of plants (Rodrigo et al., 2006; Ladygina and Hedlund, 2010). In some studies, diazotrophic abundance and community composition were found to be mainly affected by soil characteristics, such pH, inorganic N and carbon/nitrogen (C/N) ratio, especially salinity and water content (Moisander et al., 2007; Collavino et al., 2014; Levy-Booth et al., 2014; Wang et al., 2017; Che et al., 2018; Lin et al., 2018). The effects of plants on microbial community in plant rhizosphere were species specific, and a synergistic relationship between plant species and environmental conditions existed (Morina et al., 2018). In addition, diazotroph assemblages were also strongly influenced by seasons, abiotic environmental parameters and host plants (Debra et al., 2011; Lin et al., 2017).

One of the major causes for soil salinization in the coastal region was the intrusion of seawater into coastal aquifers (Omuto et al., 2020). With the increase of distance from the vertical coastline, soil salinity and moisture of coastal wetlands changed significantly (Xian et al., 2019). In coastal sediments, higher rate of sediment N-fixation, which could be a significant N source, has been detected (Mortazavi et al., 2012; Bhavya et al., 2016). In coastal seagrass beds, microbial N-fixing provided 50% of the N requirements (Whiting et al., 1986). The biological N fixation (BNF) rates in coastal region can be affected by many biotic and abiotic factors, such as diazotroph diversity, soil C:N ratio and soil P level (Dang et al., 2013; Huang et al., 2016). Microbially-mediated N-dynamics were particular important to the biogeochemical functions in coastal marine wetlands (Affourtit et al., 2001; Moisander et al., 2007; Moseman-Valtierra et al., 2009). Nitrogen-fixing bacteria constituted a key functional group of microorganisms relevant to the functions of wetland ecosystems (Moseman et al., 2009). Meanwhile, human activity also generated a great amount of nitrogen, causing numerous ecological and environmental problems, such as eutrophication, in coastal region (Newell et al., 2016; Huang et al., 2021; Lin and Lin, 2022). Salinization could affect the transformation and uptake of N, and ultimately restrain the growth and decrease the production of plants (Midgley, 2012). To adapt to the salt stress condition, halophyte plants could shape specific rhizospheric microbiomes and increase the microbial diversities (Wang et al., 2010; Anburaj et al., 2012; Qiu et al., 2022). The growth of halophyte plants is usually limited by the availability of N, which is supplemented by the introduction of 'new' N in the ecosystems through plant associated diazotrophs (Debra et al., 2011; Rejmánková et al., 2018; Zhang et al., 2020; Qiu et al., 2022). The rate of microbial N fixation is correlated to plant photosynthetic activity, and the structure of diazotroph assemblage is significantly influenced by the variety of carbon sources associated with plant species. According to the mechanisms of salt tolerance, halophytes are divided into secretohalophyte, pseudohalophyte and euhalophyte. Dicotyledonous plants have more developed root system than monocotyledonous plants, and annual halophyte plants have developed a set of mechanisms safer than those of perennial halophyte plants, including seed dormancy when subjected to high salt stress, fast germination after rehydration, polymorphism in morphology and germination, and persistent seed bank and plastic resource allocation (Cao et al., 2021).

Since the 1980s, the coastal zone of Laizhou Bay-Yellow River Estuary, which cover an area of 2,870 km^2, has become one of the most serious seawater intruded regions in China (Guo and Gong, 2014). In this area, coastal saline soils show a gradient of salinity and water content from land to sea, accompanied with an apparent species succession of native plants. Although some studies on the characterization and evolution of vegetation in this area have been carried out for saline soil bioremediation, limited work has been done on the microbial community structure in the rhizosphere of plants grown in this area (Zhang et al., 2006; Ravit et al., 2007; Cao et al., 2015; Jing et al., 2018). In this study, we investigated the physicochemical factors, as well as the diversity and composition of rhizospheric N-fixing microbes

in the coastal wetland. We demonstrate that the key driving factors affecting diazotrophic community structure in the coastal saline soil are physicochemical factors but not host plant traits.

Materials and methods

Research site and sample collection

The research area was located at the coastal zone of Laizhou Bay - Yellow River Estuary in China, with an average annual rainfall of 415.9 -842 mm and a mean annual temperature of 12.3°C-12.9°C (Figure 1A). Four sampling sites, Changyi (CY) and Shouguang (SG), which possess silt and low or non-saline soils, and Dongying (DY) and Binzhou (BZ), which possess rigid and high salinity soils, were chosen in this study (Figure 1B). For sample collection, surface soil was removed from each individual plant in a given plot, and plant roots together with rhizospheric soil were carefully excavated. Rhizospheric soil was obtained by shaking plants vigorously to separate the soil that not tightly adhered to the roots. Soils remaining attached to the roots after this were considered as rhizospheric soils (Jing et al., 2018). Finally, a total number of 18 samples corresponding to 8 different plant species, including *Chenopodium L., Phragmites australis, Tamarix austromongolica Nakai, Tamarix austromongolica Nakai, Suaeda salsa, Limonium sinens, Imperata* sp., and *Typha* sp., were collected (Figure 1C; Table 1). Host plants were morphologically identified and classified based their salt tolerance (6 halophytic and 2 non-halophytic), life style (3 annual and 5 perennial) and cotyledon number (5 dicotyledon and 3 monocotyledon), according to the Subject Database of Chinese Plant (http://www.plant.csdb.cn/) and Plant Collection Database (http://www.plantpic.csdb.cn/), as described previously (Zhang et al., 2006).

Rhizospheric soil analyses

Soil samples with different soil salinity and moisture were collected in April, 2021. In each sampling area, five replication blocks (10×10 m) were established, and the rhizospheric soils of the most abundant plant species (4–5) available in the blocks were sampled. Fresh soil pH and salinity were determined with a soil to $CaCl_2$ (0.01mol L^{-1}) ratio of 1:5 (w:v). Soil moisture was measured gravimetrically as described previously (Gardner, 1986). Total carbon (TC), total sulphur (TS) and total N (TN) were determined using the Thermo Scientific™ Flash*Smart*™ Elemental Analyzers. Concentrations of nitrate (NO_3^--N), nitrite (NO_2^--N) and ammonium (NH_4^+-N) in the soils were extracted with KCl solution (2 mol L^{-1}) and determined with the auto-analyzer (Seal, Germany) (Mulvaney, 1996). Soil types was classified as non-saline (Sal<1.2‰), slight saline (1.2‰–2.4‰), moderate saline (2.4‰–4.8‰), strong saline (4.8‰–9.6‰) and severe saline (Sal>9.6‰) as described previously (Richards, 1954). Soil moisture was divided into low moisture (<8%), medium moisture (8%–12%) and high moisture (>12%).

DNA isolation and quantitative real-time PCR analysis

Total soil DNA was isolated using the FastDNA® SPIN Kit for Soil (MP Biomedicals, Solon, OH, USA) following the manufacturer's protocol. DNA concentrations were determined with spectrophotometer Nanodrop 2000c (Thermo-Fisher, USA). To quantify the abundance of *nifH* gene in the rhizospheric soils, quantitative real-time PCR (qPCR) was performed with the forward (5'-TGCGAYCCSAARGCBGACTC-3') and reverse (5'-ATSGCCATCATYTCRCCGG A-3') primers (Poly et al., 2001). For each reaction, a total volume of 20 μL TB Green™ Premix Ex Taq™ II (TaKaRa, Japan) supplemented with 0.8 μL of each primer and 1μL of soil DNA template was generated. Thermal cycling conditions was as follows: pre-incubation at 50° C for 2 min, pre-denaturation at 95°C for 10min, then reaction for 40 cycles consisting of denaturation at 94°C for 30 s, annealing at 60°C for 30 s and extension at 72°C for 60 s, followed by melting curve analysis at 65-95°C (0.5°C per reading). The reactions were carried out in an BioRAD CFX96 fast real-time PCR system (Applied Biosystems, USA). Standard curves for the genes were obtained using serial dilutions of linearized plasmids (pTZ57R/T, Fermentas, USA) containing the target gene amplified from environmental clones (R^2 = 0.99 for all standard curves).

High-throughput sequencing and bioinformatic analysis

For high-throughput sequencing analysis, the forward and reverse primers (5'-TGYGAYCCNAARGCNGA-3' and 5'-ADNGCCATCATYTCNCC-3') were used to amplify the *nifH* gene with the barcode. All PCR reactions were carried out in 30μL reactions with 15μL of Phusion®High-Fidelity PCR Master Mix (New England Biolabs), 0.2μM of forward and reverse primers, and about 10 ng template DNA. Thermal cycling consisting of initial denaturation at 98°C for 1 min, followed by 30 cycles of denaturation at 98°C for 10 s, annealing at 50°C for 30s, and elongation at 72°C for 60s, was performed as described previously (Gaby and Buckley, 2012). PCR products was purified with GeneJET Gel Extraction Kit (Thermo Scientific) and sequenced on the Illumina MiSeq PE250 platform at Biozeron Company (Shanghai, China).

Sequence analysis were performed with UPARSE software package using the UPARSE-OTU and UPARSE-OTUref algorithms. In-house Perl scripts were used to analyze alpha

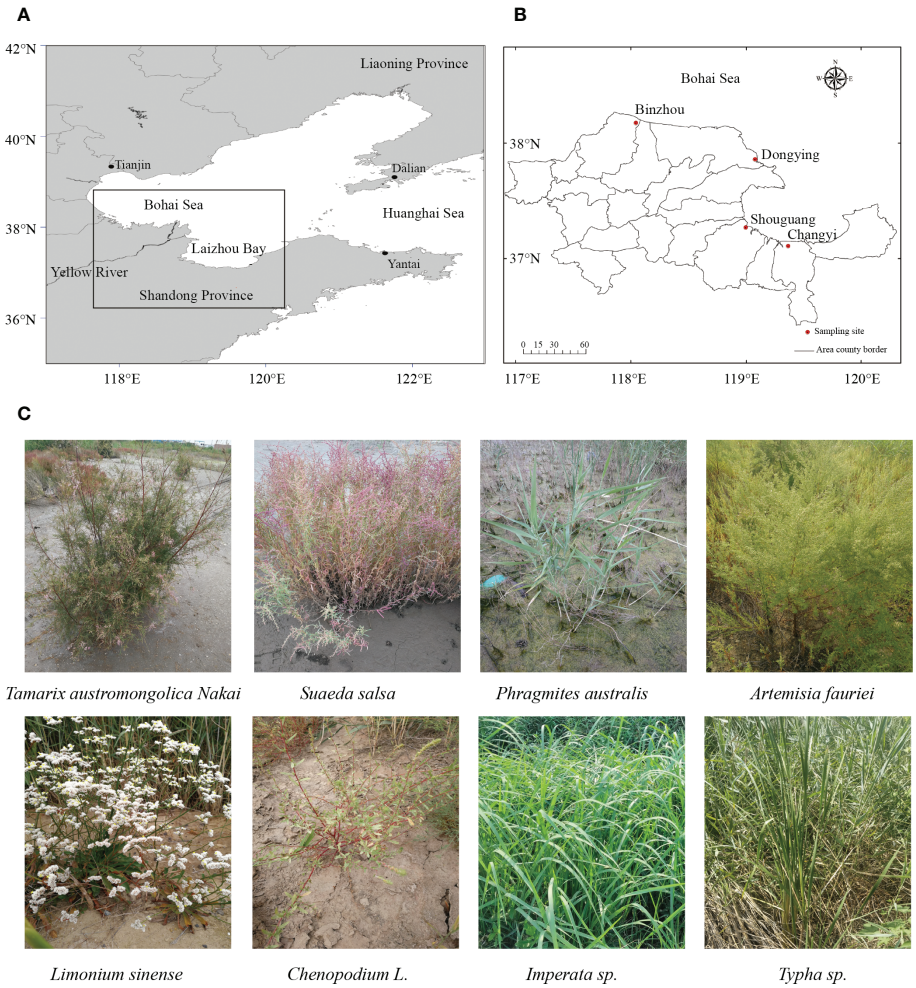

FIGURE 1
Images showing the locations and plants of sampling sites. **(A, B)** Geographic maps showing the sampling positions at the south coastal plain of the Laizhou Bay and the mouth of the Yellow River in China. **(C)** Phenotypes of representative plants for ryhizospheric soil samplings.

(within samples) and beta (among samples) diversity. Sequences with ≥97% similarity were assigned to the same operational taxonomic units (OTUs). A representative sequence for each OTU was picked and classified using the Ribosomal Database Project (RDP) classifier. Alpha diversity indexes (Chao 1, Shannon, Simpson) were calculated using the R software. Beta diversity was calculated based on Bray-Curtis dissimilarities and visualized using non-metric multidimensional scaling (NMDS) in PRIMER v.6 (Primer-E, UK). To confirm the difference in the abundance of individual taxonomy between the two groups, Metastats 2.0 was used. LEfSe was taken for the quantitative analysis of biomarkers in different groups. This method was designed to analyze data in which the number of species is much higher than the number of samples, and to provide biological class explanation to establish statistical significance, biological consistency and effect-size estimation of predicted biomarkers. To identify the differences of microbial communities between the two groups, ANOSIM were performed based on the Bray-Curtis dissimilarity distance matrices (Laurent et al., 2013).

Statistical analysis

The normality of all variables was tested using Shapiro-Wilk analysis. One-way analysis of variance (ANOVA) (for normally distributed variables) and non-parametric Kruskal-Wallis test (for the variables showing non-normal distribution) were performed to identify the differences between environmental factors, alpha diversity estimators, and soil salinity and moisture levels. Spearman's correlations between diazotrophs abundance, alpha diversity and environmental factors were performed using SPSS v.11.5 (SPSS, Chicago, IL, United States). Following detrended correspondence analysis determining the length of the environmental gradient, canonical correspondence analysis

(CCA) was performed to establish which environmental parameters played an important role in the variation of diazotrophic compositions using Canoco 5.0.

Results

Different soil properties are observed in coastal saline lands

To assess the diversity and community composition of diazotrophic microbes in the rhizospheres of plants grown in the coastal saline area, rhizospheric soil samples from four sites, Changyi (CY), Shouguang (SG), Dongying (DY) and Binzhou (BZ), located at the coastal zone of Laizhou Bay-Yellow River Estuary in China, were collected (Figures 1A, B). In this sampling area, plant community is dominated by halophyte plants such as *Suaeda salsa*, *Phragmites australis*, *Tamarix austromongolica Nakai*, *Chenopodium L.*, *Artemisia fauriei*, *Limonium sinense*, and some non-halophyte plants such as *Imperata* sp. and *Typha* sp. (Figure 1C; Table 1). Accompanied with the gradient of salinity and water moisture from land to sea, the host plant community showed obvious species succession. Since halophytes can survive in saline soils with low nutrient loads and water holding capacity, we first compared the property of the soil samples collected from different saline sites. Generally, all rhizospheric soil samples were slightly alkaline, with pH values ranged from 7.18 to 7.77, and their salinity and water content varied greatly, ranged from 0.5‰ to 15.14‰ and 1.10‰ to 13.38%, respectively (Table 1). Soils from DY and BZ sampling sites showed strong and severe salinity (5.38‰~15.14‰), and medium and high moisture (8.96% ~13.38%), whereas soils from CY and SG sampling sites showed low saline (0.50‰~0.99‰) and moisture (1.1%~4.13%). The fertility of each sampling site was poor and the content of inorganic N was low, ranged from 2.78 to 14.05 $mg{\cdot}kg^{-1}$, with NO_3^-N as the dominant inorganic N ranged from 2.25 to 9.18 $mg{\cdot}kg^{-1}$ (Table 1). The highest salinity and moisture, with a percentage of 15.14% and 13.38%, was detected in the soil samples collected from DY-01 and DY-02, respectively. Whereas the lowest salinity and moisture, with a percentage of 0.50% and 1.10%, was detected in the soil samples collected from SG-03 and SG-01, respectively. The highest TN and TC, with a percentage of 0.069% and 2.007%, respectively, was detected in the soil samples collected from BZ-03. Whereas the lowest TN (0.016%) and TC (0.635%) was detected in the soil samples collected from SG03 and CY02, respectively (Table 1).

nifH gene abundance is significantly affected by soil physiochemical factors

To assess the abundance of diazotrophic microbes in the rhizosphere of plants grown in the coastal saline area, we examined the copy numbers of *nifH* gene in the collected soil samples. The copy numbers of *nifH* gene varied widely, ranged from 1.99×10^6 to 3.80×10^8 copies g^{-1} dry soil across all the collected samples, with the highest *nifH* gene copy number detected in the rhizospheric soil samples of *Tamarix austromongolica Nakai* collected in Binzhou area (Figure 2). Further ANOVA and Kruskal-Wallis analyses revealed that the copy numbers of *nifH* gene were significantly affected by soil salinity and moisture, not plant traits (Table 2). A higher *nifH* gene copy number was observed in soil samples with high salinity and moisture than in soil samples with non-saline and low moisture. Spearman's correlation analysis exhibited that the copy numbers of *nifH* gene were significantly related to pH value, soil salinity, moisture, and the levels of TN, TC, TS (total sulphur), NH_4^+-N and NO_3^-N (Table 3).

Different diazotrophic community structures are observed

To further understand the richness and diversity of diazotrophic communities in the rhizosphere of plants grown in the selected coastal saline area, we carried out high-throughput sequencing analysis. A total number of 812554 raw reads were obtained from 18 samples. At a cut-off of 97% sequence similarity, 5007 OTUs representing 10 phyla were obtained. We analyzed the diversity (Shannon and Simpson) and richness (Chao1) indices with two-way ANOVA and Kruskal-Wallis tests, and found that Shannon, Simpson and Chao1 indices were remarkably influenced by soil salinity and moisture, whereas alpha-diversities were not significantly affected by plant traits such as halophyte type, life span and cotyledon type (Table 2). Overall, the most abundant phylum was *Proteobacteria* (mean ± SE, 85.0% ± 13.1%; n = 18), followed by *Cyanobacteria* (6.71% ± 11.3%), unclassified phylum (5.86% ± 3.61%) and Firmicutes (1.21% ± 1.96%). Two phyla, *Chloroflexi* and *Fibrobacteres*, appeared to be the minor components (<1%) across all the soil samples (Figure S1). At genus level, *Bradyrhizobium* was found to be the most abundant genus (16.1%), followed by *Halorhodospira* (8.36%), *Desulfovibrio* (6.81%) and *Azospirillum* (5.98%), in the soil samples (Figure 3A).

The diversity of diazotrophs is affected by soil salinity and moisture

Based on the OTUs from the 16S rRNA gene sequences, we further generated non-metric multidimensional scaling (NMDS) ordination plot of diazotrophic community dissimilarities. We observed that diazotrophic communities in all the soil samples were clearly divided into two groups based on their soil salinity and moisture levels (Figure 3B). Further ANOSIM test also demonstrated that the diversity of diazotrophic community was significantly affected by soil salinity and soil moisture, but not by plant traits (Table 4). A higher diversity of diazotrophic

TABLE 1 Characteristics of host plants and rhizospheric soils.

Sample ID	Scientific name	Halophytes type	Life span	Cotyledon type	pH value	Salinity (‰)	Moisture (%)	TN(%)	TC(%)	TS(%)	NH_4^+-N (mg/kg)	NO_2^-N (mg/kg)	NO_3^-N (mg/kg)
CY-01	*Chenopodium L.*	Secretohalophyte	Annual	Dicotyledon	7.34 ± 0.19	0.53 ± 0.00	2.99 ± 0.08	0.055 ± 0.00	0.841 ± 0.11	0.004 ± 0.00	0.86 ± 0.04	0.024 ± 0.01	3.12 ± 0.22
CY-02	*Phragmites australis*	Pseudohalophyte	Perennial	Monocotyledon	7.18 ± 0.20	0.58 ± 0.00	4.13 ± 0.12	0.031 ± 0.00	0.635 ± 0.00	0.003 ± 0.00	0.22 ± 0.12	0.021 ± 0.01	2.53 ± 0.13
CY-03	*Tamarix austromongolica Nakai*	Secretohalophyte	Perennial	Dicotyledon	7.28 ± 0.19	0.63 ± 0.00	3.65 ± 0.31	0.044 ± 0.01	0.754 ± 0.01	0.008 ± 0.00	1.44 ± 0.35	0.14 ± 0.06	3.61 ± 0.61
CY-04	*Artemisia fauriei*	Pseudohalophyte	Perennial	Dicotyledon	7.18 ± 0.19	0.51 ± 0.12	2.75 ± 0.10	0.044 ± 0.00	0.79 ± 0.02	0.003 ± 0.00	0.97 ± 0.36	0.089 ± 0.04	3.38 ± 0.09
SG-01	*Suaeda salsa*	Euhalophyte	Annual	Dicotyledon	7.61 ± 0.13	0.99 ± 0.00	1.1 ± 0.03	0.032 ± 0.03	1.186 ± 0.02	0.008 ± 0.00	0.81 ± 0.10	0.034 ± 0.01	6.83 ± 0.51
SG-02	*Phragmites australis*	Pseudohalophyte	Perennial	Monocotyledon	7.22 ± 0.13	0.67 ± 0.00	1.88 ± 0.02	0.018 ± 0.00	0.998 ± 0.06	0.005 ± 0.00	–	0.01 ± 0.00	2.44 ± 0.04
SG-03	*Tamarix austromongolica Nakai*	Secretohalophyte	Perennial	Dicotyledon	7.29 ± 0.13	0.50 ± 0.00	2.32 ± 0.05	0.016 ± 0.00	0.998 ± 0.02	0.003 ± 0.00	0.31 ± 0.00	0.031 ± 0.00	2.25 ± 0.35
SG-04	*Artemisia fauriei*	Pseudohalophyte	Perennial	Dicotyledon	7.38 ± 0.13	0.71 ± 0.01	2.75 ± 0.02	0.021 ± 0.01	1.058 ± 0.15	0.004 ± 0.00	3.09 ± 0.39	0.042 ± 0.01	5.41 ± 0.20
SG-05	*Chenopodium L.*	Secretohalophyte	Annual	Dicotyledon	7.41 ± 0.13	0.66 ± 0.00	2.22 ± 0.02	0.018 ± 0.00	0.98 ± 0.00	0.004 ± 0.00	1.08 ± 0.00	0.015 ± 0.00	2.66 ± 0.18
DY-01	*Suaeda salsa*	Euhalophyte	Annual	Dicotyledon	7.55 ± 0.17	15.14 ± 0.02	11.47 ± 0.39	0.05 ± 0.01	1.522 ± 0.22	0.083 ± 0.01	1.77 ± 0.75	0.031 ± 0.03	9.18 ± 1.03
DY-02	*Phragmites australis*	Pseudohalophyte	Perennial	Monocotyledon	7.52 ± 0.18	11.22 ± 0.02	13.38 ± 0.45	0.05 ± 0.01	1.543 ± 0.03	0.047 ± 0.01	5.88 ± 0.52	0.034 ± 0.02	8.13 ± 0.25
DY-03	*Tamarix austromongolica Nakai*	Secretohalophyte	Perennial	Dicotyledon	7.70 ± 0.18	10.40 ± 0.02	12.62 ± 0.03	0.05 ± 0.00	1.652 ± 0.05	0.047 ± 0.00	2.27 ± 1.11	0.017 ± 0.00	6.04 ± 0.34
DY-04	*Limonium sinense*	Secretohalophyte	Annual	Dicotyledon	7.73 ± 0.16	11.78 ± 0.03	12.07 ± 0.25	0.042 ± 0.00	1.55 ± 0.35	0.046 ± 0.01	1.23 ± 0.36	0.02 ± 0.00	3.2 ± 0.16
DY-05	*Imperata* sp.	Non-halophyte	Perennial	Monocotyledon	7.59 ± 0.15	8.47 ± 0.02	12.48 ± 0.06	0.046 ± 0.00	1.606 ± 0.40	0.039 ± 0.00	4.51 ± 0.18	0.022 ± 0.00	3.31 ± 0.31
BZ-01	*Suaeda salsa*	Euhalophyte	Annual	Dicotyledon	7.77 ± 0.19	7.88 ± 0.03	11.33 ± 0.26	0.042 ± 0.01	1.557 ± 0.04	0.079 ± 0.01	0.79 ± 0.27	0.021 ± 0.01	3.75 ± 0.07
BZ-02	*Phragmites australis*	Pseudohalophyte	Perennial	Monocotyledon	7.58 ± 0.18	5.38 ± 0.03	10.3 ± 0.56	0.042 ± 0.00	1.498 ± 0.19	0.086 ± 0.02	–	0.015 ± 0.01	2.52 ± 0.02

(Continued)

10.3389/fmars.2022.1100289

TABLE 1 Continued

Sample ID	Scientific name	Halophytes type	Life span	Cotyledon type	pH value	Salinity (‰)	Moisture (%)	TN(%)	TC(%)	TS(%)	NH_4^+-N (mg/kg)	NO_2^-N (mg/kg)	NO_3^-N (mg/kg)
BZ-03	*Tamarix austromongolica Nakai*	Secretohalophyte	Perennial	Dicotyledon	7.42 ± 0.18	14.93 ± 0.04	12.15 ± 0.35	0.069 ± 0.02	2.007 ± 0.10	0.135 ± 0.04	2.85 ± 1.00	0.055 ± 0.01	11.39 ± 0.26
BZ-04	*Typha* sp.	Non-halophyte	Perennial	Monocotyledon	7.31 ± 0.19	5.73 ± 0.01	8.96 ± 0.26	0.044 ± 0.00	1.452 ± 0.05	0.083 ± 0.01	1.24 ± 0.59	0.033 ± 0.01	4.02 ± 0.22

community was observed in the soil samples with strong saline and high moisture, whereas no significant difference was observed in the overall diazotrophic composition among the soil samples collected from the rhizosphere of plants with different traits (Table 4).

We also performed Venn diagram analysis and a total number of 495 shared OTUs among the soil samples with different salinity and moisture levels were identified (Figures 4A, B). Samples collected at high salinity site showed the highest numbers of unique OTUs. Among the samples collected from the rhizospheric soils of different plant species, the highest number of unique OTUs (732) was observed in the rhizospheric soil samples of *Secretohalophyte* (Figure 4C). Higher numbers of unique OTUs were also observed in the rhizospheric soil samples of perennial and dicotyledonous plants than in those of annual and monocotyledonous plants, with a number of 4359 versus 2895, and 3970 versus 3555, respectively (Figures 4D, E). We further compared the unique OTUs in the soil samples collected from the rhizosphere of the same plant species grown at different sites. Higher numbers of unique OTUs were observed in the rhizospheric soil samples of *Suaeda salsa*, *Phragmites australis* and *Tamarix austromongolica Nakai* at high salinity and moisture sites in Binhzou and Dongying (Figures 4F-H).

Differentiated taxa are identified in the diazotrophic community

To verify the potential discriminating species in the relative abundance between different groups, we carried out Linear discriminant analysis (LDA) effect size (LEfSe) analysis. A total number of 92 and 87 potential diazotrophic biomarkers distinguishing soil salinity and moisture levels were identified (Figures 5A, B). Among them, *Cyanobacteria*, *Spirochaetes* and *Euryarchaeota* was respectively found to be the main biomarker for the diazotrophic community in the samples collected at non-saline and low soil moisture, strong saline and medium soil moisture, and severe saline and high soil moisture sites (Figures 5A, B).

In the samples collected from the rhizospheric soils of euhalophyte plants, the abundance of *Ectothiorhodospira* was found to be significantly different (Figure 5C). *Dechloromonas*, *Desmonostoc*, *Rhodobacter*, *Methylosinus*, *Erwiniaceae* and *Pantoea* were specifically identified in the samples collected from the rhizospheric soils of monocotyledonous plants (Figure 5D). In addition, four potential diazotrophic biomarkers distinguishing the rhizospheric soil samples of annual and perennial plants were identified (Figure 5E). In the samples collected from the rhizospheric soils of annual plants, the biomarkers were mostly clustered in *Cyanobacteria* and *Gammaproteobacteria*, including *Synechococcale* and *Marichromatium*, whereas in those of perennial plants, the biomarkers were mostly clustered in *Gammaproteobacteria*, including *Pseudomonas* and *Methylococcus* (Figure 5E).

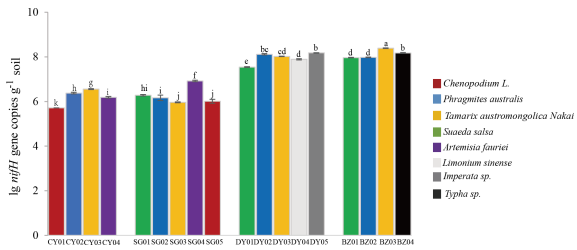

FIGURE 2
Quantification of *nifH* gene in the rhizospheric soil samples collected at different locations. Four sampling locations, Changyi (CY) and Shouguang (SG) with silt and low or non-saline soils, and Dongying (DY) and Binzhou (BZ) with rigid and high salinity soils, were selected. CY01, CY02, CY03, CHY04, SG01, SG02, SG03, SG04, SG05, DY01, DY02, DY03, DY04, DY05, BZ01, BZ02, BZ03 and BZ04 represent the soil samples respectively collected from the four locations. Values were means and standard deviations of three biological replicates (n=3). Lowercase letters denote significant differences of *nifH* gene copy numbers (Student's *t*-test, $P<0.05$).

TABLE 2 Comparison of the abundance and diversity of nitrogen-fixing bacteria from the rhizosphere of different plant species.

	lg *nifH* gene copies	Richness (chao 1)	Shannon index	Simpson index
Types of halophytes				
Secretohalophyte	7.06 ± 0.24^{b}	808.33 ± 256.49	4.55 ± 0.45	0.052 ± 0.024
Pseudohalophyte	6.96 ± 0.20^{b}	746.63 ± 254.62	4.33 ± 0.47	0.054 ± 0.019
Euhalophyte	7.26 ± 0.25^{b}	1094.25 ± 382.76	5.27 ± 0.31	0.013 ± 0.003
Non-halophyte	8.18 ± 0.13^{a}	1657.54 ± 348.39	5.86 ± 0.41	0.010 ± 0.0057
P Value	**0.043**	0.361	0.30	0.503
Monocotyledon/Dicotyledon				
Monocotyledon	7.50 ± 0.21	1202.59 ± 269.24	5.19 ± 0.39	0.026 ± 0.14
Dicotyledon	7.03 ± 0.16	793.36 ± 154.18	4.52 ± 0.33	0.493 ± 0.16
P Value	0.079	0.221	0.235	0.364
Life span				
Annual	7.05 ± 0.23	838.50 ± 228.79	4.89 ± 0.32	0.027 ± 0.012
Perennial	7.25 ± 0.16	975.41 ± 206.51	4.67 ± 0.36	0.049 ± 0.016
P Value	0.47	0.689	0.703	0.370
Saline grade				
Non-saline	6.28 ± 0.065^{b}	350.19 ± 33.04^{c}	3.71 ± 0.24^{b}	0.073 ± 0.02^{a}
Strong saline	8.07 ± 0.031^{a}	1724.14 ± 147.41^{a}	5.81 ± 0.17^{a}	0.01 ± 0.002^{b}
Severely saline	7.99 ± 0.075^{a}	929.77 ± 154.19^{b}	5.58 ± 0.10^{a}	0.01 ± 0.001^{b}
P Value	**<0.001**	**0.001**	**<0.001**	**0.002**
Soil moisture grade				
Low moisture	6.28 ± 0.07^{c}	350.19 ± 33.04^{b}	3.80 ± 0.24^{b}	0.07 ± 0.018^{a}
Medium moisture	7.91 ± 0.070^{a}	1337.53 ± 166.82^{a}	5.78 ± 0.19^{a}	0.0086 ± 0.0014^{b}
High moisture	8.12 ± 0.045^{b}	1724.14 ± 166.82^{a}	5.60 ± 0.93^{a}	0.0113 ± 0.0015^{b}
P Value	**<0.001**	**0.002**	**<0.001**	**0.001**

One-way ANOVA and Kruskal-Wallis test was performed. Lowercase letters and the values highlighted in bold indicate significant difference (P<0.05).

TABLE 3 Spearman's correlation between the physiochemical factors and community structure of nitrogen-fixing bacteria.

Physiochemical factor	pH	Salinity	Moister	TN	TC	TS	NH_4^+-N	NO_2^--N	NO_3^--N
lg nifH gene copies	0.50*	0.80**	0.82**	0.51**	0.80**	0.81**	0.67**	0.07	0.55*
Shannon index	0.66**	0.76**	0.62**	0.36	0.87**	0.84**	0.39	-0.27	0.41

*P<0.05, ** P<0.01.

Diazotrophic community is closely correlated with environmental parameters

To dissect the relationships between diazotrophic communities and environmental parameters, we performed canonical correlation analysis (CCA). A remarkable correlation between diazotrophic communities and environmental parameters was observed. As shown in the CCA results, a percentage of 28.5% and 24.2% variation in the diazotrophic community was respectively described in the two CCA canonical axes, suggesting a remarkable correlation between diazotrophic communities and environmental parameters (Figure 6). The major environmental parameters closely correlated with diazotrophic community were soil salinity (P=0.002), soil moisture (P=0.002), TC (P=0.002), TN (P=0.008), TS (P=0.002) and pH value (P=0.002).

Discussion

The growth and health of plants are largely affected by soil physiochemical properties and microbial community structure (Marasco et al., 2018; Jing et al., 2018; Wang et al., 2020). And plant invasion and N enrichment can considerably affect BNF (Xu et al., 2012; Huang et al., 2016). To date, a number of studies based on the diversity and abundance of diazotrophic community in the soils of different habitats, such as paddy field, forest and desert, have been carried out (Wang et al., 2016; Meng et al., 2019; Wang et al., 2021).However, the knowledge about the diazotrophic community structures in the rhizosphere of plants grown in coastal saline soil is limited. In this work, we assess the diversity and community composition of diazotrophic microbes in the rhizosphere of plants grown at the coastal zone of Laizhou Bay-Yellow River estuary in China (Figures 1A, B). Similar to that of other coastal lands in the north part of China, the host plant community is mainly composed of various halophytes in this area, and the soil physiochemical properties are obviously varied at different sampling locations (Figure 1C; Table 1).

Previously it was found that the abundance of *nifH* gene was also significantly related to the BNF rates of in the temperate coastal region of the northwestern North Pacific (Shiozaki et al., 2015). Consistent with the soil physiochemical properties, we found that *nifH* gene copy numbers in the collected soil samples varied widely, with the highest *nifH* gene copy number observed in the rhizospheric soils of plants grown in high salinity and medium moister area (Figure 2; Table 2). To further understand the correlation between the *nifH* gene copy numbers and soil physiochemical properties, we performed Spearman's correlation analysis. The results demonstrated that, in addition to soil salinity and moister, the copy numbers of *nifH* gene were also closely related to the value of soil pH, and the levels of TN, TC, TS, NH_4^+-N and NO_3^--N (Table 3).

Due to its strong persistence across various soil environments, *Bradyrhizobium* has been shown to be the dominant diazotroph in soil system (Pereira et al., 2013; Piromyou et al., 2015). *Bradyrhizobium* was generally detected in the rhizosphere of plants forming root nodules with legumes for N fixation or plants participating in N fixation under non-symbiotic condition (Davis et al., 2011; Meng et al., 2019; Wang et al., 2020; Wang et al., 2021). *Halorhodospira* was also dominantly identified in the rhizospheric soils of coastal salt tolerant plants due to its strong salinity resistance (Imhoff and Truper, 1997). *Azospirillum* has been found to be associated with a variety of crops, and performed an important role in the non-symbiotic N fixation (Steenhoudt and Vanderleyden, 2000; Di Salvo et al., 2018). Our results expanded the distribution range of *Bradyrhizobium* and *Azospirillum* to the rhizosphere of coastal halophyte plants. In addition, *Alpha-* and *Gammaproteobacteria* have been identified as the dominant N fixers in coastal saline soil ecosystem (Yousuf et al., 2014). Similarly, a total number of 10 phyla, with *Bradyrhizobium*, *Desulfovibrio*, *Halorhodospira* and *Azospirillum* were the dominant diazotrophic groups at genus level, were identified in the collected rhizospheric soil samples (Figures 3A, B).

The growth and photosynthetic activity of plants driven by the energy from the sulfide oxidation in root tissues was stimulated by rhizodeposition (Mendelssohn and Morris, 2000; Rolando et al., 2022). In our study, some sulfate reducing bacteria, such as *Desulfovibrio*, *Desulfomicrobium* and *Desulfobacter*, were observed in the diazotrophic community (Figure 3A). This is consistent with previous reports that plant rhizodeposition stimulated N fixation by root-associated sulfate reducers in marsh and hypersaline soda lake environments, and *Desulfovibrio*, *Desulfobulbus* and *Desulfatitalea* coupled sulfate or sulfur respiration to N fixation (Gandy and Yoch, 1988; Tourova et al., 2014; Thajudeen et al., 2017; Rolando et al., 2022). A percentage of 17% energy produced in sulfate reduction was provided to the nitrogen fixation process (Nielsen et al., 2001). *Thioalkalispira*, the typical haloalkaliphilic sulfur-oxidizing bacteria (SOB), could remove the toxic sulphides from the

root zone of plants, and couple S oxidation with C and N fixation (Barbieri et al., 2010; Petersen et al., 2016; Thajudeen et al., 2017). In all the collected rhizospheric soil samples, *Thioalkalispira*, were found to be the core diazotrophs (Figure 3A). Similar results were also observed in the coastal sediments of Bohai Bay, China (Wang et al., 2015). Furthermore, in the rhizosphere of each coastal host species grown under different salinity and moisture conditions, a high proportion of

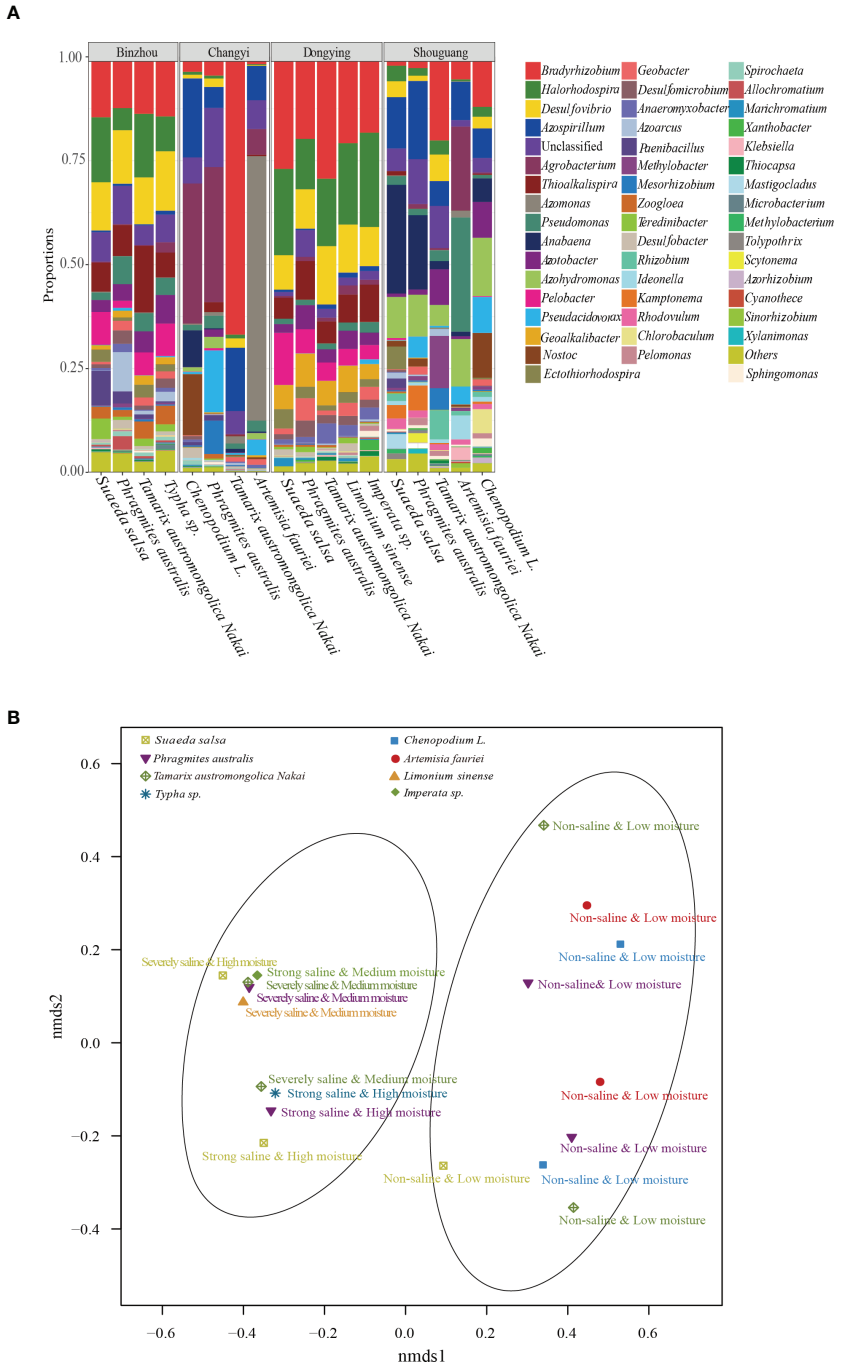

FIGURE 3
Diazotrophic community structure assays. **(A)** Diazotrophic genera in different soil samples collected from the four locations. Dominant diazotrophic genera with high relative abundance (>1%) were shown. **(B)** Non-metric multidimensional scaling analysis (nNMDS). The diazotrophic community dissimilarities based on OTUs from the *nifH* gene sequences were shown. All the samples were clearly divided into two groups based on soil salinity and moisture levels.

TABLE 4 Taxonomic analysis of the diazotrophic community structures.

Group pairs	R	*P value*
Annual vs. perennial	-0.052	0.639
Monocotyledon vs. *dicotyledon*	-0.108	0.936
Types of halophytes	-0.019	0.504
Euhalophyte vs. *pseudohalophyte*	0.099	0.20
Euhalophyte vs. *secretohalophyte*	-0.044	0.49
Euhalophyte vs. *non-halophyte*	-0.333	0.90
Pseudohalophyte vs. *secretohalophyte*	0.058	0.22
Pseudohalophyte vs. *non-halophyte*	0.01	0.43
Secretohalophyte vs. *non-halophyte*	-0.286	1.00
Salinity	0.469	**0.003**
Strong saline vs. severely saline	0.231	0.11
Strong saline vs. non-saline	0.643	**0.001**
Severely saline vs. non-saline	0.72	**0.001**
Soil moisture	0.47	**0.003**
Medium moisture vs. high moisture	0.275	0.08
Medium moisture vs. low moisture	0.664	**0.001**
High moisture vs. low moisture	0.704	**0.002**

The community structure of diazotrophs based plant life span (annual and perennial), cotyledons number (monocotyledon and dicotyledon), halophyte type, salinity and soil moisture was assessed using ANOSIM test. The values highlighted in bold are statistically significant (P<0.05).

unclassified taxa (5.86%) was observed, suggesting that a substantially high and novel diversity of diazotrophic taxa existed in the coastal ecosystem (Figures 3A, B). This is possibly attributed to the special soil physicochemical and plant community property of the coastal ecosystem. Indeed, a total number of 495 shared OTUs among the soil samples with different salinity levels were identified, as indicated by the Venn diagram analysis (Figures 4A-H).

Under stress condition, specific root related microbial community could be formed in the rhizosphere of a certain plant. And in return, this microbiota may help to improve plant resistance to the corresponding stress (Bai et al., 2022). *Ectothiorhodospira* species were found in all kinds of aquatic environments, especially in the stagnant littoral, estuarine and highly saline area (Trüper & Imhoff, 1981). They were also found in the rhizospheric soils of plants grown on Ebinur Lake Wetlands, but not in the paddy fields (Davis et al., 2011; Wang et al., 2020; Zhang et al., 2021). In coastal alkaline soil, *Ectothiorhodospira* attached to anoxygenic purple sulfur bacteria and played a role in the process of N fixation (Tourova et al., 2014; Zhou et al., 2021). We observed that the community structure of diazotrophic microbes in the tested rhizospheric soil samples were significantly affected by the types of halophytes, and as indicated by the high throughput sequencing analysis, *Ectothiorhodospira* was significantly different in the diazotrophic microbial community of halophyte rhizosphere (Table 2; Figures 5A-C). No significant difference was found in the diazotrophic abundance and diversity between monocotyledon and dicotyledon, or perennial and annual plant rhizosphere (Table 2; Figures 5D, E).

When either NO_3^--N or NH_4^+-N as N source was insufficient, N fixation occurred (Zhivotchenko et al., 1995). In the rhizosphere of annual halophytes, *Synechococcales* and *Marichromatium* might play an important role in N fixation, especiall in coastal saline soils (Rigonato et al., 2013). We observed that, for the community structure of diazotrophic microbes, more diazotrophic genus, such as *Dechloromonas*, *Desmonostoc*, *Rhodobacter*, *Methylosinus*, *Erwiniaceae* and *Pantoea*, were found in the rhizospheric soils of monocotyledonous plants, and the biomarkers were mostly clustered in *Synechococcale* and *Marichromatium* in the rhizospheric soils of annual plants (Figures 5D, E). These results may be largely explained by the adventitious root systems of monocotyledonous plants, the main organs for the absorption of nutrient and water, and for the recruiting of specific N-fixing microbes in the rhizosphere.

Previous study has showed that low salinity promoted, whereas high salinity inhibited, the growth of soil N-fixing bacteria (Hou et al., 2018). In addition to the salinity, soil electrical conductivity (EC) also functioned as the main factor driving the variation of microbial community composition (Wang et al., 2020). In our study,

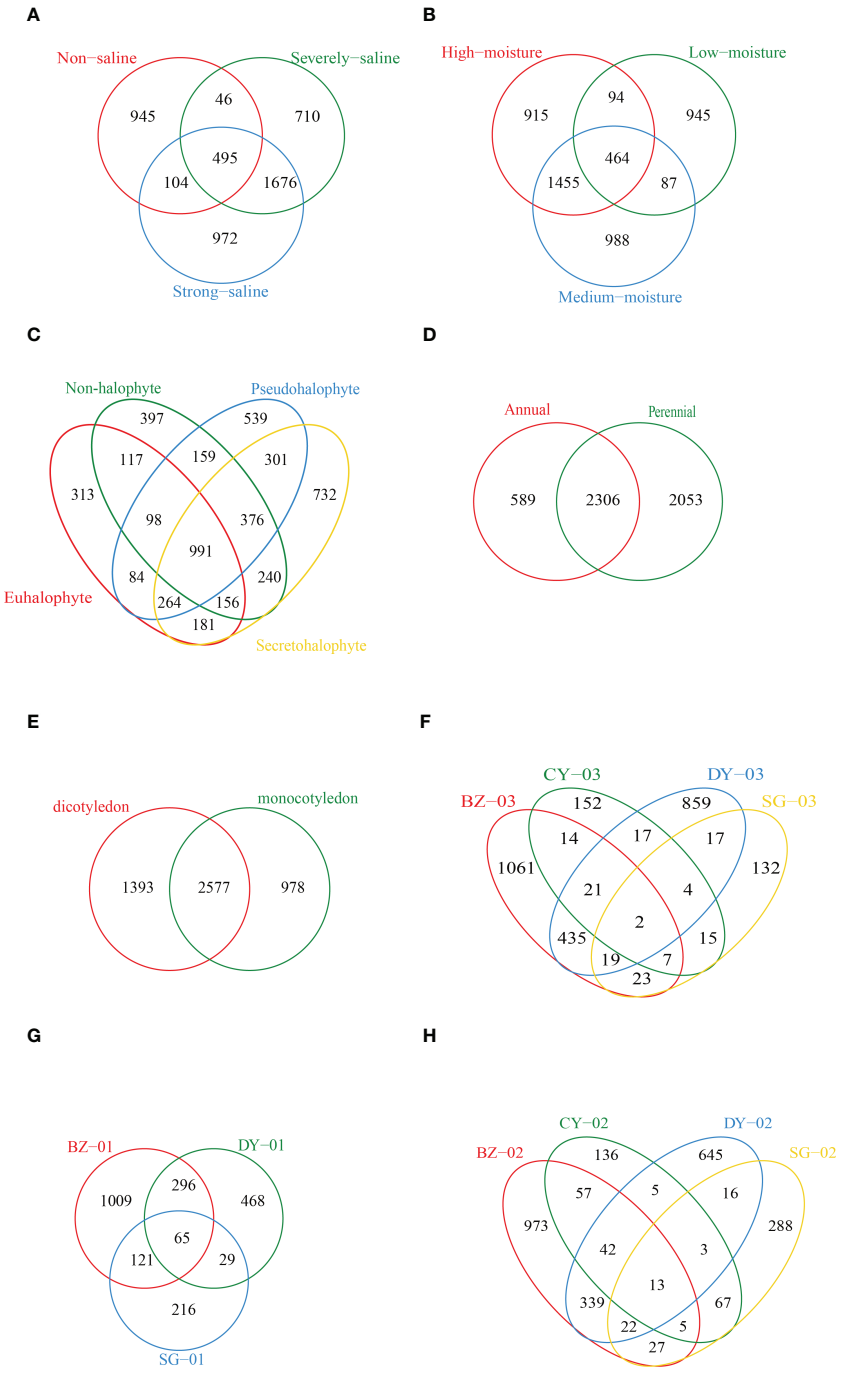

FIGURE 4
Venn diagrams showing the numbers of shared and unique diazotrophic OTUs among the soil samples. **(A)** Different salinity levels. **(B)** Different soil moistures. **(C)** Different plant types based on salt resistance. **(D)** Different plant types based on life span. **(E)** Different plant types based on cotyledon number. **(F-H)** Soil samples respectively collected from the rhizosphere of *Tamarix austromongolica Nakai*, *Suaeda salsa* and *Phragmites australis* grown at different sampling locations. CY02, CY03, SG01, SG02, SG03, DY01, DY02, DY03, BZ01, BZ02 and BZ03 represent the soil samples respectively collected from Changyi (CY), Shouguang (SG), Dongying (DY) and Binzhou (BZ).

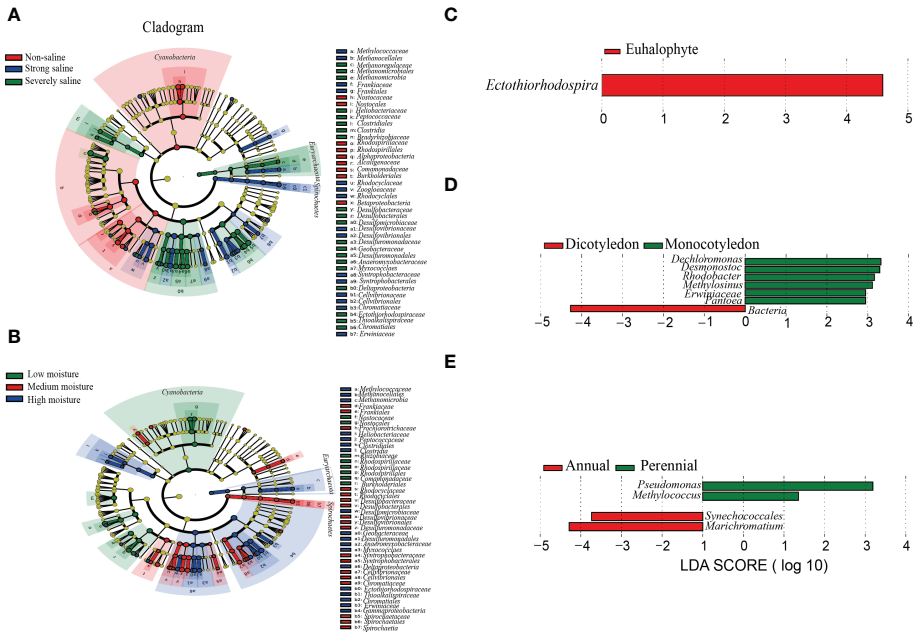

FIGURE 5
Phylogenetic dendrograms showing the biomarkers of diazotrophic microbes in the rhizospheric soil samples collected from Changyi (CY), Shouguang (SG), Dongying (DY) and Binzhou (BZ). **(A)** Different salinity levels. **(B)** Different soil moistures. **(C)** Different plant types based on salt resistance. **(D)** Different plant types based on cotyledon number. **(E)** Different plant types based on life span. The diazotrophic taxonomic levels from phylum to genus were exhibited with the circles from inside to outside. Diazotrophic abundance with no significant difference among individual soil samples was marked with yellow dots. The biomarkers were classified with different colors and shown on the right.

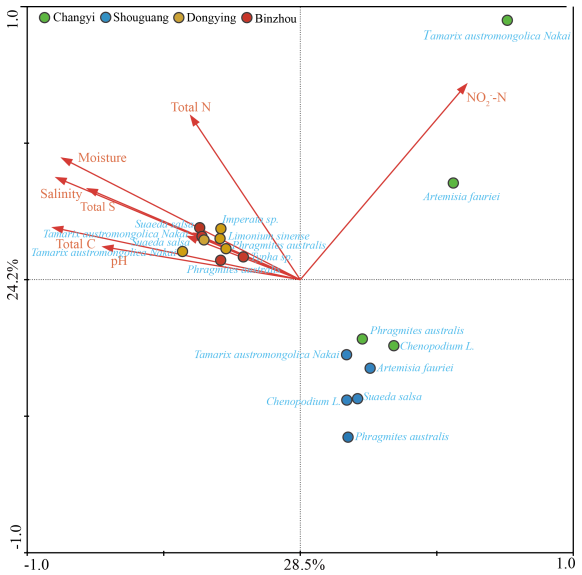

FIGURE 6
Canonical correspondence analysis (CCA) based on diazotrophic microbes and environmental parameters in different plant host habitats at Changyi (CY), Shouguang (SG), Dongying (DY) and Binzhou (BZ).

an influence of soil salinity and moisture on the abundance and community composition of diazotrophic microbes was observed (Table 2; Figure 3B). In coastal saline soils, the influence of soil salinity and moisture on diazotrophic community could be explained by several reasons (Herbert et al., 2015; Rolando et al., 2022). First, salinization increased NH_4^+ release through ion substitution, which subsequently inhibited N fixation, leading to decreased *nifH* copies under severely saline environment. Second, seawater infiltration increased soil SO_4^{2-} content, which affected the coupling of chemolithotrophic S oxidation with N fixation, a sulfate reduction process by diazotrophic microorganisms. Third, salinity changed the stability of microbial extracellular enzymes, and affected the mineralization and decomposition of macromolecular organic matter. And fourth, the increase of ionic strength reduced the adsorption of organic matters, and affected the availability of organic substrates for the growth of heterotrophs including diazotrophs.

In conclusion, using high throughput sequencing and quantitative real-time PCR targeting *nifH* genes, we investigated the diazotrophic abundance and community composition in the coastal saline soils of Laizhou Bay-Yellow River estuary. A strong correlation between diazotrophic abundance and soil physicochemical factors was observed. The physicochemical factors were significantly co-varied with the OTU based community composition of diazotrophs. Our findings demonstrate that in coastal saline soils, the community structure of diazotrophic microbes in the rhizosphere of plants grown in coastal saline soil is mainly affected by soil physicochemical factors but not by the host plant traits.

Data availability statement

The datasets presented in this study can be found at NCBI Sequence Read Archive, with accession number SRP411732.

Author contributions

YS, LM, HYZ, RF, XL, YS, ML and JuL conducted the experiments. YS, RF and JL analyzed data. YS, JC and HXZ wrote the manuscript. All authors contributed to the article and approved the submitted version.

Funding

This work has been jointly supported by the following grants: the National Key Research & Development Program of China (2021YFD1900903; 2019YFD1002703); the Natural Science Foundation of Shandong Province, China (ZR2020QC062; ZR2021QD157); the Science and Technology Demonstration Project of "Bohai Granary" of Shandong Province (2019BHLC002); the Science and Technology Innovation Project of Shandong Academy of Agricultural Sciences (CXGC2022F06; CXGC2022E19); the National Natural Science Foundation of China (41807083; 31870576, 32071733).

Conflict of interest

The authors declare that the research was conducted in the absence of any commercial or financial relationships that could be construed as a potential conflict of interest.

Publisher's note

All claims expressed in this article are solely those of the authors and do not necessarily represent those of their affiliated organizations, or those of the publisher, the editors and the reviewers. Any product that may be evaluated in this article, or claim that may be made by its manufacturer, is not guaranteed or endorsed by the publisher.

Supplementary material

The Supplementary Material for this article can be found online at: https://www.frontiersin.org/articles/10.3389/fmars.2022.1100289/full#supplementary-material

References

Affourtit, J., Zehr, J. P., and Paerl, H. W. (2001). Distribution of nitrogen-fixing microorganisms along the neuse river estuary, north Carolina. *Microb. Ecol.* 41, 114–123. doi: 10.1007/s002480000090

Anburaj, R., Nabeel, M. A., Sivakumar, T., and Kathiresan, K. (2012). The role of rhizobacteria in salinity effects on biochemical constituents of the halophyte sesuvium portulacastrum. *Russ. J. Plant Physl.* 59 (1), 115–119. doi: 10.1134/s1021443712010025

Bai, B., Liu, W. D., Qiu, X. Y., Zhang, J., Zhang, J. Y., and Bai, Y. (2022). The root microbiome: Community assembly and its contributions to plant fitness. *J. Integr. Plant Biol.* 64, 230–243. doi: 10.1111/jipb.13226

Barbieri, E., Ceccaroli, P., Saltarelli, R., Guidi, C., Potenza, L., Basaglia, M., et al. (2010). New evidence for nitrogen fixation within the Italian white truffle tuber magnatum. *Fungal Biol.* 114 (11-12), 936–942. doi: 10.1016/j.funbio.2010.09.001

Bhavya, P. S., Kumar, S., Gupta, G. V. M., Sudheesh, V., Sudharma, K. V., Varrier, D. S., et al. (2016). Nitrogen uptake dynamics in a tropical eutrophic estuary (Cochin, India) and adjacent coastal waters. *Estuaries Coasts* 39, 54–67. doi: 10.1007/s12237-015-9982-y

Cao, J., Lv, X. Y., Chen, L., Xing, J. J., and Lan, H. Y. (2015). Effects of salinity on the growth, physiology and relevant gene expression of an annual halophyte grown from heteromorphic seeds. *AoB Plants.* 7, plv112. doi: 10.1093/aobpla/plv112

Cao, J. J., Wang, H. R., Holden, N. M., Adamowski, J. F., Biswas, A., Zhang, X. F., et al. (2021). Soil properties and microbiome of annual and perennial cultivated grasslands on the qinghai–Tibetan plateau. *Land Degrad. Dev.* 32 (18), 5306–5321. doi: 10.1002/ldr.4110

Che, R. X., Deng, Y. C., Wang, F., Wang, W. J., Xu, Z. H., and Hao, Y. B. (2018). Autotrophic and symbiotic diazotrophs dominate nitrogen-fixing communities in Tibetan grassland soils. *Sci. Total Environ.* 639, 997–1006. doi: 10.1016/j.scitotenv.2018.05.238

Collavino, M. M., Tripp, H. J., Frank, I. E., Vidoz, M. L., Calderoli, P. A., Donato, M., et al. (2014). *nifH* pyrosequencing reveals the potential for location-specific soil chemistry to influence N_2-fixing community dynamics. *Environ. Microbiol.* 16 (10), 3211–3223. doi: 10.1111/1462-2920.12423

Dang, H., Yang, J., Li, J., Luan, X., Zhang, Y., Gu, G., et al. (2013). Environment-dependent distribution of the sediment *nifH*-harboring microbiota in the northern south China Sea. *Appl. Environ. Microbio.* 79 (1), 121–132. doi: 10.1128/AEM.01889-12

Davis, D. A., Gamble, M. D., Bagwell, C. E., Bergholz, P. W., and Lovell, C. R. (2011). Responses of salt marsh plant rhizosphere diazotroph assemblages to changes in marsh elevation, edaphic conditions and plant host species. *Microb. Ecol.* 61 (2), 386–398. doi: 10.2307/41489060

Debra, A. D., Megan, D. G., Christopher, E. B., Peter, W. B., and Charles, R. L. (2011). Responses of salt marsh plant rhizosphere diazotroph assemblages to changes in marsh elevation, edaphic conditions and plant host species. *Microb. Ecol.* 61 (2), 386–398. doi: 10.1007/s00248-010-9757-8

Di Salvo, L. P., Ferrando, L., Fernández-Scavino, A., García de, S., and Inés, E. (2018). Microorganisms reveal what plants do not: Wheat growth and rhizosphere microbial communities after *Azospirillum* brasilense inoculation and nitrogen fertilization under field conditions. *Plant Soil.* 424, 405–417. doi: 10.1007/s11104-017-3548-7

Dong, J. Y., Zhang, J. Q., Liu, Y. H., and Jing, H. C. (2022). How climate and soil properties affect the abundances of nitrogen-cycling genes in nitrogen-treated ecosystems: a meta-analysis. *Plant Soil* 477(1), 389–404. doi: 10.1007/s11104-022-05420-6

Gaby, J. C., and Buckley, D. H. (2012). A comprehensive evaluation of PCR primers to amplify the *nifH* gene of nitrogenase. *PLoS One* 7, e42149. doi: 10.1371/journal.pone.0042149

Galloway, J. N., Dentener, F. J., Capone, D. G., Boyer, E. W., Howarth, R. W., Seitzinger, S. P., et al. (2004). Nitrogen cycles: Past, present, and future. *Biogeochemistry* 70 (2), 153–226. doi: 10.2307/4151466

Gandy, E. L., and Yoch, D. C. (1988). Relationship between nitrogen-fixing sulfate reducers and fermenters in salt marsh sediments and roots of spartina alternifora. *Appl. Environ. Microb.* 54, 2031–2036. doi: 10.1002/bit.260320421

Garbeva, P., van Elsas, J. D., and van Veen, J. A. (2008). Rhizosphere microbial community and its response to plant species and soil history. *Plant Soil* 302, 19–32. doi: 10.2307/42951751

Gardner, W. H. (1986). "Water content," in *Methods of soil analysis. part i. physical and mineralogical methods*. Ed. A. Klute (Madison: American Society of Agronomy).

Guo, X. H., and Gong, J. (2014). Differential effects of abiotic factors and host plant traits on diversity and community composition of root-colonizing arbuscular mycorrhizal fungi in a salt-stressed ecosystem. *Mycorrhiza* 24, 79–94. doi: 10.1007/s00572-013-0516-9

Gupta, V. V. S. R., Roper, M. M., and Roget, D. K. (2006). Potential for non-symbiotic N_2-fixation in different agroecological zones of southern Australia. *Aust. J. Soil Res.* 44 (4), 343–354. doi: 10.1071/SR05122

Herbert, E. R., Boon, P., Burgin, A. J., Neubauer, S. C., Franklin, R. B., Ardon., M., et al. (2015). A global perspective on wetland salinization: Ecological consequences of a growing threat to freshwater wetlands. *Ecosphere* 6 (10), art206. doi: 10.1890/ES14-00534.1

Hou, L. J., Wang, R., Yin, G. Y., Liu, M., and Zheng, Y. L. (2018). Nitrogen fixation in the intertidal sediments of the Yangtze estuary: Occurrence and environmental implications. *J. Geophys. Res-Biogeo.* 123 (3), 936–944. doi: 10.1002/2018JG004418

Huang, F., Lin, X., Hu, W., Zeng, F., He, L., and Yin, K. (2021). Nitrogen cycling processes in sediments of the pearl river estuary: Spatial variations, controlling factors, and environmental implications. *Catena* 206, 105545. doi: 10.1016/j.catena.2021.105545

Huang, J., Xu, X., Wang, M., Nie, M., Qiu, S. Y., Quan, Z. X., et al. (2016). Responses of soil nitrogen fixation to *Spartina alterniflora* invasion and nitrogen addition in a Chinese salt marsh. *Sci. Rep.* 6, 20384. doi: 10.1038/srep20384

Imhoff, J. F., and Truper, H. G. (1997). *Ectothiorhodospira halochloris* sp. nov: a new extremely halophilic phototrophic bacterium containing bacteriochlorophyll. *Arch. Microbiol.* 114, 115–121. doi: 10.1007/bf00410772

Ininbergs, K., Bay, G., Rasmussen, U., Wardle, D. A., and Marie-Charlotte, W. (2011). Composition and diversity of *nifH* genes of nitrogen-fixing *Cyanobacteria* associated with Boreal forest feather mosses. *New Phytol.* 192, 507–517. doi: 10.1111/j.1469-8137.2011.03809.x

Jiang, Y. J., Li, S. Z., Li, R. P., Zhang, J., Liu, Y. H., Lv, L. F., et al. (2017). Plant cultivars imprint the rhizosphere bacterial community composition and association networks. *Soil Biol. Biochem.* 109, 145–155. doi: 10.1016/j.soilbio.2017.02.010

Jing, C. L., Xu, Z. X., Zou, P., Tang, Q., Li, Y. Q., You, X. W., et al. (2018). Coastal halophytes alter properties and microbial community structure of the saline soils in the yellow river delta, China. *Appl. Soil Ecol.* 134, 1–7. doi: 10.1016/j.apsoil.2018.10.009

Ladygina, N., and Hedlund, K. (2010). Plant species influence microbial diversity and carbon allocation in the rhizosphere. *Soil Biol. Biochem.* 42 (2), 162–168. doi: 10.1016/j.soilbio.2009.10.009

Laurent, P., Aymé, S., Catherine, H., David, B., Florian, B., Jones, C. M., et al. (2013). Loss in microbial diversity affects nitrogen cycling in soil. *ISME J.* 7 (8), 1609–1619. doi: 10.1038/ismej.2013.34

Levy-Booth, D. J., Prescott, C. E., and Grayston, S. J. (2014). Microbial functional genes involved in nitrogen fixation, nitrification and denitrification in forest ecosystems. *Soil Biol. Biochem.* 75, 11–25. doi: 10.1016/j.soilbio.2014.03.021

Li, J. Y., Chen, Q. F., Li, Q., Zhao, C. S., and Feng, Y. (2021). Influence of plants and environmental variables on the diversity of soil microbial communities in the yellow river delta wetland, China. *Chemosphere* 274, 129967. doi: 10.1016/j.chemosphere.2021.129967

Li, Y. Y., Chen, X. H., Xie, Z. X., Li, D. X., Wu, P. F., Kong, L. F., et al. (2018). Bacterial diversity and nitrogen utilization strategies in the upper layer of the northwestern pacific ocean. *Front. Microbiol.* 9. doi: 10.3389/fmicb.2018.00797

Lin, X. B., Hou, L. J., Liu, M., Li, X. F., Zheng, Y. L., Yin, G. Y., et al. (2016). Nitrogen mineralization and immobilization in sediments of the East China Sea: Spatiotemporal variations and environmental implications. *J. Geophys. Res-Biogeo.* 121, 2842–2855. doi: 10.1002/2016JG00349

Lin, X. B., Li, X. F., Gao, D. Z., Liu, M., and Lv, C. (2017). Ammonium production and removal in the sediments of shanghai river networks. *J. Geophys. Res-Biogeo* 122, 2461–2478. doi: 10.1002/2017JG003769

Lin, G. M., and Lin, X. B. (2022). Bait input altered microbial community structure and increased greenhouse gases production in coastal wetland sediment. *Water Res.* 30, 218. doi: 10.1016/j.watres.2022.118520

Lin, Y. X., Ye, G. X., Liu, D. Y., Ledgard, S., Luo, J. F., Fan, J. B., et al. (2018). Long-term application of lime or pig manure rather than plant residues suppressed diazotroph abundance and diversity and altered community structure in an acidic ultisol. *Soil Biol. Biochem.* 123, 218–228. doi: 10.1016/j.soilbio.2018.05.018

Liu, X. Y., Liu, C., Gao, W. H., Xue, C., Guo, Z. H., Jiang, L., et al. (2019). Impact of biochar amendment on the abundance and structure of diazotrophic community in an alkaline soil. *Sci. Total Environ.* 688, 944–951. doi: 10.1016/j.scitotenv.2019.06.293

Marasco, R., Mosqueira, M. J., Fusi, M., Ramond, J. B., Merlino, G., Booth, J. M., et al. (2018). Rhizosheath microbial community assembly of sympatric desert speargrasses is independent of the plant host. *Microbiome* 6 (1), 215. doi: 10.1186/s40168-018-0597-y

Mendelssohn, I. A., and Morris, J. T. (2000). "Eco-physiological controls on the productivity of spartina alternifora loisel," in *Concepts and controversies in tidal marsh ecology*. Eds. M. P. Weinstein and D. A. Kreeger (Kluwer Academic Publishers: Boston), 59–80.

Meng, H., Zhou, Z. C., Wu, R. N., Wang, Y. F., and Gu, J. D. (2019). Diazotrophic microbial community and abundance in acidic subtropical natural and re-vegetated forest soils revealed by high-throughput sequencing of *nifH* gene. *Appl. Microbiol. Biot.* 103, 995–1005. doi: 10.1007/s00253-018-9466-7

Midgley, G. F. (2012). Biodiversity and ecosystem function. *Science* 335 (6065), 174. doi: 10.1126/science.1217245

Moisander, P. H., Morrison, A. E., Ward, B. B., Jenkins, B. D., and Zehr, J. P. (2007). Spatial-temporal variability in diazotroph assemblages in Chesapeake bay using an oligonucleotide *nifH* microarray. *Environ. Microbial.* 9 (7), 1823–1835. doi: 10.1111/j.1462-2920.2007.01304.x

Morina, J. C., Morrissey, E. M., and Franklin, R. B. (2018). Vegetation effects on bacteria and denitrifier abundance in the soils of two tidal freshwater wetlands in Virginia. *Appl. Environ. Soil Sci.* 2018, 1–10. doi: 10.1155/2018/4727258

Mortazavi, B., Riggs, A. A., Caffrey, J. M., Genet, H., and Phipps, S. W. (2012). The contribution of benthic nutrient regeneration to primary production in a shallow eutrophic estuary, weeks bay, Alabama. *Estuaries Coasts* 35 (3), 862–877. doi: 10.1007/s12237-012-9478-y

Moseman-Valtierra, S. M., Johnson, R., Zhang, R., and Qian, P. Y. (2009). Differences in cordgrass structure between a mature and developing marsh reflect distinct N_2-fixing communities. *Wetlands* 29, 919–930. doi: 10.1672/08-222.1

Moseman, S. M., Zhang, R., Qian, P. Y., and Levin, L. A. (2009). Diversity and functional responses of nitrogen-fixing microbes to three wetland invasions. *Biol. Invasions.* 11, 225–239. doi: 10.1007/s10530-008-9227-0

Mulvaney, R. L. (1996). "Nitrogen: Inorganic forms," in *Methods of soil analysis*. Ed. D. L. Sparks (Madison, WI: SSSA Book Ser. 5. SSSA), 1123–1184.

Newell, S. E., McCarthy, M. J., Gardner, W. S., and Fulweiler, R. W. (2016). Sediment nitrogen fixation: a call for re-evaluating coastal N budgets. *Estuaries Coasts* 39, 1626–1638. doi: 10.1007/s12237-016-0116-y

Nielsen, L. B., Finster, K., Welsh, D. T., Donelly, A., Herbert, R. A., Wit, R., et al. (2001). Sulphate reduction and nitrogen fixation rates associated with roots, rhizomes and sediments from *Zostera noltii* and *Spartina maritima* meadows. *Environ. Microbiol.* 3 (1), 63–71. doi: 10.1046/j.1462-2920.2001.00160.x

Oliveira, J. T. C., Figueredo, E. F., Diniz, W. P., da, S., Oliveira, L. F. P., de, Andrade, P. A. M., et al. (2017). Diazotrophic bacterial community of degraded pastures. *Appl. Environ. Soil Sci.* 1, 1–10. doi: 10.1155/2017/2561428

Omuto, C. T., Vargas, R. R., El Mobarak, A. M., Mohamed, N., Viatkin, K., and Yigini, Y. (2020). *Mapping of salt-affected soils: Lesson 3-spatial modelling of soil indicators (Properties) related salt problems* (Rome: FAO).

Ospina-Betancourth, C., Acharya, K., Allen, B. D., Entwistle, J., Head, I. M., Sanabria, J., et al. (2020). Enrichment of nitrogen fixing bacteria in a nitrogen deficient wastewater treatment system. *Environ. Sci. Technol.* 54, 3539–3548. doi: 10.1021/acs.est.9b05322

Pereira, E., Silva, M. C., Schloter-Hai, B., Schloter, M., van Elsas, J. D., and Salles, J. F. (2013). Temporal dynamics of abundance and composition of nitrogen fixing communities across agricultural soils. *PloS One* 8, e74500. doi: 10.1371/journal.pone.0074500

Petersen, J. M., Kemper, A., Gruber-Vodicka, H., Cardini, U., van der Geest, M., Kleiner, M., et al. (2016). Chemosynthetic symbionts of marine invertebrate animals are capable of nitrogen fixation. *Nat. Microbiol.* 2, 16195. doi: 10.1038/nmicrobiol.2016.195

Piromyou, P., Greetatorn, T., Teamtisong, K., Okubo, T., Shinoda, R., Nuntakij, A., et al. (2015). Preferential association of endophytic *Bradyrhizobia* with different rice cultivars and its implications for rice endophyte evolution. *Appl. Environ. Microbiol.* 81 (9), 3049–3061. doi: 10.1128/AEM.04253-14

Poly, F., Monrozier, L. J., and Bally, R. (2001). Improvement in the RFLP procedure for studying the diversity of *nifH* genes in communities of nitrogen fixers in soil. *Res. Microbiol.* 152, 95–103. doi: 10.1016/S0923-2508(00)01172-4

Qiu, L. P., Kong, W. B., Zhu, H. S., Zhang, Q., Banerjee, S., Ishii, S., et al. (2022). Halophytes increase rhizosphere microbial diversity, network complexity and function in inland saline ecosystem. *Sci. Total Environ.* 831, 154944. doi: 10.1016/j.scitotenv.2022.154944

Ravit, B., Ehrenfeld, J. G., Häggblom, M. M., and Bartels, M. (2007). The effects of drainage and nitrogen enrichment on *Phragmites australis*, *Spartina alterniflora*, and their root-associated microbial communities. *Wetlands* 27, 915–927. doi: 10.1672/0277-5212(2007)27[915:TEODAN]2.0.CO;2

Rejmánková, E., Sirová, D., Castle, S. T., Bárta, J., Carpenter, H., and Bradley, R. (2018). Heterotrophic N_2-fixation contributes to nitrogen economy of a common wetland sedge, schoenoplectus californicus. *PloS One* 13 (4), e0195570. doi: 10.1371/journal.pone.0195570

Richards, L. A. (1954). *Diagnosis and improvement of saline and alkali soil, U.S* (Washington D. C: Salinity Lab. Staff, USDA HandBook 60).

Rigonato, J., Kent, A. D., Alvarenga, D. O., Andreote, F. D., and Fiore, M. F. (2013). Drivers of cyanobacterial diversity and community composition in mangrove soils in south-east Brazil. *Environ. Microbiol.* 15 (4), 1103–1114. doi: 10.1111/j.1462-2920.2012.02830.x

Rodrigo, C., Monika, G., Nicole, M., Jana, L., Gabriele, B., and Kornelia, S. (2006). Effects of site and plant species on rhizosphere community structure as revealed by molecular analysis of MicrobialGuilds. *FEMS Microbiol. Ecol.* 56 (2), 236–249. doi: 10.1111/j.1574–6941.2005.00026.x

Rolando, J. L., Kolton, M., Song, T., and Kostka, J. E. (2022). The core root microbiome of spartina alterniflora is predominated by sulfur-oxidizing and sulfate-reducing bacteria in Georgia salt marshes, USA. *Microbiome* 10, 37. doi: 10.1101/2021.07.06.451362

Shiozaki, T., Nagata, T., Ijichi, M., and Furuya, K. (2015). Nitrogen fixation and the diazotroph community in the temperate coastal region of the northwestern north pacific. *Biogeosciences* 12 (15), 4751–4764. doi: 10.5194/bg-12-4751-2015

Steenhoudt, O., and Vanderleyden, J. (2000). *Azospirillum*, a free-living nitrogen-fixing bacterium closely associated with grasses: Genetic, biochemical and ecological aspects. *FEMS Microbiol. Rev.* 24 (4), 487–506. doi: 10.1016/s0168-6445(00)00036-x

Thajudeen, ,. J., Yousuf, J., Veetil, V. P., Varghese, S., Singh, A., and Abdulla, M. H. (2017). Nitrogen fixing bacterial diversity in a tropical estuarine sediments. *World J. Microb. Biot.* 33 (2), 41. doi: 10.1007/s11274-017-2205-x

Tkacz, A., Cheema, J., Go, C., Grant, A., and Poole, P. S. (2015). Stability and succession of the rhizosphere microbiota depends upon plant type and soil composition. *ISME J.* 9(11), 2349–2359. doi: 10.1038/ismej.2015.41

Tourova, T. P., Slobodova, N. V., Bumazhkin, B. K., Sukhacheva, M. V., and Sorokin, D. (2014). Diversity of diazotrophs in the sediments of saline and soda lakes analyzed with the use of the *nifH* gene as a molecular marker. *Microbiology* 83 (5), 634–647. doi: 10.1134/S002626171404016X

Trüper, H. G., and Imhoff, J. F. (1981). "The genus ectothiorhodospira," in *The prokaryotes*. Eds. M. P. Starr, H. Stolp, H. G. Trüper, A. Balows and H. G. Schlegel (Berlin, Heidelberg: Springer). doi: 10.1007/978-3-662-13187-915

Vejan, P., Abdullah, R., Khadiran, T., Ismail, S., and Nasrulhaq Boyce, A. (2016). Role of plant growth promoting rhizobacteria in agricultural sustainability–a review. *Molecules* 21 (5), 573–590. doi: 10.3390/molecules21050573

Wang, J., Bao, J. T., Li, X. R., and Liu, Y. B. (2016). Molecular ecology of *nifH* genes and transcripts along a chronosequence in revegetated areas of the tengger desert. *Microb. Ecol.* 71 (1), 150–163. doi: 10.1007/s00248-015-0657-9

Wang, H. H., Li, X., Li, X. Y., Li, F. L., Su, Z. C., and Zhang, H. W. (2021). Community composition and Co-occurrence patterns of diazotrophs along a soil profile in paddy fields of three soil types in China. *Microb. Ecol.* 82, 961–970. doi: 10.1007/s00248-021-01716-9

Wang, X. G., Sun, R. B., Tian, Y. P., Guo, K., Sun, H. Y., Liu, X. J., et al. (2020). Long-term phytoremediation of coastal saline soil reveals plant species-specific patterns of microbial community recruitment. *mSystems* 5 (2), e00741–19. doi: 10.1128/msystems.00741-19

Wang, Z. Y., Xin, Y. Z., Gao, D. M., Li, F. M., Morgan, J., and Xing, B. S. (2010). Microbial community characteristics in a degraded wetland of the yellow river delta. *Pedosphere* 20 (4), 466–478. doi: 10.1016/s1002-0160(10)60036-7

Wang, L. P., Zheng, B. H., and Lei, K. (2015). Diversity and distribution of bacterial community in the coastal sediments of bohai bay, China. *Acta Oceanol. Sin.* 34 (10), 122–131. doi: 10.1007/s13131-015-0719-3

Wang, C., Zheng, M., Song, W. F., Wen, S. L., Wang, B., Zhu, C. Q., et al. (2017). Impact of 25 years of inorganic fertilization on diazotrophic abundance and community structure in an acidic soil in southern China. *Soil Biol. Biochem.* 113, 240–249. doi: 10.1016/j.soilbio.2017.06.019

Whiting, G. J., Gandy, E. L., and Yoch, D. C. (1986). Tight coupling of root-associated nitrogen fixation and plant photosynthesis in the salt marsh grass spartina alterniflora and carbon dioxide enhancement of nitrogenase activity. *Appl. Environ. Microbiol.* 52 (1), 108–113. doi: 10.1021/ie0002226

Xian, X. X., Pang, M. Y., Zhang, J. L., Zhu, M. K., Kong, F. L., and Xi, M. (2019). Assessing the effect of potential water and salt intrusion on coastal wetland soil quality: Simulation study. *J. Soils Sediments.* 19, 2251–2264. doi: 10.1016/j.apsoil.2011.10.021

Xu, C. W., Yang, M. Z., Chen, Y. J., Chen, L. M., Zhang, D. Z., Liang, M., et al. (2012). Changes in non-symbiotic nitrogen-fixing bacteria inhabiting rhizosphere soils of an invasive plant ageratina adenophora. *Appl. Soil Ecol.* 54, 32–38. doi:10.1016/j.apsoil.2011.10.021

Yousuf, B., Kumar, R., Mishra, A., and Jha, B. (2014). Differential distribution and abundance of diazotrophic bacterial communities across different soil niches using a gene-targeted clone library approach. *FEMS Microbiol. Lett.* 360 (2), 117–125. doi: 10.1111/1574-6968.12593

Zak, D. R., Holmes, W. E., White, D. C., Peacock, A. D., and Tilman, D. (2003). Plant diversity, soil microbial communities, and ecosystem function: Are there any links? *Ecology* 84 (8), 2042–2050. doi: 10.2307/3450029

Zhang, M. J., Chai, L. W., Huang, M., Jia, W. Q., Guo, J. B., and Huang, Y. (2020). Deciphering the archaeal communities in tree rhizosphere of the qinghai-Tibetan plateau. *BMC Microbiol.* 20 (1), 235–248. doi: 10.1186/s12866-020-01913-5

Zhang, X. L., Gu, D. Q., Feng, A. P., and Xia, D. X. (2006). Comparative research on characters and evolvement of vegetation of coastal wetlands of yellow river delta and southern laizhou bay. *Bull. Soil Water Conserv.* 26, 127–140. doi: 10.1016/S1872-2032(06)60050-4

Zhang, X., Hu, W., Jin, X. T., Chen, T., and Niu, Y. H. (2021). Diversity of soil nitrogen-fixing bacteria in the rhizosphere and non-rhizophere soils of ebinur lake wetland. *Arch. Microbiol.* 22–30), 1–14. doi: 10.1007/s00203-021-02363-x

Zhivotchenko, A. G., Nikonova, E. S., and Jørgensen, M. H. (1995). Effect of fermentation conditions on N_2 fixation by methylococcus capsulatus. *Microb. Ecol.* 14 (1), 9–15. doi: 10.1007/bf00369847

Zhou, L. T., Li, J. J., Pokhrel, G. R., Chen, J., Zhao, Y. L., Bai, Y., et al. (2021). *nifH* gene sequencing reveals the effects of successive monoculture on the soil diazotrophic microbial community in casuarina equisetifolia plantations. *Front. Plant Sci.* 11. doi: 10.3389/fpls.2020.578812

frontiers | Frontiers in Marine Science

TYPE Original Research
PUBLISHED 22 December 2022
DOI 10.3389/fmars.2022.1098508

OPEN ACCESS

EDITED BY
Jing Wei,
Sun Yat-sen University, China

REVIEWED BY
Yu Wang,
Guangzhou University, China
Jiapeng Wu,
Guangzhou University, China

*CORRESPONDENCE
Xuefeng Peng
xpeng@seoe.sc.edu

SPECIALTY SECTION
This article was submitted to Marine Biogeochemistry, a section of the journal Frontiers in Marine Science

RECEIVED 15 November 2022
ACCEPTED 05 December 2022
PUBLISHED 22 December 2022

CITATION
Lazo-Murphy BM, Larson S, Staines S, Bruck H, McHenry J, Bourbonnais A and Peng X (2022) Nitrous oxide production and isotopomer composition by fungi isolated from salt marsh sediments. *Front. Mar. Sci.* 9:1098508. doi: 10.3389/fmars.2022.1098508

Nitrous oxide production and isotopomer composition by fungi isolated from salt marsh sediments

Birch Maxwell Lazo-Murphy, Samantha Larson, Sydney Staines, Heather Bruck, Julianne McHenry, Annie Bourbonnais and Xuefeng Peng*

School of Earth, Ocean, and Environment, University of South Carolina, Columbia, SC, United States

The emissions of nitrous oxide (N_2O), a potent greenhouse gas and ozone-depleting agent, have been steadily increasing from coastal environments, such as salt marsh sediments, as a result of anthropogenic nutrient loading. Biotic processes, including nitrification and denitrification, are the largest sources of N_2O from salt marsh sediments. While it is assumed that the bulk of N_2O from salt marsh sediment is produced by nitrification and bacterial denitrification, recent reports suggest fungal denitrification may contribute significantly. In this study, four fungi capable of growth under sulfidic conditions were isolated from salt marsh sediments in North Inlet, South Carolina, USA. Fungal species included *Purpureocillium lilacinum, Trichoderma harzianum, Trichoderma virens*, and *Rhodotorula glutinis*, as determined by sequencing the18S and 28S rRNA genes. The isotopomer signatures of N_2O produced by these fungi were measured using isotope ratio mass spectrometry, which can be used to estimate the contribution of different sources of N_2O. Up to 22.8% of nitrite provided in growth media was converted to N_2O by fungal strains isolated from salt marsh sediments. The site preference (SP) of N_2O produced by salt marsh sediment fungi ranged from 7.5 $\pm$ 1.6‰ to 33.4 $\pm$ 1.2‰. These values are lower than the SP of N_2O from the model fungal denitrifier *Fusarium oxysporum* (37.1 $\pm$ 2.5‰), which is the SP typically used as an endmember in isotope mass balance considerations. The N_2O SP values we measured expand the range of N_2O SP used for isotope mass balances calculations to determine the relative contribution of fungi to N_2O production in salt marsh sediments.

KEYWORDS

nitrous oxide, fungi, stable isotop, site preference (SP), sulfidic, salt marsh, sediment, isotopomer

1 Introduction

Salt marshes represent one of the largest carbon sinks on Earth and effectively filter out excess nutrients, organic matter, and pollutants which would otherwise enter the ocean and potentially lead to coastal eutrophication, harmful algal blooms, and oxygen depletion (Vernberg, 1993; Teal and Howes, 2000; Burden et al., 2013). High amounts of primary production lead to the depletion of oxygen by aerobic respiration, allowing diverse anaerobic metabolisms to aid in the removal of nutrients, such as nitrate through denitrification (Kaplan et al., 1979; Kostka et al., 2002; Mcowen et al., 2017; Wu et al., 2021). Denitrification has been shown to impact water, sedimentary, and atmospheric chemistry by removing nitrate (NO_3^-) and producing nitrous oxide (N_2O) and N_2-gas (Philippot et al., 2013; Lecomte et al., 2018; Zheng et al., 2018). The recent increases in N_2O emissions from coastal environments is primarily due to the increases in anthropogenic N in riverine discharge (Murray et al., 2015; Martin et al., 2018; Al-Haj and Fulweiler, 2020; Tian et al., 2020). N_2O is of concern as it is a greenhouse gas with a warming potential 296 times higher than carbon dioxide (CO_2) and is an ozone-depleting agent (IPCC, 2014). Understanding N_2O sources in salt marshes and how the sources may change with climate change is, therefore, crucial. Multiple studies have indicated that anaerobic biogeochemical processes mediated by fungi are understudied in marine environments. This study focuses on marine fungal denitrifiers, which have been hypothesized to significantly contribute to salt marsh N_2O production (Gadd, 2006; Grossart et al., 2016; Wankel et al., 2017; Amend et al., 2019; Gutiérrez et al., 2020; Aldossari and Ishii, 2021).

Denitrification is a stepwise reaction where NO_3^- is reduced to nitrite (NO_2^-), nitric oxide (NO), N_2O, and dinitrogen gas (N_2) through a series of enzymatic reactions encoded by the following genes: respiratory nitrate reductase/periplasmic nitrate reductase (*narG/napA*), copper/iron containing nitrite reductase (*nirK/nirS*), nitric oxide reductase (*nor* in bacteria/*p450nor* in fungi), and nitrous oxide reductase (*nosZ*) (Nakahara et al., 1993; Zumft, 1997). Fungi differ from bacteria and archaea in that they lack *nosZ* (Shoun et al., 1992; Hayatsu et al., 2008). Fungal N_2O is thereby released into the environment where it can be consumed by N_2O-reducing bacteria or emitted to the atmosphere (Higgins et al., 2018).

$$NO_3^- \overset{narG/napA}{\rightarrow} NO_2^- \overset{nirK}{\rightarrow} NO \overset{p450nor}{\rightarrow} N_2O \; X \; N_2 \qquad \text{Eqn. 1)}$$

Since the turn of the century, terrestrial studies regarding N_2O emissions have shown that fungi, rather than bacteria, are a dominant source of soil N_2O production and account for up to 80% of released N_2O (Laughlin and Stevens, 2002; Ma et al., 2008). While bacterial and archaeal processes are considered the dominant source of N_2O from salt marshes, recent studies suggest fungal denitrification may contribute a greater share of N_2O emissions in coastal sediments than initially thought, similar to terrestrial counterparts (Wankel et al., 2017; Aldossari and Ishii, 2021). Recent advancements in sequencing technology and cultivation efforts have been instrumental in uncovering the estimated 10,000 species of undiscovered marine fungi, many of which may be capable of denitrification, a widespread trait amongst fungi (Jones, 2011; Maeda et al., 2015; Amend et al., 2019). Furthermore, recent studies have shown that the relative abundance of fungal denitrifiers is positively correlated with nutrient loading and is a significant N_2O source in estuaries (Kearns et al., 2019; Kim et al., 2020; Gao et al., 2022). The lack of fungal denitrifiers in recovering salt marshes has also been shown to limit bioavailable nitrogen (NO_3^-) removal, thus demonstrating the role denitrifying fungi play in salt marsh sediment biogeochemistry (Starr et al., 2022). These studies provide a basis to rethink salt marsh N_2O dynamics and study salt marsh fungi to determine the significance of fungi in acting as an N_2O source.

Isotopic approaches can be used to distinguish fungal N_2O production from other sources (Sutka et al., 2008; Rohe et al., 2014; Rohe et al., 2017; Wankel et al., 2017). N_2O is an asymmetric molecule where the centrally positioned alpha nitrogen (N^{α}) atom is bonded to the beta positioned nitrogen (N^{β}) and oxygen. Differences in isotopic fractionation between fungi, bacteria, and archaea produce changes in the positioning of light and heavy nitrogen atoms (^{14}N, ^{15}N) in the N_2O molecule (Sutka et al., 2006; Maeda et al., 2015). The intramolecular distribution of ^{15}N is defined by site preference (SP).

$$SP = \delta^{15}N^{\alpha} - \delta^{15}N^{\beta} \qquad \text{Eqn. 2)}$$

N_2O SP is independent of both the initial isotopic composition of the substrate and changes with subsequent consumption (Toyoda et al., 2002; Sutka et al., 2006). Therefore, N_2O SP is thought to be only process-dependent and has been used as a tracer to identify the source of N_2O in terrestrial and marine environments (Butterbach-Bahl et al., 2013; Bourbonnais et al., 2017; Casciotti et al., 2018; Kelly et al., 2021). Fungal N_2O SP measured for the model denitrifying fungi *Fusarium oxysporum* (37.1 ± 2.5‰) has been used by multiple studies to estimate the contribution of fungi to N_2O production from soil and coastal sediments (Rohe et al., 2014; Wankel et al., 2017; Rohe et al., 2021; Su et al., 2021). However, studies have indicated that *F. oxysporum* is not a well-represented species in fungal communities where *Spartina* dominates, which is a common feature of salt marshes in Europe, the United States, and China (though invasive), questioning the use of this endmember in isotope mass balances in these environments (Parrondo et al., 1978; Newell et al., 1996; Buchan et al., 2002; Buchan et al., 2003; Torzilli et al., 2006; Ge et al., 2016). Furthermore, the N_2O SP of soil-isolated *F. oxysporum* may not be representative of salt marsh fungi, as saline environments are known to cause physiological responses

in fungi, with some studies suggesting fungal denitrification may be enhanced with at higher salinities (Thiem et al., 2018; Yu et al., 2019; Pérez-Llano et al., 2020; Aldossari and Ishii, 2021; Calabon et al., 2021; Jones et al., 2022). N_2O SP from salt marsh sediment fungi would therefore be more representative of fungi isolated from saline environments. A recent metabarcoding survey showed that fungi from the families *Teratosphearíaceae*, *Mycosphaerellaceae*, *Physalacriaceae*, and *Lasiosphaeriaceae* and from the orders Capnodiales and Rhytismatales dominated sediment mycobiomes in a New England salt marsh (Kearns et al., 2019). The same study found that the relative abundance of putative denitrifying fungi from the orders Sordariales and Hypocreales were the highest (Kearns et al., 2019). In this study, we isolated four N_2O-producing fungal strains from salt marsh sediments and measured their N_2O yield and SP.

2 Materials and methods

The first part of this study is designed to isolate N_2O-producing fungi from salt marsh sediments. Published studies on fungal N_2O production obtained their isolates either from a culture collection (e.g. Maeda et al., 2015) or from the environment using aerobic media (e.g. Jirout, 2015). To the best of our knowledge, we made the first attempt using anaerobic enrichment cultures to isolate fungi from salt marsh sediments, which typically become anoxic below just a few millimeters depth. Given previous reports on the presence of fungi in anoxic parts of salt marsh sediments (e.g. Kearns et al., 2019), we expect the use of anaerobic media will select for fungal lineages well adapted to anoxia. Previous studies on N_2O-producing fungi all used complex media including undefined components such as potato infusion and peptone. To select for fungi adapted to low nutrient supply, a defined mineral media recipe (detailed below) was included in our isolation efforts.

2.1 Aerobic media

Aerobic media were prepared with an artificial seawater base containing 20 g L^{-1} sodium chloride (Fisher Scientific), 3 g L^{-1} magnesium chloride hexahydrate (Fisher Scientific), 0.15 g L^{-1} calcium chloride (Fisher Scientific), 0.5 g L^{-1} potassium chloride (Fisher Scientific) in ultrapure water produced by Milli-Q® EQ 7000 Ultrapure Water Purification System (MilliporeSigma, Merck KGaA, Darmstadt, Germany). Mineral media included 10 mM 3-(N-Morpholino)-Propanesulfonic Acid (MOPS) buffer (pH = 7.2, from 1 M stock solution (209.26 g L^{-1} MOPS free acid from EMP Millipore Corp., 100 mL L^{-1} 5 M sodium hydroxide from Spectrum Chemical Mfg Corp.), 2 mM ammonium chloride (Fisher Scientific), 0.2 mM sodium sulfate (J.T. Baker), 0.146 mM dipotassium phosphate (J.T. Baker), and 0.0588 mM monopotassium phosphate (J.T. Baker), and supplemented with trace elements. The final concentration of trace elements included: 20 µM hydrochloric acid (VWR Chemicals), 7.5 µM ferrous ammonium sulfate (Fisher Scientific), 0.48 µM boric acid (Sigma Chemical Co.), 0.5 µM manganese chloride (Fisher Scientific), 6.8 µM cobalt sulfate (Sigma Chemical Co.), 1.0 µM nickel chloride (Acros Organics), 12 nM copper chloride (Acros Organics), 0.5 µM zinc sulfate (Sigma Chemical Co.), 0.15 µM sodium molybdate (Acros Organics), 25 nM metavanadate (Acros Organics), 9 µM sodium tungstate (Acros Organics), 23 nM sodium selenite (Sigma Chemical Co.). *Spartina Alterniflora* stems, collected from North Inlet salt marshes, were cleaned and chopped to about 3 mm in size, and included as a carbon substrate in vials (1% w v^{-1}). Complex media were prepared with the same recipe and two additional components, namely 2.5 g L^{-1} of yeast extract (Fluka BioChemika) and 2.5 g L^{-1} of peptone (Fluka BioChemika). Solid media were prepared by including 2% (w v^{-1}) agar (Thermo Scientific). After autoclave sterilization and cooling (20 minutes at 121°C), a mixture of penicillin-G sodium (Alfa Aesar) and streptomycin sulfate (Acros Organics) was added to reach a final concentration of 0.2 g L^{-1} to minimize bacterial growth.

2.2 Anaerobic media

The composition of anaerobic media used to isolate and maintain fungal cultures was identical to aerobic media with the following exceptions. Resazurin, 1 µg L^{-1}, (Acros Organics) was added as a redox indicator; 0.1 mM of sodium sulfide (Acros Organics) and 1 g L^{-1} of L-cysteine (Acros Organics) were included as reducing reagents. Liquid media were purged with ultra-high purity N_2 (Airgas) for 20 to 30 minutes, and 20-ml were dispensed into N_2-flushed 65-ml serum vials sealed with butyl rubber septa and aluminum crimps. After autoclave sterilization, each vial of anaerobic media was supplemented with a mixture of 0.2 g L^{-1} of penicillin-G sodium (Alfa Aesar), 0.2 g L^{-1}streptomycin sulfate (Acros Organics), and 10 µM sodium nitrite (Fisher Chemicals). For isotopic analysis (described below), the anaerobic media were amended with 100 µM NO_2^-. Anaerobic roll tubes for colony picking were prepared as described previously (Peng et al., 2018).

2.3 Isolation and maintenance of N_2O-producing fungal strains

Triplicate 30-cm sediment cores were taken from two sites, Clambank and Oyster Landing, at the North Inlet-Winyah Bay National Estuarine Research Reserve in Georgetown, South Carolina (33.35°N, 79.20°W) on June 17th, 2021 (Figure 1). The North Inlet salt marsh is dominated by *Spartina alterniflora* (Allen et al., 2014). The cores were put on ice during transportation from Georgetown to Columbia, South

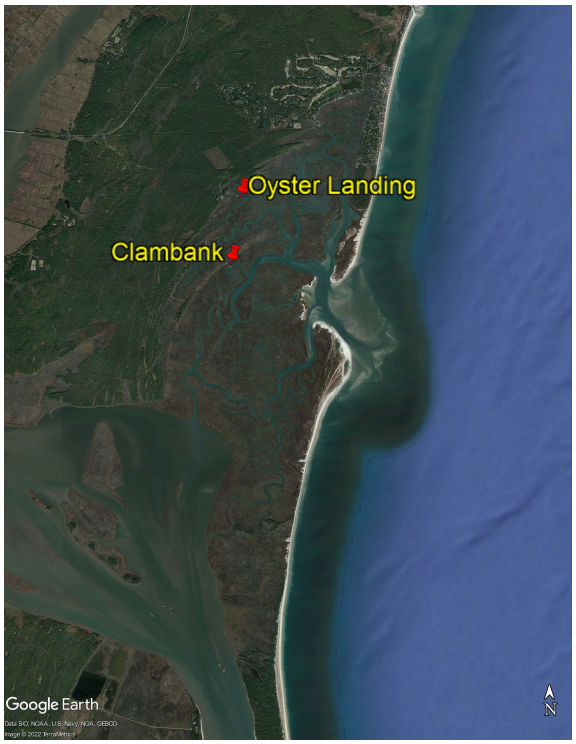

FIGURE 1
Samling locations (marked by pins) for salt marsh sediments at the North Inlet-Winyah Bay National Estuarine Research Reserve (33.35°N, 79.20°W). The image is produced using Google Earth Pro with data from SIO, NOAA, U.S. Navy, NGA, and GEBCO satellites.

Carolina, where initial enrichment culture inoculation occurred on the same day.

As marine fungi are typically hard to isolate (Edwards et al., 2017; Amend et al., 2019), we used the common plate dilution technique (Warcup, 1950) to isolate N_2O-producing fungi that are facultative anaerobes. Sediments from 1 cm and 10 cm depths were diluted in aerobic media and were used to streak agar plates. After three rounds of colony picking, isolated fungal cultures were inoculated into anaerobic media and screened for the ability to grow under sulfidic conditions and produce N_2O. Two fungal strains isolated using complex media and one fungal strain isolated using mineral media demonstrated high potential for N_2O production.

Anaerobic enrichment cultures of salt marsh sediment fungi were established in an Aldrich® AtmosBag (SKU Z555525) pre-flushed three times with ultra-high purity nitrogen (N_2). Approximately 0.1 g of sediment was placed into the serum vials containing anaerobic media using aseptic techniques. All enrichment cultures were screened for N_2O production in the headspace using a gas chromatograph (described below) equipped with an electron capture detector (ECD). N_2O-producing enrichment cultures were selected for fungal isolation using the anaerobic roll tube technique (Peng et al., 2018). One N_2O-producing fungal strain was isolated from anaerobic enrichment cultures. This was the first known case of anaerobic marine fungi isolated under sulfidic conditions.

Isolated fungal cultures were maintained in anaerobic batch cultures, which were transferred to fresh media every 7-10 days. When inoculating fresh media, 0.2 mL of media containing fungal cells were drawn from the inoculum culture using techniques that avoided oxygen contamination. For yeasts, the batch culture serving as the inoculum was thoroughly homogenized before inoculation. For filamentous fungi, we performed careful visual inspection to include similar amounts of filamentous fungi in each 0.2-ml inoculum to ensure replicate cultures had similar amount of initial biomass.

2.4 DNA extraction and rRNA gene sequencing

Fungal cells were harvested by centrifugation and DNA were extracted using the DNeasy Plant Pro kit (QIAGEN). The quantity and quality of the DNA were measured using a Nanodrop 2000C spectrophotometer (ThermoFisher Scientific).

The small (SSU) and large (LSU) subunits of the rRNA genes were amplified using the primers Fun18S1 (5'-CCATG CATGTCTAAGTWTAA-3') (Lord et al., 2002) and FR1 (5'-ANCCATTCAATCGGTANT-3') (Vainio and Hantula, 2000) targeting the V1 to V8 regions of the SSU rRNA gene and LR0R (5'-ACCCGCTGAACTTAAGC-3') and LR5 targeting the D1 to D3 regions of the LSU rRNA gene (Tedersoo et al., 2015). The PCR reactions were performed using Phusion® high-fidelity DNA polymerase (New England BioLabs, M0530, Ipswich, MA). The thermal cycle started with 30 seconds at 98°C, followed by 30 cycles of 10 seconds at 98°C, 30 seconds at 60° C, and 30 seconds at 72°C. The final elongation at 72°C was 5 minutes long. The PCR products were gel purified using Zymo DNA Clean & Concentrator -5 following the manufacturer's protocol and sent to Etonbio (Research Triangle Park, North Carolina, USA) for Sanger sequencing.

SSU and LSU sequences were searched against the NCBI nt database using the web portal for blastn (Johnson et al., 2008). Sequences for phylogenetic analysis were retrieved from the NCBI GenBank. Sequences were aligned using MUSCLE and manually trimmed using MEGA version 11 (Edgar, 2004; Tamura et al., 2021). Maximum-likelihood trees were constructed using FastTree 2.1 with default settings (1,000 bootstrap replicates, Jukes-Cantor model) (Price et al., 2010). The tree was then imported to Interactive Tree of Life (iTOL v6.6) for visualization (Letunic and Bork, 2019).

2.5 Measurements of headspace gas composition

SRI Greenhouse Gas Monitoring Gas Chromatograph, model 8610-0040, equipped with an ECD and a flame ionized detector (FID) was used to measure N_2O and CO_2 headspace gas production. Prior to gas extraction, 5 mL of ultra-high purity N_2 gas was added to vials with a gas-tight syringe and a sterilized needle to avoid air contamination. A gas-tight syringe and a sterilized needle was used to extract 5 mL of headspace gas, which was manually injected into the sampling port on the instrument. Ultra-high purity N_2 gas was used as the carrier gas, maintained at 30 psi. The column oven temperature was set at 90 °C. The ECD and FID, coupled to a methanizer for CO_2, measurements, were set at 300 °C. N_2O standard curves were constructed using 5 ppm, 10 ppm, and 100 ppm N_2O (GASCO, Cal Gas Direct Incorporated, Huntington Beach, California, USA). CO_2 standard curves were constructed using 1%, 5%, and 10% CO_2 calibration standards from GASCO. Multiple reference samples served as controls, including uninoculated media and N_2O producing fungal cultures terminated with concentrated sodium hydroxide and purged with N_2.

2.6 N_2O isotopic analysis

Analysis of N_2O stable isotopes and isotopomers were made using an Elementar Americas Inc. isoprime precisION continuous flow, multicollector, isotope-ratio mass spectrometer (CF-MC-IRMS) equipped with a custom purge-and-trap and gas extraction systems, as described in Charoenpong et al. (2014). The CF-MC-IRMS has the necessary collector configuration for simultaneous determination of masses 30, 31 for the NO^+ fragment of N_2O (determination of $\delta^{15}N^{\alpha}$) and 44, 45, and 46 (determination of bulk $\delta^{15}N$ and $\delta^{18}O$). Cultures for isotopic analysis had a final NO_2^- concentration of 100 µM. A gas tight syringe was used to extract 3-mL to 5-mL headspace gas, which was then injected into the CF-MC-IRMS injection port. N_2O was purified in a purge and trap system under helium continuous flow (40 mL/min), CO_2 was chemically removed, and H_2O vapor was eliminated with both chemical and cryogenic traps. N_2O was cryofocused with two liquid N_2 traps and passed through a capillary GC column prior to IRMS analysis. These latter steps, including GC column backflushing to eliminate interferences in the SP determination, were nearly identical to what was described by McIlvin and Casciotti (2010). Helium flow was optimized to achieve quantitative extraction and reproducible results, even at low N_2O concentrations. N_2O concentrations in our samples were calculated from relative peak heights between the samples and a dilution series of pure N_2O gas mixtures (in N_2) of known N_2O concentrations (500 and 7500 ppm). The reproducibility of bulk $\delta^{15}N$ and $\delta^{18}O$ and SP as well as any instrumental drift were determined from measurements of an internal reference gas distributed through the analytical run. The measurements were calibrated from a four-point calibration correction using N_2O standards covering a large range of SP (-92.7‰ - 18.9‰), as well as bulk $\delta^{15}N$ and $\delta^{18}O$ composition calibrated by S. Toyoda (Tokyo Institute of Technology), and obtained from Joaquim Mohn (EMPA, Swiss Federal Laboratories for Materials Science & Technology). These standards were analyzed in duplicate for each run to quantify the scrambling effect, potential offset and iteratively solve for the different calibration parameters (Frame and Casciotti, 2010; Mohn et al., 2014). Correction for isobaric interference from ^{17}O was included in these procedures. Standard deviations for triplicate measurements of our N_2O standards were typically below 0.1‰ for $\delta^{15}N$-N_2Obulk, 0.2‰ for $\delta^{18}O$-N_2O and 1‰ for SP, which were comparable to values reported by Mohn et al. (2014).

3 Results

3.1 Phylogeny and classification

The four fungal strains we isolated and investigated in this study were *Purpureocillium lilacinum BL2022*, *Trichoderma virens XP2022*, *Trichoderma harzianum MB2022*, *and Rhodotourla glutinis MT2022*, as identified by blastn and phylogenetic analysis (Supplementary Figures S1, S2, and S3; Supplementary Table 1). *T. harzianum* and *T. virens* were closely related to terrestrial and marine derived species, such as *T. polysporum* and *T. citrinoviride*. *R. glutinis MT2022* was closely related to other species which have been isolated from both marine (*R. diobovata)* and terrestrial environments (*R. graminis* and *R. babjeavae*). *P. lilacinum* was closely related to terrestrially derived species but was distinct from *P.lilacinum CBS284.36*. *T. harzianum* was the only strain isolated using mineral media (Table 1), which did not contain yeast extract or peptone.

3.2 N_2O and CO_2 production from salt marsh sediment fungi

P. lilacinum produced the greatest amount of N_2O and CO_2 (22.8 ± 7.8 nmol of N_2O and 179 ± 24 µmol of CO_2, Figures 2A, E). *T. virens*, *T. harzianum*, and *R. glutinis*. produced an average of 17.4 ± 5.4 nmol, 4.45 ± 0.48 nmol, and 4.24 ± 1.57 nmol of N_2O (Figures 2B–D) and 39.0 ± 20.0, 5.00 ± 0.44, and 88.1 ± 37.5 µmol of CO_2 (Figures 2F–H), respectively. The production of N_2O by *P. lilacinum* did not plateau until the 22nd day. The production of N_2O by *T. virens* plateaued after the 16th day. The production of N_2O by *T. harzianum* and *R. glutinis* reached a maximum in only two to three days. N_2O yield for each fungal

TABLE 1 The mean and standard deviation (n = 3) of N_2O site preference (SP) produced by salt marsh sediment fungal strains from this study.

Species	Media type	Mean (‰)	SD (‰)
T. harzianum	Mineral	7.46	1.57
T. virens	Complex	30.56	2.09
P. lilacinum	Complex	31.00	1.31
R. glutinis	Complex	33.41	1.20

The composition of complex and mineral media was the same except that yeast extract and peptone were included in complex media.

strain was calculated using the average maximum N_2O produced, where N_2O yield is the fraction of NO_2^-N converted to N_2O-N (see Supplementary Information for additional details). *P.lilacinum, T. virens*, *T. harzianum*, and *R. glutinis* had respective yields of 22.8 ± 7.8%, 17.4 ± 5.4%, 4.45 ± 0.48%, and 4.24 ± 1.57%. There was a significant correlation between N_2O and CO_2 production ($p< 0.01$) for each replicate culture of the filamentous fungi *P. lilacinum*, *T. virens*, and *T. harzianum* (Figure 3). N_2O and CO_2 production by *R. glutinis* were not significantly correlated.

To further explore the effect of concentration on fungal N_2O production, the species with the highest cumulative N_2O production, *P. lilacinum*, was cultivated with 0 µM, 10 µM, 100 µM NO_2^- in triplicate. When grown without NO_2^-, *P. lilacinum* produced <1 nmol of N_2O (Figure 4). The addition of 100 µM to growth media resulted in a >10-fold increase in N_2O production for two of the three replicates when compared to the three replicates grown with 10 µM NO_2^- (285.0 ± 20.1 nmol and 22.8 ± 7.8 nmol of N_2O, respectively).

3.3 Site preference of N_2O from salt marsh sediment fungi

Site preference (SP) values of N_2O from salt marsh sediment fungi ranged from 7.49 ± 1.57‰ for *T. harzianum*, to 33.41 ± 1.20‰ for *R. glutinis* (Table 1), which were all lower than N_2O SP values (37.1 ± 2.5‰) measured from the model fungal denitrifier *F. oxysporum* (Sutka et al., 2008).

4 Discussion

4.1 N_2O production by salt marsh sediment fungi

We used both aerobic and anaerobic cultivation techniques to isolate N_2O-producing fungi from salt marsh sediments in North Inlet, South Carolina, USA. The aerobic technique is similar to previous efforts to isolate N_2O-producing fungi from

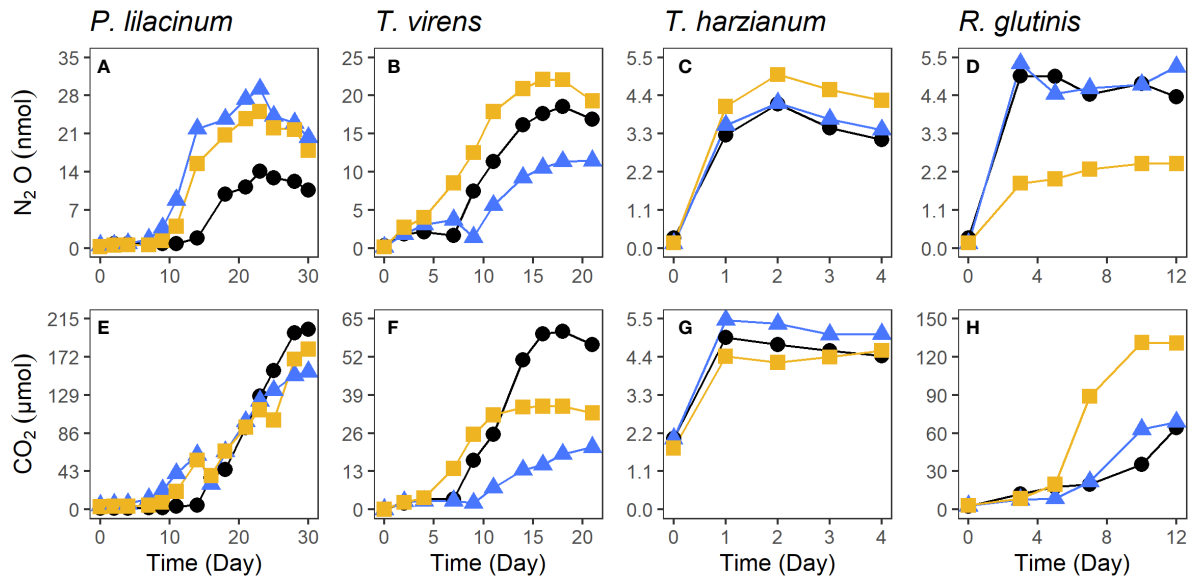

FIGURE 2
The production of N_2O and CO_2 by *P. lilacinum* **(A, E)**, *T. virens* **(B, F)**, *T. harzianum* **(C, G)**, and *R. glutinis* **(D, H)** isolated from salt marsh sediments. Each color and symbol combination represents one of the three replicates.

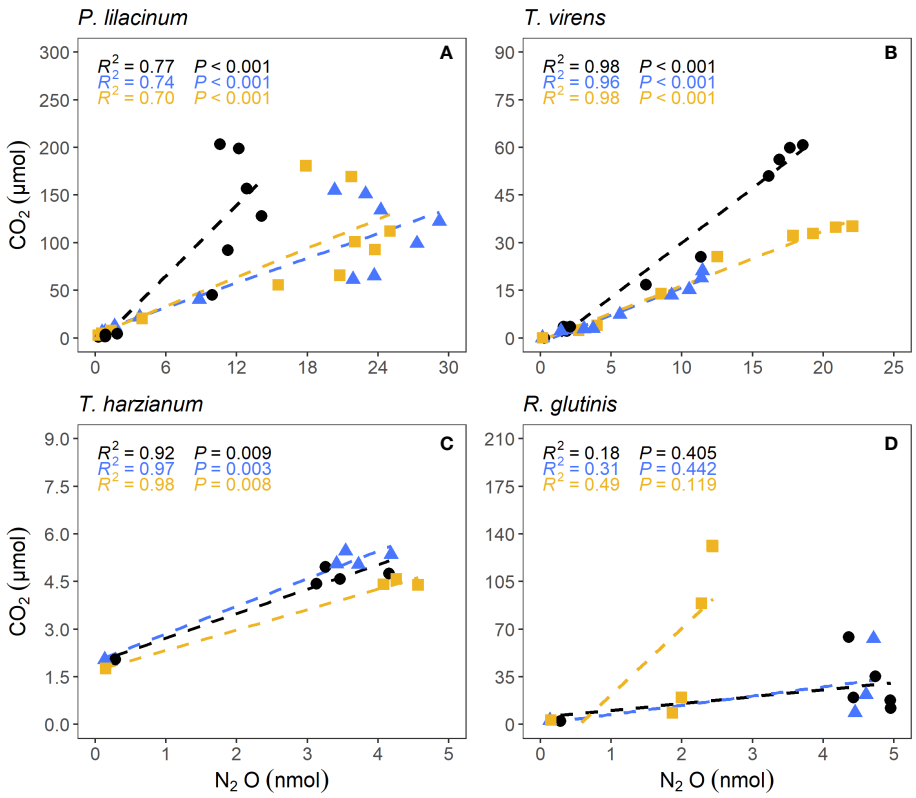

FIGURE 3
Correlation between N_2O and CO_2 production by salt marsh sediment fungi *P. lilacinum* **(A)**, *T. virens* **(B)**, *T. harzianum* **(C)**, and *R. glutinis* **(D)**. Each color represents one of the three replicates.

soil (Jirout et al., 2013; Mothapo et al., 2013) except that our media were prepared with a seawater base, which selected for fungi adapted to salinity in the range of 30 to 35 ppt. All filamentous species (*P. lilacinum*, *T. virens*, and *T. harzianum*) we isolated from salt marsh sediments have been isolated from soil and shown to produce N_2O (Lavrent'ev et al., 2008; Jirout, 2015; Maeda et al., 2015). A comparative genomics studies showed that all these three species possess the diagnostic gene for fungal denitrification, the cytochrome P450 nitric oxide reductase (*P450nor*) (Higgins et al., 2018). The positive correlations between N_2O and CO_2 production by filamentous fungi indicate respiratory denitrification is responsible for N_2O production. Variability in N_2O production, within individual strains' cultures, is likely due to small differences in the number of cells in the inoculum between triplicates. While this study was not intended as an exhaustive search for N_2O-producing fungi from salt marsh sediments, our results indicate that at least a subset of N_2O-producing fungi from terrestrial environments (Mothapo et al., 2015) are present in salt marsh sediments and have the potential to produce N_2O at high yields.

The ability to produce N_2O was widespread among the hundreds of strains tested by Maeda and colleagues (Maeda et al., 2015), but only one (Mucorales) of the 70 N_2O-producing strains in their study was not from the phylum Ascomycota. A survey of *P450nor* in over 700 fungal genomes also showed that this diagnostic gene for fungal denitrification was primarily found in Ascomycota (Higgins et al., 2018). While Ascomycota seem to be the main lineage capable of N_2O production, fungi from other phyla, particularly early diverging lineages, are poorly represented in these studies, partially due to their low abundance in terrestrial environments (Berbee et al., 2017). There is evidence that early diverging fungi play a more important role in marine environments than in terrestrial environments, and their potential to produce N_2O remains to be examined (Peng and Valentine, 2021).

To the best of our knowledge, this is the first study that used strictly anaerobic techniques to isolate fungi from salt marsh sediments, where oxygen is typically depleted a few millimeters below the surface (Peng et al., 2021). The only N_2O-producing

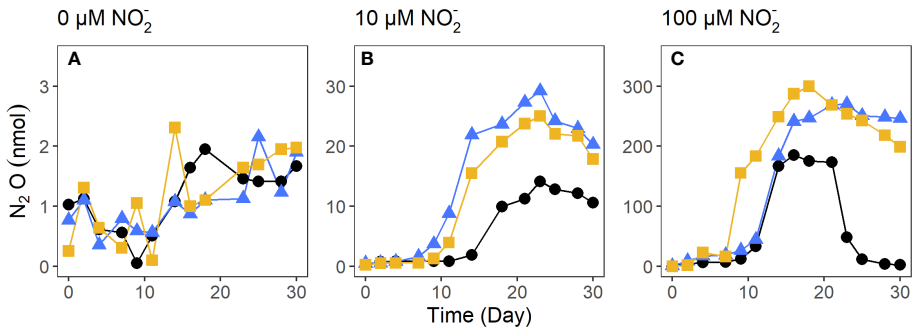

FIGURE 4
N_2O production by the salt marsh sediment fungi *P. lilacinum* cultivated with 0 μM **(A)**, 10 μM **(B)**, and 100 μM **(C)**. Each color and symbol combination represents one of the three replicates.

fungus isolated anaerobically was the basidiomycetous yeast *R. glutinis*, which is not known to possess *P450nor* in its genome (Higgins et al., 2018), but it does possess a fungal nitrite reductase (fungal *nirK*). The decoupling between N_2O and CO_2 production in *R. glutinis* cultures (Figure 3) suggests that N_2O production by *R. glutinis* may not be from respiratory denitrification. Instead, energy production by *R. glutinis*, an oleaginous yeast, was likely from fermentation (Yeeh, 1999; Xue et al., 2008). This could also explain the low N_2O yield by *R. glutinis* (3.25 ± 1.20%). While this is the first report of N_2O production by *R. glutinis* grown under sulfidic conditions, an unidentified *Rhodotorula* species grown under aerobic conditions produced N_2O after it reached stationary phase (Bleakley and Tiedje, 1982). Therefore, regardless of the mechanism of N_2O production by *R. glutinis*, it can contribute significantly to N_2O production from salt marsh sediments where the redox conditions fluctuate due to daily tides. A strong positive correlation was observed between N_2O production rate and the relative abundance of *Rhodotorula* in estuarine sediments in Xiamen, China (Su et al., 2021).

4.2 The influence of cultivation conditions on fungal N_2O production

Nearly all previous studies on N_2O production by fungi used media containing 10 mM of NO_2^- (Shoun et al., 1992; Mouton et al., 2012; Jirout et al., 2013; Mothapo et al., 2013; Maeda et al., 2015; Zou et al., 2021), which is orders of magnitude higher than the *in situ* NO_2^- concentrations in soil or marine sediments. It is known that different nutrient levels can cause different physiological responses in fungi, including changes which affect the ability of the cell to transport nutrients and degrade carbon (Ozcan and Johnston, 1999; Zaman et al., 2008). In this study we cultivated N_2O-producing fungi using sulfidic media containing NO_2^- at a level (10 μM) much closer to *in situ* conditions. Consequently, the total amounts of N_2O production in our study were lower than previously reported value, but the yield of N_2O from NO_2^- by salt marsh sediment fungi (up to 22.8 ± 7.8%) was comparable to some of the highest levels in previous studies (Mothapo et al., 2013; Jirout, 2015; Maeda et al., 2015). Furthermore, the salt marsh sediment fungi were cultivated under sulfidic conditions, demonstrating their relevance in N_2O production even at sulfidic depths of the sediments.

The ~10-fold increase in both N_2O and CO_2 production by *P. lilacinum* grown with 100 μM NO_2^- (compared to 10 μM) further supports the notion that respiratory reduction of NO_2^- was the primary mechanism for N_2O production, although we cannot rule out the possibility that secondary metabolisms also contribute to N_2O production (Higgins et al., 2018). Such a response by *P. lilacinum* implies that fungal N_2O production from salt marsh sediments will scale linearly with nutrient inputs from anthropogenic sources. A recent report demonstrated the drastic increase in N_2O production from salt marsh sediments under long-term fertilization (Peng et al., 2021), and fungi may have played a major role in the observed N_2O production by the bulk sediment community.

4.3 Site preference of fungi isolated from salt marsh sediment

Stable isotope mass balance has become a useful tool to determine the contribution of fungi to total N_2O production (Wankel et al., 2017; Rohe et al., 2021; Su et al., 2021). This approach constrains the contribution of different sources and sinks of N_2O by measuring N and O isotopes and isotopomers of N_2O from a complex system, which requires the knowledge of endmembers for each pathway (e.g. bacterial denitrification,

fungal denitrification). However, studies employing this method so far have relied primarily on the N_2O isotopomer signature determined for the model organism *F. oxysporum* (Sutka et al., 2008), which is not necessarily representative of N_2O produced by marine fungi from salt marsh sediments. A recent study using an isotope mass balance approach found that the site preference value and $\delta^{18}O$ of N_2O from estuarine sediments sometimes exceeded the values for the fungal endmember based on *F. oxysporum* (Su et al., 2021). We interpret this as additional evidence for the need to evaluate the N_2O isotopologue composition produced by fungi from salt marsh sediments.

A study on soil fungi showed that N_2O SP ranged from 15.8‰ - 37.1‰, depending on the species (Maeda et al., 2015). Yet, work by Maeda and colleagues (Maeda et al., 2015) has since not been used in any published isotope mass balances calculations. Our findings add to evidence presented by Maeda et al. (2015) that N_2O SP depends on the fungal isolate at the species and even strain level. We further present evidence that N_2O SP may differ based on growth conditions, even for fungi of the same species. N_2O SP values measured by Maeda et al. (2015) for several strains of *T. harzianum* ranged from 30 - 33.4‰. In contrast, the SP values of N_2O produced by the salt marsh sediment *T. harzianum* from this study (7.46 ± 1.57‰) was much lower, and was the lowest fungal N_2O SP reported to date. This may be attributed to two factors. Firstly, the *T. harzianum* isolated from salt marsh sediments in this study is the first and only N_2O-producing fungal culture grown on mineral media to the best of our knowledge. It has been shown that different organic nitrogen sources can impact N_2O emissions, though little is known about how N_2O SP values would be impacted (Pelster et al., 2012). Secondly, fungal culture media we prepared did not include any soluble sugars (e.g. dextrose), which was a staple ingredient in all previously published studies (Sutka et al., 2008; Rohe et al., 2014; Maeda et al., 2015). Instead, the stems of *Spartina alterniflora* (lignocellulose) was provided as the sole carbon source to *T. harzianum* grown on mineral media. It has recently been shown that the type of carbon substrates used to cultivate freshwater bacteria has a significant impact on the SP values of bacterial N_2O (Li et al., 2022). It is possible that this is true for N_2O-producing fungi as well, though future work is needed to verify.

Along with *T. harzianum*, other salt marsh sediment fungi in this study produced N_2O SP values lower than that from the model fungal denitrifier *F. oxysporum* (Sutka et al., 2008), indicating that it is inaccurate and oversimplifying to use the N_2O SP from one single strain as an endmember for stable isotope mass balance calculations. Many of the N_2O SP values measured from core incubations by Wankel and colleagues (Wankel et al., 2017) are within the range of the N_2O SP values reported in this study and by Maeda et al. (2015). Future work is needed to determine how carbon and nitrogen substrate types influence fungal N_2O SP values. While the range of fungal N_2O SP values overlaps with the N_2O SP range from abiotic N_2O production, abiotic denitrification is favored in high pH conditions with solid iron (III) or copper (II) catalysts (Zhu-Barker et al., 2015) and hence irrelevant or negligible in our cultures (pH buffered at 7.2) and in salt marsh sediments (typically < 7.5). Given the wide range of fungal N_2O SP values, the selection of endmember is therefore critical in studies using stable isotope mass balance calculations. The endmember selection can be informed by metabarcoding analysis of the fungal community in general (e.g. targeting the rRNA gene) and the functional genes for fungal denitrification (e.g. *nirK* gene) (Long et al., 2015; Chen et al., 2016; Maeda et al., 2017).

Data availability statement

The datasets presented in this study are deposited at NCBI GenBank with accession number PRJNA901534. The code to generate figures and calculations implemented in R is deposited at https://github.com/birchmaxwell/SaltMarshFungiN2O.

Author contributions

BL-M is a PhD student supervised by XP and AB. Samples were collected and maintained by BL-M, SL, SS, HB, and XP. BL-M, SS, HB, and JM conducted headspace gas analysis. BL-M and AB conducted IRMS analysis. XP and BL-M conducted sequencing analysis. BL-M conducted data analysis and led the writing of the manuscript. All authors contributed to the article and approved the submitted version.

Funding

This work was supported by the Advanced Support Program for Innovative Research Excellence-I (ASPIRE-I) at the University of South Carolina (Award #216100-21-56788).

Acknowledgments

The authors are grateful for the assistance of Erik Smith during sediment core collection.

Conflict of interest

The authors declare that the research was conducted in the absence of any commercial or financial relationships that could be construed as a potential conflict of interest.

Publisher's note

All claims expressed in this article are solely those of the authors and do not necessarily represent those of their affiliated organizations, or those of the publisher, the editors and the reviewers. Any product that may be evaluated in this article, or claim that may be made by its manufacturer, is not guaranteed or endorsed by the publisher.

Supplementary material

The Supplementary Material for this article can be found online at: https://www.frontiersin.org/articles/10.3389/fmars.2022.1098508/full#supplementary-material

References

Aldossari, N., and Ishii, S. (2021). Fungal denitrification revisited – recent advancements and future opportunities. *Soil Biol. Biochem.* 157, 108250. doi: 10.1016/j.soilbio.2021.108250

Allen, D. M.Allen, W.B.Feller, R. F.Plunket, J. S., editors. (2014). *Site Profile of the North Inlet – Winyah Bay National Estuarine Research Reserve*. Georgetown, S.C.: North Inlet – Winyah Bay National Estuarine Research Reserve. 432 pp.

Al-Haj, A. N., and Fulweiler, R. W. (2020). A synthesis of methane emissions from shallow vegetated coastal ecosystems. *Glob. Change Biol.* 26, 2988–3005. doi: 10.1111/gcb.15046

Amend, A., Burgaud, G., Cunliffe, M., Edgcomb, V. P., Ettinger, C. L., Gutiérrez, M. H., et al. (2019). Fungi in the marine environment: Open questions and unsolved problems. *mBio* 10, e01189–e01118. doi: 10.1128/mBio.01189-18

Berbee, M. L., James, T. Y., and Strullu-Derrien, C. (2017). Early diverging fungi: Diversity and impact at the dawn of terrestrial life. *Annu. Rev. Microbiol.* 71, 41–60. doi: 10.1146/annurev-micro-030117-020324

Bleakley, B. H., and Tiedje, J. M. (1982). Nitrous oxide production by organisms other than nitrifiers or denitrifiers. *Appl. Environ. Microbiol.* 44, 1342–1348. doi: 10.1128/aem.44.6.1342-1348.1982

Bourbonnais, A., Letscher, R. T., Bange, H. W., Échevin, V., Larkum, J., Mohn, J., et al. (2017). N2O production and consumption from stable isotopic and concentration data in the Peruvian coastal upwelling system. *Glob. Biogeochem. Cycles* 31, 678–698. doi: 10.1002/2016GB005567

Buchan, A., Newell, S. Y., Butler, M., Biers, E. J., Hollibaugh, J. T., and Moran, M. A. (2003). Dynamics of bacterial and fungal communities on decaying salt marsh grass. *Appl. Environ. Microbiol.* 69, 6676–6687. doi: 10.1128/AEM.69.11.6676-6687.2003

Buchan, A., Newell, S. Y., Moreta, J. I. L., and Moran, M. A. (2002). Analysis of internal transcribed spacer (ITS) regions of rRNA genes in fungal communities in a southeastern U.S. salt marsh. *Microb. Ecol.* 43, 329–340. doi: 10.1007/s00248-001-1062-0

Burden, A., Garbutt, R. A., Evans, C. D., Jones, D. L., and Cooper, D. M. (2013). Carbon sequestration and biogeochemical cycling in a saltmarsh subject to coastal managed realignment. *Estuar. Coast. Shelf Sci.* 120, 12–20. doi: 10.1016/j.ecss.2013.01.014

Butterbach-Bahl, K., Baggs, E. M., Dannenmann, M., Kiese, R., and Zechmeister-Boltenstern, S. (2013). Nitrous oxide emissions from soils: how well do we understand the processes and their controls? *Philos. Trans. R. Soc B Biol. Sci.* 368. doi: 10.1098/rstb.2013.0122

Calabon, M. S., Jones, E. B. G., Promputtha, I., and Hyde, K. D. (2021). Fungal biodiversity in salt marsh ecosystems. *J. Fungi* 7, 648. doi: 10.3390/jof7080648

Casciotti, K. L., Forbes, M., Vedamati, J., Peters, B. D., Martin, T. S., and Mordy, C. W. (2018). Nitrous oxide cycling in the Eastern tropical south pacific as inferred from isotopic and isotopomeric data. *Deep Sea res. part II top. Stud. Oceanogr.* 156, 155–167. doi: 10.1016/j.dsr2.2018.07.014

Charoenpong, C. N., Bristow, L. A., and Altabet, M. A. (2014). A continuous flow isotope ratio mass spectrometry method for high precision determination of dissolved gas ratios and isotopic composition. *Limnology and Oceanography: Methods* 12, 323–337. doi: 10.4319/lom.2014.12.323

Chen, H., Yu, F., and Shi, W. (2016). Detection of N2O-producing fungi in environment using nitrite reductase gene (nirK)-targeting primers. *Fungal Biol.* 120, 1479–1492. doi: 10.1016/j.funbio.2016.07.012

Edgar, R. C. (2004). MUSCLE: multiple sequence alignment with high accuracy and high throughput. *Nucleic Acids Res.* 32, 1792–1797. doi: 10.1093/nar/gkh340

Edwards, J. E., Forster, R. J., Callaghan, T. M., Dollhofer, V., Dagar, S. S., Cheng, Y., et al. (2017). PCR and omics based techniques to study the diversity, ecology and biology of anaerobic fungi: Insights, challenges and opportunities. *Front. Microbiol.* 8. doi: 10.3389/fmicb.2017.01657

Frame, C. H., and Casciotti, K. L. (2010). Biogeochemical controls and isotopic signatures of nitrous oxide production by a marine ammonia-oxidizing bacterium. *Biogeosciences* 7, 2695–2709. doi: 10.5194/bg-7-2695-2010

Gadd, G. M. Ed. (2006). *Fungi in biogeochemical cycles*. (British Mycological Society symposia; No. 24) (Cambridge, England: Cambridge University Press). doi: 10.1017/CBO9780511550522

Gao, D., Hou, L., Liu, M., Zheng, Y., Yin, G., and Niu, Y. (2022). N2O emission dynamics along an intertidal elevation gradient in a subtropical estuary: Importance of N2O consumption. *Environ. Res.* 205, 112432. doi: 10.1016/j.envres.2021.112432

Ge, Z.-M., Wang, H., Cao, H.-B., Zhao, B., Zhou, X., Peltola, H., et al. (2016). Responses of eastern Chinese coastal salt marshes to sea-level rise combined with vegetative and sedimentary processes. *Sci. Rep.* 6, 28466. doi: 10.1038/srep28466

Grossart, H.-P., Wurzbacher, C., James, T. Y., and Kagami, M. (2016). Discovery of dark matter fungi in aquatic ecosystems demands a reappraisal of the phylogeny and ecology of zoosporic fungi. *Fungal Ecol.* 19, 28–38. doi: 10.1016/j.funeco.2015.06.004

Gutiérrez, M. H., Vera, J., Srain, B., Quiñones, R. A., Wörmer, L., Hinrichs, K.-U., et al. (2020). Biochemical fingerprints of marine fungi: implications for trophic and biogeochemical studies. *Aquat. Microb. Ecol.* 84, 75–90. doi: 10.3354/ame01927

Hayatsu, M., Tago, K., and Saito, M. (2008). Various players in the nitrogen cycle: Diversity and functions of the microorganisms involved in nitrification and denitrification. *Soil Sci. Plant Nutr.* 54, 33–45. doi: 10.1111/j.1747-0765.2007.00195.x

Higgins, S. A., Schadt, C. W., Matheny, P. B., and Löffler, F. E. (2018). Phylogenomics reveal the dynamic evolution of fungal nitric oxide reductases and their relationship to secondary metabolism. *Genome Biol. Evol.* 10, 2474–2489. doi: 10.1093/gbe/evy187

Intergovernmental Panel on Climate Change ed (2014). "Anthropogenic and natural radiative forcing," in *Climate change 2013 – the physical science basis: Working group I contribution to the fifth assessment report of the intergovernmental panel on climate change* (Cambridge: Cambridge University Press), 659–740. doi: 10.1017/CBO9781107415324.018

Jirout, J. (2015). Nitrous oxide productivity of soil fungi along a gradient of cattle impact. *Fungal Ecol.* 17, 155–163. doi: 10.1016/j.funeco.2015.07.003

Jirout, J., Šimek, M., and Elhottová, D. (2013). Fungal contribution to nitrous oxide emissions from cattle impacted soils. *Chemosphere* 90, 565–572. doi: 10.1016/j.chemosphere.2012.08.031

Johnson, M., Zaretskaya, I., Raytselis, Y., Merezhuk, Y., McGinnis, S., and Madden, T. L. (2008). NCBI BLAST: a better web interface. *Nucleic Acids Res.* 36, W5–W9. doi: 10.1093/nar/gkn201

Jones, E. B. G. (2011). Fifty years of marine mycology. *Fungal Divers.* 50, 73. doi: 10.1007/s13225-011-0119-8

Jones, E. B. G., Ramakrishna, S., Vikineswary, S., Das, D., Bahkali, A. H., Guo, S.-Y., et al. (2022). How do fungi survive in the Sea and respond to climate change? *J. Fungi Basel Switz.* 8, 291. doi: 10.3390/jof8030291

Kaplan, W., Valiela, I., and Teal, J. M. (1979). Denitrification in a salt marsh ecosystem. *Limnol. Oceanogr.* 24, 726–734. doi: 10.4319/lo.1979.24.4.0726

Kearns, P. J., Bulseco-McKim, A. N., Hoyt, H., Angell, J. H., and Bowen, J. L. (2019). Nutrient enrichment alters salt marsh fungal communities and promotes putative fungal denitrifiers. *Microb. Ecol.* 77, 358–369. doi: 10.1007/s00248-018-1223-z

Kelly, C. L., Travis, N. M., Baya, P. A., and Casciotti, K. L. (2021). Quantifying nitrous oxide cycling regimes in the Eastern tropical north pacific ocean with isotopomer analysis. *Glob. Biogeochem. Cycles* 35, e2020GB006637. doi: 10.1029/2020GB006637

Kim, J., Chaudhary, D. R., and Kang, H. (2020). Nitrogen addition differently alters GHGs production and soil microbial community of tidal salt marsh soil depending on the types of halophyte. *Appl. Soil Ecol.* 150, 103440. doi: 10.1016/j.apsoil.2019.103440

Kostka, J. E., Roychoudhury, A., and Van Cappellen, P. (2002). Rates and controls of anaerobic microbial respiration across spatial and temporal gradients in saltmarsh sediments. *Biogeochemistry* 60, 49–76. doi: 10.1023/A:1016525216426

Laughlin, R. J., and Stevens, R. J. (2002). Evidence for fungal dominance of denitrification and codenitrification in a grassland soil. *Soil Sci. Soc Am. J.* 66, 1540–1548. doi: 10.2136/sssaj2002.1540

Lavrent'ev, R. B., Zaitsev, S. A., Sudnitsyn, I. I., and Kurakov, A. V. (2008). Nitrous oxide production by fungi in soils under different moisture levels. *Mosc. Univ. Soil Sci. Bull.* 63, 178–183. doi: 10.3103/S0147687408040054

Lecomte, S. M., Achouak, W., Abrouk, D., Heulin, T., Nesme, X., and Haichar, F.el Z. (2018). Diversifying anaerobic respiration strategies to compete in the rhizosphere. *Front. Environ. Sci.* 6. doi: 10.3389/fenvs.2018.00139

Letunic, I., and Bork, P. (2019). Interactive tree of life (iTOL) v4: recent updates and new developments. *Nucleic Acids Res.* 47, W256–W259. doi: 10.1093/nar/gkz239

Li, S., Wang, S., and Ji, G. (2022). Influences of carbon sources on N2O production during denitrification in freshwaters: Activity, isotopes and functional microbes. *Water Res.* 226, 119315. doi: 10.1016/j.watres.2022.119315

Long, A., Song, B., Fridey, K., and Silva, A. (2015). Detection and diversity of copper containing nitrite reductase genes (nirK) in prokaryotic and fungal communities of agricultural soils. *FEMS Microbiol. Ecol.* 91, 1–9. doi: 10.1093/femsec/fiu004

Lord, N. S., Kaplan, C. W., Shank, P., Kitts, C. L., and Elrod, S. L. (2002). Assessment of fungal diversity using terminal restriction fragment (TRF) pattern analysis: comparison of 18S and ITS ribosomal regions. *FEMS Microbiol. Ecol.* 42, 327–337. doi: 10.1111/j.1574-6941.2002.tb01022.x

Maeda, K., Spor, A., Edel-Hermann, V., Heraud, C., Breuil, M.-C., Bizouard, F., et al. (2015). N2O production, a widespread trait in fungi. *Sci. Rep.* 59697. doi: 10.1038/srep09697

Maeda, K., Toyoda, S., Philippot, L., Hattori, S., Nakajima, K., Ito, Y., et al. (2017). Relative contribution of nirK- and nirS- bacterial denitrifiers as well as fungal denitrifiers to nitrous oxide production from dairy manure compost. *Environ. Sci. Technol.* 51, 14083–14091. doi: 10.1021/acs.est.7b04017

Ma, W. K., Farrell, R. E., and Siciliano, S. D. (2008). Soil formate regulates the fungal nitrous oxide emission pathway. *Appl. Environ. Microbiol.* 74, 6690–6696. doi: 10.1128/AEM.00797-08

Martin, R. M., Wigand, C., Elmstrom, E., Lloret, J., and Valiela, I. (2018). Long-term nutrient addition increases respiration and nitrous oxide emissions in a new England salt marsh. *Ecol. Evol.* 8, 4958–4966. doi: 10.1002/ece3.3955

McIlvin, M. R., and Casciotti, K. L. (2010). Fully automated system for stable isotopic analyses of dissolved nitrous oxide at natural abundance levels. *Limnology and Oceanography: Methods* 8, 54–66. doi: 10.4319/lom.2010.8.54

Mcowen, C. J., Weatherdon, L. V., Bochove, J.-W. V., Sullivan, E., Blyth, S., Zockler, C., et al. (2017). A global map of saltmarshes. *Biodivers. Data J.*, e11764. doi: 10.3897/BDJ.5.e11764

Mohn, J., Wolf, B., Toyoda, S., Lin, C.-T., Liang, M.-C., Brüggemann, N., et al. (2014). Interlaboratory assessment of nitrous oxide isotopomer analysis by isotope ratio mass spectrometry and laser spectroscopy: current status and perspectives. *Rapid Commun. Mass Spectrom.* 28, 1995–2007. doi: 10.1002/rcm.6982

Mothapo, N., Chen, H., Cubeta, M. A., Grossman, J. M., Fuller, F., and Shi, W. (2015). Phylogenetic, taxonomic and functional diversity of fungal denitrifiers and associated N2O production efficacy. *Soil Biol. Biochem.* 83, 160–175. doi: 10.1016/j.soilbio.2015.02.001

Mothapo, N. V., Chen, H., Cubeta, M. A., and Shi, W. (2013). Nitrous oxide producing activity of diverse fungi from distinct agroecosystems. *Soil Biol. Biochem.* 66, 94–101. doi: 10.1016/j.soilbio.2013.07.004

Mouton, M., Postma, F., Wilsenach, J., and Botha, A. (2012). Diversity and characterization of culturable fungi from marine sediment collected from st. Helena bay, south Africa. *Microb. Ecol.* 64, 311–319. doi: 10.1007/s00248-012-0035-9

Murray, R. H., Erler, D. V., and Eyre, B. D. (2015). Nitrous oxide fluxes in estuarine environments: response to global change. *Glob. Change Biol.* 21, 3219–3245. doi: 10.1111/gcb.12923

Nakahara, K., Tanimoto, T., Hatano, K., Usuda, K., and Shoun, H. (1993). Cytochrome p-450 55A1 (P-450dNIR) acts as nitric oxide reductase employing NADH as the direct electron donor. *J. Biol. Chem.* 268, 8350–8355. doi: 10.1016/S0021-9258(18)53102-1

Newell, S., Porter, D., and Lingle, W. l. (1996). Lignocellulolysis by ascomycetes (fungi) of a saltmarsh grass (smooth cordgrass). *Microsc. Res. Tech.* 33, 32–46. doi: 10.1002/(SICI)1097-0029(199601)33:1<32::AID-JEMT5>3.0.CO;2-2

Ozcan, S., and Johnston, M. (1999). Function and regulation of yeast hexose transporters. *Microbiol. Mol. Biol. Rev. MMBR* 63, 554–569. doi: 10.1128/MMBR.63.3.554-569.1999

Parrondo, R. T., Gosselink, J. G., and Hopkinson, C. S. (1978). Effects of salinity and drainage on the growth of three salt marsh grasses. *Bot. Gaz.* 139, 102–107. doi: 10.1086/336975

Pelster, D. E., Chantigny, M. H., Rochette, P., Angers, D. A., Rieux, C., and Vanasse, A. (2012). Nitrous oxide emissions respond differently to mineral and organic nitrogen sources in contrasting soil types. *J. Environ. Qual.* 41, 427–435. doi: 10.2134/jeq2011.0261

Peng, X., Ji, Q., Angell, J. H., Kearns, P. J., Bowen, J. L., and Ward, B. B. (2021). Long-term fertilization alters nitrous oxide cycling dynamics in salt marsh sediments. *Environ. Sci. Technol.* 55, 10832–10842. doi: 10.1021/acs.est.1c01542

Peng, X., Swift, C. L., Theodorou, M. K., and O'Malley, M. A. (2018). "Methods for genomic characterization and maintenance of anaerobic fungi," in *Fungal genomics: Methods and protocols methods in molecular biology*. Eds. R. P. de Vries, A. Tsang and I. V. Grigoriev (New York, NY: Springer), 53–67. doi: 10.1007/978-1-4939-7804-5_5

Peng, X., and Valentine, D. L. (2021). Diversity and N2O production potential of fungi in an oceanic oxygen minimum zone. *J. Fungi* 7, 218. doi: 10.3390/jof7030218

Pérez-Llano, Y., Rodríguez-Pupo, E. C., Druzhinina, I. S., Chenthamara, K., Cai, F., Gunde-Cimerman, N., et al. (2020). Stress reshapes the physiological response of halophile fungi to salinity. *Cells* 9, 525. doi: 10.3390/cells9030525

Philippot, L., Raaijmakers, J. M., Lemanceau, P., and van der Putten, W. H. (2013). Going back to the roots: the microbial ecology of the rhizosphere. *Nat. Rev. Microbiol.* 11, 789–799. doi: 10.1038/nrmicro3109

Price, M. N., Dehal, P. S., and Arkin, A. P. (2010). FastTree 2 – approximately maximum-likelihood trees for Large alignments. *PloS One* 5, e9490. doi: 10.1371/journal.pone.0009490

Rohe, L., Anderson, T.-H., Braker, G., Flessa, H., Giesemann, A., Lewicka-Szczebak, D., et al. (2014). Dual isotope and isotopomer signatures of nitrous oxide from fungal denitrification – a pure culture study. *Rapid Commun. Mass Spectrom.* 28, 1893–1903. doi: 10.1002/rcm.6975

Rohe, L., Apelt, B., Vogel, H.-J., Well, R., Wu, G.-M., and Schlüter, S. (2021). Denitrification in soil as a function of oxygen availability at the microscale. *Biogeosciences* 18, 1185–1201. doi: 10.5194/bg-18-1185-2021

Rohe, L., Well, R., and Lewicka-Szczebak, D. (2017). Use of oxygen isotopes to differentiate between nitrous oxide produced by fungi or bacteria during denitrification. *Rapid Commun. Mass Spectrom.* 31, 1297–1312. doi: 10.1002/rcm.7909

Shoun, H., Kim, D.-H., Uchiyama, H., and Sugiyama, J. (1992). Denitrification by fungi. *FEMS Microbiol. Lett.* 94, 277–281. doi: 10.1111/j.1574-6968.1992.tb05331.x

Starr, S. F., Mortazavi, B., Tatariw, C., Kuehn, K. A., Cherry, J. A., Ledford, T., et al. (2022). Poor recovery of fungal denitrification limits nitrogen removal capacity in a constructed gulf coast marsh. *Soil Biol. Biochem.* 170, 108692. doi: 10.1016/j.soilbio.2022.108692

Sutka, R. L., Adams, G. C., Ostrom, N. E., and Ostrom, P. H. (2008). Isotopologue fractionation during N2O production by fungal denitrification. *Rapid Commun. Mass Spectrom.* 22, 3989–3996. doi: 10.1002/rcm.3820

Sutka, R. L., Ostrom, N. E., Ostrom, P. H., Breznak, J. A., Gandhi, H., Pitt, A. J., et al. (2006). Distinguishing nitrous oxide production from nitrification and denitrification on the basis of isotopomer abundances. *Appl. Environ. Microbiol.* 72, 638–644. doi: 10.1128/AEM.72.1.638-644.2006

Su, X., Wen, T., Wang, Y., Xu, J., Cui, L., Zhang, J., et al. (2021). Stimulation of N2O emission *via* bacterial denitrification driven by acidification in estuarine sediments. *Glob. Change Biol.* 27, 5564–5579. doi: 10.1111/gcb.15863

Tamura, K., Stecher, G., and Kumar, S. (2021). MEGA11: Molecular evolutionary genetics analysis version 11. *Mol. Biol. Evol.* 38, 3022–3027. doi: 10.1093/molbev/msab120

Teal, J. M., and Howes, B. L. (2000). "Salt marsh values: Retrospection from the end of the century," in *Concepts and controversies in tidal marsh ecology*. Eds. M. P. Weinstein and D. A. Kreeger (Dordrecht: Springer Netherlands), 9–19. doi: 10.1007/0-306-47534-0_2

Tedersoo, L., Anslan, S., Bahram, M., Põlme, S., Riit, T., Liiv, I., et al. (2015). Shotgun metagenomes and multiple primer pair-barcode combinations of amplicons reveal biases in metabarcoding analyses of fungi. *MycoKeys* 10, 1–43. doi: 10.3897/mycokeys.10.4852

Thiem, D., Gołębiewski, M., Hulisz, P., Piernik, A., and Hrynkiewicz, K. (2018). How does salinity shape bacterial and fungal microbiomes of alnus glutinosa roots? *Front. Microbiol.* 9. doi: 10.3389/fmicb.2018.00651

Tian, H., Xu, R., Canadell, J. G., Thompson, R. L., Winiwarter, W., Suntharalingam, P., et al. (2020). A comprehensive quantification of global nitrous oxide sources and sinks. *Nature* 586, 248–256. doi: 10.1038/s41586-020-2780-0

Torzilli, A. P., Sikaroodi, M., Chalkley, D., and Gillevet, P. M. (2006). A comparison of fungal communities from four salt marsh plants using automated ribosomal intergenic spacer analysis (ARISA). *Mycologia* 98, 690–698. doi: 10.1080/15572536.2006.11832641

Toyoda, S., Yoshida, N., Miwa, T., Matsui, Y., Yamagishi, H., Tsunogai, U., et al. (2002). Production mechanism and global budget of N2O inferred from its isotopomers in the western north pacific. *Geophys. Res. Lett.* 29, 7–4. doi: 10.1029/2001GL014311

Vainio, E. J., and Hantula, J. (2000). Direct analysis of wood-inhabiting fungi using denaturing gradient gel electrophoresis of amplified ribosomal DNA. *Mycol. Res.* 104, 927–936. doi: 10.1017/S0953756200002471

Vernberg, F. J. (1993). Salt-marsh processes: A review. *Environ. Toxicol. Chem.* 12, 2167–2195. doi: 10.1002/etc.5620121203

Wankel, S. D., Ziebis, W., Buchwald, C., Charoenpong, C., de Beer, D., Dentinger, J., et al. (2017). Evidence for fungal and chemodenitrification based N2O flux from nitrogen impacted coastal sediments. *Nat. Commun.* 8, 15595. doi: 10.1038/ncomms15595

Warcup, J. H. (1950). The soil-plate method for isolation of fungi from soil. *Nature* 166, 117–118. doi: 10.1038/166117b0

Wu, J., Hong, Y., Liu, X., and Hu, Y. (2021). Variations in nitrogen removal rates and microbial communities over sediment depth in daya bay, China. *Environ. pollut.* 286, 117267. doi: 10.1016/j.envpol.2021.117267

Xue, F., Miao, J., Zhang, X., Luo, H., and Tan, T. (2008). Studies on lipid production by rhodotorula glutinis fermentation using monosodium glutamate wastewater as culture medium. *Bioresour. Technol.* 99, 5923–5927. doi: 10.1016/j.biortech.2007.04.046

Yeeh, Y. (1999). "RHODOTORULA," in *Encyclopedia of food microbiology*. Ed. R. K. Robinson (Oxford: Elsevier), 1900–1905. doi: 10.1006/rwfm.1999.1340

Yu, Y., Zhao, C., Zheng, N., Jia, H., and Yao, H. (2019). Interactive effects of soil texture and salinity on nitrous oxide emissions following crop residue amendment. *Geoderma* 337, 1146–1154. doi: 10.1016/j.geoderma.2018.11.012

Zaman, S., Lippman, S. I., Zhao, X., and Broach, J. R. (2008). How saccharomyces responds to nutrients. *Annu. Rev. Genet.* 42, 27–81. doi: 10.1146/annurev.genet.41.110306.130206

Zheng, B., Zhu, Y., Sardans, J., Peñuelas, J., and Su, J. (2018). QMEC: a tool for high-throughput quantitative assessment of microbial functional potential in c, n, p, and s biogeochemical cycling. *Sci. China Life Sci.* 61, 1451–1462. doi: 10.1007/s11427-018-9364-7

Zhu-Barker, X., Cavazos, A. R., Ostrom, N. E., Horwath, W. R., and Glass, J. B. (2015). The importance of abiotic reactions for nitrous oxide production. *Biogeochemistry* 126, 251–267. doi: 10.1007/s10533-015-0166-4

Zou, Y.-N., Wu, Q.-S., and Kuča, K. (2021). Unravelling the role of arbuscular mycorrhizal fungi in mitigating the oxidative burst of plants under drought stress. *Plant Biol.* 23, 50–57. doi: 10.1111/plb.13161

Zumft, W. G. (1997). Cell biology and molecular basis of denitrification. *Microbiol. Mol. Biol. Rev. MMBR* 61, 533–616. doi: 10.1128/mmbr.61.4.533-616.1997

frontiers | Frontiers in Marine Science

TYPE Original Research
PUBLISHED 09 January 2023
DOI 10.3389/fmars.2022.1093279

OPEN ACCESS

EDITED BY
Liyang Yang,
Fuzhou University, China

REVIEWED BY
Xiaofei Li,
East China Normal University, China
Junhong Bai,
Beijing Normal University, China

*CORRESPONDENCE
Zhuo Shen
zshen218@126.com

†These authors have contributed equally to this work

SPECIALTY SECTION
This article was submitted to Marine Biogeochemistry, a section of the journal Frontiers in Marine Science

RECEIVED 08 November 2022
ACCEPTED 12 December 2022
PUBLISHED 09 January 2023

CITATION
Lin X, Lin G, Zheng Y, Li W, Guo P, Fan S, Kong T, Tian D, Sun D and Shen Z (2023) Nitrogen mineralization and immobilization in surface sediments of coastal reclaimed aquaculture ecosystems. *Front. Mar. Sci.* 9:1093279. doi: 10.3389/fmars.2022.1093279

Nitrogen mineralization and immobilization in surface sediments of coastal reclaimed aquaculture ecosystems

Xianbiao Lin[1,2†], Genmei Lin[3†], Yijie Zheng[3], Wenjing Li[3], Peng Guo[1,2], Shiyuan Fan[1,2], Tiantian Kong[1,2], Dongfan Tian[1,2], Dongyao Sun[4] and Zhuo Shen[3*]

[1]Frontiers Science Center for Deep Ocean Multispheres and Earth System, and Key Laboratory of Marine Chemistry Theory and Technology, Ministry of Education, Ocean University of China, Qingdao, China, [2]College of Chemistry & Chemical Engineering, Ocean University of China, Qingdao, Shandong, China, [3]School of Marine Sciences, Sun Yat-sen University, and Southern Marine Science and Engineering Guangdong Laboratory (Zhuhai), Zhuhai, China, [4]School of Geography Science and Geomatics Engineering, Suzhou University of Science and Technology, Suzhou, China

Sediment nitrogen (N) mineralization and immobilization are two crucial processes driven by microorganisms, which may play significant roles in the regulation of water quality in aquaculture ecosystems. However, limited information is available about the quantitative importance of sedimentary N mineralization and immobilization in coastal aquaculture systems. Here, a combination of incubation experiments with a ^{15}N isotope dilution technique were employed, aiming to quantify N mineralization and immobilization processes in surface sediments (0–5 cm) of three types of aquaculture ecosystems (seabass, white shrimp, and green crab ponds) reclaimed within the western bank of the Pearl River Estuary. Our results showed that no significant difference in sediment N mineralization and immobilization rates, microbial abundances, and organic matter among different aquaculture types on small-scale range. Meanwhile, prolonged pond-drying significant reduced sediment N mineralization and immobilization rates, bacterial abundances, organic matter, moisture content, ferrous ion (Fe^{2+}), Fe^{2+}/Fe^{3+}, and ammonium (NH_4^+), while not strongly altered sediment percentage of NH_4^+ mineralized per day (PAM), relative ammonium immobilization (RAI), fungal abundances, TOC/TN, nitrate (NO_3^-), and $\delta^{13}C_{org}$. N mineralization and immobilization rates were both significantly related to overlying water NO_3^-, as well as sediment moisture content, bulk density, organic matter, Fe^{2+}, and microbial abundances. In addition, the total mineralized and immobilized N in aquaculture surface sediments from the Guangdong-Hong Kong-Macao Greater Bay Area were estimated to be approximately 4.55×10^4 and 3.68×10^4 t N yr^{-1}, respectively. Higher N mineralization relative to N immobilized fluxes indicated that the sediment serves as an important source of eutrophication in reclaimed aquaculture system of coastal wetlands.

KEYWORDS

N mineralization and immobilization, available organic carbon fractions, sediment, reclaimed aquaculture ecosystem, 15N isotope dilution technique

1 Introduction

Since the last century, anthropogenic activities have already become one of the major factors driving the change of global nitrogen (N) cycling and caused more than tripled N-flows higher than those caused by natural processes, and thus resulting in a total globally fixed N of about 413 Tg N y^{-1} (Zilio et al., 2020). The increasing reactive N load disrupts the N balance in both marine and terrestrial ecosystems. Meanwhile, a series of ecological problems, such as the loss of habitats and biodiversity (Galloway et al., 2008), eutrophication and the expansion of periodic or permanent low oxygen zone (Diaz and Rosenberg, 2008), the outbreak of toxic algae (Li et al., 2014), and the strengthened emission of greenhouse gases (Murray et al., 2015; Mao et al., 2022) were caused in the latest century. Therefore, coastal N pollution is one of the global significant and urgent environmental problem. Studies regarding N biogeochemical processes of estuarine and coastal ecosystems have become a cutting-edge scientific issue, which is also a key topic of many international research programs such as International Geophere-Biosphere Programme/Land-Ocean Interactions in Coastal Zone (IGBP/LOICZ), Integrated Marine Biogeochemistry and Ecosystem Research (IMBER) and Future Earth (Howarth et al., 2011; Buzzelli et al., 2013).

N mineralization and immobilization processes of N biogeochemical cycle in estuarine and coastal sediments. N mineralization is an important N-cycling process by which organic N is converted into inorganic forms available to organisms, which can exacerbate water eutrophication (Mishra et al., 2005). Conversely, microbial N immobilization is an important N-cycling process in which microorganisms convert inorganic N into organic N (e.g., amino acid and proteins) (Zhu et al., 2013), Meanwhile, some previous studies indicated that ammonium (NH_4^+) immobilization is considered as the major process of anaerobic ammonia consumption, which can effectively transform NH_4^+ into organic N and maintain the health of ecosystem (Matheson et al., 2003; Huang et al., 2021; Yang et al., 2022). These two important N biogeochemical processes have important ecological and environmental significance for maintaining N balance in estuarine and coastal ecosystems. Previous studies have reported that sediment N mineralization and immobilization are mainly affected by the physicochemical properties of sediment (e.g., soil texture, total carbon and N, C/N, pH, and water content) (Paul et al., 2003; Rutigliano et al., 2009; Huang et al., 2021), environmental climate factors (e.g., temperature, precipitation) (Gao et al., 2014; Lin et al., 2016a), and microorganisms in complex estuarine and coastal ecosystems (Cufrey and Kemp, 1992; Herbert, 1999; Bai et al., 2012; Qi et al., 2019). Thus, it is necessary to fully understand these two processes and their controlling factors for evaluation of N balance and prediction of N dynamics with the ever-changing environmental conditions in estuaries and coasts.

A large area of coastal wetlands has been reclaimed for development over the past few decades, and aquaculture use is one of the major reclamation purposes. In China, more than 1,260 km^2 of coastal wetlands was reclaimed for aquaculture every year (Cao et al., 2011; Zuo et al., 2013). In order to meet the unprecedented demand of aquatic products supply, large amount of nitrogen- and phosphorus-rich bait is added into these ecosystems. When the nutrients in the water column exceed the requirment of plankton and aquacultured organisms, several disadvantages including water quality deterioration, frequent disease occurrence, and aquaculture benefits decline appeared (Amano et al., 2011). Coastal aquaculture ecosystem is generally regarded as a major source of N pollutants, and subsequent environemntal problems have attracted widespread concerns nowadays (Wu et al., 2014; Lin and Lin, 2022). Sediment is a vital place where N mineralization and immobilization occurred, representing frequent transformation between inorganic N and organic N, which could aggravate eutrophication to some extent. Coastal wetlands in the Pearl River Estuary are reclamation hotspots for aquaculture and have been significantly affected by anthropogenic activities. Investigation of N mineralization and immobilization around this area could refelct both regional and typical characteristics. In this study, relcaimed brackish aquaculture ecosystems located on the west river bank of the Pearl River Estuary were selected, and a combination of sediment incubation experiment and ^{15}N stable isotope dilution method was employed. The main objectives of this study are to: (1) quantify sediment N mineralization and immobilization rates; (2) compare the effects of different cultured species (seabass, white shrimp, and green crab) on sediment N mineralization and immobilization, and identify the key controlling factors of these two processes; (3) preliminarily estimate sediment N mineralization and immobilization fluxes in the Guangdong-Hong Kong-Macao Greater Bay Area, and provide scientific basis for ecological effect evaluation as well as policy formulation and management in the area.

2 Materials and method

2.1 Study area and sampling

The Pearl River Delta (PRD, 112.9–114.4°E, 21.82–23.25°N) located on southern China covers an area of ~54,754 km^2 and is surrounded by several highly populated cities such as Hong Kong, Guangzhou, Macau, and Shenzhen with a total population of over 78.61 million people in 2021 (Li et al., 2000; Liu et al., 2018). It is plain river network area with the slope of 0.1–0.2‰

and the density of river network of ~0.8 km km^{-2}, which is characterized by subtropical humid climate with an annual average temperature of 21.8°C and an annual average rainfall of 1747.4 mm (Wang et al., 2012). A small irregular semidiurnal tide dominates this area with the average of 0.86 to 1.6 m and maximum of 2.29 to 3.36 m (Wang et al., 2012). The shallow aquaculture pools that were created by the removal of original marsh vegetation (mangrove). The PRD is experiencing massive industrialization and urbanization nowadays and makes great contributions to China's economy. Take the year of 2021 as an example, this area provided ~12.3% of the national gross domestic product ($1406.18 billion) according to the China Statistical Yearbook 2022. Meanwhile, the coastal habitats of the PRD have been highly productive ecosystems, being an extremely important aquaculture area of China (Zhou et al., 2019). Coastal wetlands reclamation for aquaculture pond took the largest proportion of the total conversion from natural wetlands (estuarine water, mangrove forest and salt marsh) towards constructed wetlands in this region. For example, the breeding area of the PRD increased about threefold from 256.01 km^2 in 1980 to 826.72 km^2 in 2015 (Zhou et al., 2019). With rapid economic growth and urbanization of the PRD, local environment has suffered from serious environmental problems, especially the high N loading, which has great effects on water quality and N cycling processes (Dai et al., 2008; Li et al., 2013; Wu et al., 2020).

Our samples were selected from three separate coastal ponds aquaculturing different economic species on the western bank of the Pearl River Estuary, one for fish (*Perca fluviatilis*), one for shrimp (*Penaeus vannamei*), and one for crab (*Scylla serrata*) (Figure 1). The sediments were collected using a core cylinder, a PVC pipe handle and a one-way valve from these sites in winter (January 19, 2019) and summer (July 12, 2019). At each site, triplicate surface sediments (0–5 cm) were taken from the cores, and sealed with air-tight, acid-cleaned plastic bags. Overlying water samples of each site were also collected in polyethylene bottles and filtered through 0.2 μm filters (Millipore, Bedford, United States). All the samples were transported to the laboratory on ice within 8 h. In the laboratory, filter samples were immediately stored at -20°C. Sediments of each sampling site were mixed thoroughly under a helium condition, and subsequently divided into three parts. One part was stored at 4°C for measuring microbial biomass carbon (MBC) and N-cycling rates, the second part was frozen at -20°C for determination of physicochemical parameters, and the third part was preserved at -80°C for molecular analysis.

2.2 Determination of physicochemical properties

Sediment water content was determined according to the weight loss from fresh sediment after freeze-drying until constant weight. Sediment pH was determined by measuring the pH of the mixture of fresh sediment and Milli-Q (MQ) water (1:2.5 in v/v) (Zhang et al., 2015). Sediment NH_4^+, NO_2^-, and NO_3^- were extracted by 2 M KCl purged with N_2 for 30 min and measured using 2 M KCl as standard curve substrate (Hou et al., 2013). Total extractable iron (Fe) and ferrous oxide (Fe^{2+}) were extracted by 0.5 M HCl and 0.25 M hydroxylamine hydrochloride (both purged with N_2 for ~15 min) from fresh sediments, and the concentrations were determined using ferrozine-based colorimetric method using the spectrophotometer. The concentrations of ferric iron (Fe^{3+}) were calculated by subtracting Fe^{2+} from Fe (Lovley and Phillips, 1987; Hu et al., 2022). Sediment texture was determined by laser particle size analyzer LS13 320 (Hou et al., 2013). After effective leaching of carbonates with 1 M HCl, sediment total organic carbon (TOC) and total nitrogen (TN) were measured on an elemental analyzer (Vario EL, Elementar, Germany) (Zhang et al., 2015; Wu et al., 2021). Sediment stable organic carbon isotopic composition ($\delta^{13}C_{org}$) were analyzed on a Thermo MAT 253Plu isotope ratio mass spectrometer. After oxidation with 333 mmol L^{-1} $KMnO_4$, sediment easily oxidized organic carbon (EOC) was measured on a spectrophotometer colorimetry (Vieira et al., 2007). Sediment dissolved organic carbon (DOC) was extracted with MQ water and determined with a Shimadzu TOC-TN analyzer (Shimadzu Crop., Kyoto, Japan). Sediment MBC were extracted with K_2SO_4 and determined through chloroform fumigation-extraction method (Vance et al., 1987; Beck et al., 1997).

2.3 Measurements of N transformation rates

Gross N mineralization (GNM) and NH_4^+ immobilization (GAI) rates were determined using ^{15}N isotope dilution technique (Kirkham and Bartholomew, 1954). Briefly, twelve centrifuge tubes (50 mL) were prepared for each sample, and 5 g fresh sediment was weighed into each centrifuge tube. For determination of the GNM and GAI rates, six centrifuge tubes with a mixture of sediment and saltwater (1:5 in w/w) were vortexed thoroughly. Tubes were sealed and preincubated for 24 h under *in situ* temperature in dark on a shaker table (150 rpm). After the preincubation, $^{15}NH_4^+$ (99 atom%, $^{15}NH_4Cl$) was added into the tubes, the final concentration of ^{15}N was about 2 μg g^{-1} and the final percentage of ^{15}N was about 10–15%. Triplicate initial samples were terminated by adding 1 mL 50% Zinc chloride ($ZnCl_2$) solution and immediately frozen at -20°C, and triplicates incubation samples were sealed and were put back to the incubator. After 24-hour incubation, final samples were terminated and immediately frozen at -20°C.

$$GNM = \frac{M_i - M_f}{t} \times \frac{log(H_i M_f / H_f M_i)}{log(M_i / M_f)} \quad (1)$$

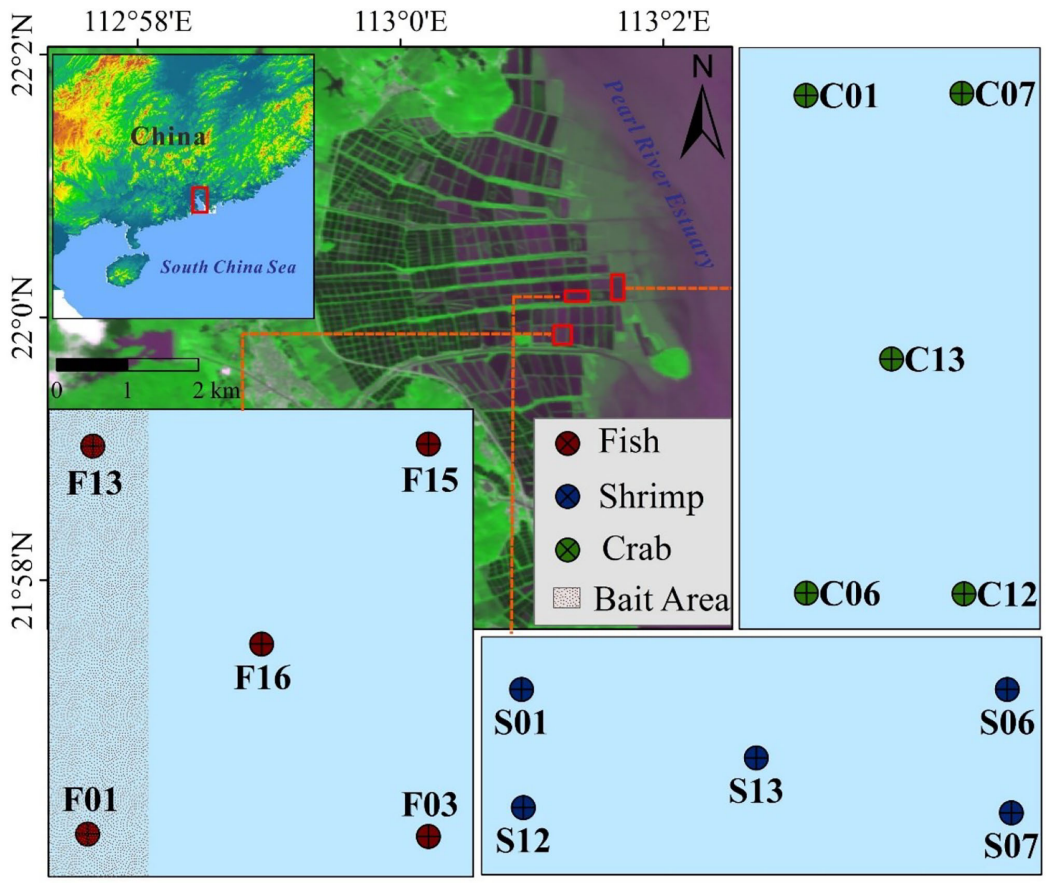

FIGURE 1
Study area and sampling sites of three types of reclaimed aquaculture ecosystem in the Pearl River Estuary.

$$GAI = \frac{Mi - Mf}{t} \times \frac{log(H_i/H_f)}{log(M_i/M_f)} \quad (2)$$

M_i and M_f (μg N g^{-1} dry weight) are total NH_4^+ concentrations of initial (before incubation) and final (after incubation) samples; $H_i$and H_f (μg N g^{-1} dry weight) are $^{15}NH_4^+$ concentrations of initial and final samples; t (d) is the incubation time (24 h).

The relative NH_4^+ immobilization (RAI) is calculated as the ratio of GAI to GNM rates, and RAI value of ≥ 1 indicates a N-limited sediment, whereas a value of approximately 0.5 indicates N saturation (Aber, 1992). The percentage of NH_4^+ mineralized per day (PAM%) was referred to as the rates of GNM divided by sediment N contents, which can indicate the sediment available N by the internal N cycle.

2.4 Microbial analysis

Sediment DNA was extracted by the FastDNA spin kit for sediment (MP Biomedical, United States) based on the manufacturer's instructions. The concentration and purity of extracted DNA were determined by NanoDrop spectrophotometer (NanoDrop 2000C, Thermo Scientific, United States), and the fragments size and quality were evaluated by 1.0% agarose gel electrophoresis. Quantitative PCR (qPCR) assays were used to measure microbial gene abundances on an ABI 7500 Fast real-time qPCR system (Applied Biosystems, United States). For bacterial 16S rRNA gene and fungal ITS gene, primer pairs 341F/519R (Bachar et al., 2010) and SSU081 and 1196R were used (Rousk et al., 2010), respectively. The standard curves for these two genes were created using a 10-fold dilution series (10^2–10^9 copies) of the

standard plasmids DNA. Each sample was measured in triplicates.

2.5 Calculations and statistical analyses

Statistical analysis was performed using SPSS 19.0 (SPSS Inc., United States). All variables were tested for normality by Shapiro-Wilk test, and the non-normality variable were normalized by using Blom's formula. Statistically significant difference of N transformation rates and sediment physicochemical properties between three ponds were determined by one-way ANOVA, Turkey test (p<0.05, equal variances assumed) or Dunnett's test (p<0.05, equal variances not assumed). The correlations were analyzed by and linear regression analyses and Pearson test (two-tailed, p<0.05). The graphs were drawn by ArcGIS 10.2 (ArcMap 10.2, ESRI, United States) and Origin 2019 (OriginLab Corporation, United States).

3 Results

3.1 Physicochemical properties of overlying water

Physicochemical properties of overlying water in the three types of relcaimed aquaculture ponds are shown in Table 1 and Table S1. During winter sampling, crab pond was in the early period of pond-drying, and only a litter overlying water was remaing in the crab ponds, while the shrimp pond was in the late drying period, and the surface sediments were dried and cracked. Therefore, overlying water of the shrimp and crab ponds in winter was not sampled because of that those two ponds were in drying and dreging period. One-way ANOVA showed that overlying water salinity, pH, NH_4^+, NO_3^-, and NO_2^- of the fish pond showed significant seasonal differences (p<0.05), while no significant seasonal difference was found for the dissolved oxygen (DO) (p>0.05). The salinity and pH in winter was higher than those in summer. Influenced by aquaculture activities, NH_4^+, NO_2^-, and NO_3^- were all significantly higher in summer than those in winter (p<0.05). In summer, both DO and salinity showed significantly differences among three ponds (p<0.05 for all). The highest DO was observed in the shrimp ponds (10.30 ± 1.05 mg L^{-1}) followed by the crab ponds (7.90 ± 0.52 mg L^{-1}) and fish ponds (5.11 ± 0.14 mg L^{-1}), which may potentailly result from the most operating waterwheel-type aerators in the shrimp and crab ponds. Consistenly, the highest salinity was measured in the crap ponds (2.85 ± 0.00 ‰) followed by the crab ponds (2.25 ± 0.18 ‰) and fish ponds (0.9 ± 0.04 ‰). The overlying water quality of these ponds were relatively well controlled. Overlying water NH_4^+ and NO_2^- of the fish ponds were both significantly higher that those in shrimp and crab ponds (p<0.05).

3.2 Physicochemical properties of sediments

Physicochemical properties of surface sediments in the relcaimed aquaculture ponds are shown in Table 2 and Table S2.

TABLE 1 Physiochemical parameters of overlying water in different reclaimed aquaculture ponds.

Physiochemical parameters		Fish		Shrimp	Crab
		Summer	Winter	Summer	Summer
DO (mg L^{-1})	Range	4.43–5.25	4.57–5.05	9.34–11.18	7.72–8.55
	Mean ± SD	4.93 ± 0.32^{Ac}	4.79 ± 0.23^{A}	10.22 ± 0.65^{a}	8.13 ± 0.30^{b}
Salinity (‰)	Range	0.84–0.94	1.53–1.56	2.01–2.57	2.85–2.85
	Mean ± SD	0.90 ± 0.04^{Bc}	1.55 ± 0.01^{A}	2.25 ± 0.20^{b}	2.85 ± 0.00^{a}
pH	Range	8.13–8.18	8.37–8.65	8.93–9.24	8.85–8.90
	Mean ± SD	8.15 ± 0.02^{Bc}	8.53 ± 0.11^{A}	9.10 ± 0.12^{a}	8.88 ± 0.02^{b}
NH_4^+ (μM)	Range	5.90–6.90	0.25–1.66	0.44–1.90	0.68–3.04
	Mean ± SD	6.34 ± 0.47^{Aa}	0.64 ± 0.58^{B}	1.03 ± 0.58^{c}	1.92 ± 0.95^{b}
NO_2^- (μM)	Range	0.59–0.64	0.20–0.27	0.04–0.09	0.02–0.09
	Mean ± SD	0.61 ± 0.02^{Aa}	0.24 ± 0.03^{B}	0.07 ± 0.02^{b}	0.04 ± 0.02^{c}
NO_3^- (μM)	Range	36.70–39.09	1.90–4.90	34.86–43.56	34.72–41.27
	Mean ± SD	37.91 ± 0.96^{Aa}	3.89 ± 1.18^{B}	37.42 ± 3.53^{a}	37.57 ± 2.76^{a}

Statistically significant difference between seasons (p<0.05 according the F statistics) is labeled in the different uppercase letters, and the significant difference between aquaculture ponds (Turkey multiple comparison p<0.05) is labeled in the different lowercase letters.

10.3389/fmars.2022.1093279

TABLE 2 Spatiotemporal variations of sediment physicochemical properties in different reclaimed aquaculture ponds.

Physicochemical properties	Fish pond		Shrimp pond		Crab pond	
	Summer	Winter	Summer	Winter	Summer	Winter
Temperature (°C)	30.64 ± 0.18^{Ac}	17.5 ± 0.07^{Ba}	32.68 ± 0.40^{Aa}	17.26 ± 0.05^{Bc}	32.22 ± 0.15^{Ab}	17.4 ± 0.07^{Bb}
Moisture content	0.36 ± 0.06^{Aa}	0.36 ± 0.04^{Ab}	0.54 ± 0.19^{Aa}	0.29 ± 0.04^{Bc}	0.44 ± 0.08^{Aa}	0.43 ± 0.05^{Aa}
Bulk density (g mL^{-1})	1.63 ± 0.14^{Aa}	1.69 ± 0.05^{Ab}	1.38 ± 0.25^{Ba}	1.85 ± 0.15^{Aa}	1.51 ± 0.10^{Aa}	1.51 ± 0.06^{Ac}
NH_4^+ (μg N g^{-1})	12.20 ± 4.12^{Aa}	6.81 ± 1.09^{Ba}	31.65 ± 18.26^{Ba}	6.30 ± 4.08^{Ab}	21.69 ± 17.22^{Aa}	1.78 ± 0.39^{Bc}
NO_2^- (μg N g^{-1})	0.04 ± 0.01^{Bb}	0.15 ± 0.03^{Aa}	0.12 ± 0.09^{Aa}	0.46 ± 0.64^{Aa}	0.04 ± 0.02^{Bb}	0.17 ± 0.08^{Aa}
NO_3^- (μg N g^{-1})	3.18 ± 0.40^{Aa}	1.58 ± 0.17^{Ba}	5.10 ± 2.19^{Aa}	7.29 ± 12.10^{Aa}	4.01 ± 0.58^{Aa}	1.77 ± 1.04^{Ba}
Fe^{2+} (mg Fe g^{-1})	8.56 ± 2.94^{Ac}	3.09 ± 0.52^{Ba}	19.62 ± 8.34^{Aa}	0.43 ± 0.28^{Ba}	13.04 ± 3.30^{Ab}	2.92 ± 0.62^{Ba}
Fe^{3+} (mg Fe g^{-1})	5.71 ± 2.20^{Ab}	2.20 ± 0.97^{Ba}	1.37 ± 0.54^{Ac}	3.28 ± 1.60^{Aa}	6.62 ± 6.62^{Aa}	1.81 ± 0.34^{Ba}
Fe^{2+}/Fe^{3+}	1.95 ± 1.80^{Ac}	1.72 ± 0.95^{Aa}	14.97 ± 6.62^{Aa}	0.13 ± 0.05^{Ba}	2.13 ± 0.98^{Ab}	1.61 ± 0.20^{Aa}
Median grain size (μm)	47.53 ± 11.17^{Aa}	24.88 ± 9.73^{Ba}	29.94 ± 13.00^{Ab}	16.29 ± 10.59^{Aa}	16.16 ± 4.02^{Ac}	18.27 ± 9.21^{Aa}
TOC (mg C g^{-1})	10.49 ± 2.10^{Aa}	11.03 ± 3.02^{Aa}	16.46 ± 7.75^{Aa}	12.30 ± 4.61^{Aa}	11.04 ± 0.80^{Aa}	10.05 ± 0.50^{Ba}
TN (mg N g^{-1})	1.00 ± 0.15^{Aa}	0.89 ± 0.17^{Aa}	2.15 ± 1.25^{Aa}	1.57 ± 0.66^{Aa}	1.28 ± 0.16^{Aa}	1.09 ± 0.09^{Ba}
TOC/TN	10.47 ± 0.66^{Aa}	12.71 ± 4.25^{Aa}	8.05 ± 1.16^{Ac}	7.93 ± 0.69^{Ac}	8.69 ± 0.72^{Ab}	9.28 ± 0.49^{Ab}
$\delta^{13}C_{org}$ (‰)	-24.65 ± 0.15^{Aa}	-24.98 ± 0.38^{Ac}	-23.77 ± 0.71^{Aa}	-24.02 ± 0.81^{Aa}	-24.32 ± 0.66^{Aa}	-24.27 ± 0.23^{Ab}
EOC (mg C g^{-1})	4.77 ± 1.95^{Aa}	3.25 ± 0.80^{Aa}	8.19 ± 4.12^{Aa}	2.52 ± 0.95^{Ba}	5.79 ± 0.74^{Aa}	2.67 ± 1.35^{Ba}
DOC (mg C g^{-1})	0.10 ± 0.04^{Aa}	0.11 ± 0.04^{Aa}	0.14 ± 0.05^{Aa}	0.06 ± 0.01^{Bc}	0.11 ± 0.01^{Aa}	0.10 ± 0.01^{Ab}
MBC (mg C g^{-1})	0.13 ± 0.05^{Aa}	0.13 ± 0.03^{Aa}	0.18 ± 0.08^{Aa}	0.06 ± 0.02^{Bc}	0.15 ± 0.04^{Aa}	0.09 ± 0.01^{Bb}
Bacterial (×10^9 copies g^{-1})	8.94 ± 4.18^{Aa}	8.31 ± 2.16^{Aa}	8.31 ± 2.65^{Aa}	3.26 ± 1.90^{Bc}	6.22 ± 2.60^{Aa}	3.80 ± 0.94^{Ab}
Fungal (×10^7 copies g^{-1})	7.11 ± 4.74^{Aa}	5.19 ± 2.44^{Aa}	6.20 ± 3.07^{Aa}	4.21 ± 2.59^{Aa}	3.07 ± 1.28^{Aa}	3.38 ± 1.23^{Aa}

Statistically significant difference between seasons (F statistical variance homogeneity test $p<0.05$) is labeled in the different uppercase letters, and the significant difference between aquaculture ponds (Turkey multiple comparison $p<0.05$) is labeled in the different lowercase letters.

Due to geographic proximity, most surface sediment physicochemical properties (excluding NO_2^-, Fe^{2+}, and TOC/TN) were found no significant spatial variation among those three ponds in summer. In winter, the shrimp and crab ponds were in the drying and dredging period, and the surface sediments of the shrimp ponds were dried and cracked. Thus we found that surface sediment moisture content, Fe^{2+}, EOC, DOC, and MBC of shrimp pond in winter were significantly lower than those in summer ($p<0.05$ for all), and the sediment bulk density in winter were significantly higher that those in summer ($p<0.05$). Meanwhile, several sediment physicochemical properties in shrimp pond were significantly higher (including bulk density and $\delta^{13}C_{org}$) or lower (including moisture content, TOC/TN, DOC, MBC, and bacterial 16S rRNA abundances) that those in other ponds in winter ($p<0.05$ for all). In crab pond, sediment temperature, NH_4^+, NO_3^-, Fe^{2+}, Fe^{3+}, TOC, TN, EOC, and MBC in summer were significantly higher that those in winter ($p<0.05$ for all). In addition, all the surface sediments in those three ponds were mainly composed of fine silt and clay with low median grain size (7.69–57.77 μm).

3.3 Spatiotemporal variations of N transformation rates and microbial abundances

The spatiotemporal distributions of sediment GNM, GAI, RAI, PAM, and microbial abundances in three reclaimed aquaculture ponds were shown in Figure 2. GNM rates varied from 5.77 to 14.58 μg N g^{-1} d^{-1} with an average value of 9.64 ± 3.31 μg N g^{-1} d^{-1} in summer and from 1.75 to 6.45 μg N g^{-1} d^{-1} with an average value of 3.60 ± 1.19 μg N g^{-1} d^{-1} in winter. Significant seasonal variations in GNM rates were observed in those three ponds, with significantly higher values in summer than in winter ($p<0.05$ for all, Figure 2A). No significant difference in GNM rates occurred among three ponds in summer ($p>0.05$ for all, Figure 2A). In comparison, in summer, the GNM rates in crab pond were significantly lower than those in the other two ponds ($p<0.05$ for both, Figure 2A).

The GAI rates ranged from 5.15 to 13.68 μg N g^{-1} d^{-1} with an average of 7.71 ± 2.49 μg N g^{-1} d^{-1} in summer and from 1.67 to 5.66 μg N g^{-1} d^{-1} with an average of 3.17 ± 1.06 μg N g^{-1} d^{-1} in

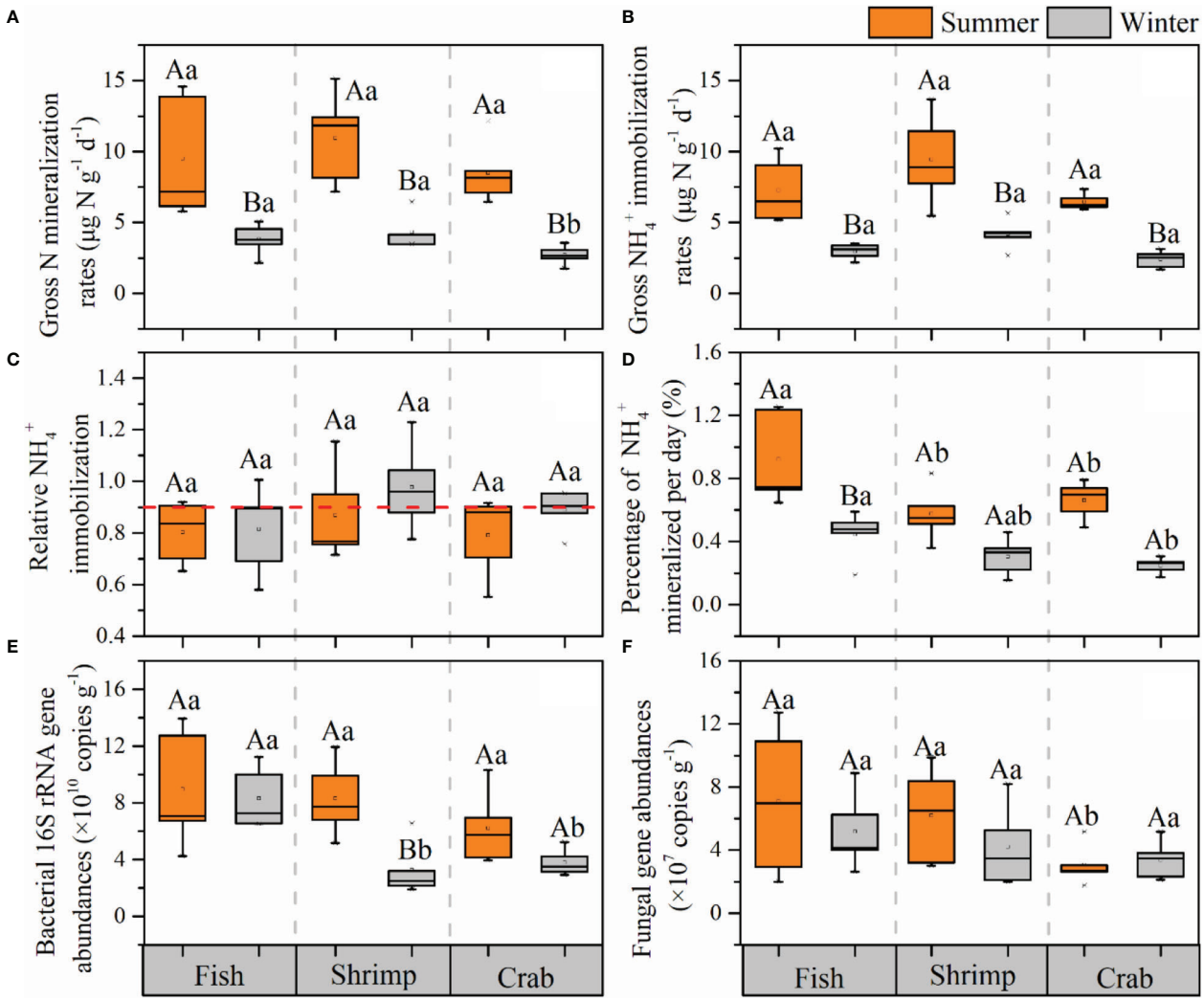

FIGURE 2
Spatiotemporal variations of gross N mineralization rates **(A)**, gross NH_4^+ immobilization rates **(B)**, relative NH_4^+ immobilization **(C)**, percentage of NH_4^+ mineralized per day **(D)**, and microbial abundances **(E, F)** in the surface sediments of different reclaimed aquaculture ponds in summer and winter. Statistically significant difference between seasons is labeled in the different uppercase letters, and the significant difference between aquaculture ponds is labeled in the different lowercase letters.

winter. Similarly, GAI rates were higher in summer than in winter with a remarkable seasonal difference within these three ponds (p<0.05 for all, Figure 2B). Spatially, no significant spatial difference in GAI rates occurred among three ponds in both summer and winter (p>0.05 for all, Figure 2B). In addition, GNM rates were significantly positively correlated with GAI rates in the whole study area in both summer and winter (p<0.05 for both, Figure S1).

The relative NH_4^+ immobilization (RAI) values ranged between 0.55 and 1.15 in summer and between 0.60 and 1.23 in winter (Figure 2C). There was no significant seasonal variation in RAI in those three ponds, and no significant spatial difference among three ponds (p > 0.05 for all; Figure 2C). A previous study has confirmed that RAI ≤ 0.5 and RAI > 0.9 indicated N-saturated environment and N-limited environment, respectively (Aber, 1992). Here, the RAI values in most sampling sites were between 0.5 and 0.9, indicating these reclaimed aquaculture ecosystems were able to maintain N balance.

PAM values ranged from 0.36% to 1.25% in summer and from 0.15% to 0.59% in winter (Figure 2D). Spatially, PAM in fish pond were significantly higher than those in other ponds (p< 0.05 for all; Figure 2D). The PAM in summer (0.92 ± 0.30%) was significantly higher than that in winter (0.45 ± 0.15%) in fish

pond ($p< 0.05$; Figure 2D). In shrimp and crab ponds, PAM in summer were also higher than those in winter, but with no significant seasonal difference ($p > 0.05$; Figure 2D).

The bacterial 16S rRNA gene abundances were in a range of 3.93–13.94×10^9 copies g^{-1} with an average of 7.82 ± 3.22×10^9 copies g^{-1} in summer. In winter, the range and average value decreased to 1.91–11.22×10^9 copies g^{-1} and 5.12 ± 2.85×10^9 copies g^{-1}. The bacterial 16S rRNA abundances in summer were significantly higher than those in winter in shrimp pond ($p<$ 0.05; Figure 2E).The values in sediment of fish pond were significantly higher than those in other two ponds in winter ($p<0.05$ for both, Figure 2E). The fungal ITS gene abundances were in a range of 1.76–12.73×10^7 copies g^{-1} with an average of 5.46 ± 3.57×10^7 copies g^{-1} in summer and in a range of 2.00–8.88×10^7 copies g^{-1} with an average of 4.26 ± 2.15×10^7 copies g^{-1} in winter, showing no significant temporal differences in those three ponds and no spatial differences among three ponds ($p<$ 0.05 for all; Figure 2F).

3.4 Effects of physicochemical properties on N-cycling processes

Considering all sampling sites, GNM and GAI rates showed significant positive correlations with sediment temperature, organic matter (TOC, TN, EOC, DOC, and MBC), microbial abundances (bacterial 16S rRNA and fungal abundances), Fe^{2+}, NH_4^+, moisture content, as well as overlying water DO and NO_3^-, while they were correlated negatively with sediment bulk density ($p<0.05$; Table 3). PAM were significantly positively correlated with sediment MBC, microbial abundances, Fe^{2+}, Fe^{3+}, as well as overlying water DIN ($p<0.05$; Table 3). RAI were positively correlated with sediment $\delta^{13}C_{org}$ and correlated negatively with sediment microbial abundances, MBC, DOC, and TOC/TN ($p<0.05$; Table 3).

4 Discussion

4.1 Effects of physicochemical properties on sediment N mineralization and immobilization

Temperature could have directly impacts on microbial physiological activities through the regulation of enzyme activities and is considered as a crucial factor of N mineralization and immobilization (Yang et al., 2010). In this study, GNM and GAI rates were both significantly higher in summer than in winter among those three ponds ($p<0.05$ for all). The seasonal variations are mainly due to temperature differences between summer (31.81 ± 0.86°C) and winter (17.54 ± 0.05°C). Also, the ratios of N-cycling rates in summer to rates in winter were used to characterize the temperature sensitivity of N mineralization and immobilization rates. A previous study found that total N immobilization rate is very sensitive to temperature while N mineralization rate shows relatively less sensitivity under low temperature condition (5–15°C) (Andersen and Jensen, 2001). However, we found that no significant difference between the temperature sensitivity of GNM and GAI (Figure 3A). The major reson is that the winter temperature in our study is over 15°C, and the temperature sensitivity of N mineralization has been found to decrease with increasing temperature (Kirschbaum, 1995). In addition, no significant spatial difference in temperature sensitivity of N mineralization and immobilization rates among those three ponds (Figure 3A). This is mainly due to similar physicochemical properties (including sediment grain size, organic matter, DIN, and TOC : TN) among those three ponds, and previous studies have found that temperature sensitivity of N mineralization and immobilization rates mainly depended on the above physicochemical properties in agricultural ecosystems (Liu et al., 2017; Miller and Geisseler, 2018).

Organic matter of aquaculture sediments originates from both autochthonous sources (microalgae, sediment and particulate organic matter) and bait inputs (Chen et al., 2016). According to the values of TOC/N ratio and $\delta^{13}C_{org}$, we found the surface sediment organic matter were mainly from marine algae, marine DOC, and marine POC (Figure 3B). This is caused mainly by the fact that the aquaculture ponds were located on the estuary, where a significant proportion of overlying water is derived from marine. More importantly, the main ingredients (~60%) of bait are fish meal and fish oil (Park et al., 2021), and they were made from marine fish (e.g. *Engraulis japonicus*).

As we all know, organic matter acting as energy source of microorganisms and substrates of N mineralization, which plays an important role in microbial-mediated N-cycling processes. To clarify how labile C impacts on N mineralization and immobilization in the reclaimed aquaculture sediments, several labile organic carbons including sediment EOC, DOC, and MBC, as well as potential N mineralization and immobilization rates, were measured. When considering all sites, the correlation strengths between labile organic carbons (EOC, DOC, and MBC) and N mineralization and immobilization rates were much higher than those between TOC and the rates. The order of above correlations was MBC>EOC>DOC>TOC (Table 3). When considering seasonal effects, we found that this regularity and trend was only found in summer (Figure 4), and the order of above correlations was changed slightly (MBC>DOC>EOC>TOC). This finding agreed well with several previous studies, which found that high availability of organic matter is favorable for soil/sediment N mineralization process in coastal wetland (Li et al., 2020; Yang et al., 2022), estuary (Huang et al., 2022) and forest (Jones and

TABLE 3 Correlations between physicochemical properties and N mineralization and immobilization rates.

Physicochemical properties		GNM	GAI	RAI	PAM
Overlying water	DO	0.49*	0.58**	0.06	-0.16
	Salinity	0.11	0.14	0.00	-0.33
	pH	0.27	0.35	0.03	-0.39
	NH_4^+	0.35	0.25	-0.17	0.70**
	NO_2^-	-0.02	-0.07	-0.01	0.49*
	NO_3^-	0.67**	0.74**	0.07	0.48*
Sediment	Temperature	0.79**	0.79**	-0.23	0.68**
	Moisture content	0.56**	0.52**	-0.27	0.00
	Bulk density	-0.55**	-0.53**	0.24	-0.14
	NH_4^+	0.65**	0.67**	-0.18	0.24
	NO_2^-	-0.19	-0.15	0.17	-0.27
	NO_3^-	0.14	0.16	0.05	-0.01
	Fe^{2+}	0.73**	0.76**	-0.17	0.39*
	Fe^{3+}	0.30	0.19	-0.28	0.52**
	Fe^{2+}/Fe^{3+}	0.27	0.31	-0.02	-0.02
	Medium grain size	0.20	0.18	-0.01	0.25
	SSA	0.11	0.12	-0.10	-0.24
	TOC	0.54**	0.52**	-0.20	-0.06
	TN	0.49**	0.50**	-0.04	-0.20
	TOC/TN	-0.13	-0.22	-0.37*	0.27
	$\delta^{13}C_{org}$	0.01	0.22	0.45*	-0.02
	EOC	0.79**	0.76**	-0.25	0.30
	DOC	0.62**	0.53**	-0.44*	0.32
	MBC	0.77**	0.64**	-0.52**	0.38*
	Bacterial	0.71**	0.53**	-0.61**	0.63**
	Fungal	0.63**	0.53**	-0.38*	0.43*

*, significant correlation (two-tail test, $p<0.05$); ** highly significant correlation (two-tail test, $p<0.01$).

Kielland, 2012). Thus, our results suggest that organic quality rather than quantity was more crucial to the control of N mineralization and immobilization in aquaculture sediments.

No significant correlations existed between organic matter and N mineralization and immobilization rates in winter, this may be probably due to the profound effect of human activities (pond-drying) on these different aquaculture ponds. As mentioned in the preceding text, fish ponds are still being farmed, and shrimp and crab ponds are in a resting state in winter. Namely, shrimp and crab ponds were in the drying and dredging period, and surface sediment of the shrimp ponds was dried and cracked. Firstly, pond-drying can significantly reduce the sediment moisture content in shrimp ponds in winter, previous studies have found that N mineralization increased with the increasing soil/sediment moisture (Jia et al., 2019; Li et al., 2020; Huang et al., 2022). Sediment moisture is involved in the metabolism of microbes and is also the irreplaceable medium linking substrates supply and microbial activity (Greaver et al., 2016). Elevated sediment moisture has also been reported to increase the decomposition and leaching of organic matter and extracellular enzyme activities, promoting soil N transformations (Mooshammer et al., 2014; Greaver et al., 2016; Jia et al., 2017). Also, increased soil moisture could limit oxygen to penetrate soils and further lead to more strongly anoxic and reducing environments, thereby facilitating denitrification and N mineralization in coastal wetlands

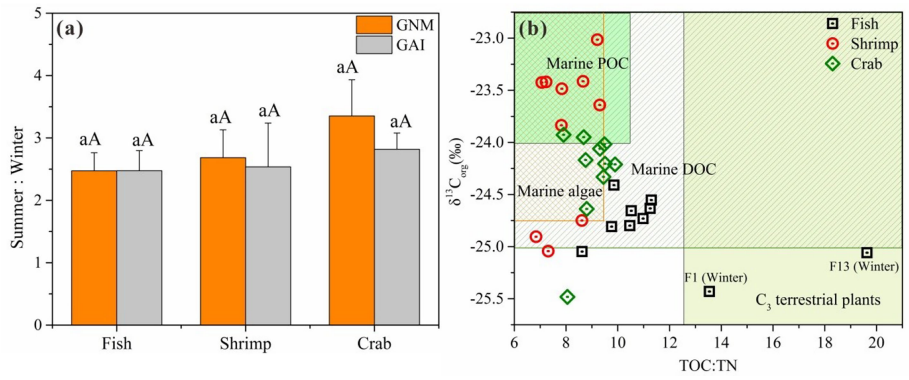

FIGURE 3
The temperature sensitivity of sediment GNM and GAI rates to seasonal change in those three ponds **(A)**; Determination of organic matter sources from autochthonous or allochthonous **(B)**. The backgrond ranges of organic matter difference sources were obtained by Lamb et al. (2006). Statistically significant difference between seasons is labeled in the different uppercase letters, and the significant difference between aquaculture ponds is labeled in the different lowercase letters. The error bar represents the standard error.

(Jia et al., 2019). Secondly, our measured sediment labile organic matter contents (including EOC, DOC, and MBC) in shrimp pond were significantly less in winter compared with those in summer (Table 2, $p<0.05$ for all). Thus, pond-drying can accelerate the decomposition of surface sediment organic matter, resulting in decreased the supply of energy source and substrate for microbial growth and mineralization. In addition, pond-drying can significantly reduce microbial biomass (MBC) and bacterial abundances in shrimp pond (Table 2, $p<0.05$ for both), thereby regulating the N mineralization and immobilization. Therefore, most physicochemical properties were significantly changed with aquaculture management activities (pond-drying), resulting in the profound reduction of sediment N mineralization and immobilization in aquaculture ecosystems.

No significant seasonal and spatial difference in microbial abundances was observed in our study excluding those in shrimp ponds in winter (Table 2), this is largely due to small summer-winter temperature differences and low spatial heterogeneity in sediment physicochemical properties. When the surface sediment was dried and cracked after long-term pond-drying, this aquaculture management activity can significantly reduce the microbial biomass and bacterial abundances, but not for fungal abundances (Table 2). This is mainly due to fungi can be remarkably drought tolerant, and they can remain active and even grow under extremely dry conditions (Treseder et al., 2010; Yuste et al., 2011). However, our study lack of data about microbial community structure and diversity. A previous study showed that pond-drying can change the sediment microbial community structure, and the abundance of *Proteobacteria*, *Nitrospirae* and *Bacteroidetes* were increased, while the pernicious microbe such as *Cyanobacteria* was decreased after pond-drying in aquaculture ecosystem (Wang et al., 2020). In addition, natural sunlight has effect on the abundance and microbial community structure in the sediments during pond-drying. Thus, we boldly speculated that pond-drying can alter microbial community composition from anaerobic, fast-growing, and copiotrophic to aerobic, slow-growing, and oligotrophic, thus promote the ecosystem reparation effectively.

Many previous studies have reported that N mineralization and immobilization rates were affected by the microbial biomass and activities, and thus they were generally closely related to the microbial respiration rates, enzymatic activities (including extracellular and intracellular enzymes), and ATP content (Bengtsson et al., 2003; Silva et al., 2005). N mineralization and immobilization rates were also controlled by the microbial biomass (MBC) and abundances (including bacterial 16S rRNA and fungal abundances) in this study (Table 4), which is consistent with previous sudies in many estuarine and coastal zone (Lin et al., 2016a; Li et al., 2020; Huang et al., 2022; Yang et al., 2022). Thus, microbial abundances could be considered as important indicators of N mineralization and immobilization rates in aquaculture sediments.

In addition, GNM and GAI rates were also positively correlated with overlying water NO_3^- (Table 3, $p<0.05$). Previous studies have revealed significant influence of environmental effective electron acceptors on N mineralization. For example, NO_3^-, as an electron acceptor of oxidized organic matter, could promote N mineralization (equation 3) and make high contribution (15 −35%) to the mineralizaiont of organic matter especially under

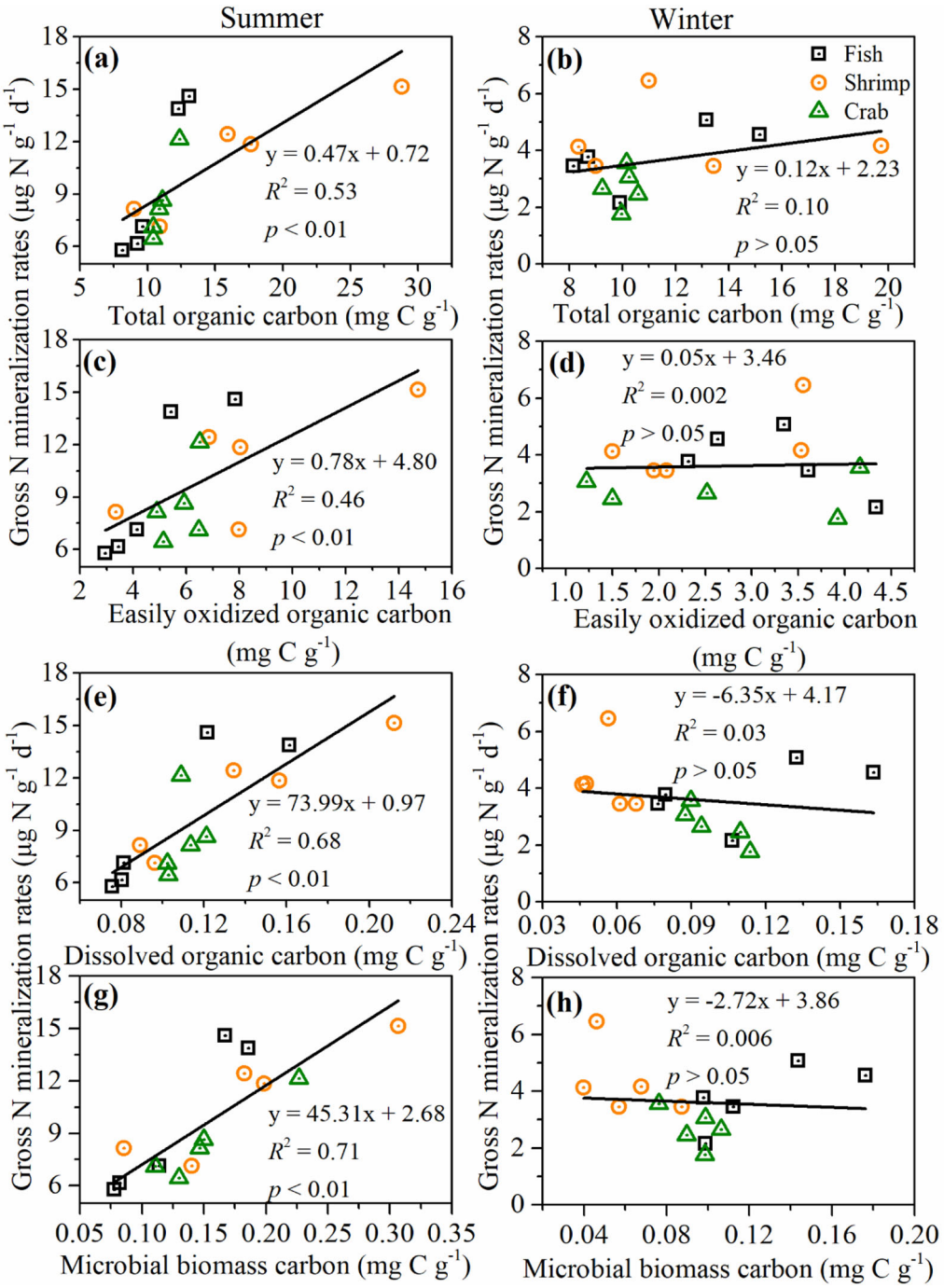

FIGURE 4
Correlations between different organic matter compounds and gross N mineralization rates in the surface sediments of different reclaimed aquaculture ponds. **(A, B)** Total organic carbon; **(C, D)** easily oxidized organic carbon; **(E, F)** dissolved organic carbon; and **(G, H)** microbial biomass carbon.

anoxic conditions (Khalil et al., 2018). Under anaerobic conditions, NO_3^-, Fe^{3+}, SO_4^{2-} as well as iron and manganese ions often work as active electron acceptors for coupling redox reactions with sediment organic matter (equation 4 and 5) (Pena et al., 2010). As sediment is flooded for long time and the vertical penetration ability of oxygen from overlying water into sediment is relatively weak, anaerobic conditions for the aforementioned reactions could be created in aquaculture ecosystem. Additional work regarding aerobic N mineralization can be done to compare the mechanisms between anoxic environments and aerobic environments.

$$(CH2O)106(NH3)16H3PO4 + 84.8HNO3 \rightarrow 106CO2 + 42.4N2 + 148.4H2O + 16NH3 + H3PO4 \quad (3)$$

$$(CH2O)106(NH3)16H3PO4 + 424FeOOH + 848H^{+} \rightarrow 106CO2 + 742H2O + 424Fe^{2+} + 16NH3 + H3PO4 \quad (4)$$

$$(CH2O)106(NH3)16H3PO4 + 53SO_4^{2-} + 106H^{+} \rightarrow 106CO2 + 106H2O + 53H2S + 16NH3 + H3PO4 \quad (5)$$

4.2 Environmental implications for N mineralization and immobilization in reclaimed aquaculture ecosystems

The average N mineralization and immobilization rates of reclaimed aquaculture ponds in this study area were lower than the rates of other aquaculture, urban river network, and mangrove wentland sediments, and higher than the rates of estuarine and coastal sediments (Table 4). The daily mineralization percentage of NH_4^+ was 0.55–1.23%, which as comparable with the value in coastal wetlands (Table 4). In addition, the value of RAI in this study (average: 0.86 ± 0.15; range: 0.58–1.23) implied that the ecosystem might be located between N limitation condition and N saturation condition (Aber, 1992). Significantly positive correlations between GNM and GAI identified in this study showed consistency with the observations in offshore seawater (Lin et al., 2016), wetlands (Jin et al., 2012), grassland (Corre et al., 2002) and forests (Bengtsson et al., 2003). It's also noteworthy that a combination of sediment incubation experiment and ^{15}N stable isotope dilution method was adopted in this study. As described in Lin et al. (2017), the added $^{15}NH_4^+$ may stimulate microbial responses, along with the dilution ratio of 1:5 (fresh sediment: water) and aerobic incubation conditions, the measured GNM and GAI might not reflect *in situ* activities. Nevertheless, it can still imply potential activities of N mineralization and immobilization in aquaculture surface sediments.

Sediment N mineralization and immobilization are important N-cycling processes in coastal wetland reclamation and aquaculture ecosystems, which plays vital roles in the reactive N balance. However, very few systematic studies investigated environmental properties, N mineralization and immobilization, and their relationships, especially in reclaimed aquaculture ecosystems. Here, based on GNM and GNI measured in this study, annual surface sediment (0–5 cm) N

TABLE 4 Comparison of N mineralization and immobilization in coastal, estuarine, and aquacultural ecosystems and our study area.

Study area	Sample type	NH_4^+ ($\mu g\ N\ g^{-1}$)	NO_3^- ($\mu g\ N\ g^{-1}$)	GNM ($\mu g\ N\ g^{-1}\ d^{-1}$)	GAI ($\mu g\ N\ g^{-1}\ d^{-1}$)	RAI	PAM %	References
Limfjorden, Denmark	Marine	–	–	2.55	–	–	–	(Blackburn, 1979)
Chesapeake Bay, United States	Marine	–	–	1.6-5.73	–	–	–	(Cufrey and Kemp, 1992)
Tilapia fish ponds, Netherlands	Aquacultural	1.15–9.33	–	9.30	–	–	–	(Jiménez-Montealegre et al., 2005)
Native coastal wetland, China	Coastal	–	–	1.71 –10.56	0.89–8.11	–	–	(Jin et al., 2012)
Yangtze Estuary, China	Coastal	–	–	0.02–5.13	–	–	0.01 –2.14	(Lin et al., 2016a)
East China Sea, China	Marine	0.45–8.58	0.62	0.11–6.10	0–9.82	–	0.01 –2.89	(Lin et al., 2016b)
River network in Shanghai, China	River	4.19 –383.25	0.11 –5.02	0.25 –25.83	0.24 –26.27	–	–	(Lin et al., 2017)
Min River Estuary, China	Estuarine	3.53–11.35	–	2.00–5.90	1.10–5.10	–	–	(Li et al., 2020)
Pearl River Estuary, China	Estuarine	3.10–6.91	0.89– 2.85	0–3.43	0.02–2.60	–	–	(Huang et al., 2021)
Pearl River Estuary, China	Estuarine	3.48–9.70	0.76 –2.11	0.15–1.99	0–1.96	0–1.81	0–0.423	(Huang et al., 2022)
Qi'ao Island, China	Coastal	10.43– 21.58	0.76– 3.14	2.69– 17.53	2.29– 21.38	0.79– 1.54	0.24– 0.86	(Yang et al., 2022)
Aquaculture ponds, China	Aquacultural	1.31–58.10	1.11 –8.72	1.75 –15.13	1.67 –13.68	0.55 –1.23	0.15 –1.25	This study

mineralization and immoblization rates in reclaimed aquaculture ecosystems of the Great Bay Area were calculated (equation 6).

$$F = \frac{1}{30}\left(\sum_{i=1}^{15} mi \cdot \quad di + \sum_{i=1}^{15} mj \cdot dj\right) \cdot \alpha \cdot s \cdot h \cdot t \qquad (6)$$

In which, F (t N yr^{-1}) is annual N mineralization or immoblization flux; mi and mj (μg N g^{-1} d^{-1}) is GNM or GAI of surface sediment (0–5 cm) in summer and winter, respectively; di and dj (g cm^{-3}) is bulk density of surface sediment (0–5 cm) in summer and winter, respectively; a is a unit conversion factor; s (m^2) is the area of reclaimed aquaculture ecosystems in the Great Bay Area (~395.57 km^2 according to remote sensing data in 2018 followed by the calclution using ArcGIS 10.2) (Figure S2); h (cm) is sampling depth (5 cm); t (d) is time (365 days).

In total, annual sediment N mineralization and immoblization rates in reclaimed aquaculture ecosystems are approximately 4.55×10^4 t N yr^{-1} and 3.68×10^4 t N yr^{-1}, respectively in the Guangdong-Hong Kong-Macao Greater Bay Area. GNM flux shows higher level than GAI flux, indicating that sediment is a nonnegligible DIN source in the aquaculture ecosystem, which plays a non-negligible role in the exacerbation of eutrophication in the estuarine and coastal ecosystems.

5 Conclusions

This study investigated N mineralization and immobilization rates in surface sediments of the reclaimed aquaculture ecosystems. GNM and GAI rates ranged from 1.75 to 15.13 μg N g^{-1} d^{-1} and from 1.67 to 13.68 μg N g^{-1} d^{-1}, respectively. Both GNM and GAI rates were significantly higher in summer than their counterparts in winter ($p<0.05$). No significant differences among three types of aquaculture ecosystems were observed ($p>0.05$). N mineralization and immobilization rates were significantly correlated with overlying water NO_3^-, as well as sediment moisture content, bulk density, organic matter, Fe^{2+}, and microbial abundances. Furthermore, this study estimated the total mineralized and immobilized N in aquaculture surface sediments from the Guangdong-Hong Kong-Macao Greater Bay Area, with the estimation of approximately 4.55×10^4 t N yr^{-1} and 3.68×10^4 t N yr^{-1}, respectively. GNM flux shows higher level than GAI flux, indicating that sediment is a crucial DIN source in the aquaculture ecosystem, which plays a non-negligible role in the exacerbation of eutrophication. Overall, this study improves the understanding of sediment N transformation processes and relevant regulation mechanisms in the reclaimed aquaculture ecosystems.

Data availability statement

The original contributions presented in the study are included in the article/Supplementary Material. Further inquiries can be directed to the corresponding author.

Author contributions

XL: Methodology, Validation, Formal analysis, Investigation, Data curation, Writing-original draft, Writing-review & editing, Funding acquisition. GL: Writing-original draft, Formal analysis, Writing-review & editing. YZ: Writing-original draft, Formal analysis, Visualization, Funding acquisition. WL: Investigation, Data curation, Writing - review & editing. PG: Data curation, Formal analysis, Writing - review & editing. SF: Writing-original draft, Formal analysis. TK: Data curation, Formal analysis. DT: Formal analysis, Data curation, Supervision. DS: Investigation, Data curation. ZS: Writing-original draft, Writing - review & editing, Funding acquisition. All authors contributed to the article and approved the submitted version.

Funding

This work was supported by the Natural Science Foundation of China (grant numbers: 31970486, 42001088), Fundamental Research Funds for the Central Universities (202262007), Innovation Group Project of Southern Marine Science and Engineering Guangdong Laboratory (Zhuhai) (311021004), the Guangdong Basic and Applied Basic Research Foundation (2020A1515010908), the Science and Technology Program of Guangzhou (No. 202002030453) and the Special fund for scientific innovation strategy-construction of high-level Academy of Agriculture Science (R2020YJ-YB3006).

Acknowledgments

We thank Prof. Jun Gong, Prof. Kedong Yin, Prof. Lijun Hou, Prof. Min Liu, and Prof. Qiangtai Huang for providing the test platform. We thank Zexin Li, Bin Wang, Rixuan Gao, Yijing Liu, Yijing Shen, Yongyi Peng, and Shuai Li for data collection. We also thank Prof. Bin Ai, Prof. Jun Zhao and Ke Huang for the help in the data about Figure S1. Thanks are given to the editor and reviewers for valuable comments on this manuscript.

Conflict of interest

The authors declare that the research was conducted in the absence of any commercial or financial relationships that could be construed as a potential conflict of interest.

Publisher's note

All claims expressed in this article are solely those of the authors and do not necessarily represent those of their affiliated organizations, or those of the publisher, the editors and the reviewers. Any product that may be evaluated in this article, or claim that may be made by its manufacturer, is not guaranteed or endorsed by the publisher.

Supplementary material

The Supplementary Material for this article can be found online at: https://www.frontiersin.org/articles/10.3389/fmars.2022.1093279/full#supplementary-material

References

Aber, J. D. (1992). Nitrogen cycling and nitrogen saturation in temperate forest ecosystems. *Trends Ecol. Evol.* 7 (7), 220–224. doi: 10.1016/0169-5347(92)90048-G

Amano, T., Yoshinaga, I., Yamagishi, T., Van Thuoc, C., Thu, P., Ueda, S., et al. (2011). Contribution of anammox bacteria to benthic nitrogen cycling in a mangrove forest and shrimp ponds, haiphong, Vietnam. *Microbes Environ.* 26 (1), 1–6. doi: 10.1264/jsme2.ME10150

Andersen, M. K., and Jensen, L. S. (2001). Low soil temperature effects on short-term gross n mineralisation-immobilisation turnover after incorporation of a green manure. *Soil Biol. Biochem.* 33 (4-5), 511–521. doi: 10.1016/S0038-0717(00)00192-9

Bachar, A., Al-Ashhab, A., Soares, M. I. M., Sklarz, M. Y., Angel, R., Ungar, E. D., et al. (2010). Soil microbial abundance and diversity along a low precipitation gradient. *Microbial Ecol.* 60, 453–461. doi: 10.1007/s00248-010-9727-1

Bai, J., Gao, H., Xiao, R., Wang, J., and Huang, C. (2012). A review of soil nitrogen mineralization as affected by water and salt in coastal wetlands: issues and methods. *CLEAN-Soil Air Water* 40 (10), 1099–1105. doi: 10.1002/clen.201200055

Beck, T., Joergensen, R. G., Kandeler, E., Makeschin, F., Nuss, E., Oberholzer, H. R., et al. (1997). An inter-laboratory comparison of ten different ways of measuring soil microbial biomass c. *Soil Biol. Biochem.* 29 (7), 1023–1032. doi: 10.1016/S0038-0717(97)00030-8

Bengtsson, G., Bengtson, P., and Månsson, K. F. (2003). Gross nitrogen mineralization-, immobilization-, and nitrification rates as a function of soil C/N ratio and microbial activity. *Soil Biol. Biochem.* 35 (1), 143–154. doi: 10.1016/S0038-0717(02)00248-1

Blackburn, T. H. (1979). Method for measuring rates of NH_4^+ turnover in anoxic marine sediments, using a ^{15}N-NH_4^+ dilution technique. *Appl. Environ. Microbiol.* 37 (4), 760–765. doi: 10.1128/aem.37.4.760-765.1979

Buzzelli, C., Wan, Y., Doering, P. H., and Boyer, J. N. (2013). Seasonal dissolved inorganic nitrogen and phosphorus budgets for two sub-tropical estuaries in south Florida, USA. *Biogeosciences* 10 (10), 6721–6736. doi: 10.5194/bg-10-6721-2013

Cao, L., Diana, J. S., Keoleian, G. A., and Lai, Q. (2011). Life cycle assessment of Chinese shrimp farming systems targeted for export and domestic sales. *Environ. Sci. Technol.* 45 (15), 6531–6538. doi: 10.1021/es104058z

Chen, Y., Dong, S., Wang, F., Gao, Q., and Tian, X. (2016). Carbon dioxide and methane fluxes from feeding and no-feeding mariculture ponds. *Environ. pollut.* 212, 489–497. doi: 10.1016/j.envpol.2016.02.039

Corre, M. D., Schnabel, R. R., and Stout, W. L. (2002). Spatial and seasonal variation of gross nitrogen transformations and microbial biomass in a northeastern US grassland. *Soil Biol. Biochem.* 34 (4), 445–457. doi: 10.1016/S0038-0717(01)00198-5

Cufrey, J. M., and Kemp, W. M. (1992). Influence of the submersed plant, potamogeton perfoliatus, on nitrogen cycling in estuarine sediments. *Limnology Oceanography* 37 (7), 1483–1495. doi: 10.4319/lo.1992.37.7.1483

Dai, M., Wang, L., Guo, X., Zhai, W., Li, Q., He, B., et al. (2008). Nitrification and inorganic nitrogen distribution in a large perturbed river/estuarine system: The pearl river estuary, China. *Biogeosciences* 5 (5), 1227–1244. doi: 10.5194/bg-5-1227-2008

Diaz, R. J., and Rosenberg, R. (2008). Spreading dead zones and consequences for marine ecosystems. *Science* 321 (5891), 926–929. doi: 10.1126/science.1156401

Galloway, J. N., Townsend, A. R., Erisman, J. W., Bekunda, M., Cai, Z., Freney, J. R., et al. (2008). Transformation of the nitrogen cycle: recent trends, questions, and potential solutions. *Science* 320 (5878), 889–892. doi: 10.1126/science.1136674

Gao, H., Bai, J., He, X., Zhao, Q., Lu, Q., and Wang, J. (2014). High temperature and salinity enhance soil nitrogen mineralization in a tidal freshwater marsh. *PloS One* 9 (4), e95011. doi: 10.1371/journal.pone.0095011

Greaver, T. L., Clark, C. M., Compton, J. E., Vallano, D., Talhelm, A. F., Weaver, C. P., et al. (2016). Key ecological responses to nitrogen are altered by climate change. *Nat. Climate Change* 6 (9), 836e843. doi: 10.1038/nclimate3088

Herbert, R. A. (1999). Nitrogen cycling in coastal marine ecosystems. *FEMS Microbiol. Rev.* 23 (5), 563–590. doi: 10.1111/j.1574-6976.1999.tb00414.x

Hou, L., Zheng, Y., Liu, M., Gong, J., Zhang, X., Yin, G., et al. (2013). Anaerobic ammonium oxidation (anammox) bacterial diversity, abundance, and activity in marsh sediments of the Yangtze estuary. *J. Geophysical Research: Biogeosciences* 118 (3), 1237–1246. doi: 10.1002/jgrg.20108

Howarth, R., Chan, F., Conley, D. J., Garnier, J., Doney, S. C., Marino, R., et al. (2011). Coupled biogeochemical cycles: eutrophication and hypoxia in temperate estuaries and coastal marine ecosystems. *Front. Ecol. Environ.* 9 (1), 18–26. doi: 10.1890/100008

Huang, F., Lin, X., Hu, W., Zeng, F., He, L., and Yin, K. (2021). Nitrogen cycling processes in sediments of the pearl river estuary: Spatial variations, controlling factors, and environmental implications. *Catena* 206, 105545. doi: 10.1016/j.catena.2021.105545

Huang, F., Lin, X., and Yin, K. (2022). Effects of algal-derived organic matter on sediment nitrogen mineralization and immobilization in a eutrophic estuary. *Ecol. Indic.* 138, 108813. doi: 10.1016/j.ecolind.2022.108813

Hu, M., Sardans, J., Le, Y., Yan, R., Zhong, Y., Huang, J., et al. (2022). Biogeochemical behavior of p in the soil and porewater of a low-salinity estuarine wetland: Availability, diffusion kinetics, and mobilization mechanism. *Water Res.* 219, 118617. doi: 10.1016/j.watres.2022.118617

Jia, J., Bai, J. H., Gao, H. F., Wang, W., Yin, S., Wang, D. W., et al. (2019). Effects of salinity and moisture on sediment net nitrogen mineralization in salt marshes of a Chinese estuary. *Chemosphere* 228, 174–182. doi: 10.1016/j.chemosphere.2019.04.006

Jia, J., Bai, J. H., Gao, H. F., Wen, X. J., Zhang, G. L., Cui, B. S., et al. (2017). *In situ* soil net nitrogen mineralization in coastal salt marshes (*Suaeda salsa*) with different flooding periods in a Chinese estuary. *Ecol. Indic.* 73, 559e565. doi: 10.1016/j.ecolind.2016.10.012

Jiménez-Montealegre, R., Verdegem, M. C., Van Dam, A. A., and Verreth, J. A. (2005). Effect of organic nitrogen and carbon mineralization on sediment organic matter accumulation in fish ponds. *Aquaculture Res.* 36 (10), 1001–1014. doi: 10.1111/j.1365-2109.2005.01307.x

Jin, X., Huang, J., and Zhou, Y. (2012). Impact of coastal wetland cultivation on microbial biomass, ammonia-oxidizing bacteria, gross n transformation and N_2O and NO potential production. *Biol. Fertility Soils* 48 (4), 363–369. doi: 10.1007/s00374-011-0631-8

Jones, D. L., and Kielland, K. (2012). Amino acid, peptide and protein mineralization dynamics in a taiga forest soil. *Soil Biol. Biochem.* 55, 60e69. doi: 10.1016/j.soilbio.2012.06.005

Khalil, K., Laverman, A. M., Raimonet, M., and Rabouille, C. (2018). Importance of nitrate reduction in benthic carbon mineralization in two eutrophic estuaries: Modeling, observations and laboratory experiments. *Mar. Chem.* 199, 24–36. doi: 10.1016/j.marchem.2018.01.004

Kirkham, D. O. N., and Bartholomew, W. V. (1954). Equations for following nutrient transformations in soil, utilizing tracer data. *Soil Sci. Soc. America J.* 18 (1), 33–34. doi: 10.2136/sssaj1954.03615995001800010009x

Kirschbaum, M. U. (1995). The temperature dependence of soil organic matter decomposition, and the effect of global warming on soil organic c storage. *Soil Biol. Biochem.* 27 (6), 753–760. doi: 10.1016/0038-0717(94)00242-S

Lamb, A. L., Wilson, G. P., and Leng, M. J. (2006). A review of coastal palaeoclimate and relative sea-level reconstructions using $\delta^{13}C$ and C/N ratios in organic material. *Earth-Science Rev.* 75 (1-4), 29–57. doi: 10.1016/j.earscirev.2005.10.003

Li, M., Cao, H., Hong, Y., and Gu, J. D. (2013). Using the variation of anammox bacteria community structures as a bio-indicator for anthropogenic/terrestrial nitrogen inputs in the pearl river delta (PRD). *Appl. Microbiol. Biotechnol.* 97 (22), 9875–9883. doi: 10.1007/s00253-013-4990-y

Li, X., Hou, L., Liu, M., and Tong, C. (2020). Biogeochemical controls on nitrogen transformations in subtropical estuarine wetlands. *Environ. pollut.* 263, 114379. doi: 10.1016/j.envpol.2020.114379

Lin, X., Hou, L., Liu, M., Li, X., Yin, G., Zheng, Y., et al. (2016a). Gross nitrogen mineralization in surface sediments of the Yangtze estuary. *PloS One* 11 (3), e0151930. doi: 10.1371/journal.pone.0151930

Lin, X., Hou, L., Liu, M., Li, X., Zheng, Y., Yin, G., et al. (2016b). Nitrogen mineralization and immobilization in sediments of the East China Sea: Spatiotemporal variations and environmental implications. *J. Geophysical Research: Biogeosciences* 121 (11), 2842–2855. doi: 10.1002/2016JG003499

Lin, X., Li, X., Gao, D., Liu, M., and Cheng, L. (2017). Ammonium production and removal in the sediments of shanghai river networks: Spatiotemporal variations, controlling factors, and environmental implications. *J. Geophysical Research: Biogeosciences* 122 (10), 2461–2478. doi: 10.1002/2017JG003769

Lin, G., and Lin, X. (2022). Bait input altered microbial community structure and increased greenhouse gases production in coastal wetland sediment. *Water Res.* 218, 118520. doi: 10.1016/j.watres.2022.118520

Li, H. M., Tang, H. J., Shi, X. Y., Zhang, C. S., and Wang, X. L. (2014). Increased nutrient loads from the changjiang (Yangtze) river have led to increased harmful algal blooms. *Harmful Algae* 39, 92–101. doi: 10.1016/j.hal.2014.07.002

Liu, B., Peng, S., Liao, Y., and Long, W. (2018). The causes and impacts of water resources crises in the pearl river delta. *J. Cleaner Production* 177, 413–425. doi: 10.1016/j.jclepro.2017.12.203

Liu, Y., Wang, C., He, N., Wen, X., Gao, Y., Li, S., et al. (2017). A global synthesis of the rate and temperature sensitivity of soil nitrogen mineralization: latitudinal patterns and mechanisms. *Global Change Biol.* 23 (1), 455–464. doi: 10.1111/gcb.13372

Li, X., Wai, O. W., Li, Y. S., Coles, B. J., Ramsey, M. H., and Thornton, I. (2000). Heavy metal distribution in sediment profiles of the pearl river estuary, south China. *Appl. Geochemistry* 15 (5), 567–581. doi: 10.1016/S0883-2927(99)00072-4

Lovley, D. R., and Phillips, E. J. (1987). Rapid assay for microbially reducible ferric iron in aquatic sediments. *Appl. Environ. Microbiol.* 53 (7), 1536–1540. doi: 10.1128/aem.53.7.1536-1540.1987

Mao, S. H., Zhang, H. H., Zhuang, G. C., Li, X. J., Liu, Q., Zhou, Z., et al. (2022). Aerobic oxidation of methane significantly reduces global diffusive methane emissions from shallow marine waters. *Nat. Commun.* 13, 7309. doi: 10.1038/s41467-022-35082-y

Matheson, F. E., Nguyen, M. L., Cooper, A. B., and Burt, T. P. (2003). Short-term nitrogen transformation rates in riparian wetland soil determined with nitrogen-15. *Biol. Fertility Soils* 38 (3), 129–136. doi: 10.1007/s00374-003-0640-3

Miller, K. S., and Geisseler, D. (2018). Temperature sensitivity of nitrogen mineralization in agricultural soils. *Biol. Fertility Soils* 54 (7), 853–860. doi: 10.1007/s00374-018-1309-2

Mishra, S., Di, H. J., Cameron, K. C., Monaghan, R., and Carran, A. (2005). Gross nitrogen mineralization rates in pastural soils and their relationships with organic nitrogen fractions, microbial biomass and protease activity under glasshouse conditions. *Biol. Fertility soils* 42 (1), 45–53. doi: 10.1007/s00374-005-0863-6

Mooshammer, M., Wanek, W., Hämmerle, I., Fuchslueger, L., Hofhansl, F., Knoltsch, A., et al. (2014). Adjustment of microbial nitrogen use efficiency to carbon: nitrogen imbalances regulates soil nitrogen cycling. *Nat. Communication* 5, 3694. doi: 10.1038/ncomms4694

Murray, R. H., Erler, D. V., and Eyre, B. D. (2015). Nitrous oxide fluxes in estuarine environments: Response to global change. *Global Change Biol.* 21 (9), 3219–3245. doi: 10.1111/gcb.12923

Park, S. J., Seo, B. S., Park, H. S., Lee, B. J., Hur, S. W., Nam, T. J., et al. (2021). Effect of fishmeal content in the diet on the growth and sexual maturation of olive flounder (*Paralichthys olivaceus*) at a typical fish farm. *Animals* 11 (7), 2055. doi: 10.3390/ani11072055

Paul, K. I., Polglase, P. J., O'connell, A. M., Carlyle, J. C., Smethurst, P. J., and Khanna, P. K. (2003). Defining the relation between soil water content and net nitrogen mineralization. *Eur. J. Soil Sci.* 54 (1), 39–48. doi: 10.1046/j.1365-2389.2003.00502.x

Pena, M. A., Katsev, S., Oguz, T., and Gilbert, D. (2010). Modeling dissolved oxygen dynamics and hypoxia. *Biogeosciences* 7 (3), 933–957. doi: 10.5194/bg-7-933-2010

Qi, X., Liu, H., Lin, Z., Liu, X., and Gong, H. (2019). Impacts of age and expansion direction of invasive spartina alterniflora on soil organic carbon dynamics in coastal salt marshes along eastern China. *Estuaries Coasts* 42 (7), 1858–1867. doi: 0.1007/s12237-019-00611-4

Rousk, J., Bååth, E., Brookes, P. C., Lauber, C. L., Lozupone, C., Caporaso, J. G, et al (2010). Soil bacterial and fungal communities across a pH gradient in an arable soil. *ISME J.* 4 (10), 1340–1351.

Rutigliano, F. A., Castaldi, S., D'ascoli, R., Papa, S., Carfora, A., Marzaioli, R., et al. (2009). Soil activities related to nitrogen cycle under three plant cover types in Mediterranean environment. *Appl. Soil Ecol.* 43 (1), 40–46. doi: 10.1016/j.apsoil.2009.05.010

Silva, R. G., Jorgensen, E. E., Holub, S. M., and Gonsoulin, M. E. (2005). Relationships between culturable soil microbial populations and gross nitrogen transformation processes in a clay loam soil across ecosystems. *Nutrient Cycling Agroecosystems* 71 (3), 259–270. doi: 10.1007/s10705-004-6378-y

Treseder, K. K., Schimel, J. P., Garcia, M. O., and Whiteside, M. D. (2010). Slow turnover and production of fungal hyphae during a Californian dry season. *Soil Bology Biochem.* 42 (9), 1657–1660. doi: 10.1016/j.soilbio.2010.06.005

Vance, E. D., Brookes, P. C., and Jenkinson, D. S. (1987). An extraction method for measuring soil microbial biomass c. *Soil Bology Biochem.* 19 (6), 703–707. doi: 10.1016/0038-0717(87)90052-6

Vieira, F. C. B., Bayer, C., Zanatta, J. A., Dieckow, J., Mielniczuk, J., and He, Z. L. (2007). Carbon management index based on physical fractionation of soil organic matter in an acrisol under long-term no-till cropping systems. *Soil Tillage Res.* 96 (1-2), 195–204. doi: 10.1016/j.still.2007.06.007

Wang, R. N., Wang, M., Huang, Q. B., Yi, M. M., Li, Z. H., Li, Q. Y., et al. (2020). Analysis of differences in microbial community structure of eel (*Anguilla japonica*) pond before and after pond-drying based on high-throughput sequencing. *J. Agric. Biotechnol.* 28 (7), 1250–1259. doi: 10.3969/j.issn.1674-7968.2020.07.011

Wang, S., Zhu, G., Peng, Y., Jetten, M. S., and Yin, C. (2012). Anammox bacterial abundance, activity, and contribution in riparian sediments of the pearl river estuary. *Environ. Sci. Technol.* 46 (16), 8834–8842. doi: 10.1021/es3017446

Wu, J. P., Hong, Y. G., Liu, X. H., and Hu, Y. H. (2021). Variations in nitrogen removalrates and microbial communities over sediment depth in daya bay, China. *Environ. pollut.* 286, 117267. doi: 10.1016/j.envpol.2021.117267

Wu, J. P., Hong, Y. G., Wen, X. M., Li, Y. B., Wang, Y., and Chang, X. Y. (2020). Activity,abundance and community composition of anaerobic ammonia-oxidizing (anammox) bacteria in sediment cores of the pearl river estuary. *Estuaries Coasts* 43, 73–85. doi: 10.1007/s12237-019-00668-1

Wu, H., Peng, R., Yang, Y., He, L., Wang, W., Zheng, T., et al. (2014). Mariculture pond influence on mangrove areas in south China: Significantly larger nitrogen and phosphorus loadings from sediment wash-out than from tidal water exchange. *Aquaculture* 426, 204–212. doi: 10.1016/j.aquaculture.2014.02.009

Yang, X., Hu, C., Wang, B., Lin, H., Xu, Y., Guo, H., et al. (2022). Sediment nitrogen mineralization and immobilization affected by non-native *Sonneratia apetala* plantation in an intertidal wetland of south China. *Environ. pollut.* 305, 119289. doi: 10.1016/j.envpol.2022.119289

Yang, C., Wang, S., Jin, X., and Wu, F. (2010). Nitrogen and phosphorus mineralization in sediments of taihu lake after the removal of light fraction organic matter. *Environ. Earth Sci.* 59 (7), 1437–1446. doi: 10.1007/s12665-009-0130-5

Yuste, J. C., Penuelas, J., Estiarte, M., Garcia-Mas, J., Mattana, S., Ogaya, R., et al. (2011). Drought-resistant fungi control soil organic matter decomposition and its response to temperature. *Global Change Biol.* 17 (3), 1475–1486. doi: 10.1111/j.1365-2486.2010.02300.x

Zhang, W. L., Zeng, C. S., Tong, C., Zhai, S. J., Lin, X., Gao, D. Z., et al. (2015). Spatial distribution of phosphorus speciation in marsh sediments along a hydrologic gradient in a subtropical estuarine wetland, China. *Estuarine, Coastal and Shelf Science* 154 (3), 30–38.

Zhou, H. H., Du, J., Nan, Y., Song, K. S., Zhao, B. Y., and Xiang, X. Y. (2019). Landscape patterns of coastal wetlands in pearl river delta and their changes for 5 periods since 1980. *Wetland Sci.* 17, 559–566. doi: 10.13248/j.cnki.wetlandsci.2019.05.009

Zhu, T., Meng, T., Zhang, J., Yin, Y., Cai, Z., Yang, W., et al. (2013). Nitrogen mineralization, immobilization turnover, heterotrophic nitrification, and microbial groups in acid forest soils of subtropical China. *Biol. Fertility Soils* 49 (3), 323–331. doi: 10.1007/s00374-012-0725-y

Zilio, M., Motta, S., Tambone, F., Scaglia, B., Boccasile, G., Squartini, A., et al. (2020). The distribution of functional n-cycle related genes and ammonia and nitrate nitrogen in soil profiles fertilized with mineral and organic n fertilizer. *PloS One* 15 (6), e0228364. doi: 10.1371/journal.pone.0228364

Zuo, P., Li, Y., Liu, C. A., Zhao, S. H., and Guan, D. M. (2013). Coastal wetlands of China: changes from the 1970s to 2007 based on a new wetland classification system. *Estuaries Coasts* 36 (2), 390–400. doi: 10.1007/s12237-012-9575-y

Frontiers in Marine Science

Explores ocean-based solutions for emerging global challenges

The third most-cited marine and freshwater biology journal, advancing our understanding of marine systems and addressing global challenges including overfishing, pollution, and climate change.

Discover the latest Research Topics

See more →

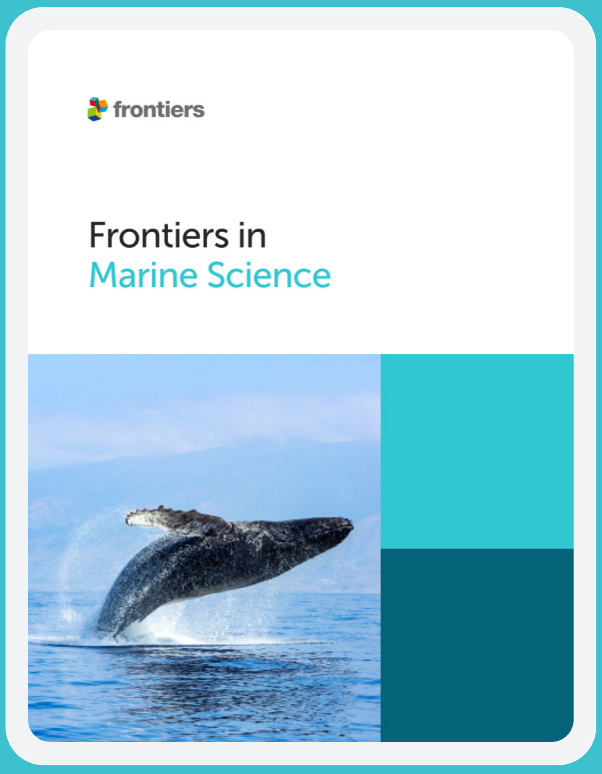

Frontiers

Avenue du Tribunal-Fédéral 34
1005 Lausanne, Switzerland
frontiersin.org

Contact us

+41 (0)21 510 17 00
frontiersin.org/about/contact